PSDF

Power Systems Development Facility

Technical Progress Report
Gasification Test Run GCT 2

April 10 - 27, 2000

DOE Cooperative Agreement Number
DE-FC21-90MC25140

SOUTHERN COMPANY

Energy to Serve Your World®

POWER SYSTEMS DEVELOPMENT FACILITY

TECHNICAL PROGRESS REPORT
GASIFICATION TEST RUN GCT2
APRIL 10 – 27, 2000

DOE Cooperative Agreement Number
DE-FC21-90MC25140

Prepared by:
Southern Company Services, Inc.
Power Systems Development Facility
P.O. Box 1069
Wilsonville, AL 35186
Tel: 205-670-5840
Fax: 205-670-5843
http://psdf.southernco.com

August 2001

POWER SYSTEMS DEVELOPMENT FACILITY

DISCLAIMER

Available to the public from the National Technical Information Service, U.S. Department of Commerce, 5285 Port Royal Road, Springfield, VA 22161. Phone orders accepted at (703) 487-4650.

ACKNOWLEDGEMENT

The authors wish to acknowledge the contributions and support provided by various project managers: Jim Longanbach (DOE), Neville Holt (EPRI), Gene Cover (KBR), Zal Sanjana (Westinghouse), and Vann Bush (SRI). Also, the enterprising solutions to problems and the untiring endeavors of many personnel at the site during commissioning of the transport reactor train in gasification mode of operation are greatly appreciated. The project was sponsored by the U.S. Department of Energy National Energy Technology Laboratory under contract DE-FC21-90MC25140.

CONTENTS

Section Page

Listing of Tables

Listing of Figures

1.0 EXECUTIVE SUMMARY

1.1 SUMMARY

This report discusses gasification characterization test 2 (GCT2) of the Kellogg Brown & Root transport reactor train with a Siemens Westinghouse Power Corporation (Siemens Westinghouse) particle filter system at the Power Systems Development Facility (PSDF) located in Wilsonville, Alabama. The transport reactor is an advanced circulating fluidized-bed reactor designed to operate as either a combustor or a gasifier using one of two possible particulate control devices (PCDs). The transport reactor was operated as a pressurized gasifier during GCT2.

GCT2 was planned as a 250-hour test run to characterize the limits of operational parameter variations using a blend of several Powder River Basin (PRB) coals and Ohio Bucyrus limestone. The primary test objectives were:

- *Gas Velocity* – Characterize the effect of gas velocity on solids collection efficiency.
- *Higher Operating Temperature and Pressure* – Evaluate the effect of higher operating temperature and pressure on process performance.

Secondary objectives included the continuation of the following reactor characterizations:

- *Operational Stability* – Characterize reactor loop and PCD operations with short-term tests by varying coal feed, air/coal ratio, riser velocity, solids circulation rate, system pressure, and air distribution.
- *Reactor Operations* – Study the devolatilization and tar cracking effects from transient conditions during transition from start-up burner to coal. Evaluate the effect of process operations on heat release, heat transfer, and accelerated fuel particle heat-up rates. Study the effect of changes in reactor conditions on transient temperature profiles, pressure balance, and product gas composition.
- *Effects of Reactor Conditions on Syngas Composition* – Evaluate the effect of air distribution, steam/coal ratio, solids circulation rate, and reactor temperature on CO/CO_2 ratio, H_2/converted carbon ratio, gasification rates, carbon conversion, and cold and hot gas efficiencies.
- *Effects of Reactor Conditions on H_2S Emissions* – Study the effect of Ca/S molar ratio, riser velocity, and solids circulation rate on sulfur capture. Evaluate effects on limits of sulfur capture dynamics in relation to CaS-H_2O-H_2S-CaO reaction's approach to equilibrium.
- *Forms of Sulfur From Reactor Operations* – Determine the effect of reactor operations on forms of sulfur (CaS, $CaSO_4$, FeS) in the reactor standpipe solids and in the fines from

the PCD. Quantify the reactive sulfide concentration in these solids streams and at the sulfator solids outlet.

Test run GCT2 was started on April 10, 2000, and was completed on April 27, 2000. This test run provided additional data necessary to analyze reactor operations and to identify necessary modifications to improve equipment and process performance. The reactor temperature was varied between 1,650 and 1,800°F at pressures from 160 to 240 psig; 313 hours of solid circulation and 217 hours of coal feed were attained.

1.2 PSDF ACCOMPLISHMENTS

The PSDF has achieved over 4,985 hours of operation on coal feed and about 6,470 hours of solids circulation in combustion mode and 673 hours of solid circulation and 450 hours of coal feed in gasification mode of operation. The major accomplishments during GCT1 and GCT2 are summarized below. For combustion related accomplishments see the technical progress report for the TC05 test campaign.

1.2.1 Transport Reactor Train

The major accomplishments and observations during GCT1 and GCT2 included the following:

1. With subbituminous coal, about 90-percent carbon conversion and 100 Btu/scf syngas heating value (corrected for aeration and instrument nitrogen) can be attained. This is sufficient to support existing pressurized syngas burners without further dilution by nitrogen or saturation by water vapor. Moisture content in the syngas is sufficient for NO_X control.

2. In GCT1, two bituminous coals and a PRB coal were tested with different sorbents. In GCT2, stable gasification reactor operation was achieved at several fuel gas-flow rates and reactor pressures up to 240 psig on PRB coal.

3. The corrected fuel gas heating values from PRB coal were in 85 to 105 Btu/scf range depending on the test condition during the 5 days of stable gasification operation in GCT2. The gas yield was between 3.0 and 3.5 lb/lb coal. In the test range, the solids circulation rates, gas and solids residence times, and reactor temperatures do not show much effect on the fuel gas-heating values.

4. As the coal-feed rate was increased from 0.85 to 1.40 times the design coal-feed rate to the transport gasifier, the apparent air/coal ratio decreased from 3.1 to 2.5 lb/lb coal (corresponding to the total oxygen from air and coal to converted carbon molar ratio from 0.72 to 0.62). The actual air/coal ratio, however, remained constant at around 2.0 after removing the effect of heat loss and energy required for heating the added nitrogen.

5. The devolatilization products evolution on unit coal-feed basis is generally invariant to an increase in PRB coal-feed rate. The observed increase in syngas heating value at high coal-feed rates is mainly due to reduced effect of added nitrogen (dilution and relatively less energy consumption for heatup).

6. For PRB coal, the corrected cold-gas efficiency (syngas latent heat to coal latent heat) remained nearly constant at around 60 percent in spite of changes in operating parameters such as reactor temperatures, pressures, gas residence time, and coal- and steam-feed rates. The corrected hot-gas efficiency (syngas latent + sensible heat-to-coal latent heat) was 80 percent and the remaining coal latent heat was mainly present in the ash/char stream from the process.

7. Steam has a major role to play in the performance of the transport gasifier. When the ratio of total steam-(steam fed and coal moisture)-to-fed PRB carbon varied from 0.42 to 0.54, the gas H_2-to-feed carbon ratio varied from 0.25 to 0.3. Based on gas analysis, test data show that for each mole of carbon converted about 0.35 moles of steam react.

8. The longest continuous run of 184 hours in gasification mode of operation at the pilot plant was achieved with PRB coal. No deposits, clinkers, or any other operational problems were encountered with either the transport reactor or the PCD operation.

9. The overall mass balance was excellent at ± 2 percent. The carbon, hydrogen, and oxygen element balances were good at ± 10 percent. The calcium balance was poor at ±60 percent and the coal ash and limestone inerts balance was marginal at ± 20 percent.

10. Tar formation could be minimized and completely eliminated during certain test periods by varying reactor operating parameters.

11. Overall the dipleg operated well with high solids flow through the dipleg due to the inefficiency of the disengager. However, there were brief cyclone dipleg upsets.

12. The reactor loop ran consistently at about 50-percent design circulation rate. Reactor operations were smooth without any incident of oxygen breakthrough or any temperature excursions.

13. The highest temperature could be maintained in the mixing zone. By increasing the coal-feed rate the highest temperature would move from lower riser to mid-mixing zone.

14. Carbon content of recirculating solids is just sufficient to maintain reactor temperature of 1,800°F at coal-feed rates tested.

15. As the coal-feed rate was increased the solids circulation rate increased, the standpipe level increased, and the loading to PCD also increased.

16. Limestone calcination of 90 to 100 percent was achieved in the transport gasifier.

17. The PCD operated extremely well at conditions tested (i.e., solids circulation rates, loading, gas flow rates, temperature and pressure).

18. The transition from the start-up burner to coal feed was smooth without any incidents of oxygen breakthrough.

19. Temperature swings were observed in the reactor even without varying operating parameters. The temperature swings may be related to cycling of the coal-feed system. At high coal-feed rates the system is designed to cycle every 5 minutes. Further study is to be done to control this variation within acceptable limits.

20. After initial problems with lines plugging with coal feed fines, the coal-feed system operated flawlessly. High coal-feed rates (up to 1.1 x design) were achieved with room to increase rates further to 1.2 x design.

21. The primary gas cooler operated well without any signs of plugging. However, there was a decrease in heat-removal rates over a period of time, likely due to tar deposits on the heat transfer area.

22. The thermal oxidizer (atmospheric syngas burner) operated well with syngas of different heating values and a small amount of propane.

23. With logic changes made to the reactor controls, the char/ash removal system (FD0510) operated well without any line plugging during gasification.

24. The fine ash/char cooling and transfer system (FD0502/FD0520) operated well; however, there were problems at times when trying to remove solids from the PCD cone. If further increases are made to solids carryover to PCD the bottleneck in the fines removal system will be the FD0502 screw cooler.

25. The heat-removal capacity of the sulfator remains too high to achieve an operating temperature of 1,600°F. Insufficient air flow to complete combustion due to greater-than-design carbon feed rates remains a problem.

26. A separate level/temperature-control system for the steam condensate system worked well. There were no sulfator-related trips due to low-steam flow.

27. Flare pilot-sensing reliability was better than for the previous run; however, additional improvements need to be made. Flow sensing of both propane and syngas flow to the flare was more reliable.

28. Unacceptably high baghouse temperature continues to be an issue. Higher temperature is the result of combination of a higher-than-design coal-feed rates to gasifier, syngas flow rates, flue gas flow rates from sulfator, and lower-than-design cooling dilution air availability.

1.2.2 PCD

The major highlights for the PCD area during GCT2 are summarized below.

1. The PCD successfully operated for about 217 on-coal hours during the GCT2 gasification test run. Stable PCD operation was maintained that was not achieved during the GCT1A and GCT1B through D gasification test runs. The PCD temperatures were controlled at stable levels. The inlet particulate loading was stable and less than that in GCT1. The solids accumulation in the PCD cone, therefore, was significantly reduced.

2. All new monolithic silicon carbide filter elements from Pall and Schumacher performed well without mechanical failure. The visual inspection showed that all filter elements kept their integrity and the clean-side surface was clean. The char cake was thin and uniform after the clean shutdown. No solids bridging was found between filter elements and plenum walls.

3. The new filter holders developed by PSDF personnel and the new fail-safe gasket developed by Siemens Westinghouse were installed on all filter elements in GCT2. These fixture assemblies performed successfully. The outlet loading never exceeded 0.5 ppmw throughout the entire run. Elimination of instrument wires through the Conax fittings on the plenums was another factor contributing to the lower char emission.

4. The pressure drop across the PCD was stabilized and controlled within an acceptable level for both the baseline and transient DP. The back-pulse parameters were adjusted according to the PCD system response and there still was room for further reduction to the back-pulse intensity and frequency, which are important to the operations in commercial plants. In comparison, stabilized DP was not achieved in GCT1 and this eventually led to unplanned system shutdowns.

5. SRI successfully measured inlet and outlet particulate loadings during the run. Char samples from the inlet sampling and from char cake were analyzed and tested. The lab measurements are consistent with actual PCD performance. A better understanding of the effects of particle size and surface area on char cake drag has been developed.

6. The ash removal system (FD0520/FD0502) worked fine in GCT2. Due to the lower inlet particulate loading to the PCD, solids accumulated in the PCD cone only on two occasions. However, the O-rings on lock hopper spheri valves failed several times during start-up, causing unnecessary system shutdowns. The system did not fail again once the hardware insert that holds the O-rings was replaced with a spare part.

7. The post-run PCD inspection showed that the shroud and liner sections were relatively clean. There was no further distortion on the shroud and liners. The plenums and tubesheet were also clean compared to the previous gasification runs.

8. Ten different types of new Siemens Westinghouse fail-safes were tested to support the development of the technology. After the exposure in GCT2 they were flow tested at Siemens Westinghouse Power Corporation. The results showed that there was no loss in their permeability. The fail-safes will be continuously tested in the following runs and their performance will be further evaluated.

9. Material testing was conducted at SRI on seven filter elements removed after GCT2. The results will be presented in a later report along with results for two elements from GCT1A and one element from GCT1B through D.

1.3 FUTURE PLANS

One additional 250-hour characterization test run with the transport reactor train operating in gasification mode is planned for late 2000. Several large-scale modifications and repairs for the transport reactor will be completed before this test. These activities include major refractory repairs to the primary cyclone and disengager and a modified loop seal on the cyclone dipleg.

2.0 INTRODUCTION

This report provides an account of the GCT2 test campaign with the Kellogg Brown & Root (KBR) transport reactor and the Siemens Westinghouse Power Corporation (Siemens Westinghouse) filter vessel at the Power Systems Development Facility (PSDF) located in Wilsonville, Alabama, 40 miles southeast of Birmingham. The PSDF is sponsored by the U. S. Department of Energy (DOE) and is an engineering-scale demonstration of two advanced coal-fired power systems. In addition to DOE, Southern Company Services, Inc., (SCS), Electric Power Research Institute (EPRI), and Peabody Holding Company are cofunders. Other cofunding participants supplying services or equipment include KBR, Foster Wheeler (FW), Siemens Westinghouse, and Combustion Power Company. SCS is responsible for constructing, commissioning, and operating the PSDF.

2.1 THE POWER SYSTEMS DEVELOPMENT FACILITY

SCS entered into an agreement with DOE/National Energy Technology Laboratory (NETL) for the design, construction, and operation of a hot-gas clean-up test facility for pressurized gasification and combustion. The purpose of the PSDF is to provide a flexible test facility that can be used to test advanced power system components and assess the integration and control issues of advanced power systems. The facility was designed as a resource for rigorous, long-term testing and performance assessment of hot-stream, clean-up devices and other components in an integrated environment.

The PSDF was designed to consist of five modules for systems and component testing. These modules include:

- An advanced pressurized fluidized-bed combustion module (APFBC).
- A transport reactor module.
- A hot-gas clean-up module.
- A compressor/turbine module.
- A fuel cell module.

The APFBC module consists of FW technology for second-generation PFBC. This module relies on the partial conversion of the coal to fuel gas in a carbonizer, with the remaining char converted in a PFBC. Both the fuel gas and PFBC exhaust gas streams are filtered to remove particulates, then combined in a topping combustor to raise the inlet gas temperature to a combustion turbine. The advanced gasifier module includes KBR transport reactor technology for pressurized combustion and gasification to provide either an oxidizing or reducing gas for parametric testing of hot particulate control devices. The filter systems that will be tested at PSDF include particulate control devices (PCD) supplied by Combustion Power Company and by Siemens Westinghouse.

2.2 TRANSPORT REACTOR SYSTEM DESCRIPTION

The transport reactor is an advanced circulating fluidized-bed reactor operating as either a combustor or as a gasifier, using one of two possible hot-gas, clean-up filter technologies (particulate control devices or PCDs) at a component size readily scaleable to commercial systems. The transport reactor train operating in either the combustion or gasification modes is shown schematically in Figure 2.2-1. A taglist of all major equipment in the process train and associated balance-of-plant is provided in Tables 2.2-1 and -2.

The transport reactor consists of a mixing zone, a riser, a disengager, a cyclone, a standpipe, a dipleg, a solids cooler, and J-legs. In the combustion mode, the fuel, sorbent, and air are mixed together in the mixing zone along with the solids from the standpipe and solids cooler J-legs. The mixing zone, located below the riser, has a slightly larger diameter compared to the top part of the riser. Provision is made to inject air at several different points along the riser to control the formation of NO_X during combustion mode of operation. The gas and solids move up the riser together, make two turns, and enter the disengager. The disengager removes larger particles by gravity separation. The gas and remaining solids then move to the cyclone, which removes most of the particles not collected by the disengager. The gas then exits the transport reactor and goes to the primary gas cooler and the PCD for final particulate clean-up. The solids collected by the disengager and cyclone are recycled back to the reactor mixing zone through the standpipe and a J-leg. In the combustion mode of operation the solids cooler controls the reactor temperature by generating steam and provides solids surge volume. A part of the solids stream from the standpipe flows through the solids cooler. The solids from the solids cooler then return to the bottom of the reactor mixing zone through another J-leg. The solids cooler is not used in gasification. The nominal transport reactor operating temperatures are 1,800 and 1,600°F for gasification and combustion modes, respectively. The reactor system is designed to have a maximum operation pressure of 294 psig with a thermal capacity of about 21 MBtu/hr for combustion mode and 41 MBtu/hr for gasification mode.

For start-up purposes, a burner (BR0201) is provided at the reactor mixing zone. Liquefied propane gas (LPG) is used as start-up fuel. The fuel and sorbent are separately fed into the transport reactor through lockhoppers. Coal is ground to a nominal average particle diameter of 300 to 400 µm when the transport reactor is operated in gasification mode and combustion mode, respectively. Sorbent is ground to a nominal average particle diameter of 20 to 60 µm. Limestone or dolomitic sorbents are fed into the reactor for sulfur capture, thus decreasing the need for downstream facilities to reduce plant sulfur emissions. The gas leaves the transport reactor cyclone and goes to the primary gas cooler which cools the gas prior to entering the Siemens Westinghouse PCD barrier filter. The PCD uses ceramic or metal elements to filter out dust from the reactor. The filters remove almost all the dust from the gas stream to prevent erosion of a downstream gas turbine in a commercial plant. The operating temperature of the PCD is controlled both by the reactor temperature and by an upstream gas cooler. For test purposes, the gas from the transport reactor can flow through the gas cooler from zero to 100 percent. The PCD gas temperature can range from 700 to 1,600°F. The filter elements are back-pulsed by high-pressure nitrogen or air in a desired time interval or at a given maximum pressure difference across the elements. There is a secondary gas cooler located behind the filter vessel to cool the gas before discharging it to the stack or thermal oxidizer. In a commercial

process, the gas from the PCD would be sent to a combustion gas turbine. The flue gas or fuel gas is sampled for on-line analysis after traveling through the secondary gas cooler.

After exiting the secondary gas cooler the gas is then let down to about 2 psig through a pressure control valve. In gasification, the fuel gas is then sent to a thermal oxidizer to burn the gas and oxidize all reduced sulfur compounds (H_2S, COS, CS_2) and reduced nitrogen compounds (NH3, HCN). The thermal oxidizer uses propane as a supplemental fuel. In combustion, the thermal oxidizer can be bypassed and fired on propane to make start-up steam. The gas from the thermal oxidizer goes to the baghouse and then to the stack.

The transport reactor produces both fine ash collected by the PCD and coarse ash extracted from the transport reactor standpipe. The two solid streams are cooled using screw coolers, reduced in pressure in lock hoppers, and then combined. The combustion solids are suitable as produced for commercial use or as landfill. In gasification, any fuel sulfur captured by sorbent should be present as calcium sulfide (CaS). The gasification solids are processed in the sulfator to oxidize the CaS to calcium sulfate ($CaSO_4$) and burn any residual carbon on the ash. The waste solids are then suitable for commercial use or disposal. Neither the sulfator nor the thermal oxidizer would be part of a commercial process. In a commercial process the gasification solids would be burned in a pressurized, fluidized bed combustor to recover the heating value of the residual carbon content.

Table 2.2-1

Major Equipment in the Transport Reactor Train

TAG NAME	DESCRIPTION
BR0201	Reactor Start-Up Burner
BR0401	Thermal Oxidizer
BR0602	Sulfator Start-Up/PCD Preheat Burner
CO0201	Main Air Compressor
CO0401	Recycle Gas Booster Compressor
CO0601	Sulfator Air Compressor
CY0201	Primary Cyclone in the Reactor Loop
CY0207	Disengager in the Reactor Loop
CY0601	Sulfator Cyclone
DR0402	Steam Drum
DY0201	Feeder System Air Dryer
FD0206	Spent Solids Screw Cooler
FD0210	Coal Feeder System
FD0220	Sorbent Feeder System
FD0502	Fines Screw Cooler
FD0510	Spent Solids Transporter System
FD0520	Fines Transporter System
FD0530	Spent Solids Feeder System
FD0602	Sulfator Solids Screw Cooler
FD0610	Sulfator Sorbent Feeder System
FL0301	PCD — Siemens Westinghouse
FL0302	PCD — Combustion Power
FL0401	Compressor Intake Filter
HX0202	Primary Gas Cooler
HX0203	Combustor Heat Exchanger
HX0204	Transport Air Cooler
HX0402	Secondary Gas Cooler
HX0405	Compressor Feed Cooler
HX0601	Sulfator Heat Recovery Exchanger
ME0540	Heat Transfer Fluid System
RX0201	Transport Reactor
SI0602	Spent Solids Silo
SU0601	Sulfator

Table 2.2-2 (Page 1 of 3)

Major Equipment in the Balance-of-Plant

TAG NAME	DESCRIPTION
BO2920	Auxiliary Boiler
BO2921	Auxiliary Boiler – Superheater
CL2100	Cooling Tower
CO2201A-D	Service Air Compressor A-D
CO2202	Air-Cooled Service Air Compressor
CO2203	High-Pressure Air Compressor
CO2601A-C	Reciprocating N_2 Compressor A-C
CR0104	Coal and Sorbent Crusher
CV0100	Crushed Feed Conveyor
CV0101	Crushed Material Conveyor
DP2301	Baghouse Bypass Damper
DP2303	Inlet Damper on Dilution Air Blower
DP2304	Outlet Damper on Dilution Air Blower
DY2201A-D	Service Air Dryer A-D
DY2202	Air-Cooled Service Air Compressor Air Dryer
DY2203	High-Pressure Air Compressor Air Dryer
FD0104	MWK Coal Transport System
FD0111	MWK Coal Mill Feeder
FD0113	Sorbent Mill Feeder
FD0140	Coke Breeze and Bed Material Transport System
FD0154	MWK Limestone Transport System
FD0810	Ash Unloading System
FD0820	Baghouse Ash Transport System
FL0700	Baghouse
FN0700	Dilution Air Blower
HO0100	Reclaim Hopper
HO0105	Crushed Material Surge Hopper
HO0252	Coal Surge Hopper
HO0253	Sorbent Surge Hopper
HT2101	MWK Equipment Cooling Water Head Tank
HT2103	SCS Equipment Cooling Water Head Tank
HT0399	60-Ton Bridge Crane
HX2002	MWK Steam Condenser
HX2003	MWK Feed Water Heater

Table 2.2-2 (Page 2 of 3)

Major Equipment in the Balance-of-Plant

TAG NAME	DESCRIPTION
HX2004	MWK Subcooler
HX2103A	SCS Cooling Water Heat Exchanger
HX2103C	MWK Cooling Water Heat Exchanger
LF0300	Propane Vaporizer
MC3001-3017	MCCs for Various Equipment
ME0700	MWK Stack
ME0701	Flare
ME0814	Dry Ash Unloader for MWK Train
ML0111	Coal Mill for MWK Train
ML0113	Sorbent Mill for Both Trains
PG2600	Nitrogen Plant
PU2000A-B	MWK Feed Water Pump A-B
PU2100A-B	Raw Water Pump A-B
PU2101A-B	Service Water Pump A-B
PU2102A-B	Cooling Tower Make-Up Pump A-B
PU2103A-D	Circulating Water Pump A-D
PU2107	SCS Cooling Water Make-Up Pump
PU2109A-B	SCS Cooling Water Pump A-B
PU2111A-B	MWK Cooling Water Pump A-B
PU2300	Propane Pump
PU2301	Diesel Rolling Stock Pump
PU2302	Diesel Generator Transfer Pump
PU2303	Diesel Tank Sump Pump
PU2400	Fire Protection Jockey Pump
PU2401	Diesel Fire Water Pump #1
PU2402	Diesel Fire Water Pump #2
PU2504A-B	Waste Water Sump Pump A-B
PU2507	Coal and Limestone Storage Sump Pump
PU2700A-B	Demineralizer Forwarding Pump A-B

Table 2.2-2 (Page 3 of 3)

Major Equipment in the Balance-of-Plant

TAG NAME	DESCRIPTION
PU2920A-B	Auxiliary Boiler Feed Water Pump A-B
SB3001	125-V DC Station Battery
SB3002	UPS
SC0700	Baghouse Screw Conveyor
SG3000-3005	4160-V, 480-V Switchgear Buses
SI0101	MWK Crushed Coal Storage Silo
SI0103	Crushed Sorbent Storage Silo
SI0111	MWK Pulverized Coal Storage Silo
SI0113	MWK Limestone Silo
SI0114	FW Limestone Silo
SI0810	Ash Silo
ST2601	N_2 Storage Tube Bank
TK2000	MWK Condensate Storage Tank
TK2001	FW Condensate Tank
TK2100	Raw Water Storage Tank
TK2300A-D	Propane Storage Tank A-D
TK2301	Diesel Storage Tank
TK2401	Fire Water Tank
XF3000A	230/4.16-kV Main Power Transformer
XF3001B-5B	4160/480-V SS Transformer No. 1-5
XF3001G	480/120-V Miscellaneous Transformer
XF3010G	120/208 Distribution Transformer
XF3012G	UPS Isolation Transformer
VS2203	High-Pressure Air Receiver

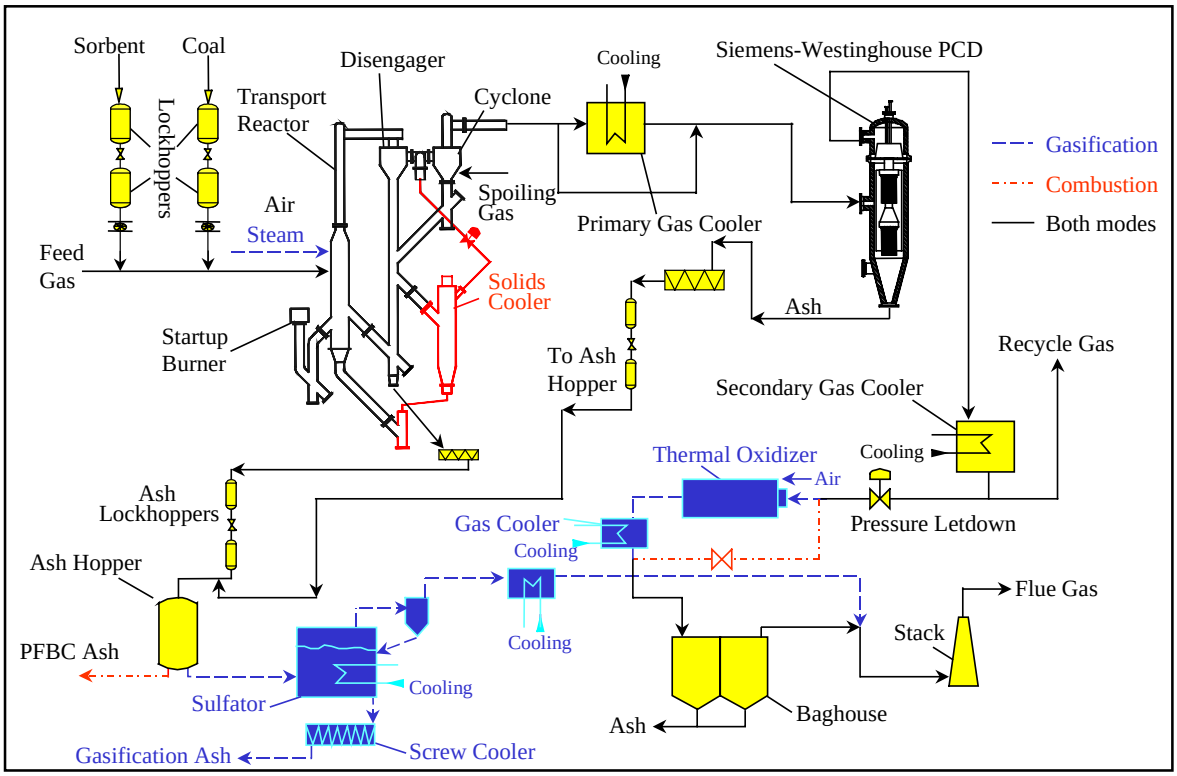

Figure 2.2-1 Flow Diagram of the Transport Reactor Train

2.3 SIEMENS WESTINGHOUSE PARTICULATE CONTROL DEVICE

Different PCDs will be evaluated on the transport reactor train. The first PCD, commissioned in 1996 and used in all of the testing to date, was the filter system designed by Siemens Westinghouse. The dirty gas enters the PCD below the tubesheet, flows through the filter elements, and the ash collects on the outside of the filter. The clean gas passes from the plenum/filter element assembly through the plenum pipe to the outlet pipe. As the ash collects on the outside surface of the filter elements the pressure drop across the filter system gradually increases. The filter cake is periodically dislodged by injecting a high-pressure gas pulse to the clean side of the filter elements. The cake then falls to the discharge hopper.

Until the first gasification run in late 1999, the transport reactor had been operated only in the combustion mode. Initially, high-pressure air was used as the pulse gas for the PCD; however, the pulse gas was changed to nitrogen early in 1997. The pulse gas was routed individually to the two-plenum/filter element assemblies via injection tubes mounted on the top head of the PCD vessel. The pulse duration was typically 0.1 to 0.5 seconds.

A sketch of the Siemens Westinghouse PCD is shown in Figure 2.3-1.

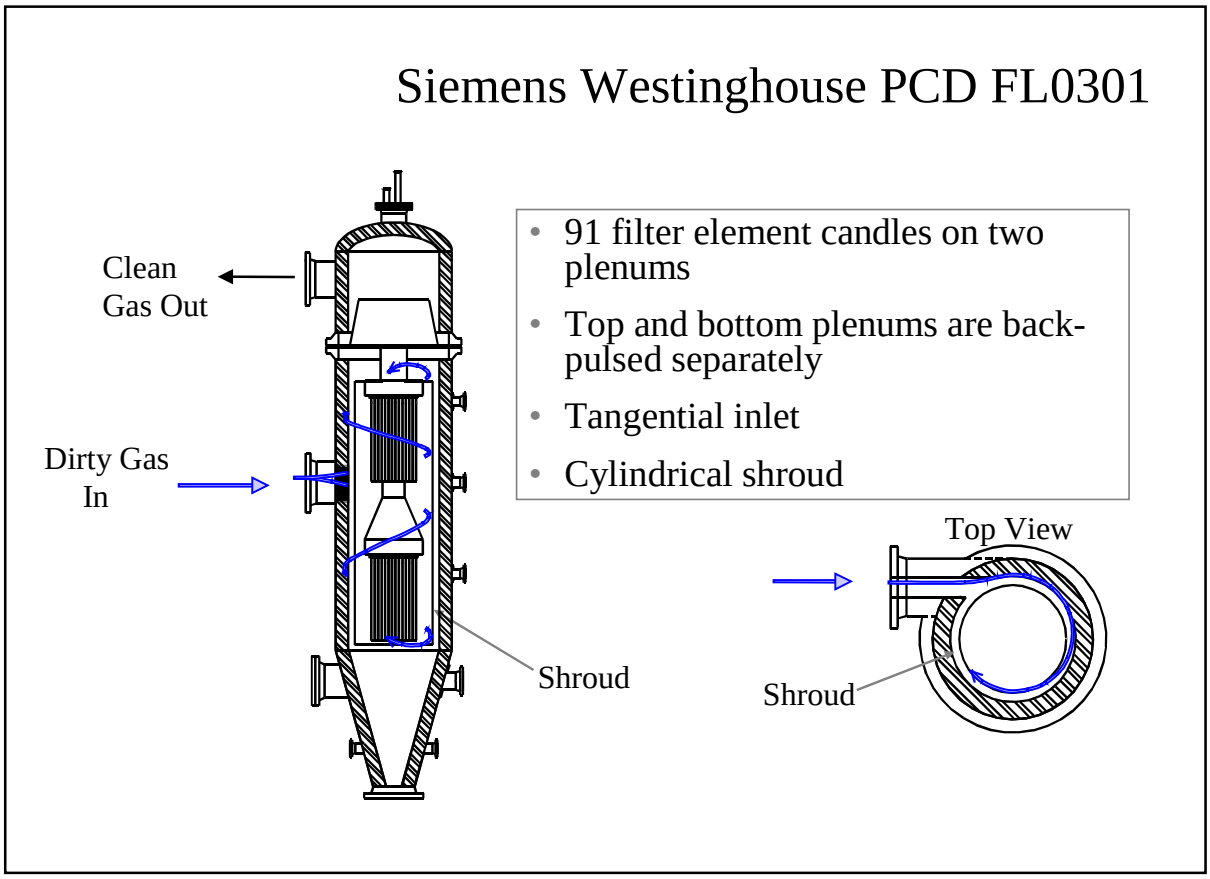

Figure 2.3-1 Siemens Westinghouse PCD

2.4 OPERATION HISTORY

Commissioning activities began in September 1995 and proceeded in parallel with construction activities. Design and construction of the transport reactor and associated equipment was completed in the early summer of 1996. All separate components and subsystems were fully operational by midsummer and commissioning work was focused on integration issues for the entire transport reactor train. The first coal fire in combustion mode of operation was achieved on August 18, 1996. A series of characterization tests was initiated to develop an understanding of reactor system operations. Test runs CCT1, CCT2, and CCT3 were completed by December 1996. Solids carryover from the reactor to the PCD was found to be excessive during these test runs. A number of start-up and design problems associated with various equipment were successfully addressed.

During 1997 three additional sets of characterization test runs (CCT4, CCT5, and CCT6) and one major test campaign (TC01) were undertaken. TC01 focused on exposing the PCD filter elements to process gas for 1,000 hours at temperatures from 1,350 to 1,400°F and achieving stable reactor operations. An Alabama bituminous coal from the Calumet mine in the Mary Lee seam and Plum Run dolomite were used in these test runs.

Two test campaigns (TC02 and TC03) were successfully completed during 1998. TC02 was planned for reactor parametric testing to better quantify the effect of different variables on reactor and filter element operation. Test run TC02 was started on April 5, 1998, and completed on May 11, 1998. Based on TC02 observations, TC03 was planned for additional reactor parametric testing to better quantify the effect of different variables on reactor and PCD operation and to evaluate operation with an Eastern Kentucky bituminous coal and a Gregg Mine limestone from Florida. The third major test campaign (TC03) was performed from May 31 to August 10, 1998. Stable operations were demonstrated using the Eastern Kentucky coal and Plum Run dolomite, Bucyrus limestone, and Ohio Bucyrus limestone during TC03. There were, however, circulation problems using the Eastern Kentucky coal and Florida Gregg Mine limestone because of deposits resulting from excessive fines (segregated) in the Eastern Kentucky feed. One additional test run (TC04) was started on October 14, 1999, but prematurely ended due to a temperature excursion in the PCD during the initial heatup of the transport reactor system.

The final combustion test campaign was started on January 10, 1999, in combustion mode of operation and was completed May 2, 1999. During TC05, steady state operations with a variety of fuel and sorbent feed materials were demonstrated (including petroleum coke with two different sorbents) and reactor parametric testing with different feed combinations was performed. Overall, TC05 was a successful test run with 10 different feed combinations tested.

Conversion of the transport reactor train to gasification mode of operations was performed from May to September 1999. The first gasification test run (GCT1) was planned as a 250-hour test run to commission the transport reactor train in gasification mode of operation and to characterize the limits of operational parameter variations. GCT1 was started on September 9, 1999, with the first part completed on September 15, 1999 (GCT1A). The

second part of GCT1 was started on December 7, 1999, and completed on December 15, 1999 (GCT1B through D). This test run provided the data necessary for preliminary analysis of reactor operations and for identification of necessary modifications to improve equipment and process performance. Five different feed combinations of coal and sorbent were tested in order to gain a better understanding of the reactor solids collection-system efficiency.

GCT2, planned as a 250-hour characterization test run, was started on April 10, 2000, and completed on April 27, 2000. Additional data was taken to analyze the effect of different operating conditions on reactor performance and operability. A blend of several PRB coals was used with Ohio Bucyrus limestone. Figure 2.4-1 is a summary of operating test hours achieved with the transport reactor at the PSDF.

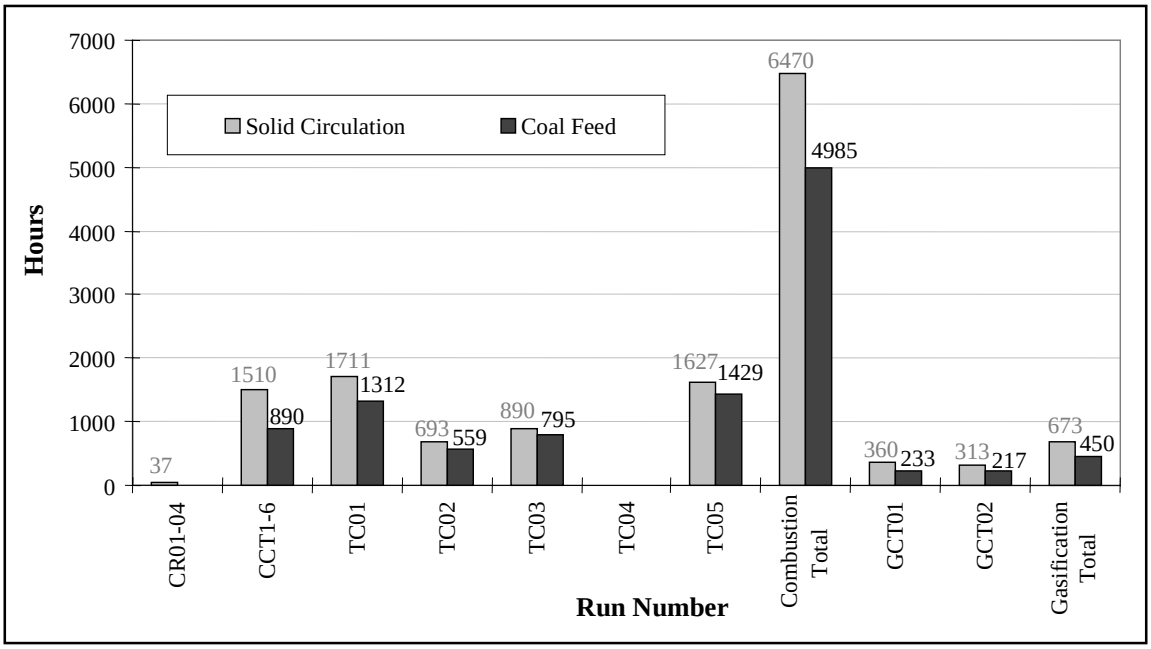

Figure 2.4-1 Operating Hours Summary for the Transport Reactor Train

3.0 PARTICLE FILTER SYSTEM

3.1 GCT2 RUN OVERVIEW

The GCT2 test run was the first gasification test run in which stable PCD operation was achieved. The success was attributed to experiences in GCT1 as well as corrective actions taken prior to GCT2. In GCT1A, some metal and composite filter elements did not perform well, causing leakage and blinding. Dust leaking through the conventional filter element holders was another contributor to the backside blinding. While the transport reactor was commissioning, the solids loading to the PCD was high and tar deposition may also have occurred. As a result, the PCD pressure drop was unacceptably high, eventually causing a system shutdown.

In tests GCT1B through D new monolithic silicon carbide filter elements were installed to eliminate the material problem. A newly developed fail-safe gasket from Siemens Westinghouse was installed on all filter elements as part of the effort to improve the sealing on the filter holders. Fourteen new holders were also proof-tested on selected filter elements. However, a considerable amount of dust loading was still present in the outlet gas stream, possibly due to the leakage through the conventional holders and Conax fittings for instrument wires across the plenums. The leakage caused some backside blinding. Furthermore, tar deposition may have occurred with two different fuel sources, PRB coal and then Illinois No. 6 coal, and in the transition between them. The pressure drop across the PCD dramatically increased to a very high level after the coal transition and eventually caused a system shutdown.

With the lessons learned during GCT1 as well as the technical readiness to address the operation difficulties, several actions were taken prior to GCT2. First, all filter elements were installed with the new filter holder designed by PSDF personnel and the new fail-safe gasket developed by Siemens Westinghouse. Second, all instrument wires were redirected through a nozzle on the vessel wall rather than through the plenums. Third, all new monolithic silicon carbide filter elements were installed, again to continue the evaluation, because this type of material showed good mechanical performance although the leakage may have vaguely affected the evaluation on the filtration. With these changes, PCD performance was significantly improved in GCT2. The outlet loading did not exceed 0.5 ppmw. Equally important, the transport reactor operated smoothly and tar formation was greatly reduced. The solids loading to the PCD was less than in GCT1 and constant. The pressure drop across the PCD was controlled within acceptable level. The ash removal system also performed better than in the previous gasification runs. Major achievements are:

1. The PCD successfully operated for about 217 on-coal hours during the GCT2 gasification test run. Stable PCD operation was maintained, which was not achieved during GCT1 gasification test runs. The PCD temperatures were controlled at stable levels. The inlet particulate loading was stable and less than that in GCT1. The solids accumulation in the PCD cone, therefore, was significantly reduced.

2. All new monolithic silicon carbide filter elements from Pall and Schumacher performed well without any mechanical failure. The visual inspection showed that all filter elements kept their integrity and the clean-side surface was clean. The char cake was thin and

uniform after the clean shutdown. No solids bridging was found between filter elements and plenum walls.

3. The new filter holders developed by PSDF personnel and the new fail-safe gasket developed by Siemens Westinghouse were installed on all filter elements in GCT2. These fixture assemblies performed successfully. The outlet loading never exceeded 0.5 ppmw throughout the entire run. Elimination of instrument wires through the Conax fittings on the plenums was another factor contributing to the lower char emission.

4. The pressure drop across the PCD was stabilized and controlled within an acceptable level for both the baseline and transient DP. The back-pulse parameters were adjusted according to the PCD system response and there still was room for further reduction to the back-pulse intensity and frequency, which are important to the operations in commercial plants. In comparison, stabilized DP was not achieved in GCT1 and this eventually led to unplanned system shutdowns.

5. SRI successfully measured inlet and outlet particulate loadings during the run. Char samples from the inlet sampling and from char cake were analyzed and tested. The lab measurements are consistent with actual PCD performance. A better understanding of the effects of particle size and surface area on char cake drag has been developed.

6. The ash removal system (FD0520/FD0502) worked fine in GCT2. Due to the lower inlet particulate loading to the PCD, solids accumulated in the PCD cone only on two occasions. However, the O-rings on lock hopper spheri valve failed several times during startup, causing unnecessary system shutdowns. The system did not fail again once the hardware insert that holds the O-rings was replaced with a spare part.

7. The post-run PCD inspection showed that the shroud and liner sections were relatively clean. There was no further distortion on the shroud and liners. The plenums and tubesheet were also clean compared to the previous gasification runs.

8. Ten different types of new Siemens Westinghouse fail-safes were tested to support the development of the technology. After the exposure in GCT2 they were flow tested at Siemens Westinghouse Power Corporation. The results showed that there was no loss in their permeability. The fail-safes will be continuously tested in the following runs and their performance will be further evaluated.

9. Material testing was conducted at SRI on seven filter elements removed after GCT2. The results will be presented in a later report along with results for two elements from GCT1A and one element from GCT1B through D.

3.2 GCT2 RUN REPORT

3.2.1 Introduction

The GCT2 gasification run was a landmark run for the PCD since some of the challenges encountered during GCT1A and GCT1B through D were solved. These challenges included high pressure drop across the PCD, high outlet loading, and char accumulation in the cone of the PCD.

The low outlet loading from the PCD, which was never above 1 ppm, was attributed to the following reasons during GCT2: (1) installation of the new filter holder design and (2) elimination of thermocouple wires through the plenums. All the filters for this run were installed with the new filter holder design that was proof-tested on 14 filter elements during GCT1B through D. The new design was believed to place adequate compression on the gasket, which would allow a better seal across the PCD.

The lower pressure drop during GCT2 was a result of several factors. The transport reactor ran at higher temperatures than GCT1A and the first part of GCT1B through D, which reduced the production of tar in the system. This lower tar production not only decreased the pressure drop, it also allowed the primary gas cooler to run as designed. The lower outlet loading mentioned above prevented the chance of any backside blinding of the filter.

During GCT1B through D char accumulation in the cone of the PCD was a problem that limited the transport reactor performance. Higher inlet loading to the PCD and a relatively smaller capacity of the ash removal system were main reasons for the char buildup in the cone. During GCT2 the inlet loading was relatively lower, which reduced the chance of char accumulation. Also, during GCT1 the nitrogen purge on the screw conveyor was determined to be too high. This high back-flow was another factor affecting the char accumulation in the cone. The nitrogen flow for the GCT2 run was decreased and the accumulation of char in the cone of the PCD was minimized.

During the startup, the ash removal system was responsible for four unplanned shutdowns. In each instance the O-ring around the top spheri valve on the FD0520 system failed. The seal pressure was believed to be too high. The seal pressure was originally 365 psig but after the fourth failure the seal pressure was decreased to 330 psig. Also, the hardware insert in the FD0520 system was worn and warped. The hardware insert was also replaced with a new spare part after the last O-ring failure. Throughout the remainder of the run the FD0520 seals did not fail.

3.2.2 Test Objectives

The primary test objectives for the run included:

- Test New Filter Holder – Based on the performance of the new filter holder during GCT1B through D, the entire PCD was installed with the new design.

- Test PCD Pressure Drop on Powder River Basin Coal – During GCT1 the pressure drop across the PCD was extremely high. During this run multiple fuel and sorbent sources made the performance evaluation difficult. Therefore, it was determined to feed one fuel source to the reactor rather than testing different fuel sources.

- Test Monolithic Silicon Carbide Ceramic Filters – New Pall and Schumacher SiC filter elements were installed for test run GCT2 in order to continue the test and evaluation of these types of filter elements. Monolithic silicon carbide filter elements were tested in GCT1B through D and showed good performance.

3.2.3 Observation/Events – 04/11/00 Through 04/27/00

A. Back-pulse system started on 4/11/00 at 22:00 – The back-pulse was started with a rate and pressure of 30 minutes and 320 psig, respectively.

B. System pressure increased to 60 psig on 04/12/00 at 00:15.

C. System pressure increased to 100 psig on 04/12/00 at 14:30.

D. Start-up burner lit on 4/12/00 at 15:15 – At this time the main air compressor was started.

E. Back-pulse pressure increased to 305 psig on 4/12/00 at 18:00.

F. Start-up burner tripped on 4/13/00 at 00:30 – Process was shut down due to a lack of nitrogen.

G. Start-up burner lit on 4/13/00 at 09:17 – The main air compressor was started. The system pressure was increased to 100 psig.

H. Coal feed started on 4/13/00 at 18:00 – At this time the start-up burner tripped. The coal and sorbent fed to the reactor were PRB coal and Ohio limestone. Back-pulse rate and pressure were increased to 5 minutes and 550 psig, respectively.

I. System pressure increased to 160 psig on 4/13/00 at 20:40.

J. Coal feeder tripped on 4/14/00 at 12:00 – FD0520 had a seal leak that shut down the process. Main air compressor shut down. Back-pulse rate and pressure were changed to 30 minutes and 410 psig, respectively.

K. Main air compressor started on 4/14/00 at 19:45 – System pressure decreased to 100 psig.

L. Start-up burner lit on 4/14/00 at 20:00 – Back-pulse timer changed to 10 minutes.

M. Coal feeder started on 4/15/00 at 00:13.

N. Coal feeder tripped on 4/15/00 at 00:45 – The coal feeder was unable to depressurize. Also, during this time an (FD0520) O-ring failed.

O. Coal feeder started on 4/15/00 at 11:30 – Start-up burner tripped. Back-pulse timer and pressure were changed to 5 minutes and 550 psig, respectively. System pressure increased to 160 psig.

P. Coal feeder stopped on 4/15/00 at 15:00 – FD0520 had a seal leak that shut down the process. Main air compressor stopped. Back-pulse timer and pressure were changed to 30 minutes and 250 psig, respectively.

Q. System pressure increased to 100 psig on 4/16/00 at 17:20.

R. Back-pulse pressure increased on 4/16/00 at 18:00 – The back-pulse pressure was increased to 340 psig. Main air compressor started and start-up burner lit.

S. Back-pulse timer and pressure changed on 4/17/00 at 02:50 – The back-pulse pressure and timer were changed to 5 minutes and 520 psig, respectively.

T. Coal feeder started on 4/17/00 at 03:00 – At this time the start-up burner tripped.

U. System pressure increased to 160 psig on 4/17/00 at 04:40.

V. Coal feeder stopped on 4/17/00 at 10:45 due to FD0520 top spheri valve O-ring failure – Back-pulse timer and pressure changed to 30 minutes and 250 psig, respectively. Main air compressor stopped. System pressure decreased to 100 psig.

W. Main air compressor started on 4/17/00 at 19:30 – The start-up burner started.

X. Coal feeder started on 4/17/00 at 23:54 – The start-up burner tripped.

Y. Back-pulse timer and pressure changed on 4/18/00 at 00:15 – The back-pulse timer and pressure were changed to 5 minutes and 550 psig, respectively. The system pressure was increased to 160 psig.

Z. Coal feeder increased to 100 percent on 4/18/00 at 14:00.

AA. System pressure increased to 180 psig on 4/18/00 at 21:00.

BB. System pressure increased to 200 psig on 4/19/00 at 10:35.

CC. Coal feeder tripped on 4/20/00 at 08:26.

DD. Back-pulse timer and pressure changed on 4/21/00 at 15:50 – The back-pulse timer and pressure were changed to 10 minutes and 400 psig, respectively.

EE. Coal feeder reduced to 50 percent on 4/21/00 at 22:30 due to low level of milled coal.

FF. System pressure increased to 220 psig on 4/22/00 at 20:25.

GG. Coal-feed rate increased to 100 percent on 4/23/00 at 09:23 – Back-pulse timer and pressure changed to 5 minutes and 620 psig, respectively.

HH. Back-pulse pressure reduced on 4/24/00 at 20:00 – The back-pulse pressure was reduced to 520 psig.

II. Increased system pressure to 240 psig on 4/25/00 at 06:30 – Increased back-pulse pressure to 540 psig.

JJ. Coal feeder tripped on 4/25/00 at 17:00 – Main air compressor stopped. System pressure decreased to zero psig. Changed back-pulse timer and pressure to 30 minutes and 250 psig, respectively.

KK. Back-pulse started on 4/26/00 at 21:00 – The back-pulse system was started with a rate and pressure of 30 minutes and 350 psig. Main air compressor started. Start-up burner lit.

LL. System pressure increased to 100 psig on 4/27/00 at 00:10.

MM. Back-pulse timer and pressure changed on 4/27/00 at 07:00 – The back-pulse timer and pressure were changed to 5 minutes and 560 psig, respectively. Coal feeder started and start-up burner tripped.

NN. Run ended on 4/27/00 at 10:15.

3.2.4 Run Summary

The GCT2 gasification run began with start-up of the main air compressor on April 10, 2000, and the PCD back-pulse system was started at 22:00 on April 11, 2000. Once the start-up burner and main air compressor were started the system began to heat up. At 12:30 on April 13, 2000, the start-up burner tripped. At this time it was determined to shut down the process due to a lack of nitrogen. At 09:17 on April 13, 2000, the start-up burner was lit. The system pressure was increased to 100 psig. Once the reactor temperature reached 1,000°F, the coal feeder was started. The coal and sorbent fed to the reactor were PRB coal and Ohio limestone, respectively. The coal and sorbent were fed at 18:00 on April 13, 2000. During this time the back-pulse rate and pressure were 5 minutes and 550 psig, respectively. The peak-pressure drop was greater than 250 inH_2O. To decrease the pressure drop, the system pressure was increased to 160 psig at 20:40 on April 13, 2000, in order to decrease the face velocity. At the same time the temperature in the PCD was approximately 1,050°F.

On April 14, 2000, at 12:00 the FD0520 system failed due to a seal leak. The O-ring around the top spheri valve on FD0520 failed. This failure resulted in the shutdown of the process. This

O-ring failed on three more occasions during the run. Apparently the seal pressure, which was set at 365 psig, was too high. The seal pressure was decreased to 330 psig at 21:30 on April 16, 2000. Also, the hardware insert that holds the O-ring was replaced with a spare part. The O-ring did not fail after these changes were made.

On April 14, 2000, at 20:00 the start-up burner was lit. The coal feeder was started at 00:13 on April 15, 2000. During this time the back-pulse rate and pressure were 5 minutes and 550 psig, respectively. The base line and peak pressure drops across the PCD were 50 and 110 inH_2O, respectively. The PCD inlet temperature was 950°F during this time and the system pressure was 160 psig. After a short period of operation the FD0520 system failed again, which shut down the process. As mentioned above, the O-ring around the top spheri valve failed. This incident occurred on April 15, 2000, at 01:45.

On April 16, 2000, at 19:40 the start-up burner was lit and the coal feeder was started at 03:00 on April 17, 2000. By 10:45 on the same day the FD0520 top spheri valve failed again and the process was shut down. After this repair the seal pressure was decreased from 365 psig to 330 psig. At 19:30 on April 17, 2000, the start-up burner was lit. By 23:50 the coal feeder was started. On April 18 at 14:00 the coal feeder rate was increased to 100 percent. During this time the base line and peak pressures were 80 and 150 inH_2O, respectively. At 08:00 on April 20, 2000, the reactor had a major dip-leg upset. This upset resulted in the PCD inlet temperature increasing ~375°F. The filter element temperature increased by ~200°F. Since there was no evidence of ceramic filters found in the ash removal system it was assumed that the ceramic filters survived the thermal event, and this was confirmed during the inspection of the PCD. Other than this one upset, the PCD temperature remained below 1,000°F except for a short period of time during startup where the inlet temperature was ~1,050°F. Due to the stable pressure drop across the PCD the back-pulse timer was changed from 5 to 10 minutes at 15:50 on April 21. Around 20:20 on the same day the back-pulse timer was changed from 10 to 20 minutes. Over the next few days the back-pulse timer was changed back to 10 and 15 minutes.

Between April 21 and April 25 the PCD operation was essentially uneventful. The base-line and peak-pressure drops were below 80 and 200 inH_2O, respectively. The process was shut down due to a plug in the transport reactor on April 25, 2000, at 17:00.

The run was resumed briefly with coal feed early on April 27 but was terminated at 10:15 on April 27, 2000.

Table 3.2-1

GCT2 Run Statistics for
04/11/00 Through 04/27/00

Start Time:	04/11/00 22:00 (for back-pulse system)
End Time:	04/27/00 10:15
Coal Type:	Powder River Basin
Hours on Coal:	Approx. 217 hrs
Sorbent Type:	Ohio limestone
Number of Filter Elements:	91
Filter Element Layout No.:	16 (Figure 3.2-1)
Filtration Area:	258.44 ft^2 (24.0 m^2)
Pulse-Valve-Open Time:	0.2 sec
Pulse-Time Trigger:	5 to 30 min
Pulse Pressure:	350 to 620 psig
Pulse-DP Trigger:	250 inWG

Table 3.2-2 (Page 1 of 2)

GCT2 Major Events for
04/11/00 Through 04/27/00

Event	Description	Date at Time
A	Back-Pulse System Started	4/11/00 at 22:00
B	System Pressure Increased to 60 psig	4/12/00 at 00:15
C	System Pressure Increased to 100 psig	4/12/00 at 14:30
D	Start-up Burner Lit	4/12/00 at 15:15
E	Back-Pulse Pressure Increased to 305 psig	4/12/00 at 18:00
F	Start-Up Burner Tripped	4/13/00 at 00:30
G	Start-Up Burner Lit	4/13/00 at 09:17
H	Coal Feeder Started	4/13/00 at 18:00
I	System Pressure Increased to 160 psig	4/13/00 at 20:40
J	Coal Feeder Tripped	4/14/00 at 12:00
K	Main Air Compressor Started	4/14/00 at 19:45
L	Start-Up Burner Lit	4/14/00 at 20:00
M	Coal Feeder Started	4/15/00 at 00:13
N	Coal Feeder Tripped	4/15/00 at 00:45
O	Coal Feeder Started	4/15/00 at 11:30
P	Coal Feeder Stopped	4/15/00 at 15:00
Q	System Pressure Increased to 100 psig	4/16/00 at 17:20
R	Back-Pulse Pressure Increased	4/16/00 at 18:00
S	Back-Pulse Timer and Pressure Changed	4/17/00 at 02:50
T	Coal Feeder Started	4/17/00 at 03:00
U	System Pressure Increased to 160 psig	4/17/00 at 04:40
V	Coal Feeder Stopped	4/17/00 at 10:45
W	Main Air Compressor Started	4/17/00 at 19:30
X	Coal Feeder Started	4/17/00 at 23:54

Table 3.2-2 (Page 2 of 2)

Y	Back-Pulse Timer and Pressure Changed	4/18/00 at 00:15
Z	Coal Feeder Increased to 100%	4/18/00 at 14:00
AA	System Pressure Increased to 180 psig	4/18/00 at 21:00
BB	System Pressure Increased to 200 psig	4/19/00 at 10:35
CC	Coal Feeder Tripped	4/20/00 at 08:26
DD	Back-Pulse Timer and Pressure Changed	4/21/00 at 15:50
EE	Coal Feeder Reduced to 50%	4/21/00 at 22:30
FF	System Pressure Increased to 220 psig	4/22/00 at 20:25
GG	Coal Feed Rate Increased to 100%	4/23/00 at 09:23
HH	Back-Pulse Pressure Reduced	4/24/00 at 20:00
II	Increased System Pressure to 240 psig	4/25/00 at 06:30
JJ	Coal Feeder Tripped	4/25/00 at 17:00
KK	Back-Pulse Started	4/26/00 at 21:00
LL	System Pressure Increased to 100 psig	4/27/00 at 00:10
MM	Back-Pulse Timer and Pressure Changed	4/27/00 at 07:00
NN	Run Ended	4/27/00 at 10:15

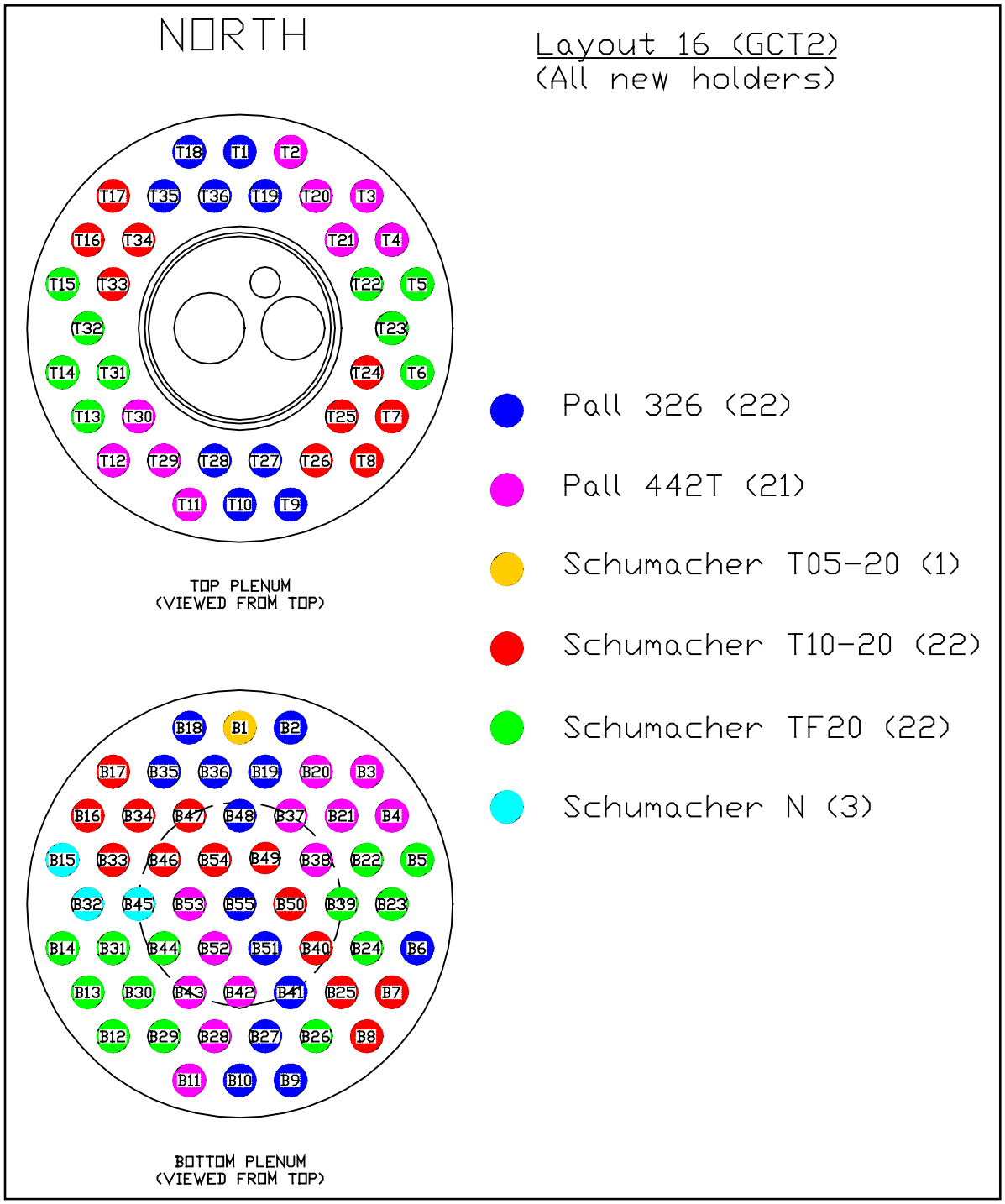

Figure 3.2-1 Filter Element Layout for GCT2

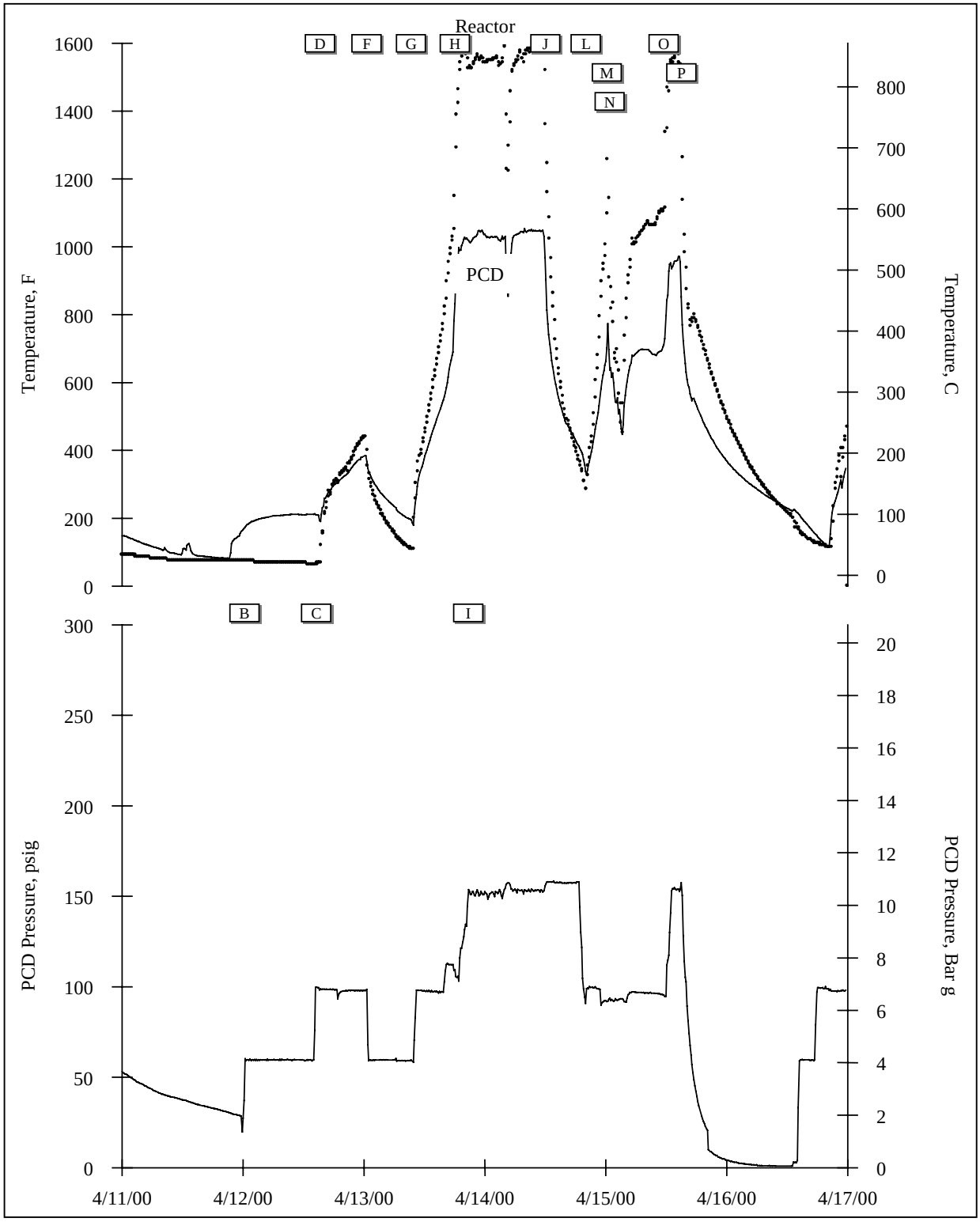

Figure 3.2-2 GCT2 Temperature and Pressure for April 11 Through April 17

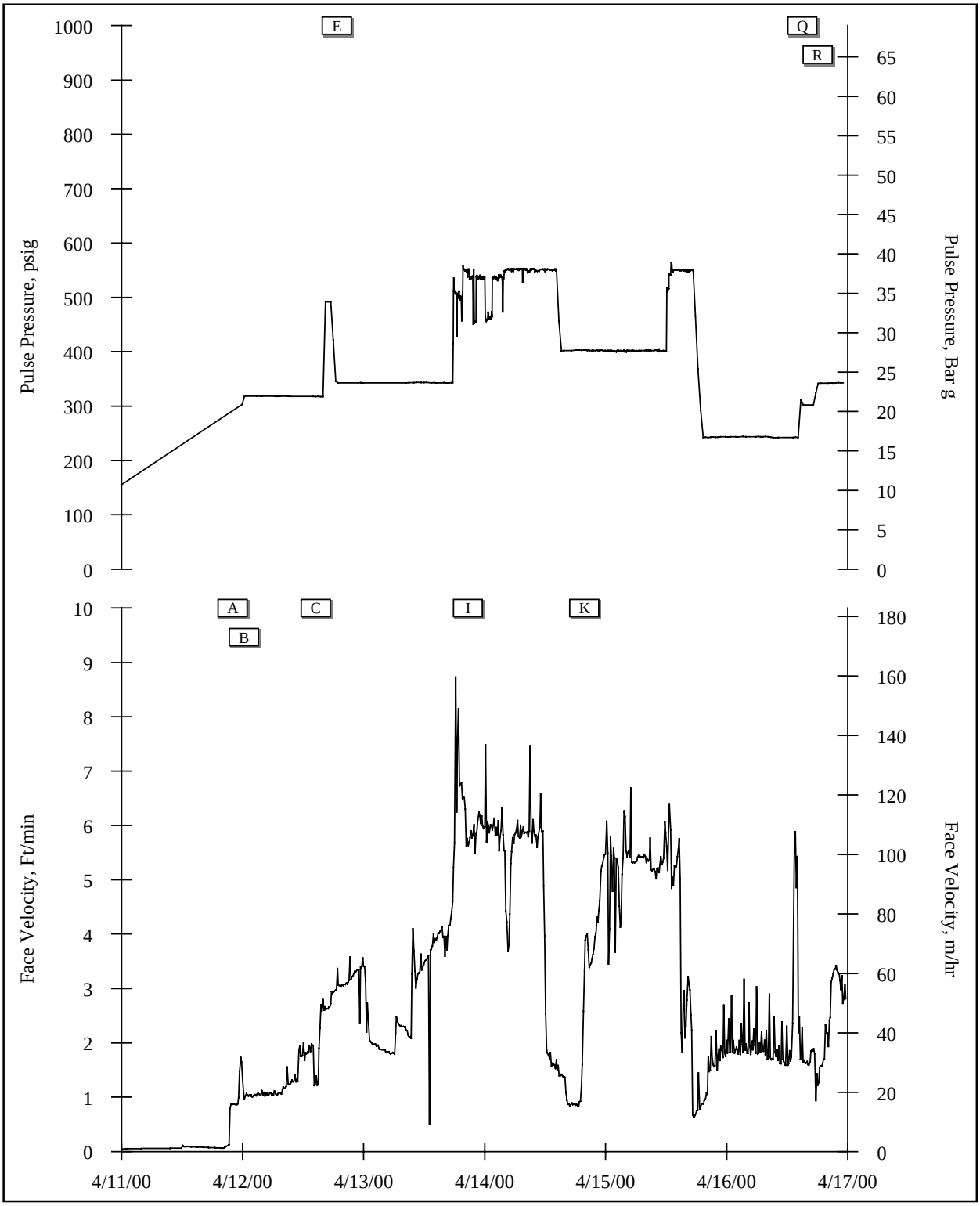

Figure 3.2-3 GCT2 Back-Pulse Pressure and Face Velocity for April 11 Through April 17

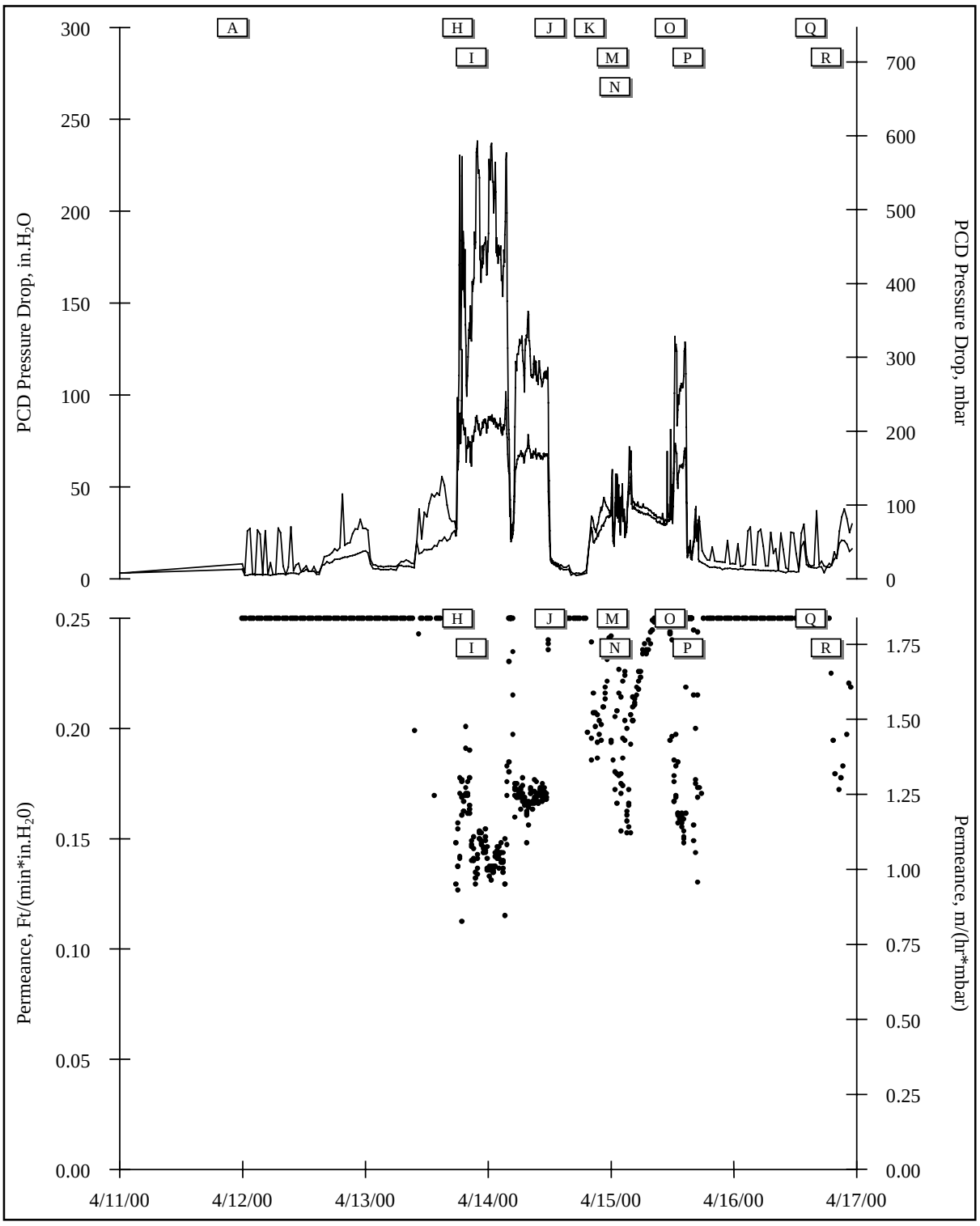

Figure 3.2-4 GCT2 Pressure Drop and Permeance for April 11 Through April 17

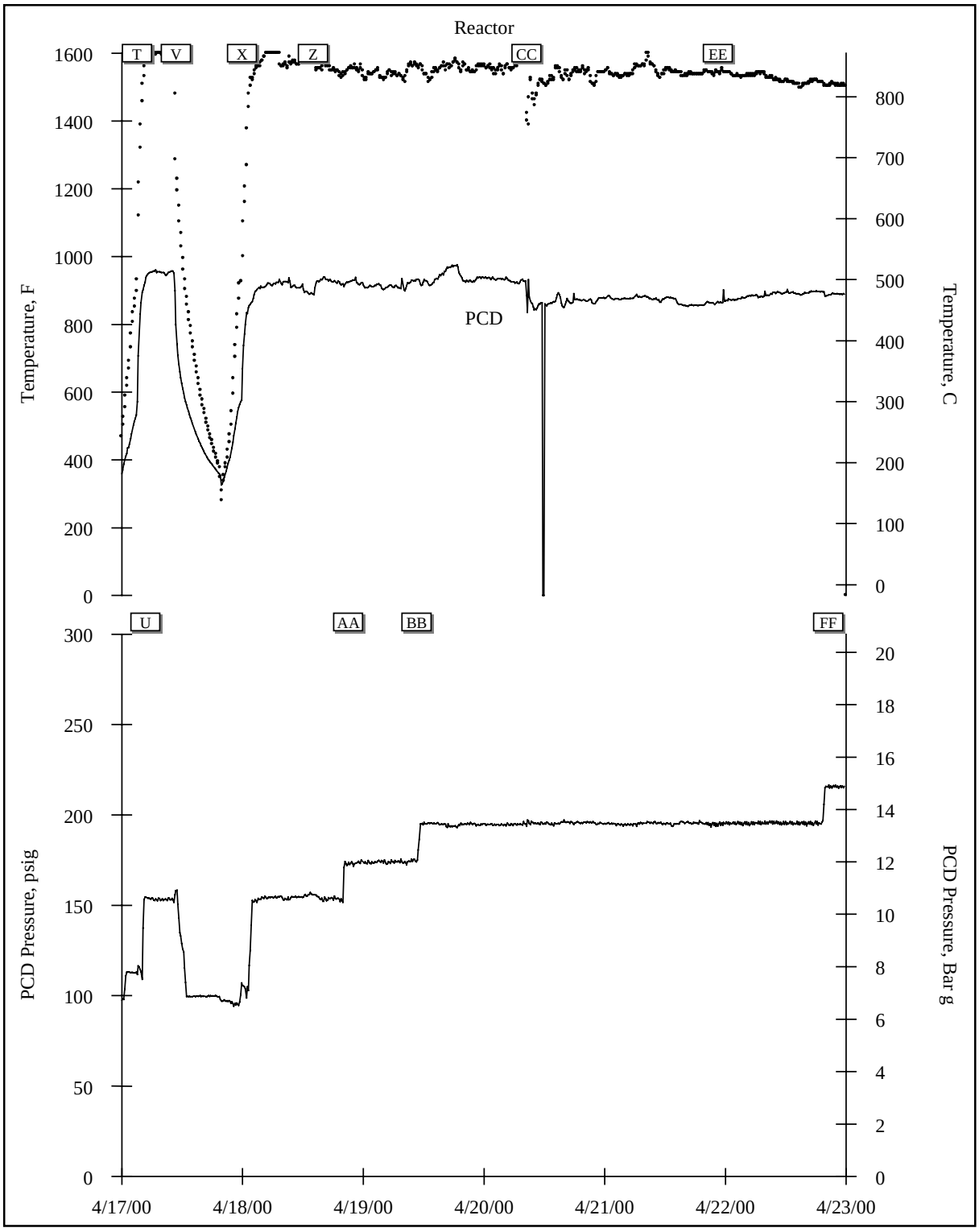

Figure 3.2-5 GCT2 Temperature and Pressure for April 17 Through April 23

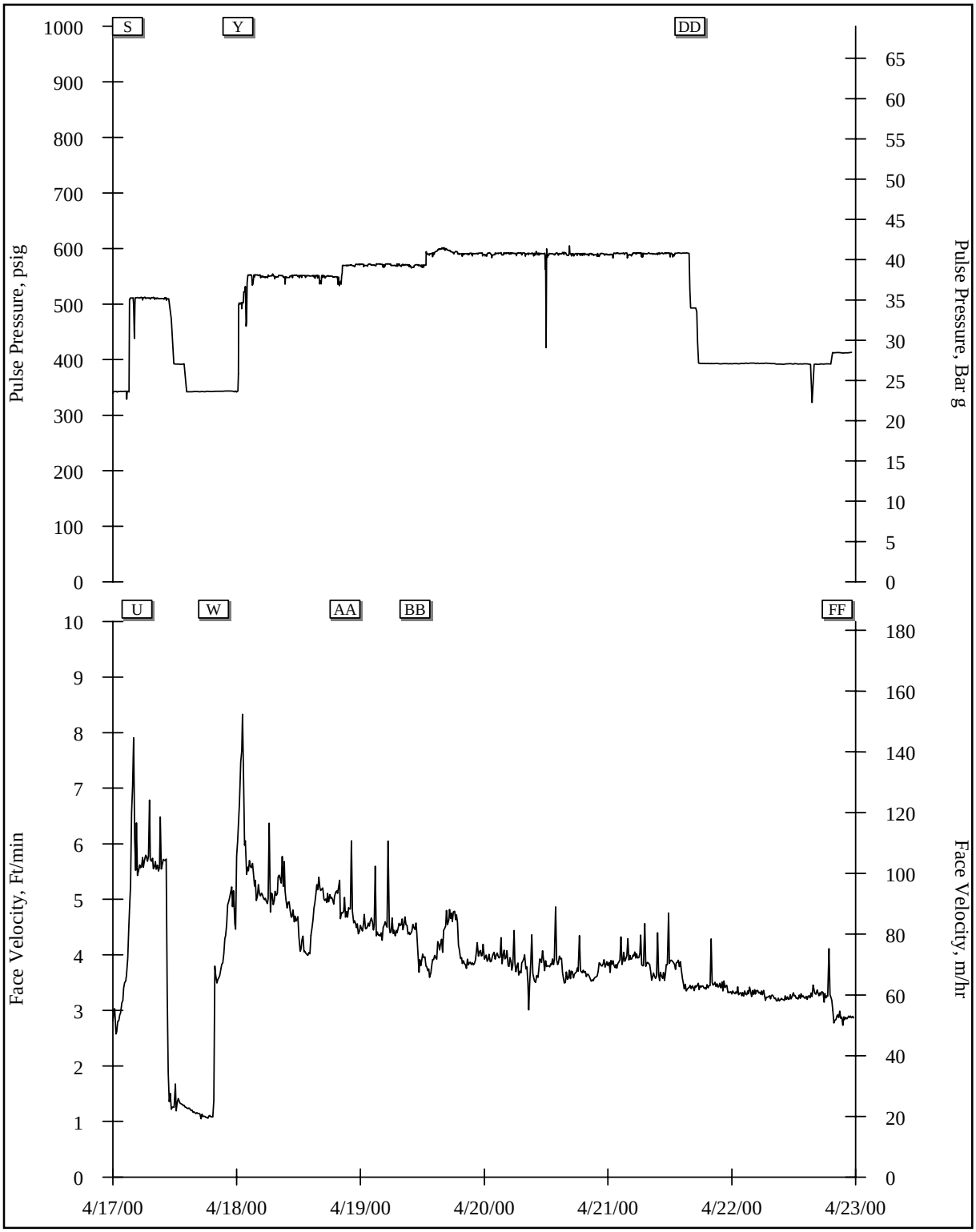

Figure 3.2-6 GCT2 Back-Pulse Pressure and Face Velocity for April 17 Through April 23

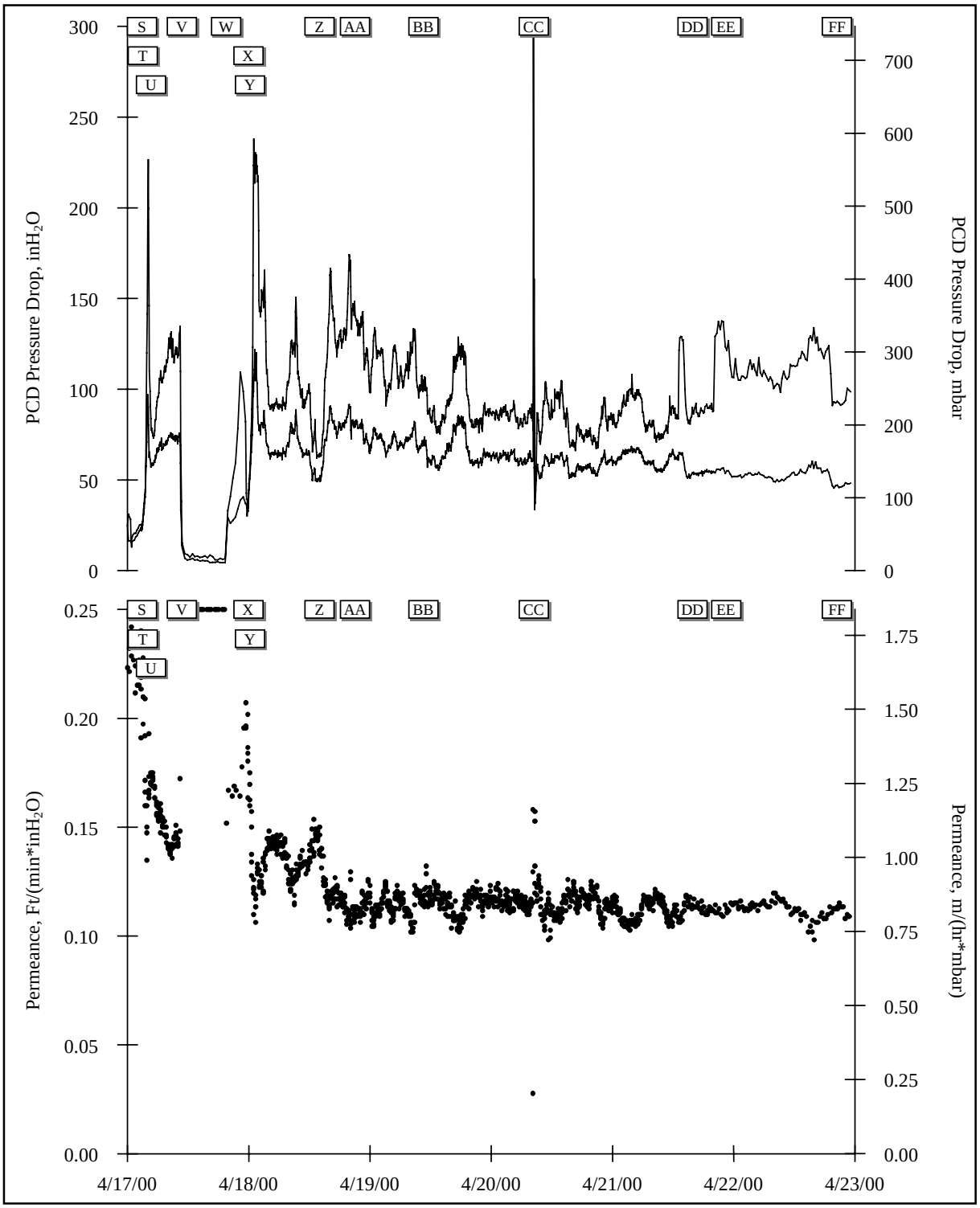

Figure 3.2-7 GCT2 Pressure Drop and Permeance for April 17 Through April 23

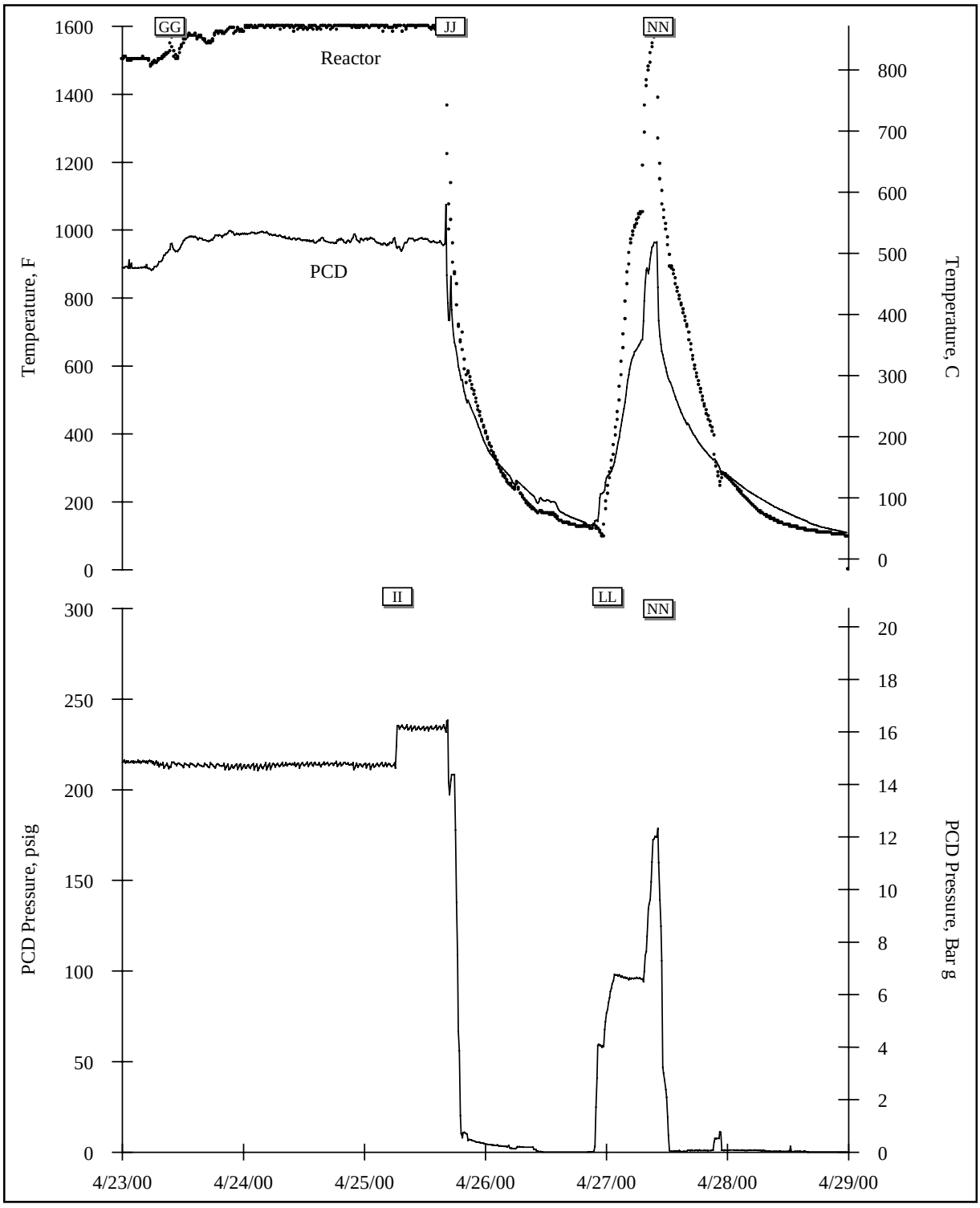

Figure 3.2-8 GCT2 Temperature and Pressure for April 23 Through April 29

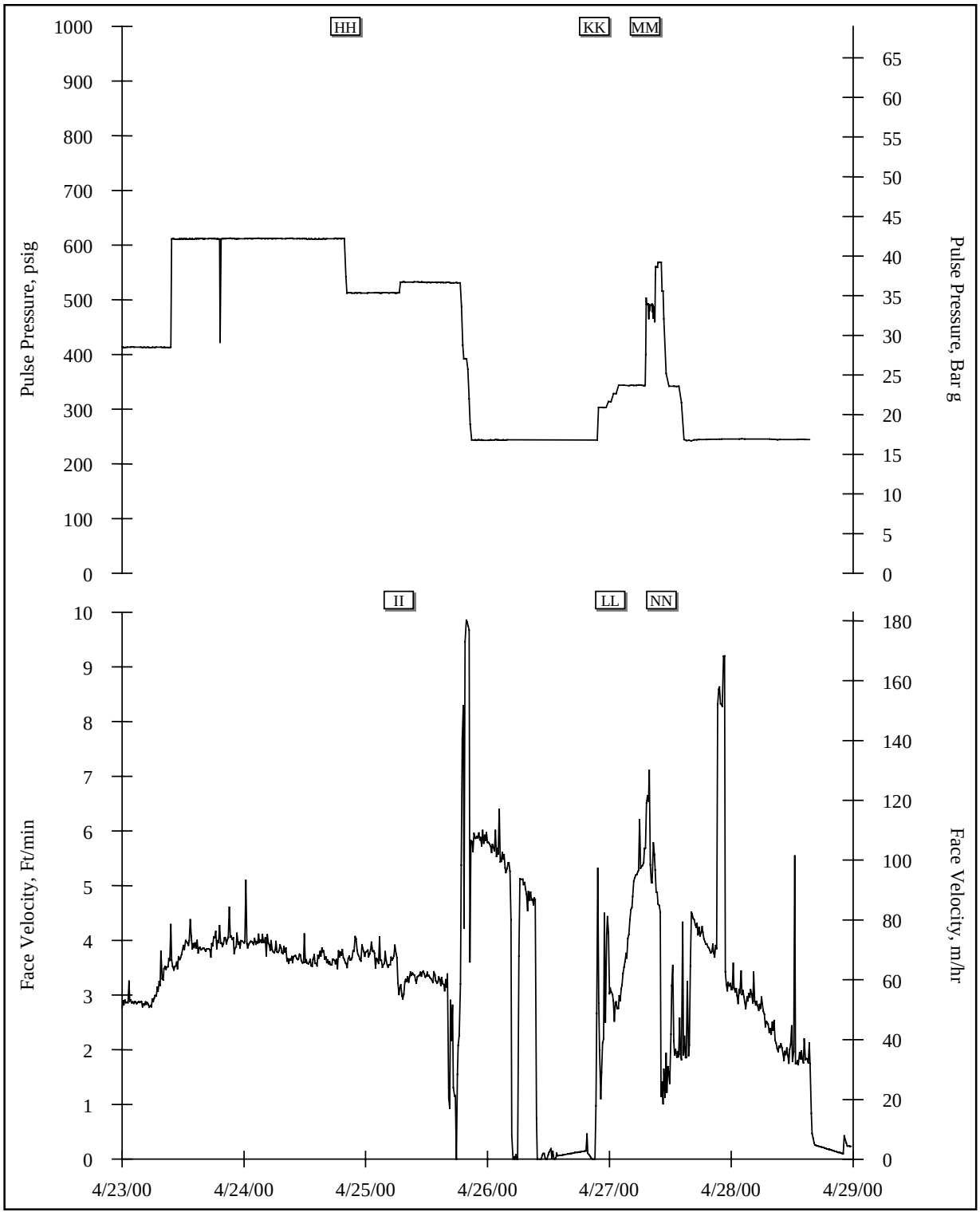

Figure 3.2-9 GCT2 Pulse-Pressure and Face Velocity for April 23 Through April 29

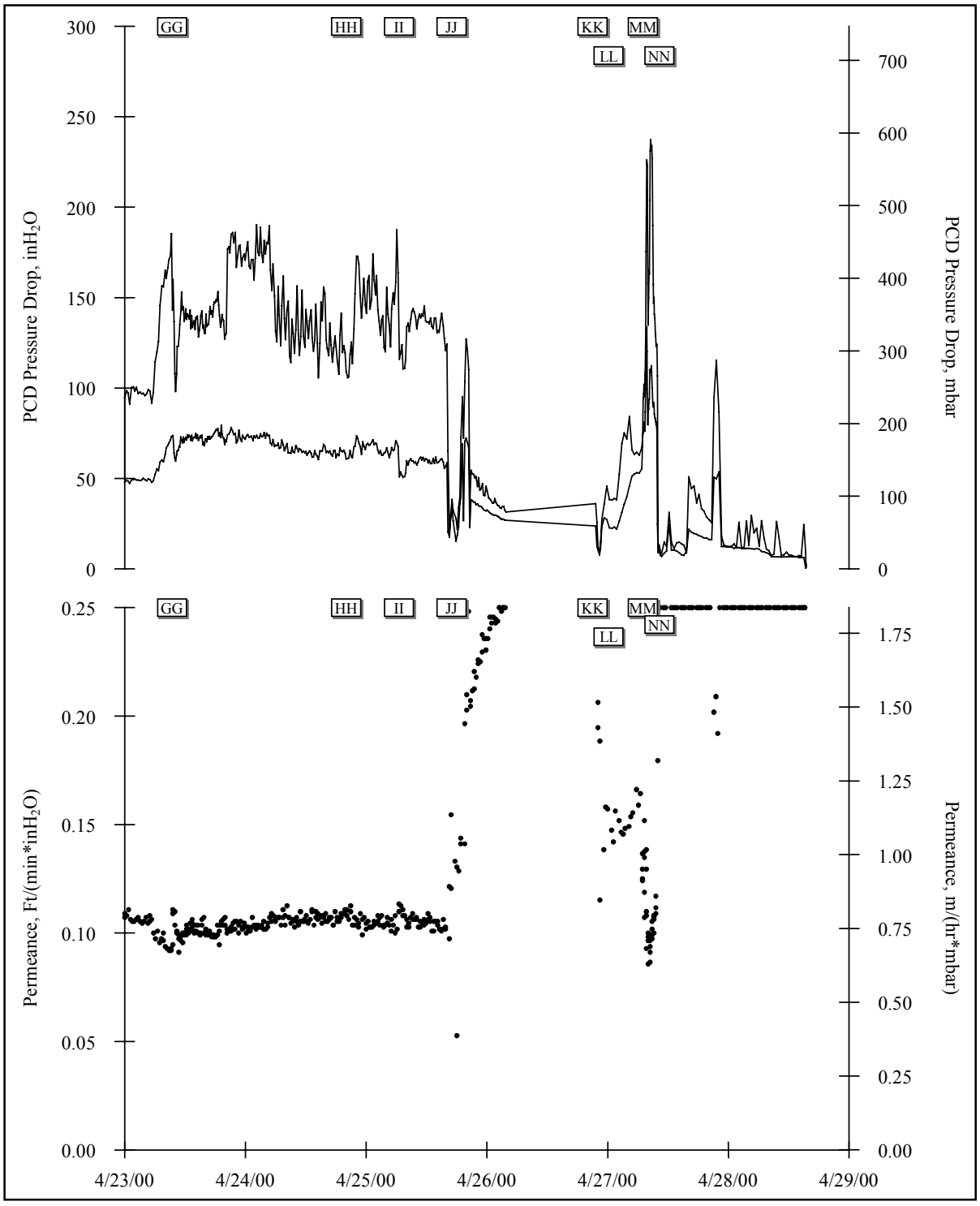

Figure 3.2-10 GCT2 Pressure Drop and Permeance for April 23 Through April 29

3.3 GCT2 INSPECTION REPORT

3.3.1 Introduction

Test run GCT2 started on April 10, 2000, (coal feed commencing on April 13) and ended on April 27, 2000. The particulate control device (PCD) was inspected after the GCT2 run. Generally, the inspection included visual examinations of the following:

- Filter element fixtures.
- Filter elements.
- Filter element gaskets.
- Fail-safes.
- Char deposition.
- PCD vessel and plenum assemblies.
- Auxiliary equipment.

3.3.2 GCT2 Inspection

The PCD operated in gasification mode for a total of 217 hours on coal during the GCT2 run. During the operation the outlet loadings were very low and there did not appear to be any significant leakage through the PCD. The system was shut down in a controlled manner on April 27, 2000. The PCD was shut down in a clean state, which means that the back-pulse equipment continued to be cycled after coal feed was stopped. The PCD was opened on May 15. GCT2 PCD operating parameters are shown in Table 3.3-1.

Prior to the GCT2 run continuing efforts were made to limit the leakage in the PCD. The modified filter-element fixtures (modified filter holders) and the "lapped-construction" primary gaskets that were proof-tested during the GCT1B through D run were installed throughout both plenums. Also, no thermocouple wires were routed from the dirty side of the PCD to the clean side in an attempt to eliminate the leakage through the Conax fittings.

3.3.2.1 Filter Element Fixtures

The original conventional filter nut filter-element fixture design compressed two different gasket types in series with one set of bolts. However, each of the different gasket types potentially required different compression values to adequately seal. Therefore, the modified filter holder filter-element fixture design was implemented to address this issue.

The modified filter holder design added an additional part called a "fail-safe holder" that allowed the primary gasket and the element flange gasket to be compressed separately. With this design the primary gasket was compressed by the fail-safe holder bolts and the element flange gasket was compressed by the "new filter nut" bolts.

Since the fail-safe holder bolts could now be torqued independently of the filter element they were torqued to 120 in-lb in order to get as much compression on the primary gaskets as possible without damaging the gaskets. The new filter nut bolts were torqued to 70 in-lb.

During inspection, the remaining bolt torque was checked on random fixtures to verify that the modified filter holders continued to provide superior sealing compression. The remaining torques are shown in Figures 3.3-3 and -4. The following observations were made:

- The remaining torque on the new fail-safe holder bolts generally ranged from 40 to 100 in-lb. This is the remaining torque that was available to compress the primary gasket.

- The remaining torque on the new filter nut bolts generally ranged from 30 to 60 in-lb. This is the remaining torque that was available to compress the element flange gasket.

As a comparison, the GCT1B through D inspection showed that the remaining torque on the conventional filter nut bolts generally ranged from below 20 to 60 in-lb, per bolt. This was the remaining torque that was available to compress both the lapped-construction primary gasket and the element flange gasket in series. (It should be noted that 20 in-lb was the lowest setting on the torque wrench. Several of the bolts had torques below 20 in-lb.)

During the GCT2 disassembly there were some minor mechanical fit-up problems with the modified filter holder parts. Seven of the new filter nuts bound slightly on the fail-safe holders and two of the fail-safe holders bound slightly in the plenums. Also, one of the fail-safe holders was noticeably loose inside the plenum. The binding of the mating parts could have been the result of the bolts not being tightened uniformly during installation.

The modified filter holder parts were machined from 310 stainless steel. After the GCT1B through D run it was noticed that the color of the parts had changed from a shiny stainless steel color to a dull black color. However, the parts did not discolor during the GCT2 run.

There was a "shiny coating or film" inside many of the fail-safe holders which could be flaked off in pieces. This coating may have been caused by tar deposition inside the fail-safe holder. No further analysis has been performed on the film at this time. Any additional information will be reported at a later date.

3.3.2.2 Filter Elements

Based on the successful operation of the monolithic silicon carbide (SiC) filter elements during the GCT1B through D gasification run, monolithic SiC elements were also installed for the GCT2 run. All new, unused elements were installed. A tubesheet map and a filter element layout drawing (Layout 16) are shown in Figures 3.3-1 and -2. The letters T and B preceding the numbers denote the top and bottom plenums, respectively.

The monolithic SiC elements performed well during the GCT2 gasification run. The elements were visually inspected and no obvious damage was found. All of the elements were considered to be "clean" inside. There was no loose char inside any of the elements, and there was no char accumulated on the inside walls of the elements.

3.3.2.3 Filter Element Gaskets

During the GCT1A inspection, there was evidence that the original fiberfrax ring primary gasket did not provide effective sealing after exposure to the operating atmosphere and repeated back-pulse cycles. Siemens Westinghouse lapped-construction primary gaskets were used to replace the fiberfrax ring gaskets on all elements during the GCT1B through D run. Compared to the original fiberfrax ring gaskets, these lapped-construction gaskets provided better sealing during the GCT1B through D run. Therefore, lapped-construction gaskets were also installed with all filter elements prior to the GCT2 run. The gasket types used during the GCT2 run are defined below:

GASKET TYPE	GASKET LOCATION
Lapped-construction	Plenum-to-Fail-safe (Primary Gasket)
Top Donut	Fail-safe-to-Fail-safe Holder
Bottom Donut (No. 1)	Fail-safe Holder-to-Element
Bottom Donut (No. 2)	New Filter Nut-to-Element
Sock Gasket	Element-to-Bottom Donut Gasket (No. 2)

Similar to the GCT1B through D run, the lapped-construction primary gaskets provided good sealing. There were no obvious leak paths in the area of the new fail-safe holder flanges that would have indicated leakage past the primary gaskets. After the filter elements were removed each individual gasket was visually inspected. Also, selected gaskets were cut open to visually inspect the internals of the gaskets. The following observations were made regarding the gaskets:

- There were broken fibers on approximately half of the lapped-construction primary gaskets. However, this does not necessarily mean that the sealing capability of the gasket was compromised. It should also be noted that some, or all, of this damage could have occurred during disassembly.

- There was a small amount of loose char on the fail-safe flanges (plenum-to-fail-safe side) of elements T3 and T8. There were also small amounts of loose char on several of the lapped-construction primary gaskets. However, there did not appear to be significant leakage past the contact surfaces of the element flange gaskets or the lapped-construction gaskets. (It should be noted that char could deposit on the outer edges of the gaskets since these edges were exposed to the dirty-side gas.)

- Loose char was found inside the element flange gaskets and lapped-construction gaskets. The color of the gaskets had changed from white to light black and gasket fiber patterns could be seen on some of the fail-safe sealing surfaces. It appeared that fine char particles had penetrated through the gasket structure, since the element flange gaskets and the lapped-construction gaskets were dust-tight, not gas-tight seals.

- The element flange gaskets were retained inside a machined cavity. On a few of the elements there was loose char between the outside diameter of this gasket and the inside diameter of the cavity. However, the char did not seem to be on the downstream

face of the gasket. (It should be noted that char could deposit on the outer edges of the gaskets since these edges were exposed to the dirty-side gas.)

3.3.2.4 Fail-safes

None of the fail-safes were damaged during the GCT2 run. Compared to previous gasification runs the fail-safes were cleaner after this run. Only two of the fail-safes had loose particles on the downstream end (top plates) of the fail-safes.

3.3.2.5 Char Deposition

No char bridging was found in the PCD. Compared to the GCT1B through D inspection, the filter elements and the nonfiltration surfaces were generally cleaner.

The char that accumulated on the filter element fixtures had a "fluffy" appearance and did not appear to be compressed (Figure 3.3-5). Start-up material, such as sand, could be seen under a layer of char on some of the nonfiltration surfaces (Figure 3.3-5).

The filter element char cake was generally thin, approximately 0.040 to 0.065 in. (see Section 3.4). Distinct "peaks and valleys" could be seen in the char cake on all of the elements (Figure 3.3-6). However, viewing the elements on the outer periphery of each plenum, the char cake had a smoother appearance on the leading edge of the elements.

The char build-up on the top ash shed and the top plenum wall was not severe. There were vertical paths in the accumulated char on the top ash shed. Also, flow patterns could be seen at the bottom of the top ash shed splitter bars (Figure 3.3-7). The build-up on the bottom plenum wall was even thinner than the build-up on the top plenum wall.

Very little char was accumulated on the inside wall of the shroud and there was only minimal char build-up on the liner sections (Figure 3.3-8). Also, the clean-side of the tubesheet was very clean compared to previous gasification runs.

3.3.2.6 PCD Vessel and Plenum Assemblies

With the PCD head removed, the shroud and liner were visually inspected from the top of the PCD vessel. The liner section repairs that were performed after TC05 were still intact. There was no obvious change in the liner shape.

The clean-side of the tubesheet had a shiny coating or "film" on the metal surfaces. This coating may have been caused by tar deposition inside the PCD head.

3.3.2.7 Auxiliary Equipment

Prior to the GCT2 run 14 thermocouples were installed on individual filter elements in order to monitor the local temperatures. Seven thermocouples were installed on top plenum elements and seven on bottom plenum elements. For previous gasification runs the thermocouple wires

were routed from the dirty-side of the PCD to the clean-side through the plenum. Conax fittings with lava sealant were used to seal the wires and maintain the pressure boundary inside the PCD. The lava sealant was used due to the high temperatures inside the PCD. However, there was evidence that the lava-sealant Conax fittings were leaking and were attributing to the high outlet loadings. Therefore, for the GCT2 run the thermocouple wires were not routed through the clean-side of the PCD. They were routed from the dirty-side of the PCD directly to atmosphere through a nitrogen-purged flange on the PCD. Conax fittings with Teflon sealant were used due to the lower temperatures in the nitrogen-purged nozzle. During the run no leaks were noticed on the Teflon-sealed Conax fittings. Also, all 14 thermocouples gave accurate readings throughout the run.

There was tar accumulation on the back-pulse pipes. The tar will be removed to verify that there is no corrosion in this area. If there is any evidence of corrosion this data will be reported at a later date.

3.3.3 GCT2 Inspection Summary

During the GCT2 run there did not appear to be any significant leakage through the PCD and the outlet loadings were very low. This was a drastic improvement compared to previous gasification runs.

The modified-filter-holder filter-element fixtures allowed the primary gasket and the element flange gasket to be compressed separately. This design also resulted in higher residual torques on both gaskets after repeated back-pulse cycles. Consequently, there did not appear to be significant leakage past the contact surfaces of the element flange gaskets or the lapped-construction primary gaskets. It was decided that modified-filter-holder fixtures would be used throughout both plenums in the subsequent GCT3 gasification run.

Similar to the GCT1B through D run, the Westinghouse lapped-construction primary gaskets provided good sealing during the GCT2 run. There were no obvious leak paths in the area of the new fail-safe-holder flanges that would have indicated leakage past the primary gaskets. It was decided that lapped-construction primary gaskets would be used for the subsequent GCT3 gasification run.

The monolithic SiC filter elements performed well during the GCT2 gasification run. The elements were visually inspected and no obvious damage was found. There was no loose char inside any of the elements and all of the elements were considered to be "clean" inside.

The filter element char cake was generally thin approximately 0.040 to 0.065 in. (see Section 3.4). The char build-up on the nonfiltration surfaces was not severe.

The liner section repairs that were performed after the TC05 test campaign were still intact. There was no obvious change in the liner shape. It was decided to continue to use the existing liner sections and to delay the planned modifications to the PCD vessel refractory.

The element thermocouple wires were routed from the dirty-side of the PCD directly to atmosphere through a nitrogen-purged PCD vessel flange. The Teflon-sealant Conax fittings that were used to maintain the pressure boundary between the dirty-side of the PCD and atmosphere provided satisfactory sealing. It was decided that this method of sealing the element thermocouple wires would also be used in the subsequent GCT3 gasification run.

Table 3.3-1

GCT2 PCD Operating Parameters

Element Layout	Layout 16 (Figure 3.3-2)
Filtration Area	258.4 ft^2
Back-pulse Pressure	200 to 400 psig Above Reactor Pressure (Approximate)
Back-pulse Timer	Set to 5 min (Varied Between 5 and 20 min)
Back-pulse High-Pressure Trigger Point	250 inH_2O
Back-pulse Valve-Open Time	0.2 sec
Inlet Gas Temperature	700 to 1,050°F (Approximate)
Face Velocity	2.5 to 6.0 ft/min (Approximate)
Baseline DP	50 to 125 inH_2O (Approximate)
Peak DP	50 to 250 inH_2O
Inlet Loading (SRI Sampling)	25,700 to 34,000 ppmw
Outlet Loading (SRI Sampling)	0.10 to 0.37 ppmw
Coal/Sorbent	PRB/Dolomite

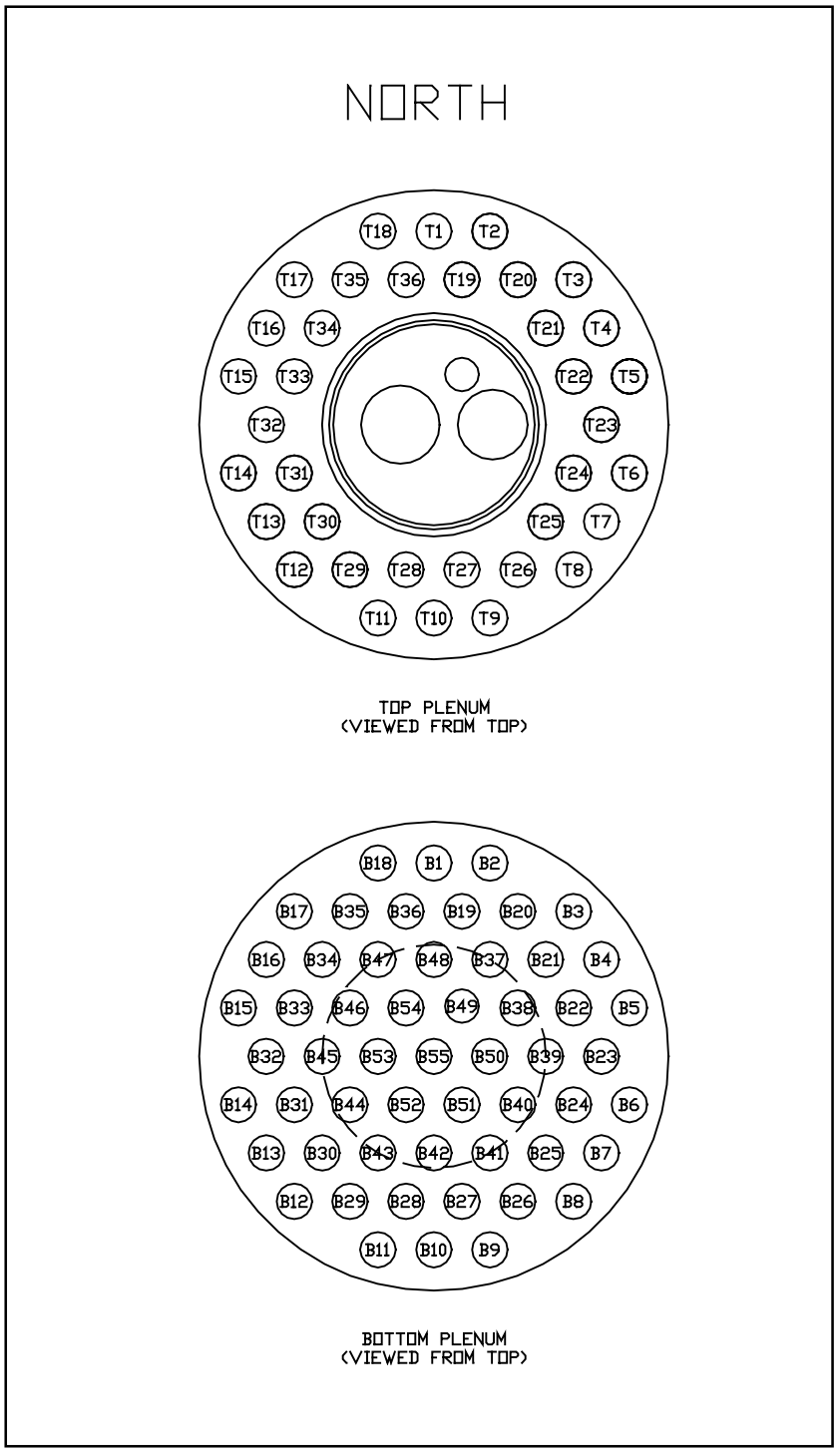

Figure 3.3-1 Tubesheet Layout

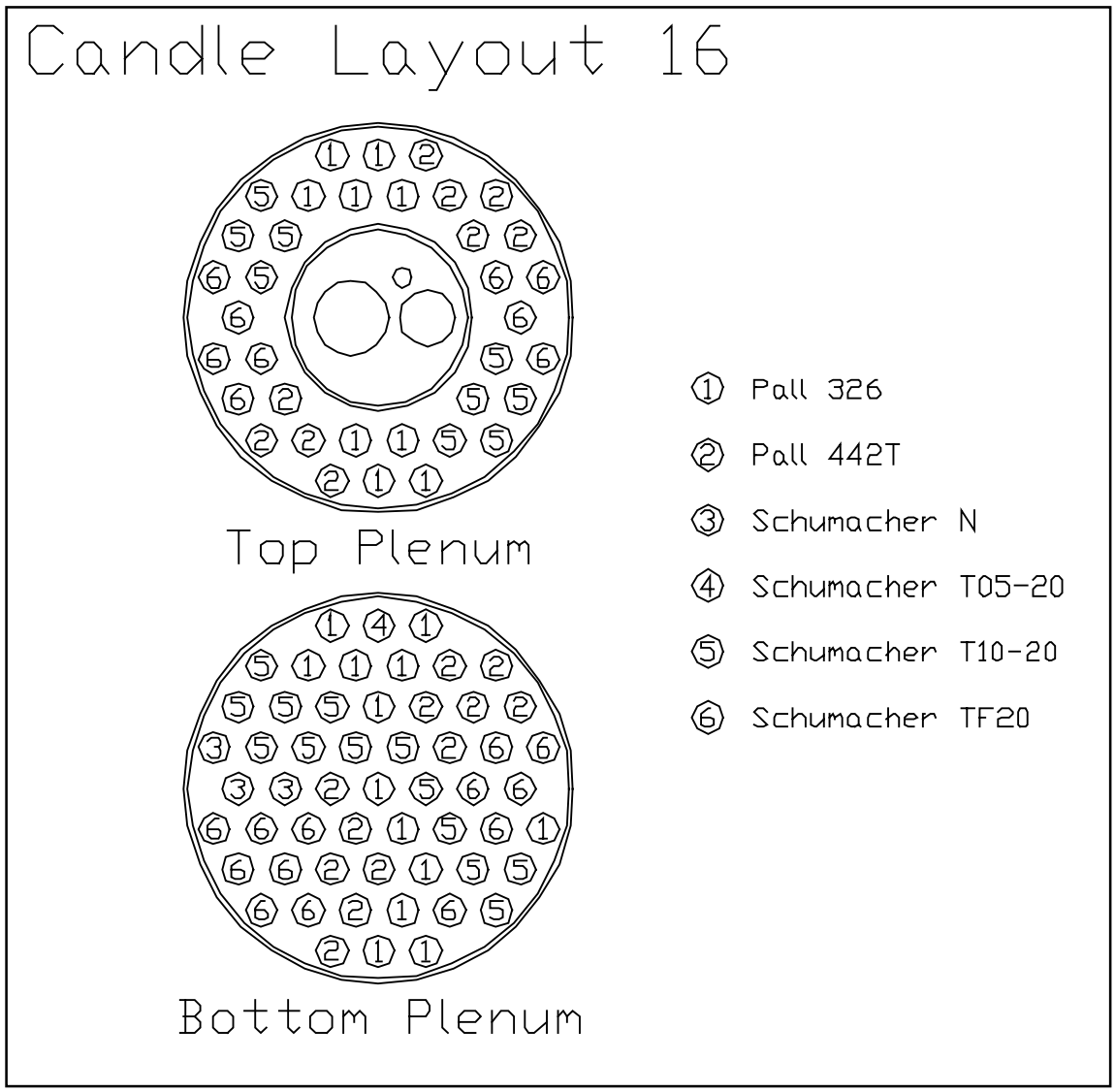

Figure 3.3-2 Filter Element Layout 16

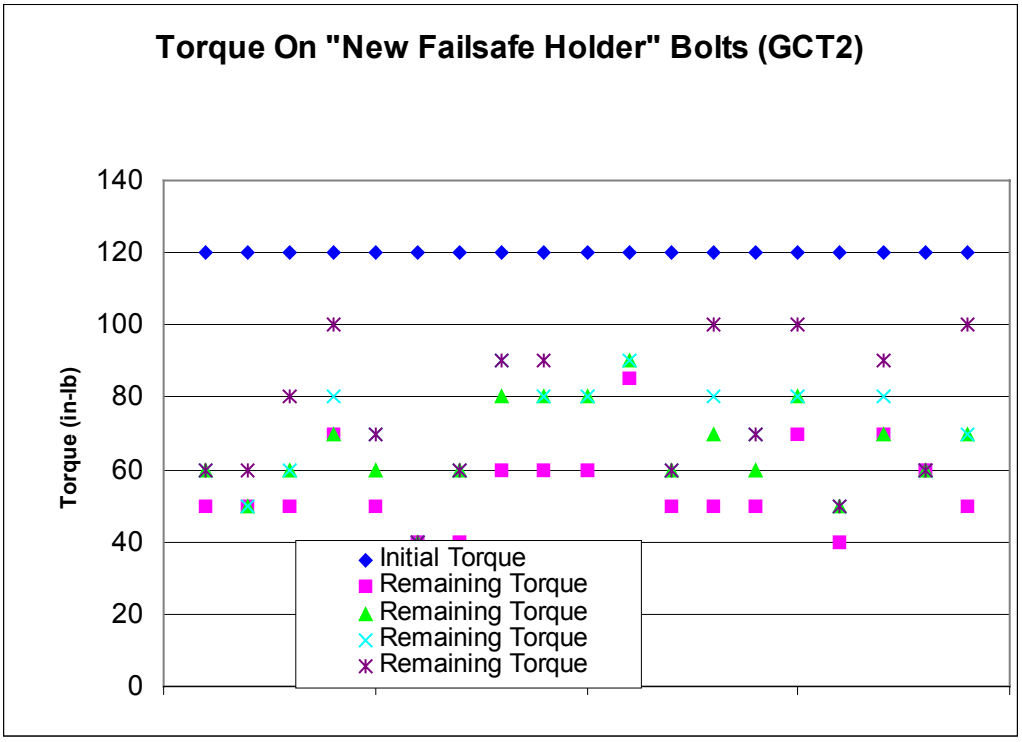

Figure 3.3-3 Remaining Torque on "New Fail-safe Holder" Bolts

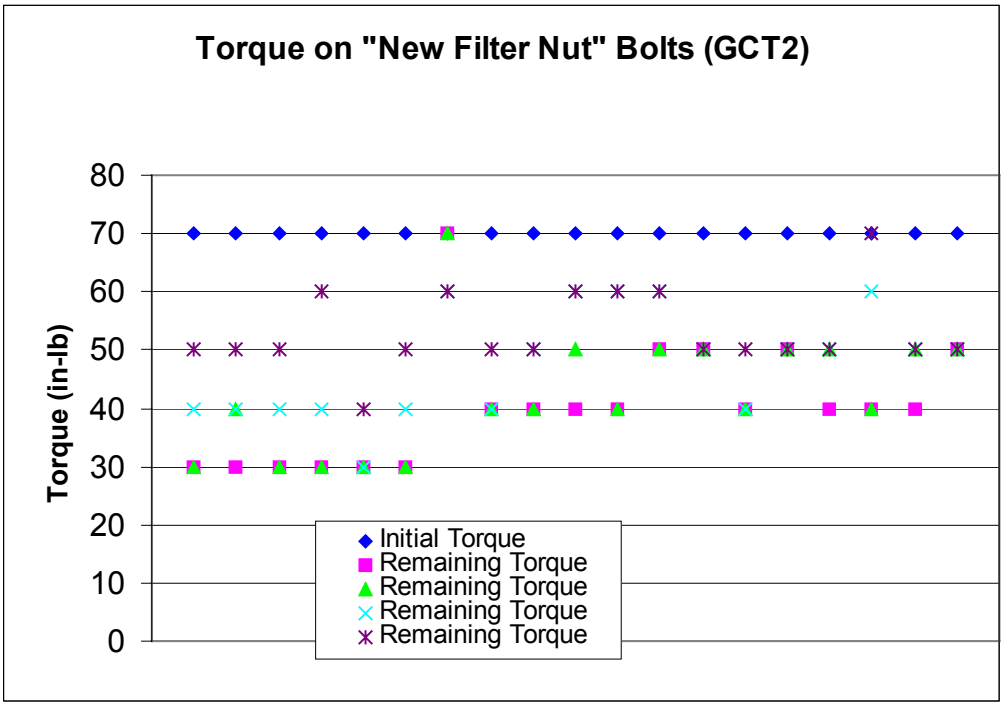

Figure 3.3-4 Remaining Torque on "New Filter Nut" Bolts

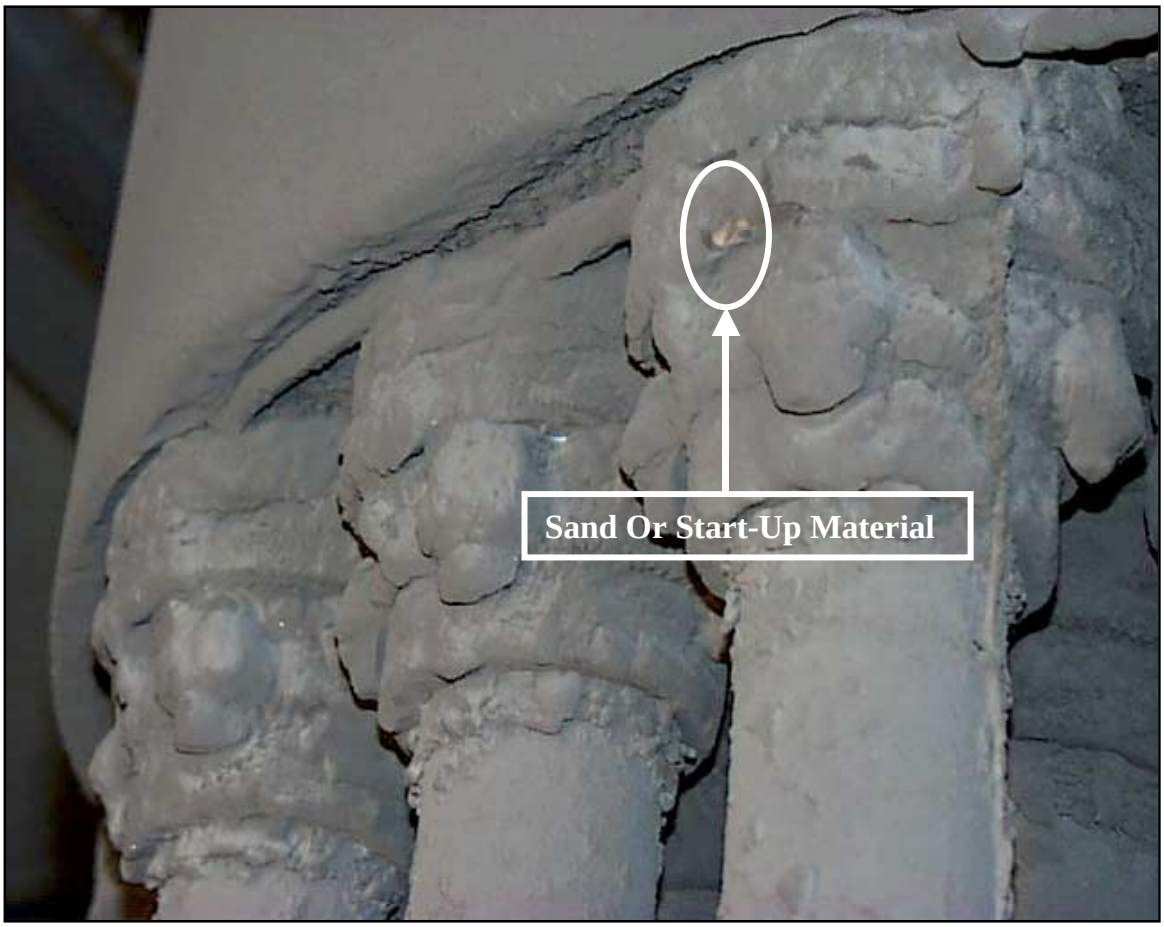

Figure 3.3-5 Char Accumulation on Modified Filter Holders

Figure 3.3-6 Char Accumulation on Monolithic SiC Filter Elements

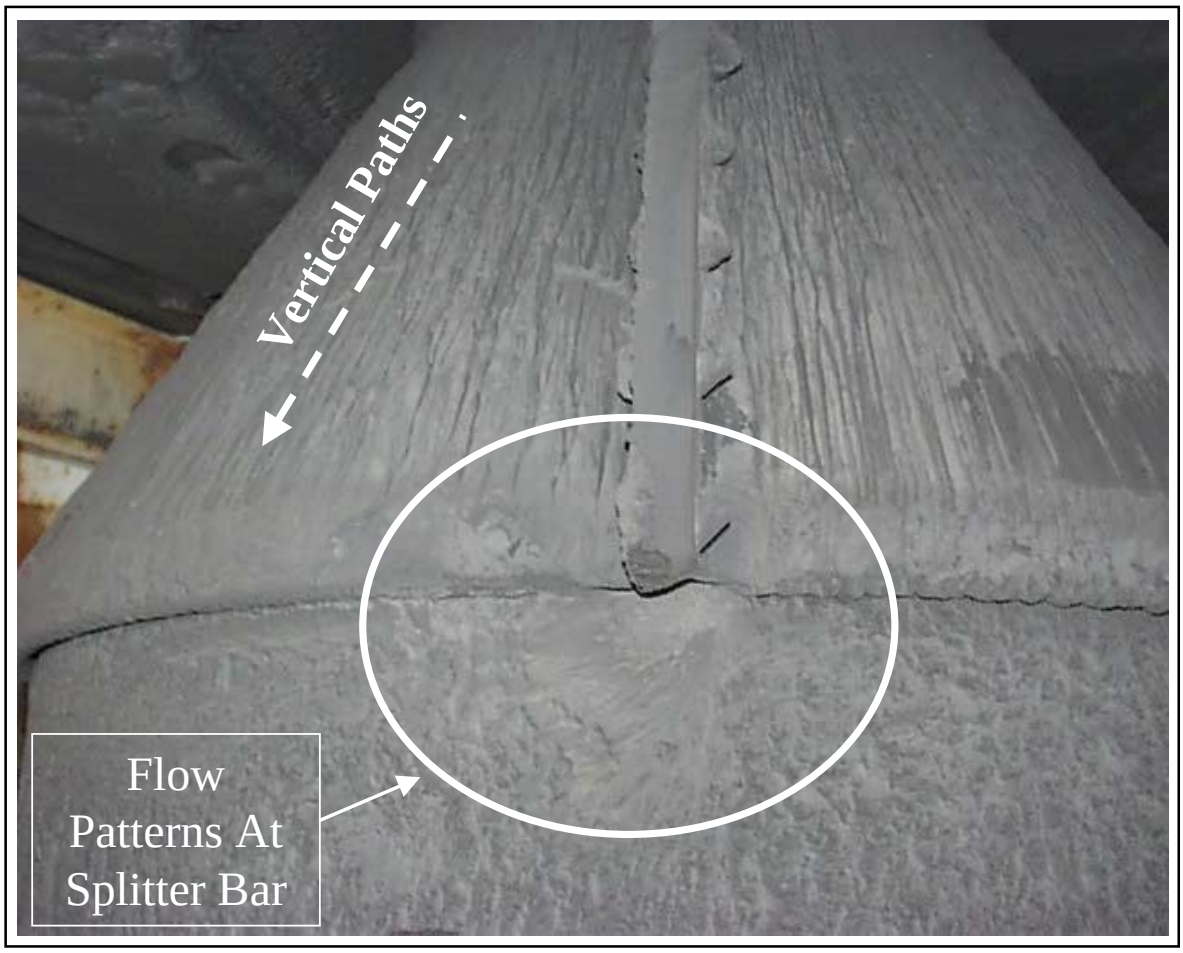

Figure 3.3-7 Char Accumulation on Top Ash Shed and Top Plenum Wall

Figure 3.3-8 Char Accumulation on Shroud and Liner Sections

3.4 GCT2 CHAR CHARACTERISTICS AND PCD PERFORMANCE

This section deals with the characteristics of the char produced in GCT2 and the relationship between char characteristics and PCD performance. As in previous tests, in situ char samples and dustcake samples from GCT2 were thoroughly characterized in an effort to better understand the effects of the char characteristics on PCD performance. In situ char samples were collected at the PCD inlet and at the PCD outlet throughout GCT2. In addition to the in situ samples, residual dustcake samples were obtained following shutdown and removal of the PCD internals. Characterization of the in situ particulate samples and dustcake samples included: chemical analysis; particle-size analysis; laboratory drag/porosity measurements; and measurements of the true particle density, bulk density, uncompacted bulk porosity, and specific-surface area. As in GCT1, drag measurements on the GCT2 char included the use of both the compressed ash permeability tester (CAPTOR) and the new resuspended ash permeability tester (RAPTOR). These measurements were used to better understand the relative contribution of the dustcake to the total PCD pressure drop and to gain insight into the effects of dustcake buildup on drag.

In addition to the char characterization mentioned above, the GCT2 testing included one attempt to analyze the process gas for alkali vapor which is also discussed in this section.

3.4.1 In situ Particulate Sampling

As in previous test campaigns, in situ particulate sampling runs were performed on a regular basis at the PCD inlet and at the PCD outlet throughout GCT2. The system and procedures used for the in situ particulate sampling have been described in previous reports. Seven particulate sampling runs were performed at the PCD inlet and eight were performed at the PCD outlet. All of the GCT2 samples were produced by gasification of Powder River Basin (PRB) coal with addition of Ohio (Bucyrus) limestone for in-bed sulfur capture.

Table 3.4-1 is a summary of the particulate loadings measured in the process gas stream during GCT2. Compared to previous test programs, the mass concentrations entering the PCD were quite stable. All of the loadings were in the range of 25,700 to 34,000 ppmw, producing a mean value of 31,100 and a standard deviation of 2,600 (coefficient of variation of 0.08). The high degree of consistency is attributed to improved transport reactor operation, use of only one coal/sorbent combination, and relatively minor changes in the operating conditions from day to day.

Also shown in Table 3.4-1 are the particle concentrations measured at the outlet of the PCD along with the PCD collection efficiency calculated from the corresponding inlet and outlet measurements. During GCT2 the PCD operated with very low outlet loadings consistent with an absence of significant leaks. The measured outlet loading during all tests was less than 0.37 ppmw with an average collection efficiency of >99.999 percent. During many tests the measured loading was close to the lower limit of resolution, determined during GCT2 to be 0.13 ppmw.

The water vapor content of the flue gas was determined during most of the outlet particulate test runs. This was done by collecting the condensate from the flue gas in an ice-bath condenser and

calculating the vapor concentration from the volume of gas and condensate. During GCT2 the values ranged from 8.7 to 10.3 percent by volume during normal operation. The high value (14.7 percent) was collected during a period of maximum-steam injection.

3.4.2 Sampling of Residual Dustcakes

In addition to the in situ particulate samples discussed above, residual dustcake samples were collected when the PCD filter cluster was removed after the conclusion of GCT2. Prior to the test conclusion there was a system shutdown on April 25 that was caused by solids plugging in the transport reactor system. After clearing the blockage the system was restarted and coal feed was reestablished on April 27. After running for only a few hours on coal the system was again shut down. Back-pulsing of the PCD continued throughout the initial shutdown period (about 16 hours without coal feed) and the PCD was back-pulsed extensively after the final shutdown (about 30 hours after tripping the coal feeder). Because of the two shutdowns and the extensive back-pulsing associated with both shutdowns it is possible that the remaining dustcake may not be representative of the residual dustcake that was present during the run. On the other hand, it is also possible that the residual dustcake is a relatively static layer laid down during the early part of the run and was relatively unaffected by the shutdown, restart, and additional back-pulsing. To investigate how well the remaining dustcake represents the residual cake, dustcake samples were thoroughly characterized to evaluate their contribution to PCD drag. In a subsequent section of this report the dustcake drag measured in the laboratory is compared to the dustcake drag estimated from PCD-pressure drop.

During the GCT2 dustcake sampling, in situ single-point measurements of the dustcake thickness and areal loading were made on six selected filter elements. More extensive, multi-point measurements were also made on two filter elements after they were carefully removed and transported to the laboratory for evaluation. The latter measurements involved multi-point thickness measurements along with the determination of the areal loading by recovery of the entire dustcake. Based on the single-point measurements, the dustcake thickness varied from 0.040 to 0.065 in. with an average value of 0.051 in. Dustcake areal loading varied from 0.068 to 0.13 lb/ft^2 with an average value of 0.088 lb/ft^2. Dustcake porosity values determined from the corresponding values of thickness and areal loading varied from 78 to 88 percent, with an average value of 85 percent. These single-point measurements were in reasonable agreement with the more extensive measurements made on the two selected filter elements. Average dustcake thicknesses for the two selected elements were 0.046 and 0.051 in. and average dustcake areal loadings were 0.092 to 0.099 lb/ft^2. Based on these values, the calculated dustcake porosity was in the range of 81 to 84 percent.

As in previous tests, porosity measurements were also made using the absorption of isopropyl alcohol (IPA) into nodules. These measurements were made using small, intact nodules of char removed from selected dustcake samples. Porosities determined by IPA absorption varied from 71 to 75 percent, with an average value of 73 percent. These values are substantially lower than the porosity values calculated from the dustcake thicknesses and areal loadings, which yielded average values of 81 to 85 percent. These results suggest that the intact nodules removed from the GCT2 dustcake samples were more consolidated, or more compressed, than was the bulk GCT2 dustcake. Therefore, at least for the GCT2 dustcake, the IPA absorption technique may not be a suitable method of estimating dustcake porosity.

3.4.3 Chemical Analysis of In situ Samples and Dustcakes

As in previous test runs, chemical analyses were performed on in situ particulate samples and residual dustcake samples from GCT2. PCD hopper samples were also analyzed, but the compositions of the hopper samples were not used in the evaluation of PCD performance since previous tests have shown that hopper samples are generally not useful for this purpose. The samples were analyzed for carbon, hydrogen, nitrogen, sulfur, and ash; and ashes from the ignited samples were subjected to a standard ash minerals analysis. The standard ash minerals analysis included: aluminum, calcium, iron, magnesium, phosphorous, potassium, silicon, sodium, and titanium. Only the results for aluminum, calcium, iron, magnesium, and silicon are reported here because the concentrations of the other elements were generally less than 0.5 wt percent in the original sample. The elemental analyses reported here are expressed as weight percent of the element in the original sample on an as-received basis.

Using the elemental analyses along with an analysis of CO_2 content, the chemical composition of each sample was calculated as follows:

- $CaCO_3$ content was calculated assuming that all of the CO_2 originated from $CaCO_3$.
- CaS content was calculated assuming that all of the sulfur was present in the form of CaS.
- Any remaining Ca was assumed to take the form of CaO.
- All carbon not accounted for in $CaCO_3$ was assumed to be present as elemental carbon.
- All metals were assumed to be present as the oxides.

The assumption that all of the CO_2 originated from $CaCO_3$ seems reasonable since the relatively small amount of $MgCO_3$ that is contained in the Ohio limestone would completely calcine before the $CaCO_3$ would begin to calcine. The assumption that all of the sulfur is present as CaS may not be valid if some of the sulfur is contained in MgS or FeS, although the relatively low concentrations of magnesium and iron in these samples suggest that the contribution of these sulfides is probably small compared to the contribution of CaS. The assumption that the other metals are present in the form of the oxides could be questioned on the basis that the process conditions in the transport gasifier might favor reduction of certain oxides. For example, Fe_2O_3 could be reduced to FeO or even to elemental iron. It is also possible that the iron could be sulfidized to FeS. Although these uncertainties involve relatively minor constituents of the PCD solids, they may be important in resolving material balances and questions concerning the fate of sulfur and other species. Therefore, PSDF process engineers are working with researchers at the National Energy Technology Laboratory in Morgantown to determine the actual compounds that should be present in the gasifier solids by using free-energy minimization techniques. Since these predictions are not yet available the calculated chemical compositions given here should be regarded as preliminary estimates. The elemental analyses should still be reliable.

3.4.3.1 In situ Samples

Table 3.4-2 summarizes the analytical results for the in situ particulate samples obtained during GCT2. The first two samples collected on April 17 and 19 may not be reliable since these samples were obtained between system startups when sand was being added to make up the solids in the transport gasifier. If these two samples are excluded the remaining samples are fairly consistent in terms of their elemental analyses and they show interesting differences when compared to the analytical results obtained on in situ samples from GCT1.

	GCT1 PRB Char (Dolomite)	GCT2 PRB Char (Ohio Limestone)	GCT1 IL Char (Ohio Limestone)
Avg Carbon (Wt %)	58.5	39.7	41.4
Avg Sulfur (Wt %)	0.85	0.47	4.2
Avg Calcium (Wt %)	4.9	14.3	12.7
Avg Magnesium (Wt %)	1.1	2.0	2.0
Avg Silicon (Wt %)	7.0	8.3	6.1

It is interesting to compare the elemental analysis of the GCT1 char that was generated from PRB coal and dolomite with that of the GCT2 char generated from the same coal with Ohio limestone. In particular, the difference in sulfur content is noteworthy and may suggest a difference in sulfur capture obtained with the dolomite versus the limestone. As expected, the coal/limestone solids are higher in calcium than are the coal/dolomite solids, but contrary to expectations, the magnesium content is also higher in the coal/limestone solids. Comparison of the GCT2 char with GCT1 char from Illinois coal shows that the GCT2 char contains much less sulfur, which is to be expected given the much lower sulfur content of the PRB coal compared to the Illinois coal. Calcium and magnesium contents are reasonably similar for these two chars that were both generated using Ohio limestone. The calculated compositions suggest that the GCT2 char entering the PCD contains on average about 38-percent elemental carbon, about 14-percent calcium carbonate, about 11-percent free lime, about 1-percent calcium sulfide, and about 36-percent inerts.

3.4.3.2 Dustcake Samples

Table 3.4-3 summarizes the analytical results obtained on the residual dustcake samples removed during the post-GCT2 PCD inspection. One bulk dustcake sample was obtained by scraping the dustcakes from selected filter elements in the top plenum and another by scraping elements in the bottom plenum. Separate dustcake samples were also obtained from two elements in the bottom plenum as indicated below. In terms of elemental analysis, all of the samples had fairly consistent compositions. The average elemental analysis is summarized below along with comparable data from the PRB and bituminous coal portions of GCT1.

	GCT1A PRB Dustcake	GCT2 PRB Dustcake	GCT1B-D Bit Dustcake
Avg Carbon (Wt %)	51.4	39.0	48.0
Avg Sulfur (Wt %)	0.41	0.66	1.9
Avg Calcium (Wt %)	8.2	11.8	5.6
Avg Magnesium (Wt %)	2.2	1.8	1.1
Avg Silicon (Wt %)	4.3	7.5	6.8

It is interesting that the GCT2 dustcake contains more sulfur than does the GCT1A (PRB) dustcake since the in situ samples showed the opposite relationship. That is, the GCT2 in situ samples contained less sulfur than the GCT1A in situ samples. These results suggest that the amount of sulfur captured in the gas phase ahead of the PCD was higher during GCT1A, while the amount of sulfur removed by the dustcake was higher during GCT2. As expected, the PRB/limestone dustcake from GCT2 is higher in calcium than is the PRB/dolomite dustcake from GCT1A but, contrary to expectations, the magnesium content of the GCT2 (PRB/limestone) dustcake is only slightly lower than that of the GCT1A (PRB/dolomite) dustcake. This discrepancy may be related to the shutdown/restart situation and extensive pulsing experienced by the dustcake at the conclusion of GCT2. Comparison of the GCT2 dustcake with the GCT1B through D dustcake from Illinois coal shows that the GCT2 dustcake contains much less sulfur, which again is to be expected given the much lower sulfur content of the PRB coal compared to the Illinois coal. Unlike the in situ samples, calcium and magnesium contents are significantly different for the two dustcakes even though both dustcakes were generated using Ohio limestone. Again, this may be related to the shutdown/restart situation near the end of GCT2 and the extensive back-pulsing after shutdown. The calculated compositions suggest that the GCT2 dustcake contains on average about 39-percent elemental carbon, about 2-percent calcium carbonate, about 14 percent free lime, about 1.5-percent calcium sulfide, and about 44 percent inerts. This composition is compared to that of the in situ samples listed below.

	GCT2 Dustcake	GCT2 In situ
Avg Elemental Carbon (Wt %)	38.7	38.1
Avg $CaCO_3$ (Wt %)	2.0	13.7
Avg Free Lime (CaO) (Wt %)	14.2	11.5
Avg CaS (Wt %)	1.5	1.1
Avg Inerts (Wt %)	43.6	35.6

This comparison suggests that the GCT2 residual dustcake contains less sorbent and more inerts than the GCT2 in situ samples. This difference cannot be attributed to sand carryover because the dustcake samples actually contain less silica than do the in situ samples (approximately 16 versus 18 percent). As expected, the dustcake contains more sulfur than do the in situ samples as a result of the additional sulfur capture by the cake. Actually, the major compositional difference between the GCT2 dustcake and the GCT2 in situ samples is in the $CaCO_3$ content, which is much lower in the dustcake (2 versus 14 percent). The additional sulfidation of the cake is not nearly sufficient to account for the difference in $CaCO_3$. The difference is obviously

not attributable to a simple dilution with inert material (e.g., sand) since the level of inerts is not dramatically different between the dustcake and in situ samples (44 versus 36 percent). One possible explanation could be that $CaCO_3$ in the dustcake decomposed during shutdown. This decomposition could occur when the CO_2 level in the process gas drops after the coal feed is turned off. As the dustcake cools in the absence of CO_2, decomposition of the $CaCO_3$ would be favored thermodynamically. This decomposition should produce a higher level of CaO in the dustcake as the $CaCO_3$ decomposes to CaO. In fact, the dustcake does have a higher CaO content (14 versus 11 percent for the in situ samples). This difference in CaO would be sufficient to produce a change in the $CaCO_3$ content from 14 to about 9 percent assuming that all of the additional CaO came from decomposition of $CaCO_3$. The extra sulfidation of the dustcake would be sufficient to account for a further reduction in $CaCO_3$ from 9 to about 8 percent. From these results it may be concluded that the combined effects of decomposition and sulfidation are not sufficient to completely account for the low-$CaCO_3$ content of the dustcake, which is only 2 percent. One possible explanation for this discrepancy is that there was preferential dropout of $CaCO_3$ in the PCD vessel before the dust reached the filter elements. Preferential dropout of the $CaCO_3$ would be possible if the $CaCO_3$ (unreacted limestone) were concentrated in the larger particle-size fractions. This possibility is being investigated through the chemical analysis of size-segregated particulate samples; however, the results of the analyses are not yet available. If the unreacted limestone is preferentially dropping out in the PCD vessel, as suggested here, this could have implications on sorbent utilization. Therefore, it may be possible to improve sorbent utilization by eliminating the dropout through changes in the particle-size distribution of the limestone.

3.4.4 Physical Properties of In situ Samples and Dustcakes

As in previous tests, the GCT2 in situ particulate samples and dustcake samples were subjected to the standard suite of physical measurements, including true particle density, bulk density, uncompacted bulk porosity, specific-surface area, particle-size analysis, and dustcake drag measurements as a function of dustcake porosity. The instruments and procedures used for making these measurements have been described in previous reports.

3.4.4.1 In situ Particulate Samples

Physical properties of the in situ particulate samples are summarized in Table 3.4-4. As discussed previously, sample GCT2IMT-1 was collected between system startups when sand was being added to make up solids in the transport reactor. Therefore, the results obtained for this sample were not included in calculating the average values for GCT2. The remaining samples are fairly consistent in terms of their physical properties. Average values of the various physical properties are given below along with similar data from GCT1 for comparison.

Physical Property	GCT1 PRB Char	GCT2 PRB Char	GCT1 IL Char
Bulk Density (g/cc)	0.33	0.36	0.31
Skeletal Particle Density (g/cc)	2.02	2.24	2.23
Uncompacted Bulk Porosity (%)	84	84	86
Specific Surface Area (m^2/g)	92.9	93.4	19.0
Mass-Median Diameter (μm)	20.6	17.9	23.3

Based on the above comparison, the PRB chars produced from GCT1 and GCT2 seem to have fairly similar physical properties even though they were generated using two different sorbents (dolomite in GCT1 and limestone in GCT2). The GCT1 char from Illinois coal also appears to be fairly similar to the PRB chars in most respects except that it has substantially less surface area (19 versus 93 m^2/g for the PRB chars) and a slightly larger mass-median diameter (MMD) (23 μm versus 18 to 21 μm for the PRB chars). Compared to combustion ashes, all of these chars have relatively low bulk densities, relatively high bulk porosities, and relatively high specific-surface areas. Although there does not appear to be large differences in the MMD of the various char samples, this result does not necessarily mean that there are not other significant differences in the particle-size distributions that are not reflected in the MMD. A more detailed comparison of the particle-size distributions of the char is presented in a subsequent section.

3.4.4.2 Dustcake Samples

Table 3.4-5 is a summary of the physical properties of the residual dustcake samples. The first two samples listed in the table are bulk dustcake samples scraped from five to eight randomly selected filter elements. Bulk dustcake samples were obtained in this manner from both the top and bottom plenums as indicated in the table. The last two samples listed in the table were obtained by scraping the entire dustcake from two selected elements after they were removed from the PCD plenum and transported to the laboratory for evaluation. Care was taken to ensure that the dustcake was not disturbed during the removal and transport of these elements. As shown in the summary below, the GCT2 dustcake had a higher bulk density (and therefore a lower uncompacted bulk porosity) than either of the dustcakes from GCT1.

Physical Property	GCT1A Dustcake	GCT2 Dustcake	GCT1B-D Dustcake
Bulk Density (g/cc)	0.33	0.43	0.28
Skeletal Particle Density (g/cc)	2.11	2.15	2.25
Uncompacted Bulk Porosity (%)	84	80	88
Specific Surface Area (m^2/g)	54.6	23.9	10.8
Mass Median Diameter (μm)	6.2	7.4	8.8

Comparison of the GCT2 and GCT1A dustcakes reveals differences that are more appreciable than might be expected, given that both dustcakes were generated from PRB coal, albeit with two different sorbents (limestone in GCT2 and dolomite in GCT1A). These differences could be at least partially attributable to differences in the reacted sorbents. It is also possible that the

properties of the GCT2 dustcake may have been affected by the shutdown, restart, and extensive back-pulsing at the end of GCT2. Compared to dustcakes from combustion ashes, all of the char dustcakes listed above have relatively low bulk density, relatively high bulk porosity, relatively high specific-surface area, and relatively low MMD.

Comparing the properties of the GCT2 dustcakes to those of the GCT2 in situ samples reveals several interesting differences. First, the GCT2 dustcake has a much smaller MMD than do the GCT2 in situ samples (7 versus 18 μm). This difference in MMD has been seen in previous tests and has been attributed to the dropout of larger particles in the PCD vessel. Secondly, the dustcake has a much lower surface area than do the in situ samples (24 versus 93 m^2/g). This difference in surface area was also seen in the comparison of GCT1 dustcakes and in situ samples. The most likely explanation appears to be that the larger particles, which tend to drop out in the PCD vessel, actually have higher specific-surface areas than do the smaller particles. This trend is contrary to what might be expected (that smaller particles would have a higher specific-surface area as a result of their higher surface-to-volume ratio). Moreover, the measured values of surface area are much higher than expected for solid spheres. For example, the specific-surface area of a solid, 1μm sphere with a true density of 2.1 g/cc is only 2.86 m^2/g. Therefore, it is clear that most of the char surface area must be either in the form of pores or have considerable surface texture. The differences in surface area and other properties are summarized below.

Physical Property	GCT2 Dustcake	GCT2 In situ
Bulk Density (g/cc)	0.43	0.36
Skeletal Particle Density (g/cc)	2.15	2.24
Uncompacted Bulk Porosity (%)	80	84
Specific Surface Area (m^2/g)	23.9	93.4
Mass Median Diameter (μm)	7.4	17.9

Comparing in situ samples and residual dustcake samples generated from combustion ashes has revealed trends in the MMD that are similar to those reported here for the chars. Therefore, there appears to be significant dropout of larger particles in the PCD vessel with gasification chars as well as combustion ashes. While previous testing has succeeded in quantifying the dropout that occurs with combustion ashes, this has not been possible with gasification chars due to the engineering and safety problems associated with the on-line collection of all PCD solids arriving during a given filtration cycle. Because of this limitation it is not possible to accurately calculate the amount of char that is collected during a given filtration cycle, which makes it impossible to calculate the actual drag of the transient dustcake based on the transient ΔP. To date, the transient drag (or ΔP) has not been a critical issue because increasing baseline ΔP has been the major factor limiting PCD operations. If transient drag becomes an issue in the future, however, it may be necessary to design a system for measuring particle dropout in the PCD vessel during future gasification runs.

3.4.5 Particle Size Analysis of In situ Samples and Dustcakes

The size distribution of the particles that make up the PCD dustcake is a critical factor in determining the drag properties of that dustcake. In addition, the particle-size distributions of the various particulate samples can aid in understanding operating characteristics of the entire system. Particle-size distribution measurements were made using the Microtrac size analyzer on samples collected in situ in the gas stream at the inlet of the PCD and on the dustcake samples removed from the candles at the end of the test program.

The particle-size distributions of the seven in situ samples collected at the inlet of the PCD are shown in Figure 3.4-1. The open symbols on the plot are the results for the seven individual samples while the closed symbols and line indicate the average distribution. Good agreement is seen among all of the samples except for one outlier at the minimum particle size, which was excluded from the mean to prevent skewing of the distribution. The average in situ distribution from GCT2 is compared to the in situ size distribution from GCT1A in Figure 3.4–2. Both of these test periods were while gasifying PRB coal in the transport reactor and produced very similar distributions at the PCD inlet. Few apparent differences can be attributed to the different sorbents (dolomite in GCT1A versus Ohio limestone in GCT2) used during the two periods.

After shutdown at the end of GCT2, samples were collected from the residual dustcake that remained in the PCD. Two samples were collected that included large quantities of dust from both the upper and lower plenums. The particle size distributions of these two samples are shown by the open symbols in Figure 3.4-3. As before, the average of the two distributions is indicated on the figure by the solid symbols and line. Although the two distributions are very similar there are some relatively subtle differences between the upper and lower plenums. The upper plenum has a somewhat finer size distribution than the lower plenum, one consistent with more large particles reaching the lower plenum. The upper plenum has about 20 percent more particles around 2.5 µm while there are about three times as many 60-µm particles in the lower plenum sample. The MMD of the two distributions likewise reflect these subtle differences with a value of 6.6 µm for the upper plenum and 7.4 µm for the lower.

Previously, size segregation has been observed in this PCD that produced a dustcake that has a finer size distribution and thus has higher drag than the dust that is collected from the inlet gas stream. Although this segregation (dropout) cannot be measured directly in gasification mode as was done in combustion, comparison of these particle-size distributions can provide information regarding this phenomenon. Figure 3.4-4 compares the size distribution measured at the PCD inlet with the dustcake distribution. Although the collection efficiency of the PCD cyclonic flow system cannot be calculated from these distributions because of a lack of information regarding the relative masses involved, these data do suggest that particles larger than 10 to 20 µm are not reaching the dustcake at the same levels as smaller particles. This dropout of large particles is consistent with results from previous test programs and suggests that changes in the design of the disengager/cyclone system may not produce a directly proportional effect on the operation of the PCD, since the larger particles may drop out in the PCD anyway.

Because the transport reactor was shut down, restarted briefly, and then back-pulsed repeatedly after the final shutdown of GCT2, there was a question about what effect this activity had on

the residual dustcake that remained for inspection. Figure 3.4-5 compares the particle-size distribution of the PCD dustcake samples collected at the end of the GCT2 and GCT1A test programs. The two distributions are virtually identical suggesting that the attempted restart (with sand carryover, etc.) probably did not affect this parameter of the dustcake in a significant way.

3.4.6 Drag Characteristics of In situ Samples and Dustcakes

Drag measurements were made in the laboratory on the upper and lower plenum dustcake samples collected from the PCD at the end of GCT2. As previously described in the report on GCT1, laboratory drag measurements were made with two different techniques. The conventional measurement CAPTOR measures the drag as a function of porosity on a sample that is poured into a cup-shaped measurement cell and mechanically compressed by increasing amounts. The newer measurement RAPTOR measures both the drag and porosity that result from collecting a dustcake of resuspended dust from a flowing-gas stream.

The results of the CAPTOR measurements on the GCT2 dustcake samples are shown by the curves plotted in Figure 3.4-6. The dashed curve shows data for the upper plenum sample while the lower plenum sample is represented by the solid curve. The CAPTOR data indicate that the upper plenum sample has almost twice the inherent drag (at the same porosity) as the sample from the lower plenum. However, the porosity of the samples must be known (estimated) before these data can be used to assess the effect on PCD operation.

One measure of porosity that is determined from the CAPTOR measurement is termed "flow-compacted porosity." This is the minimum amount of compression of the sample that will allow a drag measurement to be made without cracking or other failure of the dustcake when it is subjected to flowing conditions. Most samples must be compressed significantly to sustain typical face velocities without failing under the stress of the pressure gradient in the dustcake. The open symbols superimposed on the two CAPTOR curves in Figure 3.4-6 represent the values obtained at these highest-porosity data points of each CAPTOR test. According to this measure, both dustcake samples have about the same drag but at different porosities. The dustcake drag from this technique was about 58 $inWC/(ft/min)/(lb/ft^2)$ (average for both samples) at an average porosity of 71 percent.

The porosity values obtained from the CAPTOR measurement (flow-compacted porosity) are significantly lower than those indicated by other measurements. As discussed in a previous section, both the uncompacted bulk porosities and the areal loading measurements on the actual PCD residual dustcakes returned average values of 80 to 84 percent. At these higher porosities the dustcake drag taken from the CAPTOR curve would be 8 to 18 $inWC/(ft/min)/(lb/ft^2)$, significantly lower than the 58 $inWC/(ft/min)/(lb/ft^2)$ obtained at the flow-compacted porosity.

The drag measurements made with the RAPTOR device are shown by the solid symbols in Figure 3.4-6. The test was run twice on each of the two dustcake samples resulting in four total data points. The RAPTOR results are compared to the various CAPTOR measurements/ estimates listed below.

Measurement/Estimation Technique	Sample Porosity (%)	Normalized Drag, $\frac{\text{inWC}}{(\text{ft/min})(\text{lb/ft}^2)}$
CAPTOR Measurement at Areal Loading Porosity	84	8
CAPTOR Measurement at Uncompacted- Bulk Porosity	80	18
CAPTOR Measurement at Flow-Compacted Porosity	71	58
RAPTOR Measurement of Drag and Porosity	82	56

The RAPTOR data indicate about the same drag as the CAPTOR results taken at the flow-compacted porosity, slightly less than 60 inWC/(ft/min)/(lb/ft^2). However, the RAPTOR results suggest that the porosity is much higher than the flow-compacted porosity obtained from CAPTOR (82 versus 71 percent). The porosity of the dustcake collected in the RAPTOR device under flowing conditions agrees with the porosity of the PCD residual dustcake determined from the dustcake thickness and areal loading measurements. Interestingly, the RAPTOR measurements do not suggest a significant difference between the upper and lower plenum samples.

It seems reasonable that different results might be obtained with the two drag measurement techniques. When a dustcake is collected under flowing conditions, collection of large particles (which are too massive to follow flow streamlines) would form a pore structure through which the gas must flow. Smaller particles, which can partially follow the streamlines before collection, would tend to flow into and then to fill these pore structures. This would produce a dustcake with a drag and porosity dependent on how the particles actually deposit. When this dustcake is removed, sieved, and poured into a cup (as in the CAPTOR measurement) the small particles will tend to be distributed evenly over the surfaces of the large particles rather than in clusters inside the flow channels. Therefore, when the uniformly distributed sample is compressed to the same average porosity as the flow-deposited dustcake it has a lower drag. The uniformly distributed sample must undergo compression to a lower porosity to produce the same drag as the flow-deposited dustcake. With this in mind, these various laboratory drag measurements will be compared to the actual PCD drag in the next section.

3.4.7 Analysis of PCD Pressure Drop

As in the GCT1 analysis, the contribution of the GCT2 residual dustcake to the baseline PCD pressure drop (ΔP) was estimated by subtracting out the contributions of vessel losses and irreversible increases in the filter element ΔP and the fail-safe ΔP. As in GCT1, vessel losses were estimated from the baseline ΔP recorded during the GCT2 startup prior to the initiation of coal feed. To put both the final baseline ΔP and the startup baseline ΔP on the same basis, both values of ΔP were normalized to a temperature of 1,000°F and to a face velocity of 3.5 ft/min. Unlike GCT1, the changes in filter element and fail-safe ΔP were negligible in GCT2. Since there was no particle leakage through the PCD during GCT2 there was no potential for backside blinding of the elements and fail-safes. There was no potential for filter element pore plugging by nickel sulfidation because no metal elements were installed during GCT2. Without these

complications the contribution of the residual dustcake to the baseline ΔP may be determined by simply subtracting the vessel losses. The drag of the residual dustcake may then be calculated by simply dividing the dustcake ΔP by the areal loading (0.09 lb/ft^2) and by the face velocity (3.5 ft/min). To allow direct comparison of this drag value with laboratory drag measurements, the dustcake drag obtained in this manner may then be adjusted to room temperature using the ratio of gas viscosities at 1,000 and 70°F. To adjust from process gas conditions at 1,000°F where the gas viscosity is 345 μP to room conditions at 70°F where the viscosity of air is 184 μP, the drag values obtained at process conditions must be divided by a factor of 345/184 = 1.88. The results of the calculations outlined above are summarized below.

1. Final baseline ΔP normalized to 1,000°F and 3.5 ft/min (inWC)	76
2. Vessel losses (start-up baseline ΔP normalized to same conditions) (inWC)	32
3. Irreversible filter element and fail-safe ΔP (inWC)	0
4. Dustcake ΔP (Item 1 – Item 2 – Item 3) (inWC)	44
5. Dustcake drag (Item 4/areal loading/face velocity) (inWC/(ft/min)/(lb/ft^2))	140
6. Dustcake drag at room temperature (Item 5/1.88) (inWC/(ft/min)/(lb/ft^2))	74

Based on the analysis summarized above, the dustcake drag at room temperature is estimated to be 74 inWC/(ft/min)/(lb/ft^2). This value may be compared directly to the drag measurements made on the dustcake samples in the laboratory.

	Porosity (%)	Drag, $\frac{\text{inWC}}{(\text{ft}/\text{min})(\text{lb}/\text{ft}^2)}$
CAPTOR at areal loading porosity	84	8
CAPTOR at uncompacted-bulk porosity	80	18
CAPTOR at flow-compacted porosity	71	58
RAPTOR	82	56
Actual PCD	84	74

Based on the results summarized above, the RAPTOR appears to give the best agreement with the actual PCD dustcake porosity and drag. The CAPTOR measurement made at the flow-compacted porosity gives similar agreement with drag but at a much lower value of porosity. Based on the CAPTOR measurements of drag versus porosity the drag values at the areal loading porosity and at the uncompacted-bulk porosity are much lower than the actual PCD dustcake drag. As discussed previously, there may be fundamental differences in the structure of dustcakes formed under flowing conditions and dustcakes formed by packing a bulk sample of dust with a piston. These differences in dustcake structure probably play a key role in determining the relationship between dustcake porosity and drag. Once these differences are thoroughly understood it may not be surprising that CAPTOR measurements made at 71-percent porosity yield about the same drag as RAPTOR measurements made at 82-percent porosity. If it can be demonstrated that the CAPTOR drag values obtained at the flow-

compacted porosity (FCP) consistently agree with RAPTOR drag values then it may be possible to use the CAPTOR measurements at the FCP to evaluate dustcake drag. Until such agreement can be demonstrated, however, the RAPTOR appears to provide the best prediction of dustcake porosity and drag that can be expected in actual operation.

3.4.8 Alkali Vapor Sampling

In addition to the gas analysis discussed above, the GCT2 testing included one attempt to analyze the process gas for alkali vapor. For this measurement, a cartridge containing activated alumina beads was mounted at the outlet of the particulate sampler to adsorb any alkali vapor present in the sample gas. Extraction of the activated alumina beads after the run suggested that alkali vapor was successfully adsorbed from the process gas, but the alumina beads were found to be contaminated with a surface coating of a gray substance. Subsequent testing revealed that the beads could be restored to their original beige color by baking them in air at 1,000°F. Based on this result, it was suggested that the gray-surface contamination may have been carbon or soot from the cracking of tar vapor. In view of this contamination problem, results of the alkali sampling will not be reported for this run. Additional alkali sampling runs will be performed during subsequent test programs to investigate the extent of the surface-contamination problem and to determine whether the contamination has any effect on the alkali vapor measurement.

3.4.9 Conclusions

The GCT2 test program successfully demonstrated that very low levels of particulate emissions (< 1 ppmw) can be achieved during operation of the PCD on gasification char. While the test results do not prove that the modified filter holders were responsible for eliminating particle leakage through the PCD it is noteworthy that substantial particle penetration occurred during the two previous gasification tests (GCT1A and GCT1B through D) with the old-style holders. Another major accomplishment of GCT2 was the demonstration of stable-PCD operation (stable-baseline ΔP) during operation of the transport reactor in gasification mode. Stable operation was achieved with a corrected, normalized baseline ΔP of about 76 inWC. Based on the analysis given here the residual dustcake accounted for about 60 percent of the baseline ΔP and vessel losses accounted for about 40 percent of the baseline ΔP. Unlike as in GCT1, there was no irreversible increase in filter element ΔP or in failsafe ΔP. This result was expected, since there was no potential for backside blinding from particle leakage and there were no metal elements that could become plugged by reactions with H_2S.

Particulate loadings and size distributions measured at the PCD inlet were much more consistent in GCT2 than in previous test programs. The chemical composition and physical properties of the particulate matter also showed improved uniformity. This consistency is attributed to the use of a single coal and sorbent along with only minor changes in transport reactor operating conditions.

Comparison of the actual dustcake drag and porosity with laboratory drag and porosity measurements suggests that the best agreement is obtained with the RAPTOR measurements.

Good agreement in drag values may also be obtained by using the CAPTOR measurements at the flow-compacted porosity (FCP), but this value of porosity is much lower than the porosity determined from thickness and areal loading measurements on the residual dustcake. One possible explanation for these results is that there is a fundamental difference in the structure of dustcakes developed under flowing conditions and dustcakes developed by physically compressing a bulk sample of the dust. Additional testing is needed to investigate the correlation between actual drag, RAPTOR drag, and CAPTOR drag at the FCP.

Table 3.4-1

PCD Inlet and Outlet Particulate Measurements

	PCD Inlet				PCD Outlet					PCD
Test Date	SRI Run No.	Start Time	End Time	Particle Loading, ppmw	SRI Run No.	Start Time	End Time	H2O Vapor (vol %)	Particle Loading (ppmw [1])	Collection Efficiency (%)
4/14/00	--	--	--	--	1	9:00	10:00	--	0.28	--
4/17/00	1	9:55	10:00	34000	2	9:00	10:30	10.3	< 0.13	> 99.999 6
4/19/00	2	10:00	10:15	31100	3	9:50	11:35	14.7	0.30	99.9990
4/20/00	3	13:35	13:50	31000	4	13:30	14:50	8.7	0.23	99.9993
4/21/00	4	8:21	8:36	28300	5	8:00	11:30	9.8	0.18	99.9994
4/22/00	5	10:10	10:30	25700	7	9:51	12:48	9.0	0.37	99.9986
4/24/00	6	12:35	12:50	29600	8	10:50	12:55	10.0	0.16	99.9995
4/25/00	7	10:07	10:20	30900	9	8:45	12:45	9.2	0.22	99.9993

Note 1. Average blank filter correction = 0.13 ppmw.

Table 3.4-2

Analytical Results on In situ Particulate Samples From GCT2
(Weight %)

Elemental Analysis (As-Received Basis)

Lab ID	SRI Run No.	Date	C	H	N	S	Al	Ca	Fe	Mg	Si
AB06810	GCT2IMT-1	04/17/00	36.52	0.35	0.26	0.79	3.82	17.26	1.90	2.44	8.34
AB06811	GCT2IMT-2	04/19/00	43.58	0.45	0.31	0.77	3.87	7.34	1.83	0.88	11.40
AB06812	GCT2IMT-3	04/20/00	42.38	0.40	0.30	0.35	3.28	13.12	1.62	1.28	6.80
AB06813	GCT2IMT-4	04/21/00	36.06	0.26	0.22	0.33	3.51	16.40	1.50	1.92	9.01
AB06814	GCT2IMT-5	04/22/00	44.99	0.46	0.31	0.12	2.89	13.93	1.37	2.04	6.19
AB06815	GCT2IMT-6	04/24/00	36.93	0.32	0.20	0.28	3.96	15.81	1.88	2.81	8.30
AB06816	GCT2IMT-7	04/25/00	37.52	0.25	0.21	0.66	3.56	16.01	1.96	2.93	8.06
Average			39.71	0.36	0.26	0.47	3.55	14.27	1.72	2.04	8.30

Chemical Composition Calculated from Elemental Analysis*

Lab ID	SRI Run No.	Date	CO_2	$CaCO_3$	CaS	CaO	Al_2O_3	Fe_2O_3	MgO	SiO_2	Elem C**
AB06810	GCT2IMT-1	04/17/00	3.02	6.86	1.77	18.94	7.21	2.72	4.07	17.87	35.70
AB06811	GCT2IMT-2	04/19/00	7.06	16.05	1.73	-0.05	7.32	2.61	1.46	24.43	41.65
AB06812	GCT2IMT-3	04/20/00	9.77	22.20	0.78	5.33	6.19	2.31	2.14	14.57	39.72
AB06813	GCT2IMT-4	04/21/00	4.23	9.61	0.73	17.01	6.62	2.14	3.21	19.31	34.91
AB06814	GCT2IMT-5	04/22/00	6.76	15.36	0.27	10.70	5.45	1.95	3.40	13.26	43.15
AB06815	GCT2IMT-6	04/24/00	5.31	12.07	0.62	14.89	7.48	2.68	4.68	17.78	35.48
AB06816	GCT2IMT-7	04/25/00	6.03	13.70	1.49	13.58	6.72	2.79	4.88	17.27	35.88
Average			6.03	13.69	1.06	11.48	6.71	2.46	3.41	17.79	38.07

*Assumes that all CO_2 is present as $CaCO_3$, all sulfur is present as CaS, and remaining calcium is present as CaO.

**Assumes that all carbon that is not contained in $CaCO_3$ is present in elemental form.

Table 3.4-3

Analytical Results on Residual Dustcake Samples From GCT2
(Weight %)

Elemental Analysis (As-Received Basis)

Plenum	Element	Date	C	H	N	S	Al	Ca	Fe	Mg	Si
Bottom	Various	05/15/00	39.55	0.47	0.45	0.58	3.06	12.92	1.35	2.00	6.76
Top	Various	05/15/00	42.58	0.50	0.44	0.74	2.46	10.43	1.26	1.60	4.96
Bottom	B-28	05/16/00	37.15	0.38	0.44	0.75	3.30	12.19	1.29	1.91	9.00
Bottom	B-38	05/16/00	36.38	0.36	0.40	0.56	3.28	11.57	1.31	1.82	9.07
Average			38.92	0.43	0.43	0.66	3.02	11.78	1.30	1.83	7.45

Chemical Composition Calculated from Elemental Analysis*

Plenum	Element	Date	CO_2	$CaCO_3$	CaS	CaO	Al_2O_3	Fe_2O_3	MgO	SiO_2	Elem C**
Bottom	Various	05/15/00	1.14	2.59	1.31	15.61	5.78	1.92	3.33	14.48	39.24
Top	Various	05/15/00	1.36	3.09	1.67	11.58	4.64	1.81	2.67	10.63	42.21
Bottom	B-28	05/16/00	0.44	1.00	1.69	15.20	6.23	1.84	3.19	19.29	37.03
Bottom	B-38	05/16/00	0.50	1.14	1.26	14.58	6.20	1.88	3.03	19.44	36.24
Average			0.86	1.95	1.48	14.24	5.71	1.86	3.06	15.96	38.68

*Assumes that all CO_2 is present as $CaCO_3$, all sulfur is present as CaS, and remaining calcium is present as CaO.

**Assumes that all carbon that is not contained in $CaCO_3$ is present in elemental form.

Table 3.4-4

Physical Properties of GCT2 In situ Samples

Lab ID	SRI Run No.	Date	Bulk Density, g/cm^3	True Density, g/cm^3	Uncompacted Bulk Porosity, %	BET Surface Area, m^2/g	Mass-Median Diameter, μm
AB06810	GCT2IMT-1	04/17/00	0.60	2.46	75.6	98.5	17.4
AB06811	GCT2IMT-2	04/19/00	0.34	2.17	84.3	77.2	17.6
AB06812	GCT2IMT-3	04/20/00	0.39	2.18	82.1	55.1	16.3
AB06813	GCT2IMT-4	04/21/00	0.33	2.29	85.6	131.0	15.8
AB06814	GCT2IMT-5	04/22/00	0.37	2.20	83.2	57.7	19.9
AB06815	GCT2IMT-6	04/24/00	0.35	2.29	84.7	151.0	19.3
AB06816	GCT2IMT-7	04/25/00	0.36	2.31	84.4	88.2	18.6
GCT2 Average*			0.36	2.24	84.1	93.4	17.9
Average for GCT1A**			0.46	2.25	79.6	47.8	27.2
Average for GCT1B-D PRB Portion			0.33	2.02	83.7	92.9	20.6
PRB Char from TRDU			0.29	2.35	87.7	N.M.***	4.7

* Run No. GCT2IMT-1 excluded from average due to probable startup influences.

** Conditions generally unstable throughout GCT1A; values are probably not representative.

*** Not measured.

Table 3.4-5

Physical Properties of GCT2 Dustcake Samples

Plenum	Element No.	Date	Bulk Density, g/cc	Particle Density, g/cc	Uncompacted Bulk Porosity, %	Specific Surface Area, m^2/g	Mass-Median Diameter, μm
Bottom	Various	05/15/00	0.43	2.15	80	23.9	7.4
Top	Various	05/15/00	0.39	2.15	82	17.1	6.6
Bottom	B-28	05/16/00	0.47	2.24	79	20.2	11.4
Bottom	B-38	05/16/00	0.44	2.23	80	31.4	9.9
GCT2 Average			0.43	2.15	80	23.9	7.4
Average for GCT1A			0.33	2.11	84	54.6	6.2
Average for GCT1B-D			0.28	2.25	88	10.8	8.8

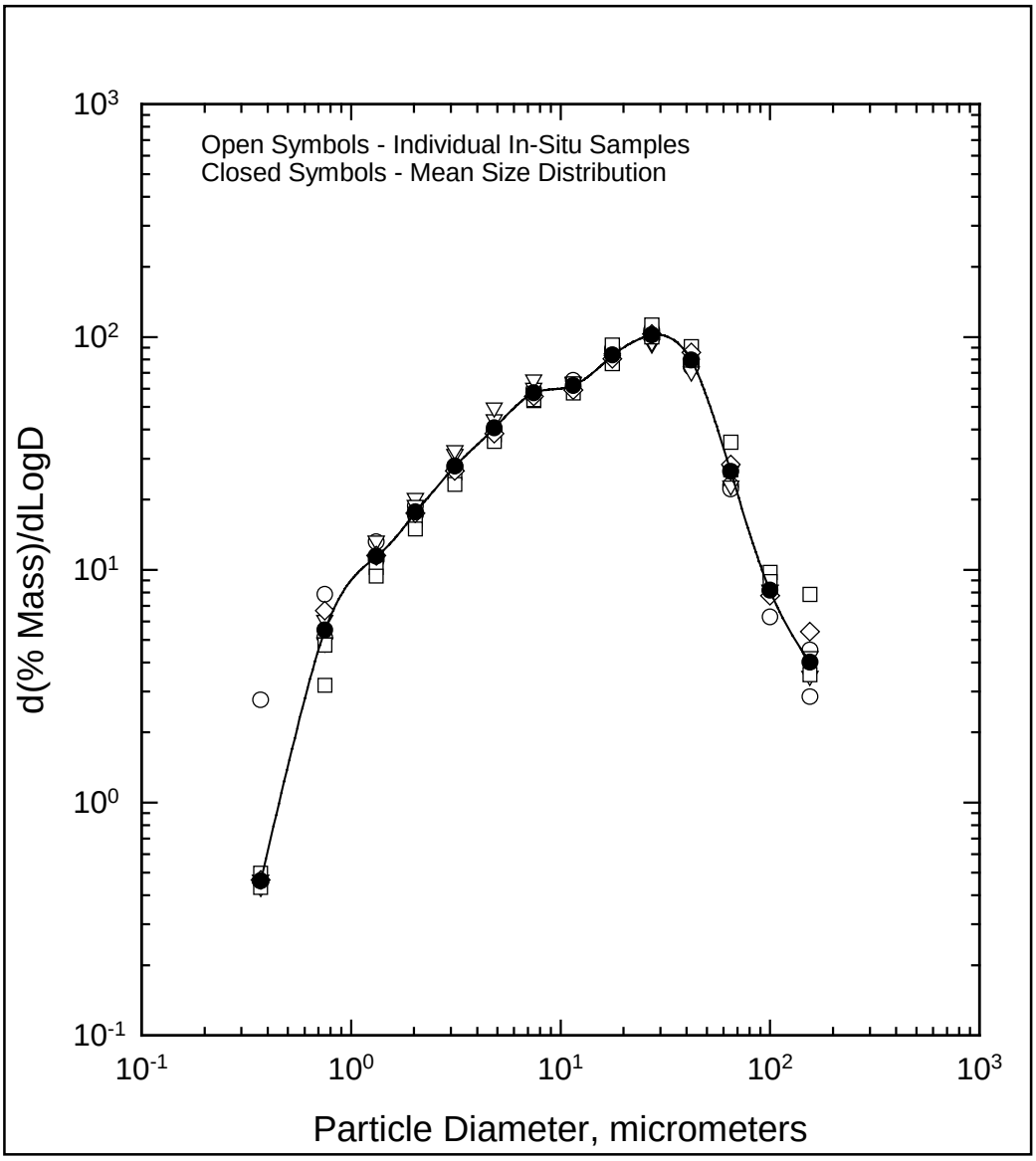

Figure 3.4-1 Particle Size Distribution of In situ Particulate Samples

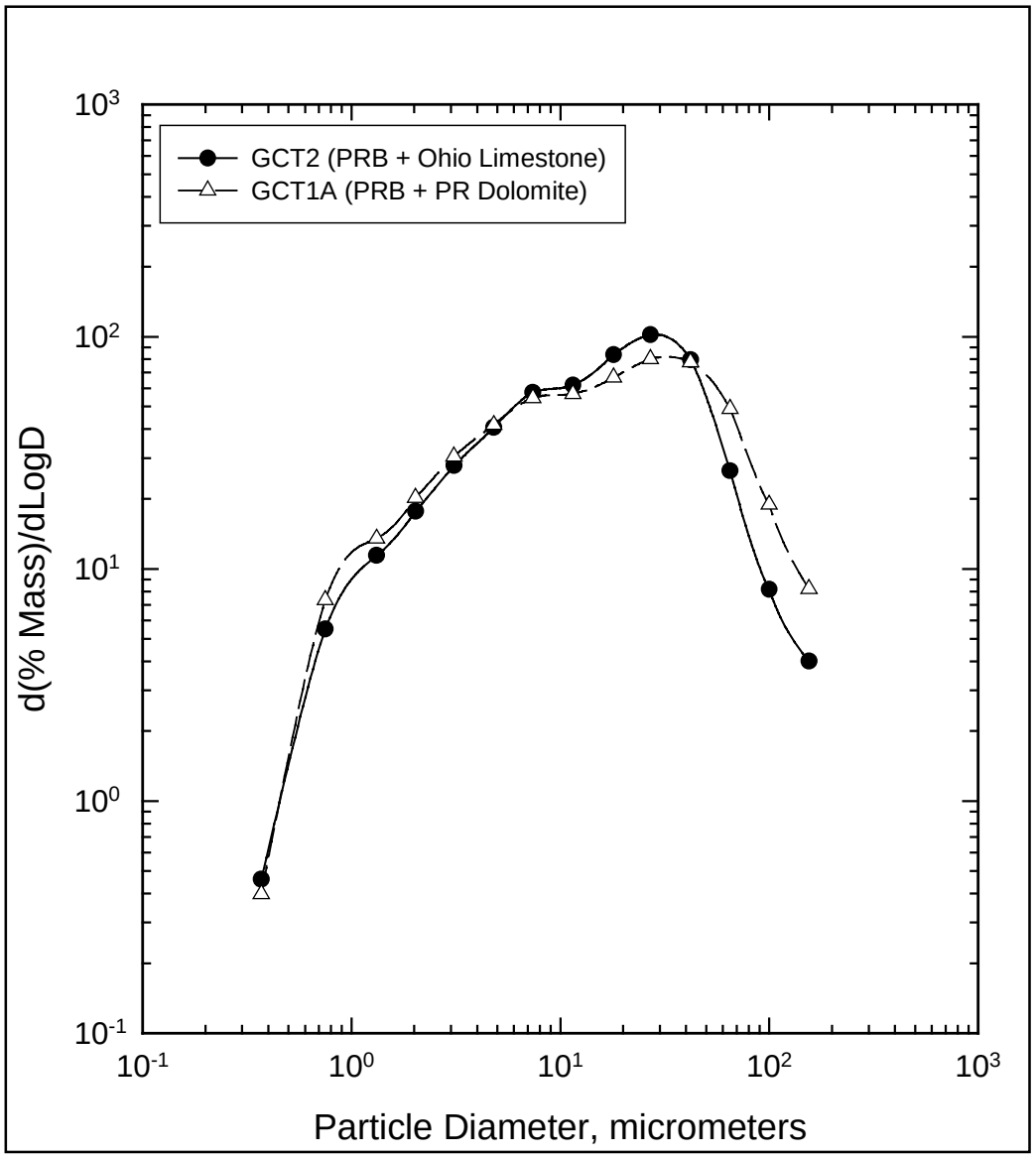

Figure 3.4-2 Comparison of Particle Size Distributions of GCT2 and GCT1A In situ Particulate Samples

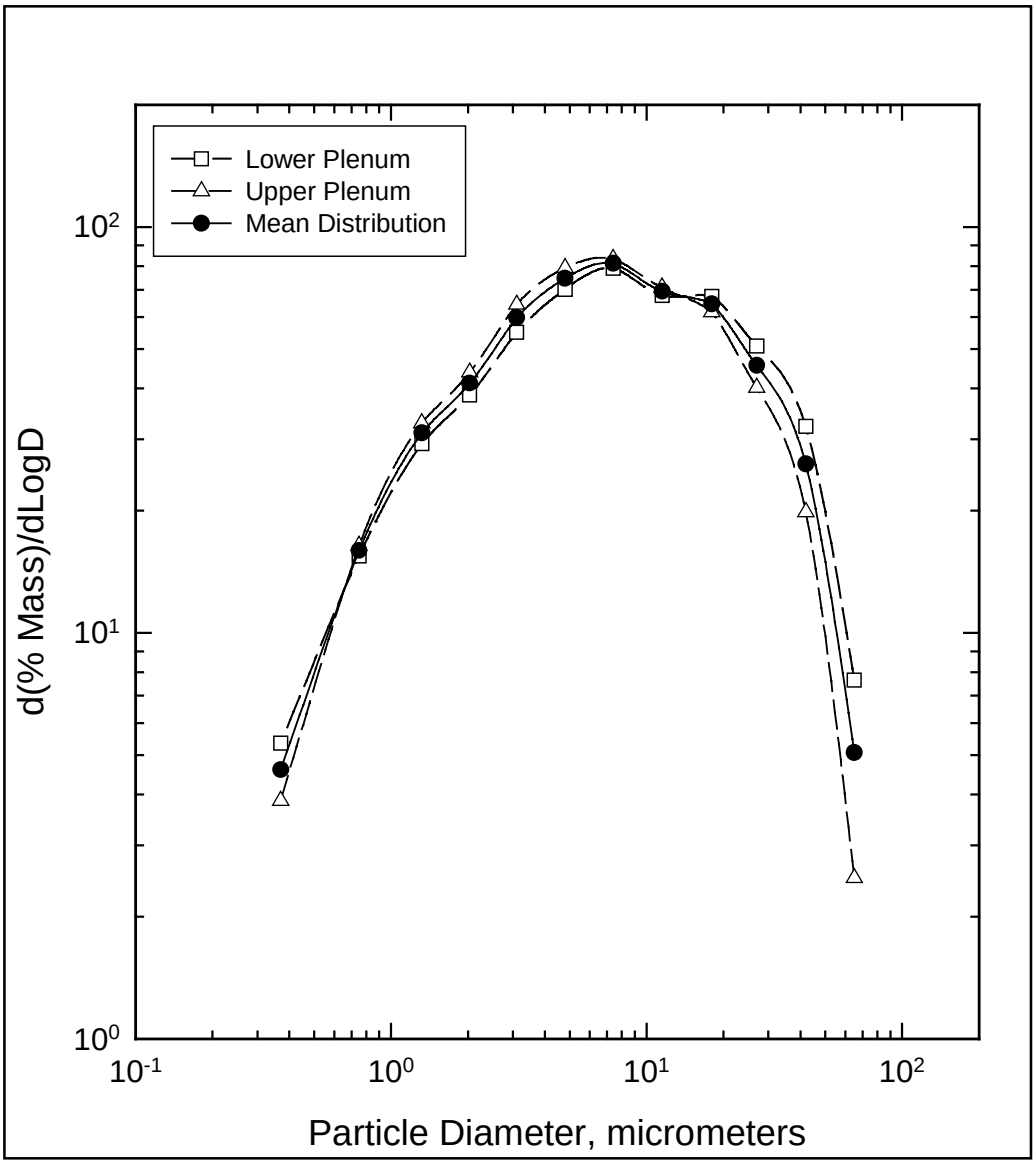

Figure 3.4-3 Particle Size Distribution of Candle Dustcake Samples

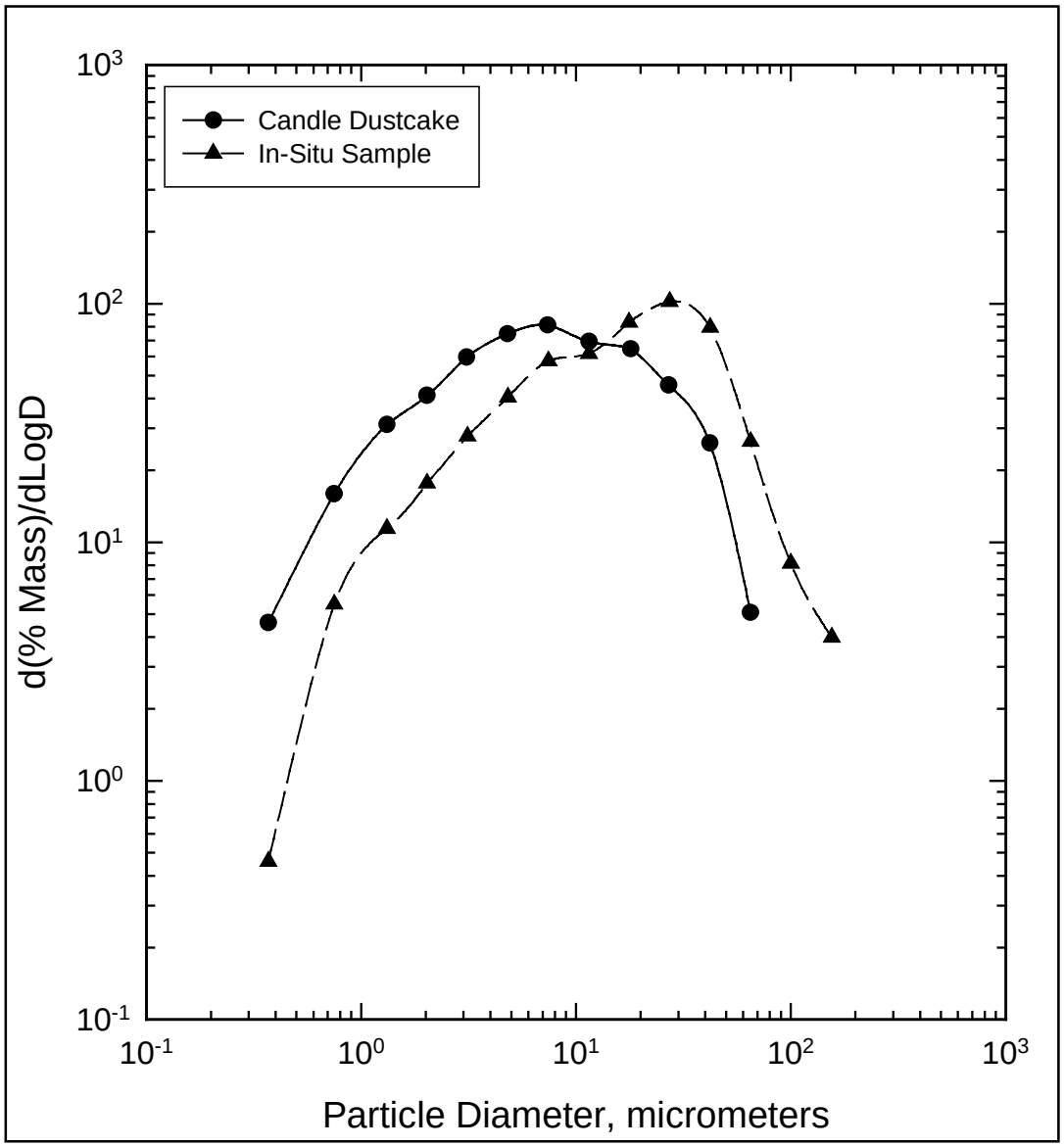

Figure 3.4-4 Comparison of Particle Size Distributions of In situ and Candle Dustcake Samples

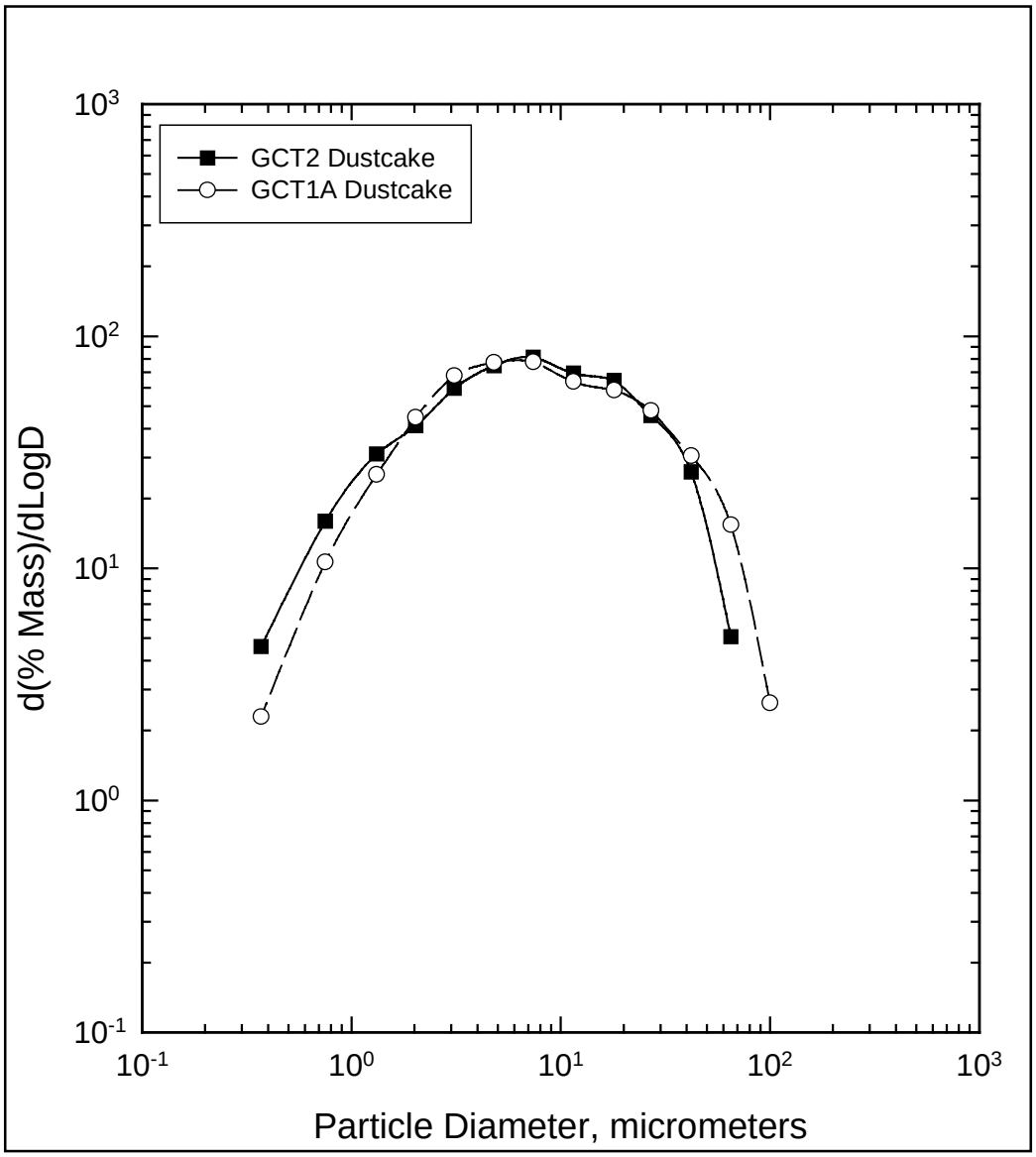

Figure 3.4-5 Comparison of Particle Size Distributions of GCT2 and GCT1A Candle Dustcakes

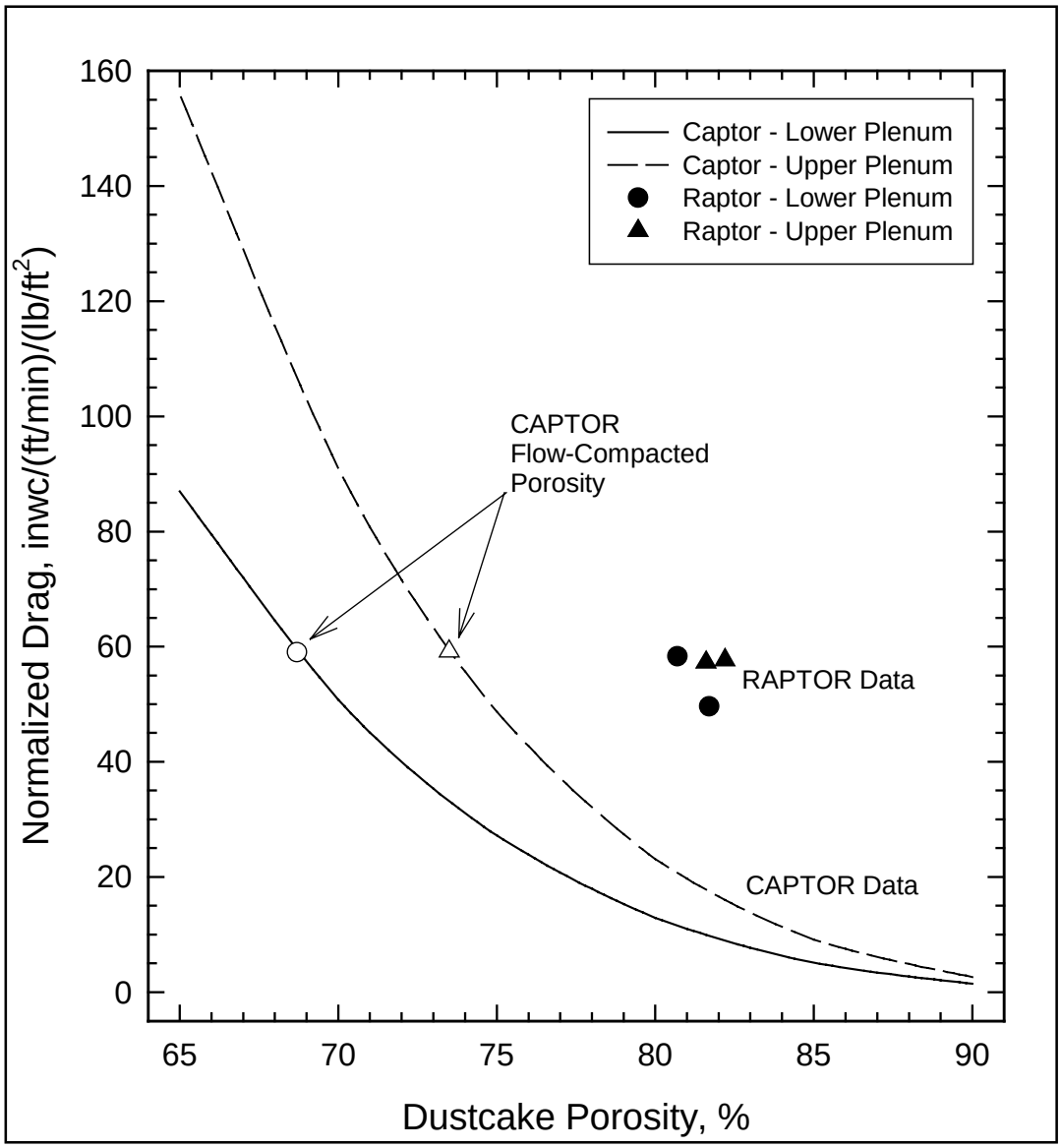

Figure 3.4-6 GCT2 Residual Dustcake Drag Measurements

3.5 FINES HANDLING SYSTEM

3.5.1 Operational Summary

The spent fines ash removal system required significant maintenance during the GCT2 run. Most of the problems were associated with the FD0520 lock vessel system. The problems included: (1) lock vessel leakage, (2) slow vent time, (3) vent line failure, and (4) frequent cycle timer changes. The screw cooler required minimal maintenance relative to the FD0520 system. The major problem associated with the screw cooler was the occasional leakage of the drive-side seals.

During start-up of GCT2, the FD0520 lock vessel leaked on four different occasions, which resulted in the shutdown of the process. The cause of this leak was due to the upper spheri valve O-ring failure. It was determined that warping and wearing of the hardware fitting as well as higher nitrogen-seal pressure may have contributed to the O-ring damage. The nitrogen-seal pressure was decreased from 365 to 330 psig. After the nitrogen-seal pressure was decreased the problem did not appear again throughout the rest of the run.

Just as in GCT1A and GCT1B through D, problems associated with slow-vent times reoccurred in the lock vessel. If the venting time is too slow, the logic of this system is programmed to trip the screw cooler and lock vessel system and thus decrease the PCD ash-removal rate. The vent orifice valve (XV8539) was further opened to facilitate faster vent times. This action resulted in more char going through the vent line. Over time this propagates pipe erosion. Eventually, the vent valve did fail during the run and had to be repaired.

A suitable level probe was not found in time for this run. Therefore, the FD0520 system had to be placed on a timer. This required excessive attention of the operators and engineers to ensure that char was being removed from the PCD. At the same time, the timer had to be placed at a rate that would not excessively cycle the valves. A new level probe design will be installed before the next run. Two options are currently being explored:

1. Nuclear Detection – This type of level detection uses a nuclear source to determine the solids level. This type of probe is mounted on the outside of the vessel. Therefore, it is not affected by the process conditions in the lock vessel.

2. Temperature Difference – This design measures a temperature difference to cycle the vessel. As the solids level rises in the lock vessel and covers the probe, a temperature difference is detected. The probe then sends a signal to begin the cycling process.

Attention given to the screw cooler was mainly due to leakage on the drive-side seals. On some occasions the bolts on the packing follower had to be tightened. Modifications to the sealing arrangement are currently being explored.

The main modification made to the ash-removal system following the GCT1B through D tests is the addition of a flow restriction to the nitrogen purge on the first lantern rings on both sides of the screw cooler. After GCT1B through D the nitrogen flow to the seal purges on FD0502 was determined to be too high. This caused the char to fluff and accumulate on the walls of the

PCD. As the char covered the thermocouples the temperature would drop, giving the impression that the PCD cone was full. This modification successfully reduced the amount of nitrogen to this purge. By keeping the thermocouples uncovered, accurate determination of the char level in the PCD cone was achieved.

3.5.2 Spent Fines Transport System (FD0520) – Observations and Events

A. April 13, 2000, at 19:00 – Lock vessel vented slowly causing the FD0520 and screw cooler to trip. The vent orifice valve (XV8539) was opened to allow faster venting.

B. April 14, 2000, at 15:30 – Lock vessel seal leaked. The upper spheri valve O-ring failed. The seal insert was still in good condition. The O-ring was replaced.

C. April 15, 2000, at 04:20 – Lock vessel seal leaked. Once again the spheri valve O-ring failed.

D. April 15, 2000, at 14:45 – Lock vessel seal leaked when the O-ring failed again. The nitrogen-seal pressure was determined to be too high. The nitrogen-seal pressure was decreased from 365 to 330 psig.

E. April 17, 2000, at 10:12 – Lock vessel seal leaked. The O-ring failed again.

F. April 18, 2000, at 07:15 – FD0520 vent line leaked. The "A" vent valve was leaking around the flange. This valve was isolated and "B" valve was opened.

G. April 19, 2000, at 08:00 – Discharge line plugged.

H. April 21, 2000, at 11:35 – Discharge line plugged.

I. April 22, 2000, at 00:09 – FD0520 tripped. The high-level switch in the FD0530 vessel alarmed. The logic is programmed to trip the FD0520 system whenever the char level gets too high in FD0530.

3.5.3 Spent Fines Screw Cooler (FD0502) – Observations and Events

A. April 13, 2000, at 10:55 – Drive-side seal leaked. The seal leaked between the packing and the shaft. The bolts on the packing follower were tightened to 80 in-lb.

B. April 14, 2000, at 11:40 – FD0502 seal pressure dropped below the system pressure. During this time the system pressure could have forced char into the seals. Over time, the seals would erode and fail.

C. April 14, 2000, at 18:30 – FD0502 seal pressure dropped below the system pressure. The seal pressure dropped below the system pressure due to low-nitrogen-header pressure.

D. April 15, 2000, at 03:40 – FD0502 seal pressure dropped below the system pressure.

E. April 15, 2000, at 12:55 – Drive-side seal leaked. The bolts on the packing follower were tightened to 80 in-lb. This action stopped the leakage.

F. April 17, 2000, at 10:00 – FD0502 seal pressure dropped below the system pressure.

G. April 19, 2000, at 09:00 – FD0502 seal pressure dropped below the system pressure.

H. April 19, 2000, at 12:40 – FD0502 seal pressure increased. The nitrogen that supplies the seal pressure to the screw cooler was increased to 180 lb/hr. This was done to maintain 20-psig-pressure differential between the seal pressure and the system pressure.

I. April 22, 2000, at 03:39 – Drive-side seal leaked. The gas leaking from the screw cooler was nitrogen. (This was based on the fact that the gas did not have a smell. Also, the portable gas detector only detected low oxygen near the leak.)

3.6 FILTER ELEMENT DATA

Physical, mechanical, and thermal properties of many different types of filter elements have been measured at SRI. For most of the element types testing has been conducted on as-manufactured elements and on elements from PFBC or PCFBC operation. Test results have been reported as they were generated in several reports to the DOE, NETL and the SCS, PSDF (See references 1 through 5). All of these previously reported results are compiled and presented in the Appendix to provide access to the data in a single source. Results are presented for the following types of filter elements:

- Pall 442T.
- Pall 326.
- Pall 181.
- Schumacher F40.
- Schumacher TF20 and T10-20.
- Schumacher N10-20.
- Inductrial Filter and Pump (IF&P) REECER™.
- Coors P-100A-1.
- Blasch 4-270.
- Ensto.
- Specific Surface.
- Techniweave N610/mullite.
- McDermott ceramic composite.
- Honeywell PRD-66C.
- 3M oxide-oxide composite.
- Pall iron aluminide.

A brief description of each material is given in the section where the results are presented. In all of the previous reports considerable data analysis was provided to assess how the results relate to performance in the operating environment. No analysis is provided in the Appendix. Results are presented in tabular and graphical formats with no comment. A list summarizing the properties for each filter is presented on page 3.6-3.

References

1.0 Spain, J.D. and Starrett, H.S., "Physical, Mechanical, and Thermal Properties of Schumacher SiC Filter Material," Report Number SRI-MME-94-253-6938.20.1-I-F, Prepared for U.S. DOE/METC under Contract No. DE-AC21-89MC26233, March 1994.

2.0 Spain, J.D. and Starrett, H.S., "Physical, Mechanical, and Thermal Properties of Refractron SiC Filter Material," Report Number SRI-MME-94-253-6938.20.1-I-F, Prepared for U.S. DOE/METC under Contract No. DE-AC21-89MC26233, May 1994.

3.0 Spain, J.D. and Starrett, H.S., "Physical, Mechanical, and Thermal Properties of Coors Alumina Mullite Filter Material," Report Number SRI-MME-94-480-6938.20.1-III-F, Prepared for U.S. DOE/METC under Contract No. DE-AC21-89MC26233, August 1994.

4.0 "Technical Progress Report for Kellogg Brown & Root Transport Reactor Train With Siemens Westinghouse Particulate Control Device: TC04 Report, October 14 – 17, 1998, " Section 3.4. Prepared by Southern Company Services, DOE Cooperative Agreement Number DE-FC21-90MC25140.

5.0 "Technical Progress Report for Kellogg Brown & Root Transport Reactor Train With Siemens Westinghouse Particulate Control Device: TC05 Report, January 10 – May 2, 1999," Appendix. Prepared by Southern Company Services, DOE Cooperative Agreement Number DE-FC21-90MC25140.

	Pall 442T	Pall 326	Pall 181	Schum. F40	Schum. TF20 and T10-20	Schum. N10-20	IF&P REECER	Coors P-100A-1	Blasch 4-270	Ensto	Specific Surface	AIT N610/ mullite	McDermott	Honeywell PRD-66C	3M Oxide/ Oxide	Pall Fe_3Al
Bulk density (lbm/ft^3)	110	113	113	117	121	123	137	103	111	118	77	108	51	89		245
Hoop tensile strength at RT[1] (psi)	2,450	2,060	2,800	2,280	1,900	2,530	2,040	1,900	500	990	320	3,460	700	830	2530[5]	17,300[6]
Axial tensile strength at RT (psi)	2,000	1,300	2,570	1,120	900		2,120	2,480	270	920		5,450[4]	600	290		19,000[6]
Axial Young's Modulus at RT (10^6 psi)	6.0	5.7	6.0	5.9	4.0		14	4.3	0.90	2.3		6.2	0.45	0.35		5.2
Axial tensile strain-to-failure at RT (mils/in.)	0.35	0.24	0.45	0.21	0.22		0.16	0.62	0.37	0.50		0.84[4]	2.1	1.5		9.5
Axial tensile strength at 1,500°F (psi)	1,750	2,200	2,060	1,360	1,200		1,980	2,390		900						6,300[6,7]
Axial Young's Modulus at 1,500°F (10^6 psi)	4.4	2.8	5.0	3.9	2.3		18	2.5		2.3						3.6[7]
Axial tensile strain-to-failure at 1,500°F (mils/in)	0.46	1.4	0.47	0.41	0.40		0.10	1.0		0.40						14.8[7]
Axial compressive strength at RT (psi)	12,100			9,540				17,200				2650	580		3180[5]	
Axial compressive strain-to-failure at RT (mils/in.)	2.1			1.7				4.4				0.53	2.3		3.4	
Axial CTE[2], 500 to 1,500°F (10^{-6} in./in.-°F)	2.6	2.8	2.8	2.5	2.6	2.5	2.4	2.8	4.1	3.9	1.0	4.7	4.6	2.2		13.1
Radial thermal conductivity at 1,000°F (Btu-in./hr-ft^2-°F)	38	38	32	38	52	28	120	10	5.2	6.0	3.8	2.3	1.6	3.4		
Pressure drop at 5 ft/min face velocity[3] (inH_2O)	0.6	1.3			2.1 TF20 4.4 T10-20		1.5	3.3	7.7				1.7	0.9	1.1	4.1

1.) RT = Room temperature. 2.) CTE = Coefficient of thermal expansion. 3.) Using air at ambient conditions. 4.) Only one value. 5.) Stress calculations were based on measured specimen I.D. values and a nominal thickness of the inside structural wall of 0.055 in. The stress calculations assume that all load was carried by the inside structural wall. 6.) Ultimate strength shown; yielding occurred at lower stress level. 7.) Results at 1,400°F for Pall Fe_3Al.

4.0 TRANSPORT REACTOR

4.1 GCT2 RUN SUMMARY

Test run GCT2 began on April 10 with startup of the main air compressor. Coal feed was started on April 13, 2000, at 17:50 and ended on April 25, 2000, at 16:16 due to a piece of refractory plugging the cyclone dipleg. The reactor was restarted on coal feed for 3 hours on April 27, 2000. Total time on coal was 217.5 hours and 413 tons of PRB coal was processed. The sorbent for the run was Ohio Bucyrus limestone.

Primary objectives of test run GCT2 were as follows:

- *Gas Velocity* – Characterize the effect of gas velocity on solids collection efficiency.
- *Higher Operating Temperature and Pressure* – Evaluate the effect of higher operating temperature and pressure on process performance.

Secondary objectives included the continuation of the following reactor characterizations:

- *Operational Stability* – Characterize reactor loop and PCD operations with short-term tests by varying coal feed, air/coal ratio, riser velocity, solids circulation rate, system pressure, and air distribution.
- *Reactor Operations* – Study the devolatilization and tar cracking effects from transient conditions during transition from start-up burner to coal. Evaluate the effect of process operations on heat release, heat transfer, and accelerated fuel particle heatup rates. Study the effect of changes in reactor conditions on transient temperature profiles, pressure balance, and product gas composition.
- *Effects of Reactor Conditions on Syngas Composition* – Evaluate the effect of air distribution, steam/coal ratio, solids circulation rate, and reactor temperature on CO/CO_2 ratio, H_2/converted carbon ratio, gasification rates, carbon conversion, and cold and hot gas efficiencies.
- *Effects of Reactor Conditions on H_2S Emissions* – Study the effect of Ca/S molar ratio, riser velocity, and solids circulation rate, on sulfur capture. Evaluate the effects on limits of sulfur capture dynamics in relation to $CaS\text{-}H_2O\text{-}H_2S\text{-}CaO$ reaction approach to equilibrium.
- *Forms of Sulfur From Reactor Operations* – Determine the effect of reactor operations on forms of sulfur (CaS, $CaSO_4$, FeS) in the reactor standpipe solids and in the fines from the PCD. Quantify the reactive sulfide concentration in these solids streams and at the sulfator solids outlet.

Activities during the outage preceding test run GCT2 included about 47 equipment revisions. Those affecting the process the most are as follows:

- The sulfator fuel-oil injection tubing was increased in size, and with fuel oil addition the sulfator temperature could be increased above 1,500°F.

- The eight thermowells which failed in GCT1 were changed. Five were changed to Inconel 600 (with the last 2 inches coated with chrome carbide). Three were changed to a ceramic tube with an Inconel inner shell. The thermowells were removed and photographed. Only the thermowells in the riser and crossovers were damaged. The ceramic-covered thermowells cracked and the ends were worn off. The chromium carbide-coated ends were worn off in most of the riser thermocouples. However, thermowells from the standpipe and other parts of the reactor system were only slightly worn.

- Due to flow constrictions, separate pipes were run to the start-up burner for nitrogen and another for propane. Other parts of the plant were not upset as these changes were made.

- Due to possible plugging of the coal feed nozzle, a steam shroud was made for the coal feed nozzle. Either nitrogen or steam could be added. Nitrogen was used in the shroud for this test run and no plugging was detected.

- The maximum temperature for the steam from the hot-gas heat exchanger on the sulfator gas was limited to 750°F. The trip point was increased to 950°F to eliminate the operating restrictions encountered in test run GCT1. The piping metallurgy is designed for the higher temperature.

- Several alarm and interlock enhancements were made to allow higher temperature operation and to fine tune the alarm set points.

Seal failure of the O-ring on the FD0520 spheri valve seals resulted in five shutdowns and startups between April 13 and April 17, 2000, before getting the spheri valve O-ring to hold. All of these failures occurred on the second generation of O-ring seals that distribute seal-pressurization nitrogen to spheri seals. The original version of the spheri valve with a silicone seal was used. The first coal feed started on April 13, 2000, at 17:50. The first test period, GCT2A, was designated for April 13 from 20:55 to April 14 at 11:30. This period was split into six operating periods (designated GCT2A-1 to GCT2A-6) for various feed rates at 160 psig. Continuous coal feed started on April 17, 2000, at 23:54.

After startup, flows and pressure were adjusted on April 18, when it was decided to fix two leaks. One was on the FD0520 pressurization line and the other was on the FD0520 vent valve. The repairs were made on-line at low-coal feed. By 14:07 the coal feed rate was increased to 100 percent of feeder speed at 160 psig (4,300 lb per hour). Samples were labeled GCT2B-1 to -4. Pressure was increased at 20:03 to 180 psig and maintained until 10:52 on April 19 for periods GCT2C-1 to -8. There were four cyclone dipleg upsets on April 18.

Reactor pressure of 200 psig was maintained from 11:24 on April 19 until 19:42 on April 22 for periods GCT2D-1 through GCT2D-22. On April 19 some difficulties were met in keeping the baghouse temperature low. Heat from burning the syngas in the thermal oxidizer caused too great a temperature for the baghouse. The coal-feed rate was reduced at 19:30 to lower the heat input. Excess air and air quench were reduced on the thermal oxidizer to reduce the amount of heat going to the baghouse.

On April 20 operation for periods GCT2D-7 through -12 was stable until 08:26, when it was decided to blow out some instrument legs since the PDTs did not look good. One of the PDTs blown out had a common leg with the PT287 pressure transmitter. This caused the reactor pressure to suddenly drop but it recovered within 10 minutes. The coal-feed rate was reduced for about 30 minutes to 65 percent to remove solids from the PCD cone. During feeding problems with the limestone the limestone was found to be slightly moist. The limestone in storage was drummed and new limestone was not available until 13:30, when the limestone was fed at 20 percent of feeder speed. There were three dipleg upsets during that day.

On April 21 the coal-feed rate was reduced due to the coal mill not being able to grind coal fast enough. The as-received coal was wet, and the coal rate was reduced to 60 percent (3,000 to 3,400 lb per hour of coal) for periods GCT2D-16 to -22. There were nine dipleg upsets during that day.

On April 22 the limestone rate was reduced to 8 percent at 7:55 which started period GCT2D-19. The coal-feed rate was 51 percent or about 3,000 pph. The coal rate was low because of slow grinding in the coal mills. The limestone rate was further reduced at 18:19 to 4 percent for the start of period GCT2D-22. At 19:00 small amounts of tar were being formed. At 19:42 the reactor pressure was increased to 220 psig to start period GCT2E. There were eight dipleg upsets that day.

On April 23 the coal mills ground enough to accumulate 37 tons so the coal and limestone feed rates were slowly increased at 5:25. At 07:13 there was a lot of tar in the gas sampling system. At 9:35 the coal feed rate was increased to 100 percent (4,300 lb per hour of coal) with signs of tar formation. At 18:00 the reactor temperature was increased to between 1,740 and 1,750°F. The limestone rate was reduced from 30 percent (250 pph) to 10 percent to start GCT2E-5. With the higher temperature, the tar formation disappeared in the gas analyzer. The mixing zone temperature (TI349) was operating between 1,750 and 1,760°F at 20:50 with small amounts of tar formation.

On April 24 the TI349 (mixing zone) was increased to around 1,770°F, which started test GCT2E-6. Minimum amounts of tar were still flowing along the usual sample line to the gas analyzer. At 14:10 the coal rate was reduced to 80 percent (4,000 lb per hour of coal) with a mixing zone temperature around 1,744°F and 220 psig, which preceded period GCT2E-9. At 21:55 coal feed rate was increased to 100 percent (4,300 lb per hour of coal) to start period GCT2E-11. At 22:30 there was no tar in the sample lines.

On April 25 at 06:20 the reactor pressure was increased to 240 psig to start period GCT2F. At 12:17 tar formation was apparent. At 16:02 the dipleg was not functional; coal feed was stopped at 16:16. Standpipe and disengager were borescoped but no blockage was found. The cyclone dipleg was also borescoped. A piece of refractory was found in the end of the cyclone dipleg. The refractory was pushed out into the standpipe. The piece looked to be about 12 inches long and probably 3 to 5 inches in diameter. The reactor was buttoned up.

On April 27 coal feed was started at 07:15 and stopped at 10:15 to end the test run.

Table 4.1-1

GCT2 Operating Conditions for Transport Reactor

Start-up Bed Material	Sand (~ 120 μm)
Fuel Type	Powder River Basin
Fuel Particle Size (MMD)	300 to 400 μm
Average Fuel-Feed Rate	Maximum possible without accumulating ash/char in PCD cone
Sorbent Type	Ohio Bucyrus limestone
Sorbent Particle Size	30 to 60 μm
Average Sorbent Feed Rate	0 to 200 pph
Ca/S Molar Ratio	Ratio required for 90%+ sulfur capture
Reactor Temperature	1,700 to 1,800°F
Reactor Pressure	160 to 240 psig
Riser Gas Velocity (fps)	40 to 50 ft/s
Solids Circulation Rate (lb/hr)	Maximum possible without accumulating ash/char in PCD cone
Primary Gas Cooler Bypass	0%
PCD Temperature	800 to 1,000°F
Total Gas Flow Rate	20,000 to 25,000 lb/hr
Air/Coal Ratio	2.4 to 3.2
Primary Air Split ($1^{st}/2^{nd}$ levels)	50/50 to 90/10
Steam/Coal Ratio	0.15 to 0.35
Sulfator Operating Temperature	1,100 to 1,600°F
Planned Duration of Coal Feed	217 hours

Table 4.1-2

Coal Analyses as Fed

	PRB
Moisture	17.7
Ash	7.0
Sulfur	0.5
C	55.6
H	4.1
N	0.8
O	14.4
Vol	34.3
Fix C	41.0
Heating Value(Btu/lb)	9621

Table 4.1-3

Sorbent Analyses

	Bucyrus Limestone From Ohio
$CaCO_3$ (wt %)	74.1
$MgCO_3$ (wt %)	17.8
Inerts (wt %)	8.1

Table 4.1-4
Operating Periods

	MZ temp deg F	Riser Temp deg F	Pres psig	Coal Feed Rate lb/hr	Air Flow lb/hr	Air/Coal	Air/Carbon	Steam Flow lb/hr	Steam/Coal
GCT2A-1	1696	1596	160	4900	12502	2.55	4.64	790	0.16
GCT2A-2	1721	1623	160	4902	12768	2.60	4.74	1046	0.21
GCT2A-3	1706	1612	160	4917	12526	2.55	4.63	1240	0.25
GCT2A-4	1694	1599	160	4768	12156	2.55	4.64	1272	0.27
GCT2A-5	1705	1656	160	3861	12060	3.12	5.68	1998	0.52
GCT2A-6	1719	1676	160	3880	12091	3.12	5.67	2000	0.52
GCT2B-1	1744	1730	160	3343	10996	3.29	5.98	875	0.26
GCT2B-2	1733	1662	160	3787	10557	2.79	5.07	705	0.19
GCT2B-3	1729	1703	160	2625	9043	3.44	6.26	710	0.27
GCT2B-4	1720	1652	160	4477	11130	2.49	4.52	841	0.19
GCT2C-1	1699	1633	180	4744	11972	2.52	4.59	786	0.17
GCT2C-2	1716	1652	180	4762	12032	2.53	4.59	783	0.16
GCT2C-3	1728	1656	180	4499	11303	2.51	4.57	779	0.17
GCT2C-4	1698	1628	180	4557	11255	2.47	4.49	776	0.17
GCT2C-5	1728	1650	180	4435	11035	2.49	4.52	748	0.17
GCT2C-6	1701	1619	180	4489	10895	2.43	4.41	764	0.17
GCT2C-7	1705	1579	180	4483	10992	2.45	4.46	765	0.17
GCT2C-8	1737	1615	180	3912	10920	2.79	5.08	1253	0.32
GCT2D-1	1708	1603	200	3731	10178	2.73	4.96	1687	0.45
GCT2D-2	1708	1603	200	3559	10218	2.87	5.22	1877	0.53
GCT2D-3	1716	1610	200	4488	11920	2.66	4.83	2196	0.49
GCT2D-4	1727	1620	200	4375	11830	2.70	4.92	2063	0.47
GCT2D-5	1727	1606	200	3692	10141	2.75	4.99	1379	0.37
GCT2D-6	1743	1621	200	3732	10473	2.81	5.10	1400	0.37
GCT2D-7	1735	1613	200	3652	10417	2.85	5.19	1375	0.38
GCT2D-8	1738	1613	200	3606	10216	2.83	5.15	1351	0.37

Table 4.1-4 (Page 2 of 2)

	MZ temp deg F	Riser Temp deg F	Pres psig	Coal Feed Rate lb/hr	Air Flow lb/hr	Air/Coal	Air/Carbon	Steam Flow lb/hr	Steam/Coal
GCT2D-9	1704	1591	200	4422	11351	2.57	4.67	745	0.17
GCT2D-10	1742	1615	200	3965	10569	2.67	4.85	756	0.19
GCT2D-11	1754	1619	200	3799	10221	2.69	4.89	753	0.20
GCT2D-12	1742	1608	200	4236	10852	2.56	4.66	742	0.18
GCT2D-13	1700	1588	200	4411	11275	2.56	4.65	750	0.17
GCT2D-14	1739	1616	200	3920	11004	2.81	5.10	739	0.19
GCT2D-15	1705	1587	200	4343	10893	2.51	4.56	742	0.17
GCT2D-16	1718	1589	200	3463	9706	2.80	5.10	738	0.21
GCT2D-17	1714	1599	200	3262	9615	2.95	5.36	735	0.23
GCT2D-18	1721	1589	200	2987	9015	3.02	5.49	727	0.24
GCT2D-19	1719	1570	200	2969	8654	2.92	5.30	737	0.25
GCT2D-20	1699	1548	200	3040	8741	2.88	5.23	746	0.25
GCT2D-21	1713	1565	200	3055	8860	2.90	5.27	752	0.25
GCT2D-22	1710	1567	200	3051	8877	2.91	5.29	752	0.25
GCT2E-1	1730	1552	220	3035	8663	2.85	5.19	688	0.23
GCT2E-2	1734	1547	220	3025	8693	2.87	5.22	672	0.22
GCT2E-3	1737	1598	220	4523	11828	2.61	4.75	988	0.22
GCT2E-4	1715	1580	220	4605	11684	2.54	4.61	984	0.21
GCT2E-5	1754	1616	220	4595	12069	2.63	4.78	990	0.22
GCT2E-6	1768	1631	220	4480	12117	2.70	4.92	976	0.22
GCT2E-7	1741	1635	220	4251	11777	2.77	5.04	984	0.23
GCT2E-8	1743	1626	220	4174	11385	2.73	4.96	996	0.24
GCT2E-9	1744	1625	220	4049	11419	2.82	5.13	1015	0.25
GCT2E-10	1745	1634	220	3998	11596	2.90	5.27	1002	0.25
GCT2E-11	1749	1627	220	4320	11800	2.73	4.97	1000	0.23
GCT2E-12	1738	1612	220	4349	11747	2.70	4.91	1013	0.23
GCT2F-1	1765	1610	240	4475	11955	2.67	4.86	470	0.11
GCT2F-2	1768	1611	240	4511	12057	2.67	4.86	471	0.10

4.2 HEAT BALANCE

To gain a better understanding of the transport reactor operations, a heat balance was performed for the reactor mixing zone and riser. Each thermocouple was taken as an independent control volume. Assumptions were made as to the amount of gas and feed solids heated within each control volume based on gas and solids velocities and orientation of nozzles and thermocouples. The actual gas analysis was used to calculate heat-release rates based on CO and CO_2 production. Heat loss to the atmosphere and heat consumption from steam-char gasification were also taken into account. Figures 4.2-1 and 4.2-2 show plots of actual and predicted temperatures for the middle mixing zone and upper riser during GCT2. The plots show a good agreement between the actual and predicted temperatures.

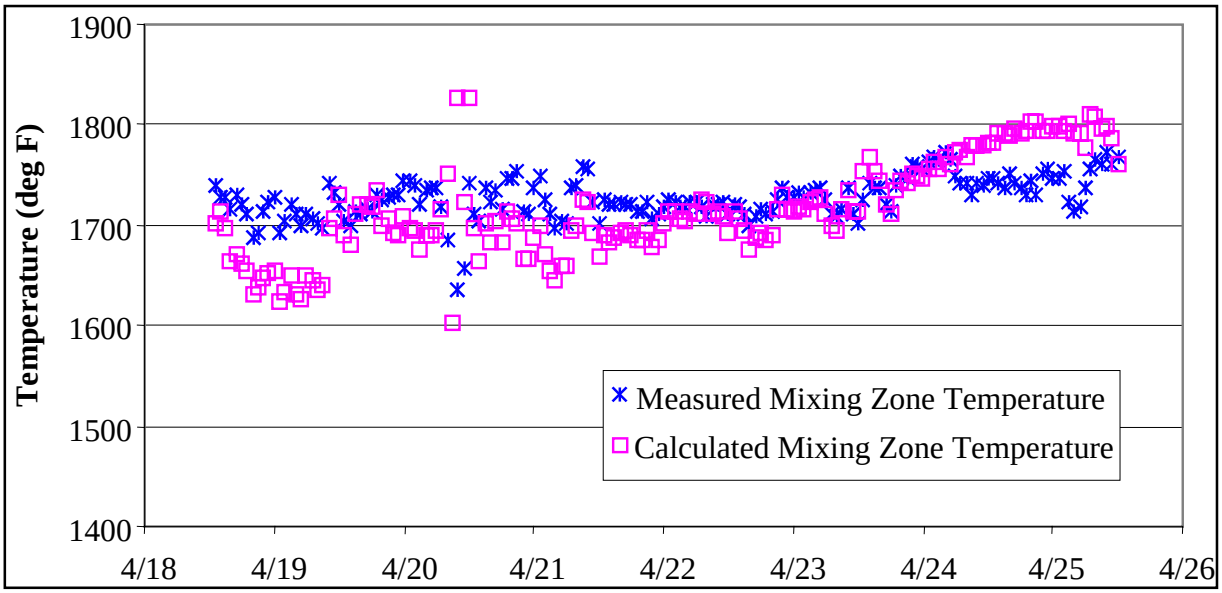

Figure 4.2-1 Mixing Zone Temperature, Actual vs. Predicted

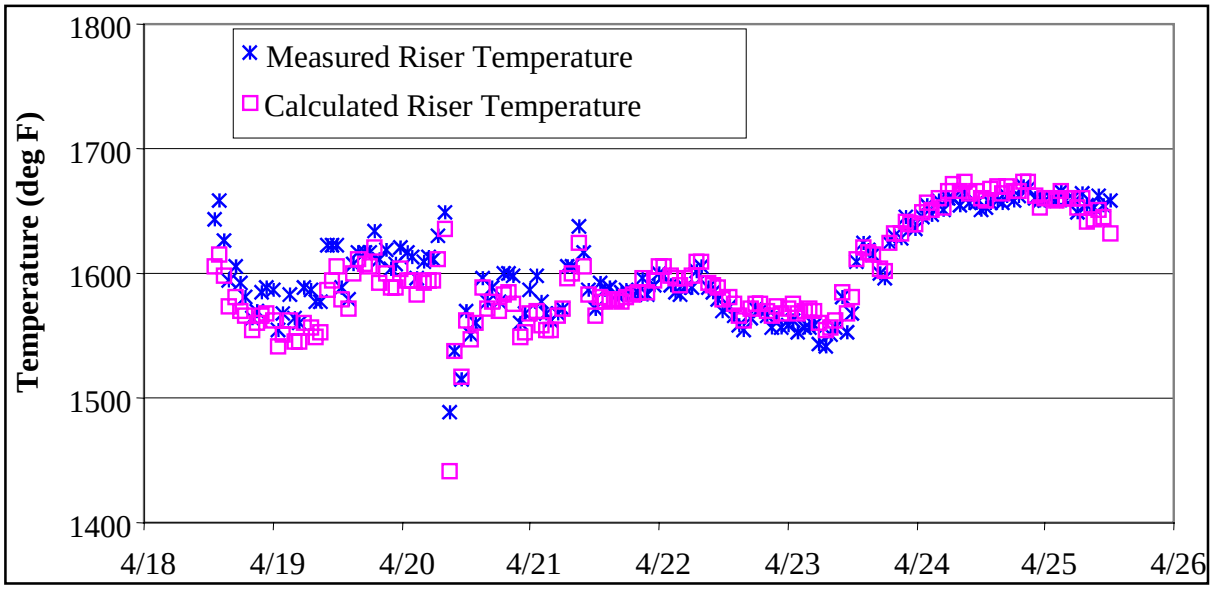

Figure 4.2-2 Riser Temperature, Actual vs. Predicted

4.3 GAS ANALYSES

During GCT2 synthesis gas analyzers were continuously monitored and results recorded by the plant information system (PI). Several in situ grab samples of synthesis gas moisture were measured during the PCD outlet loading sampling. This section will use the gas analyzer data and gas canister data to show:

- Synthesis gas heating value.
- Synthesis gas molecular weight.
- Synthesis gas compositions for CO, H_2, CO_2, H_2O, N_2, CH_4, and $C_2H_6^+$.
- Cold gas gasification efficiency.
- Hot gas gasification efficiency.

Run GCT2 began on April 13, 2000, ended on April 27, 2000, and consisted of five separate test periods. The first four periods of operation were very short, lasting from 6 to 12 hours. This section will concentrate on the long-term operation from April 18 to 25 due to the lack of steady state data during the shorter periods of operations. The only fuel used during GCT2 was a blend of several Powder River Basin coals.

Hourly averages for the mixing zone temperatures, PCD (particulate control device, FL0301) temperatures, and reactor pressures are shown on Figure 4.3-1. The reactor mixing zone temperature quickly increased to 1,750°F a few hours after startup and was maintained between 1,700 and 1,775°F for the entire run. Note the reactor upset at 08:30 on April 20 when the pressure control impulse line was inadvertently opened and closed quickly, causing the reactor pressure to cycle between 86 and 208 psig. It then took a few hours for the reactor and PCD temperatures to return to steady values. The reactor pressure was increased in several increments from 160 to 240 psig. The majority of the run was done at either 200 or 220 psig. The pressure at the end of the run (240 psig) was the highest pressure at which the reactor had been operated to date. The PCD inlet temperature had several long periods at constant temperatures. During the first several days of operation from April 18 to 20 the PCD inlet was at 925 to 975°F. After the upset at 08:30 on April 20 the PCD temperature decreased to 850°F and then slowly increased to 875°F by 12:00 on April 22. On April 23 the PCD temperature increased to 1,000°F due to the increase in both coal and air rates (see Figure 4.3-2), which of course increased the synthesis gas rate (see Figure 4.5-3). The PCD temperature was constant at just under 1,000°F from 12:00 on April 24 until the end of the test.

Hourly averages for the coal-feed rate and the air rate are shown in Figure 4.3-2. The coal-feed rate was calculated from the coal feeder speed and a correlation from the FD0210 weight cell. The air rate was obtained from FI205. The air rate steadily decreased from 13,000 to 9,000 lb per hour during the first 14 hours of operation on April 18, while the coal rate varied from 2,800 to 4,000 lb per hour. After 16:00 on April 18 the coal rate leveled out at 4,300 lb per hour. For the next several days the air rate was maintained at 10,000 to 12,000 lb per hour and the coal rate at 3,700 to 4,300 lb per hour. At 16:00 on April 21 the coal rate was decreased to 3,400 lb per hour and then at 00:00 on April 22 reduced again to 3,000 lb per hour. The coal rate was reduced because the coal milling systems could not keep up with the desired coal-feed rate due to problems with the coal milling system. The air rate followed the coal rate down to 10,000 lb per hour and then to 8,700 lb per hour. On the morning of April 23 the problems with the coal

milling had been resolved and the coal-feed rate could be increased to the maximum value of 4,300 lb per hour. The air rate was also increased to 12,000 lb per hour at the same time and both coal and air rates were maintained at these rates until the end of the run.

The plant gas analyzer system analyzed the following gases during GCT2 using the associated analyzers:

N_2	AI464B
CO	AI425, AI434B, AI453G, AI464C
CO_2	AI434C, AI464D
CH_4	AI464E
$C_2H_6^+$	AI464F
H_2	AI464G

The AI464B-G analyzers use a gas chromatograph and typically have about a 6-minute delay. The other three CO analyzers (AI425, AI434B, and AI464C) and CO_2 analyzer (AI434C) are IR which give more real time measurements. All analyzers require that the gas sample is conditioned to remove water vapor, so all the analyzers report gas compositions on a dry basis. During the run the gas analyzer conditioning system frequently plugged with tar and naphthalene, which required the analyzer technicians to clean the gas analyzer conditioning systems. There was less gas analyzer plugging in GCT2 than in GCT1, as the gas analyzer-conditioning system had been improved to handle tar.

The raw synthesis gas analyzer data was adjusted to produce the best estimate of the actual gas composition in the following four steps:

1. Choice of CO and CO_2 analyzers.
2. Correction of GC H_2 data taken before 20:00 on April 20.
3. Normalization of gas compositions (force to 100 percent total).
4. Conversion of dry compositions to wet compositions.

With four CO analyzers there is a measure of self-consistency when all or several of the four analyzers read the same value. There is also the choice of which analyzer to use when problems with other analyzers arise due to tar condensation. The raw data hourly averages for three of the four CO analyzers are given in Figure 4.3-3. The CO analyzer AI434B was not in operation from April 18 to 25 and is not shown in the plots in Figure 4.3-3. The other three CO analyzers agreed with each other very well during the first 6 days of operation, until 10:00 on April 23 when AI425 suddenly dropped in value and remained lower than the other two analyzers (AI464C and AI434B). During the last 3 days of testing, after the AI425 started disagreeing with the other two analyzers, the values from either AI464C or AI434B were used to determine the CO compositions. Carbon monoxide analyzers (AI464C and AI434B) agreed during the entire period from April 18 to 25. There were several periods when the gas analyzers were calibrated, which show up as low CO measurements. The CO compositions used in calculations were interpolated for times when the gas analyzers were being calibrated.

Data from both of the CO_2 analyzers is shown on Figure 4.3-4. There was excellent agreement between the two analyzers for the entire testing period. Note that AI434C had more calibration dips than AI464D.

During the evening of April 20 the analyzer technician noticed that the H_2 peak was overlapping another peak. Once the H_2 peak was resolved, the H_2 concentration increased to about three times its previous value (see Figure 4.3-5). Figure 4.3-5 plots the raw H_2 analyzer data (AI464G) the best estimate CO concentration data, and the ratio of H_2/CO. Before the H_2 analyzer recalibration on April 20 the H_2 concentration was from 2.0 to 2.5 percent and the H_2/CO ratio was 0.3 to 0.5. After the recalibration the H_2 concentration increased to 6 to 8 percent and the H_2/CO ratio increased to 0.8 to 1.0. Prior to the recalibration the H_2 concentration did not seem to follow the CO concentration, and after the recalibration the H_2 seemed to track the CO concentration better, especially on the morning of April 23 when they both increased together. The H_2 and CO seemed to stop tracking at 07:00 on April 25 when the CO concentration increased to 11 percent, the H_2 concentration remained at 8 percent, and the H_2/CO ratio decreased to 0.7. The change might have been caused by the decrease in steam rate on April 25 (see Figure 4.3-8).

In an attempt to estimate the H_2 concentration prior to the recalibration, the CO and H_2 concentrations were correlated using post recalibration data. The data were correlated using the analyzer H_2 data and the best estimate of the CO concentration using the data between 20:00 on April 20 (the recalibration) and 07:00 on April 25 (when the H_2 - CO trend seemed to change). The result of this calibration is shown on Figure 4.3-6. All GCT2 H_2 concentration data prior to 20:00 on April 20 were calculated from the following correlation:

$$H_2 = CO \times 0.7318 + 1.5361 \quad (1)$$

This correlation is not valid for the CO and H_2 concentrations for the last few hours of April 25.

Figure 4.3-7 shows the sum of the dry-gas compositions for GCT2 using the corrected H_2 and selected CO and CO_2 concentrations. For the first day and a half the sum of the dry-gas compositions were centered around 100 percent, indicating that H_2 correction improved the consistency of the data. For the next several hours, from 11:00 on April 19 to 08:30 on April 20, the sum of the gas compositions added up to 98 percent, indicating possibly that there was not enough H_2 correction. After the recalibration on April 20 the sum of the gas compositions increased to 100.5 percent for 2 days, until 16:00 on April 22 when it dropped to 100 percent. For the rest of the run the gas compositions remained between 100.0 and 100.5 percent, indicating very consistent gas analyzer data for this period.

All gas compositions were normalized by dividing each gas composition by the sum of the mole fractions. This forces the dry-gas compositions to add up to 100 percent. This is a minor correction for most of GCT2 when the sums of the gas compositions were already close to 100 percent. The only period of significant corrections was when the gas compositions added up to 98 percent from 11:00 on April 19 to 08:00 on April 20.

The water-vapor content of the synthesis gas was measured seven times during GCT2 while measuring the PCD outlet particulate measurements. Since the KBR transport reactor does not have a working on-line H_2O analyzer, this is the only H_2O measurement of the synthesis gas during GCT2. Water-gas shift equilibrium constants were calculated for each moisture

measurement using the wet normalized CO_2, H_2, and CO concentrations and are shown in Table 4.3-1. The water-gas shift reaction:

$$CO + H_2O \leftrightarrow H_2 + CO_2 \quad (2)$$

The water-gas shift equilibrium constant:

$$Kp = \frac{(H_2)(CO_2)}{(H_2O)(CO)} \quad (3)$$

( ) = Partial pressure, mole percent, or mole fraction.

The water-gas shift equilibrium temperatures for a given gas composition can be determined from literature thermodynamic data (see Table 4.3-1). Typically, in design, the water-gas shift equilibrium is estimated from an approach-to-equilibrium temperature. There does not appear to be any process temperature that matches the water-gas-shift equilibrium temperature, so the approach-to-equilibrium was arbitrarily determined from the riser inlet temperature (TI367). To estimate moisture content in the synthesis gas for times when the moisture content was not measured an average approach temperature of 0.0°F was used because it seemed to fit the measured data better than the average value. The measured- and calculated-H_2O concentrations and the steam rates are shown in Figure 4.3-8.

The first measured H_2O point taken on April 17 is not shown on Figure 4.3-8 because it was taken during a brief period of operation. Of the six remaining points there was a nonconforming measured H_2O concentration taken on April 19. This moisture measurement was taken during an increase in steam rate from 800 to 1,400 lb per hour, which may have upset the moisture measurements. The next four moisture measurements agreed well with the calculated moisture values. The final moisture measurement did not agree well with the calculated moisture measurement. This is probably due to the high measured CO that was not consistent with typical values for H_2 and CO_2. It is also possible that this moisture measurement was taken too close to a change in steam rate from 1,000 to 450 lb per hour.

The normalized- and corrected-for-water-vapor gas compositions for CO_2, H_2, CO, CH_4, and C_2H_6 are shown in Figure 4.3-9. The analyzer CO_2 concentrations were fairly constant at about 10 percent for the entire test except for one increase of up to nearly 12 percent on April 19 during a period when the H_2 and CO concentrations dipped down to 5 to 6 percent. This was at the same time that the gas analyzers added up to 98 percent (prior to the system upset) (see Figure 4.3-7).

The H_2 and CO concentrations tracked each other very closely except for the last several hours of operation on April 25 when the CO concentration rose to about 2 percent above the H_2 concentration. The H_2 and CO concentrations started the run between 6 and 8 percent on April 18 and then both seemed to level off at 7 percent on the morning of April 19. When the CO_2 increased on April 19 both the CO and H_2 decreased to 5 percent and then rose to 6 percent until the upset at 08:30 on April 20. The upset and resulting changes in operation raised the CO and H_2 up to 7 to 8 percent for about 24 hours. Note that the recalibration of the H_2 analyzer at

20:00 on April 20 is not apparent from the H_2 plot. In the morning of April 22 both the H_2 and CO decreased to 5 to 6 percent and remained in that range for several days until April 23 when both concentrations increased up to 7 to 8 percent due to an increase in coal and air rates. The H_2 remained constant at 7 percent until the end of the run. The CO remained constant at 8 percent until 07:00 on April 25 when the pressure was increased to 240 psig, the steam rate was decreased, and the CO concentration increased to 10 percent.

The CH_4 concentrations were very constant during the entire test at from 1.5 to 2.0 percent. There was a slight dip in the CH_4 before the upset and then the value increased back to the steady trend after the upset. The $C_2H_6^+$ gas analyzer data was consistently very low at about 0.25 to 0.5 percent for the entire run.

The gas molecular weight and N_2 concentration plots are shown in Figure 4.3-10. The analyzer N_2 concentrations were fairly constant at between 60 and 70 percent for the entire test. The gas molecular weight values are from 26.5 to 27.2 during the test and inversely followed the H_2 concentrations in that as the H_2 concentrations increased the molecular weight decreased due to the low molecular weight of H_2.

The FI465 transmitter molecular weight was not changed from the combustion value of 30 lb/mole, so a correction factor was developed using a thermal oxidizer oxygen balance. The correction was to multiply the measured FI465 reading by 1.03, which increased the flow rate to produce a better thermal oxidizer oxygen balance. This is described in Section 4.5, Mass Balances (see Figure 4.5-2).

The PSDF transport reactor adds more N_2 per pound to synthesis gas than a commercial reactor because of the additional PSDF sampling purges, additional PSDF instrument purges, and the need to aerate the lower portion of the reactor. Instrument purges would be proportionally smaller in a commercial design due to the scale factor (instruments stay the same size as plant size increases). Any additional N_2 added to the riser also requires additional fuel to bring the additional N_2 up to operating temperatures. This additional fuel then requires additional air, which then adds more N_2 from air to the reactor and further dilutes the synthesis gas. In a commercial reactor aeration N_2 would only be used for startup. To determine a commercial synthesis LHV, the following gas components are deleted from the raw synthesis gas:

- Nitrogen that is added through FI609.
- Nitrogen that is added with the air required for burning coal required to heat FI609 nitrogen to reactor process temperature.
- Carbon dioxide from burning the coal required for heating FI609 nitrogen.
- Water vapor from burning the coal required for heating FI609 nitrogen.

A demonstration reactor also has a much larger heat loss per pound of synthesis gas produced than a commercial reactor. This additional heat loss requires additional coal to heat up the reactor to process temperatures. The heat loss of the transport reactor was about 1.5 million Btu/hr, which was estimated from a PSDF transport reactor combustion test. To compare the LHV from different sizes of transport reactors, an adiabatic LHV is calculated that assumes zero heat loss. Naturally, no reactor, no matter how large, will have zero heat loss. The amount of coal that must be burned to balance the transport reactor heat loss and its required combustion

air was calculated. To determine the adiabatic LHV, the following were subtracted from the N_2 corrected flue gas:

- Air nitrogen added to burn the coal required for the reactor heat loss.
- Carbon dioxide from burning the coal required for the reactor heat loss.
- Water vapor from burning the coal required for the reactor heat loss.

The flow indicator FI609 that reports the medium pressure N_2 was not in operation during GCT2. The N_2 added to the reactor was determined from a nitrogen balance on the system, since the air rate, synthesis gas rate, and synthesis gas nitrogen are known. The calculated N_2 rate is shown in the plot in Figure 4.5-3 in Section 4.5, Mass Balance.

The lower gas heating (LHV) value was calculated from the measured (raw) gas compositions, nitrogen corrected gas compositions, and adiabatic gas compositions using the formula:

$$\mathrm{LHV(Btu/SCF)} = \left\{ \begin{matrix} 275\times(\mathrm{H_2\%}) + 322\times(\mathrm{CO\%}) + \\ 913\times(\mathrm{CH_4\%}) + 1641\times(\mathrm{C_2H_6^+\%}) \end{matrix} \right\} /100 \qquad (4)$$

The raw synthesis gas LHV, the N_2-corrected LHV, and the adiabatic LHV are plotted in Figure 4.3-11. The raw gas LHV was usually between 50 and 70 Btu/SCF and increased to nearly 80 Btu/SCF during the last few hours of operation. After the upset on April 20 the N_2-corrected LHV was between 90 and 120 Btu/SCF and the adiabatic LHV was between 100 and 130 Btu/SCF. Note the intermittent spikes in both the N_2-corrected and adiabatic LHV. This was caused by short spikes in the C_2^+ concentration, whose importance is amplified when corrections are made in the gas composition by reducing N_2, CO_2, and H_2O compositions. The hourly averages of these short spikes can be seen in Figure 4.3-9, but they are not too clear due to the low range of the C_2^+ concentrations. These spikes could be short bursts of hydrocarbons that are either produced in the reactor at the time of analysis or have collected in the sampling system and then suddenly blow into the C_2^+ analyzer.

The N_2 correction adds about 40 Btu/SCF to the raw LHV and the adiabatic correction adds about 10 Btu/SCF to the N_2-corrected LHV. The corrected LHV was from 80 to 121 Btu/SCF during the first day of operation on April 18. Early on April 19 the corrected LHV leveled off at 110 Btu/SCF, then dropped to 90 Btu/SCF at the middle of the day where it stayed until the system upset at 08:30 on April 20. After the April 20 upset the corrected LHV increased to around 115 Btu/SCF where it stayed in the 100 to 120 Btu/SCF range until 24:00 on April 21. The LHV then steadily decreased to 90 Btu/SCF at 12:00 on April 24 where it slowly increased to 100 Btu/SCF. On April 23 the LHV increased to 115 Btu/SCF at 12:00 hours (when the coal and air rates increased), then decreased back to 100 Btu/SCF by 00:00 on April 24. The slow decrease in LHV continued until 12:00 on April 24 when the LHV leveled off at 90 to 100 Btu/SCF. The LHV then increased to 115 Btu/SCF for the last few hours of testing when the steam rate was lowered to 800 lb per hour and the reactor pressure increased to 240 psig.

The gasification efficiency is defined as the percent of the coal heating value recovered in the synthesis gas. The synthesis gas has both latent heat and sensible heat as it exits the transport reactor cyclone (CY0201). The cold gas gasification efficiency is based on the latent heat of the

synthesis gas and the hot gas gasification efficiency is based on the sum of the synthesis gas latent and sensible heats. The N_2 and adiabatic corrections to the synthesis gas compositions both reduce the N_2, CO_2, and H_2O content of the synthesis gas, thus increasing the LHV. Since the total synthesis gas rate also decreases, the total latent heat of the synthesis gas does not change much as the two gas composition corrections are made. The sensible heat does decrease with each correction because the total gas rate decreases. The major change with the two corrections is that the coal rate decreases. The N_2 correction decreases the coal rate by the amount of coal required to:

- Heat the FI609 nitrogen.
- Heat the coal required to heat up the FI609 nitrogen.
- Heat the air required to burn the coal required to heat the FI609 nitrogen.

The adiabatic correction includes (1) the amount of coal rate decrease for the N_2 correction and (2) any further decreases in the coal rate, by the amount of coal required to:

- Balance the reactor heat loss.
- Heat the additional coal required to balance the reactor heat loss.
- Heat the additional air required to burn the coal required to balance the reactor heat loss.

The cold gas gasification efficiencies for the raw synthesis gas, the N_2-corrected synthesis gas, and the adiabatic synthesis gas are shown in Figure 4.3-12. The N_2 correction adds about 10 percent to the raw cold gas efficiency and the adiabatic correction adds about 5 percent to the N_2-corrected cold gas efficiency. The raw cold gas gasification efficiencies were from 40 to 60 percent with most of the run at around 50 percent. The N_2-corrected cold gas gasification efficiency was between 55 and 65 percent for the last 5 days of GCT2. The adiabatic-cold gas gasification efficiency was between 60 and 70 percent for the last 5 days of GCT2. Again, there are short spikes in the N_2-corrected and adiabatic cold gas gasification efficiencies due to the spikes in C_2^+ measurements.

The N_2-corrected cold gas gasification efficiency was from 58 to 75 percent during the first day of operation on April 18. Early on April 19 the corrected LHV leveled off at 58 percent, dropped to 50 percent in the middle of the day, then increased to 50 percent until the system upset at 08:30 on April 20. After the April 20 upset the corrected-cold gas gasification efficiency increased to around 60 percent. For most of the run the corrected cold gas efficiency stayed in the 55 to 65 percent range. The large increase in coal rate on April 23 increased the N_2-corrected and the adiabatic cold gas gasification efficiencies by 5 percent, while the raw cold gas gasification efficiency increased from 50 to 60 percent. All the cold gas gasification efficiencies increased for the last few hours of testing when the steam rate was lowered to 800 lb per hour and the reactor pressure increased to 240 psig.

The hot gas-gasification efficiencies for the raw synthesis gas, the N_2-corrected synthesis gas, and the adiabatic synthesis gas are shown in Figure 4.3-13. The N_2 correction subtracts about 1.0 percent from the raw hot gas efficiency and the adiabatic correction adds about 3 percent to the N_2-corrected hot gas efficiency. This is due to the compensating effects of higher synthesis gas heating value and lower synthesis flow rate. All three hot gas-gasification efficiencies are essentially the same. The hot gas-gasification efficiencies were from 70 to 85

percent with most of the run at around 80 percent. During the first day of operation (April 18) there were a few hours of above 100-percent hot-gas-gasification efficiencies. This was likely due to changes in the char inventory, when during this period the reactor gave poor carbon and hydrogen balances (see Figures 4.5-7 and -8). Again, there are short spikes in the adiabatic cold gas gasification efficiencies due to the spikes in C_2^+ measurements.

Two main sources of losses in efficiency are the heat loss and the latent heat of the PCD solids. The reactor heat loss of 1.5 MBtu/hr is about 3.5 percent of the feed coal energy, while the latent heat of the PCD solids is about 9 percent of the feed coal energy. The heat loss percentage will decrease as the reactor size is increased. While the transport reactor does not recover the latent heat of the PCD solids, this latent heat could be recovered in a combustor. The latent heat of the PCD solids can be decreased by decreasing both the PCD solids carbon content (heating value) and the PCD solids rate. The improvements to the transport reactor disengager, cyclone, and cyclone dipleg currently underway should decrease the PCD solids rate and thus increase the transport reactor efficiency and carbon conversion.

Since neither the transport reactor H_2S analyzer nor the thermal oxidizer SO_2 analyzer were working during GCT2, the H_2S concentration and the sulfur emissions in the transport reactor were not directly measured. The sulfur emissions can be calculated from the coal rate, coal sulfur, PCD solids sulfur, and PCD solids rate. The calculated sulfur emissions data are shown in Figure 4.3-14. Coal sulfur values are provided in Section 4.4, Solids Analyses, in Figure 4.4-1. The PCD solids rate is provided in Section 4.5, Mass Balances, in Figure 4.5-4. The maximum sulfur emissions possible are also shown in Figure 4.3-14. The maximum sulfur emissions were calculated from the coal-feed rate, coal-sulfur level, and the synthesis gas rate assuming that all of the coal sulfur left the system with the synthesis gas (no sulfur removal). A comparison of the sulfur emissions calculated from the solids data and the maximum sulfur emissions from the coal sulfur indicate very little sulfur removal for most of GCT2. This low removal is inconsistent with results from GCT1 (40-percent sulfur removal with PRB coal) and KRW reactor results (40- to 50-percent sulfur removals with 0.6-percent sulfur coal).

The main sulfur species in coal gasification are considered to be H_2S and carbon oxysulfide (COS). There should also be only a minor amount of carbon disulfide (CS_2). KRW data indicates that the majority of the gaseous sulfur is present as H_2S, with the balance COS. KRW typically measured concentrations of 100 to 200 ppm COS for 0.6- to 1.0-percent sulfur fuels. The PSDF plans to get the H_2S analyzer operational and take COS grab samples for the next gasification run to determine the gasification sulfur emissions of the transport reactor.

Table 4.3-1

Water Gas Shift Equilibrium

Date	H_2O Meas. (%)	H_2 Wet (%)	CO Wet (%)	CO_2 Wet (%)	Kp	Equilibrium Temperature (°F)	Riser Temperature (°F)	Approach Temperature (°F)
4/17/00	10.3	6.5	7.5	9.7	0.82	1,600	1,648	-48
4/19/00	14.7	5.5	5.7	10.1	0.66	1,736	1,607	130
4/20/00	8.7	6.6	7.5	10.1	1.01	1,477	1,552	-75
4/21/00	9.8	6.0	6.9	9.6	0.86	1,568	1,520	47
4/22/00	9.0	5.4	5.2	9.7	1.13	1,421	1,426	-5
4/24/00	10.0	6.9	6.4	9.8	1.06	1,456	1,459	-3
4/25/00	9.2	6.8	9.5	9.3	0.73	1,671	1,461	210

Notes:

1. H_2O measured during PCD outlet particulate-loading sampling.
2. H_2, CO, and CO_2 are hourly averages measured by plant analyzers.

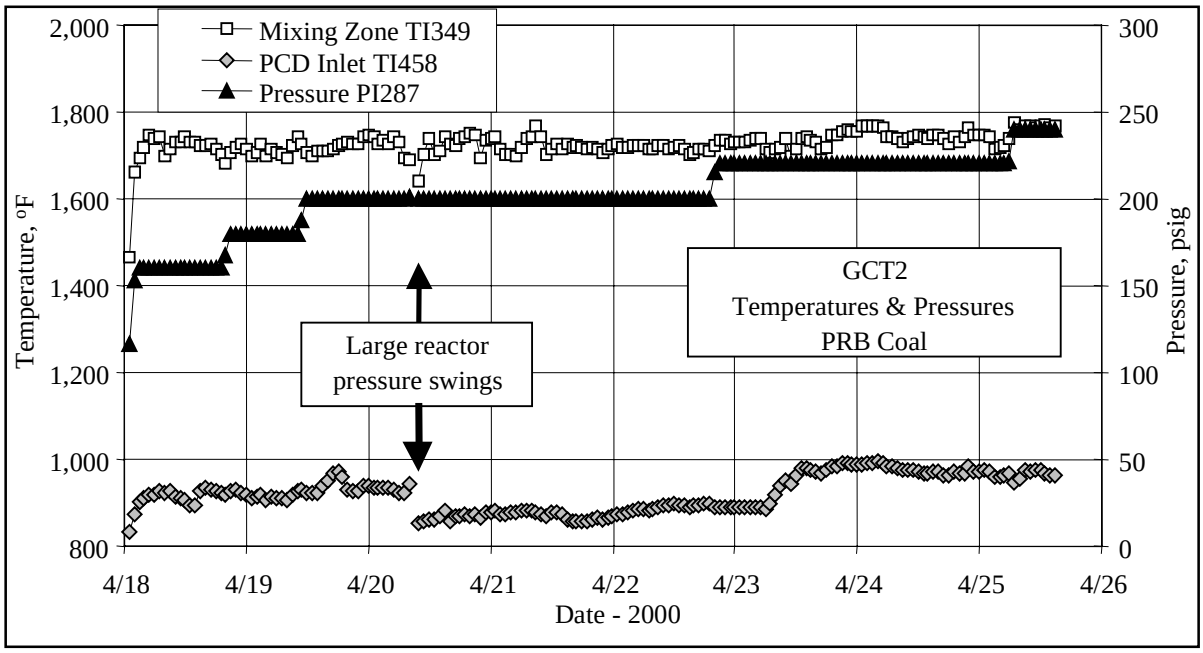

Figure 4.3-1 Temperature and Pressures

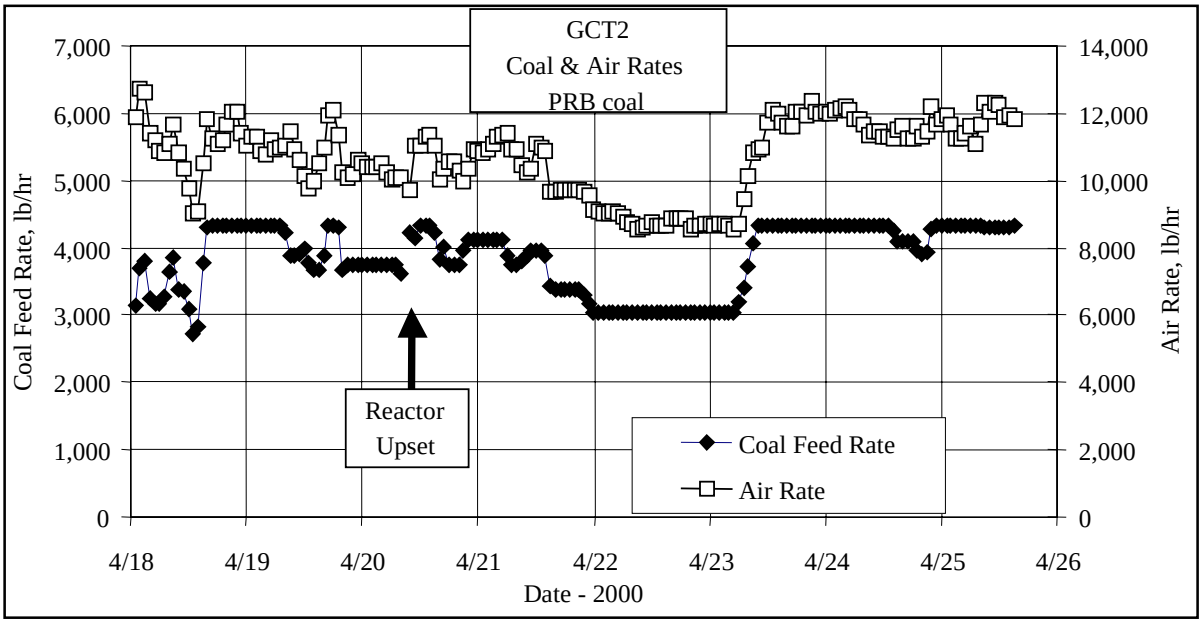

Figure 4.3-2 Air and Coal Rates

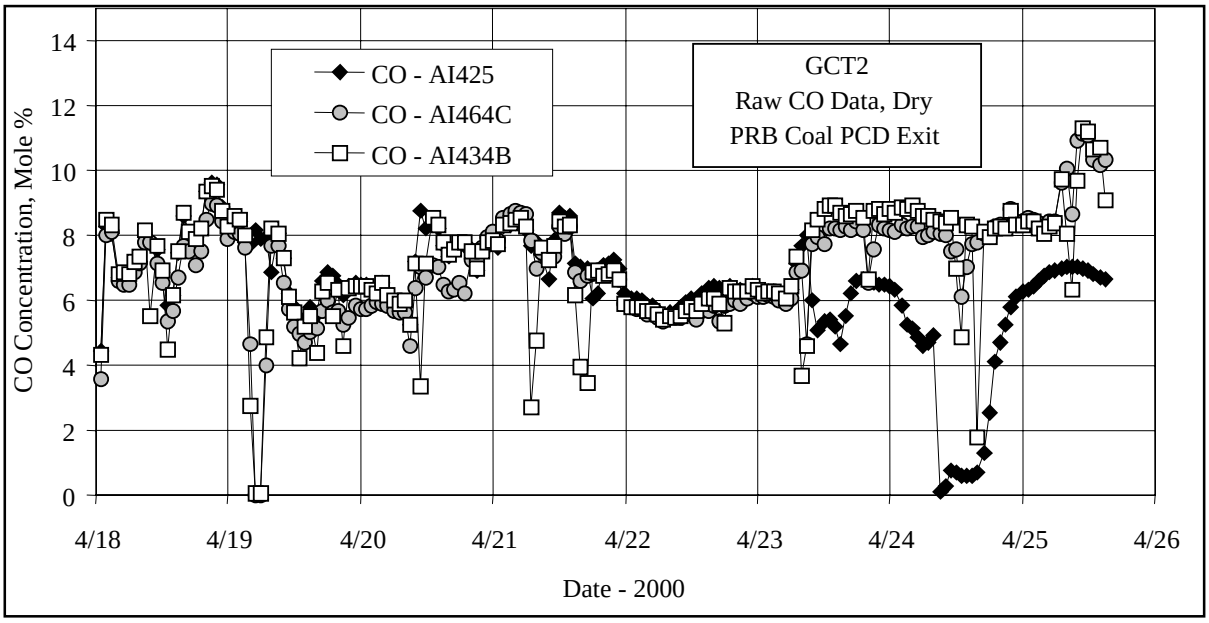

Figure 4.3-3 Dry, Raw Carbon Monoxide Gas Analyzer Data

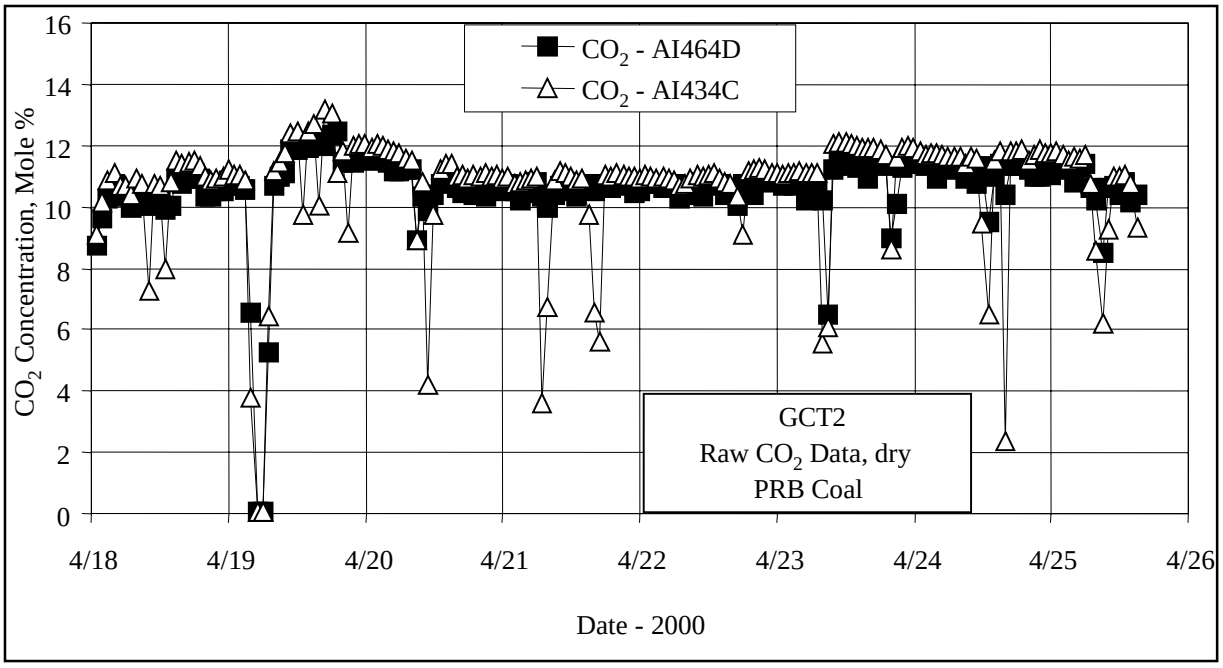

Figure 4.3-4 Dry, Raw Carbon Dioxide Gas Analyzer Data

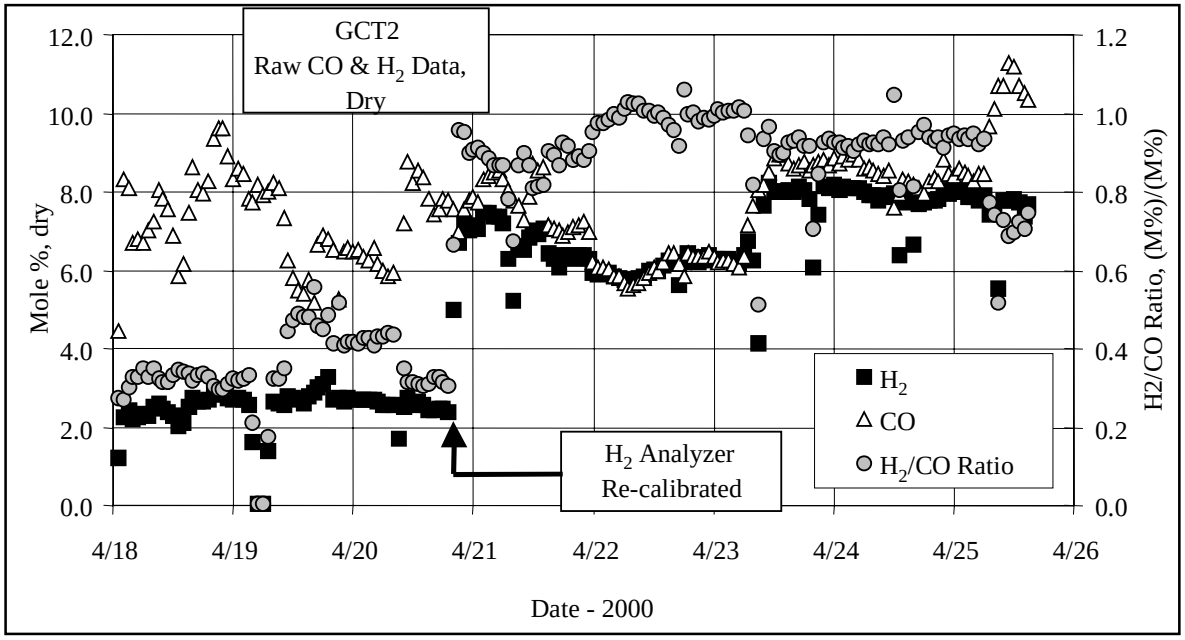

Figure 4.3-5 Hydrogen and Carbon Monoxide Concentrations

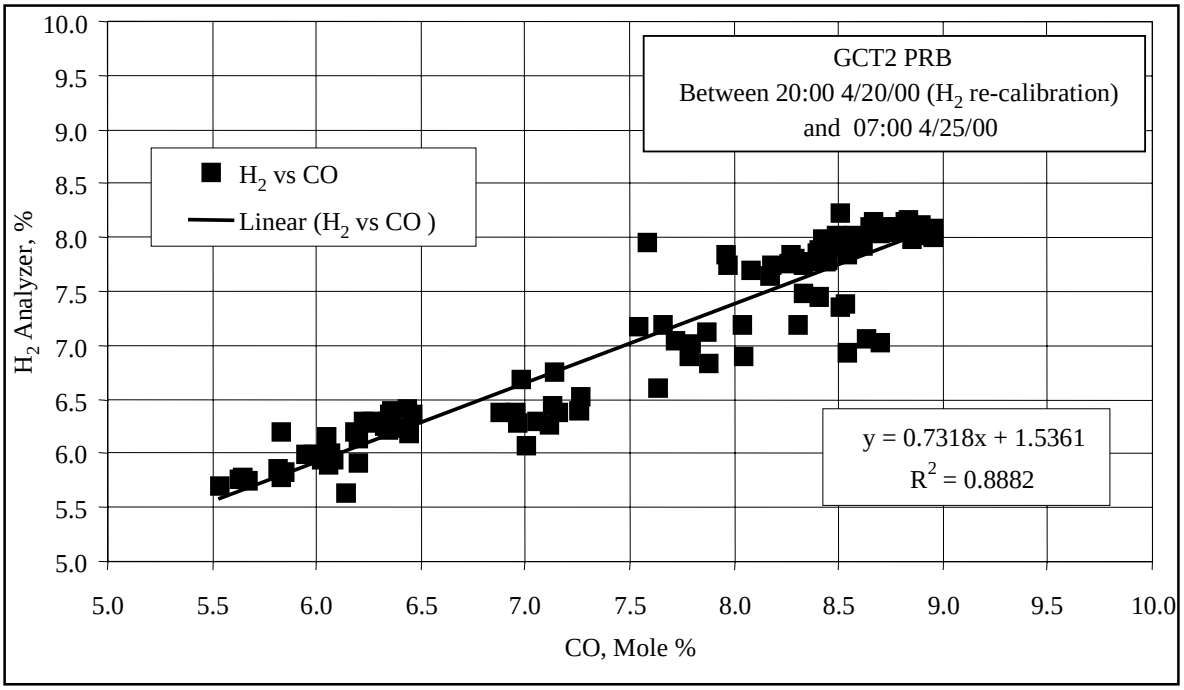

Figure 4.3-6 Hydrogen-Carbon Monoxide Correlation

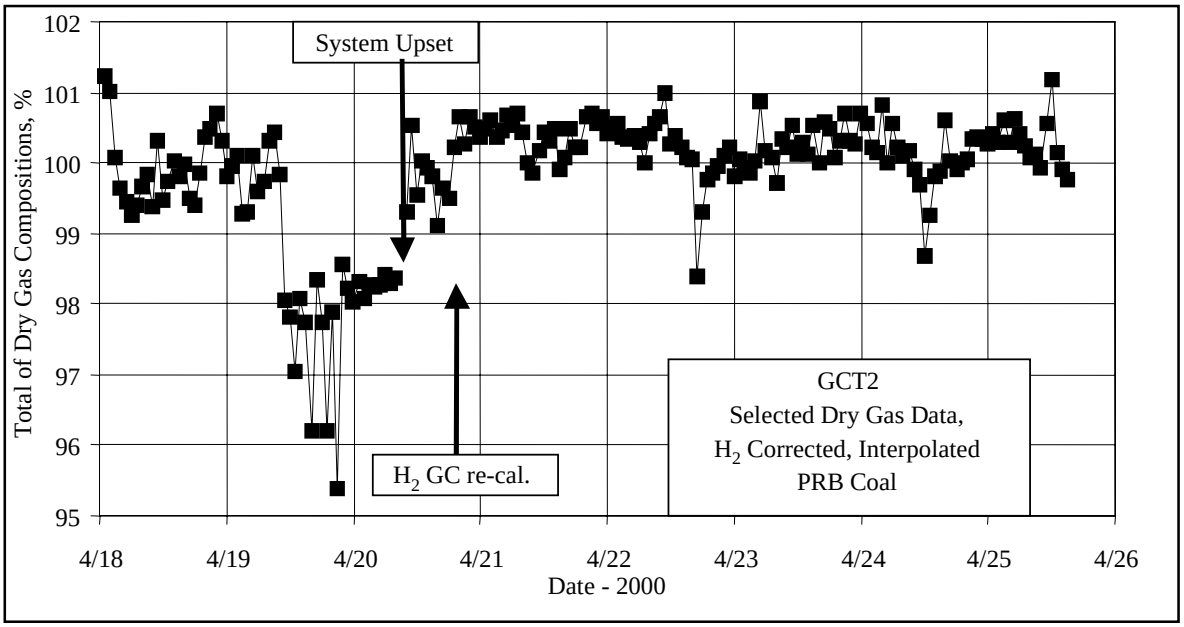

Figure 4.3-7 Sum of Dry Gas Compositions After H_2 Correction

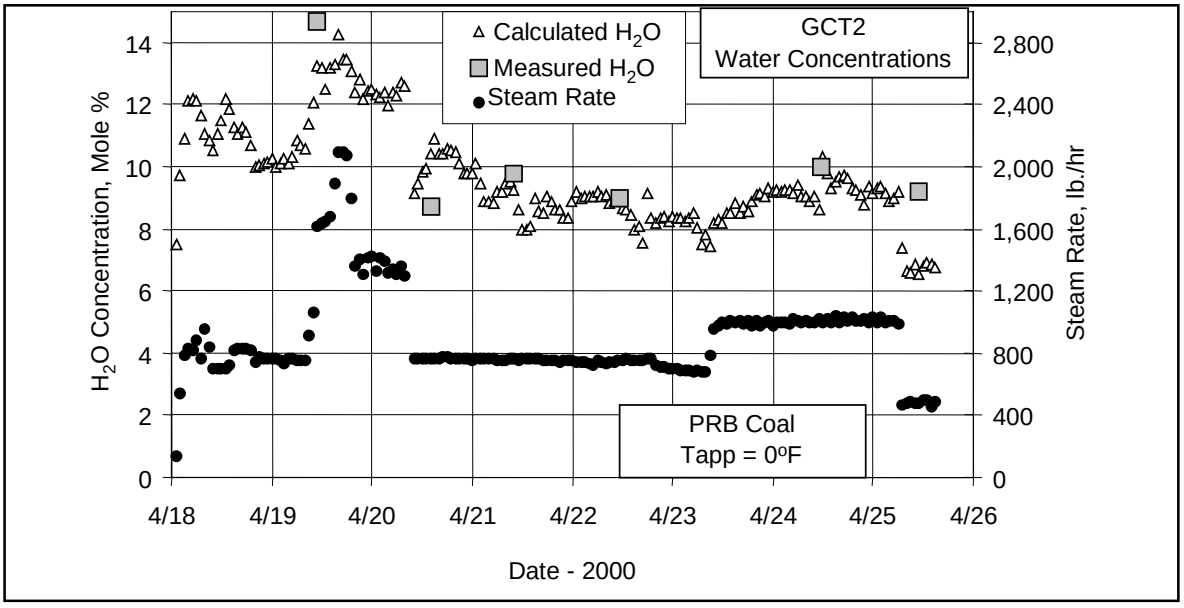

Figure 4.3-8 Measured and Calculated Water Vapor Concentrations and Steam Rate

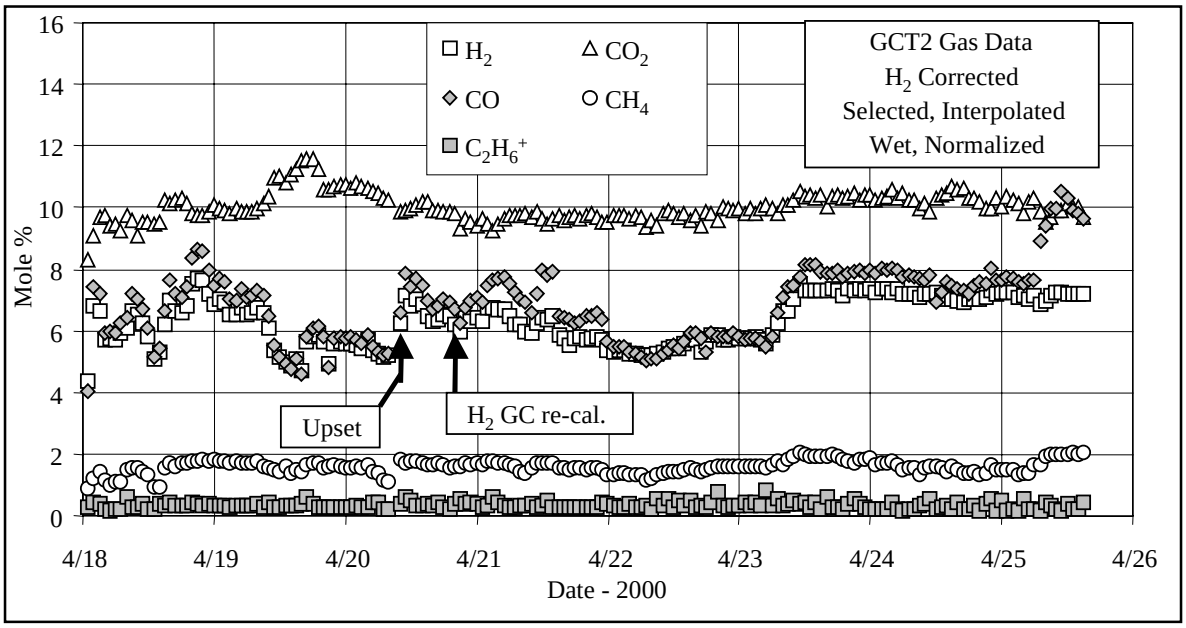

Figure 4.3-9 Synthesis Gas Compositions

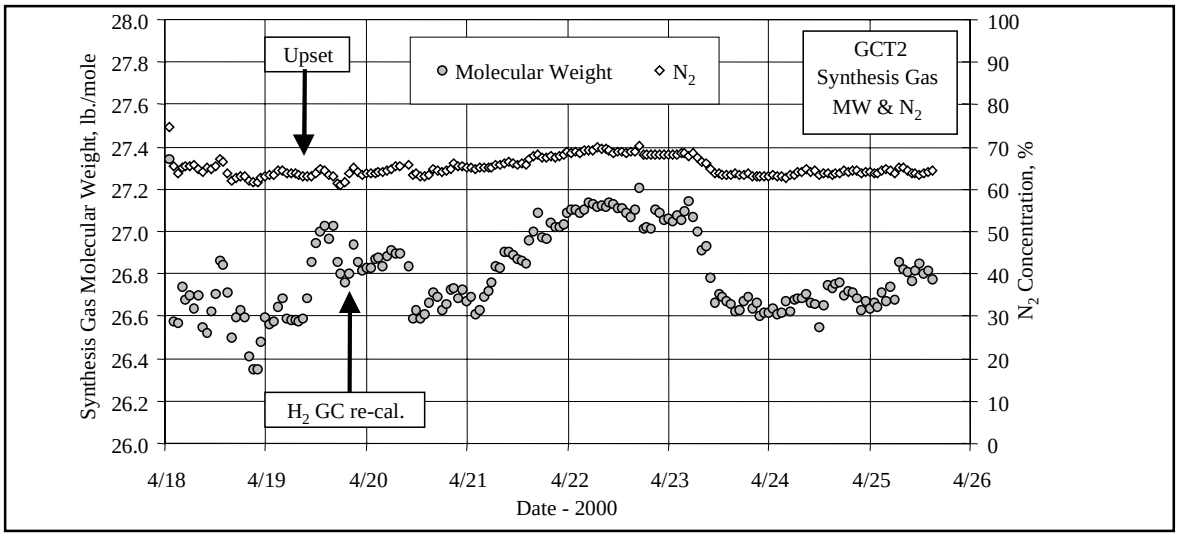

Figure 4.3-10 Synthesis Gas Molecular Weights and Nitrogen Composition

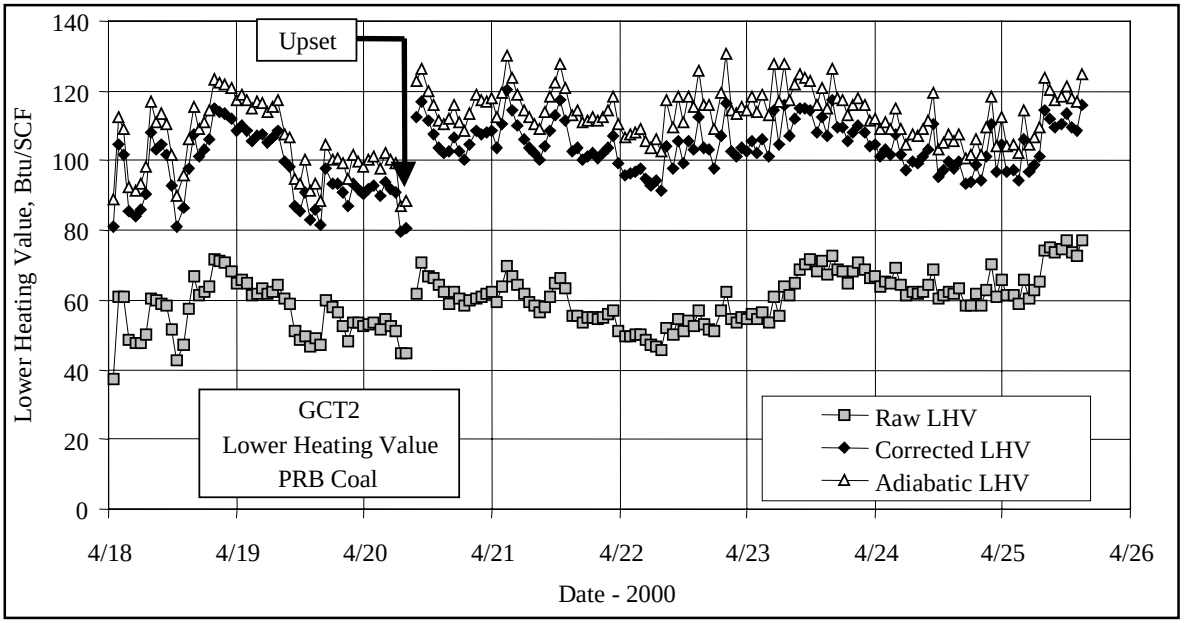

Figure 4.3-11 Measured Gas LHV and Corrected Gas LHV

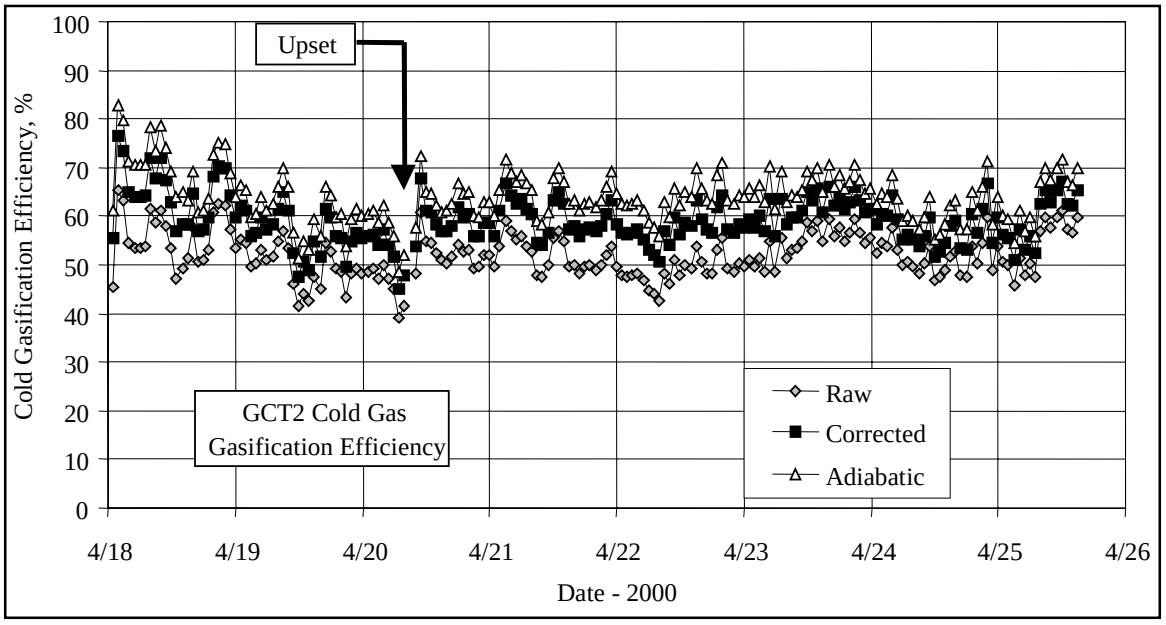

Figure 4.3-12 Raw, Corrected, and Adiabatic Cold Gas Gasification Efficiencies

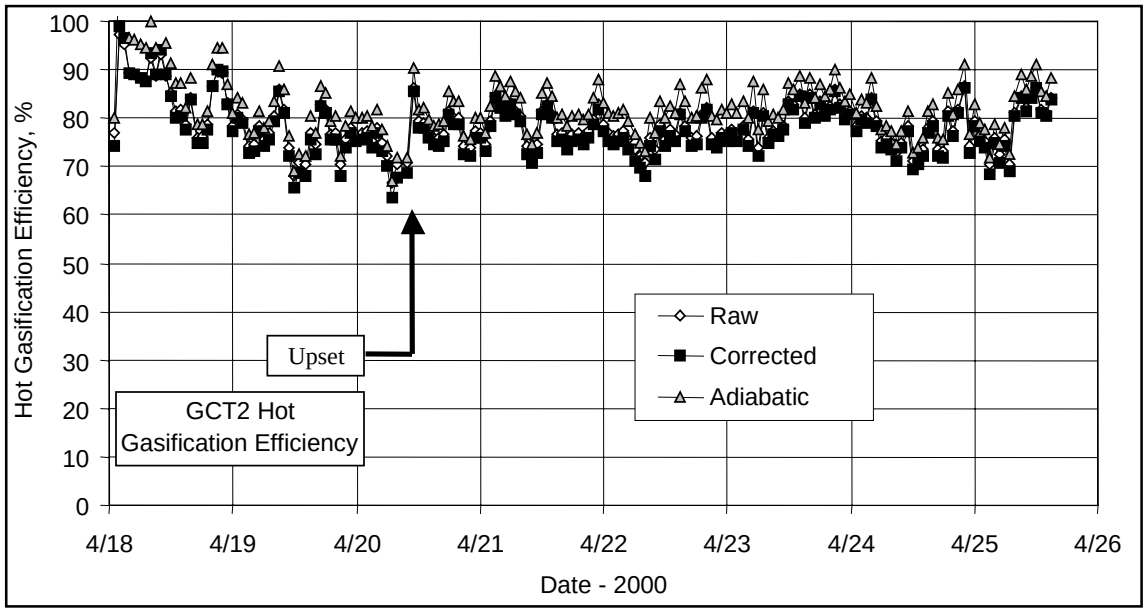

Figure 4.3-13 Raw, Corrected, and Adiabatic Hot Gas Gasification Efficiencies

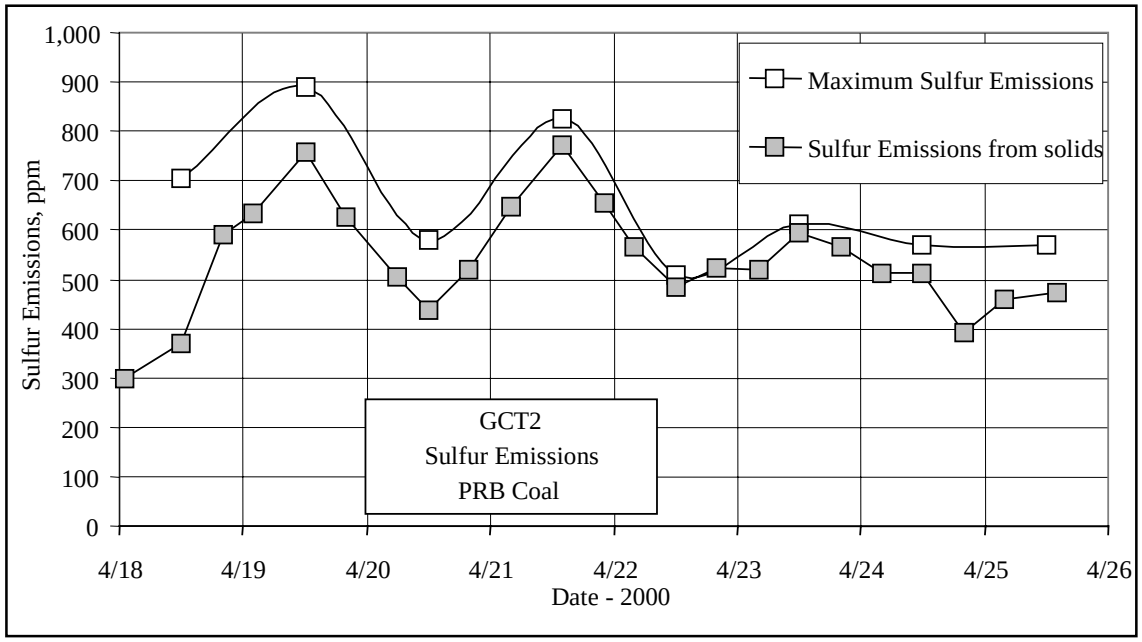

Figure 4.3-14 Synthesis Gas Sulfur Emissions

4.4 SOLIDS ANALYSES

During GCT2 solids were collected from the fuel feed system (FD0210), the sorbent feed system (FD0220), the standpipe spent solids transport system (FD0510), and the PCD fine solids transport system (FD0520). These solids were analyzed for chemical composition and particle size. This section will use the chemical analysis data to show:

- Chemical composition changes.
- Sulfur removal.
- Particle size and bulk density changes.

Figure 4.4-1 shows the fuel sulfur and ash as sampled from the fuel feed system during GCT2. The Powder River Basin (PRB) coal had from 0.35 to 0.6 percent sulfur and from 6-to 7-percent ash. The sulfur and the ash decreased during the test. The PRB sulfur level was higher in GCT2 than in GCT1.

The coal carbon and hydrogen contents as sampled from FD0210 are shown in Figure 4.4-2. The carbon was between 53 and 58 weight percent and decreased during the run. The hydrogen content was steady at about 4.0 to 4.3 weight percent until the final sample on April 25, where it dropped off to 3.25 percent. The hydrogen is reported as received and does not include the hydrogen in the coal moisture.

The coal oxygen and moisture contents as sampled from FD0210 are shown in Figure 4.4-3. The coal oxygen was between 11 and 17 weight percent and was slightly increasing during the run. The oxygen is reported as received and does not include the oxygen in the coal moisture. Oxygen is also not directly measured but is the value required to make the elemental analysis add up to 100 percent. Therefore it is the least accurate of the elemental analyses. The coal moisture was between 17 and 20 weight percent for GCT2 and seemed to be slightly increasing during GCT2.

The Sauter mean diameter (SMD) and mass mean diameter (D_{50}) particle size of ground coal sampled from the feed to silo SI0112 during GCT2 are shown in Figure 4.4-4. These samples were analyzed for particle size during coal grinding. If the particle size was found to be out of the target range grinding operational changes were made immediately and samples taken again and analyzed. Most of the ground coal samples were between 300 and 400 µm SMD and D_{50}.

The SMD and D_{50} particle size of the coal feed to the transport reactor in GCT2 are shown in Figure 4.4-5. The general trend was of decreasing SMD and D_{50} during the test. The coal SMD diameter started the test at 500 µm then decreased to 400 µm by the end of GCT2. The D_{50} started the test at 400 µm and ended the test at around 300. There were two dips in the SMD down to 300 µm on April 20 and April 23, which might indicate segregated fines in the coal feed.

A comparison of the average mass mean particle sizes measured during GCT2 for the two milling systems, SI0111 and SI0112, with the D_{50} measured at the coal feed system FD0210 is shown in Table 4.4-1. The standard deviation for each sample is also shown to give an estimate

of the variation in D_{50} during the coal grinding and testing. For most of GCT2, SI0112 was operated rather than SI0111, so the D_{50} for SI0112 should be more consistent than SI0111 when compared with FDO210. The D_{50} for SI0112 was 358 µm and the D_{50} for FD0210 was 354 µm, which is excellent agreement. The coal ground by SI0111 was finer at 272 µm than the coal ground by SI0112. The GCT1 FD0210 D_{50} were slightly finer than those for GCT2 by about 26 µm, which was about one-half of the standard deviation of both sample sets.

FD0220 was used during GCT2 to feed Ohio Bucyrus limestone and Wisconsin sand into the transport reactor. Analyses for the last 5 days of operation are shown in Figure 4.4-6. The first four samples are remarkably consistent at 77-weight percent $CaCO_3$, 18-weight percent $MgCO_3$, and 5-weight percent inerts. In the last sample on April 25 the inerts rose to 10 percent, the $CaCO_3$ dropped to 65 percent, and the $MgCO_3$ dropped to 16 percent.

The SMD and D_{50} of the solids sampled from the sorbent feeder FD0220 are shown in Figure 4.4-7. There was a wide variation in the SMD and D_{50} for the FD0220 solids. It was expected that the SMD diameter would be around 20 µm. The SMD began the run at 20 µm, rose to 130 on April 22, then slowly fell back to 20 on April 25. There would appear to be a large variation of the limestone grind during GCT2, but this could be due to 100-µm sand mixed with the sorbent. The D_{50} tracks the SMD, starting the run at 10 µm and peaking at 65.

FD0510 was not run much during GCT2 and there were very few FD0510 samples taken. Since the reported solids analyses might reflect operation several days before actually sampled the FD0510 solids were not analyzed.

Figure 4.4-8 shows the plot of the SMD, D_{50}, and bulk density for the PCD solids sampled from FD0520. The SMD was fairly constant at 10 to 15 µm from April 18 to 22. On April 22, in the early morning, the SMD went up to above 20 µm and then decreased to about 10. This was the same time that the FD0220 solids increased in size, then decreased in size. From April 23 to the end of GCT2 the SMD was about 15 µm. The D_{50} tracked the SMD, starting the test at about 20 µm, peaking at 34 on April 23, then leveling off at 20 to 25.

The GCT2 average D_{50} PCD solids as sampled from FD0520 are shown in Table 4.4-1. The GCT2 average D_{50} was 21.5 µm, which was slightly finer than the GCT1 D_{50} at 27.7 µm. The GCT1 D_{50} standard deviation was higher than the GCT2 D_{50} standard deviation due to the multiple fuels (PRB, Illinois No. 6, and Alabama bituminous) processed in GCT1 as opposed to only PRB being fired in GCT2. The size reduction of the coal feed to PCD solids was about 18:1.

The bulk density varied between 18 and 30 lb/ft^3 for the entire run with a few outliers. The bulk density started the run at 20 lb/ft^3, then increased to 24 lb/ft^3 at 12:00 April 20 where it stayed for about 24 hours. At 12:00 on April 21 the bulk density increased to 27 lb/ft^3 where it stayed until late on April 23. After April 23 the bulk density varied between 22 and 28 lb/ft^3 for the rest of the run.

The average bulk density of the PCD solids sampled from FD0520 is shown in Table 4.4-2 as compared with both the GCT1 PCD solids bulk density and the coal-feed bulk density. The bulk density of the GCT2 PCD solids was slightly less than the bulk density of the GCT1 PCD

solids but almost within the standard deviation. The bulk density of both runs PCD solids was about one-half of the feed-coal bulk densities.

The solid compounds produced by the transport reactor were determined using the solids analysis and the following assumptions.

1. All carbon dioxide measured came from $CaCO_3$, hence moles CO_2 = moles $CaCO_3$.
2. All sulfide sulfur measured came from CaS.
3. All sulfate sulfur measured came from $CaSO_4$.
4. All calcium not taken by CaS, $CaSO_4$, and $CaCO_3$ came from CaO.
5. All magnesium came from MgO.
6. Total carbon is measured as the sum of organic and inorganic (CO_2) carbon; the organic carbon is the total carbon minus the CO_2 (inorganic) carbon).
7. Inerts are the sum of the Al_2O_3, Fe_2O_3, P_2O_5, K_2O, SiO_3, Na_2O, and TiO_2 contents.

Figure 4.4-9 shows the organic carbon (total carbon minus CO_2 carbon) and the inerts (ash containing no calcium, magnesium, or sulfur compounds) for the PCD solids sampled from FD0520. Since FD0520 ran continuously during GCT2, solid samples were taken often with a goal of one sample every 2 hours. About half of the GCT2 PCD solids that were sampled were analyzed.

The PCD solids organic carbon content started out at about 50 percent, and was fairly constant for the first 4 days of operation at between 40 and 50 percent. The PCD solids carbon content then decreased from 50 to nearly 30 percent from April 23 to April 25. Lower carbon content will generally result in higher carbon conversions. The FD0520 PCD solids carbon contents are consistent with the in situ solids carbon content reported in Table 3.4-2. The in situ solids were sampled upstream of the PCD. The inerts were fairly constant for the entire run at between 22 and 32 percent, with a few nonconforming points. The first nonconforming point on April 20 might have been caused by the April 20 sand addition. Constant inert PCD solids compositions indicate that the coal rate, the PCD solids rate, and the reactor inerts inventory were fairly constant during GCT2.

Figure 4.4-10 provides the amounts of $CaCO_3$, CaS, CaO, and $CaSO_4$ in the PCD solids as sampled from FD0520. The CaO started the run at 5 weight percent and then rose to 25 to 30 weight percent by the end of the run. The $CaCO_3$ started the run at 5 percent, then increased to 14 percent at 12:00 on April 19, and seemed to level off at from 8 to 14 percent. On April 21 the $CaCO_3$ dropped down to 3 to 5 percent (except for one nonconforming point) until April 24 when it decreased to less than 3 percent. The CaO and $CaCO_3$ values indicate that the calcium was nearly entirely calcined for the last 4 days of GCT2 (April 22 to 25). The FD0520 PCD solids CaS contents were consistent with in situ solids CaS contents. The FD0520 CaO and $CaCO_3$ contents were not consistent with the in situ solids. This is due to the larger CO_2 measured in the in situ solids. There appears to be an inconsistency in the in situ solids, since the CO_2 measured at the end-of-the-run dust cake solids agreed with the FD0520 solids CO_2 content.

Both the CaS and $CaSO_4$ were at very low levels of less than 3 percent, indicating very poor reactor sulfur capture. The beginning and end of the run had slightly higher levels of CaS and

$CaSO_4$. It is probable that the $CaSO_4$ levels in the PCD solids are inorganic sulfur that came in the PRB coal ash that was not reduced to CaS.

The PCD solids nitrogen and hydrogen concentrations are provided in Figure 4.4-11. As expected, they are lower than the coal nitrogen and hydrogen (see Figure 4.4-2). The PCD solids hydrogen was typically about 10 percent of the coal hydrogen.

The PCD solids and coal higher heating value (HHV) are provided in Figure 4.4-12. The HHV of the PCD solids started GCT2 at about 80 percent of the coal HHV and then slowly decreased to about 60 percent of the coal HHV.

The removal of H_2S in coal gasification using limestone is governed by three reactions:

$$CaCO_3 \rightarrow CaO + CO_2 \quad (1)$$

$$H_2S + CaCO_3 \rightarrow CaS + H_2O + CO_2 \quad (2)$$

$$H_2S + CaO \rightarrow CaS + H_2O \quad (3)$$

Reaction (1) is the limestone calcination reaction. At thermodynamic equilibrium, the CO_2 partial pressure should be a function of temperature as long as there are both $CaCO_3$ and CaO present. Reaction (2) is the reaction of CaO with H_2S, and reaction (3) is the reaction of $CaCO_3$ with H_2S. Reaction (3) is simply the overall $CaCO_3$ reaction and is the sum of reactions (1) and (2). Whether reaction (2) or (3) controls H_2S removal depends on the temperature and carbon dioxide partial pressure.

Figure 4.4-13 provides the CO_2 partial pressure and percent limestone calcination for GCT2. The CO_2 partial pressure is the system pressure times the mole fraction CO_2. The percent-limestone calcination is mole-percent CaO divided by the sum of the mole percents of CaO and $CaCO_3$, or

$$\%\ \text{Calcination} = \frac{\text{M}\%\ \text{CaO}}{\text{M}\%\ \text{CaO} + \text{M}\%\ \text{CaCO}_3} \quad (4)$$

Since a large amount of the PCD calcium solids came from the PRB coal it is very likely that a large fraction of the PCD calcium is from the PRB ash, not the sorbent feed (Ohio limestone). The GCT2 calcination started at about 70 percent, then decreased to 50 percent on April 19. The calcination then increased to 90 percent on April 22, and the calcination was from 90 to 100 percent until the end of the run. The CO_2 partial pressure increased from 15 to 25 psia during the first 2 days of operation until April 19, while the calcination was decreasing. The CO_2 partial pressure then decreased from 25 to 20 psia while the calcination was increasing, until April 21. On April 21 the CO_2 partial pressure leveled off at 20 psia until late on April 22 when the system pressure was increased from 200 to 220 psig (see Figure 4.3-1). There was a slight increase in CO_2 partial pressure on April 25 when the system pressure was again increased from 220 to 240 psig.

The percent calcium sulfidation was calculated as the mole percent of calcium compounds containing sulfur and is shown in Figure 4.4-14 along with the sulfur removal calculated from the coal-feed rate, coal sulfur, PCD solids rate, and PCD solids sulfur content.

The percent sulfidation is defined as:

$$\%\ \text{Sulfidation} = \frac{\text{M\% CaS} + \text{M\% CaSO}_4}{\text{M\% CaO} + \text{M\% CaCO}_3 + \text{M\% CaS} + \text{M\% CaSO}_4} \quad (5)$$

The sulfur removal and the calcium sulfidation tracked each other well during GCT2 because they were both calculated from the PCD solids sulfur. Since much of the calcium present in the PCD solids came as PRB coal ash, this is not a complete indication of the utilization of the fresh limestone added. The first-day sulfur removals of 40 to 50 percent were extrapolated from PCD solids sulfur data of 20:00 on April 18, and could be incorrect. On April 19 the sulfur removal decreased from 30 to 12 percent and the calcium sulfidation decreased from 20 to 5 percent. At 12:00 on April 20 the sulfur removal peaked at 25 percent, while the calcium sulfidation peaked at 12 percent. The sulfur removal and the calcium sulfidation then decreased to 5-percent removal and nearly zero-percent sulfidation. For 2 days the sulfur remained at 5 percent and the sulfidation at nearly zero percent. Late on April 23 the sulfur removal started increasing and peaked at 22 percent at around 22:00 April 24. The sulfidation increased to about 3 percent during the same period. For the last day of operation the sulfur capture leveled off at 20 percent and the sulfidation leveled off at 3 percent.

Table 4.4-1

Coal and PCD Solids Particle Sizes

Test		GCT2		GCT1	
		D_{50}	Standard Deviation	D_{50}	Standard Deviation
Location	Description	μm	μm	μm	μm
SI0111	Ground Coal	272	43		
SI0112	Ground Coal	358	78		
FD0210	Coal Feed	354	42	338	41
FD0520	Fine Solids	21.5	3.8	26.9	6.5

Table 4.4-2

Coal and PCD Solids Bulk Densities

Test		GCT2		GCT1	
		Bulk Density	Standard Deviation	Bulk Density	Standard Deviation
Location	Description	lb/ft^3	lb/ft^3	lb/ft^3	lb/ft^3
FD0210	Coal Feed	44.9	0.8	44.7	0.9
FD0520	Fine Solids	24.3	3.3	27.7	5.7

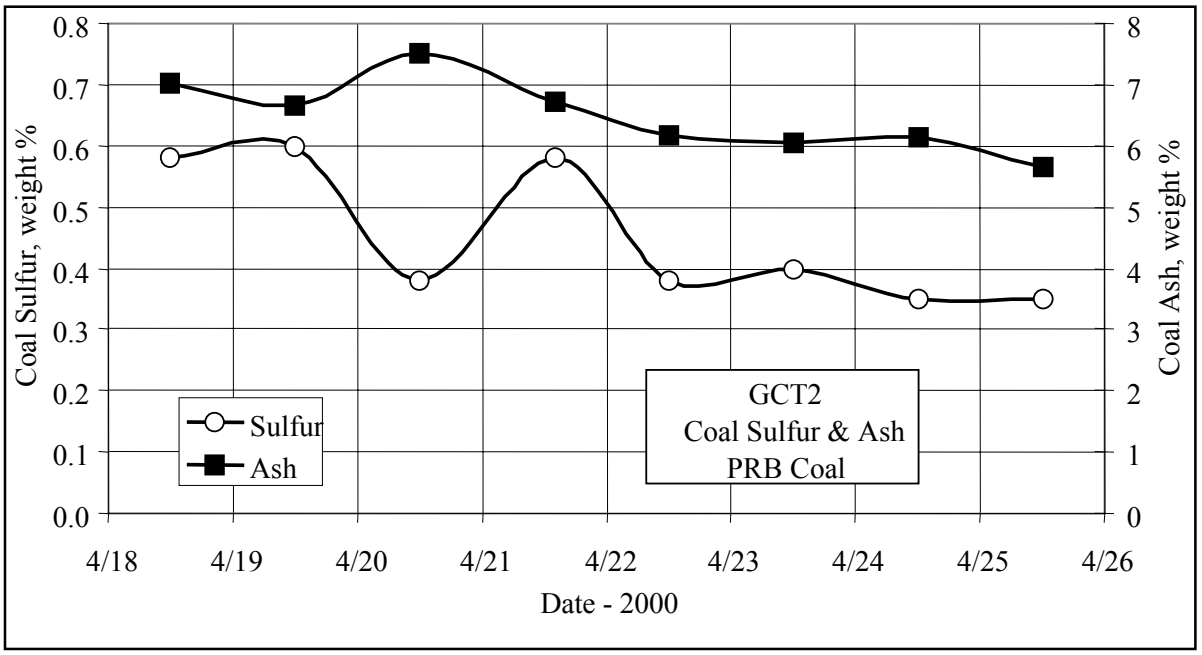

Figure 4.4-1 Coal Sulfur and Ash Contents

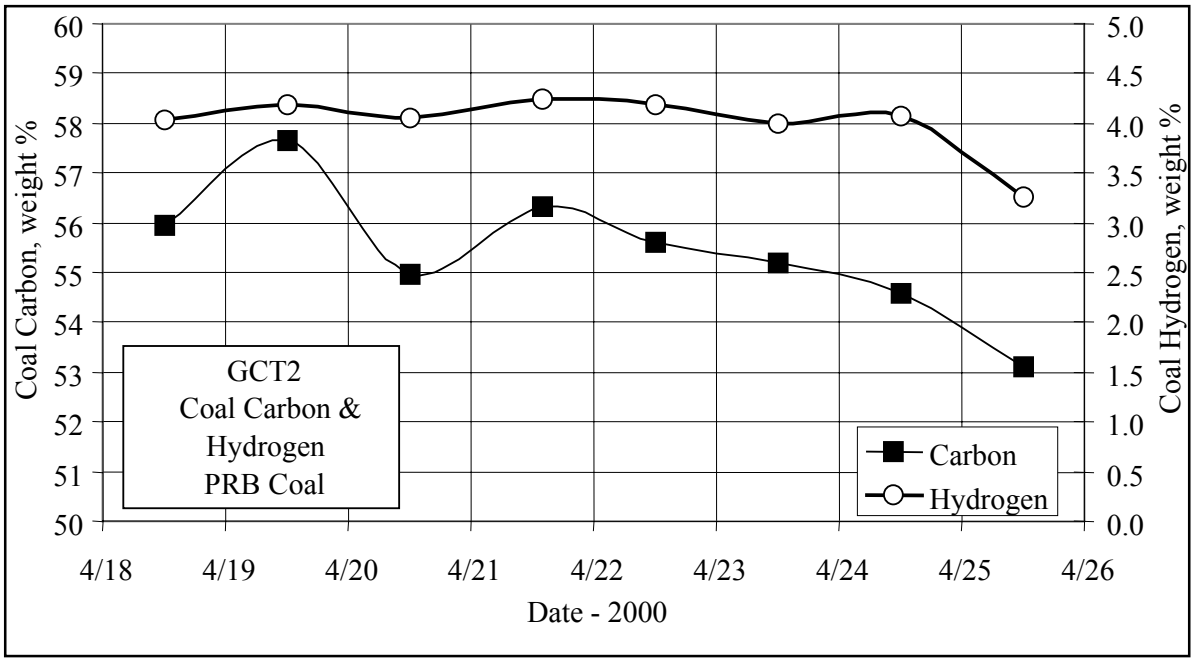

Figure 4.4-2 Coal Carbon and Hydrogen Contents

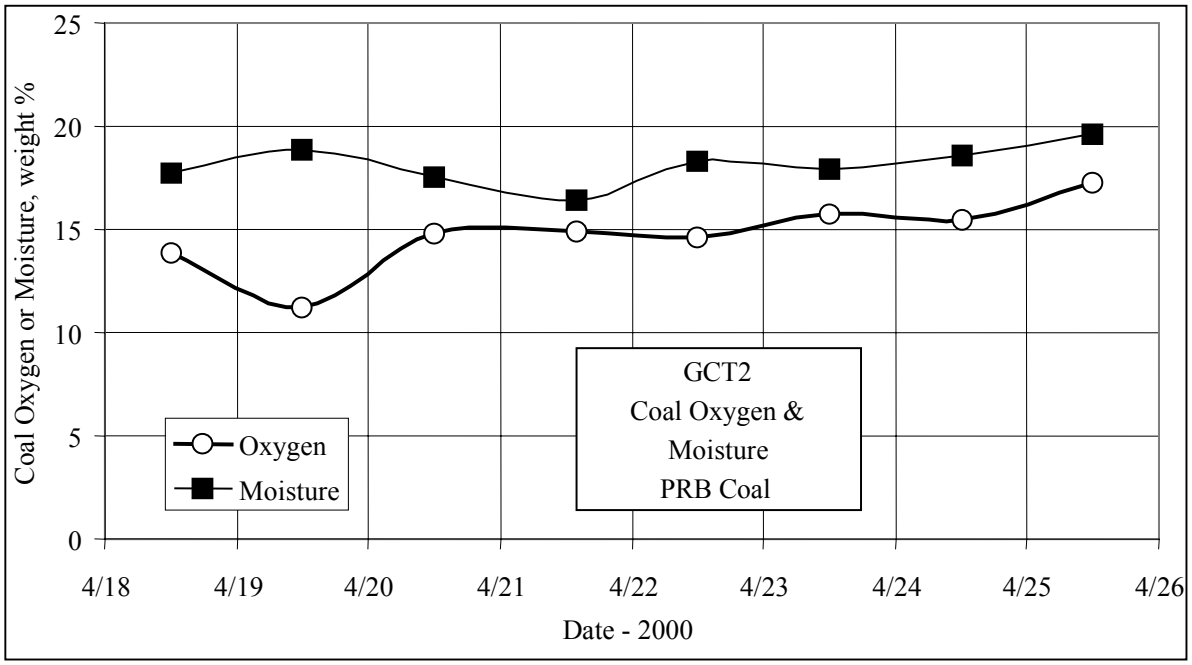

Figure 4.4-3 Coal Oxygen and Moisture Contents

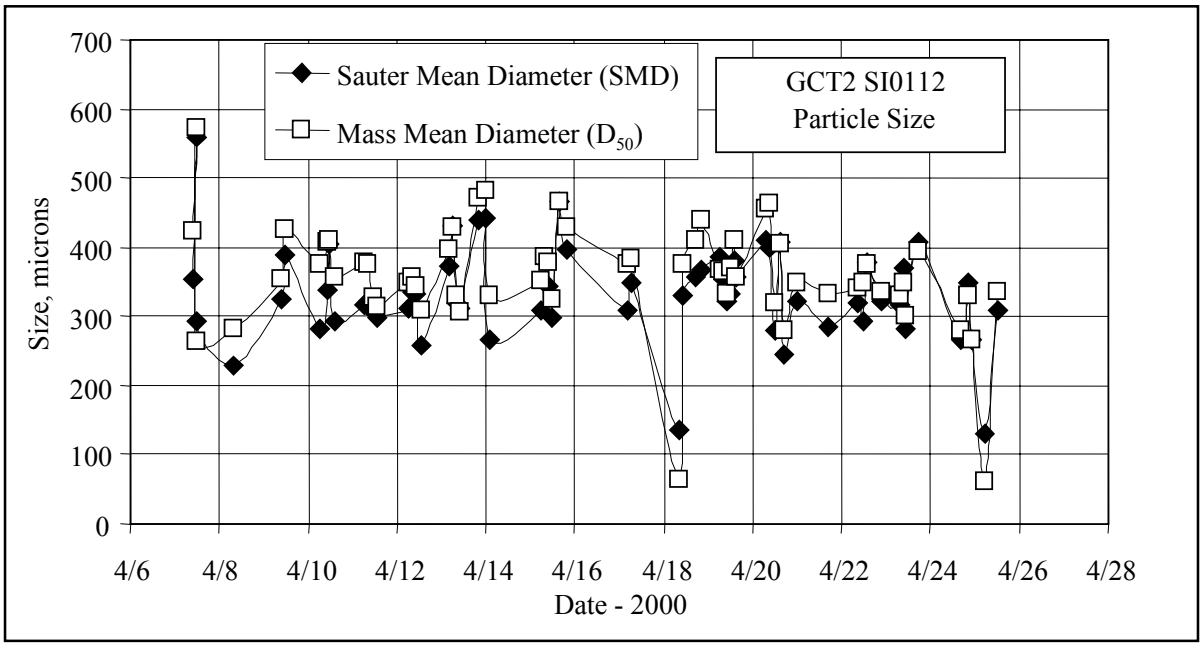

Figure 4.4-4 Ground Coal Mass Mean and Sauter Mean Diameters

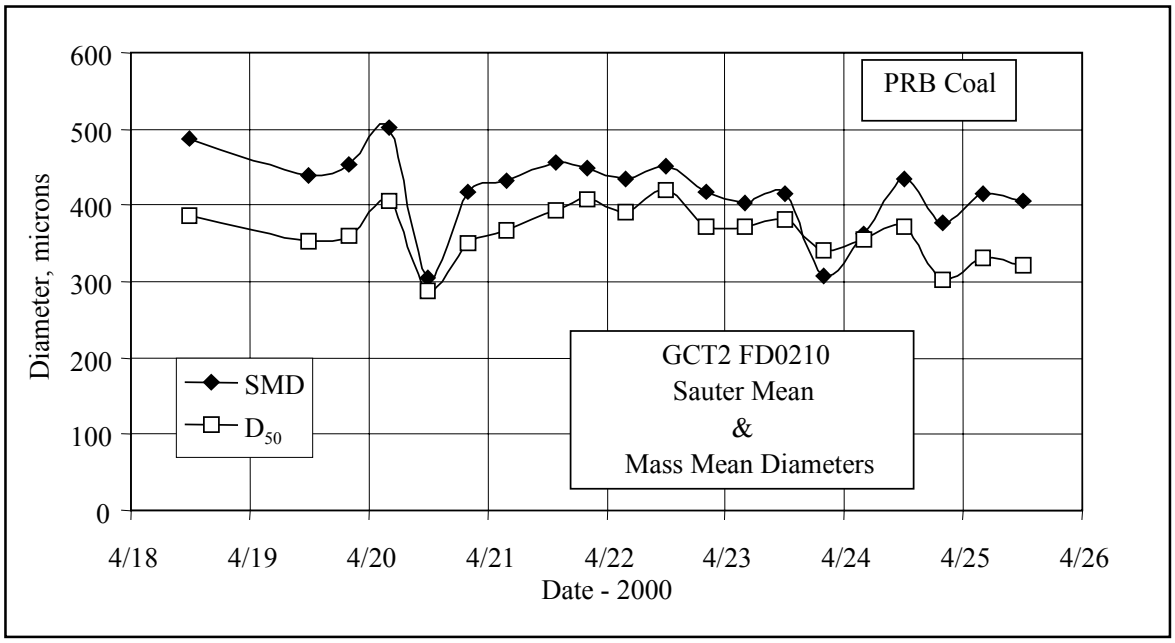

Figure 4.4-5 FD0210 Coal Mass Mean and Sauter Mean Diameters

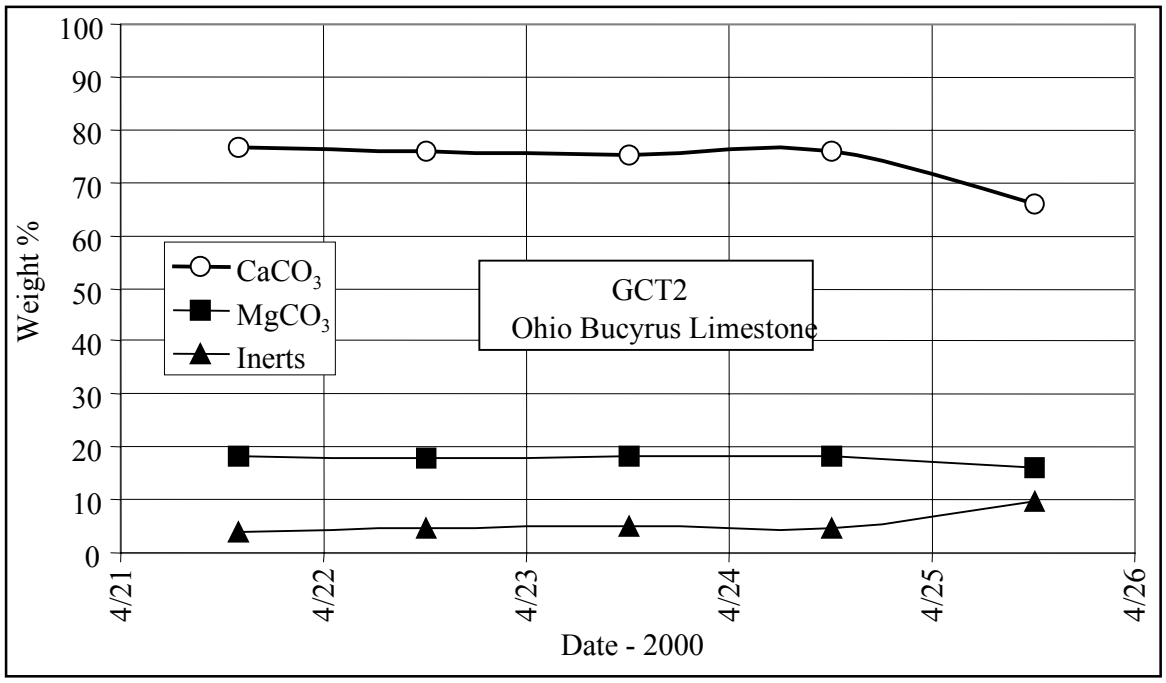

Figure 4.4-6 Limestone Compositions

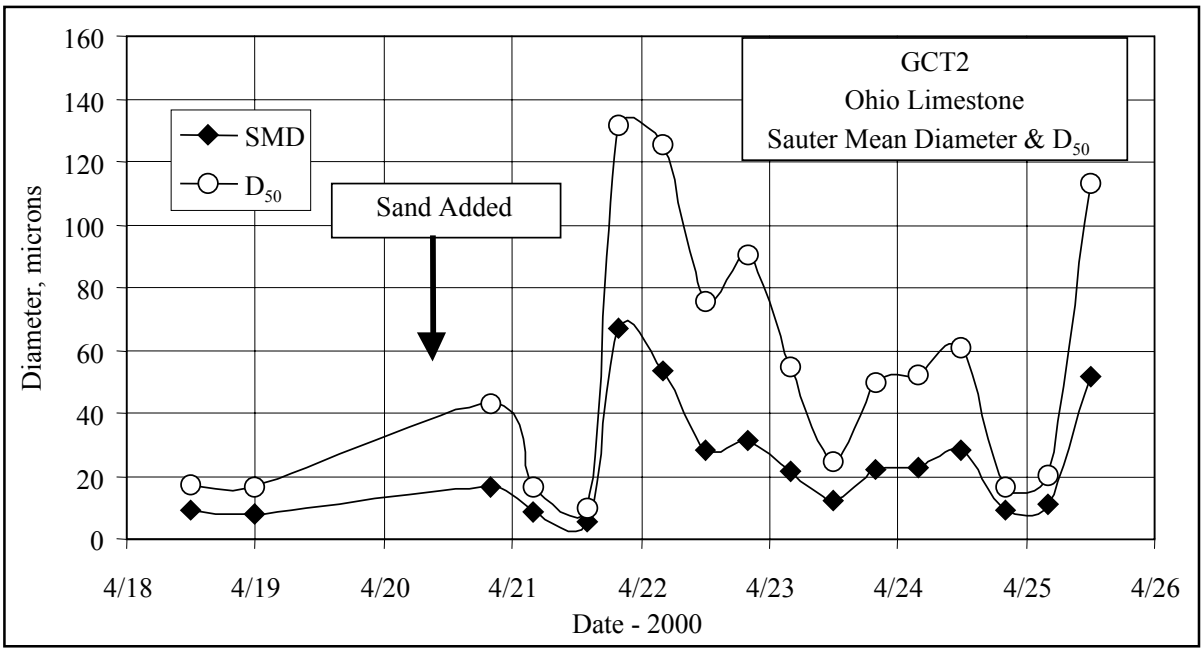

Figure 4.4-7 Limestone Sauter Mean and D_{50} Diameters

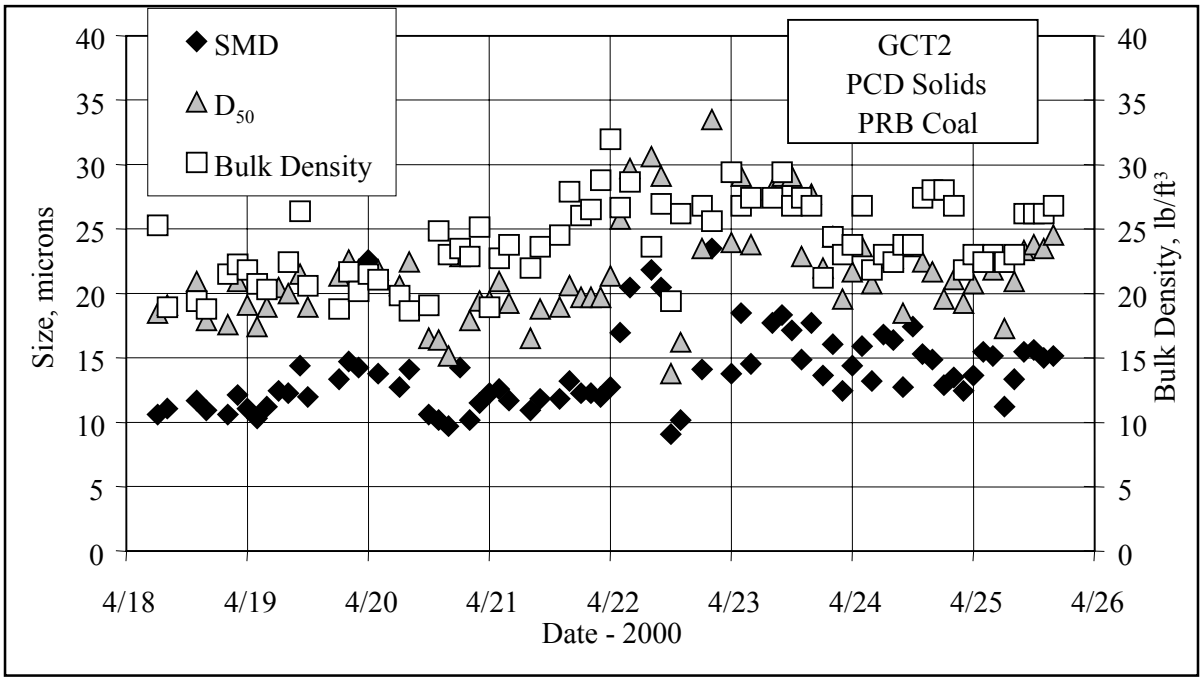

Figure 4.4-8 PCD Solids SMD, D_{50}, and Bulk Density

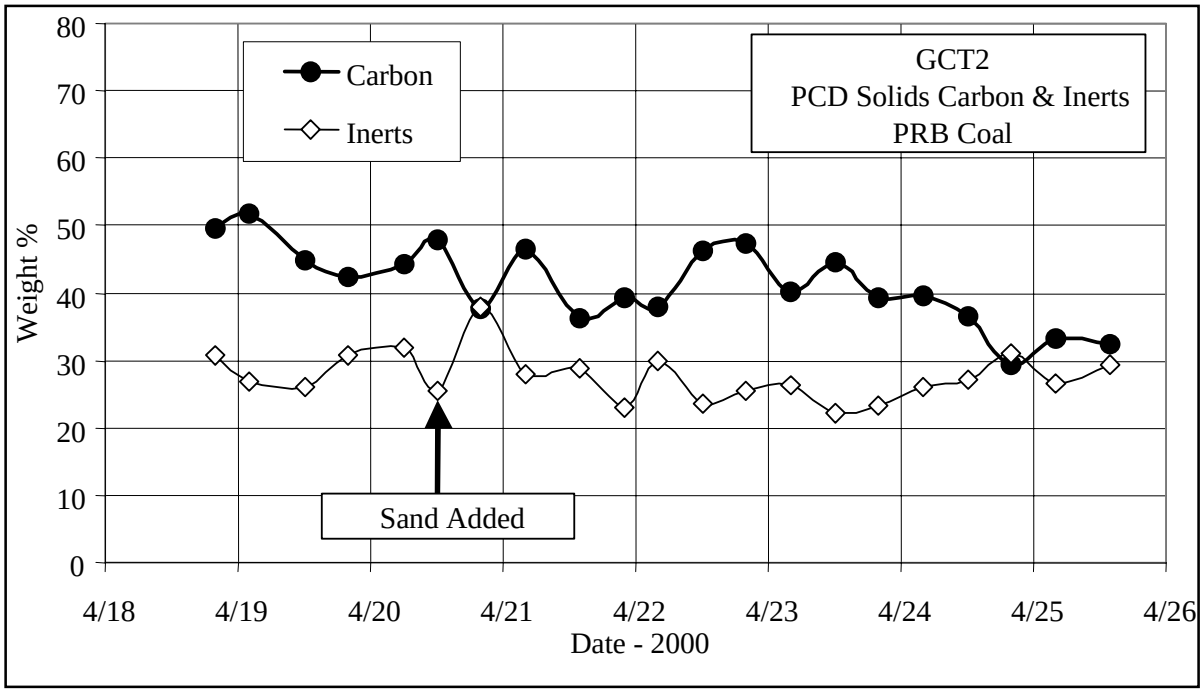

Figure 4.4-9 PCD Solids Organic Carbon and Inerts

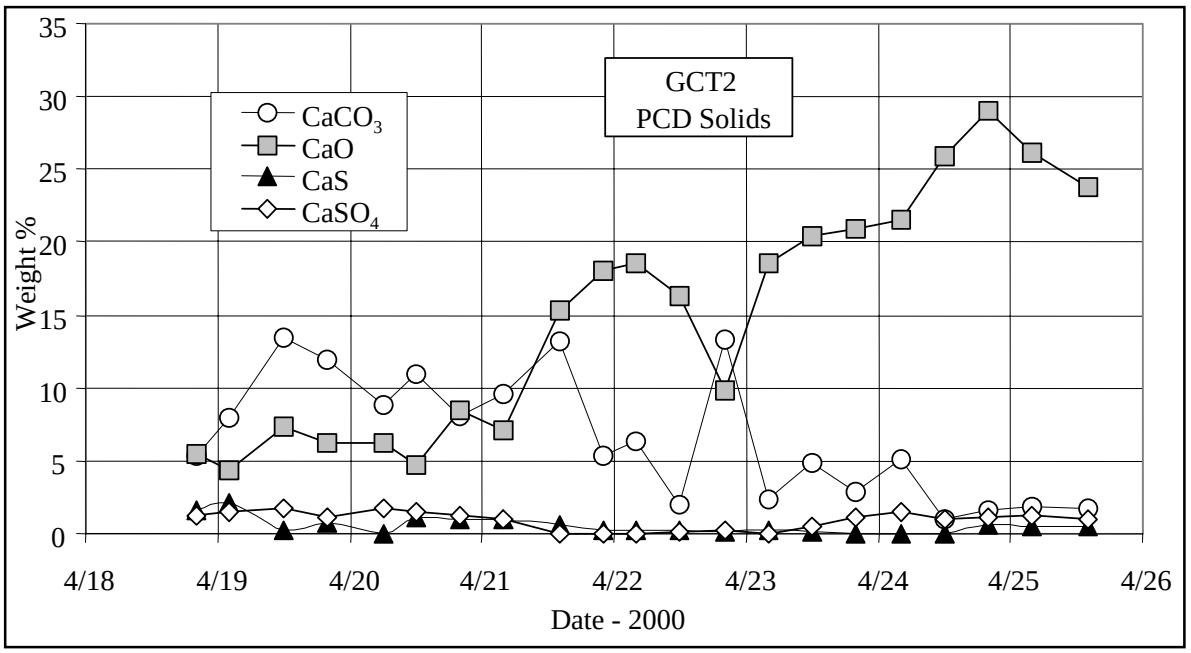

Figure 4.4-10 PCD Solids $CaCO_3$, CaS, CaO, and $CaSO_4$

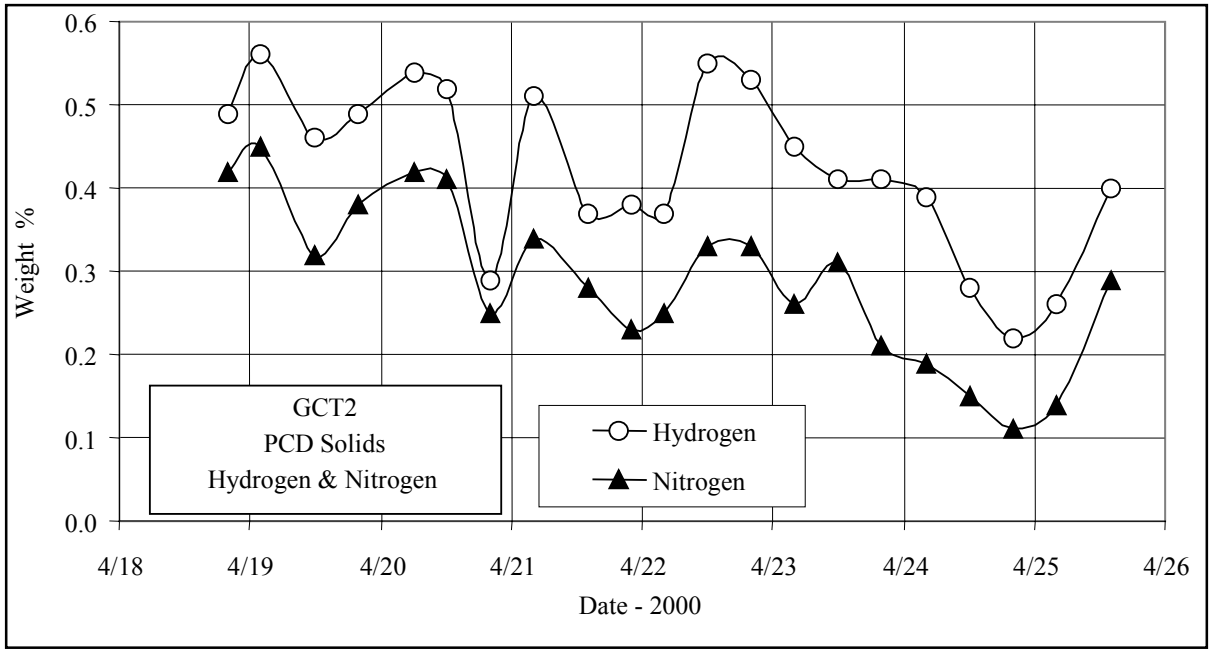

Figure 4.4-11 PCD Solids Hydrogen and Nitrogen

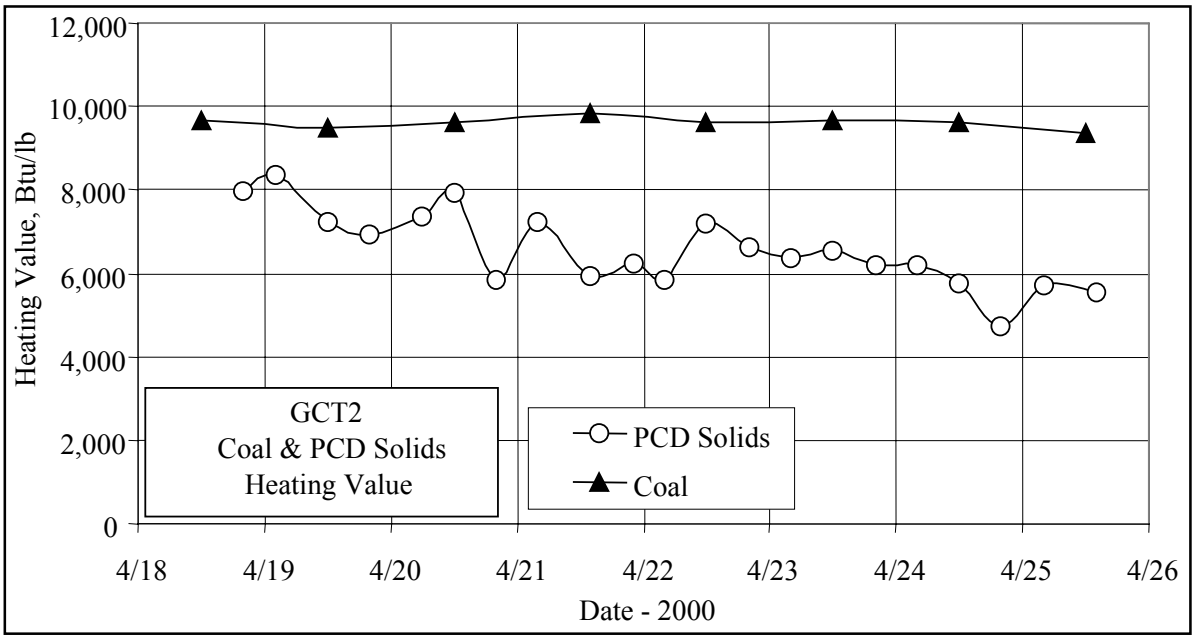

Figure 4.4-12 Coal and PCD Higher Heating Value

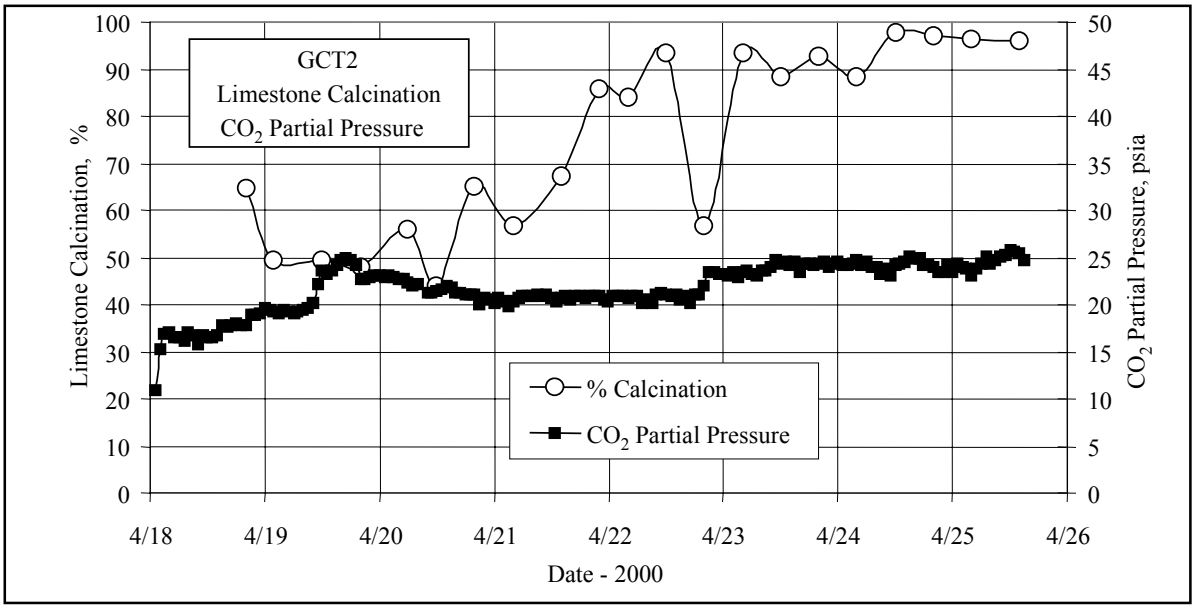

Figure 4.4-13 PCD Solids Calcination and Reactor CO_2 Partial Pressure

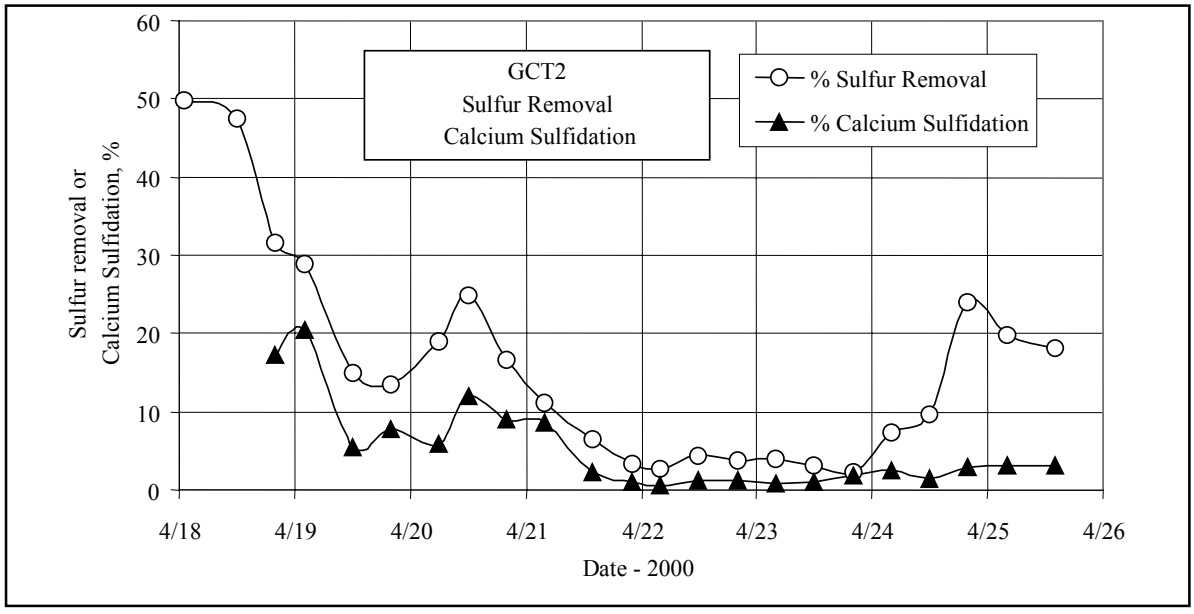

Figure 4.4-14 PCD Solids Calcium Sulfidation and Reactor Sulfur Removal

4.5 MASS BALANCES

The carbon utilization and mass balance determinations were made using gas analyses, solids analyses, and process flows entering and leaving the KBR transport reactor.

The process flows entering the KBR transport reactor are:

- Coal flow through FD0210.
- Sorbent flow through FD0220.
- Air flow measured by FI205.
- Nitrogen flow measured by FI609.
- Steam flow measured by FIC204.

The process flows leaving the KBR transport reactor are:

- Synthesis gas flow from the PCD (measured by FI465).
- PCD solids flow through FD0520.
- Reactor solids flow through FD0510.

The coal flow through FD0210 was determined from a correlation between feeder speed and coal dumps from the FD0210 storage bin. The coal and air flows are shown in Figure 4.3-2 (Section 4.3, Gas Analysis).

Typically, the sorbent-flow rate is determined similarly to the coal-feed rate, that is by a correlation of weigh cell and feeder speed data. In GCT2 the sorbent feeder leaked through and the feeder dumps could not be correlated with the feeder speed. The operator log of FD0220 fills was used to develop an estimate of the sorbent-flow rate. The estimated FD0220 feed rates are shown in Figure 4.5-1. There was no sorbent fed on April 18 except for the first 2 hours of operation. The sorbent flow was increased to 225 lb per hour for several hours on April 19. For the last half of April 19 and the first half of April 20 there was no sorbent flow except for a few brief periods. From April 21 until the end of the run limestone was fed to the reactor continuously at rates from 100 to 250 lb per hour.

The synthesis gas-flow indicator (FI465) settings had not been corrected from combustion settings so a correction factor was required to determine the correct synthesis gas-flow rate. The synthesis-gas rate was calculated by forcing an oxygen balance on the thermal oxidizer (BR0401) by using the following thermal oxidizer process tags:

Primary air flow	FI8773
Secondary air flow	FFIC8772MEAS
Quench air flow	FI8771
Propane flow	FI8753
Oxygen concentration	AIT8775

The best fit of the calculated thermal oxidizer exit O_2 and the measured thermal oxidizer exit O_2 was obtained by multiplying the FI465 reading by 1.03. The measured- and mass-balance calculated O_2 values are shown in Figure 4.5-2. All process calculations in Sections 4.3, 4.4, 4.5,

and 4.7 corrected the synthesis gas-flow rate by multiplying the value from FI465 by 1.03. A correction of only 3 percent is less than other errors in the system, and not making this correction should not significantly change any results.

The nitrogen flow reported by FI609 was clearly in error (reading larger than the flue-gas rate from FI465), so a nitrogen balance was done using the air, coal, and corrected synthesis-gas rates. The hourly average nitrogen flow and corrected synthesis-gas rates are shown in Figure 4.5-3. Once the reactor operation was stabilized on April 18 the nitrogen rate was steady at 7,500 lb per hour until the afternoon of April 22 when the rate was decreased to about 6,700 lb per hour. The nitrogen rate was held constant for about a day, then slowly decreased to 6,300 lb per hour at around 12:00 on April 24. The nitrogen rate was then held constant until the steam rate was decreased on April 25 when the nitrogen rate was decreased to 5,600 lb per hour. The nitrogen rate is important when the synthesis gas heating value is corrected for added nitrogen since the more nitrogen added the larger the heating value correction.

The synthesis-gas rates shown in Figure 4.5-3 follows the air and nitrogen rate. The synthesis-gas rate varied from 18,000 to 25,000 lb per hour depending on the air and nitrogen rates. When the air rate was lowered on April 21 the synthesis-gas rate also went down. When the air and coal rates were increased on April 23 the synthesis-gas rate increased from 19,000 to 24,000 lb per hour.

Since FD0510 was rarely used during GCT1, it will be ignored in the determination of the mass balances and carbon conversion by solids analysis.

The solids flow from the PCD can be determined from two different methods by using:

1. In situ particulate sampling data upstream of the PCD.
2. FD0530 weigh cell data.

The best measurement of the solids flow to the PCD is the in situ PCD inlet particulate determination. Using the synthesis gas-flow rate, the solids flow to the PCD can be determined because the PCD is capturing all of the solids.

The FD0530 weigh cell data can be used to determine the PCD solids flow only if both the FD0530 feeder and the FD0510 feeder (standpipe solids) are off because the FD0520 and FD0510 both feed into FD0530 and FD0530 feeds the sulfator. This method assumes that the PCD solids level in the PCD and FD0502 screw cooler are constant (that is, the PCD solids level is neither increasing nor decreasing). The results for the first two methods are compared in Figure 4.5-4. The data from both methods were smoothed for use in mass balance and carbon conversion calculations.

The in situ particulate and weigh cell data generally compare well and approximately track the coal-feed rate because most of the PCD solids are coal char and coal ash. There was a lot of scatter in the FD0530 weigh cell data on April 18. The PCD solids rate was at about 800 lb per hour on April 19, then began decreasing to 600 lb per hour from 12:00 to 24:00 on April 20. There was a gradual coal-rate decrease from 12:00 to 24:00 on April 21, which produced a gradual PCD solids-rate decrease as expected. For most of April 22 the PCD-solids rate slowly

decreased to about 400 lb per hour. There was a coal-rate increase on the morning of April 23 that produced an increase in PCD solids rate to 600 lb per hour. The PCD-solids rate was then steady for the last 2 days of operation while the coal rate was held constant.

Carbon conversion is defined as the percent fuel carbon that is gasified to CO, CO_2, CH_4, C_2H_6, and higher hydrocarbons. The commercial goal is 90 percent or greater carbon conversion. Carbon utilization is important because carbon conversion is the measure of how much carbon is rejected by the gasifier. This carbon is typically burned in a less efficient combustor and is a less efficient use of the fuel. Carbon conversion can be calculated two ways:

- From gas analysis using the fuel-feed rate, fuel-carbon content, synthesis-gas rate, and synthesis-gas composition.

- From solids analysis using the fuel-feed rate, fuel-carbon content, PCD solids-flow rate, and PCD solids-carbon content.

The results for the gas and solid analyses are shown in Figure 4.5-5. The gas compositions used are determined using procedures described in Section 4.3. Solids compositions are provided in Section 4.4.

The carbon conversions calculated from the solids balance showed little scatter during the test period and slowly rose from 80 to 90 percent during the first few days of operation. After April 21 the carbon conversion leveled off at 90 percent for the remainder of the run. The carbon conversion from the gas analyses was more scattered than from the solids analyses. The gas-analyses-based carbon conversions were above 100 percent at the beginning of the test, indicating some data errors or a depletion of carbon from the circulating solids. Excluding the first day of operation, the differences between the carbon conversion calculated from the gas and solids balances were very small.

Material balances are useful in checking the accuracy and consistency of the data obtained as well as determining periods of steady operation where the data are suitable for model development or commercial plant design.

Hourly overall material balances are provided in Figure 4.5-6, showing the relative difference (relative error) of transport reactor feeds in, minus products out, divided by the feeds ({ In-Out } / In) and the absolute difference (absolute error) of the feeds and the products (In-Out). The overall material balance was excellent, within ± 2 percent for the relative difference (± 500 lb per hour for the absolute difference) for the last 5 days of operation from April 21 to 25. The run started with a negative relative difference of about -7 percent and then decreased to -4 percent by the end of April 18. For April 19 and 20 the relative difference was fairly constant at about -3 percent (-750 lb per hour absolute difference). The relative mass balance changed from -3 to zero percent at 20:00 on April 20 when the H_2 analyzer was recalibrated (see Figure 4.3-5, section 4.3, Gas Analyses).

Some values for a 1-hour total mass balances are shown in Table 4.5-1. The air, nitrogen, and fuel rate dominate the "in" streams while the synthesis gas dominates the "out" ' streams. No material balances were done for nitrogen and sulfur. Nitrogen could not be done because the

medium-pressure nitrogen-flow indicator (FI609) was malfunctioning and not providing meaningful results. Nitrogen flow to the reactor was calculated from a nitrogen balance, essentially forcing the nitrogen balance to be perfect. The sulfur balance could not be done because both the reactor H_2S analyzer and the thermal oxidizer SO_2 analyzer were out of service. The sulfur emissions reported were calculated by difference, using the coal and PCD solids sulfur analyses.

Hourly carbon balances are shown in Figure 4.5-7. The overall carbon balance is good, with the relative difference between inlet and outlet carbon usually within ± 10 percent (± 200 lb carbon per hour absolute difference) for all days except the first day of operation. As expected from the comparison of the carbon conversions calculated from the gas and solids analyses (Figure 4.5-5), the carbon balances were not good on the first day of operation on April 18. The carbon balance was more scattered within the ±10-percent relative difference on April 19 and 20 than during the rest of the run. Some values for a 1-hour carbon balance are shown in Table 4.5-1. The coal and synthesis gas dominate the carbon balance. Since there was no standpipe solids composition data the carbon and other solids standpipe accumulation term could not be calculated.

Hourly hydrogen balances are shown in Figure 4.5-8. The hydrogen balance was good in that the relative balance was within ±10-percent relative difference (±50 lb per hour hydrogen absolute difference) from April 20 through April 25. The period of April 21 through April 24 was consistently about +7 percent (25 lb per hour of hydrogen) above perfect agreement at zero percent, in that 25 lb per hour more hydrogen leaving the reactor would produce perfect agreement. This could be explained if the hydrogen analyzer was reading slightly low. The jump in feeds-minus-products differences on April 19 was during an increase in steam rate from 800 to 1,600 lb per hour, which increased the hydrogen rate by about 90 lb per hour. The fall in feeds-minus-products differences on April 20 was just after the process upset at 08:30. The steam rate was decreased from 1,350 to 775 lb per hour after the upset, thus decreasing the feed hydrogen by about 65 lb per hour. The coal rate was also increased, which increased the feed hydrogen by about 25 lb per hour. The jump in relative hydrogen differences on April 21 seemed to be a result of the slow decrease in coal rate, which resulted in a lower hydrogen concentration in the synthesis gas. Surprisingly, the hydrogen balance is excellent at the end of the test on April 25 when the measured and calculated synthesis gas H_2O values were different (see Figure 4.3-8). Some values for a 1-hour hydrogen balance are provided in Table 4.5-1. The coal, steam, and synthesis gas streams dominate the hydrogen balance.

The steam rate can be calculated by a hydrogen energy balance, as shown in Figure 4.5-9 where it is compared to the measured steam rate. There is poor agreement with the two steam rates on the first day of operation (April 18), with the calculated steam rate higher than the measured steam rate. During the first day of operation the calculated steam rate decreased from 1,500 to 1,000 lb per hour, while the measured steam rate was fairly steady at 700 to 900 lb per hour. The calculated steam rate tracked the increase in steam rate on April 19 a few hours after the measured steam rate increased, although the calculated value did not reach the maximum measured steam rate of 2,100 lb per hour. The calculated steam rate tracked the decrease in steam rate on April 19 as they both decreased together and leveled out together, but the calculated steam rate was about 200 lb per hour less than the measured steam rate. From April

20 to April 23 the measured steam was constant at 750 lb per hour, while the calculated steam rate decreased from about 1,000 to about 500 lb per hour on April 21, then was constant at 500 lb per hour until April 23. The steam-rate increase on April 23 was seen in both steam rates, and during the second half of April 23 both steam rates were at 1,000 lb per hour. The measured steam rate was constant from April 23 to April 25 at 1,000 lb per hour, while the calculated steam rate dipped to 500 lb per hour at around 12:00 on April 24 and then increased to 1,000 on the evening of April 24. The measured steam rate decreased to 500 lb per hour on April 25 which the calculated steam rate did not track. This is probably due to the calculated decrease in synthesis gas H_2O concentration on April 25, which differed significantly from the measured synthesis gas H_2O concentration (see Figure 4.3-8).

Hourly oxygen balances are shown in Figure 4.5-10. The oxygen balance was generally quite good at ±10 percent (±500 lb per hour) from April 21 to 25. The oxygen balance started off poorly on April 18 at -20-percent relative difference (-1,000 lb per hour oxygen absolute difference). The oxygen balance slowly improved from April 18 (-20 percent) to April 21 (-10 percent) to April 22 (-3 percent). The system upset on April 19 decreased the relative difference to -10 percent (-1,000 lb per hour oxygen absolute difference), where the differences remained for about 24 hours. From April 21 to the end of the run the absolute difference was between -10 and +10 percent and for most of the time was between -5 and +5 percent, indicating an excellent oxygen balance. Typical values for the oxygen balance are shown in Table 4.5-1. Note the large oxygen contribution of the feed coal because of the PRB coal high oxygen content. The coal-oxygen concentration is determined by difference, so it is typically a less accurate value than the other elemental analyses.

Hourly calcium balances are shown in Figure 4.5-11. PRB coal operation is characterized by very low flow rates of calcium due to low required sorbent-feed rates because of low sulfur in the PRB coal. The first 2 1/2 days had intermittent sorbent feed that resulted in very poor calcium balances because the reactor was alternately charged and then run down in calcium levels. After continuous sorbent feed was started on April 20 the calcium balances were reasonable, but still poor at ± 60 percent. Typical calcium rates are shown in Table 4.5-1. Note the low total-calcium rates with about half of the inlet calcium coming from fuel and half from sorbent. The main error in calcium balance is from the sorbent feed rate, which is about 30-percent calcium. The sudden jumps in relative and absolute differences on April 23, 24, and 25 are at the same times when sudden changes in sorbent feed rate occurred. Calcium is likely to accumulate in the reactor during periods of high sorbent feed and to bleed off from the reactor during low periods of sorbent feed, which adds to deviation from the steady state assumption for the mass balance.

The inerts balance is shown in Figure 4.5-12. The inerts are all the solid compounds that do not have carbon, calcium, magnesium, sulfur, oxygen, or hydrogen. The inerts balance mainly reflects the coal and PCD solids rate, since the limestone sorbent typically has less than 10-percent inerts. The first 12 hours of operation on April 18 had a scattered-inerts balance that was very negative. For the first 2 days of operation the inerts balance was very bad and varied from -60 to -20 percent (-120 to -40 lb per hour inerts) for 2 days from 12:00 on April 18 to 08:30 on April 20 (process upset). After the process upset the inerts balance became acceptable for the remainder of the run, varying from ± 20 percent (± 40 lb per hour

inerts). The peaks and valleys seen in Figure 4.5-12 are due to the variations in the PCD solids inerts concentrations (see also Figure 4.4-6).

Another measure of the steadiness of the transport reactor is the number and severity of the cyclone dipleg upsets. A dipleg upset is when the pressure drop across the vertical section of the cyclone dipleg (DPI253) is zero for more than a few seconds. (The normal pressure drop across the vertical cyclone dipleg was 25 to 40 inH_2O.) During a cyclone dipleg upset the cyclone stops removing solids from the disengager gas stream and sends all cyclone feed solids to the PCD. The severity of a dipleg upset can be determined by the change in the standpipe and cyclone solids levels (found in DP measurements) from before the dipleg upset to after the upset. The change in reactor solids is essentially the solids that are lost from the reactor due to the upset. Figure 4.5-13 shows a plot of the time and severity of each GCT2 dipleg upset. There were no dipleg upsets during the first day of operation, April 18, probably due to the start-up sand still in the reactor making the reactor more stable. The reactor became less stable on April 22, possibly due to the low coal-feed rate and lower solids-circulation rates. Once the coal-feed rate increased on April 23, and remained at a high coal-feed rate, there were no dipleg upsets and the reactor became much more stable.

In general, the mass balances were quite good, especially for the last 5 days of operation from April 21 to 25. As expected, the gas-flow rates were self consistent, as shown by the excellent overall mass balance which is dominated by the gas flow-rate measurements (± 2 percent for the last 5 days). This of course was helped by forcing the nitrogen balance which is a large part of all the larger gas-flow rates (air and synthesis gas). Elements found in both solids and gases (carbon, oxygen, and hydrogen) had good balances (± 10 percent for the last 5 days). Elements dominated by the solids-flow rates (calcium and inerts) were not as good, probably due to the ignored reactor accumulation term and the errors in the sorbent and PCD solids rates.

The heat loss of the thermal oxidizer can be calculated from the LHV of the synthesis gas, air rate to the thermal oxidizer, thermal oxidizer outlet temperature, and propane flow rate. The thermal oxidizer propane flow and exit temperatures are provided in Figure 4.5-14. An increase in thermal oxidizer temperature or a decrease in propane rate would indicate an increase in synthesis gas heating value. The thermal oxidizer outlet temperature increased from 1,600 to about 2,000°F during the run. The propane-flow rate was essentially constant at 1,160 SCFH for the first 5 days of operation and then was decreased to 700 SCFH. During the final few hours of operation on April 25 the thermal oxidizer outlet temperature increased, which agrees with the synthesis gas LHV increase at the same time.

The hourly averages of the thermal oxidizer heat losses are provided in Figure 4.5-15. The heat losses are scattered between 0.0 and 6.5 x 10^6 Btu/hour for the first 2 days of operation, but settled down to between 1.5 and 5.0 x 10^6 Btu/hour for the last 5 days of operation. There seems to be a slow trend of increasing heat loss during the run as the thermal oxidizer exit temperature increased.

The transport reactor energy balance for the GCT2 test run is provided in Figure 4.5-16, with standard conditions chosen to be ambient pressure and temperature. The "energy in" consisted of the coal, air, and steam fed to the transport reactor. The nitrogen and sorbent fed to the

reactor was considered to be at ambient conditions and hence have no energy above the basis condition. The energy to calcine and sorbent limestone was neglected, as the sorbent-feed rate was low and only a small portion of the sorbent fed was calcined. Energy out consisted of the synthesis gas and PCD solids. The lower heating value of the coal and PCD solids were used in order to be consistent with the lower heating value of the synthesis gas. The energy of the synthesis gas and PCD solids was determined at the transport reactor cyclone exit. The synthesis gas and PCD solids energy consists of both latent and sensible heat. The heat loss in the reactor was estimated to be $1.5x10^6$ Btu/hr during a previous combustion transport reactor test.

The GCT2 energy balance started with more heat out of the reactor than in by 10 to 25 percent (3 to 8 x 10^6 Btu/hr) for the first 12 hours of operation. The energy balance went from negative 10-percent (-3.0 x 10^6 Btu/hr) to positive 10-percent (+3.0 x 10^6 Btu/hr) from 12:00 on April 18 to 12:00 on April 19. The energy balance then leveled off at being consistently high by about 10 percent ($3.3x10^6$ Btu/hr) until early on April 24. The energy balance was acceptable at +5 percent off (+1.5 x 10^6 Btu/hr) during the rapid increase in coal and air rates on April 23. Early on April 24 the energy balance was off by about +15 percent (4.5 x 10^6 Btu/hr), where it stayed until the steam rate was decreased on April 25. Once the steam rate was decreased at 07:00 on April 25 the energy balance improved to 1.0 to 5.0 percent (0.5 to 2.0 x 10^6 Btu/hr) due to an increase in LHV because of an increase in CO, CH_4, and C_2^+ concentrations. During the period between 12:00 on April 24 and 07:00 on April 25 the mass balance was high by about 1.0 to 2.0 percent (250 to 500 lb per hour). The energy balance would be significantly improved if the heat loss were to be increased to 4.5 x 10^6 Btu/hr. It is more likely that the synthesis-gas rate is actually higher or the coal-feed rate is lower than used in the energy balance.

Table 4.5-2 provides the typical energy balance for a 1-hour period in GCT2. The synthesis gas latent and sensible heat are shown separately.

The enthalpies of the synthesis gas and the coal are provided in Figure 4.5-17. The enthalpies follow the synthesis gas and coal-flow rates, as expected. Note the increase and decrease of the coal enthalpies on April 24 caused by the decrease and increase of the coal rates (see Figure 4.3-2).

The enthalpies of the PCD solids and the steam are provided in Figure 4.5-18. The enthalpy of the PCD solids consists of the latent heat of the PCD solids (char) and the sensible heat. Most of the enthalpy is from the latent heat due to the residual carbon in the char.

Table 4.5-1

Typical Total and Component Mass Balances

Mass Balance Type	Total	Carbon	Hydrogen	Oxygen	Calcium	Inerts
Date	4/23/00	4/23/00	4/23/00	4/23/00	4/23/00	4/23/00
Time Start	11:30	11:30	11:30	11:30	11:30	11:30
Time End	12:30	12:30	12:30	12:30	12:30	12:30
Fuel	PRB	PRB	PRB	PRB	PRB	PRB
Sorbent	OH LS	OH LS	OH LS	OH LS	OH LS	OH LS
Mixing Zone Temperature, ^{O}F	1,712	1,712	1,712	1,712	1,712	1,712
Pressure, psig	220	220	220	220	220	220
In, pounds/hr						
Fuel	4,322	2,385	258	1,368	41	146
Sorbent	167	20		78	50	8
Air	11,753		17	2,806		
Nitrogen	6,777					
Steam	1,001		111	889		
Total	24,020	2,405	386	5,141	91	154
Out, pounds/hr						
Fuel Gas	23,551	2,263	368	5,227		
PCD Solids	600	271	2	61	99	133
Total	24,151	2,534	370	5,288	99	133
Accumulation	-36					
(In-Out)/In, %	-0.4%	-5.4%	4.1%	-2.9%	-8.8%	13.6%
(In-Out), pounds per hour	-95	-129	16	-147	-8	21

Notes:
1. Nitrogen balance was forced, to determine nitrogen feed.
2. Sulfur balance could not be done because there was no reactor H_2S measurement.

Table 4.5-2

Typical Energy Balances

Date	4/23/00
Time Start	11:30
Time End	12:30
Fuel	PRB
Sorbent	OH LS
Mixing Zone Temperature, ^{O}F	1,712
Pressure, psig	220
Energy "In", 10^6 Btu/hr	
Fuel	39.3
Steam	1.2
Air	0.6
Total	41.1
Energy "Out", 10^6 Btu/hr	
Synthesis Gas Latent	24.5
Synthesis Gas Sensible	10.0
PCD Solids	4.2
Heat Loss[2]	1.5
Total	40.2
(In-Out)/In, %	2.3%
(In-Out), 10^6 Btu/hr	0.9

Notes:
1. Sorbent and nitrogen are at standard conditions and have zero enthalpy.
2. Heat loss by previous testing.

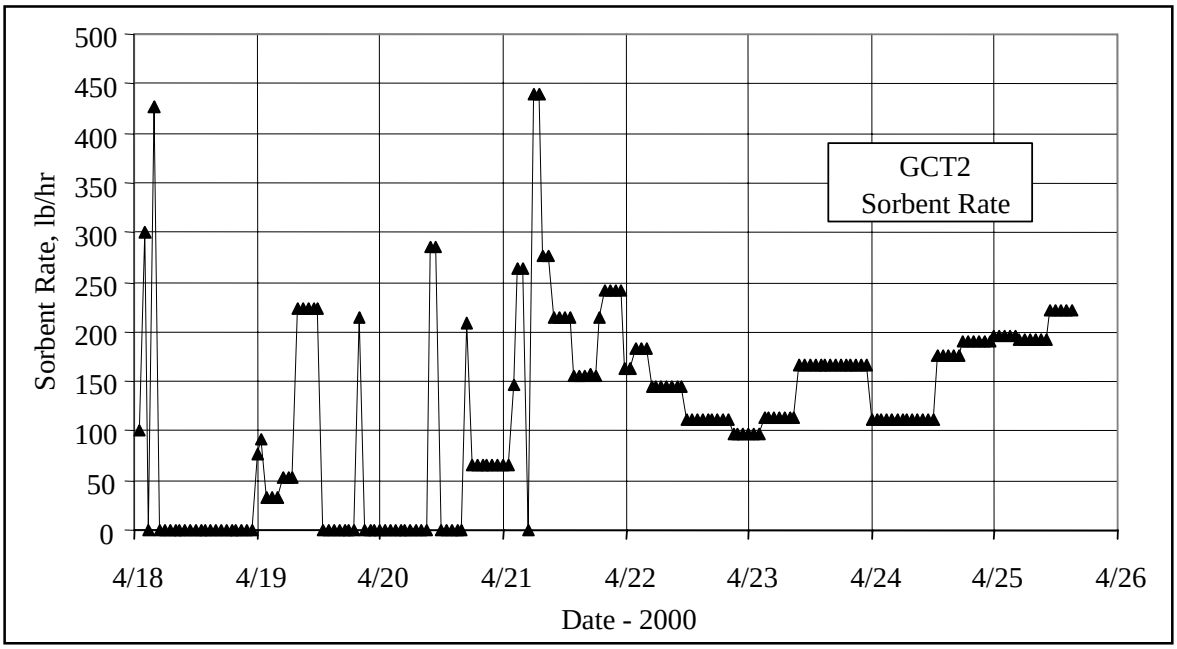

Figure 4.5-1 FD0220 Sorbent Rate

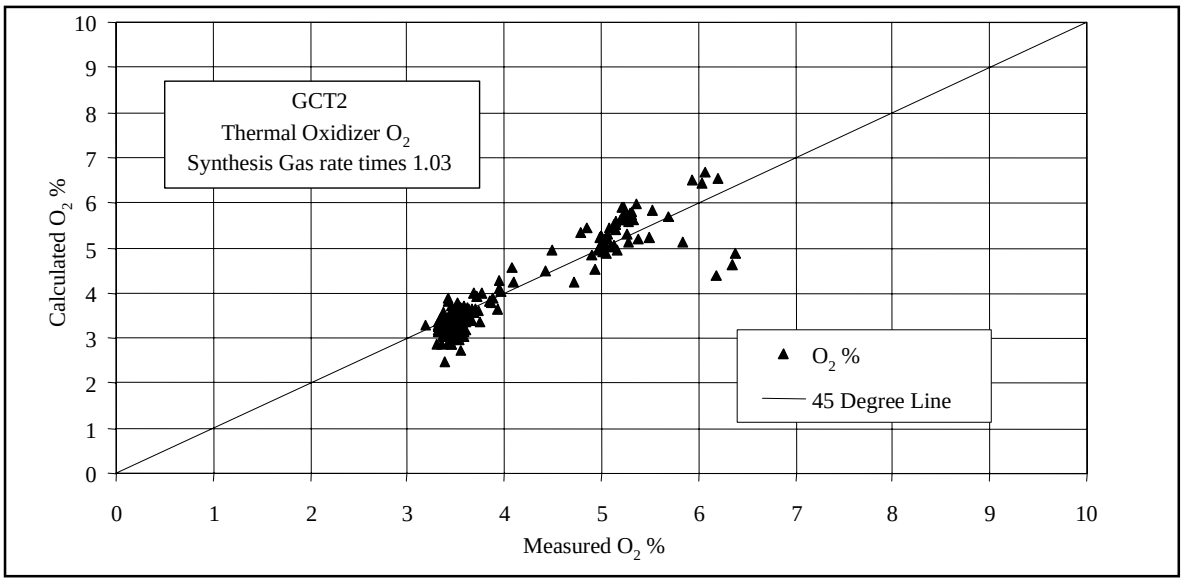

Figure 4.5-2 Measured and Calculated Thermal Oxidizer O_2

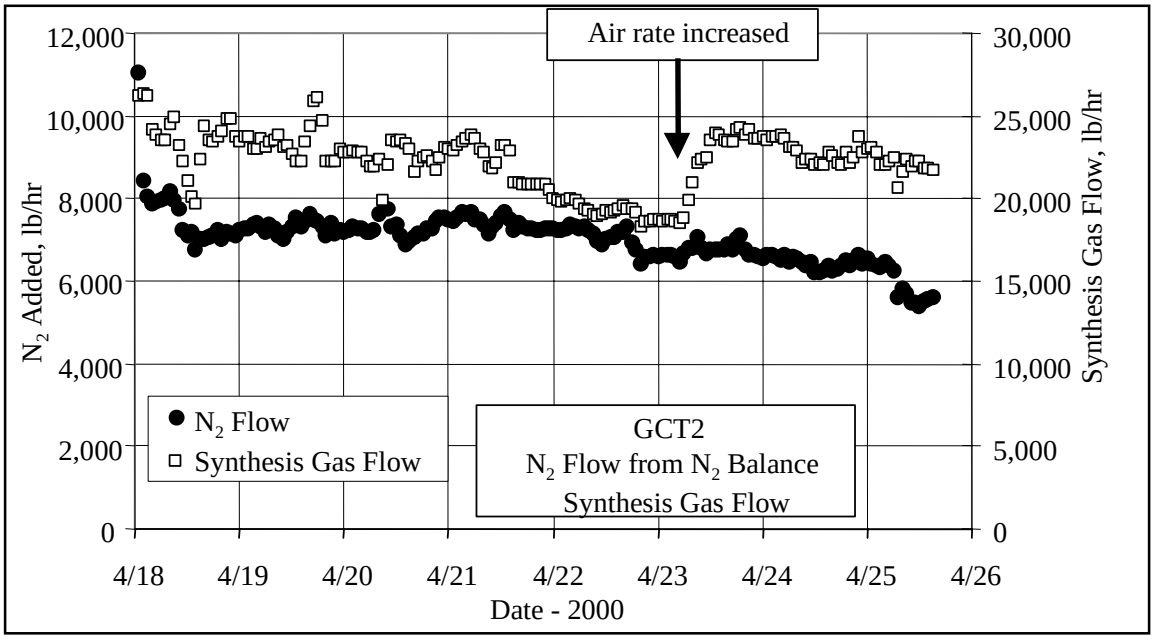

Figure 4.5-3 Nitrogen and Synthesis Gas Flows

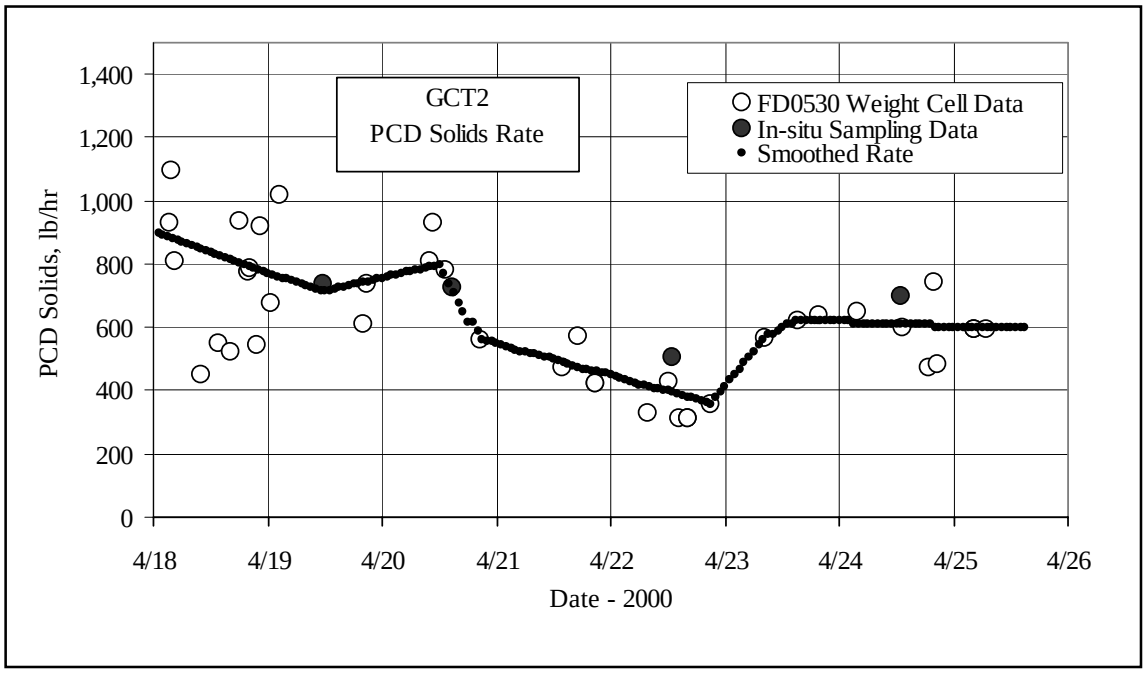

Figure 4.5-4 PCD Solids Rate

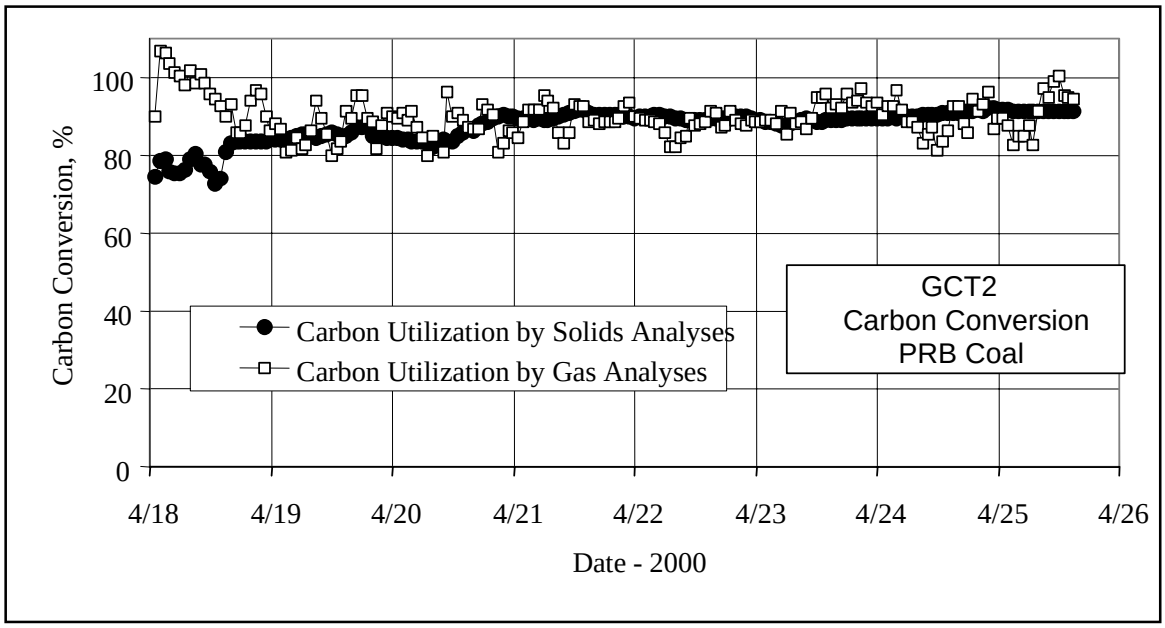

Figure 4.5-5 Carbon Conversion

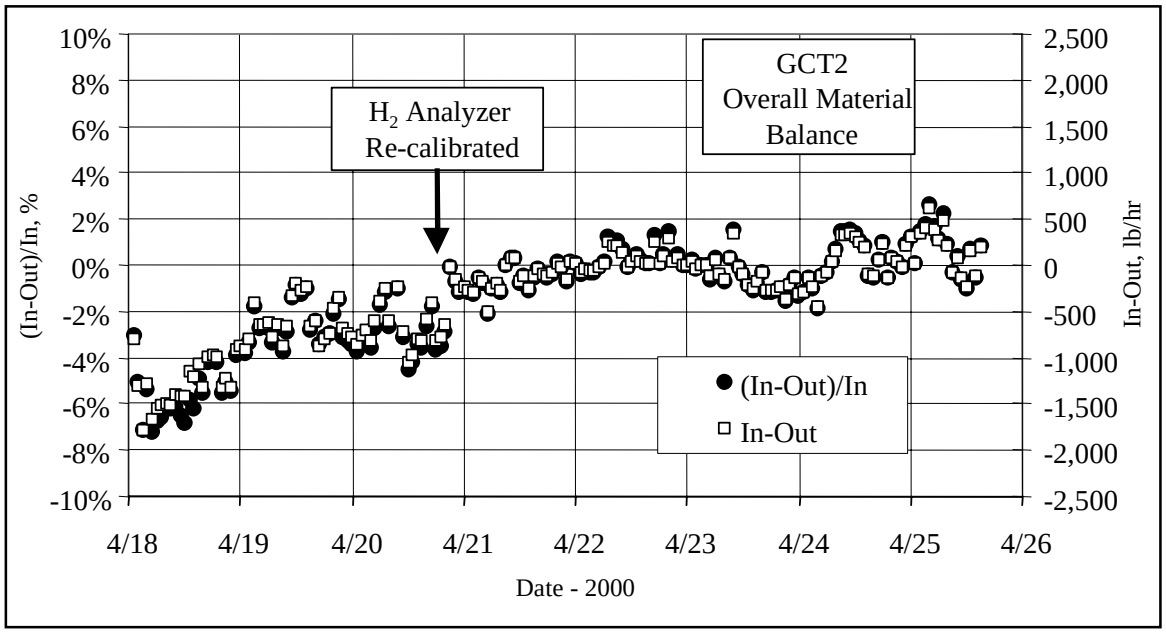

Figure 4.5-6 Overall Material Balance

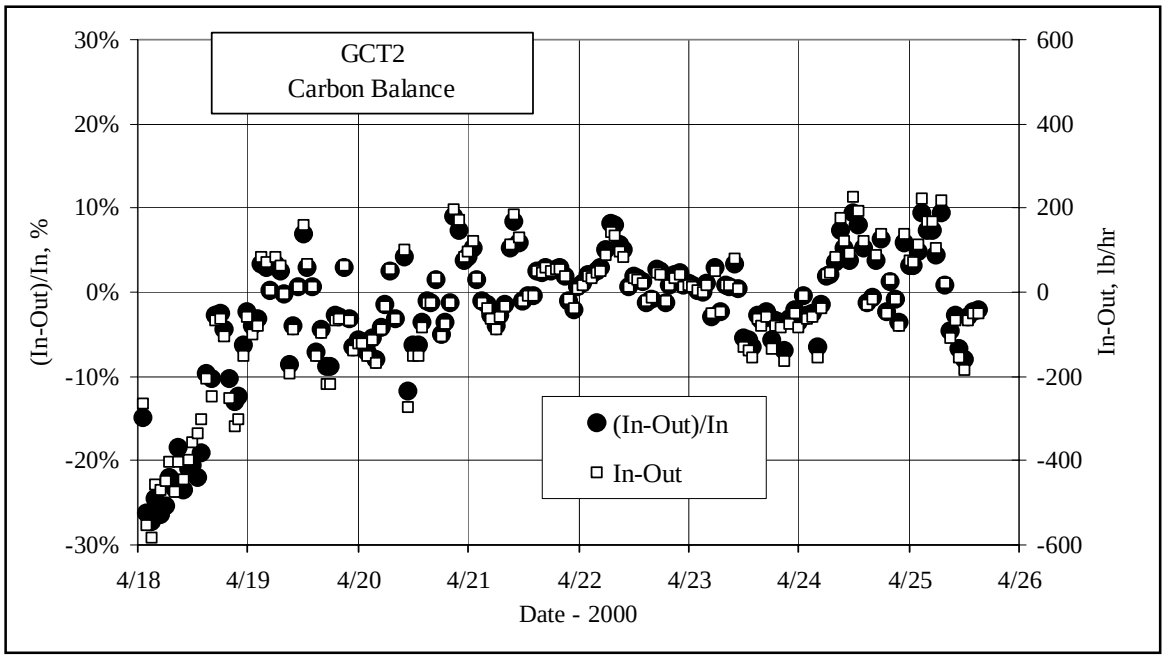

Figure 4.5-7 Carbon Balance

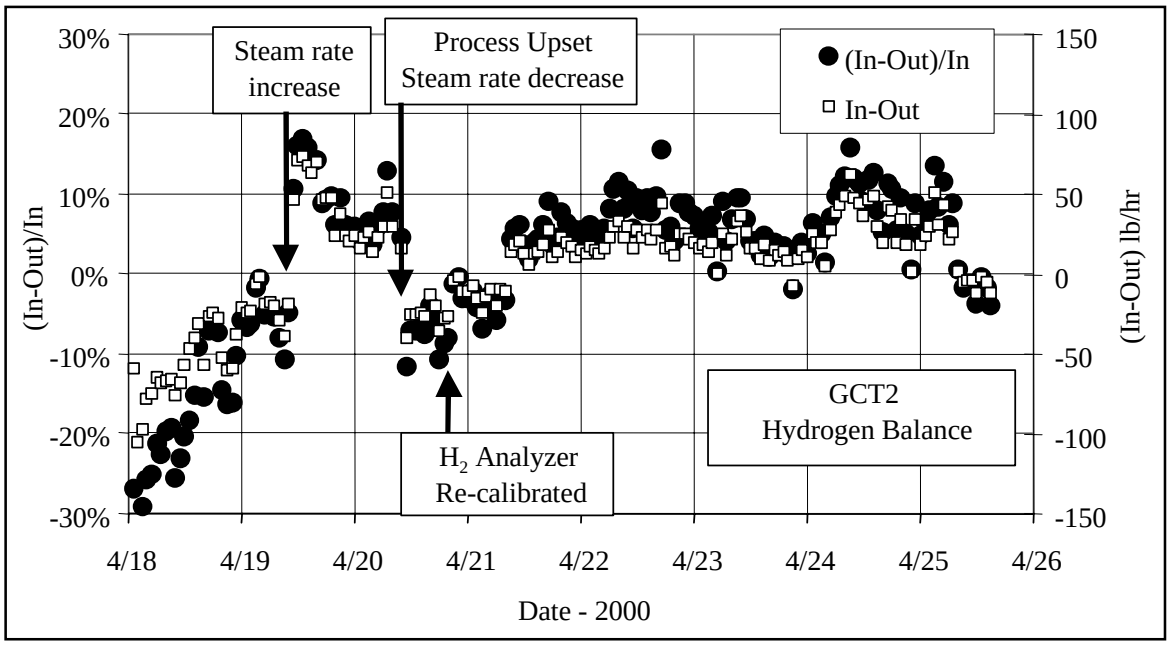

Figure 4.5-8 Hydrogen Balance

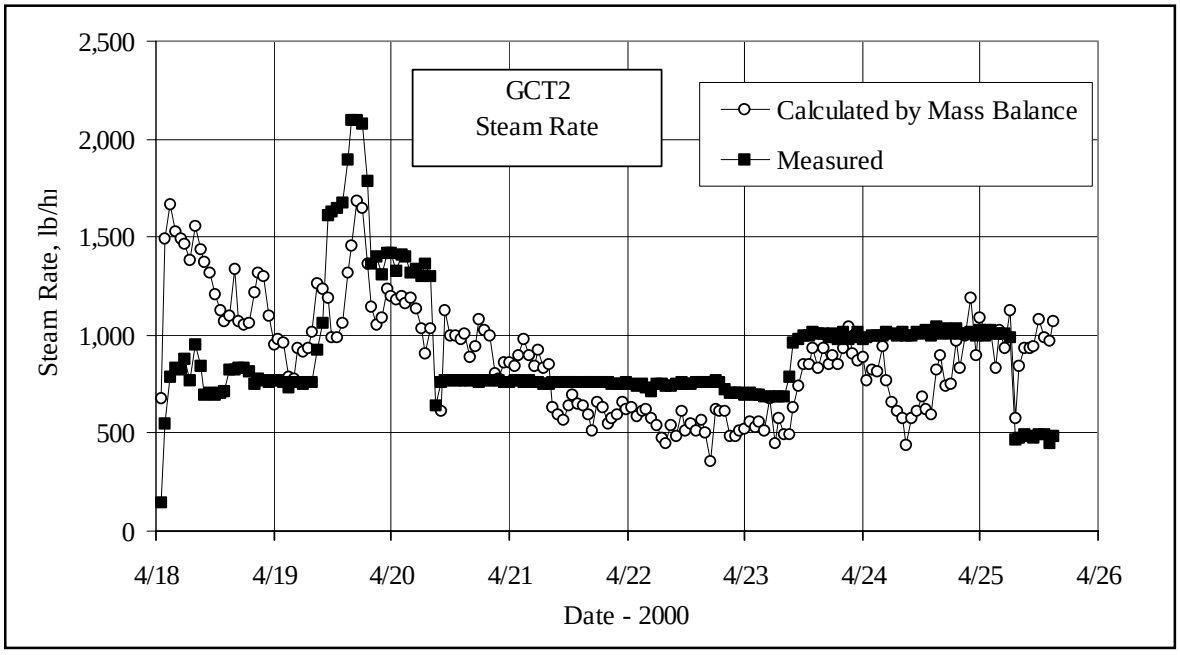

Figure 4.5-9 Steam Rates

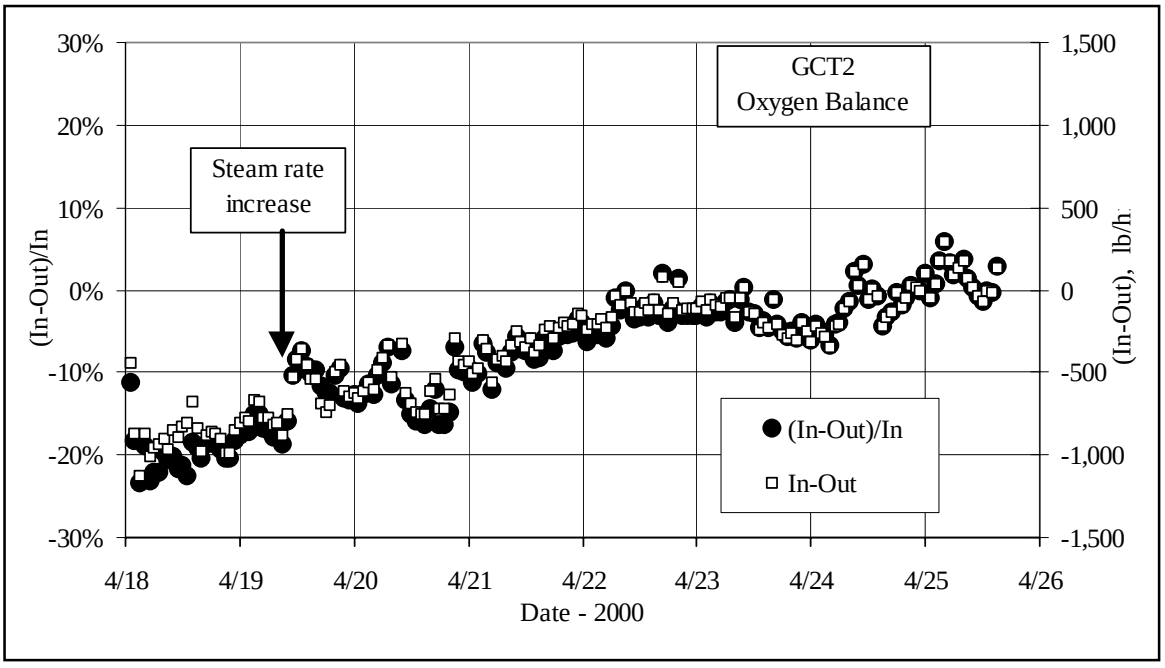

Figure 4.5-10 Oxygen Balance

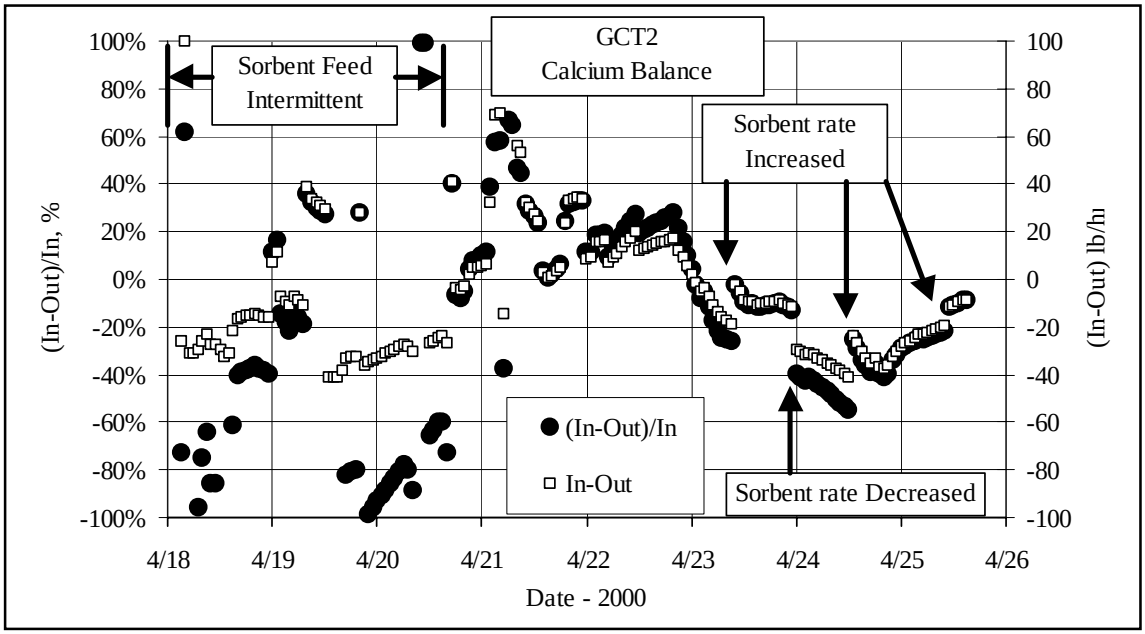

Figure 4.5-11 Calcium Balance

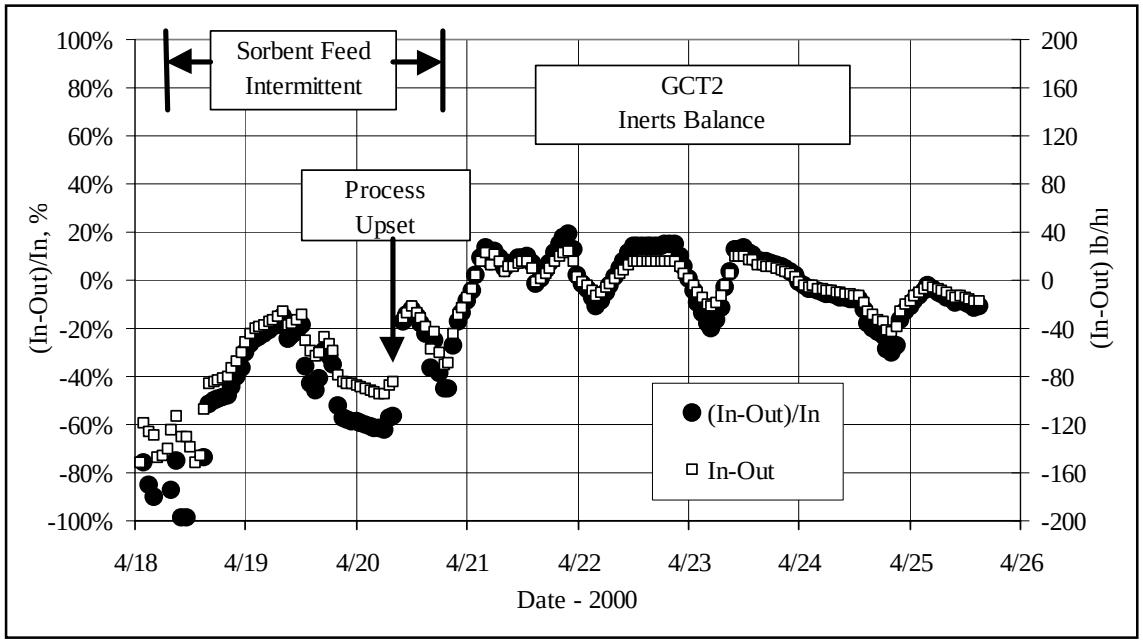

Figure 4.5-12 Inerts Balance

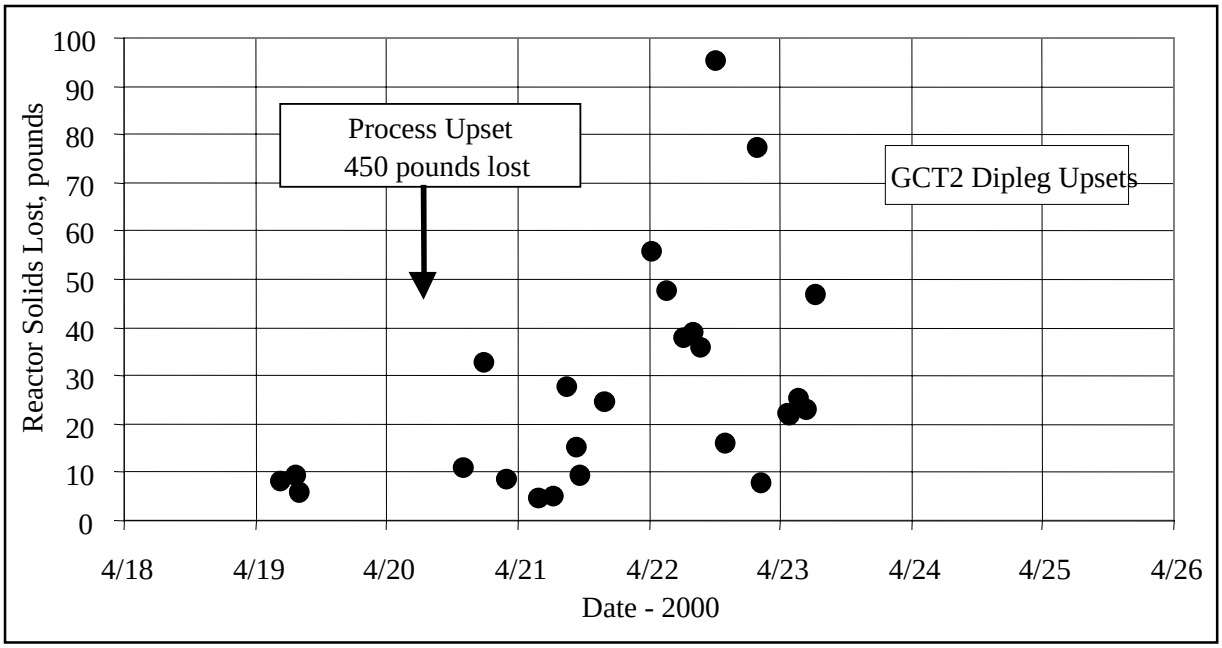

Figure 4.5-13 Dipleg Upsets

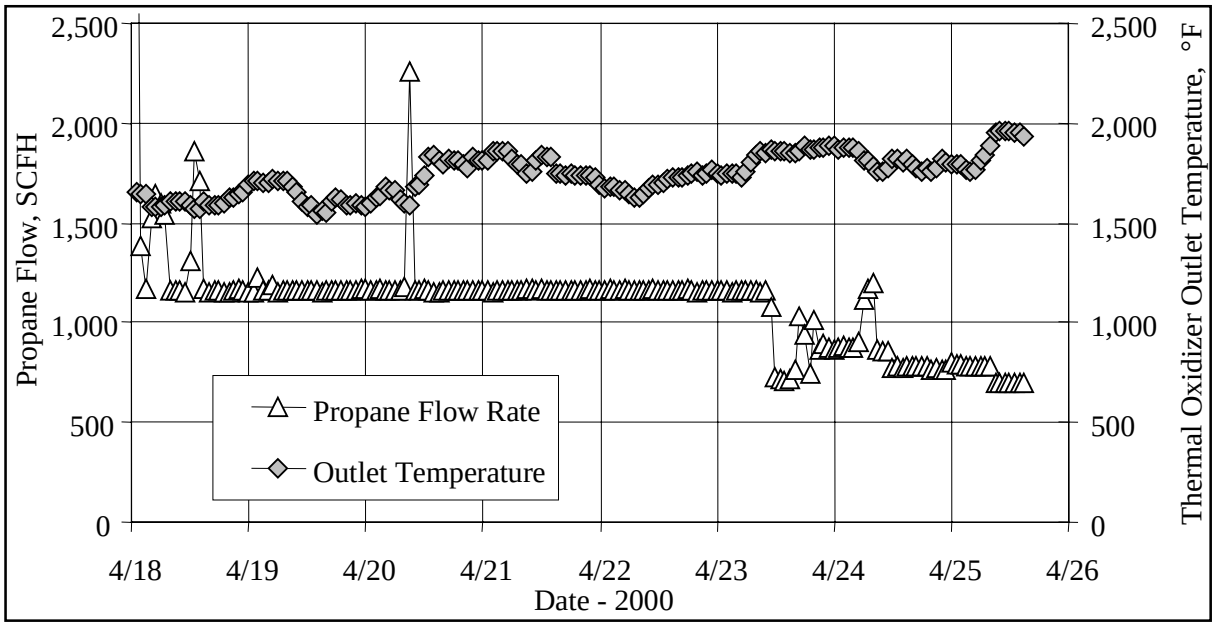

Figure 4.5-14 Thermal Oxidizer Propane Flow and Exit Temperature

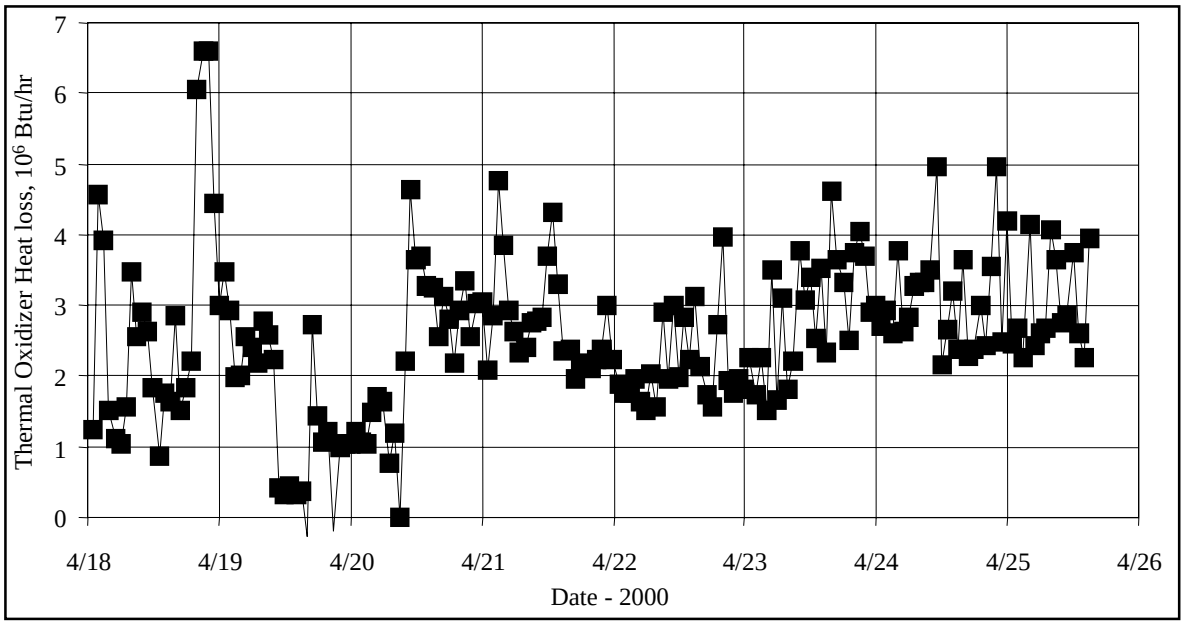

Figure 4.5-15 Thermal Oxidizer Heat Loss

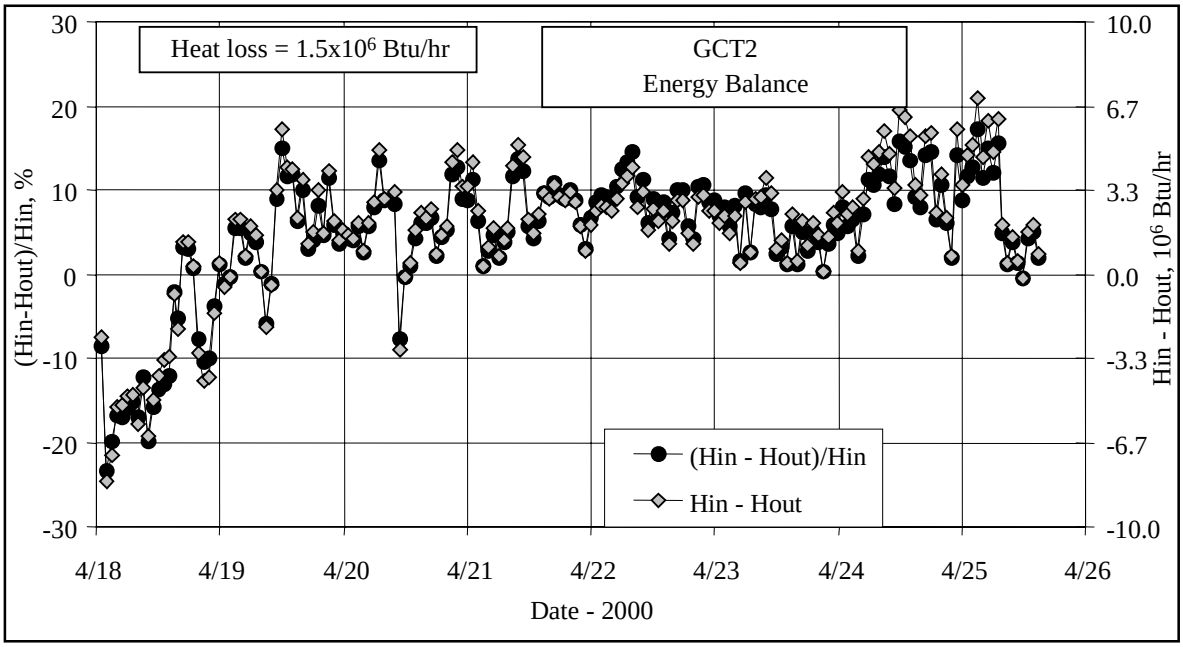

Figure 4.5-16 Energy Balance

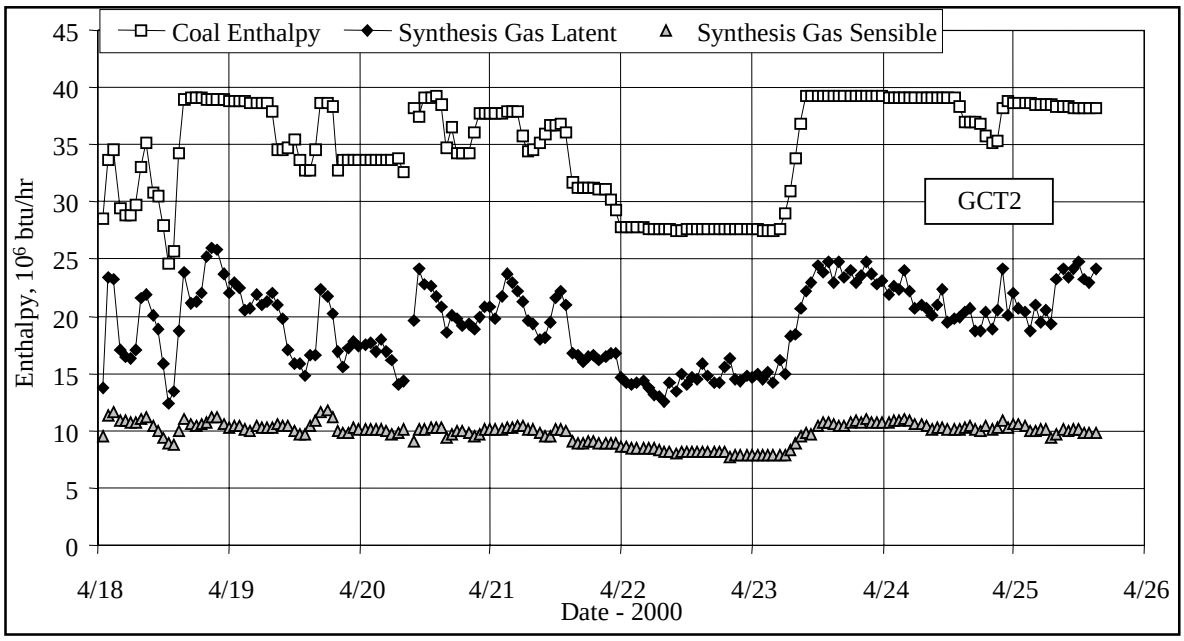

Figure 4.5-17 Coal and Synthesis Gas Enthalpies

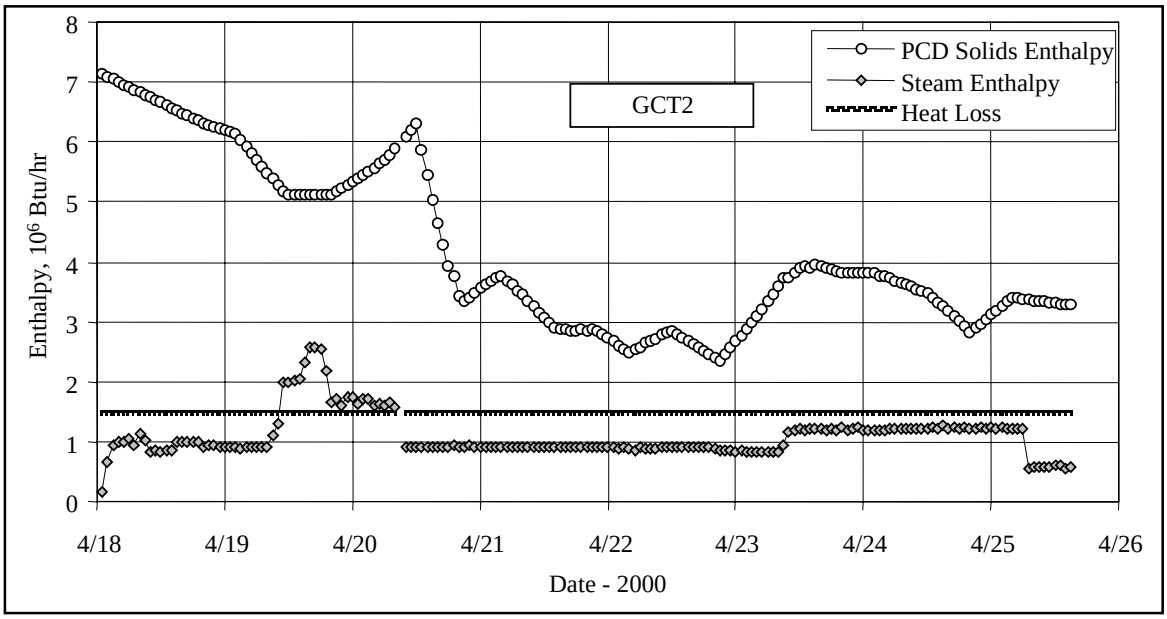

Figure 4.5-18 PCD Solids and Steam Enthalpies

4.6 GCT2 SULFATOR OPERATIONS

During GCT1 the sulfator experienced lower than expected bed temperatures due to oversized steam-superheating coils used for bed cooling. Between GCT1A and GCT1B about 35 percent of the surface area of the coils were removed. This improved the bed temperature from an average of about 1,100 to about 1,400°F. The design bed temperature is 1,600°F. To increase bed temperatures further, the superheated steam-exit temperature was raised from 700 to 900°F for GCT2. During two steady-state periods under partial load the bed temperature increased to 1,500 to 1,600°F (acceptable for char combustion).

The increase in superheated-steam temperature reduced the range of steam consumption from 23,000 to 27,000 pph in GCT1 to 10,000 to 14,000 pph during GCT2. The steam flow during GCT1 was higher at times than the saturated steam generation in the transport reactor and thermal oxidizer, resulting in decreasing steam-drum pressures. The lower steam-flow rates allowed the steam-drum-pressure control to operate normally. The lower steam-flow rates also lowered the heat duty of the superheating coils from 4.5 to 5.0 MBtu/hr to 2 to 3 MBtu/hr.

The sulfator bed continues to show signs of not being well mixed, although for the first few days of operation the bed temperature profile showed the bed to be well mixed. On April 18 the value of TI370, the lowest thermocouple in the sulfator, began to drop below the bulk bed temperature. It became much less responsive to changes in operating temperature and was about 600°F below the other bed temperatures. Two days later TI568 and TI567, the next two lowest thermocouples in the sulfator, began to show the same pattern.

Prior to GCT2 the sulfator heat recovery boiler-gas exit was changed from a side exit to a bottom exit to prevent the solids buildup in the cone of the heat exchanger. During GCT1 solids settled in the cone and blocked most heat exchanger tubes, resulting in high gas-exit temperatures. A post-GCT2 run inspection showed that the modification eliminated the solids buildup problem although a few tubes were still blocked with loose ash. The gas-exit temperature was also acceptable, remaining in the 500 to 550°F range for most of the run. There were a few instances early in the run in which the gas-exit temperature approached 800°F. The design gas exit temperature is 490°F. The higher temperatures are attributed to higher-than-design gas flows through the heat exchanger.

After the end of GCT2 the sulfator refractory was visually inspected. The inspection found a worsening of the refractory damage seen after GCT1 (see Figure 4.6-1). After only a few hundred hours of operation much of the refractory in the lower third of the sulfator was badly cracked. Large sections of refractory have come loose and fallen to the bottom of the sulfator. The lower 10 feet of refractory is to be completely replaced during the outage before GCT3.

Three other modifications will be made to the sulfator prior to GCT3. First, the steam-flow control valve is being moved downstream of the sulfator so that superheated steam from the sulfator can be used in the transport gasifier. Second, provision is being made to supplement

the sulfator combustion air with instrument air. This should increase the char capacity of the sulfator by about 20 percent. Third, the motor for the char feed system is being modified to give better control at partial-load conditions. Currently, during times of low-char production, the feed system feeds char to the sulfator at a faster rate than production resulting in unsteady operation as char is fed in batches to the sulfator.

Figure 4.6-1 Sulfator Refractory Damage Following GCT2

4.7 PROCESS GAS COOLERS

Heat transfer calculations were done on the primary gas cooler, HX0202, and the secondary gas cooler, HX0402, to determine if their performance had deteriorated during GCT2 due to tar or other compounds depositing on the tubes.

The primary gas cooler (HX0202) is between the transport reactor cyclone (CY0201) and the Siemens Westinghouse PCD (FL0301). During GCT2 the primary gas cooler was not bypassed and took the full gas flow from the transport reactor. The primary gas cooler is a single-flow heat exchanger with hot gas from the transport reactor flowing through the tubes and with the plant steam system operating on the shell side. The pertinent equations are:

$$Q = UA\Delta T_{LM} \tag{1}$$

$$Q = c_p M(T_1 - T_2) \tag{2}$$

$$\Delta T_{LM} = \frac{(T_1 - t_2) - (T_2 - t_1)}{\ln \frac{(T_1 - t_2)}{(T_2 - t_1)}} \tag{3}$$

Q = Heat transferred, Btu/hour
U = Heat transfer coefficient, Btu/hr/ft^2/°F
A = Heat exchanger area, ft^2
ΔT_{LM} = Log mean temperature difference, °F
c_p = Gas heat capacity, Btu/lb/°F
M = Mass flow of gas through heat exchanger, lb/hr
T_1 = Gas inlet temperature, °F
T_2 = Gas outlet temperature, °F
$t_1 = t_2$ = Steam temperature, °F

Using equations (1) through (3) and the process data, the product of the heat transfer coefficient and the heat exchanger area (UA) can be calculated. The UA for GCT2 is shown in Figure 4.7-1 as hourly averages along with the design UA of 5,200 Btu/hr/°F and the pressure drop across HX0202. The synthesis gas-flow rate was corrected by multiplying the measured-synthesis-gas rate by 1.03 (as explained in Section 4.5). If HX0202 is plugging the UA should decrease and the pressure drop should increase. The UA deterioration is a better indication of heat exchanger plugging during GCT1 because the pressure drop is calculated by the difference of two numbers of about the same size, usually from 150 to 240 psig, resulting in pressure drops of 1 to 2 psi.

The exchanger pressure drop tracked the synthesis gas rate fairly well. The UA slowly decreased from 5,500 to 4,500 Btu/hr/°F during the first 2 days of testing, slightly less than the design value of 5,200 Btu/hr/°F. The pressure drop was essentially constant during the first 2 days at 1.5 to 2.0 psi. The process upset at 09:00 on April 20 increased the exchanger UA to the design

value for about a day, while the process upset decreased the exchanger pressure drop from 1.75 to 0.9 psi. From 12:00 on April 21 to 12:00 on April 22 the exchanger UA decreased from 5,500 to 4,000 Btu/hr/°F and the pressure drop decreased from 1.5 to 1.0 psi. This was the same time period that the coal and air rates were decreased, thus decreasing the synthesis gas rate (see Figures 4.3-2 and 4.5-3). The pressure drop decrease is expected from the decrease in synthesis gas flow through the heat exchanger. Once the coal, air, and synthesis gas rate increased on April 23 the exchanger pressure drop increased to 2 psi, while the heat exchanger UA slightly increased to 4,400 Btu/hr/°F. The last 2 days of operation had the exchanger UA constant at 4,400 Btu/hr/°F, while the pressure tracked the decreasing synthesis gas rate and decreased to 1.5 psi. There appeared to be no clear evidence of exchanger fouling since at no time did the pressure drop increase while UA decreased. Overall, the UA seemed to decrease from 5,000 Btu/hr/°F at the start of the run, while ending the run at 4,400 Btu/hr/°F, which would indicate some plugging.

The GCT1 HX0202 UA was between 2,500 and 4,500 Btu/hr/°F, with the last day of PRB run at 4,500 Btu/hr/°F, which is quite comparable to GCT2 HX0202 operation at 4,000 to 5,000 Btu/hr/°F. The UA in GCT1 deteriorated to 2,500 Btu/hr/°F after the transition to Illinois coal and slowly increased to 3,000 Btu/hr/°F by the end of GCT1. The GCT1 HX0202 pressure drop at 3 to 4 psi was higher than during GCT2. After the GCT1 coal transition the pressure drop was as high as 6 psi and then dropped to 4.5 psi at the end of GCT1. In GCT1, after the coal transition from PRB to Illinois coal, the UA decreased while the pressure drop increased, indicating exchanger plugging.

The secondary gas cooler (HX0402) is a single-flow heat exchanger with hot gas from the PCD flowing through the tubes and with the plant steam system operating on the shell side. Some heat transfer and pressure drop calculations were done around HX0402 to determine if there was any plugging or heat exchanger performance deterioration during GCT2. HX0402 is not part of the combustion gas turbine commercial flow sheet. In the commercial gas turbine flow sheet the hot synthesis gas from the PCD would be sent directly to a combustion gas turbine. HX0402 would be used commercially if the synthesis gas was to be used in a fuel cell or as a chemical plant feedstock.

Using equations (1) through (3) and the process data, the product of the heat transfer coefficient and the heat exchanger area (UA) can be calculated. The UA for the GCT2 testing is shown in Figure 4.7-2 as hourly averages along with the design UA of 13,100 Btu/hr/°F and the pressure drop across HX0402. The synthesis gas-flow rate was corrected by multiplying the measured-synthesis-gas rate by 1.03 (as explained in Section 4.5). If HX0402 is plugging the UA should decrease and the pressure drop should increase.

Both the UA and pressure drop seemed to track to the synthesis gas rate fairly closely. The UA was steady during the first 3 1/2 days of testing (April 18 to 12:00 on April 21) at 14,000 to 17,000 Btu/hr/°F, above the design UA of 13,100 Btu/hr/°F. The pressure drop decreased from 4.0 to 2.5 during the first 2 days of testing, then remained constant from April 20 until 12:00 on April 21 at 2.0 to 2.5 psia. At 12:00 on April 21 both the UA and pressure drop decreased as the synthesis gas rate was decreased due to the lower air rates. The UA quickly

decreased from 16,000 to 13,800 Btu/hr/°F, and slowly decreased to 12,500 Btu/hr/°F until the coal and air rate were increased on April 23. The exchanger pressure drop decreased from 2.5 psi on April 21 to 1.2 on April 23. The increase in coal rate on April 23 increased the UA to 16,500 Btu/hr/°F. On April 24 the UA decreased to 15,500 Btu/hr/°F where it remained until the end of the run. The increase in coal and air rates increased the pressure drop from 1.2 to 2.5 psi. During the remainder of the run the pressure drop slowly decreased to 2.0 psi. There was no evidence of heat exchanger plugging during the run since the UA was essentially the same at the end of the run as at the start and the pressure drop decreased during the run.

The GCT1 test run had HX0402 UAs lower than GCT2 for PRB coal operation at 8,000 to 10,000 Btu/hr/°F, while for Illinois coal operation the UA was comparable to GCT2 at around 12,000 to 14,000 Btu/hr/°F. The pressure drops for GCT1 HX0402 were also comparable with GCT2 with pressure drops of 1 to 2 psi during the PRB operation and most of the Illinois coal operation.

During GCT1 the steam system was operated from 350 to 400 psig while in GCT2 the steam system was operated at from 200 to 275 psig.

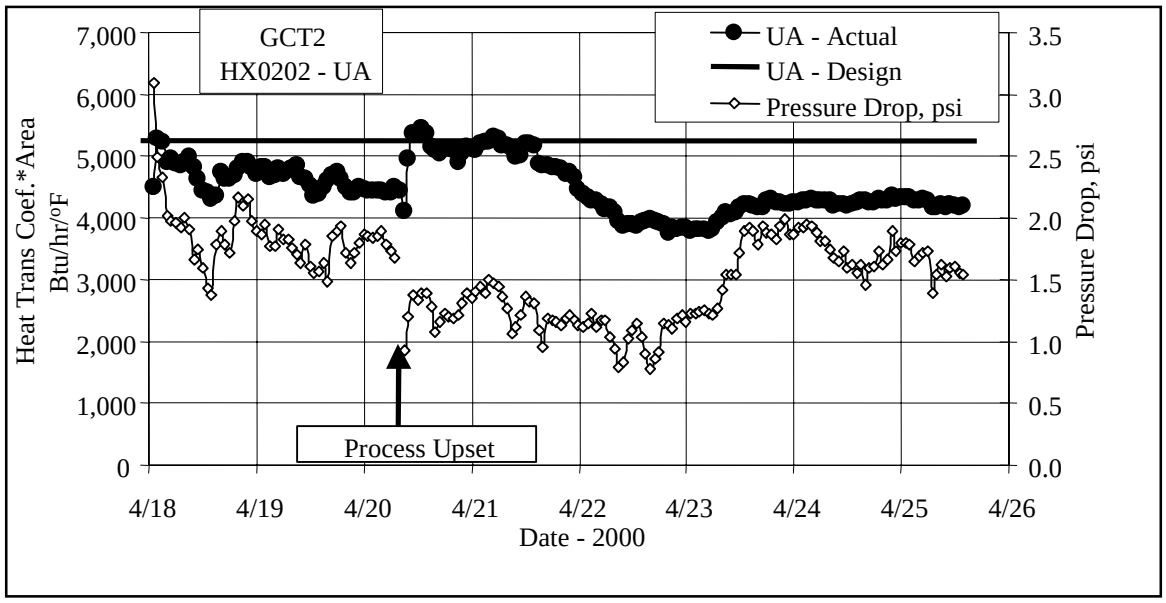

Figure 4.7-1 HX0202 Heat Transfer and Pressure Drop

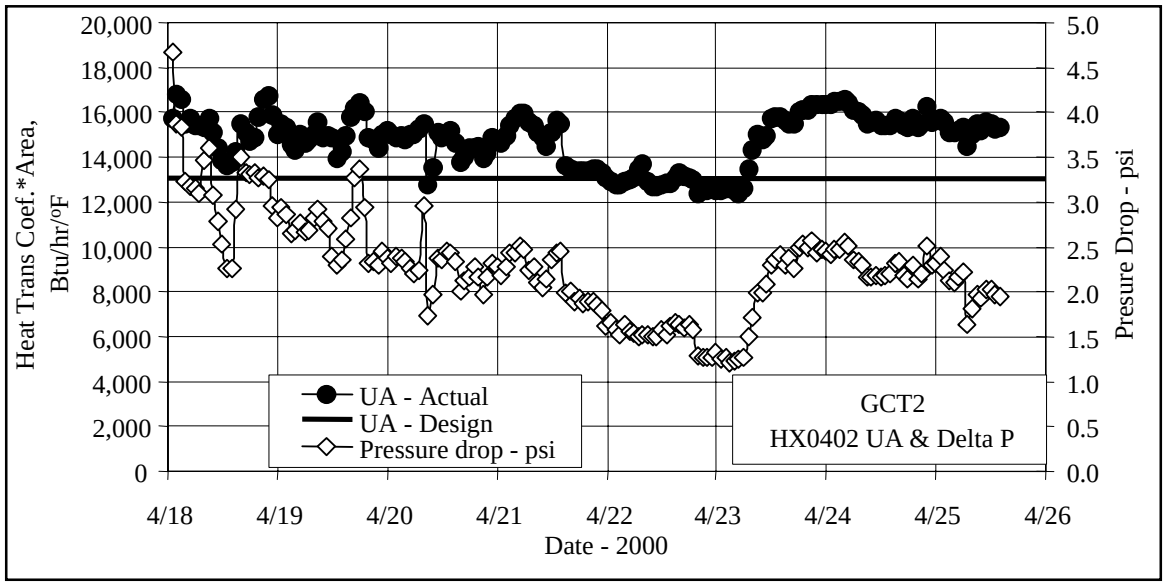

Figure 4.7-2 HX0402 Heat Transfer and Pressure Drop

TERMS

Listing of Abbreviations

AAS	Automated Analytical Solutions
ADEM	Alabama Department of Environmental Management
APC	Alabama Power Company
APFBC	Advance Pressurized Fluidized-Bed Combustion
ASME	American Society of Mechanical Engineers
AW	Application Workstation
BFI	Browning-Ferris Industries
BFW	Boiler Feed Water
BMS	Burner Management System
BOC	BOC Gases
BOP	Balance-of-Plant
BPIR	Ball Pass Inner Race, Frequencies
BPOR	Ball Pass Outer Race, Frequencies
BSF	Ball Spin Frequency
CAD	Computer-Aided Design
CEM	Continuous Emissions Monitor
CFB	Circulating Fluidized Bed
CFR	Code of Federal Regulations
CHE	Combustor Heat Exchanger
COV	Coefficient of Variation (Standard Deviation/Average)
CPC	Combustion Power Compay
CPR	Cardiopulmonary Resuscitation
CTE	Coefficient of Thermal Expansion
DC	Direct Current
DCS	Distributed Control System
DOE	U.S. Department of Energy
E & I	Electrical and Instrumentation
EERC	Energy and Environmental Research Center
EPRI	Electric Power Research Institute
EDX	Energy-Dispersive X-Ray
ESCA	Electron Spectroscopy for Chemical Analysis
FCC	Fluidized Catalytic Cracker
FCP	Flow-Compacted Porosity
FETC	Federal Energy Technology Center
FFG	Flame Front Generator
FI	Flow Indicator
FIC	Flow Indicator Controller
FOAK	First-of-a-Kind
FTF	Fundamental Train Frequency
FW	Foster Wheeler
GBF	Granular Bed Filter
GC	Gas Chromatograph
GEESI	General Electric Environmental Services, Inc.

HP	High Pressure
HRSG	Heat Recovery Steam Generator
HTF	Heat Transfer Fluid
HTHP	High-Temperature, High-Pressure
I/O	Inputs/Outputs
ID	Inside Diameter
IF&P	Industrial Filter & Pump
IGV	Inlet Guide Vanes
IR	Infrared
KBR	Kellogg Brown & Root
LAN	Local Area Network
LIMS	Laboratory Information Management System
LOC	Limiting Oxygen Concentration
LOI	Loss on Ignition
LPG	Liquefied Propane Gas
LSLL	Level Switch, Low Level
MAC	Main Air Compressor
MCC	Motor Control Center
MS	Microsoft Corporation
NDIR	Nondestructive Infrared
NETL	National Energy Technology Laboratory
NFPA	National Fire Protection Association
NOx	Nitrogen Oxides
NPDES	National Pollutant Discharge Elimination System
NPS	Nominal Pipe Size
OD	Outside Diameter
OSHA	Occupational Safety Health Administration
OSI	OSI Software, Inc.
P&IDs	Piping and Instrumentation Diagrams
PC	Pulverized Coal
PCD	Particulate Control Device
PDI	Pressure Differential Indicator
PDT	Pressure Differential Transmitter
PFBC	Pressurized Fluidized-Bed Combustion
PI	Plant Information
PLC	Programmable Logic Controller
PPE	Personal Protection Equipment
PRB	Powder River Basin
PSD	Particle Size Distribution
PSDF	Power Systems Development Facility
ΔP	Pressure Drop
PT	Pressure Transmitter
RFQ	Request for Quotation
RO	Restriction Orifice
RSSE	Reactor Solid Separation Efficiency
RT	Room Temperature
SCS	Southern Company Services, Inc.

SEM	Scanning Electron Microscopy
SMD	Sauter Mean Diameter
SRI	Southern Research Institute
SUB	Start-up Burner
TCLP	Toxicity Characteristic Leaching Procedure
TR	Transport Reactor
TRDU	Transport Reactor Demonstration Unit
TSS	Total Suspended Solids
UBP	Uncompacted Bulk Porosity
UND	University of North Dakota
UPS	Uninterruptible Power Supply
UV	Ultraviolet
VFD	Variable Frequency Drive
VOCs	Volatile Organic Compounds
WPC	William's Patent Crusher
XRD	X-Ray Diffraction
XXS	Extra, Extra Strong

Listing of Units

acfm	actual cubic feet per minute
Btu	British thermal units
°C	degrees celsius or centigrade
°F	degrees fahrenheit
ft	feet
FPS	feet per second
gpm	gallons per minute
g/cm^3	grams per cubic centimeter
g	grams
GPa	gigapascals
hp	horsepower
hr	hour
in.	inches
inWg	inches, water gauge
°K	degrees kelvin
kg	kilograms
kJ	kilojoules
kPa	kilopascals
ksi	thousand pounds per square inch
m	meters
MB	megabytes
mm	millimeters
MPa	megapascals
msi	million pounds per square inch
MW	megawatts
m/s	meters per second
MBtu	Million British thermal units
m^2/g	square meters per gram
μ or μm	microns or micrometers
dp_{50}	particle size distribution at 50 percentile
ppm	parts per million
ppm (v)	parts per million (volume)
ppm (w)	parts per million (weight)
lb	pounds
pph	pounds per hour
psia	pounds per square inch
psig	pounds per square inch gauge
ΔP	pressure drop
rpm	revolutions per minute
s or sec	seconds
scf	standard cubic feet
scfm	standard cubic feet per minute
V	volts
W	watts

APPENDIX – FILTER ELEMENT DATABOOK

Physical, mechanical, and thermal properties of many different types of filter elements have been measured at SRI. For most of the element types, testing has been conducted on as-manufactured elements and on elements from PFBC or PCFBC operation. Test results have been reported as they were generated in several reports to the DOE NETL and the SCS PSDF, references 1 through 5. All of these previously reported results are compiled and presented in this appendix to provide access to the data in a single source. Results are presented for the following types of filter elements:

1. Pall 442T.
2. Pall 326.
3. Pall 181.
4. Schumacher F40.
5. Schumacher TF20 and T10-20.
6. Schumacher N10-20.
7. Industrial Filter and Pump (IF&P) REECER™.
8. Coors P-100A-1.
9. Blasch 4-270.
10. Ensto.
11. Specific Surface.
12. Techniweave N610/mullite.
13. McDermott ceramic composite.
14. Honeywell PRD-66C.
15. 3M oxide-oxide composite.
16. Pall iron aluminide.

A brief description of each material can be found in the following sections, where the results are presented for each element. A table summarizing the properties for each filter is presented on page 3 of this Appendix. In all of the previous reports considerable data analysis was provided to assess how the results relate to performance in the operating environment. No analysis is given in this appendix; results are presented in tabular and graphical formats with no comment.

References

1. Spain, J.D. and Starrett, H.S., "Physical, Mechanical, and Thermal Properties of Schumacher SiC Filter Material," Report Number SRI-MME-94-253-6938.20.1-I-F, Prepared for U.S. DOE/METC under Contract No. DE-AC21-89MC26233, March 1994.

2. Spain, J.D. and Starrett, H.S., "Physical, Mechanical, and Thermal Properties of Refractron SiC Filter Material," Report Number SRI-MME-94-253-6938.20.1-I-F, Prepared for U.S. DOE/METC under Contract No. DE-AC21-89MC26233, May 1994.

3. Spain, J.D. and Starrett, H.S., "Physical, Mechanical, and Thermal Properties of Coors Alumina Mullite Filter Material," Report Number SRI-MME-94-480-6938.20.1-III-F, Prepared for U.S. DOE/METC under Contract No. DE-AC21-89MC26233, August 1994.

4. Technical Progress Report for Kellogg Brown & Root Transport Reactor Train With Siemens Westinghouse Particulate Control Device: TC04 Report: October 14-17, 1998, Section 3.4. Prepared by Southern Company Services, DOE Cooperative Agreement Number DE-FC21-90MC25140.

5. Technical Progress Report for Kellogg Brown & Root Transport Reactor Train With Siemens Westinghouse Particulate Control Device: TC05 Report: January 10-May 2, 1999, Appendix. Prepared by Southern Company Services, DOE Cooperative Agreement Number DE-FC21-90MC25140.

	Pall 442T	Pall 326	Pall 181	Schum. F40	Schum. TF20 and T10-20	Schum. N10-20	IF&P REECER	Coors P-100A-1	Blasch 4-270	Ensto	Specific Surface	AIT N610/ mullite	McDermott	Honeywell PRD-66C	3M Oxide/ Oxide	Pall Fe_3Al
Bulk density (lbm/ft^3)	110	113	113	117	121	123	137	103	111	118	77	108	51	89		245
Hoop tensile strength at RT[1] (psi)	2,450	2,060	2,800	2,280	1,900	2,530	2,040	1,900	500	990	320	3,460	700	830	2530[5]	17,300[6]
Axial tensile strength at RT (psi)	2,000	1,300	2,570	1,120	900		2,120	2,480	270	920		5,450[4]	600	290		19,000[6]
Axial Young's Modulus at RT (10^6 psi)	6.0	5.7	6.0	5.9	4.0		14	4.3	0.90	2.3		6.2	0.45	0.35		5.2
Axial tensile strain-to-failure at RT (mils/in.)	0.35	0.24	0.45	0.21	0.22		0.16	0.62	0.37	0.50		0.84[4]	2.1	1.5		9.5
Axial tensile strength at 1,500°F (psi)	1,750	2,200	2,060	1,360	1,200		1,980	2,390		900						6,300[6,7]
Axial Young's Modulus at 1,500°F (10^6 psi)	4.4	2.8	5.0	3.9	2.3		18	2.5		2.3						3.6[7]
Axial tensile strain-to-failure at 1,500°F (mils/in)	0.46	1.4	0.47	0.41	0.40		0.10	1.0		0.40						14.8[7]
Axial compressive strength at RT (psi)	12,100			9,540				17,200				2650	580		3180[5]	
Axial compressive strain-to-failure at RT (mils/in.)	2.1			1.7				4.4				0.53	2.3		3.4	
Axial CTE[2], 500 to 1,500°F (10^{-6} in./in.-°F)	2.6	2.8	2.8	2.5	2.6	2.5	2.4	2.8	4.1	3.9	1.0	4.7	4.6	2.2		13.1
Radial thermal conductivity at 1,000°F (Btu-in./hr-ft^2-°F)	38	38	32	38	52	28	120	10	5.2	6.0	3.8	2.3	1.6	3.4		
Pressure drop at 5 ft/min face velocity[3] (inH_2O)	0.6	1.3			2.1 TF20 4.4 T10-20		1.5	3.3	7.7				1.7	0.9	1.1	4.1

1.) RT = Room temperature. 2.) CTE = Coefficient of thermal expansion. 3.) Using air at ambient conditions. 4.) Only one value. 5.) Stress calculations were based on measured specimen I.D. values and a nominal thickness of the inside structural wall of 0.055 in. The stress calculations assume that all load was carried by the inside structural wall. 6.) Ultimate strength shown; yielding occurred at lower stress level. 7.) Results at 1,400°F for Pall Fe_3Al.

PROPERTIES OF FILTER ELEMENTS

1.0 PALL 442T

Pall 442T is a clay-bonded SiC particle material. The microstructure consists of individual SiC particles or clusters of SiC particles connected by clay or glass bridges. The elements have a structural wall with a nominal I.D. of 1.575 in. (40 mm) and a nominal wall thickness of 0.40 in. (10 mm). Mechanical and thermal properties of the elements are controlled by the structural wall and a relatively thin membrane layer applied to the outside surface provides filtration. Probable values of selected properties of virgin Pall 442T are as follows:

Bulk Density (lbm/ft^3)	110
Hoop Tensile Strength at Room Temperature (psi)	2,450
Axial Tensile Strength at Room Temperature (psi)	2,000
Axial Young's Modulus at Room Temperature (10^6 psi)	6.0
Axial Tensile Strain-to-Failure at Room Temperature (mils/in.)	0.35
Axial Tensile Strength at 1,500°F (psi)	1,750
Axial Young's Modulus at 1,500°F (10^6 psi)	4.4
Axial Tensile Strain-to-Failure at 1,500°F (mils/in.)	0.46
Axial Compressive Strength at Room Temperature (psi)	12,100
Axial Compressive Strain-to-Failure at Room Temperature (mils/in.)	2.1
Axial Coefficient of Thermal Expansion, 500 to 1,500°F (10^{-6} in./in./°F)	2.6
Radial Thermal Conductivity at 1,000°F (Btu-in./hr-ft^2-°F)	38
Pressure Drop at 5 ft/min Face Velocity, Air at Ambient Conditions(inWG)	0.6

Table 1-1 (Page 1 of 4)

Density of Pall 442T

Candle	Specimen Number	Hours in Operation	I.D. (in.)	O.D. (in.)	Density (gr/cm³)	Density (lb/ft³)	Remarks
1-94	Tn-hoop-6	virgin	1.56	2.33	1.77	110	
1-94	Tn-hoop-7	virgin	1.55	2.33	1.76	110	
1-94	Tn-hoop-8	virgin	1.55	2.32	1.77	111	
1-94	Tn-hoop-9	virgin	1.56	2.33	1.78	111	
1-94	Tn-hoop-10	virgin	1.56	2.33	1.76	110	
1-94	Tn-hoop-11	virgin	1.56	2.33	1.76	110	
1-94	Tn-hoop-12	virgin	1.57	2.32	1.77	110	
1-94	Tn-hoop-13	virgin	1.56	2.32	1.77	110	
1-94	Tn-hoop-14	virgin	1.57	2.32	1.78	111	
1-94	Tn-hoop-15	virgin	1.56	2.32	1.76	110	
1-94	Tn-hoop-16	virgin	1.56	2.32	1.76	110	
1-94	Tn-hoop-17	virgin	1.60	2.35	1.77	110	
		Average			1.77	110	
		Standard Deviation			0.01	0.39	
		Coefficient of Variation (COV)			0.35%	0.35%	
6-93	Tn-hoop-18	virgin	1.52	2.35	1.79	112	
6-93	Tn-hoop-19	virgin	1.53	2.35	1.79	112	
6-93	Tn-hoop-20	virgin	1.53	2.35	1.78	111	
6-93	Tn-hoop-21	virgin	1.53	2.34	1.79	111	
6-93	Tn-hoop-22	virgin	1.53	2.34	1.76	110	
6-93	Tn-hoop-23	virgin	1.53	2.34	1.78	111	
6-93	Tn-hoop-24	virgin	1.53	2.34	1.78	111	
6-93	Tn-hoop-25	virgin	1.53	2.34	1.78	111	
6-93	Tn-hoop-26	virgin	1.53	2.34	1.78	111	
6-93	Tn-hoop-27	virgin	1.53	2.34	1.78	111	
6-93	Tn-hoop-28	virgin	1.53	2.34	1.78	111	
6-93	Tn-hoop-29	virgin	1.54	2.33	1.79	112	
6-93	Tn-hoop-30	virgin	1.54	2.33	1.78	111	
6-93	Tn-hoop-58	virgin	1.54	2.33	1.78	111	
		Average			1.78	111	
		Standard Deviation			0.01	0.48	
		Coefficient of Variation (COV)			0.43%	0.43%	

Table 1-1 (Page 2 of 4)

Density of Pall 442T

Candle	Specimen Number	Hours in Operation	I.D. (in.)	O.D. (in.)	Density (gr/cm^3)	Density (lb/ft^3)	Remarks
8-95	Tn-hoop-31	virgin	1.54	2.36	1.74	109	
8-95	Tn-hoop-33	virgin	1.55	2.36	1.75	109	
8-95	Tn-hoop-34	virgin	1.56	2.36	1.75	109	
8-95	Tn-hoop-35	virgin	1.55	2.36	1.75	109	
8-95	Tn-hoop-36	virgin	1.54	2.35	1.76	110	
8-95	Tn-hoop-37	virgin	1.54	2.35	1.76	110	
8-95	Tn-hoop-38	virgin	1.54	2.35	1.76	110	
8-95	Tn-hoop-39	virgin	1.54	2.35	1.76	110	
8-95	Tn-hoop-40	virgin	1.54	2.35	1.76	110	
8-95	Tn-hoop-41	virgin	1.54	2.34	1.75	109	
8-95	Tn-hoop-42	virgin	1.54	2.34	1.76	110	
8-95	Tn-hoop-43	virgin	1.54	2.33	1.76	110	
8-95	Tn-hoop-44	virgin	1.56	2.33	1.75	109	
8-95	Tn-hoop-45	virgin	1.57	2.32	1.75	109	
		Average			1.75	109	
		Standard Deviation			0.01	0.35	
		Coefficient of Variation (COV)			0.29%	0.32%	
9-93	Tn-hoop-46	virgin	1.52	2.34	1.78	111	
9-93	Tn-hoop-47	virgin	1.53	2.34	1.79	112	
9-93	Tn-hoop-48	virgin	1.53	2.33	1.79	112	
9-93	Tn-hoop-49	virgin	1.53	2.33	1.79	112	
9-93	Tn-hoop-50	virgin	1.53	2.33	1.79	112	
9-93	Tn-hoop-51	virgin	1.53	2.33	1.78	111	
9-93	Tn-hoop-52	virgin	1.53	2.33	1.78	111	
9-93	Tn-hoop-53	virgin	1.53	2.33	1.78	111	
9-93	Tn-hoop-54	virgin	1.53	2.33	1.78	111	
9-93	Tn-hoop-55	virgin	1.53	2.33	1.78	111	
9-93	Tn-hoop-56	virgin	1.54	2.33	1.78	111	
9-93	Tn-hoop-57	virgin	1.54	2.32	1.77	110	
		Average			1.78	111	
		Standard Deviation			0.01	0.42	
		Coefficient of Variation (COV)			0.38%	0.38%	

Table 1-1 (Page 3 of 4)

Density of Pall 442T

Candle	Specimen Number	Hours in Operation	I.D. (in.)	O.D. (in.)	Density (gr/cm³)	Density (lb/ft³)	Remarks
R1-0077	Tn-Hoop-1	227	1.52	2.34	1.83	114	See Notes 1,2
R1-0077	Tn-Hoop-2	227	1.52	2.34	1.84	115	See Notes 1,2
R1-0077	Tn-Hoop-3	227	1.52	2.34	1.88	117	See Notes 1,2
R1-0077	Tn-Hoop-4	227	1.52	2.34	1.88	117	See Notes 1,2
R1-0077	Tn-Hoop-5	227	1.53	2.34	1.86	116	See Notes 1,2
R1-0077	Tn-Hoop-6	227	1.54	2.34	1.86	116	See Notes 1,2
R1-0077	Tn-Hoop-7	227	1.53	2.34	1.86	116	See Notes 1,2
R1-0077	Tn-Hoop-8	227	1.54	2.35	1.84	115	See Notes 1,2
R1-0077	Tn-Hoop-9	227	1.54	2.34	1.85	115	See Notes 1,2
R1-0077	Tn-Hoop-10	227	1.54	2.34	1.84	115	See Notes 1,2
		Average			1.85	116	
		Standard Deviation			0.02	0.99	
		Coefficient of Variation (COV)			0.86%	0.86%	
1A-4	Tn-Hoop-28	616	1.55	2.37	1.84	115	See Notes 1,3
1A-4	Tn-Hoop-29	616	1.53	2.35	1.84	115	See Notes 1,3
1A-4	Tn-Hoop-30	616	1.53	2.36	1.84	115	See Notes 1,3
1A-4	Tn-Hoop-31	616	1.55	2.37	1.85	116	See Notes 1,3
1A-4	Tn-Hoop-32	616	1.55	2.37	1.85	115	See Notes 1,3
1A-4	Tn-Hoop-33	616	1.56	2.37	1.85	116	See Notes 1,3
1A-4	Tn-Hoop-34	616	1.58	2.36	1.85	116	See Notes 1,3
1A-4	Tn-Hoop-35	616	1.58	2.36	1.85	116	See Notes 1,3
1A-4	Tn-Hoop-36	616	1.58	2.36	1.86	116	See Notes 1,3
		Average			1.85	115	
		Standard Deviation			0.01	0.38	
		Coefficient of Variation (COV)			0.33%	0.33%	

Table 1-1(Page 4 of 4)

Density of Pall 442T

Candle	Specimen Number	Hours in Operation	I.D. (in.)	O.D. (in.)	Density (gr/cm³)	Density (lb/ft³)	Remarks
5-948	Tn-Hoop-37	1438	1.52	2.35	1.88	117	See Notes 1,3
5-948	Tn-Hoop-38	1438	1.53	2.35	1.88	117	See Notes 1,3
5-948	Tn-Hoop-39	1438	1.53	2.35	1.89	118	See Notes 1,3
5-948	Tn-Hoop-40	1438	1.55	2.36	1.89	118	See Notes 1,3
5-948	Tn-Hoop-41	1438	1.55	2.36	1.89	118	See Notes 1,3
5-948	Tn-Hoop-42a	1438	1.55	2.36	1.89	118	See Notes 1,3
5-948	Tn-Hoop-42b	1438	1.55	2.36	1.89	118	See Notes 1,3
5-948	Tn-Hoop-43	1438	1.57	2.36	1.89	118	See Notes 1,3
5-948	Tn-Hoop-44	1438	1.57	2.35	1.89	118	See Notes 1,3
5-948	Tn-Hoop-45	1438	1.59	2.35	1.92	120	See Notes 1,3
		Average			1.89	118	
		Standard Deviation			0.01	0.63	
		Coefficient of Variation (COV)			0.53%	0.53%	
2-1018	Tn-Hoop-46	1867	1.52	2.36	1.84	115	See Notes 1,3
2-1018	Tn-Hoop-47	1867	1.52	2.36	1.84	115	See Notes 1,3
2-1018	Tn-Hoop-48	1867	1.52	2.36	1.84	115	See Notes 1,3
2-1018	Tn-Hoop-49	1867	1.55	2.37	1.83	114	See Notes 1,3
2-1018	Tn-Hoop-50	1867	1.55	2.37	1.83	114	See Notes 1,3
2-1018	Tn-Hoop-51	1867	1.55	2.37	1.82	114	See Notes 1,3
2-1018	Tn-Hoop-52	1867	1.57	2.36	1.82	114	See Notes 1,3
2-1018	Tn-Hoop-53	1867	1.59	2.37	1.81	113	See Notes 1,3
2-1018	Tn-Hoop-54	1867	1.56	2.34	1.83	114	See Notes 1,3
		Average			1.83	114	
		Standard Deviation			0.01	0.60	
		Coefficient of Variation (COV)			0.53%	0.53%	

Notes:

1. Elements were water washed before density measurements but some ash remained in the pores. Density values were calculated based on weights measured with ash in the pores and, therefore, do not represent a material property. The values are for comparison only.
2. All operation in the Siemens Westinghouse advanced particulate filtration system at the Foster Wheeler PCFBC test facility in Karhula, Finland. Nominal-operating temperature unknown.
3. All operation at the SCS PSDF in combustion mode at a nominal-operating temperature of 1,400°F.

Table 1-2

Axial Tensile Properties of Virgin Pall 442T

Candle Identification	Specimen Number	Temperature (°F)	Ultimate Strength (psi)	Young's Modulus (Msi)	Strain-to-Failure (mils/in.)	Remarks
1-94	Tn-ax-1	70	1680	6.63	0.26	
1-94	Tn-ax-6	70	2000	5.38	0.38	
1-94	Tn-ax-8	70	2120	6.22	0.35	
1-94	Tn-ax-15	70	2150	5.68	0.40	
1-94	Tn-ax-21	70	2080	6.10	0.35	
Average			2006	6.00	0.35	
Standard Deviation			171	0.4	0.05	
Coefficient of Variation (COV)			9%	7%	14%	
1-94	Tn-ax-4	1500	1910	4.42	0.50	
1-94	Tn-ax-9	1500	1810	4.88	0.46	
1-94	Tn-ax-17	1500	1900	4.85	0.45	
1-94	Tn-ax-20	1500	1760	4.07	0.46	
1-94	Tn-ax-23	1500	1330	3.58	0.41	
Average			1742	4.36	0.46	
Standard Deviation			213	0.5	0.03	
Coefficient of Variation (COV)			12%	11%	6%	
1-94	Tn-ax-3	1600	1530	2.24	0.75	
1-94	Tn-ax-10	1600	1510	3.12	0.67	
1-94	Tn-ax-18	1600	1580	2.71	0.64	
1-94	Tn-ax-22	1600	1640	2.56	0.81	
1-94	Tn-ax-26	1600	900	2.18	0.42	
Average			1432	2.56	0.66	
Standard Deviation			270	0.3	0.13	
Coefficient of Variation (COV)			19%	13%	20%	
1-94	Tn-ax-2	1700	1440	1.19	2.05	
1-94	Tn-ax-5	1700	1340	1.49	1.20	
1-94	Tn-ax-7	1700	1560	1.22	2.48	
1-94	Tn-ax-12	1700	1520	1.44	2.00	
1-94	Tn-ax-19	1700	1300	1.66	1.51	
Average			1432	1.40	1.85	
Standard Deviation			100	0.2	0.45	
Coefficient of Variation (COV)			7%	13%	24%	

Table 1-3

Room Temperature Axial Tensile Properties of Pall 442T
Virgin and After Combustion Operation

Candle Identification	Specimen Number	Hours in Operation	Ultimate Strength (psi)	Young's Modulus (Msi)	Strain-to-Failure (mils/in.)	Remarks
1-94	Tn-ax-1	Virgin	1680	6.63	0.26	
1-94	Tn-ax-6	Virgin	2000	5.38	0.38	
1-94	Tn-ax-8	Virgin	2120	6.22	0.35	
1-94	Tn-ax-15	Virgin	2150	5.68	0.40	
1-94	Tn-ax-21	Virgin	2080	6.10	0.35	
Average			2006	6.00	0.35	
Standard Deviation			171	0.43	0.05	
Coefficient of Variation (COV)			9%	7%	14%	
R1-0077	Tn-ax-2	227	1130	5.26	0.28	See Note 1
R1-0077	Tn-ax-4	227	1030	9.40	0.11	See Note 1
R1-0077	Tn-ax-10	227	1380	4.93	0.34	See Note 1
Average			1180	6.53	0.24	
1A-4	Tn-ax-11	616	2470	7.34	0.36	See Note 2
1A-4	Tn-ax-12	616	2170	7.84	0.27	See Note 2
1A-4	Tn-ax-13	616	2270	7.17	0.32	See Note 2
1A-4	Tn-ax-14	616	2340	6.45	0.36	See Note 2
1A-4	Tn-ax-15	616	2220	6.81	0.34	See Note 2
Average			2294	7.12	0.33	
Standard Deviation			104	0.5	0.03	
Coefficient of Variation (COV)			5%	7%	10%	
2-1018	Tn-ax-16	1867	1880	6.35	0.29	See Note 2
2-1018	Tn-ax-17	1867	2390	6.64	0.36	See Note 2
2-1018	Tn-ax-18	1867	2250	6.25	0.36	See Note 2
2-1018	Tn-ax-19	1867	2160	6.61	0.32	See Note 2
Average			2170	6.46	0.33	
Standard Deviation			186	0.2	0.03	
Coefficient of Variation (COV)			9%	3%	9%	

Notes:
1. All operation in the Siemens Westinghouse advanced particulate filtration system at the Foster Wheeler PCFBC test facility in Karhula, Finland. Nominal-operating temperature unknown.
2. All operation at the SCS PSDF in combustion mode at a nominal-operating temperature of 1,400°F.

Table 1-4

Room and Elevated Temperature Axial Tensile Properties of Pall 442T After Combustion Operation

Candle Identification	Specimen Number	Hours in Operation	Test Temperature (°F)	Ultimate Strength (psi)	Young's Modulus (Msi)	Strain-to-Failure (mils/in.)	Remarks
R1-0077	Tn-ax-2	227	70	1130	5.26	0.28	See Note 1
R1-0077	Tn-ax-4	227	70	1030	9.40	0.11	See Note 1
R1-0077	Tn-ax-10	227	70	1380	4.93	0.34	See Note 1
Average				1180	6.53	0.24	
R1-0077	Tn-ax-3	227	1600	1320	1.69	1.29	See Note 1
R1-0077	Tn-ax-6	227	1600	1210	1.88	1.18	See Note 1
R1-0077	Tn-ax-7	227	1600	1100	3.22	0.59	See Note 1
Average				1210	2.26	1.02	
R1-0077	Tn-ax-1	227	1700	1300	0.95	4.16	See Note 1
R1-0077	Tn-ax-2	227	1700	1290	1.12	2.94	See Note 1
R1-0077	Tn-ax-5	227	1700	790	1.41	1.96	See Note 1
R1-0077	Tn-ax-9	227	1700	1120	0.78	3.41	See Note 1
Average				1125	1.07	3.12	

Notes:

1. All operation in the Siemens Westinghouse advanced particulate filtration system at the Foster Wheeler PCFBC test facility in Karhula, Finland. Nominal-operating temperature unknown.

Table 1-5 (Page 1 of 3)

Room Temperature Hoop Tensile Strength for Pall 442T

Element	Specimen Number	Hours in Operation	Maximum Hydrostatic Pressure (psig)	Ultimate Strength (psi)	Remarks
1-94	Tn-hoop-1	Virgin	970	2360	
1-94	Tn-hoop-2	Virgin	920	2230	
1-94	Tn-hoop-3	Virgin	1020	2530	
1-94	Tn-hoop-4	Virgin	950	2390	
1-94	Tn-hoop-5	Virgin	550	1320	
1-94	Tn-hoop-7	Virgin	870	2266	
1-94	Tn-hoop-8	Virgin	930	2420	
1-94	Tn-hoop-9	Virgin	700	1820	
1-94	Tn-hoop-10	Virgin	840	2200	
1-94	Tn-hoop-11	Virgin	940	2450	
1-94	Tn-hoop-12	Virgin	970	2540	
1-94	Tn-hoop-13	Virgin	970	2590	
1-94	Tn-hoop-14	Virgin	990	2630	
1-94	Tn-hoop-15	Virgin	830	2190	
1-94	Tn-hoop-16	Virgin	970	2580	
1-94	Tn-hoop-17	Virgin	960	2590	
Average			899	2319	
Standard Deviation			118	329	
Coefficient of Variation (COV)			13%	14%	
6-93	Tn-hoop-18	Virgin	1000	2440	
6-93	Tn-hoop-19	Virgin	1080	2650	
6-93	Tn-hoop-21	Virgin	1060	2610	
6-93	Tn-hoop-22	Virgin	1040	2550	
6-93	Tn-hoop-23	Virgin	1050	2580	
6-93	Tn-hoop-24	Virgin	1020	2540	
6-93	Tn-hoop-26	Virgin	870	2160	
6-93	Tn-hoop-27	Virgin	1050	2620	
6-93	Tn-hoop-29	Virgin	1000	2530	
6-93	Tn-hoop-30	Virgin	1020	2580	
6-93	Tn-hoop-58	Virgin	960	2450	
Average			1014	2519	
Standard Deviation			55	130	
Coefficient of Variation (COV)			5%	5%	

Table 1-5 (Page 2 of 3)
Room Temperature Hoop Tensile Strength for Pall 442T

Candle	Specimen Number	Hours in Operation	Maximum Hydrostatic Pressure (psig)	Ultimate Strength (psi)	Remarks
8-95	Tn-hoop-33	Virgin	930	2330	
8-95	Tn-hoop-34	Virgin	850	2140	
8-95	Tn-hoop-35	Virgin	900	2270	
8-95	Tn-hoop-36	Virgin	1040	2600	
8-95	Tn-hoop-37	Virgin	1010	2530	
8-95	Tn-hoop-38	Virgin	970	2410	
8-95	Tn-hoop-39	Virgin	1070	2680	
8-95	Tn-hoop-40	Virgin	1070	2680	
8-95	Tn-hoop-41	Virgin	1020	2560	
8-95	Tn-hoop-42	Virgin	1090	2740	
8-95	Tn-hoop-43	Virgin	1070	2730	
8-95	Tn-hoop-45	Virgin	890	2410	
Average			993	2507	
Standard Deviation			79	186	
Coefficient of Variation (COV)			8%	7%	
9-93	Tn-hoop-46	Virgin	900	2240	
9-93	Tn-hoop-47	Virgin	1020	2510	
9-93	Tn-hoop-48	Virgin	980	2420	
9-93	Tn-hoop-49	Virgin	1080	2690	
9-93	Tn-hoop-50	Virgin	1090	2730	
9-93	Tn-hoop-51	Virgin	980	2460	
9-93	Tn-hoop-52	Virgin	1050	2620	
9-93	Tn-hoop-54	Virgin	990	2500	
9-93	Tn-hoop-55	Virgin	950	2410	
9-93	Tn-hoop-57	Virgin	930	2380	
Average			997	2496	
Standard Deviation			60	142	
Coefficient of Variation (COV)			6%	6%	
R1-0077	Tn-Hoop-1	227	590	1460	See Note 1
R1-0077	Tn-Hoop-2	227	590	1450	See Note 1
R1-0077	Tn-Hoop-3	227	690	1700	See Note 1
R1-0077	Tn-Hoop-4	227	570	1420	See Note 1
R1-0077	Tn-Hoop-5	227	620	1550	See Note 1
R1-0077	Tn-Hoop-6	227	620	1560	See Note 1
R1-0077	Tn-Hoop-7	227	630	1580	See Note 1
R1-0077	Tn-Hoop-8	227	590	1470	See Note 1
R1-0077	Tn-Hoop-9	227	620	1560	See Note 1
R1-0077	Tn-Hoop-10	227	700	1750	See Note 1
Average			622	1550	
Standard Deviation			41	102	
Coefficient of Variation (COV)			7%	7%	

Table 1-5 (Page 3 of 3)
Room Temperature Hoop Tensile Strength for Pall 442T

Candle	Specimen Number	Hours in Operation	Maximum Hydrostatic Pressure (psig)	Ultimate Strength (psi)	Remarks
1A-4	Tn-Hoop-28	616	930	2313	See Note 2
1A-4	Tn-Hoop-29	616	920	2257	See Note 2
1A-4	Tn-Hoop-30	616	890	2199	See Note 2
1A-4	Tn-Hoop-31	616	890	2233	See Note 2
1A-4	Tn-Hoop-32	616	890	2262	See Note 2
1A-4	Tn-Hoop-33	616	870	2206	See Note 2
1A-4	Tn-Hoop-34	616	880	2296	See Note 2
1A-4	Tn-Hoop-35	616	910	2363	See Note 2
1A-4	Tn-Hoop-36	616	920	2406	See Note 2
Average			900	2282	
Standard Deviation			19	66	
Coefficient of Variation (COV)			2%	3%	
5-948	Tn-Hoop-37	1438	1060	2607	See Note 2
5-948	Tn-Hoop-38	1438	1010	2466	See Note 2
5-948	Tn-Hoop-39	1438	1100	2766	See Note 2
5-948	Tn-Hoop-40	1438	1100	2759	See Note 2
5-948	Tn-Hoop-41	1438	1110	2795	See Note 2
5-948	Tn-Hoop-42a	1438	1100	2769	See Note 2
5-948	Tn-Hoop-42b	1438	1050	2646	See Note 2
5-948	Tn-Hoop-43	1438	1000	2604	See Note 2
5-948	Tn-Hoop-44	1438	1120	2916	See Note 2
5-948	Tn-Hoop-45	1438	1130	3021	See Note 2
Average			1078	2735	
Standard Deviation			43	153	
Coefficient of Variation (COV)			4%	6%	
2-1018	Tn-Hoop-46	1867	890	2159	See Note 2
2-1018	Tn-Hoop-47	1867	890	2157	See Note 2
2-1018	Tn-Hoop-48	1867	800	1951	See Note 2
2-1018	Tn-Hoop-49	1867	870	2160	See Note 2
2-1018	Tn-Hoop-50	1867	820	2026	See Note 2
2-1018	Tn-Hoop-51	1867	880	2174	See Note 2
2-1018	Tn-Hoop-52	1867	800	2074	See Note 2
2-1018	Tn-Hoop-53	1867	820	2145	See Note 2
2-1018	Tn-Hoop-54	1867	850	2215	See Note 2
Average			847	2118	
Standard Deviation			35	79	
Coefficient of Variation (COV)			4%	4%	

Notes:
1. All operation in the Siemens Westinghouse advanced particulate filtration system at the Foster Wheeler PCFBC test facility in Karhula, Finland. Nominal-operating temperature unknown.
2. All operation at the SCS PSDF in combustion mode at a nominal-operating temperature of 1,400°F.

Table 1-6
Axial Compressive Properties of Virgin Pall 442T

Candle Identification	Specimen Number	Temperature (°F)	Ultimate Strength (psi)	Young's Modulus (Msi)	Strain-to-Failure (mils/in.)	Remarks
1-94	Cm-ax-1	70	11000	5.92	1.91	
1-94	Cm-ax-3	70	12940	6.26	2.19	
1-94	Cm-ax-5	70	12350	5.73	2.21	
Average			12097	5.97	2.10	
1-94	Cm-ax-2	1700	9200	3.32	8.54	
1-94	Cm-ax-4	1700	8400	3.28	8.63	
1-94	Cm-ax-6	1700	8880	2.98	8.99	
Average			8827	3.19	8.72	

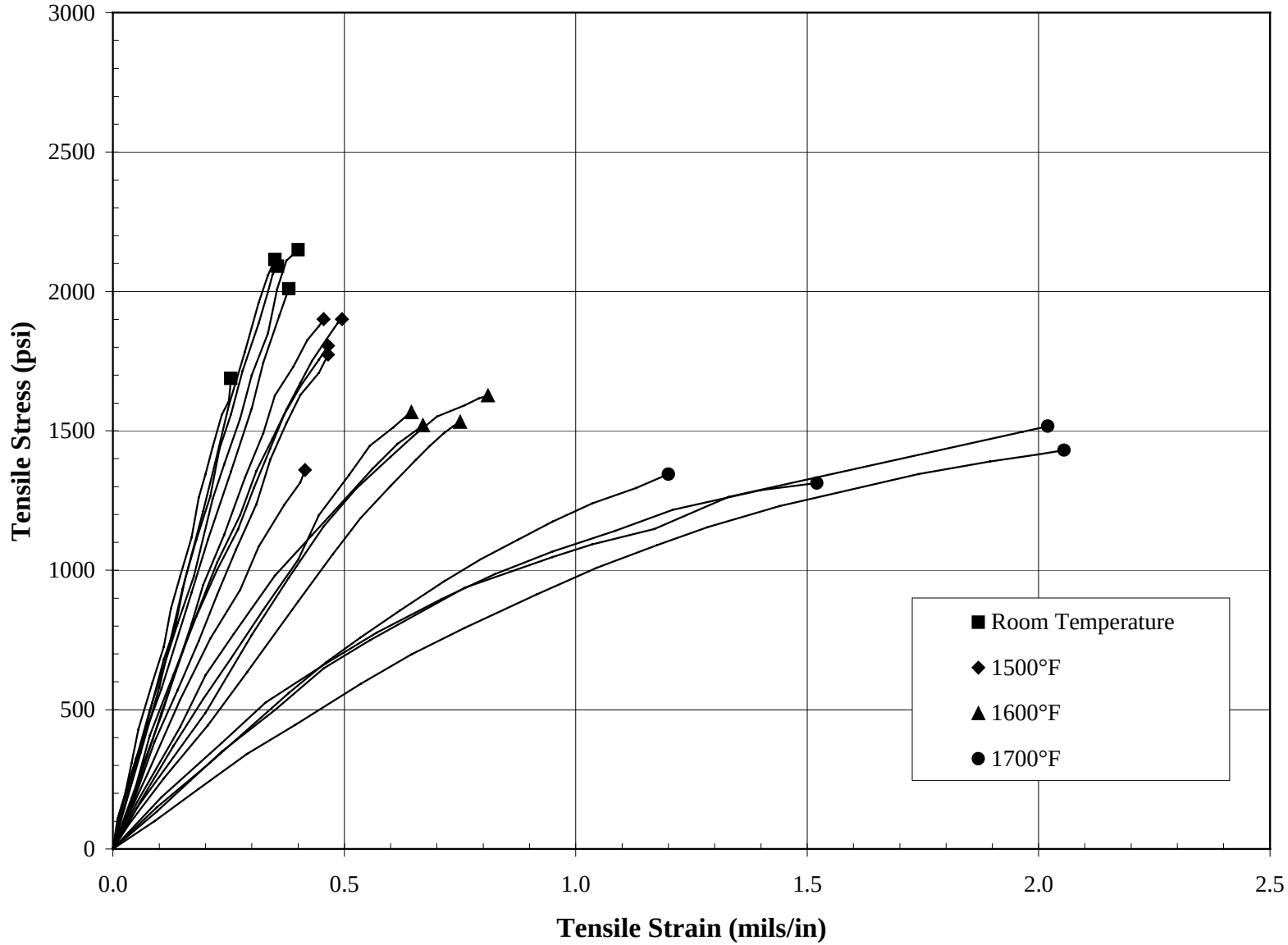

Figure 1-1 Room and Elevated Temperature Axial Tensile Stress-Strain Responses for Virgin Pall442T

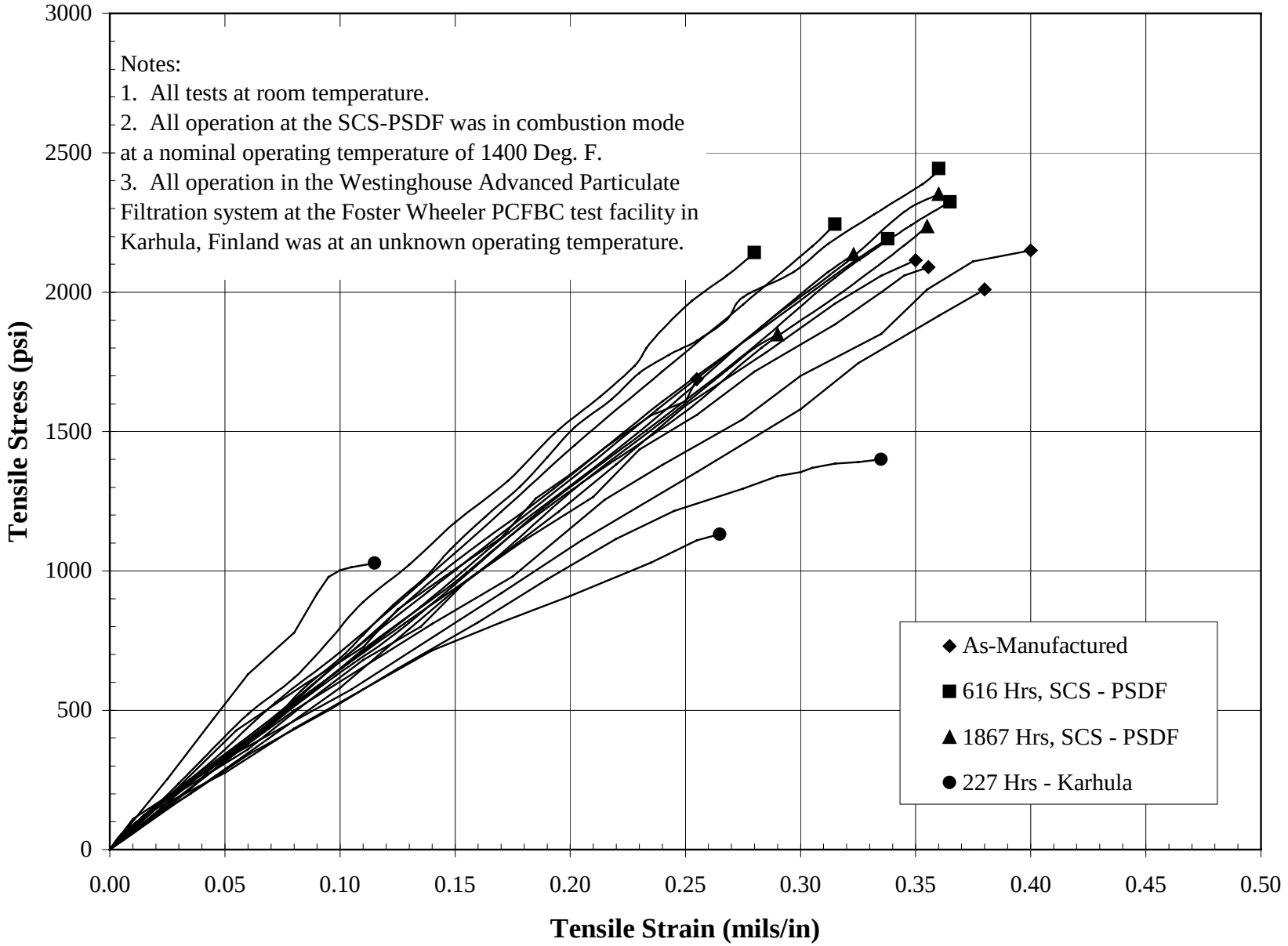

Figure 1-2 Room Temperature Axial Tensile Stress-Strain Responses for Pall 442T Virgin and After Operation

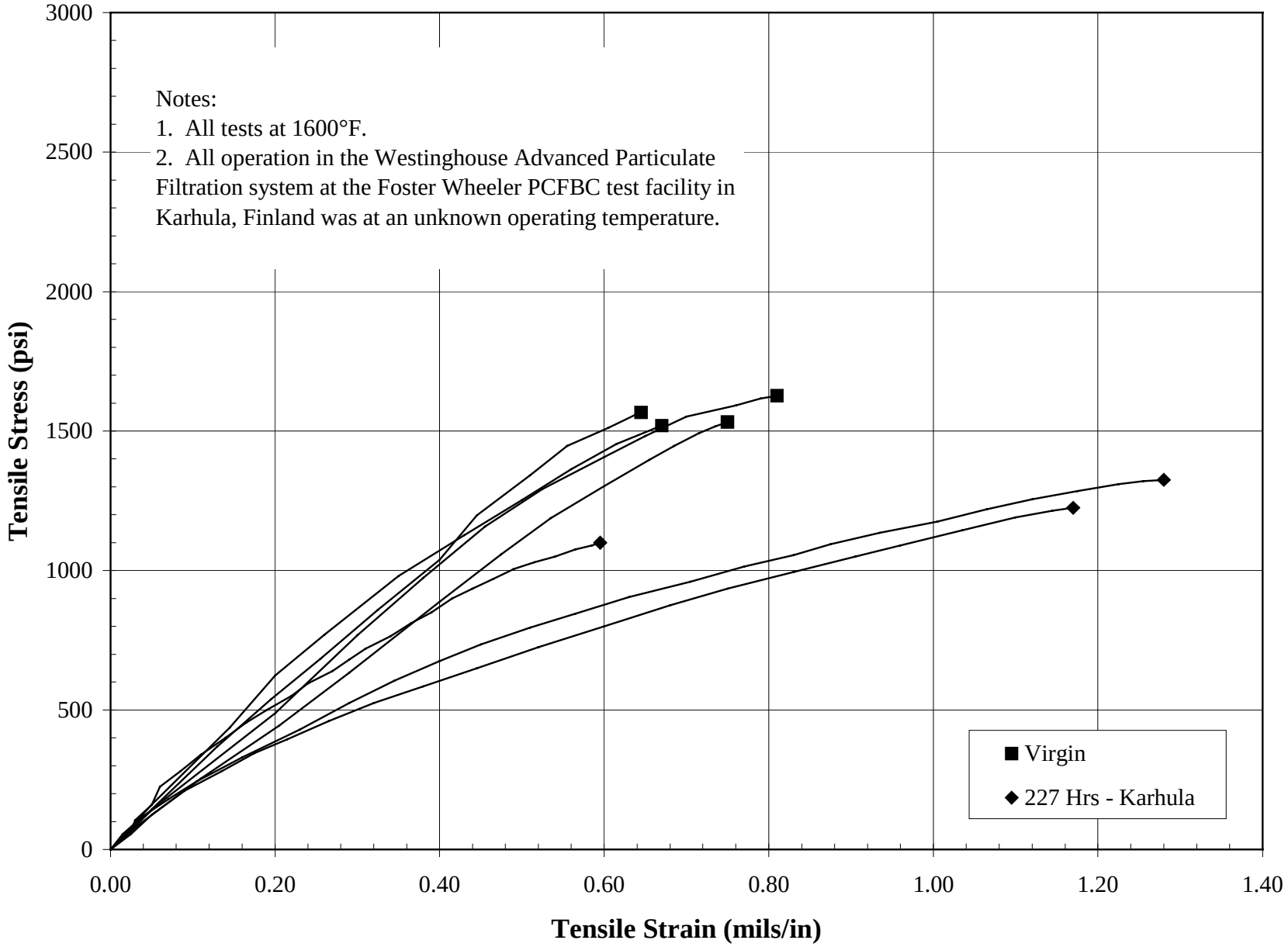

Figure 1-3 Axial Tensile Stress-Strain Responses at 1,600°F for Pall 442T After-Combustion Operation

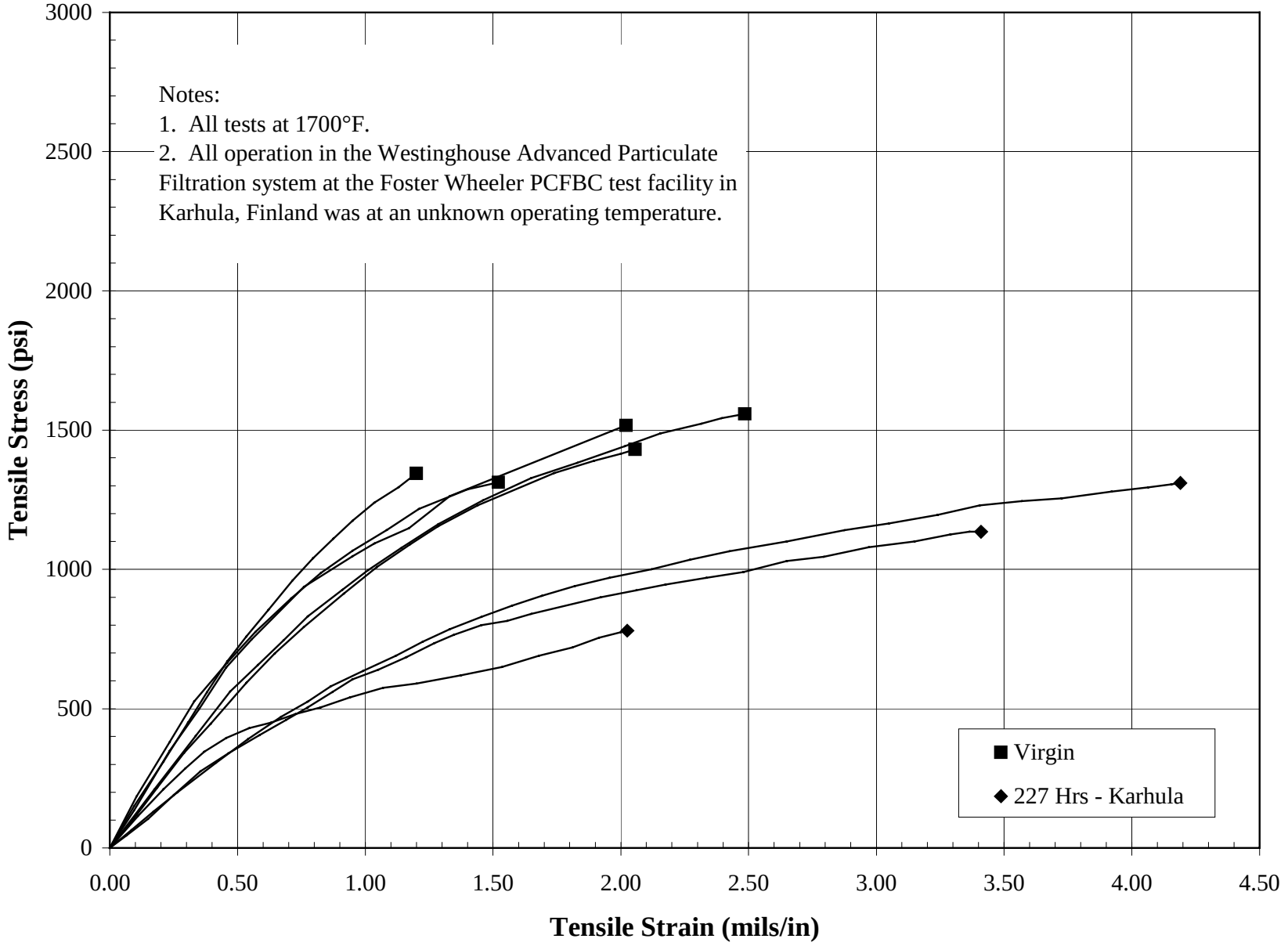

Figure 1-4 Axial Tensile Stress-Strain Responses at 1,700°F for Pall 442T After-Combustion Operation

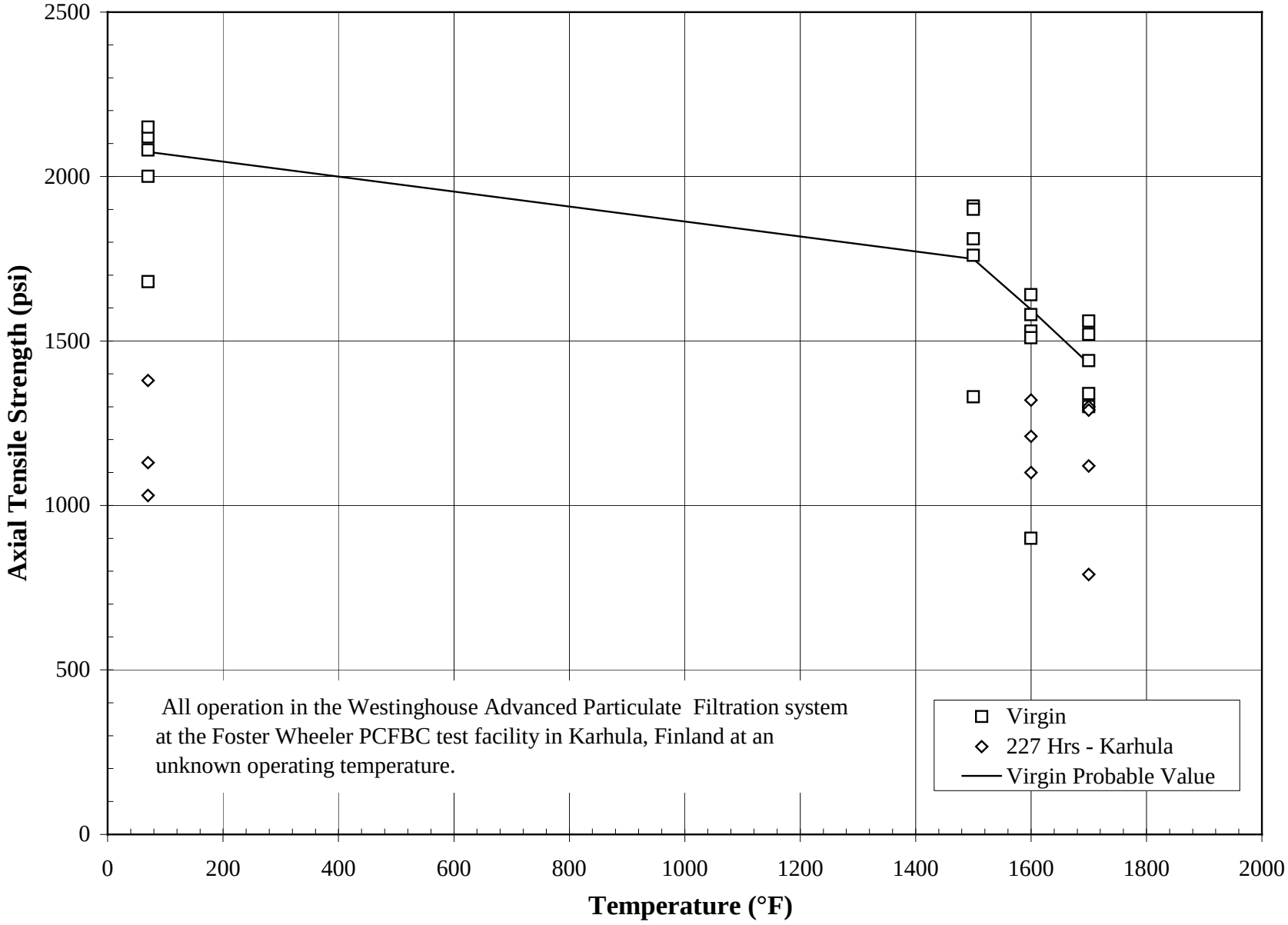

Figure 1-5 Axial Tensile Strength Versus Temperature for Pall 442T

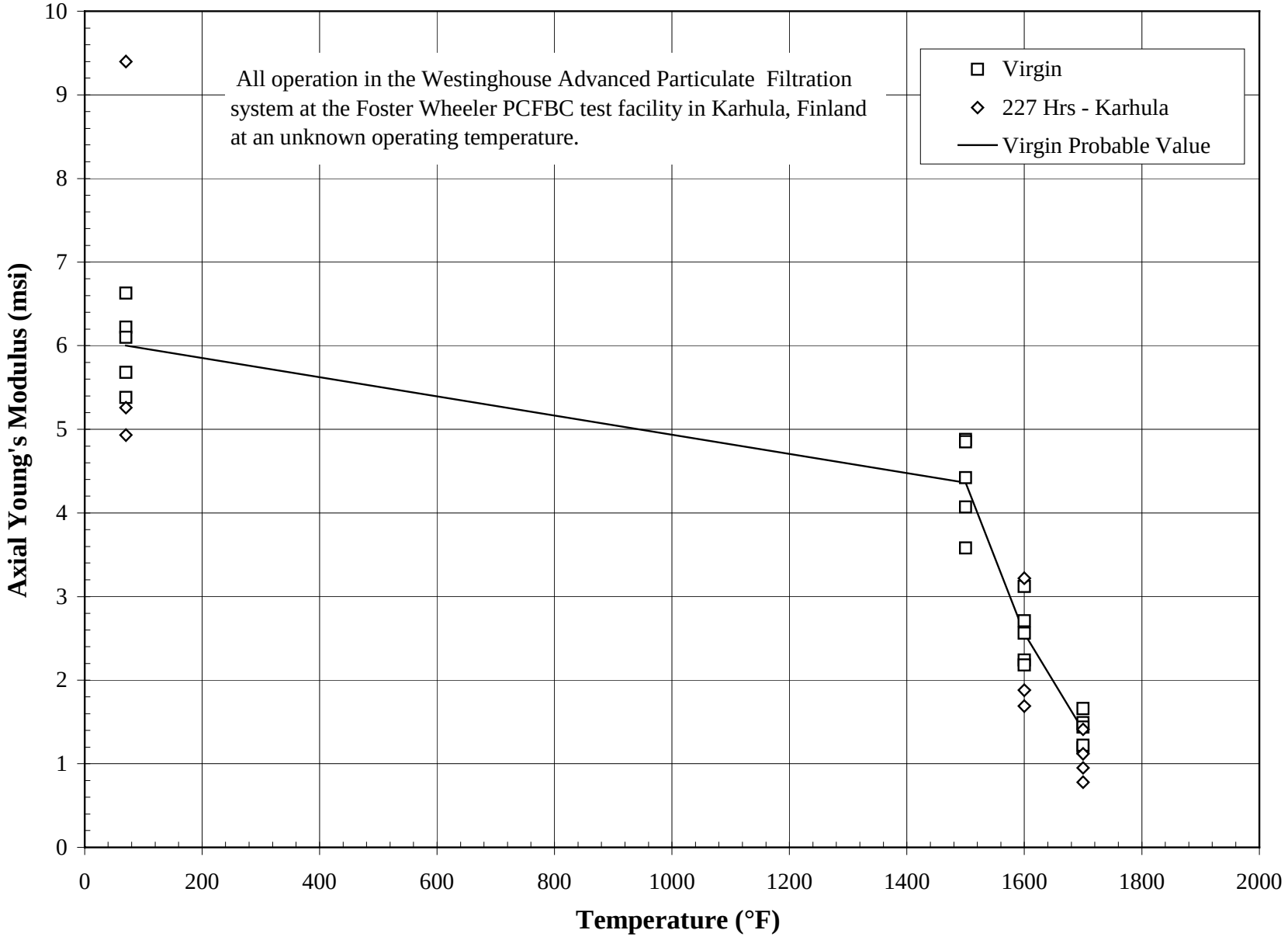

Figure 1-6 Young's Modulus Versus Temperature for Pall 442T

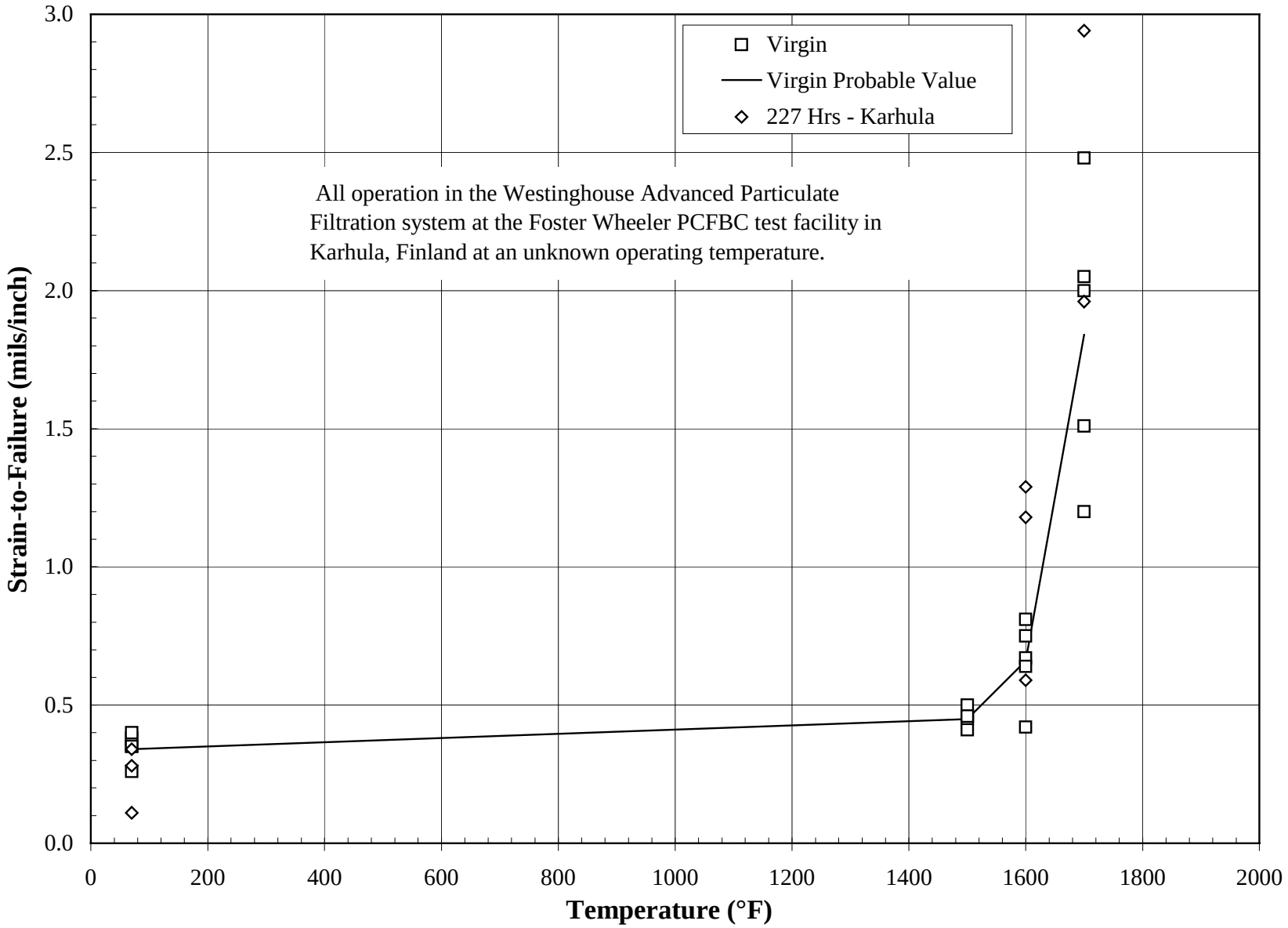

Figure 1-7 Axial Tensile Strain-to-Failure Versus Temperature for Pall 442T

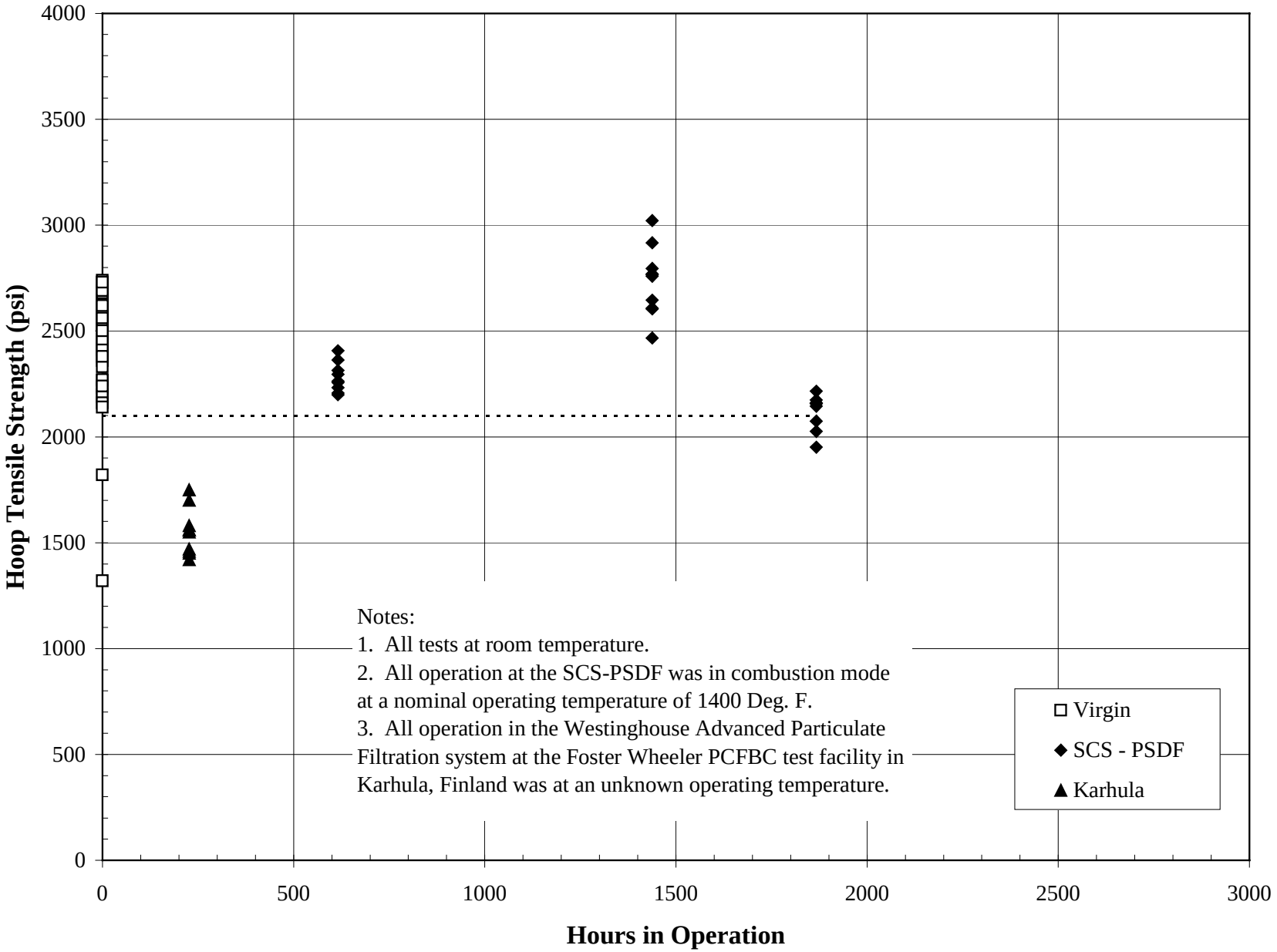

Figure 1-8 Room Temperature Hoop Tensile Strength Versus Hours in Operation for Pall 442T

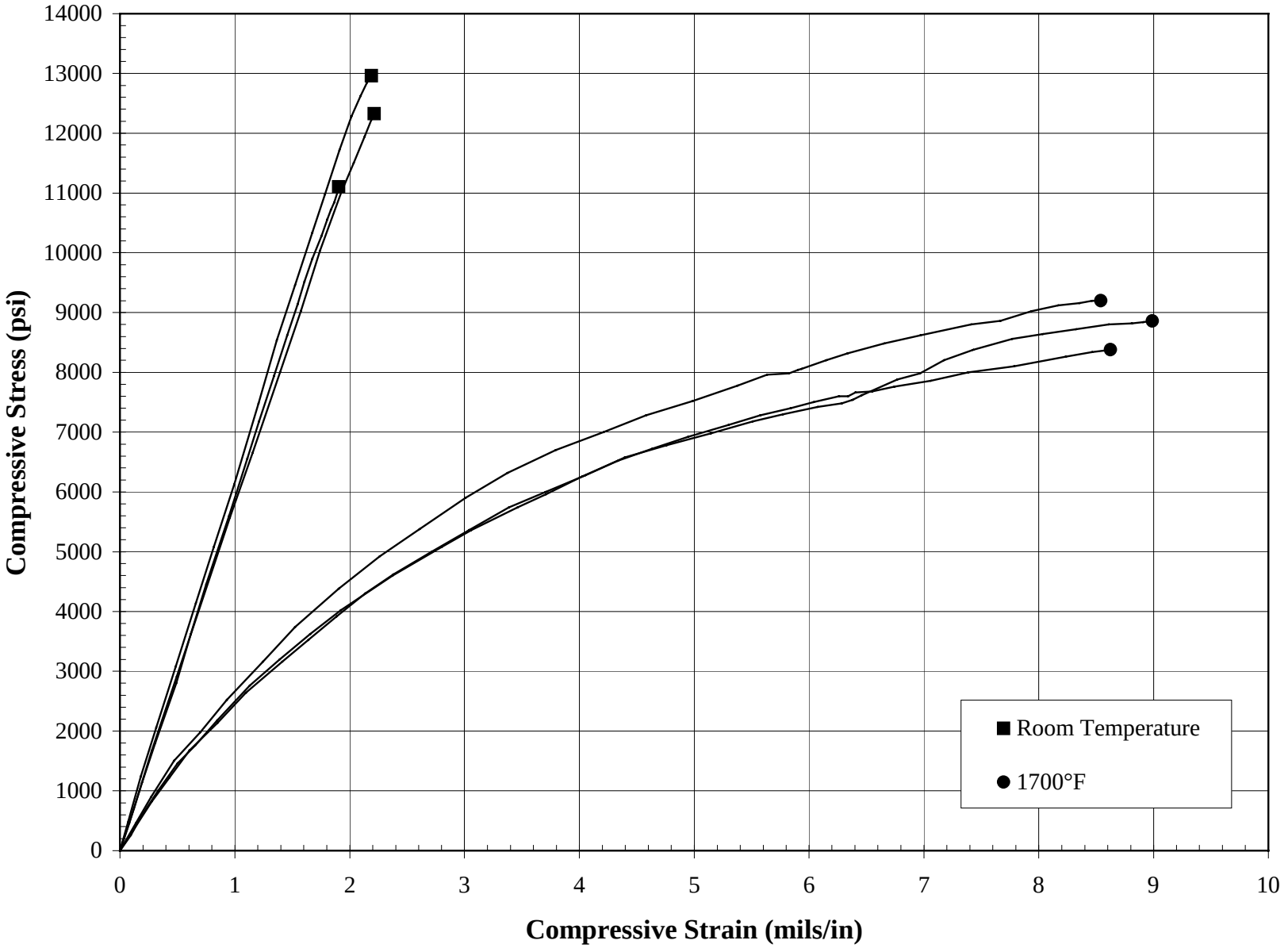

Figure 1-9 Axial Compressive Stress-Strain Responses for Virgin Pall 442T

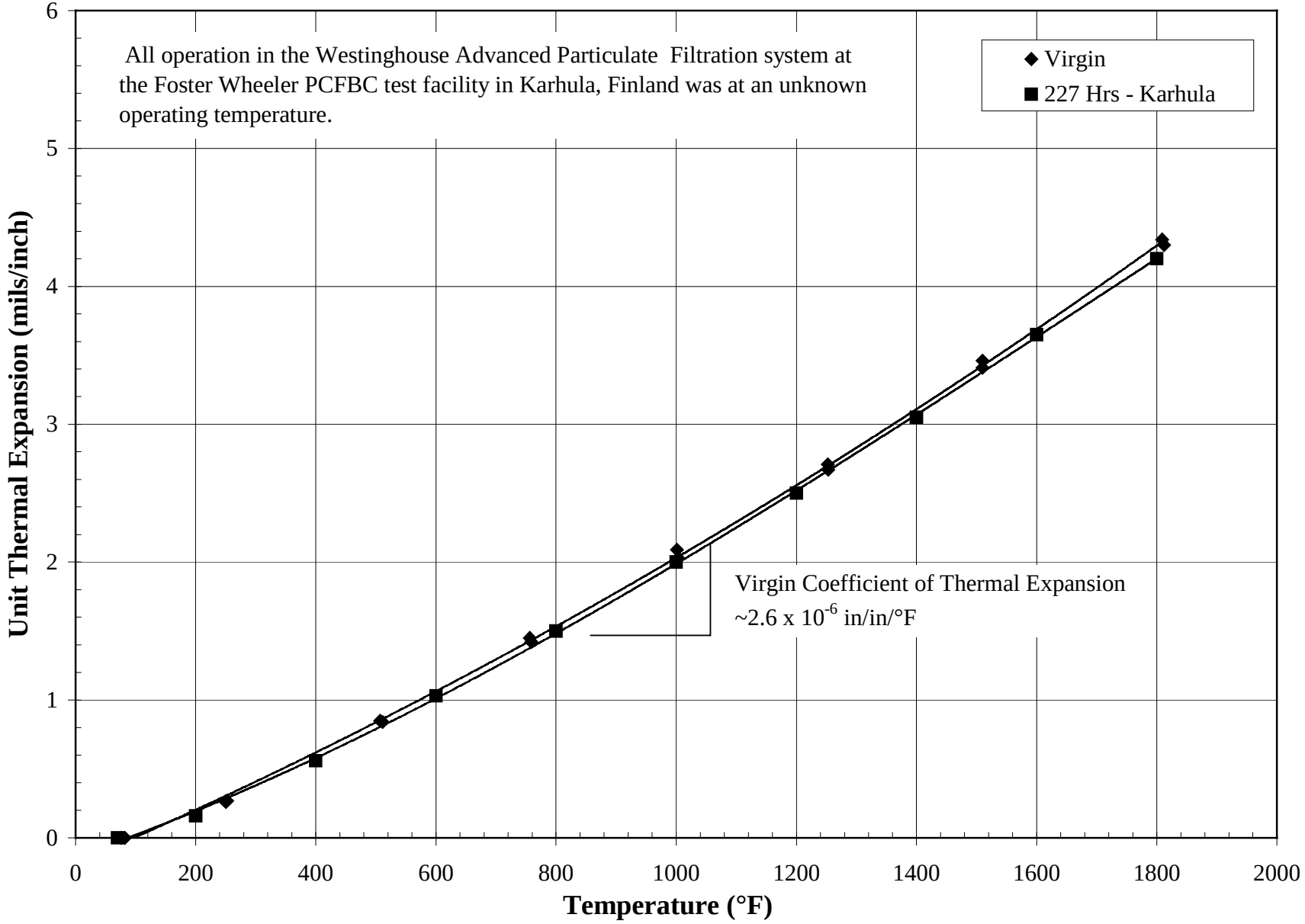

Figure 1-10 Unit Thermal Expansion of Pall 442T

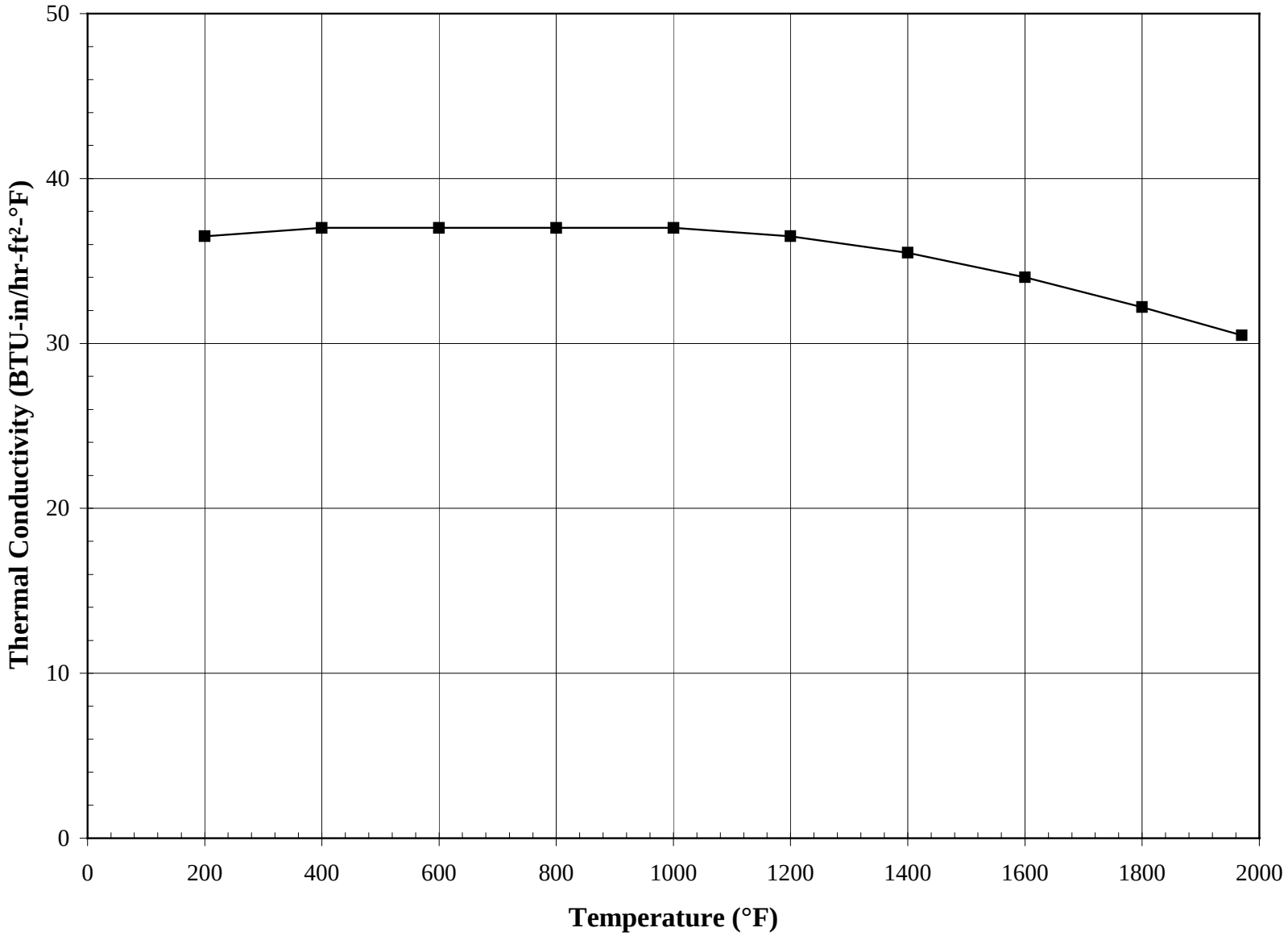

Figure 1-11 Radial Thermal Conductivity Versus Temperature for Virgin Pall 442T

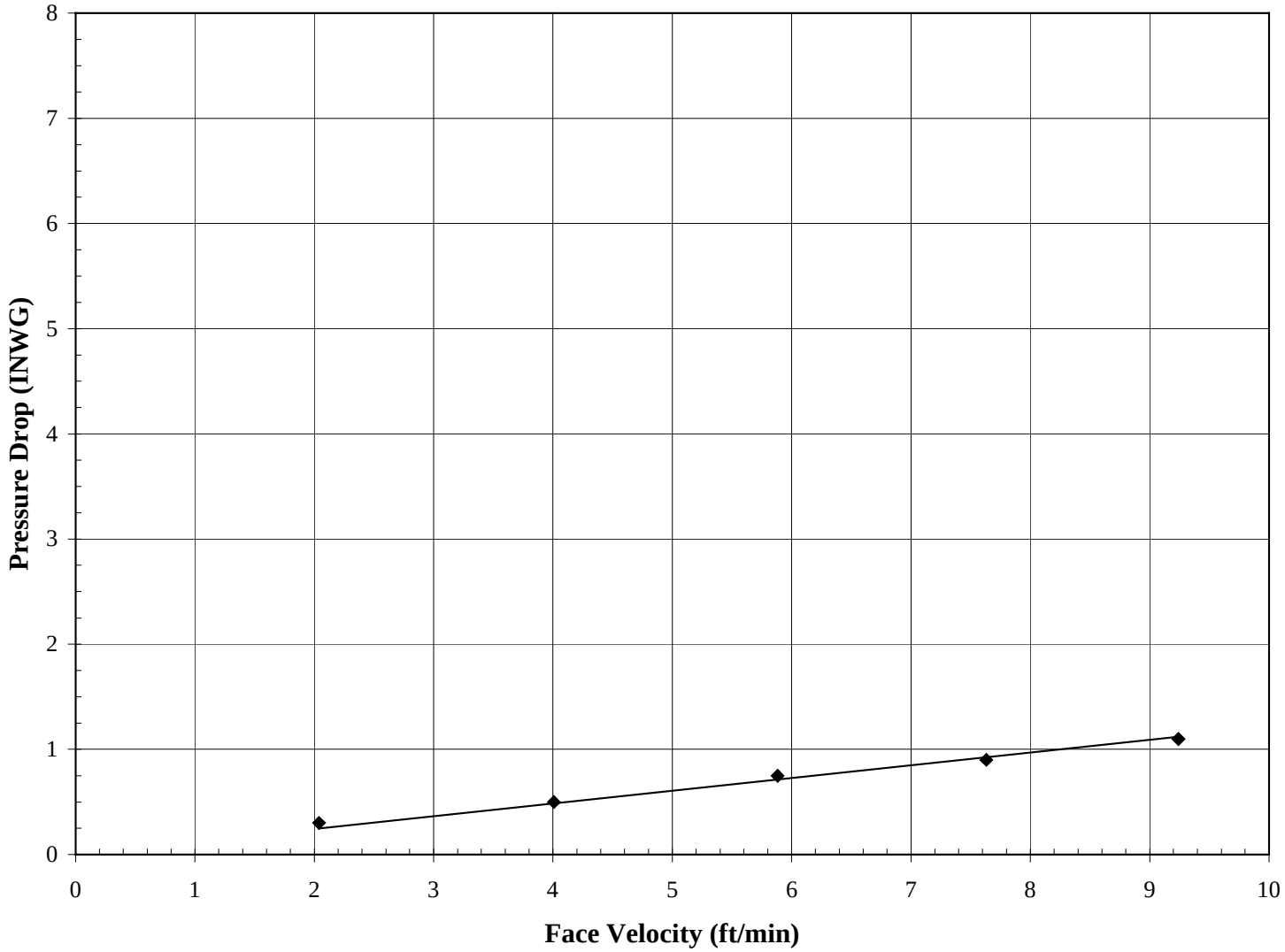

Figure 1-12 Pressure Drop Versus Face Velocity for Virgin Pall 442T Using Air at Ambient Temperature and Pressure

2.0 PALL 326

Pall 326 is a clay-bonded SiC particle material similar to Pall 442T except with a different binder to reduce creep. The microstructure consists of individual SiC particles or clusters of SiC particles connected by clay or glass bridges. The elements have a structural wall with a nominal I.D. of 1.575 in. (40 mm) and a nominal wall thickness of 0.40 in. (10 mm). Mechanical and thermal properties of the elements are controlled by the structural wall and a relatively thin membrane layer applied to the outside surface provides filtration. Probable values of selected properties of virgin Pall 326 are as follows:

Bulk Density (lbm/ft^3)	113
Hoop Tensile Strength at Room Temperature (psi)	2,060
Axial Tensile Strength at Room Temperature (psi)	1,300
Axial Young's Modulus at Room Temperature (10^6 psi)	5.7
Axial Tensile Strain-to-Failure at Room Temperature (mils/in.)	0.24
Axial Tensile Strength at 1,500°F (psi)	2,200
Axial Young's Modulus at 1,500°F (10^6 psi)	2.8
Axial Tensile Strain-to-Failure at 1,500°F (mils/in.)	1.4
Axial Coefficient of Thermal Expansion, 500 to 1,500°F, (10^{-6} in./in./°F)	2.8
Radial Thermal Conductivity at 1,000°F (BTU-in./hr-ft^2-°F)	38
Pressure Drop at 5 ft/min Face Velocity, Air at Ambient Conditions(inWG)	1.3

Table 2-1 (Page 1 of 4)

Density of Pall 326

Element	Specimen Number	Hours in Operation	I.D. (in.)	O.D. (in.)	Density (gr/cm³)	Density (lb/ft³)	Remarks
2-469	Tn-Hoop-1	Virgin	1.54	2.39	1.86	116	
2-469	Tn-Hoop-2	Virgin	1.54	2.38	1.86	116	
2-469	Tn-Hoop-3	Virgin	1.54	2.38	1.86	116	
		Average			1.86	116	
		Standard Deviation			0.004	0.24	
		Coefficient of Variation (COV)			0.21%	0.21%	
4-471	Tn-Hoop-4	Virgin	1.54	2.38	1.85	116	
4-471	Tn-Hoop-5	Virgin	1.55	2.38	1.85	116	
4-471	Tn-Hoop-6	Virgin	1.54	2.38	1.86	116	
		Average			1.86	116	
		Standard Deviation			0.003	0.19	
		COV			0.16%	0.16%	
1366-5	Tn-Hoop-201	Virgin	1.549	2.355	1.82	113	
1366-5	Tn-Hoop-202	Virgin	1.550	2.357	1.81	113	
1366-5	Tn-Hoop-203	Virgin	1.555	2.359	1.82	114	
1366-5	Tn-Hoop-204	Virgin	1.575	2.350	1.80	112	
1366-5	Tn-Hoop-205	Virgin	1.575	2.362	1.80	112	
1366-5	Tn-Hoop-206	Virgin	1.579	2.364	1.81	113	
1366-5	Tn-Hoop-207	Virgin	1.596	2.356	1.80	112	
1366-5	Tn-Hoop-208	Virgin	1.597	2.357	1.80	112	
1366-5	Tn-Hoop-209	Virgin	1.599	2.352	1.81	113	
		Average			1.81	113	
		Standard Deviation			0.007	0.14	
		COV			0.38%	0.13%	
1333-4	Tn-Hoop-210	Virgin	1.562	2.355	1.83	114	
1333-4	Tn-Hoop-211	Virgin	1.550	2.359	1.81	113	
1333-4	Tn-Hoop-212	Virgin	1.553	2.362	1.80	113	
1333-4	Tn-Hoop-213	Virgin	1.573	2.362	1.82	113	
1333-4	Tn-Hoop-214	Virgin	1.573	2.360	1.81	113	
1333-4	Tn-Hoop-215	Virgin	1.575	2.367	1.81	113	
1333-4	Tn-Hoop-216	Virgin	1.591	2.365	1.80	112	
1333-4	Tn-Hoop-217	Virgin	1.592	2.359	1.81	113	
1333-4	Tn-Hoop-218	Virgin	1.598	2.361	1.81	113	
		Average			1.81	113	
		Standard Deviation			0.009	0.31	
		COV			0.47%	0.27%	

Table 2-1 (Page 2 of 4)

Density of Pall 326

Element	Specimen Number	Hours in Operation	I.D. (in.)	O.D. (in.)	Density (gr/cm³)	Density (lb/ft³)	Remarks
1324-7	Tn-Hoop-219	Virgin	1.552	2.364	1.82	113	
1324-7	Tn-Hoop-220	Virgin	1.551	2.366	1.82	114	
1324-7	Tn-Hoop-221	Virgin	1.555	2.370	1.82	113	
1324-7	Tn-Hoop-222	Virgin	1.571	2.378	1.81	113	
1324-7	Tn-Hoop-223	Virgin	1.574	2.383	1.80	113	
1324-7	Tn-Hoop-224	Virgin	1.576	2.382	1.81	113	
1324-7	Tn-Hoop-225	Virgin	1.596	2.372	1.81	113	
1324-7	Tn-Hoop-226	Virgin	1.596	2.368	1.81	113	
1324-7	Tn-Hoop-227	Virgin	1.599	2.362	1.81	113	
		Average			1.81	113	
		Standard Deviation			0.005	0.11	
		COV			0.27%	0.09%	
1324-4	Tn-Hoop-228	Virgin	1.574	2.386	1.79	112	
1324-4	Tn-Hoop-229	Virgin	1.577	2.391	1.78	111	
1324-4	Tn-Hoop-230	Virgin	1.578	2.394	1.78	111	
1324-4	Tn-Hoop-231	Virgin	1.575	2.379	1.81	113	
1324-4	Tn-Hoop-232	Virgin	1.576	2.378	1.81	113	
1324-4	Tn-Hoop-233	Virgin	1.580	2.379	1.80	112	
1324-4	Tn-Hoop-234	Virgin	1.622	2.397	1.78	111	
1324-4	Tn-Hoop-235	Virgin	1.625	2.395	1.78	111	
1324-4	Tn-Hoop-236	Virgin	1.627	2.393	1.78	111	
		Average			1.79	111	
		Standard Deviation			0.011	0.04	
		COV			0.63%	0.04%	
1291-3	Tn-Hoop-237	Virgin	1.546	2.377	1.85	115	
1291-3	Tn-Hoop-238	Virgin	1.550	2.377	1.85	116	
1291-3	Tn-Hoop-239	Virgin	1.552	2.379	1.84	115	
1291-3	Tn-Hoop-240	Virgin	1.571	2.389	1.85	115	
1291-3	Tn-Hoop-241	Virgin	1.570	2.387	1.84	115	
1291-3	Tn-Hoop-242	Virgin	1.571	2.387	1.85	115	
1291-3	Tn-Hoop-243	Virgin	1.587	2.372	1.85	116	
1291-3	Tn-Hoop-244	Virgin	1.590	2.372	1.86	116	
1291-3	Tn-Hoop-245	Virgin	1.617	2.397	1.84	115	
		Average			1.85	115	
		Standard Deviation			0.006	0.53	
		COV			0.32%	0.46%	

Table 2-1 (Page 3 of 4)

Density of Pall 326

Element	Specimen Number	Hours in Operation	I.D. (in.)	O.D. (in.)	Density (gr/cm³)	Density (lb/ft³)	Remarks
3-24A	Tn-Hoop-1	429	1.549	2.374	1.87	117	See Notes 1,2
3-24A	Tn-Hoop-2	429	1.551	2.377	1.86	116	See Notes 1,2
3-24A	Tn-Hoop-3	429	1.554	2.381	1.86	116	See Notes 1,2
3-24A	Tn-Hoop-4	429	1.576	2.380	1.85	115	See Notes 1,2
3-24A	Tn-Hoop-5	429	1.577	2.382	1.85	115	See Notes 1,2
3-24A	Tn-Hoop-6	429	1.578	2.377	1.85	116	See Notes 1,2
3-24A	Tn-Hoop-7	429	1.601	2.377	1.86	116	See Notes 1,2
3-24A	Tn-Hoop-8	429	1.601	2.375	1.85	115	See Notes 1,2
3-24A	Tn-Hoop-9	429	1.603	2.377	1.84	115	See Notes 1,2
		Average			1.85	115	
		Standard Deviation			0.008	0.38	
		COV			0.45%	0.33%	
1-36A	Tn-Hoop-10	429	1.549	2.373	1.88	117	See Notes 1,2
1-36A	Tn-Hoop-11	429	1.545	2.374	1.88	118	See Notes 1,2
1-36A	Tn-Hoop-12	429	1.552	2.375	1.88	117	See Notes 1,2
1-36A	Tn-Hoop-13	429	1.570	2.384	1.87	117	See Notes 1,2
1-36A	Tn-Hoop-14	429	1.571	2.385	1.87	117	See Notes 1,2
1-36A	Tn-Hoop-15a	429	1.575	2.388	1.87	117	See Notes 1,2
1-36A	Tn-Hoop-15b	429	1.577	2.387	1.87	117	See Notes 1,2
1-36A	Tn-Hoop-16	429	1.597	2.365	1.87	117	See Notes 1,2
1-36A	Tn-Hoop-17	429	1.597	2.365	1.87	117	See Notes 1,2
1-36A	Tn-Hoop-18	429	1.600	2.361	1.88	117	See Notes 1,2
		Average			1.88	117	
		Standard Deviation			0.005	0.27	
		COV			0.28%	0.23%	
7-676	Tn-Hoop-1	540	1.599	2.359	1.86	116	See Notes 1,3
7-676	Tn-Hoop-2	540	1.601	2.364	1.86	116	See Notes 1,3
7-676	Tn-Hoop-3	540	1.597	2.364	1.85	116	See Notes 1,3
7-676	Tn-Hoop-4	540	1.569	2.380	1.85	116	See Notes 1,3
7-676	Tn-Hoop-5	540	1.568	2.378	1.87	117	See Notes 1,3
7-676	Tn-Hoop-6	540	1.567	2.379	1.86	116	See Notes 1,3
7-676	Tn-Hoop-7	540	1.554	2.379	1.85	116	See Notes 1,3
7-676	Tn-Hoop-8	540	1.547	2.373	1.86	116	See Notes 1,3
7-676	Tn-Hoop-9	540	1.545	2.371	1.86	116	See Notes 1,3
		Average			1.86	116	
		Standard Deviation			0.005	0.24	
		COV			0.25%	0.21%	

Table 2-1 (Page 4 of 4)

Density of Pall 326

Element	Specimen Number	Hours in Operation	I.D. (in.)	O.D. (in.)	Density (gr/cm³)	Density (lb/ft³)	Remarks
4-991	Tn-Hoop-19	1251	1.545	2.363	1.97	123	See Notes 1,2
4-991	Tn-Hoop-20	1251	1.545	2.363	1.97	123	See Notes 1,2
4-991	Tn-Hoop-21	1251	1.545	2.365	1.97	123	See Notes 1,2
4-991	Tn-Hoop-22	1251	1.568	2.367	1.98	123	See Notes 1,2
4-991	Tn-Hoop-23	1251	1.573	2.369	1.98	124	See Notes 1,2
4-991	Tn-Hoop-24	1251	1.571	2.367	1.98	124	See Notes 1,2
4-991	Tn-Hoop-25	1251	1.601	2.370	1.97	123	See Notes 1,2
4-991	Tn-Hoop-26	1251	1.594	2.367	1.96	122	See Notes 1,2
4-991	Tn-Hoop-27	1251	1.596	2.364	1.96	122	See Notes 1,2
		Average			1.97	122	
		Standard Deviation			0.008	0.28	
		COV			0.40%	0.23%	
1075-3	Tn-Hoop-246	2830	1.572	2.398	1.94	121	See Notes 1,2
1075-3	Tn-Hoop-247	2830	1.551	2.375	1.99	124	See Notes 1,2
1075-3	Tn-Hoop-248	2830	1.555	2.376	1.99	124	See Notes 1,2
1075-3	Tn-Hoop-249	2830	1.574	2.390	1.95	122	See Notes 1,2
1075-3	Tn-Hoop-250	2830	1.574	2.389	1.94	121	See Notes 1,2
1075-3	Tn-Hoop-251	2830	1.577	2.386	1.94	121	See Notes 1,2
1075-3	Tn-Hoop-252	2830	1.597	2.378	1.94	121	See Notes 1,2
1075-3	Tn-Hoop-253	2830	1.599	2.371	1.95	121	See Notes 1,2
1075-3	Tn-Hoop-254	2830	1.598	2.367	1.95	122	See Notes 1,2
		Average			1.96	121	
		Standard Deviation			0.019	0.37	
		Coefficient of Variation (COV)			0.96%	0.31%	
1069-3	Tn-Hoop-255	2834	1.553	2.377	1.87	116	See Notes 1,2,4
1069-3	Tn-Hoop-256	2834	1.556	2.380	1.87	117	See Notes 1,2,4
1069-3	Tn-Hoop-257	2834	1.558	2.384	1.86	116	See Notes 1,2,4
1069-3	Tn-Hoop-258	2834	1.575	2.392	1.85	116	See Notes 1,2,4
1069-3	Tn-Hoop-259	2834	1.576	2.393	1.85	116	See Notes 1,2,4
1069-3	Tn-Hoop-260	2834	1.576	2.388	1.86	116	See Notes 1,2,4
1069-3	Tn-Hoop-261	2834	1.597	2.380	1.85	116	See Notes 1,2,4
1069-3	Tn-Hoop-262	2834	1.598	2.378	1.85	115	See Notes 1,2,4
1069-3	Tn-Hoop-263	2834	1.600	2.374	1.86	116	See Notes 1,2,4
		Average			1.86	116	
		Standard Deviation			0.007	0.16	
		COV			0.39%	0.14%	

Notes:

1. Elements were water washed before density measurements but some ash remained in the pores. Density values were calculated based on weights measured with ash in the pores and, therefore, do not represent a material property. The values are for comparison only.
2. All operation at the SCS PSDF in combustion mode at a nominal-operating temperature of 1,400°F.
3. All operation in the Siemens Westinghouse advanced particulate filtration system at the Foster Wheeler PCFBC test facility in Karhula, Finland. Nominal-operating temperature was 1,550°F.
4. In operation during October 1998 PCD fire.

Table 2-2

Axial Tensile Properties of Virgin Pall 326

Element	Specimen Number	Temp. (°F)	Ultimate Strength (psi)	Young's Modulus (Msi)	Strain-to-Failure, (mils/in.)	Notes
4-471	Tn-Ax-12	70	1150	5.88	0.20	
4-471	Tn-Ax-17	70	1250	6.67	0.19	
2-469	Tn-Ax-5	70	910	4.82	0.19	
2-469	Tn-Ax-11	70	1270	5.06	0.25	
2-470	Tn-Ax-22	70	1990	6.22	0.35	
Average			1314	5.73	0.24	
Standard Deviation			361	0.7	0.06	
Coefficient of Variation (COV)			28%	12%	26%	
2-470	Tn-Ax-24	1400	1890	2.88	0.88	
2-470	Tn-Ax-26	1400	1840	2.72	0.72	
2-470	Tn-Ax-28	1400	2110			See Note 1
2-470	Tn-Ax-30	1400	1940	2.85	0.70	
Average			1945	2.82	0.77	
Standard Deviation			102			
COV			5%			
2-470	Tn-Ax-25	1500	2330	2.68	1.76	
2-470	Tn-Ax-27	1500	2180	2.74	1.65	
2-470	Tn-Ax-29	1500	2110	2.74	1.21	
2-470	Tn-Ax-31	1500	2140	2.96	1.16	
Average			2190	2.78	1.45	
Standard Deviation			85	0.1	0.26	
COV			4%	4%	18%	
4-471	Tn-Ax-18	1600	1390	1.82	1.30	
4-471	Tn-Ax-13	1600	1750	1.68	1.40	
2-469	Tn-Ax-7	1600	1600	3.48	2.25	
4-471	Tn-Ax-21	1600	1520	2.72	1.64	
Average			1565	2.43	1.65	
Standard Deviation			130	0.7	0.37	
COV			8%	30%	22%	
2-469	Tn-Ax-2	1700	770	1.79		See Note 1
4-471	Tn-Ax-20	1700	800	2.77	0.69	
2-469	Tn-Ax-6	1700	950	2.45	0.98	
4-471	Tn-Ax-19	1700	1210	4.30	0.93	
2-470	Tn-Ax-32	1700	1260	2.36	0.98	
Average			998	2.73	0.90	
Standard Deviation			204	0.84	0.12	
COV			20%	31%	13%	
2-469	Tn-Ax-10	1800	970	2.24	0.60	
4-471	Tn-Ax-14	1800	990	3.33	0.40	
2-470	Tn-Ax-23	1800	1070	2.04	0.71	
Average			1010	2.54	0.57	

Notes:
1. Strain measurements were not obtained because strain flags slipped during test.

Table 2-3

Room Temperature Axial Tensile Properties of Pall 326 –
Virgin and After Combustion Operation

Element	Specimen Number	Hours in Operation	Ultimate Strength (psi)	Young's Modulus (Msi)	Strain-to-Failure (mils/in.)	Notes
4-471	Tn-Ax-12	Virgin	1150	5.88	0.20	
4-471	Tn-Ax-17	Virgin	1250	6.67	0.19	
2-469	Tn-Ax-5	Virgin	910	4.82	0.19	
2-469	Tn-Ax-11	Virgin	1270	5.06	0.25	
2-470	Tn-Ax-22	Virgin	1990	6.22	0.35	
Average			1314	5.73	0.24	
Standard Deviation			361	0.7	0.06	
Coefficient of Variation (COV)			28%	12%	26%	
3-24A	Tn-Ax-1	429	1150	5.12	0.26	See Note 1
3-24A	Tn-Ax-2	429	1120	5.30	0.21	See Note 1
3-24A	Tn-Ax-3	429	1480	5.86	0.31	See Note 1
3-24A	Tn-Ax-4	429	1420	4.55	0.36	See Note 1
3-24A	Tn-Ax-5	429	1410	5.37	0.31	See Note 1
Average			1316	5.24	0.29	
Standard Deviation			150	0.42	0.05	
COV			11%	8%	18%	
7-676	Tn-Ax-1	540	870	3.98	0.39	See Note 2
7-676	Tn-Ax-2	540	1020	4.26	0.38	See Note 2
7-676	Tn-Ax-3	540	1070	4.06	0.38	See Note 2
Average			987	4.10	0.38	
R6-674	Tn-Ax-1	1166	790	3.12	0.40	See Note 2
R6-674	Tn-Ax-2	1166	860	3.09	0.42	See Note 2
R6-674	Tn-Ax-3	1166	930	3.26	0.50	See Note 2
Average			860	3.16	0.44	
4-991	Tn-Ax-6	1251	2560	7.27	0.38	See Note 1
4-991	Tn-Ax-7	1251	2420	7.55	0.33	See Note 1
4-991	Tn-Ax-8	1251	2620	5.84	0.50	See Note 1
4-991	Tn-Ax-9	1251	1830	7.34	0.27	See Note 1
4-991	Tn-Ax-10	1251	2070	7.21	0.32	See Note 1
Average			2300	7.04	0.36	
Standard Deviation			303	0.61	0.08	
COV			13%	9%	22%	

Notes:

1. All operation at the SCS PSDF in combustion mode at a nominal-operating temperature of 1,400°F.
2. All operation in the Siemens Westinghouse advanced particulate filtration system at the Foster Wheeler PCFBC test facility in Karhlua, Finland. Nominal-operating temperature was 1,550°F.

Table 2-4 (Page 1 of 4)

Room Temperature Hoop Tensile Strength of Pall 326

Element	Specimen Number	Hours in Operation	Maximum Hydrostatic Pressure (psig)	Ultimate Strength (psi)	Remarks
2-469	Tn-Hoop-1	virgin	830	2000	
2-469	Tn-Hoop-2	virgin	860	2100	
2-469	Tn-Hoop-3	virgin	810	1980	
	Average		833	2027	
4-471	Tn-Hoop-4	virgin	900	2190	
4-471	Tn-Hoop-5	virgin	1000	2470	
4-471	Tn-Hoop-6	virgin	840	2040	
	Average		913	2233	
1366-5	Tn-Hoop-201	virgin	840	2110	
1366-5	Tn-Hoop-202	virgin	870	2190	
1366-5	Tn-Hoop-203	virgin	820	2070	
1366-5	Tn-Hoop-204	virgin	830	2180	
1366-5	Tn-Hoop-205	virgin	820	2120	
1366-5	Tn-Hoop-206	virgin	830	2160	
1366-5	Tn-Hoop-207	virgin	780	2100	
1366-5	Tn-Hoop-208	virgin	770	2080	
1366-5	Tn-Hoop-209	virgin	810	2210	
	Average		819	2136	
	Standard Deviation		28	48	
	Coefficient of Variation (COV)		3.5%	2.2%	
1333-4	Tn-Hoop-210	virgin	750	1930	
1333-4	Tn-Hoop-211	virgin	790	1990	
1333-4	Tn-Hoop-212	virgin	790	1990	
1333-4	Tn-Hoop-213	virgin	780	2020	
1333-4	Tn-Hoop-214	virgin	780	2020	
1333-4	Tn-Hoop-215	virgin	800	2080	
1333-4	Tn-Hoop-216	virgin	790	2100	
1333-4	Tn-Hoop-217	virgin	790	2120	
1333-4	Tn-Hoop-218	virgin	710	1900	
	Average		776	2017	
	Standard Deviation		27	70	
	COV		3.4%	3.5%	

Table 2-4 (Page 2 of 4)

Room Temperature Hoop Tensile Strength of Pall 326

Element	Specimen Number	Hours in Operation	Maximum Hydrostatic Pressure (psig)	Ultimate Strength (psi)	Remarks
1324-7	Tn-Hoop-219	virgin	790	1980	
1324-7	Tn-Hoop-220	virgin	720	1810	
1324-7	Tn-Hoop-221	virgin	760	1910	
1324-7	Tn-Hoop-222	virgin	770	1960	
1324-7	Tn-Hoop-223	virgin	800	2050	
1324-7	Tn-Hoop-224	virgin	780	1990	
1324-7	Tn-Hoop-225	virgin	750	1990	
1324-7	Tn-Hoop-226	virgin	760	2030	
1324-7	Tn-Hoop-227	virgin	730	1950	
	Average		762	1963	
	Standard Deviation		25	67	
	COV		3.3%	3.4%	
1324-4	Tn-Hoop-228	virgin	850	2160	
1324-4	Tn-Hoop-229	virgin	870	2210	
1324-4	Tn-Hoop-230	virgin	810	2060	
1324-4	Tn-Hoop-231	virgin	790	2030	
1324-4	Tn-Hoop-232	virgin	800	2050	
1324-4	Tn-Hoop-233	virgin	810	2080	
1324-4	Tn-Hoop-234	virgin	700	1880	
1324-4	Tn-Hoop-235	virgin	660	1780	
1324-4	Tn-Hoop-236	virgin	660	1790	
	Average		772	2004	
	Standard Deviation		75	145	
	COV		9.6%	7.2%	
1291-3	Tn-Hoop-237	virgin	880	2160	
1291-3	Tn-Hoop-238	virgin	890	2200	
1291-3	Tn-Hoop-239	virgin	850	2110	
1291-3	Tn-Hoop-240	virgin	830	2090	
1291-3	Tn-Hoop-241	virgin	850	2150	
1291-3	Tn-Hoop-242	virgin	840	2120	
1291-3	Tn-Hoop-243	virgin	830	2170	
1291-3	Tn-Hoop-244	virgin	820	2160	
1291-3	Tn-Hoop-245	virgin	810	2170	
	Average		844	2148	
	Standard Deviation		25	33	
	COV		3.0%	1.5%	

Table 2-4 (Page 3 of 4)

Room Temperature Hoop Tensile Strength of Pall 326

Element	Specimen Number	Hours in Operation	Maximum Hydrostatic Pressure (psig)	Ultimate Strength (psi)	Remarks
3-24A	Tn-Hoop-1	429	660	1650	Note 1
3-24A	Tn-Hoop-2	429	710	1760	Note 1
3-24A	Tn-Hoop-3	429	610	1510	Note 1
3-24A	Tn-Hoop-4	429	640	1630	Note 1
3-24A	Tn-Hoop-5	429	670	1710	Note 1
3-24A	Tn-Hoop-6	429	680	1750	Note 1
3-24A	Tn-Hoop-7	429	610	1630	Note 1
3-24A	Tn-Hoop-8	429	610	1620	Note 1
3-24A	Tn-Hoop-9	429	660	1750	Note 1
	Average		650	1668	
	Standard Deviation		33	78	
	COV		5%	5%	
1-36A	Tn-Hoop-10	429	830	2070	Note 1
1-36A	Tn-Hoop-11	429	910	2240	Note 1
1-36A	Tn-Hoop-12	429	900	2240	Note 1
1-36A	Tn-Hoop-13	429	890	2250	Note 1
1-36A	Tn-Hoop-14	429	860	2180	Note 1
1-36A	Tn-Hoop-15a	429	860	2180	Note 1
1-36A	Tn-Hoop-15b	429	870	2220	Note 1
1-36A	Tn-Hoop-16	429	830	2210	Note 1
1-36A	Tn-Hoop-17	429	790	2110	Note 1
1-36A	Tn-Hoop-18	429	840	2260	Note 1
	Average		858	2196	
	Standard Deviation		35	60	
	COV		4%	3%	
7-676	Tn-Hoop-1	540	580	1560	Note 2
7-676	Tn-Hoop-2	540	540	1460	Note 2
7-676	Tn-Hoop-3	540	570	1520	Note 2
7-676	Tn-Hoop-4	540	550	1390	Note 2
7-676	Tn-Hoop-5	540	530	1340	Note 2
7-676	Tn-Hoop-6	540	550	1400	Note 2
7-676	Tn-Hoop-7	540	510	1270	Note 2
7-676	Tn-Hoop-8	540	610	1510	Note 2
7-676	Tn-Hoop-9	540	580	1440	Note 2
	Average		558	1432	
	Standard Deviation		29	87	
	COV		5%	6%	

Table 2-4 (Page 4 of 4)

Room Temperature Hoop Tensile Strength of Pall 326

Element	Specimen Number	Hours in Operation	Maximum Hydrostatic Pressure (psig)	Ultimate Strength (psi)	Remarks
4-991	Tn-Hoop-19	1251	960	2400	Note 1
4-991	Tn-Hoop-20	1251	960	2400	Note 1
4-991	Tn-Hoop-21	1251	900	2240	Note 1
4-991	Tn-Hoop-22	1251	900	2320	Note 1
4-991	Tn-Hoop-23	1251	940	2410	Note 1
4-991	Tn-Hoop-24	1251	940	2430	Note 1
4-991	Tn-Hoop-25	1251	850	2270	Note 1
4-991	Tn-Hoop-26	1251	890	2370	Note 1
4-991	Tn-Hoop-27	1251	910	2430	Note 1
	Average		917	2363	
	Standard Deviation		34	66	
	COV		4%	3%	
1075-3	Tn-Hoop-247	2830	1000	2479	Note 1
1075-3	Tn-Hoop-248	2830	950	2369	Note 1
1075-3	Tn-Hoop-249	2830	830	2102	Note 1
1075-3	Tn-Hoop-250	2830	810	2054	Note 1
1075-3	Tn-Hoop-251	2830	810	2066	Note 1
1075-3	Tn-Hoop-252	2830	700	1848	Note 1
1075-3	Tn-Hoop-253	2830	720	1911	Note 1
1075-3	Tn-Hoop-254	2830	740	1983	Note 1
	Average		820	2102	
	Standard Deviation		100	204	
	Coefficient of Variation (COV)		12.2%	9.7%	
1069-3	Tn-Hoop-255	2834	720	1794	Notes 1,3
1069-3	Tn-Hoop-256	2834	720	1784	Notes 1,3
1069-3	Tn-Hoop-257	2834	670	1658	Notes 1,3
1069-3	Tn-Hoop-258	2834	690	1749	Notes 1,3
1069-3	Tn-Hoop-259	2834	680	1729	Notes 1,3
1069-3	Tn-Hoop-260	2834	660	1689	Notes 1,3
1069-3	Tn-Hoop-261	2834	650	1702	Notes 1,3
1069-3	Tn-Hoop-262	2834	630	1658	Notes 1,3
1069-3	Tn-Hoop-263	2834	680	1816	Notes 1,3
	Average		678	1731	
	Standard Deviation		28	55	
	COV		4.2%	3.2%	

Notes:

1. All operation at the SCS PSDF in combustion mode at a nominal-operating temperature of 1,400°F.
2. All operation in the Siemens Westinghouse advanced particulate filtration system at the Foster Wheeler PCFBC test facility in Karhula, Finland. Nominal-operating temperature was 1,550°F.
3. In operation during October 1998 PCD fire.

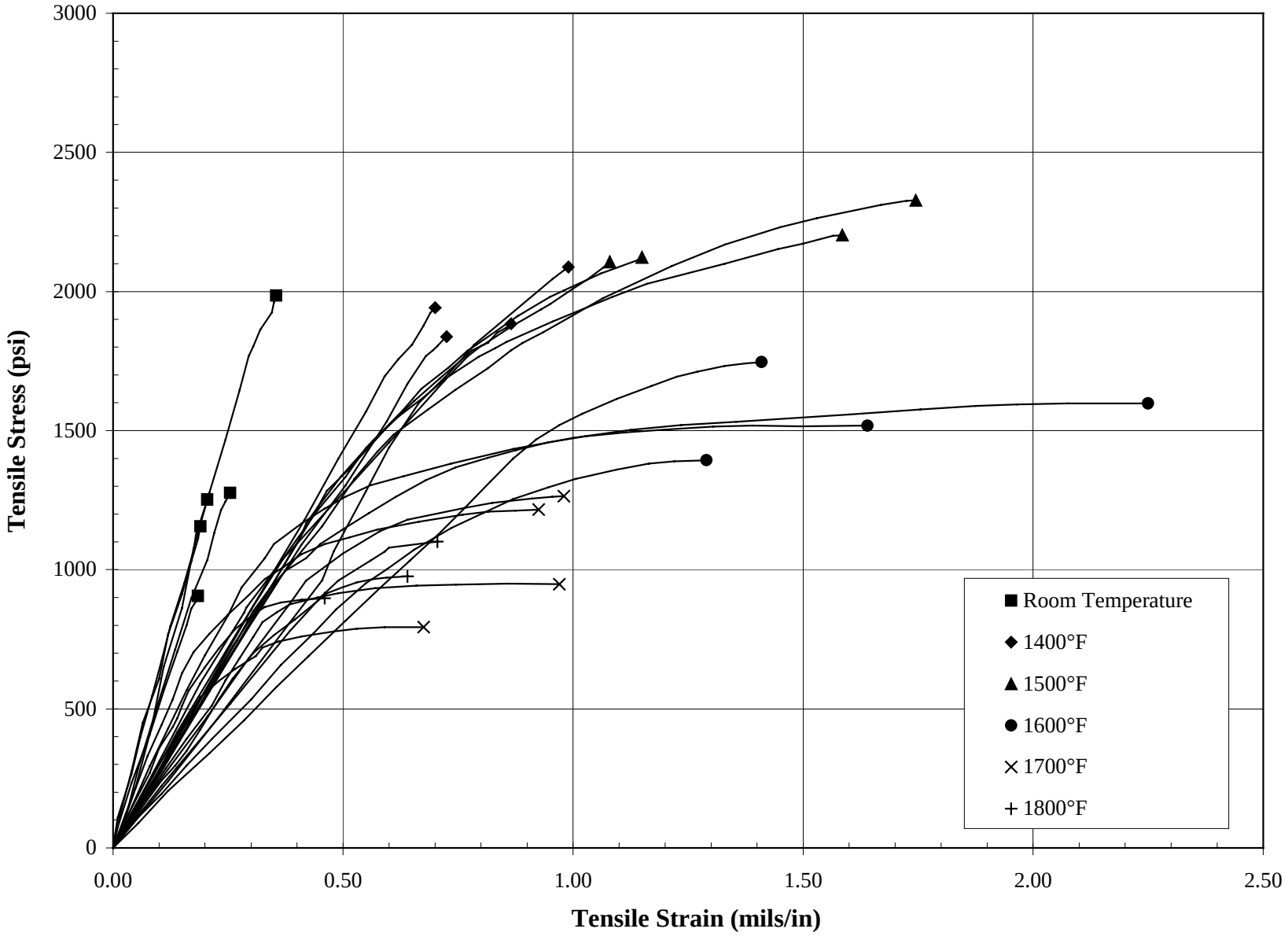

Figure 2-1 Room and Elevated Temperature Axial Stress-Strain Responses for Virgin Pall 326

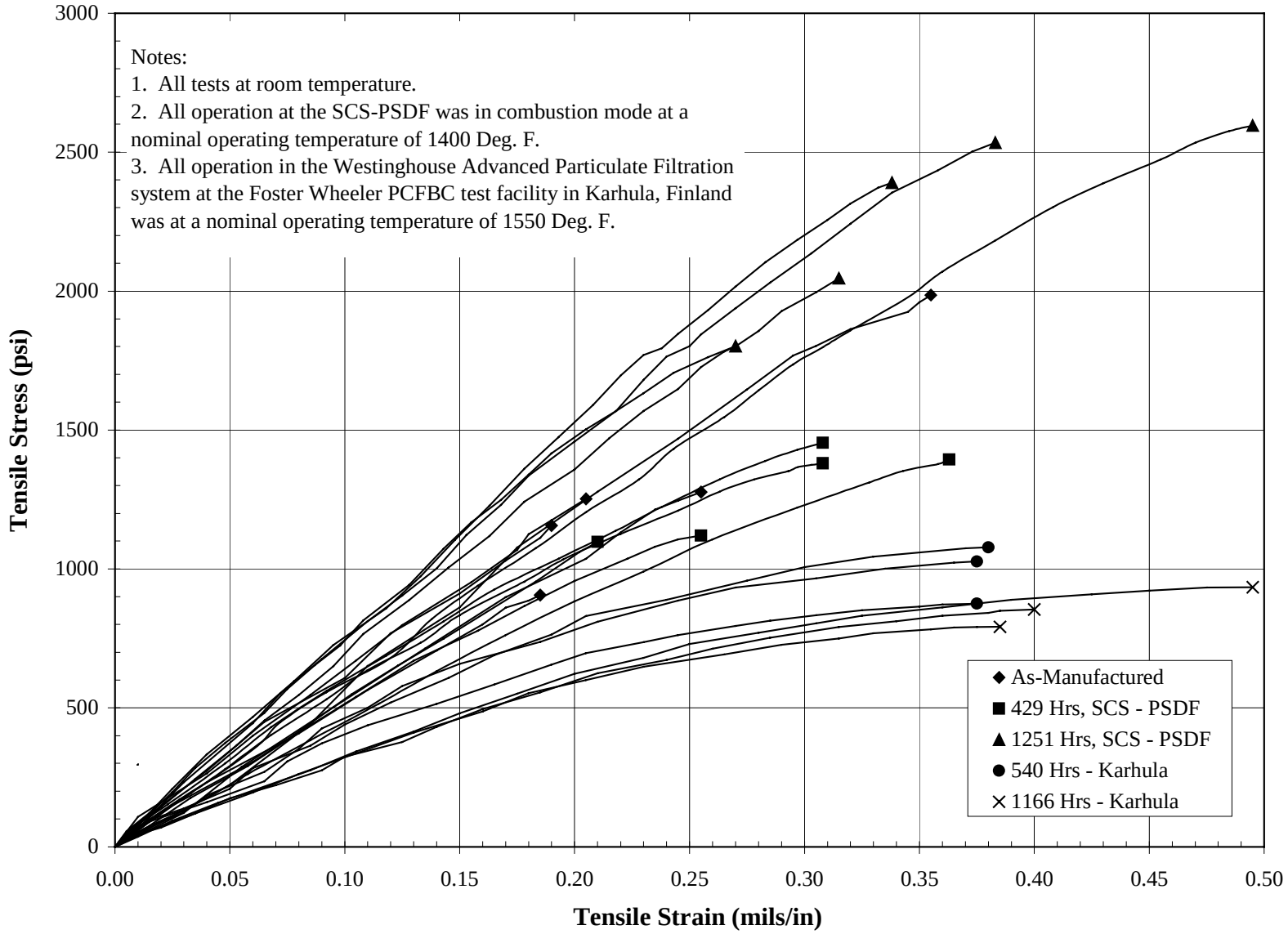

Figure 2-2 Room Temperature Tensile Stress-Strain Responses for Pall 326 Virgin and After-Combustion Operation

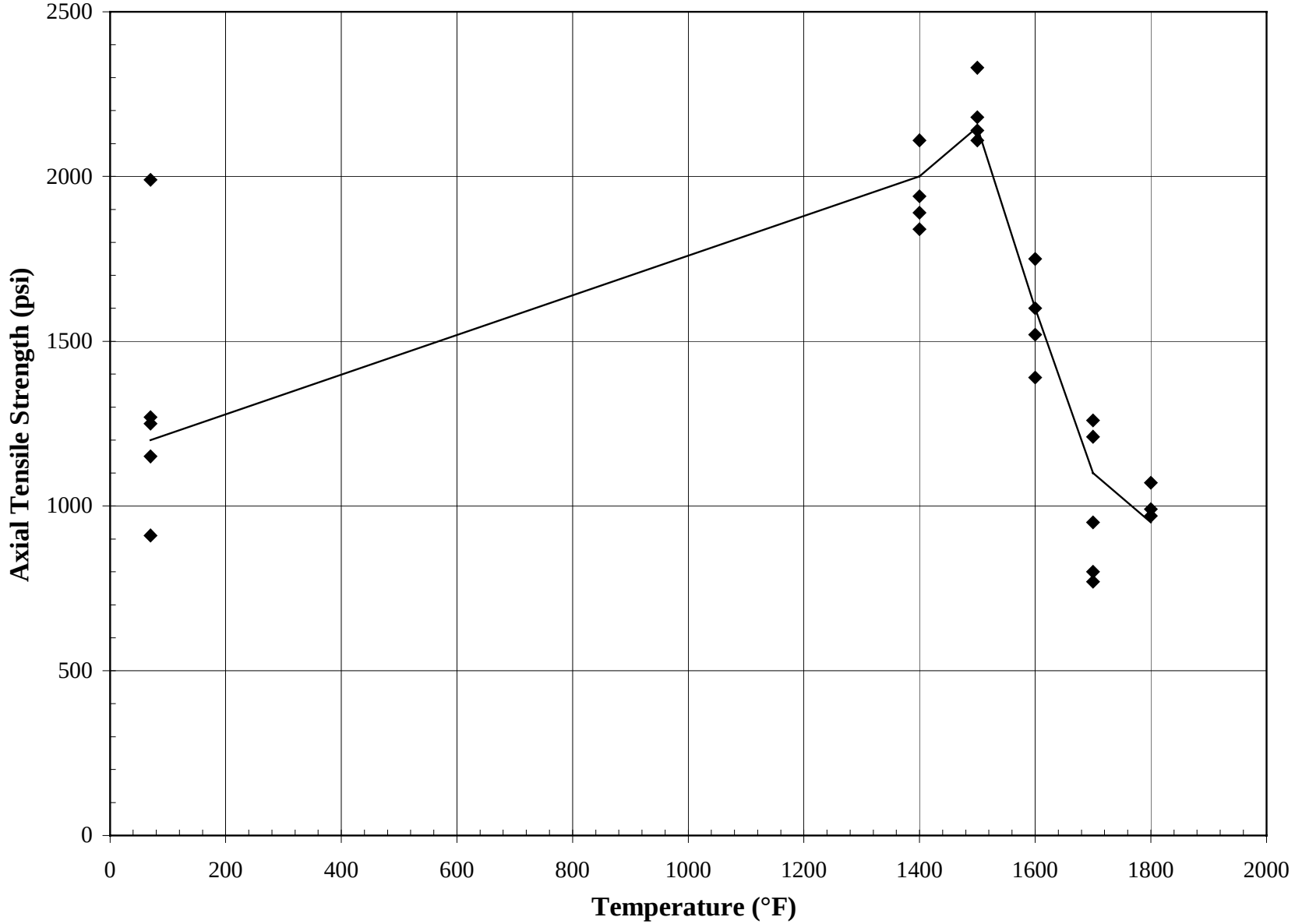

Figure 2-3 Axial Tensile Strength Versus Temperature for Virgin Pall 326

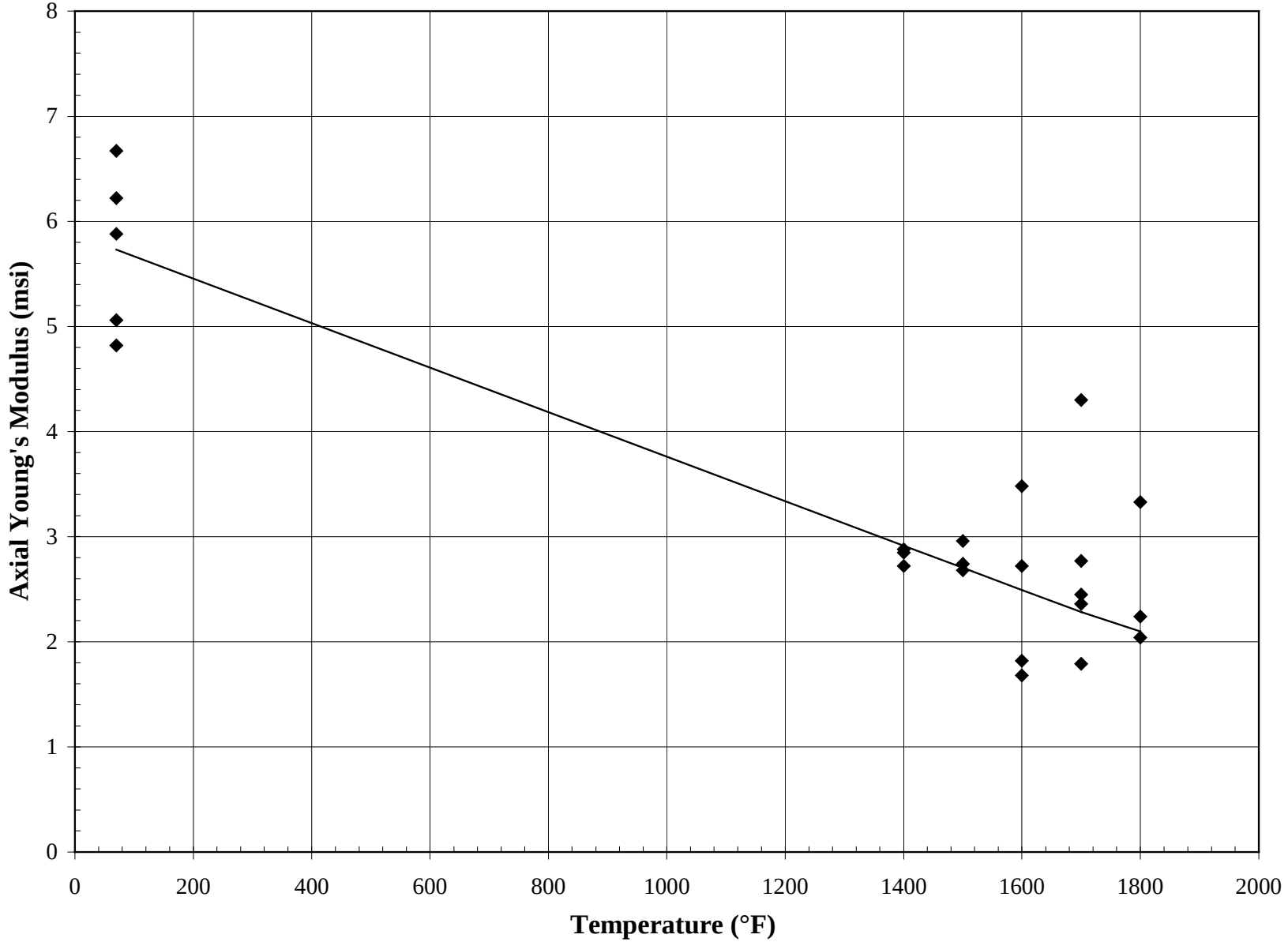

Figure 2-4 Young's Modulus Versus Temperature for Virgin Pall 326

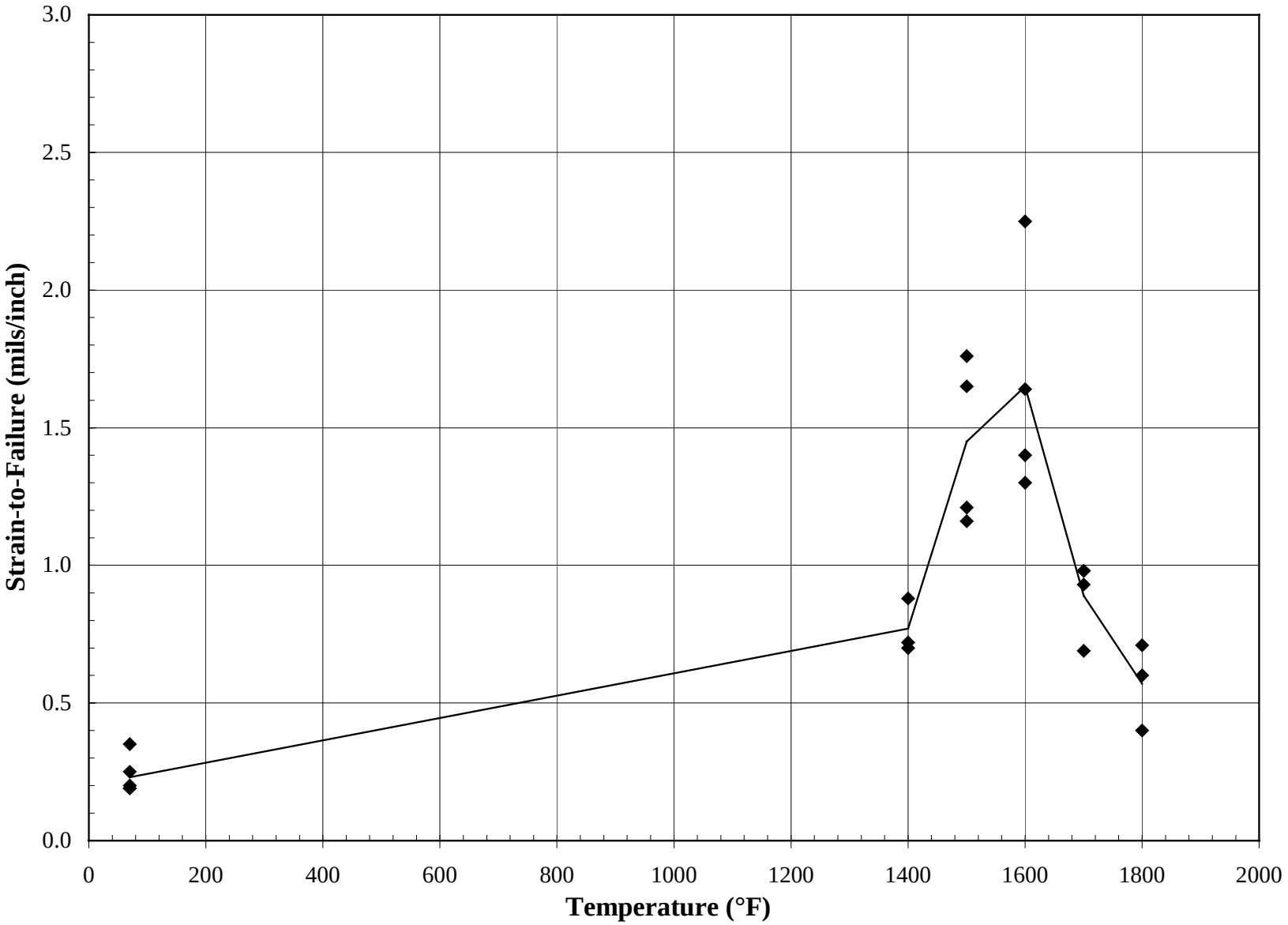

Figure 2-5 Axial Tensile Strain-to-Failure Versus Temperature for Virgin Pall 326

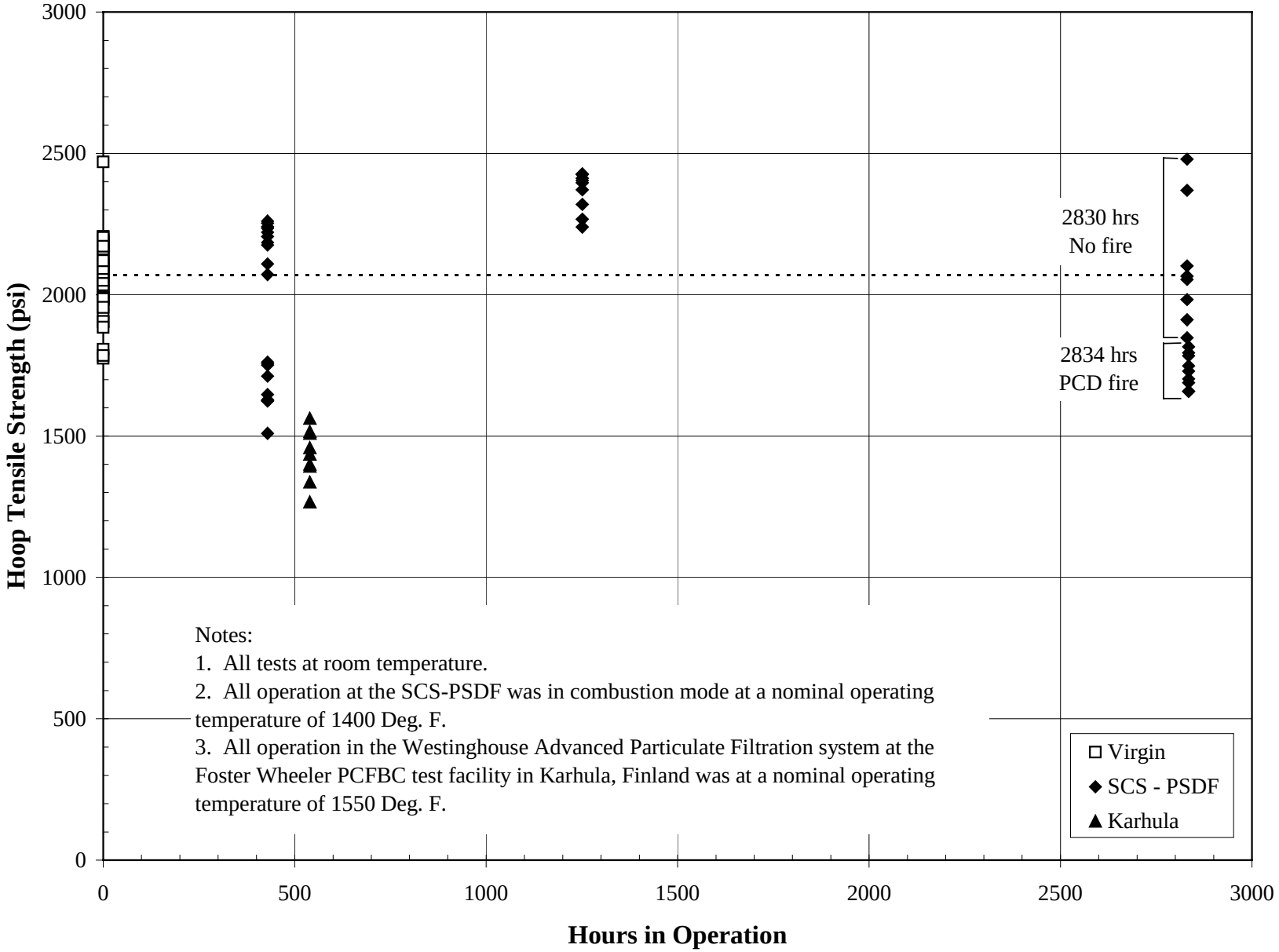

Figure 2-6 Room Temperature Hoop Tensile Strength Versus Hours in Operation for Pall 326

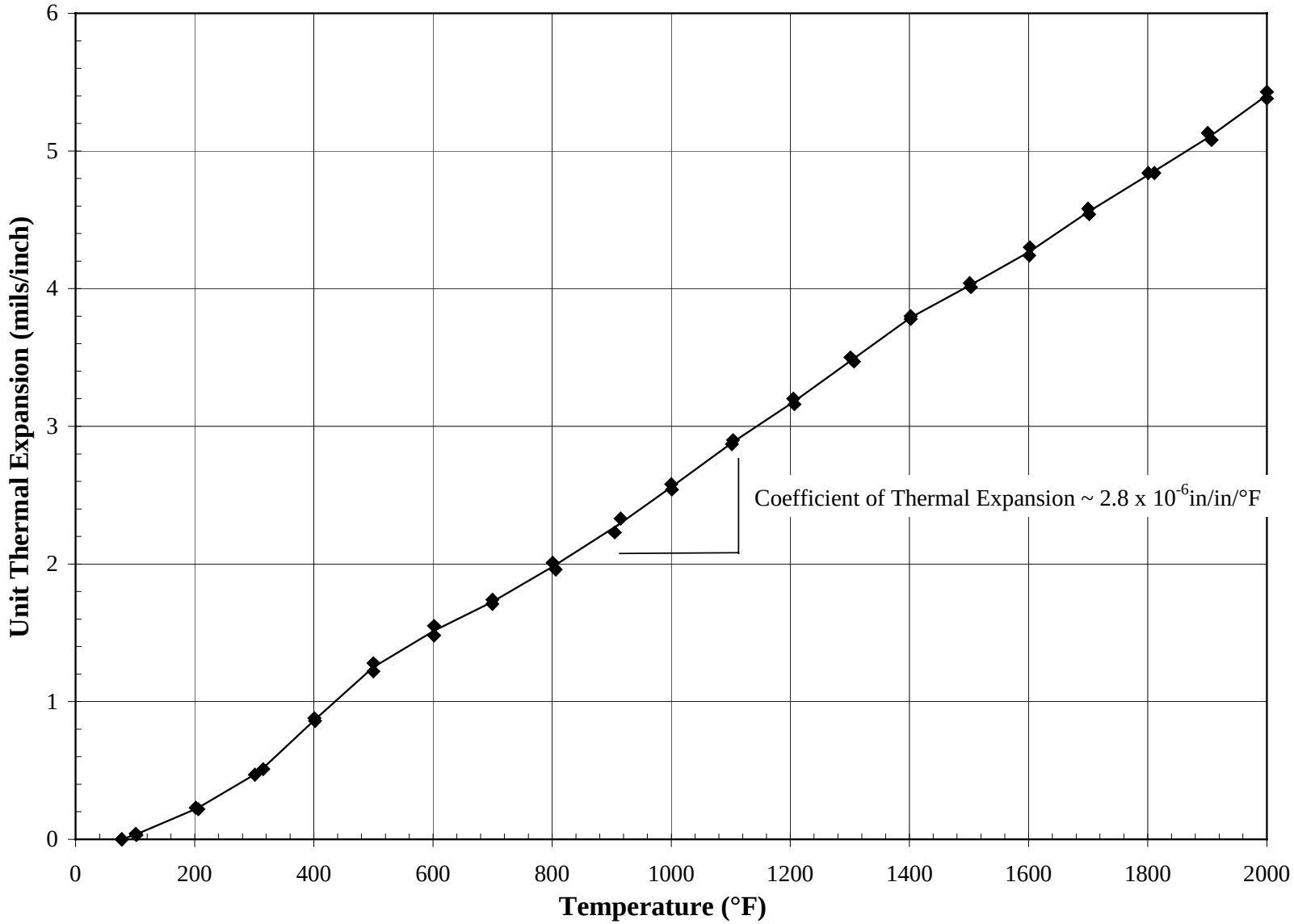

Figure 2-7 Unit Thermal Expansion of Virgin Pall 326

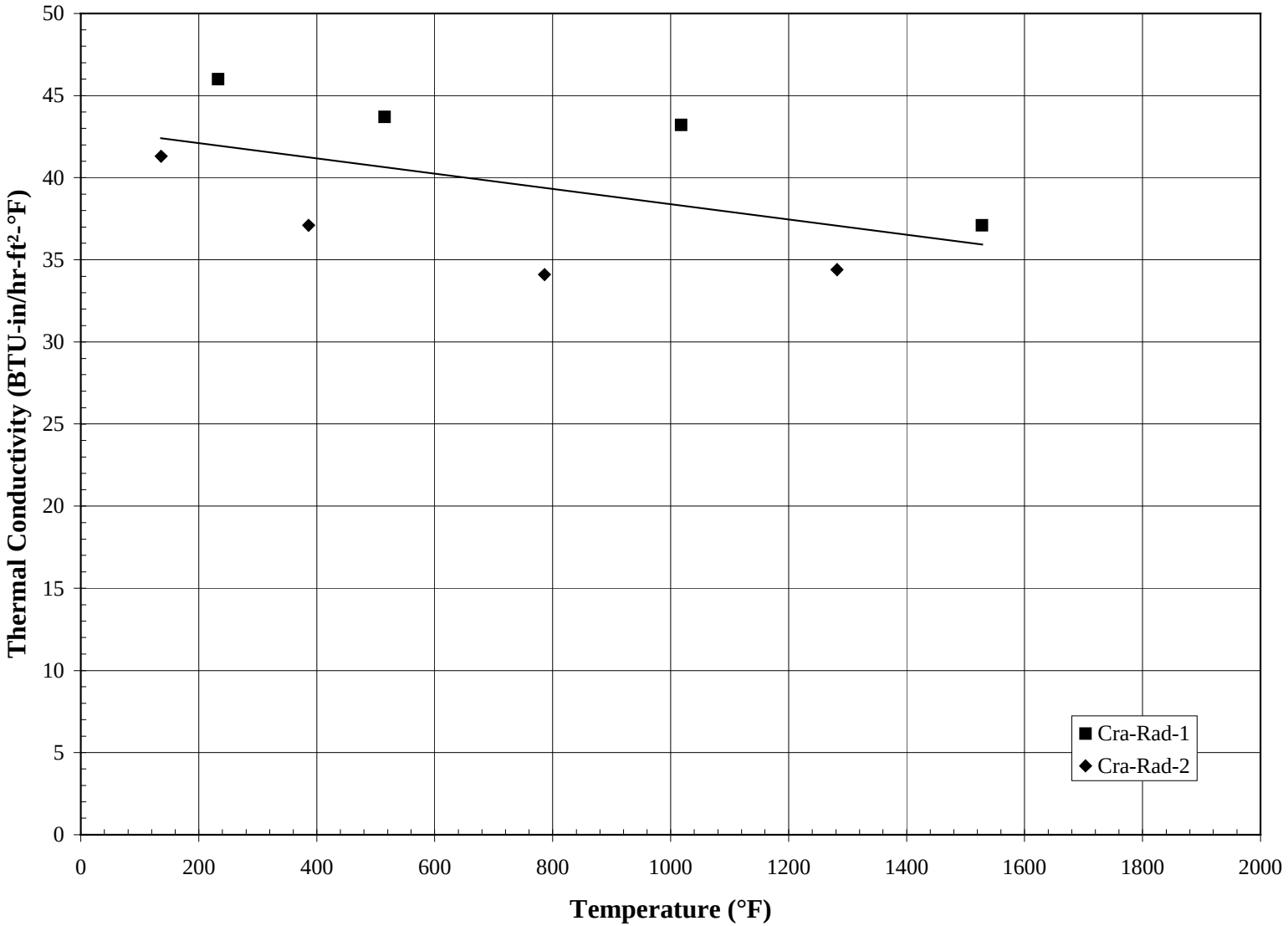

Figure 2-8 Radial Thermal Conductivity Versus Temperature for Virgin Pall 326

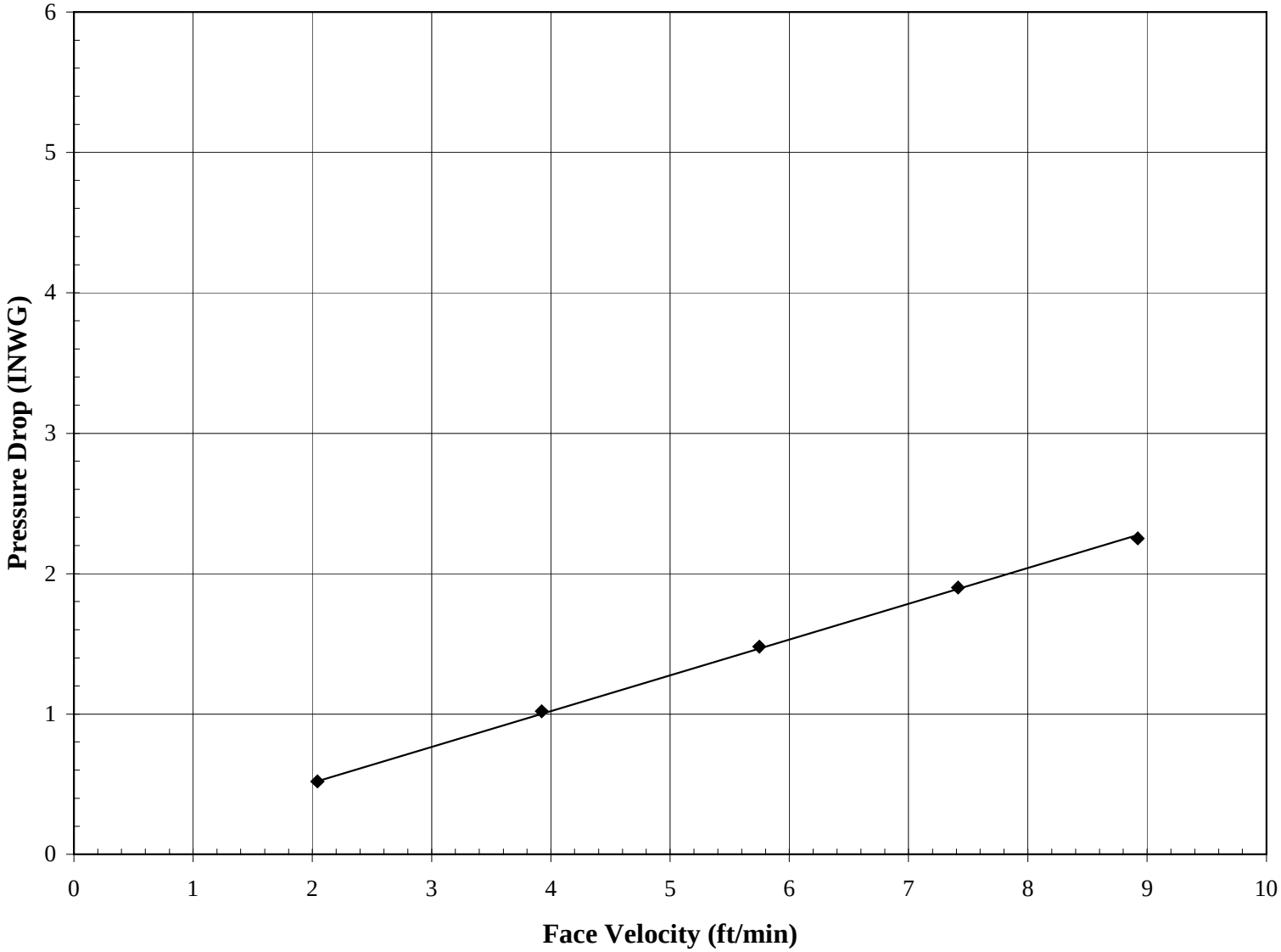

Figure 2-9 Pressure Drop Versus Face Velocity for Virgin Pall 326 Using Air at Ambient Temperature and Pressure

3.0 PALL 181

Pall 181 is a clay-bonded SiC particle material consisting of individual SiC particles or clusters of SiC particles connected by clay or glass bridges. Pall 181 is manufactured with a more crystalline binder containing more mullite than Pall 326. The elements have a structural wall with a nominal I.D. of 1.575 in. (40 mm) and a nominal wall thickness of 0.40 in. (10 mm). Mechanical and thermal properties of the elements are controlled by the structural wall and a relatively thin membrane layer applied to the outside surface provides filtration. Probable values of selected properties of virgin Pall 181 are as follows:

Bulk Density (lbm/ft^3)	113
Hoop Tensile Strength at Room Temperature (psi)	2,800
Axial Tensile Strength at Room Temperature (psi)	2,570
Axial Young's Modulus at Room Temperature (10^6 psi)	6.0
Axial Tensile Strain-to-Failure at Room Temperature (mils/in.)	0.45
Axial Tensile Strength at 1,500°F (psi)	2,060
Axial Young's Modulus at 1,500°F (10^6 psi)	5.0
Axial Tensile Strain-to-Failure at 1,500°F (mils/in.)	0.47
Axial Coefficient of Thermal Expansion, 500 to 1,500°F, (10^{-6} in./in./°F)	2.8
Radial Thermal Conductivity at 1,000°F (Btu-in./hr-ft^2-°F)	32

Table 3-1

Density of Pall 181

Element	Specimen Number	Hours in Operation	I.D. (in.)	O.D. (in.)	Density (gr/cm³)	Density (lb/ft³)	Remarks
7-1405H	Tn-Hoop-190	Virgin	1.55	2.36	1.83	114	
7-1405H	Tn-Hoop-191	Virgin	1.55	2.36	1.82	113	
7-1405H	Tn-Hoop-192	Virgin	1.55	2.36	1.82	114	
7-1405H	Tn-Hoop-193	Virgin	1.55	2.36	1.83	114	
7-1405H	Tn-Hoop-194	Virgin	1.54	2.36	1.82	114	
7-1405H	Tn-Hoop-195	Virgin	1.54	2.36	1.82	113	
7-1405H	Tn-Hoop-196	Virgin	1.52	2.34	1.79	112	
7-1405H	Tn-Hoop-197	Virgin	1.52	2.34	1.80	112	
7-1405H	Tn-Hoop-198	Virgin	1.52	2.33	1.80	112	
7-1405H	Te-Hoop-1	Virgin	1.55	2.37	1.82	114	
7-1405H	Te-Hoop-2	Virgin	1.52	2.34	1.81	113	
		Average			1.81	113	
		Standard Deviation			0.01	0.78	
		Coefficient of Variation (COV)			1%	1%	

Table 3-2

Room Temperature Hoop Tensile Strength of Pall 181

Element	Specimen Number	Hours in Operation	Maximum Hydrostatic Pressure (psig)	Ultimate Strength (psi)	Remarks
7-1405H	Tn-Hoop-190	Virgin	1120	2790	
7-1405H	Tn-Hoop-191	Virgin	1150	2860	
7-1405H	Tn-Hoop-192	Virgin	1180	2930	
7-1405H	Tn-Hoop-193	Virgin	1140	2970	
7-1405H	Tn-Hoop-194	Virgin	1160	2990	
7-1405H	Tn-Hoop-195	Virgin	1140	2920	
7-1405H	Tn-Hoop-196	Virgin	960	2470	
7-1405H	Tn-Hoop-197	Virgin	950	2610	
7-1405H	Tn-Hoop-198	Virgin	990	2700	
Average			1088	2804	
Standard Deviation			88	168	
Coefficient of Variation (COV)			8%	6%	

Table 3-3

Axial Tensile Properties of Virgin Pall 181

Element	Specimen Number	Temp. (°F)	Ultimate Strength (psi)	Young's Modulus (Msi)	Strain-to-Failure (mils/in.)	Remarks
7-1405H	Tn-Ax-76	70				See Note 1
7-1405H	Tn-Ax-80	70	2480	5.19	0.48	
7-1405H	Tn-Ax-84	70	2900	5.56	0.59	
7-1405H	Tn-Ax-87	70				See Note 1
7-1405H	Tn-Ax-90	70	2360	6.20	0.40	
7-1405H	Tn-Ax-92	70	2550	6.59	0.39	
7-1405H	Tn-Ax-93	70				See Note 1
7-1405H	Tn-Ax-94	70	2580	6.67	0.39	
Average			2574	6.04	0.45	
Standard Deviation			180	0.6	0.08	
Coefficient of Variation (COV)			7%	10%	17%	
7-1405H	Tn-Ax-77	1400	2520	4.76	0.54	
7-1405H	Tn-Ax-85	1400	2590	5.74	0.42	
Average			2555	5.25	0.48	
7-1405H	Tn-Ax-78	1500	2210	3.29	0.66	
7-1405H	Tn-Ax-81	1500	2110	5.46	0.39	
7-1405H	Tn-Ax-82	1500	1650	5.25	0.34	
7-1405H	Tn-Ax-83	1500	2270	5.49	0.49	
7-1405H	Tn-Ax-86	1500	2030	4.36	0.49	
7-1405H	Tn-Ax-89	1500	1920	5.96	0.41	
7-1405H	Tn-Ax-91	1500	2230	5.00	0.52	
Average			2060	4.97	0.47	
Standard Deviation			202	0.8	0.10	
COV			10%	17%	21%	
7-1405H	Tn-Ax-79	1600	2170	3.14	0.87	
7-1405H	Tn-Ax-88	1600	2220	4.03	0.89	
7-1405H	Tn-Ax-95	1600	2000	3.64	0.73	
Average			2130	3.60	0.83	
Standard Deviation			94	0.4	0.07	
COV			4%	10%	9%	

Notes:
1. Specimen broke in handling.

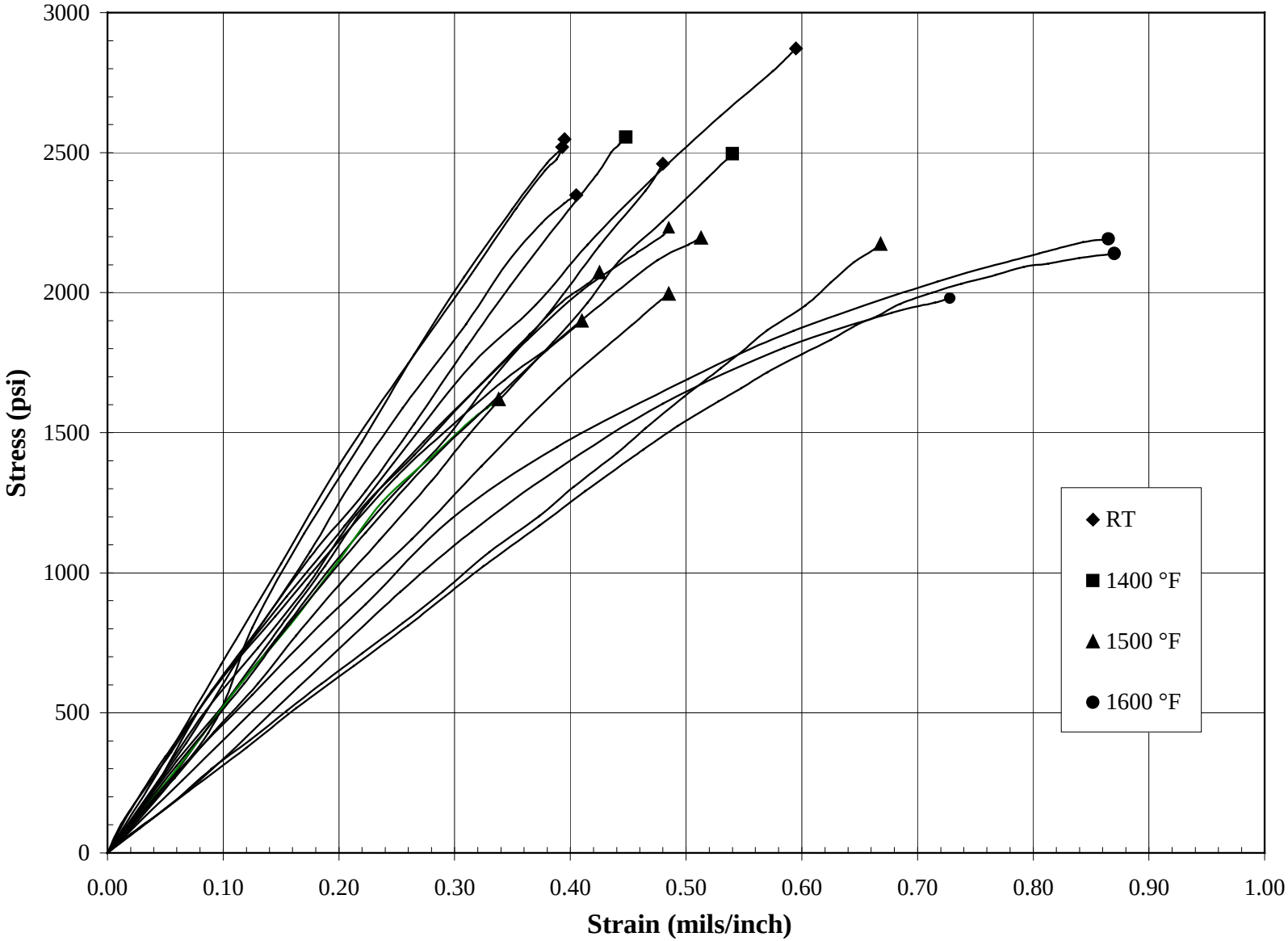

Figure 3-1 Room and Elevated Temperature Axial Tensile Stress-Strain Responses for Virgin Pall 181

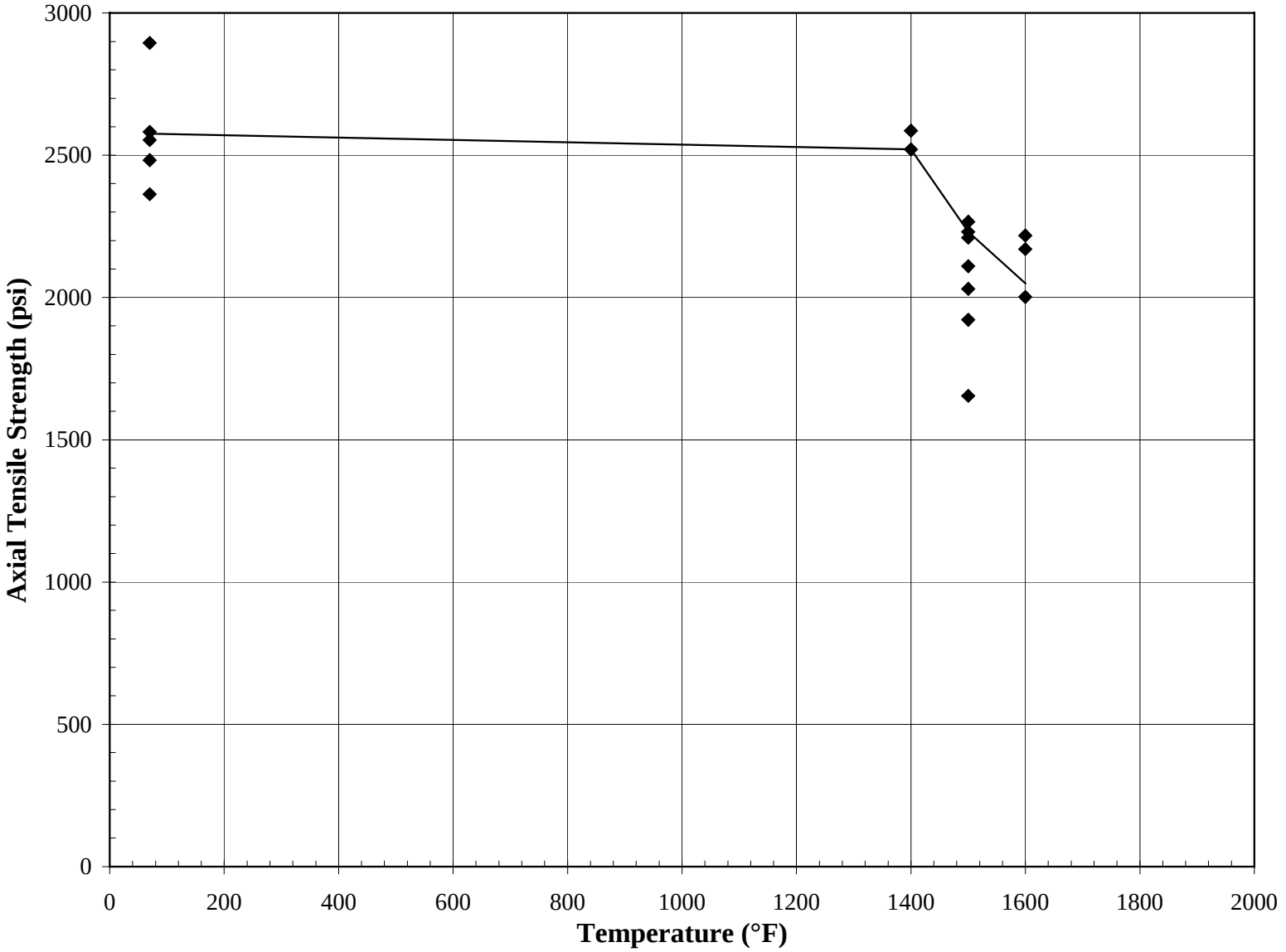

Figure 3-2 Axial Tensile Strength Versus Temperature for Virgin Pall 181

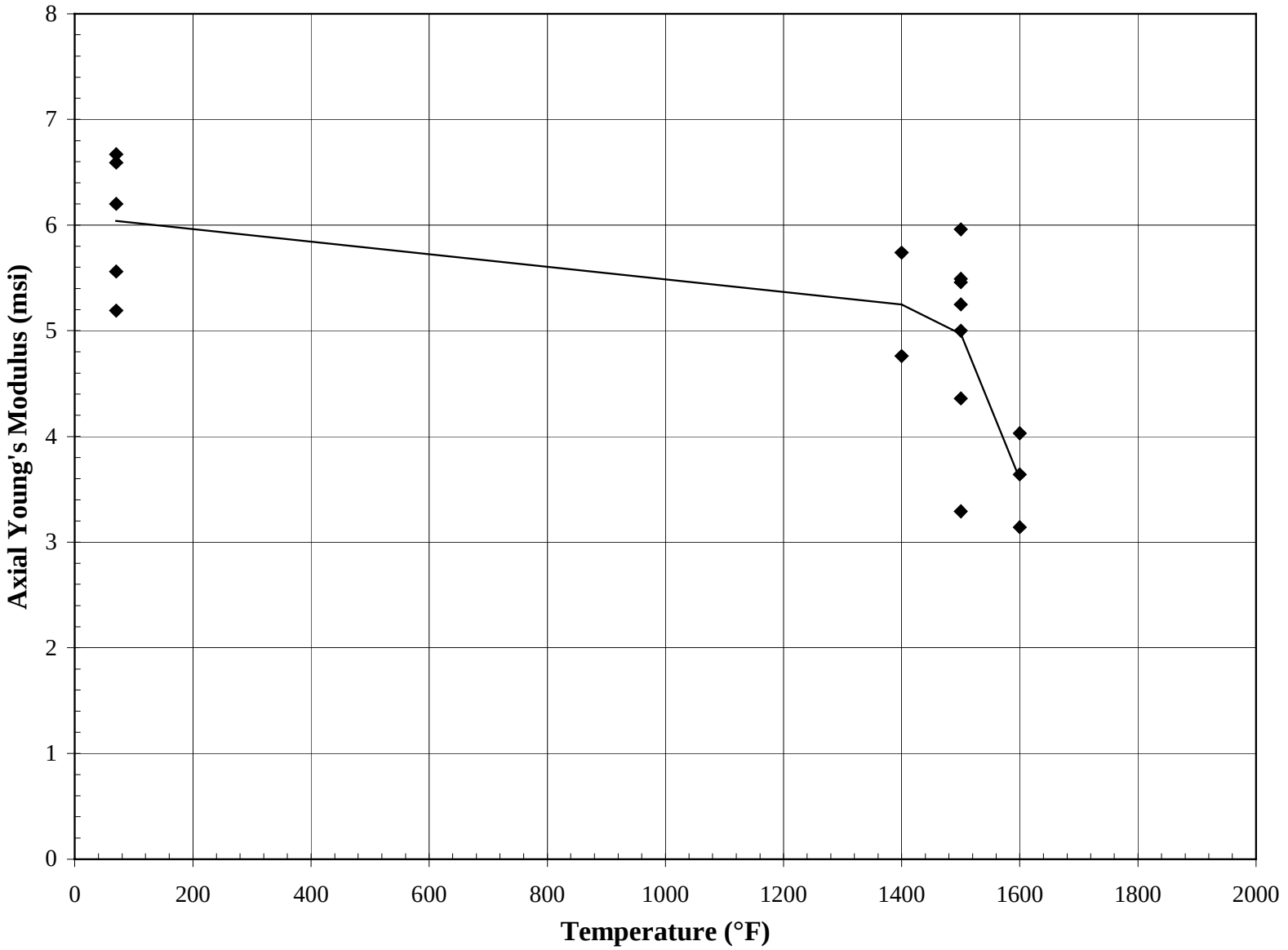

Figure 3-3 Young's Modulus Versus Temperature for Virgin Pall 181

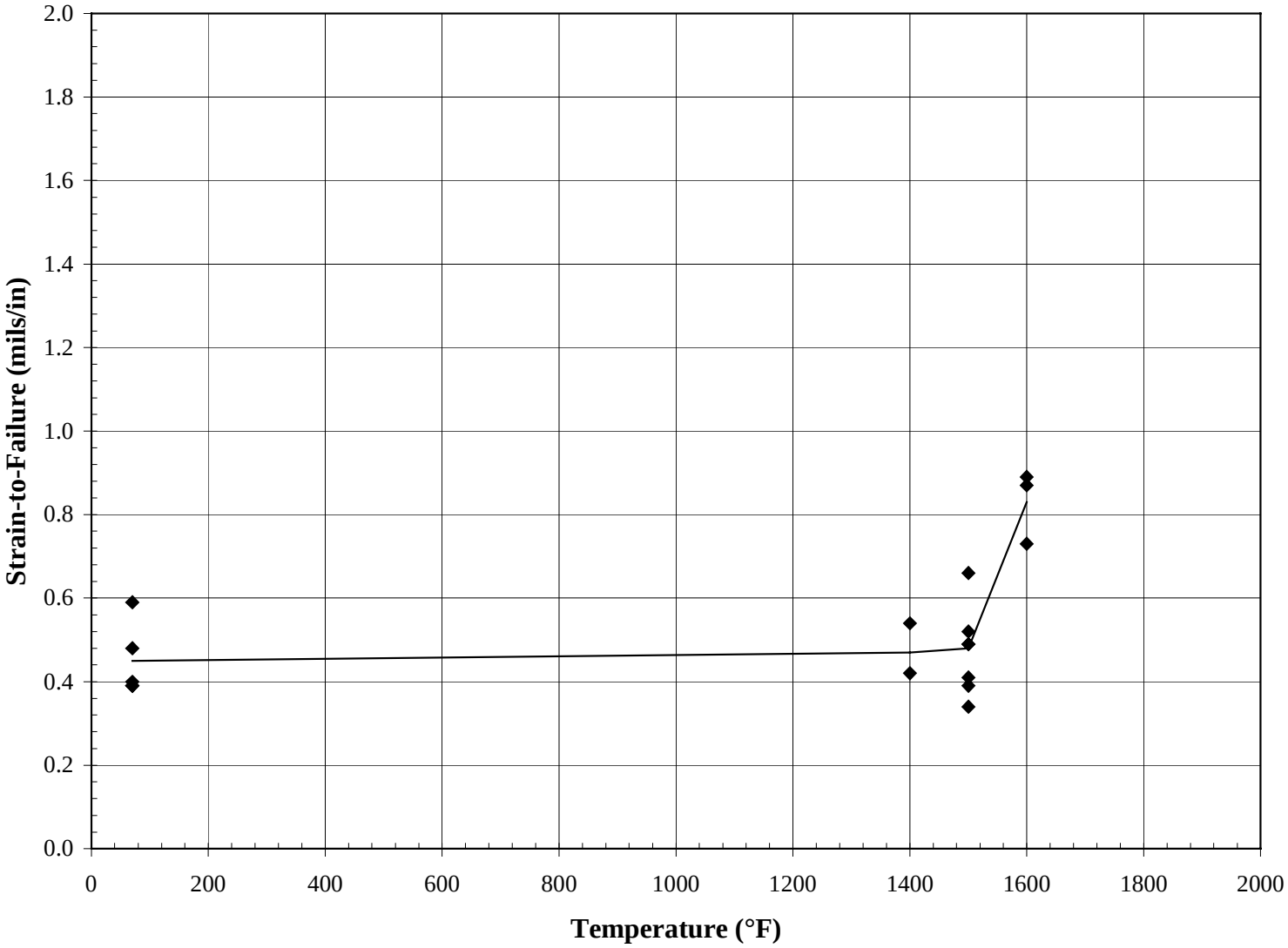

Figure 3-4 Axial Tensile Strain-to-Failure Versus Temperature for Virgin Pall 181

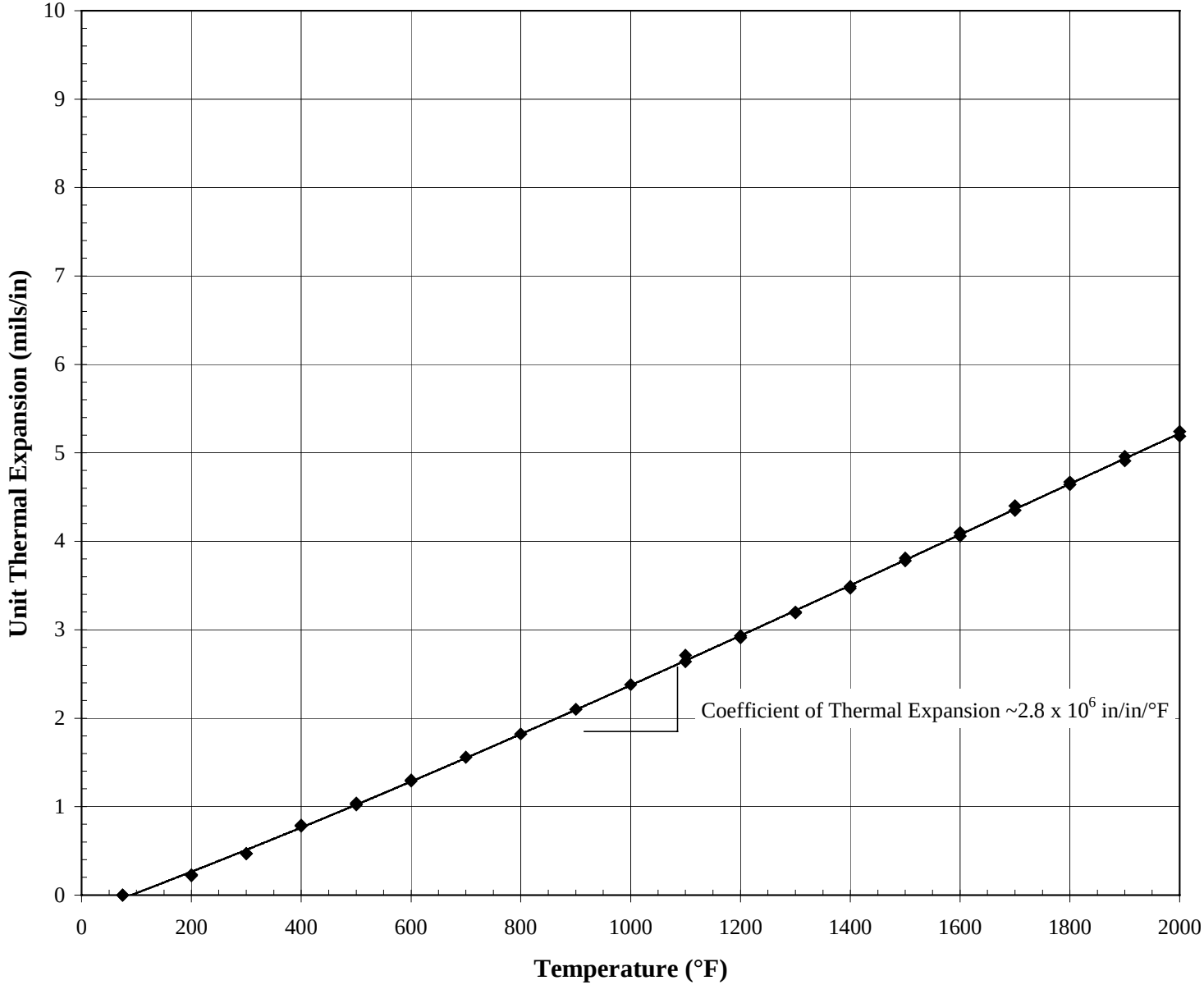

Figure 3-5 Unit Thermal Expansion of Pall 181

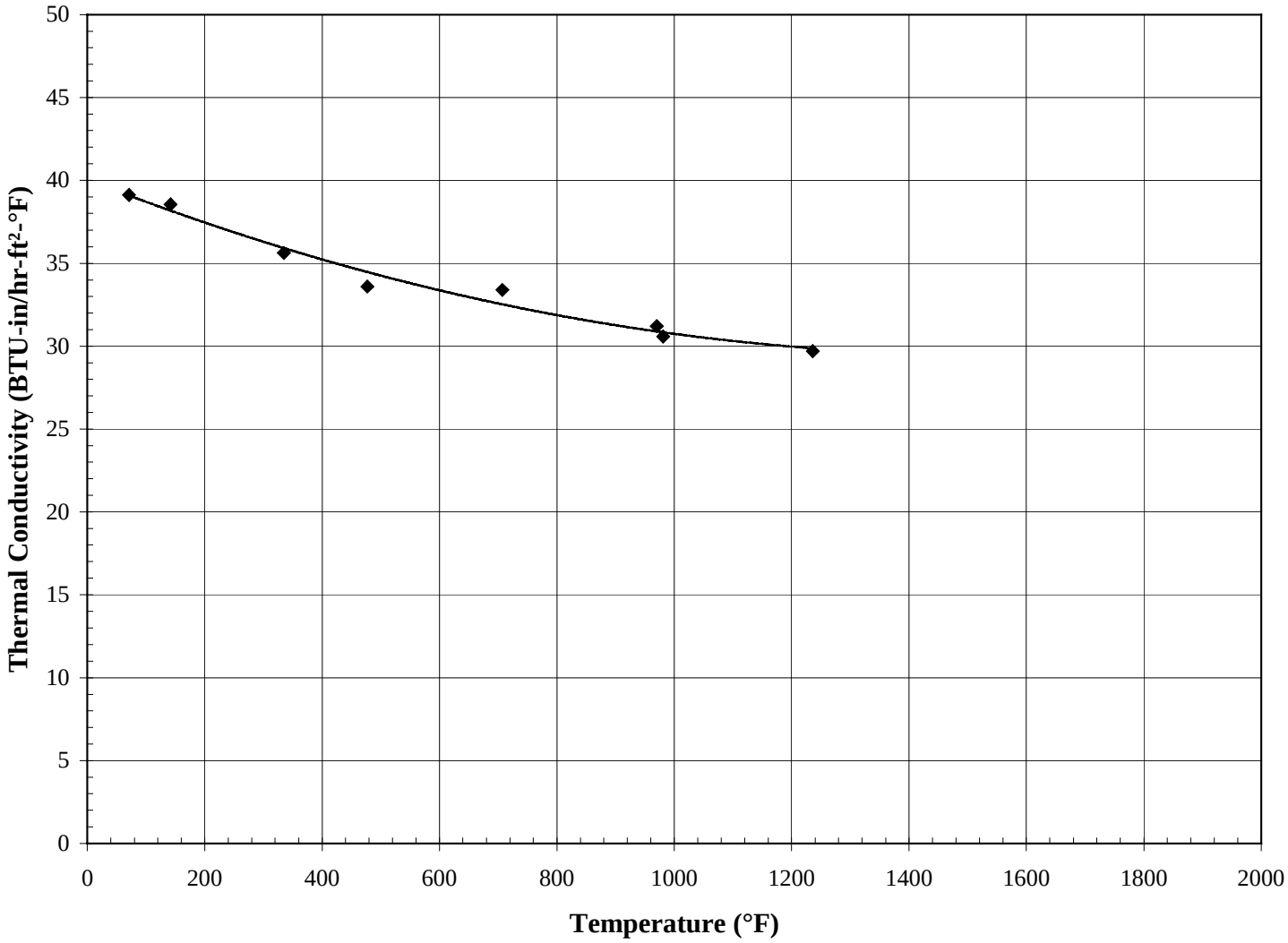

Figure 3-6 Radial Thermal Conductivity Versus Temperature for Virgin Pall 181

4.0 SCHUMACHER F40

Schumacher F40 is a clay-bonded SiC particle material consisting of individual SiC particles connected by clay or glass bridges. The elements have a structural wall with a nominal I.D. of 1.181 in. (30 mm) and a nominal wall thickness of 0.59 in. (15 mm). Mechanical and thermal properties of the elements are controlled by the structural wall and a relatively thin membrane layer applied to the outside surface provides filtration. Probable values of selected properties of virgin Schumacher F40 are as follows:

Bulk Density (lbm/ft^3)	117
Hoop Tensile Strength at Room Temperature (psi)	2,280
Axial Tensile Strength at Room Temperature (psi)	1,120
Axial Young's Modulus at Room Temperature (10^6 psi)	5.9
Axial Tensile Strain-to-Failure at Room Temperature (mils/in.)	0.21
Axial Tensile Strength at 1,500°F (psi)	1,360
Axial Young's Modulus at 1,500°F (10^6 psi)	3.9
Axial Tensile Strain-to-Failure at 1,500°F (mils/in.)	0.41
Axial Compressive Strength at Room Temperature (psi)	9,540
Axial Compressive Strain-to-Failure at Room Temperature (mils/in.)	1.7
Axial Coefficient of Thermal Expansion, 500 to 1,500°F (10^{-6} in./in./°F)	2.5
Radial Thermal Conductivity at 1,000°F (Btu-in./hr-ft^2-°F)	38

Table 4-1

Density of Schumacher F40

Element	Specimen Number	Hours in Operation	Density (gr/cm^3)	Density (lb/ft^3)	Notes
322/314C	Cm-Ax-1	Virgin	1.87	117	
322/314C	Cm-Ax-2	Virgin	1.89	118	
322/314C	Cm-Ax-3	Virgin	1.88	117	
322/314C	Cm-Ax-4	Virgin	1.89	118	
322/314C	Cm-Ax-5	Virgin	1.89	118	
322/314C	Cm-Ax-6	Virgin	1.88	117	
322/314C	Cra-Rad-1	Virgin	1.89	118	
322/314C	Cra-Rad-2	Virgin	1.88	117	
322/314C	Flx-1	Virgin	1.90	118	
322/314C	Flx-2	Virgin	1.87	117	
322/314C	Flx-3	Virgin	1.88	117	
Average			1.88	117	
Standard Deviation			0.007	0.41	
Coefficient of Variation (COV)			0.35%	0.35%	
BB21	Tn-Hoop-18	Unknown	1.893	118	See notes 1,2,3,4
BB21	Tn-Hoop-21	Unknown	1.879	117	See notes 1,2,3,4
BB21	Tn-Hoop-27	Unknown	1.871	117	See notes 1,2,3,4
Average			1.88	117	

Notes:

1. Elements were not washed out before density measurements. Some ash remained in the pores. Density values were calculated based on weights measured with ash in the pores and, therefore, do not represent a material property. The values are for comparison only.
2. BB21 refers to the plenum location during operation and is not an element identification number.
3. All operation in the Siemens Westinghouse advanced particulate filtration system at the American Electric Power PFBC Tidd demonstration plant in Brilliant, Ohio.
4. The operating temperature was < 1,500°F.

Table 4-2

Axial Tensile Properties of Virgin Schumacher F40

Element	Specimen Number	Temp. (°F)	Ultimate Strength (psi)	Young's Modulus (Msi)	Strain-to-Failure, (mils/in.)	Notes
322/314C	Tn-Ax-1	70	1230	5.20	0.26	
322/314C	Tn-Ax-6	70	1160	6.25	0.21	
322/314C	Tn-Ax-12	70	910	6.59	0.15	
322/314C	Tn-Ax-15	70	1020	5.79	0.18	
322/314C	Tn-Ax-21	70	1270	5.54	0.23	
Average			1118	5.87	0.21	
Standard Deviation			134	0.5	0.04	
Coefficient of Variation (COV)			12%	8%	19%	
322/314C	Tn-Ax-4	1500	1080	4.36	0.27	
322/314C	Tn-Ax-11	1500	1360	4.73	0.34	
322/314C	Tn-Ax-14	1500	1370	2.48	0.58	
322/314C	Tn-Ax-18	1500	1510	4.65	0.42	
322/314C	Tn-Ax-20	1500	1460	3.23	0.45	
Average			1356	3.89	0.41	
Standard Deviation			149	0.9	0.10	
COV			11%	23%	25%	
322/314C	Tn-Ax-3	1600	1100	3.95	0.57	
322/314C	Tn-Ax-10	1600	1200	2.83	0.61	
322/314C	Tn-Ax-17	1600	1200	2.52	0.70	
322/314C	Tn-Ax-19	1600	1340	3.03	0.64	
322/314C	Tn-Ax-22	1600	1280	2.66	0.57	
Average			1224	3.00	0.62	
Standard Deviation			81	0.5	0.05	
COV			7%	17%	8%	
322/314C	Tn-Ax-2	1700	1120	1.23	1.63	
322/314C	Tn-Ax-5	1700	1170	1.43	1.66	
322/314C	Tn-Ax-9	1700	1080	1.10	2.28	
322/314C	Tn-Ax-13	1700	1180	1.30	1.61	
322/314C	Tn-Ax-16	1700	1190	1.46	2.13	
Average			1148	1.30	1.86	
Standard Deviation			42	0.13	0.28	
COV			4%	10%	15%	
322/314C	Tn-Ax-24	1800	1150			
322/314C	Tn-Ax-27	1800	1130	0.57	10.0	
322/314C	Tn-Ax-30	1800	1010	0.87	5.0	
322/314C	Tn-Ax-36	1800	1120	0.81	6.8	
Average			1103	0.75	7.3	
Standard Deviation			54	0.13	2.07	
COV			5%	17%	28%	

Table 4-3

Axial Tensile Properties of Schumacher F40 After Combustion Operation

Element	Specimen Number	Temp. (°F)	Ultimate Strength (psi)	Young's Modulus (Msi)	Strain-to-Failure (mils/in.)	Notes
BB21	Tn-Ax-54	70	440	4.60	0.10	See Notes 1,2,3
BB21	Tn-Ax-55	70	380	3.88	0.11	See Notes 1,2,3
BB21	Tn-Ax-40	1500	740	2.29	0.43	See Notes 1,2,3
BB21	Tn-Ax-43	1500	780	1.69	0.52	See Notes 1,2,3

Notes:
1. BB21 refers to the plenum location during operation and is not an element identification number.
2. All operation in the Siemens Westinghouse advanced particulate filtration system at the American Electric Power PFBC Tidd demonstration plant in Brilliant, Ohio.
3. The operating temperature was < 1,500°F. Time in operation was unknown.

Table 4-4

Room Temperature Hoop Tensile Strength of Schumacher F40

Element	Specimen Number	Hours in Operation	Maximum Hydrostatic Pressure (psig)	Ultimate Strength (psi)	Notes
322/314C	Tn-Hoop-1	virgin	1410	2250	
322/314C	Tn-Hoop-2	virgin	1420	2340	
322/314C	Tn-Hoop-4	virgin	1340	2210	
322/314C	Tn-Hoop-5	virgin	1390	2310	
	Average		1390	2278	
	Standard Deviation		31	51	
	Coefficient of Variation (COV)		2.2%	2.2%	
BB21	Tn-Hoop-18	Unknown	780	1250	See Notes 1,2,3
BB21	Tn-Hoop-22	Unknown	750	1220	See Notes 1,2,3
BB21	Tn-Hoop-27	Unknown	640	1050	See Notes 1,2,3
	Average		723	1173	

Notes:
1. BB21 refers to the plenum location during operation and is not an element identification number.
2. All operation in the Siemens Westinghouse advanced particulate filtration system at the American Electric Power PFBC Tidd demonstration plant in Brilliant, Ohio.
3. The operating temperature was < 1,500°F.

Table 4-5

Axial Compressive Properties of Virgin Schumacher F40

Element	Specimen Number	Temp. (°F)	Ultimate Strength (psi)	Young's Modulus (Msi)	Strain-to-Failure, (mils/in.)	Notes
322/314C	Cm-Ax-1	70	9260	6.06	1.6	
322/314C	Cm-Ax-3	70	9820	6.10	1.8	
322/314C	Cm-Ax-5	70				See Note 1
Average			9540	6.08	1.7	
322/314C	Cm-Ax-2	1700	7400	2.50	7.3	
322/314C	Cm-Ax-4	1700	7860	3.00	8.0	
322/314C	Cm-Ax-6	1700	7860	2.83	7.7	
Average			7707	2.78	7.7	

Notes:
1. Broken during setup.

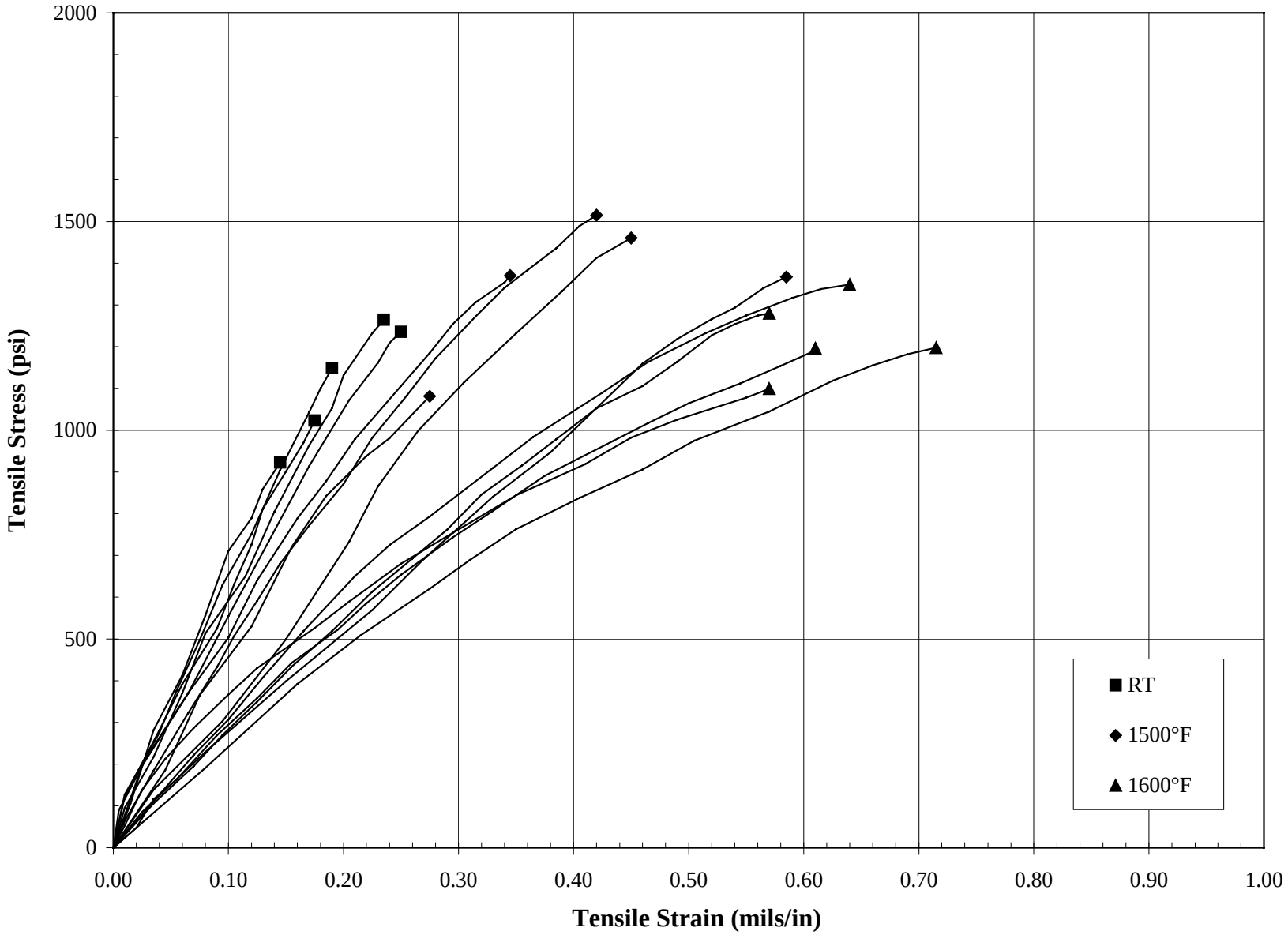

Figure 4-1 Axial Tensile Stress-Strain Responses of Virgin Schumacher F40 at Room Temperature, 1,500 and 1,600°F.

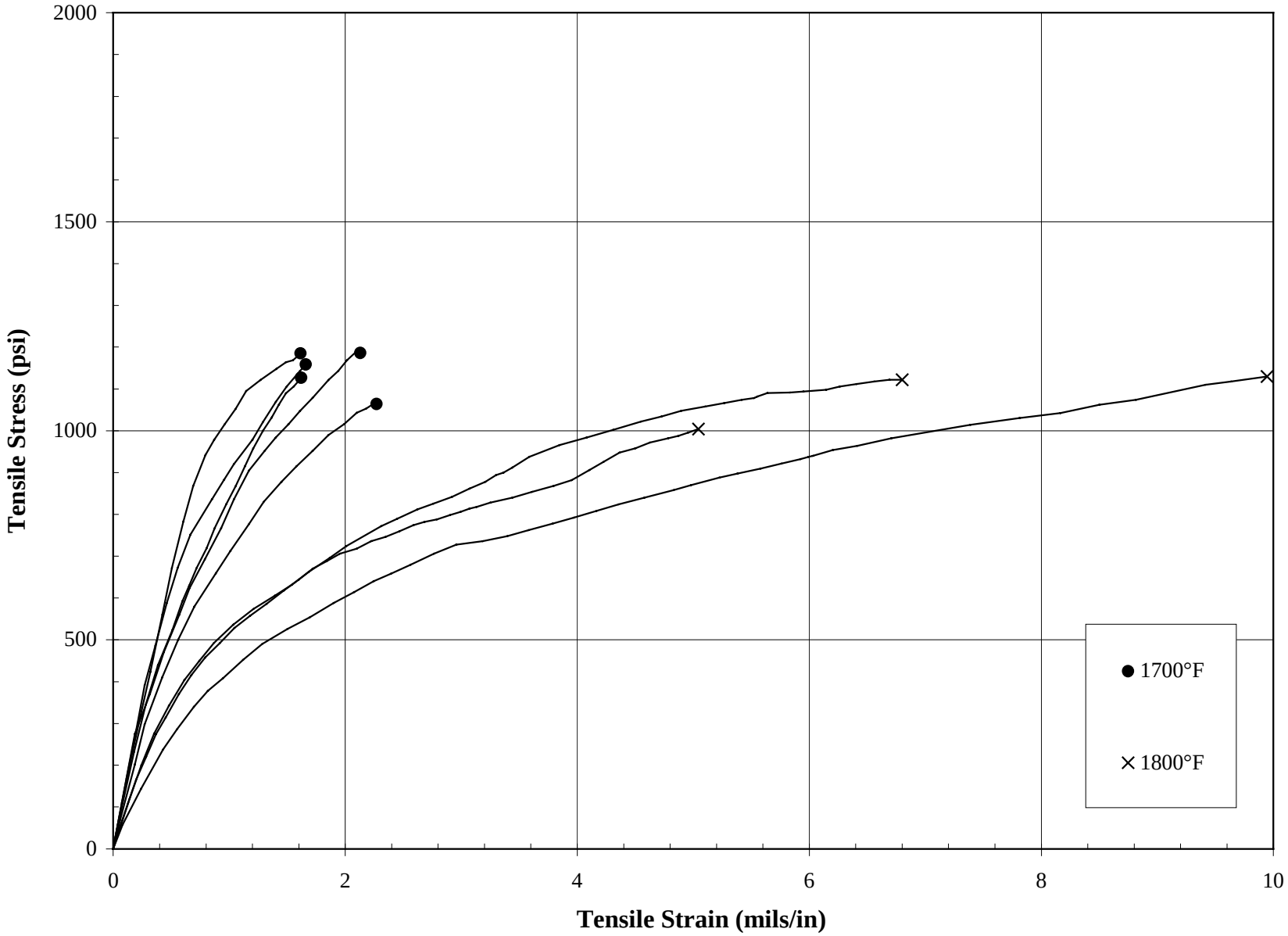

Figure 4-2 Axial Tensile Stress-Strain Responses of Virgin Schumacher F40 at 1,700 and 1,800°F

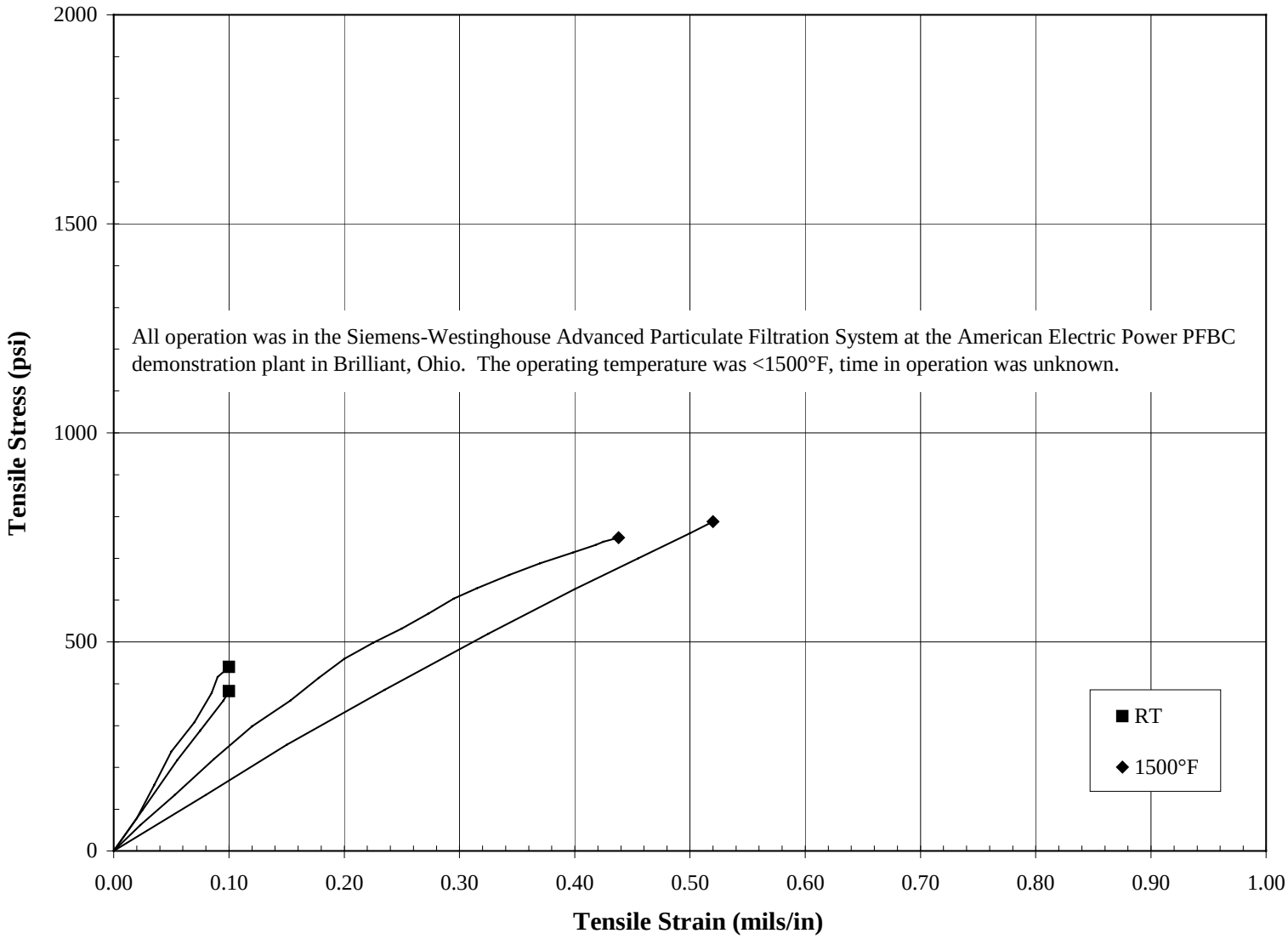

Figure 4-3 Axial Tensile Stress-Strain Responses of Schumacher F40 After Combustion Operation

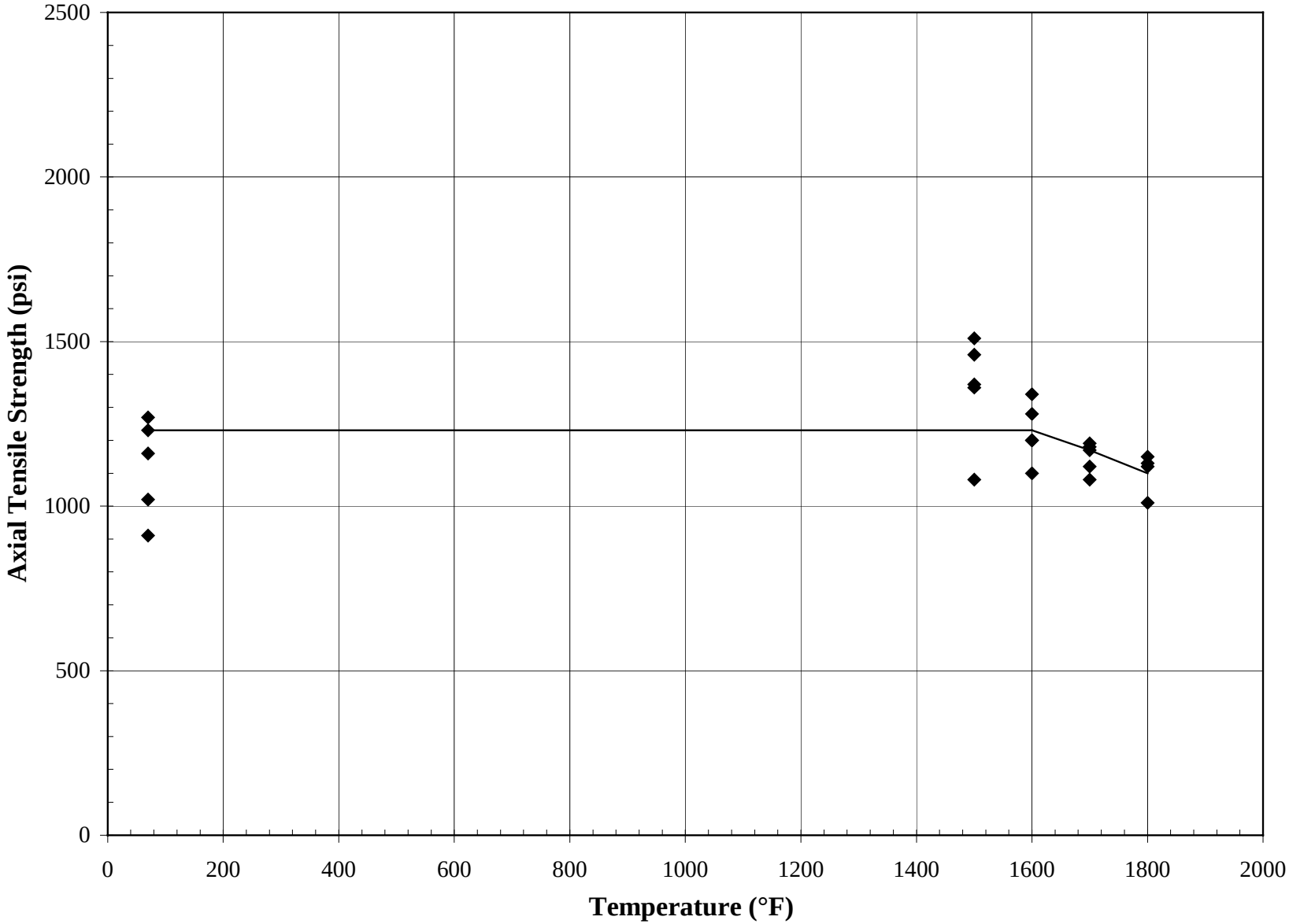

Figure 4-4 Axial Tensile Strength Versus Temperature for Virgin Schumacher F40

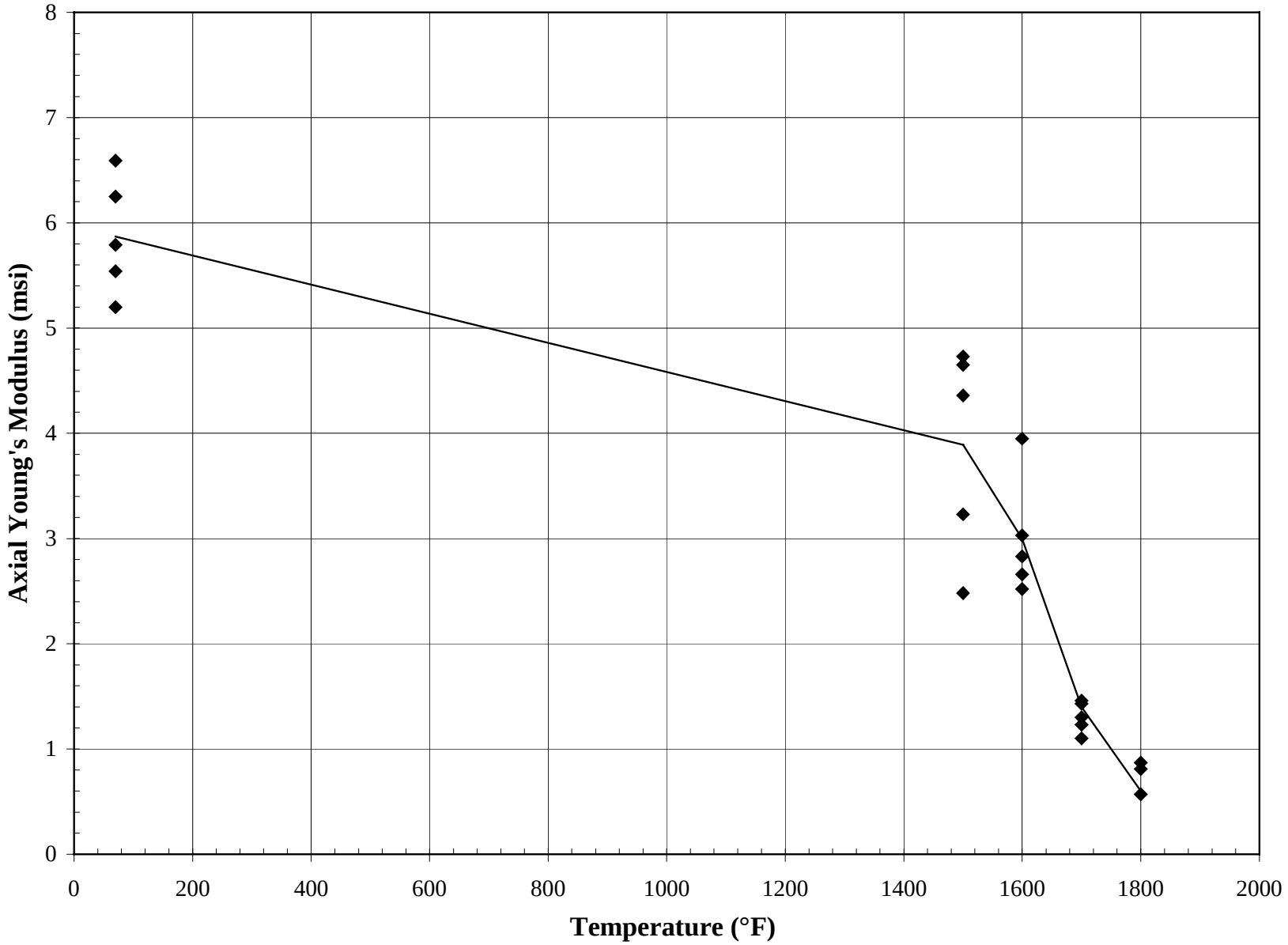

Figure 4-5 Young's Modulus Versus Temperature for Virgin Schumacher F40

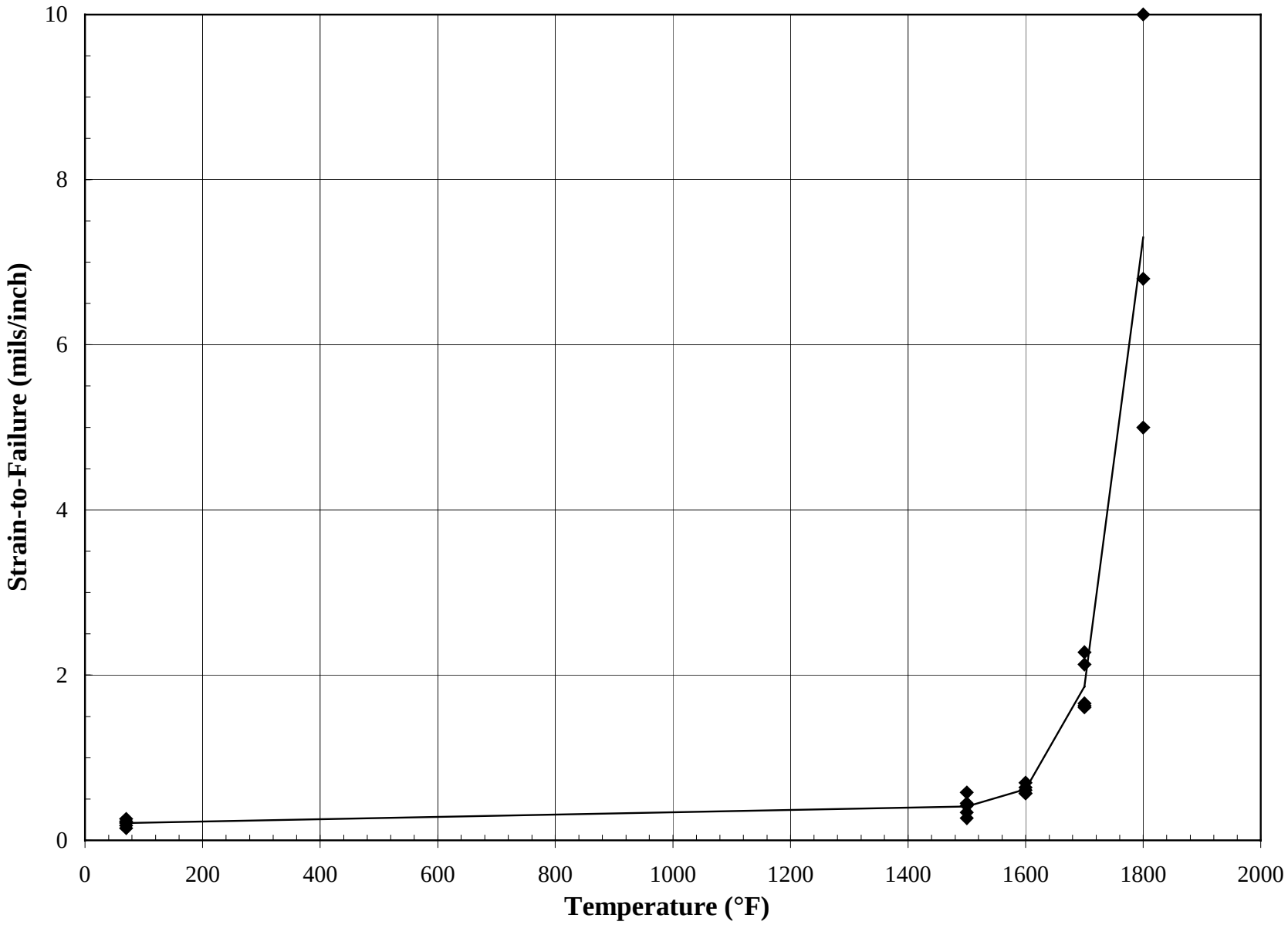

Figure 4-6 Axial Tensile Strain-to-Failure Versus Temperature for Virgin Schumacher F40

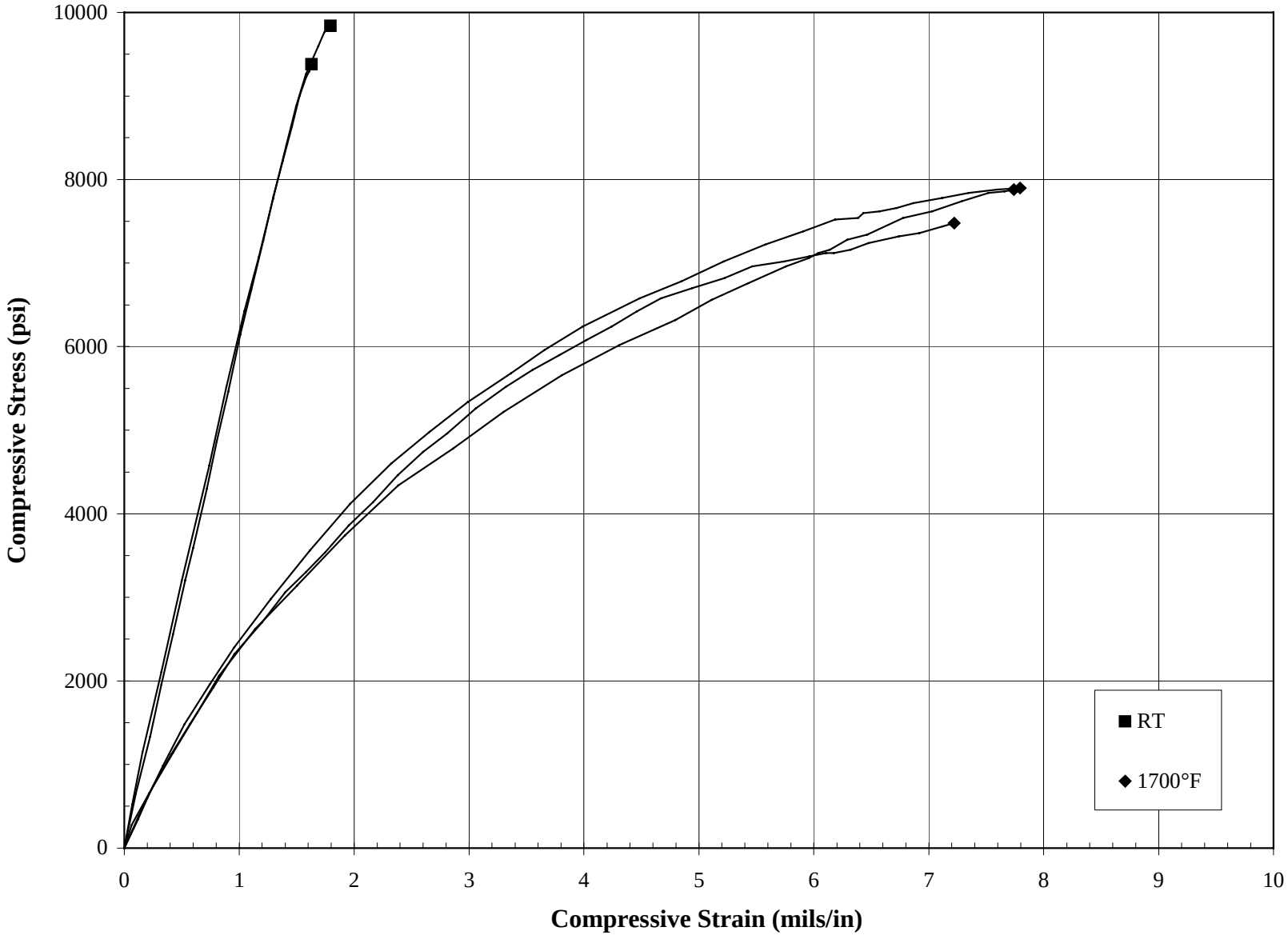

Figure 4-7 Axial Compressive Stress-Strain Response of Virgin Schumacher F40 at Room Temperature and 1,700°F

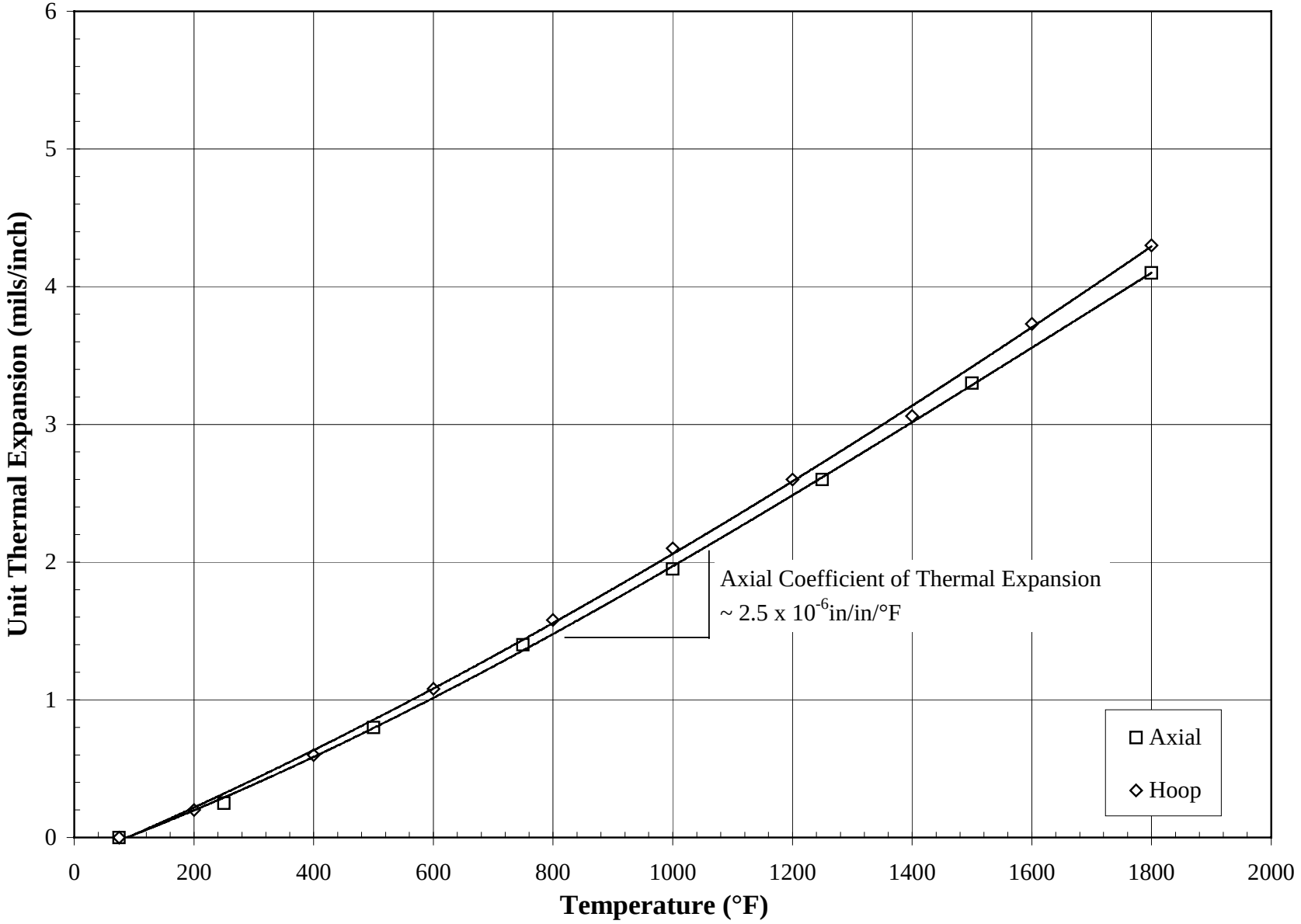

Figure 4-8 Unit Thermal Expansion of Virgin Schumacher F40

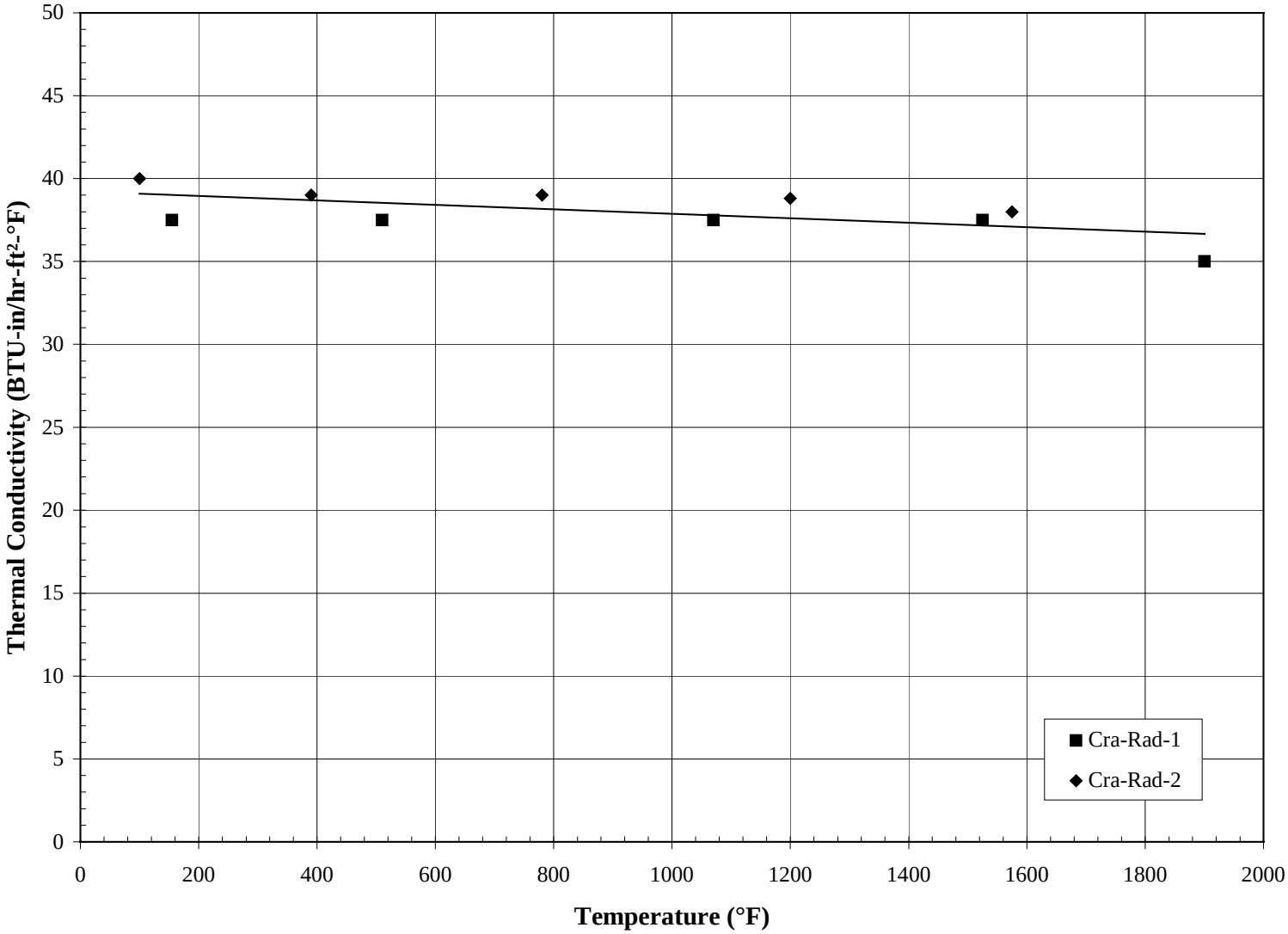

Figure 4-9 Radial Thermal Conductivity Versus Temperature for Virgin Schumacher F40

5.0 SCHUMACHER TF20 AND T10-20

Schumacher TF20 and T10-20 are clay-bonded SiC particle materials similar to Schumacher F40 except with a different binder to reduce creep. The microstructure consists of individual SiC particles connected by clay or glass bridges. The elements have a structural wall with a nominal I.D. of 1.575 in. (40 mm) and a nominal wall thickness of 0.40 in. (10 mm). Mechanical and thermal properties of the elements are controlled by the structural wall and a relatively thin-membrane layer applied to the outside surface provides filtration. The structural walls of TF20 and T10-20 are the same, but the filtration membranes are different in chemical composition and pore size. Since mechanical and thermal properties are controlled by the structural walls, properties of these two materials are tabulated together in one section. Probable values of selected properties of virgin Schumacher TF20 and T10-20 are as follows:

Bulk Density (lbm/ft^3)	121
Hoop Tensile Strength at Room Temperature (psi)	1,900
Axial Tensile Strength at Room Temperature (psi)	900
Axial Young's Modulus at Room Temperature (10^6 psi)	4.0
Axial Tensile Strain-to-Failure at Room Temperature (mils/in.)	0.22
Axial Tensile Strength at 1,500°F (psi)	1,200
Axial Young's Modulus at 1,500°F (10^6 psi)	2.3
Axial Tensile Strain-to-Failure at 1,500°F (mils/in.)	0.40
Axial Coefficient of Thermal Expansion, 500 to 1,500°F (10^{-6} in./in./°F)	2.6
Radial Thermal Conductivity at 1,000°F (Btu-in./hr-ft^2-°F)	52
Pressure Drop at 5 ft/min Face Velocity, Air at Ambient Conditions(inWG)	2.1 TF20
Pressure Drop at 5 ft/min Face Velocity, Air at Ambient Conditions(inWG)	4.4 T10-20

Table 5-1 (Page 1 of 2)

Density of Schumacher TF20 and T10-20

Material	Element	Specimen Number	Hours in Operation	I.D. (in.)	O.D. (in.)	Density (gr/cm³)	Density (lb/ft³)	Remarks
TF20	S199/315E PT-20	Tn-Hoop-1	Virgin	1.54	2.37	1.94	121	
TF20	S199/315E PT-20	Tn-Hoop-2	Virgin	1.54	2.37	1.94	121	
TF20	S199/315E PT-20	Tn-Hoop-3	Virgin	1.53	2.37	1.94	121	
TF20	344E-295	Tn-Hoop-1	Virgin	1.54	2.38	1.95	122	
TF20	344E-295	Tn-Hoop-2	Virgin	1.54	2.38	1.95	122	
TF20	344E-295	Tn-Hoop-3	Virgin	1.54	2.38	1.96	122	
TF20	344E-309	Tn-Hoop-4	Virgin	1.53	2.38	1.93	120	
TF20	344E-309	Tn-Hoop-5	Virgin	1.53	2.38	1.93	120	
TF20	344E-309	Tn-Hoop-6	Virgin	1.53	2.38	1.93	120	
			Average			1.94	121	
			Standard Deviation			0.011	0.68	
			Coefficient of Variation (COV)			0.57%	0.57%	
TF20	324H21	Tn-Hoop-264	491	1.561	2.386	1.94	121	See Notes 1,2,3
TF20	324H21	Tn-Hoop-265	491	1.568	2.384	1.94	121	See Notes 1,2,3
TF20	324H21	Tn-Hoop-266	491	1.572	2.379	1.95	122	See Notes 1,2,3
TF20	324H21	Tn-Hoop-267	491	1.587	2.387	1.94	121	See Notes 1,2,3
TF20	324H21	Tn-Hoop-268	491	1.585	2.381	1.94	121	See Notes 1,2,3
TF20	324H21	Tn-Hoop-269	491	1.591	2.387	1.94	121	See Notes 1,2,3
TF20	324H21	Tn-Hoop-270	491	1.605	2.389	1.93	120	See Notes 1,2,3
TF20	324H21	Tn-Hoop-271	491	1.601	2.384	1.93	120	See Notes 1,2,3
TF20	324H21	Tn-Hoop-272	491	1.607	2.385	1.93	120	See Notes 1,2,3
			Average			1.94	121	
			Standard Deviation			0.008	0.48	
			Coefficient of Variation (COV)			0.40%	0.40%	
TF20	S-350 F/33	Tn-Hoop-1	540	1.63	2.39	1.99	124	See Notes 1,4
TF20	S-350 F/33	Tn-Hoop-2	540	1.63	2.39	1.98	123	See Notes 1,4
TF20	S-350 F/33	Tn-Hoop-3	540	1.62	2.39	1.99	124	See Notes 1,4
TF20	S-350 F/33	Tn-Hoop-4	540	1.60	2.39	1.99	124	See Notes 1,4
TF20	S-350 F/33	Tn-Hoop-5	540	1.60	2.39	1.98	124	See Notes 1,4
TF20	S-350 F/33	Tn-Hoop-6	540	1.60	2.39	1.99	124	See Notes 1,4
TF20	S-350 F/33	Tn-Hoop-7	540	1.58	2.39	1.97	123	See Notes 1,4
TF20	S-350 F/33	Tn-Hoop-8	540	1.57	2.38	1.98	123	See Notes 1,4
TF20	S-350 F/33	Tn-Hoop-9	540	1.58	2.38	1.98	123	See Notes 1,4
			Average			1.98	124	
			Standard Deviation			0.006	0.35	
			Coefficient of Variation (COV)			0.28%	0.28%	
TF20	324H01	Tn-Hoop-273	994	1.558	2.384	1.95	121	See Notes 1,2,3
TF20	324H01	Tn-Hoop-274	994	1.567	2.381	1.94	121	See Notes 1,2,3
TF20	324H01	Tn-Hoop-275	994	1.574	2.379	1.96	122	See Notes 1,2,3
TF20	324H01	Tn-Hoop-276	994	1.586	2.381	1.95	122	See Notes 1,2,3
TF20	324H01	Tn-Hoop-277	994	1.584	2.383	1.94	121	See Notes 1,2,3
TF20	324H01	Tn-Hoop-278	994	1.586	2.386	1.94	121	See Notes 1,2,3
TF20	324H01	Tn-Hoop-279	994	1.615	2.393	1.93	121	See Notes 1,2,3
TF20	324H01	Tn-Hoop-280	994	1.609	2.382	1.94	121	See Notes 1,2,3
TF20	324H01	Tn-Hoop-281	994	1.591	2.362	1.96	122	See Notes 1,2,3
			Average			1.94	121	
			Standard Deviation			0.008	0.50	
			COV			0.41%	0.41%	

Table 5-1 (Page 2 of 2)

Density of Schumacher TF20 and T10-20

Material	Candle	Specimen Number	Hours in Operation	I.D. (in.)	O.D. (in.)	Density (gr/cm³)	Density (lb/ft³)	Remarks
TF20	324H04	Tn-Hoop-282	1234	1.556	2.381	1.93	121	See Notes 1,2,3
TF20	324H04	Tn-Hoop-283	1234	1.545	2.379	1.93	121	See Notes 1,2,3
TF20	324H04	Tn-Hoop-284	1234	1.584	2.389	1.94	121	See Notes 1,2,3
TF20	324H04	Tn-Hoop-285	1234	1.585	2.380	1.94	121	See Notes 1,2,3
TF20	324H04	Tn-Hoop-286	1234	1.587	2.384	1.94	121	See Notes 1,2,3
TF20	324H04	Tn-Hoop-287	1234	1.587	2.387	1.94	121	See Notes 1,2,3
TF20	324H04	Tn-Hoop-288	1234	1.603	2.381	1.95	121	See Notes 1,2,3
TF20	324H04	Tn-Hoop-289	1234	1.606	2.381	1.96	122	See Notes 1,2,3
TF20	324H04	Tn-Hoop-290	1234	1.606	2.379	1.94	121	See Notes 1,2,3
			Average			1.94	121	
			Standard Deviation			0.007	0.41	
			COV			0.34%	0.34%	
T10-20	324H02	Tn-Hoop-291	1788	1.564	2.378	1.98	123	See Notes 1,2
T10-20	324H02	Tn-Hoop-292	1788	1.566	2.370	1.98	124	See Notes 1,2
T10-20	324H02	Tn-Hoop-293	1788	1.570	2.368	1.98	124	See Notes 1,2
T10-20	324H02	Tn-Hoop-294	1788	1.588	2.380	1.98	123	See Notes 1,2
T10-20	324H02	Tn-Hoop-295	1788	1.590	2.379	1.98	124	See Notes 1,2
T10-20	324H02	Tn-Hoop-296	1788	1.585	2.376	1.99	124	See Notes 1,2
T10-20	324H02	Tn-Hoop-297	1788	1.600	2.376	1.99	124	See Notes 1,2
T10-20	324H02	Tn-Hoop-298	1788	1.606	2.382	1.98	123	See Notes 1,2
T10-20	324H02	Tn-Hoop-299	1788	1.602	2.375	1.98	124	See Notes 1,2
			Average			1.98	124	
			Standard Deviation			0.004	0.23	
			Coefficient of Variation (COV)			0.19%	0.19%	
T10-20	324H01	Tn-Hoop-300	1792	1.562	2.381	1.97	123	See Notes 1,2,3
T10-20	324H01	Tn-Hoop-301	1792	1.569	2.380	1.97	123	See Notes 1,2,3
T10-20	324H01	Tn-Hoop-302	1792	1.571	2.381	1.97	123	See Notes 1,2,3
T10-20	324H01	Tn-Hoop-303	1792	1.588	2.383	1.98	124	See Notes 1,2,3
T10-20	324H01	Tn-Hoop-304	1792	1.589	2.385	1.97	123	See Notes 1,2,3
T10-20	324H01	Tn-Hoop-305	1792	1.592	2.386	1.98	124	See Notes 1,2,3
T10-20	324H01	Tn-Hoop-306	1792	1.604	2.391	1.99	124	See Notes 1,2,3
T10-20	324H01	Tn-Hoop-307	1792	1.605	2.390	1.99	124	See Notes 1,2,3
T10-20	324H01	Tn-Hoop-308	1792	1.608	2.389	1.98	124	See Notes 1,2,3
			Average			1.98	124	
			Standard Deviation			0.007	0.43	
			COV			0.35%	0.35%	

Notes:

1. Elements were water washed before density measurements but some ash remained in the pores. Density values were calculated based on weights measured with ash in the pores and, therefore, do not represent a material property. The values are for comparison only.
2. All operation at the SCS PSDF in combustion mode at a nominal-operating temperature of 1,400°F.
3. In operation during October 1998 PCD fire.
4. All operation in the Siemens Westinghouse advanced particulate filtration system at the Foster Wheeler PCFBC test facility in Karhula, Finland. Nominal-operating temperature was 1,550°F.

Table 5-2

Axial Tensile Properties of Virgin Schumacher TF20 and T10-20

Material	Candle Identification	Specimen Number	Temperature (°F)	Ultimate Strength (psi)	Young's Modulus (Msi)	Strain-to-Failure (mils/in.)	Remarks
TF20	344E-295	Tn-Ax-3	70	430	3.22	0.15	
TF20	344E-295	Tn-Ax-7	70	410	3.70	0.11	
TF20	344E-309	Tn-Ax-12	70	800	4.28	0.20	
TF20	344E-309	Tn-Ax-17	70	500	5.00	0.10	
TF20	344E-309	Tn-Ax-21	70	900	3.92	0.23	
	Average			608	4.02	0.16	
	Standard Deviation			202	0.6	0.05	
	COV			33%	15%	32%	
T10-20	360H071	Tn-Ax-28	70	970	3.85	0.26	
T10-20	360H071	Tn-Ax-29	70	900	4.10	0.22	
	Average			935	3.98	0.24	
TF20	344E-311	Tn-Ax-24	1400	1260	1.87	0.68	
TF20	344E-311	Tn-Ax-26	1400	1240	3.79	0.35	
TF20	344E-311	Tn-Ax-28	1400	1140	2.88	0.43	
	Average			1213	2.85	0.49	
TF20	344E-295	Tn-Ax-2	1500	1400	2.20	0.64	
TF20	344E-309	Tn-Ax-18	1500	890	2.32	0.38	
TF20	344E-311	Tn-Ax-30	1500	880	2.35	0.40	
	Average			1057	2.29	0.47	
TF20	344E-309	Tn-Ax-14	1600	1260			See Note 1
TF20	344E-295	Tn-Ax-6	1600	1420	2.25	0.73	
TF20	344E-311	Tn-Ax-31	1600	1210	2.92	0.49	
	Average			1297	2.59	0.61	
TF20	344E-295	Tn-Ax-4	1700	1270	1.77	1.30	
TF20	344E-311	Tn-Ax-32	1700	1170	1.72	0.91	
	Average			1220	1.75	1.11	

Notes:
1. Strain measurements wee not obtained because strain flags slipped during test.

Table 5-3

Room Temperature Axial Tensile Properties of Schumacher TF20 and T10-20
Virgin and After-Combustion Operation

Material	Element	Specimen Number	Hours in Operation	Ultimate Strength (psi)	Young's Modulus (Msi)	Strain-to-Failure, (mils/in.)	Remarks
TF20	344E-295	Tn-Ax-3	Virgin	430	3.22	0.15	
TF20	344E-295	Tn-Ax-7	Virgin	410	3.70	0.11	
TF20	344E-309	Tn-Ax-12	Virgin	800	4.28	0.20	
TF20	344E-309	Tn-Ax-17	Virgin	500	5.00	0.10	
TF20	344E-309	Tn-Ax-21	Virgin	900	3.92	0.23	
	Average			608	4.02	0.16	
	Standard Deviation			202	0.6	0.05	
	Coefficient of Variation (COV)			33%	15%	32%	
TF20	S-350 F/33	Tn-Ax-1	540				See Notes 1,2
TF20	S-350 F/33	Tn-Ax-2	540	800	3.22	0.32	See Note 1
TF20	S-350 F/33	Tn-Ax-3	540	810	3.83	0.31	See Note 1
	Average			805	3.53	0.32	
TF20	324H12	Tn-Ax-21	822				See Notes 2,3
TF20	324H12	Tn-Ax-22	822				See Notes 2,3
TF20	324H12	Tn-Ax-23	822	420	4.12	0.09	See Note 3
TF20	324H12	Tn-Ax-24	822	730	3.39	0.22	See Note 3
TF20	324H12	Tn-Ax-25	822	920	3.72	0.30	See Note 3
	Average			690	3.74	0.20	
TF20	S-350 F/30	Tn-Ax-1	1166				See Notes 1,2
TF20	S-350 F/30	Tn-Ax-2	1166	830	3.52	0.26	See Note 1
TF20	S-350 F/30	Tn-Ax-3	1166	830	4.09	0.28	See Note 1
	Average			830	3.81	0.27	
T10-20	360H071	Tn-Ax-26	Virgin				See Note 2
T10-20	360H071	Tn-Ax-27	Virgin				See Note 2
T10-20	360H071	Tn-Ax-28	Virgin	970	3.85	0.26	
T10-20	360H071	Tn-Ax-29	Virgin	900	4.10	0.22	
T10-20	360H071	Tn-Ax-30	Virgin				See Note 2
	Average			935	3.98	0.24	
T10-20	324H018	Tn-Ax-31	1239	800	4.19	0.21	See Note 3
T10-20	324H018	Tn-Ax-32	1239	910	4.04	0.28	See Note 3
T10-20	324H018	Tn-Ax-33	1239	880	3.60	0.27	See Note 3
T10-20	324H018	Tn-Ax-34	1239				See Notes 2,3
T10-20	324H018	Tn-Ax-35	1239	770	3.53	0.24	See Note 3
	Average			840	3.84	0.25	
	Standard Deviation			57	0.3	0.03	
	COV			7%	7%	11%	

Notes:

1. All operation in the Siemens Westinghouse advanced particulate filtration system at the Foster Wheeler PCFBC test facility in Karhula, Finland. Nominal-operating temperature was 1,550°F.
2. Specimen was broken in handling.
3. All operation at the SCS PSDF in combustion mode at a nominal-operating temperature of 1,400°F.

Table 5-4 (Page 1 of 4)

Room Temperature Hoop Tensile Strength of Schumacher TF20 and T10-20

Material	Element	Specimen Number	Hours in Operation	Maximum Hydrostatic Pressure (psig)	Ultimate Strength (psi)	Remarks
TF20	S199/315E PT-20	Tn-Hoop-1	Virgin	710	1740	
TF20	S199/315E PT-20	Tn-Hoop-2	Virgin	700	1720	
TF20	S199/315E PT-20	Tn-Hoop-3	Virgin	670	1620	
TF20	344E-295	Tn-Hoop-1	Virgin	660	1600	
TF20	344E-295	Tn-Hoop-2	Virgin	670	1630	
TF20	344E-295	Tn-Hoop-3	Virgin	670	1630	
TF20	344E-309	Tn-Hoop-4	Virgin	730	1750	
TF20	344E-309	Tn-Hoop-5	Virgin	730	1750	
TF20	344E-309	Tn-Hoop-6	Virgin	740	1790	
Average				698	1692	
Standard Deviation				29	67	
Coefficient of Variation (COV)				4%	4%	
T10-20	360H071	Tn-Hoop-73	Virgin	970	2370	
T10-20	360H071	Tn-Hoop-74	Virgin	950	2350	
T10-20	360H071	Tn-Hoop-75	Virgin	820	2060	
T10-20	360H071	Tn-Hoop-76	Virgin	900	2310	
T10-20	360H071	Tn-Hoop-77	Virgin	870	2240	
T10-20	360H071	Tn-Hoop-78	Virgin	940	2430	
T10-20	360H071	Tn-Hoop-79	Virgin	740	1830	
T10-20	360H071	Tn-Hoop-80	Virgin	680	1800	
T10-20	360H071	Tn-Hoop-81	Virgin	700	1840	
Average				841	2137	
Standard Deviation				105	242	
COV				12%	11%	
TF20	324H21	Tn-Hoop-264	491	570	1420	See Notes 1,3
TF20	324H21	Tn-Hoop-265	491	570	1430	See Notes 1,3
TF20	324H21	Tn-Hoop-266	491	450	1140	See Notes 1,3
TF20	324H21	Tn-Hoop-267	491	530	1380	See Notes 1,3
TF20	324H21	Tn-Hoop-268	491	540	1390	See Notes 1,3
TF20	324H21	Tn-Hoop-269	491	520	1360	See Notes 1,3
TF20	324H21	Tn-Hoop-270	491	510	1360	See Notes 1,3
TF20	324H21	Tn-Hoop-271	491	500	1310	See Notes 1,3
TF20	324H21	Tn-Hoop-272	491	460	1230	See Notes 1,3
Average				517	1336	
Standard Deviation				40	90	
Coefficient of Variation (COV)				8%	7%	

Table 5-4 (Page 2 of 4)

Room Temperature Hoop Tensile Strength of Schumacher TF20 and T10-20

Material	Candle	Specimen Number	Hours in Operation	Maximum Hydrostatic Pressure (psig)	Ultimate Strength (psi)	Remarks
TF20	S-350 F/33	Tn-Hoop-1	540	570	1570	See Note 2
TF20	S-350 F/33	Tn-Hoop-2	540	540	1480	See Note 2
TF20	S-350 F/33	Tn-Hoop-3	540	580	1570	See Note 2
TF20	S-350 F/33	Tn-Hoop-4	540	570	1500	See Note 2
TF20	S-350 F/33	Tn-Hoop-5	540	580	1520	See Note 2
TF20	S-350 F/33	Tn-Hoop-6	540	610	1600	See Note 2
TF20	S-350 F/33	Tn-Hoop-7	540	590	1510	See Note 2
TF20	S-350 F/33	Tn-Hoop-8	540	590	1500	See Note 2
TF20	S-350 F/33	Tn-Hoop-9	540	600	1530	See Note 2
Average				581	1531	
Standard Deviation				19	38	
Coefficient of Variation (COV)				3%	2%	
T10-20	324H016	Tn-Hoop-82	810	480	1194	See Note 1
T10-20	324H016	Tn-Hoop-83	810	490	1230	See Note 1
T10-20	324H016	Tn-Hoop-84	810	500	1260	See Note 1
T10-20	324H016	Tn-Hoop-85	810	480	1250	See Note 1
T10-20	324H016	Tn-Hoop-86	810	360	950	See Note 1
T10-20	324H016	Tn-Hoop-87A	810	490	1270	See Note 1
T10-20	324H016	Tn-Hoop-87B	810	470	1230	See Note 1
T10-20	324H016	Tn-Hoop-88	810	490	1310	See Note 1
T10-20	324H016	Tn-Hoop-89	810	490	1300	See Note 1
T10-20	324H016	Tn-Hoop-90	810	340	910	See Note 1
Average				459	1190	
Standard Deviation				55	134	
COV				12%	11%	
TF20	324H12	Tn-Hoop-55	822	520	1300	See Note 1
TF20	324H12	Tn-Hoop-56	822	490	1220	See Note 1
TF20	324H12	Tn-Hoop-57	822	490	1250	See Note 1
TF20	324H12	Tn-Hoop-58	822	440	1150	See Note 1
TF20	324H12	Tn-Hoop-59	822	450	1180	See Note 1
TF20	324H12	Tn-Hoop-60	822	460	1210	See Note 1
TF20	324H12	Tn-Hoop-61	822	450	1220	See Note 1
TF20	324H12	Tn-Hoop-62	822	460	1240	See Note 1
TF20	324H12	Tn-Hoop-63	822	440	1180	See Note 1
Average				467	1217	
Standard Deviation				26	42	
COV				6%	3%	

Table 5-4 (Page 3 of 4)

Room Temperature Hoop Tensile Strength of Schumacher TF20 and T10-20

Material	Candle	Specimen Number	Hours in Operation	Maximum Hydrostatic Pressure (psig)	Ultimate Strength (psi)	Remarks
TF20	324H13	Tn-Hoop-64	822	580	1440	See Note 1
TF20	324H13	Tn-Hoop-65	822	560	1390	See Note 1
TF20	324H13	Tn-Hoop-66	822	480	1200	See Note 1
TF20	324H13	Tn-Hoop-67	822	480	1260	See Note 1
TF20	324H13	Tn-Hoop-68	822	500	1300	See Note 1
TF20	324H13	Tn-Hoop-69A	822	480	1240	See Note 1
TF20	324H13	Tn-Hoop-69B	822	500	1310	See Note 1
TF20	324H13	Tn-Hoop-70	822	490	1310	See Note 1
TF20	324H13	Tn-Hoop-71	822	520	1380	See Note 1
TF20	324H13	Tn-Hoop-72	822	470	1260	See Note 1
Average				506	1309	
Standard Deviation				35	71	
COV				7%	5%	
TF20	324H01	Tn-Hoop-273	994	540	1360	See Notes 1,3
TF20	324H01	Tn-Hoop-274	994	520	1310	See Notes 1,3
TF20	324H01	Tn-Hoop-275	994	540	1370	See Notes 1,3
TF20	324H01	Tn-Hoop-276	994	490	1260	See Notes 1,3
TF20	324H01	Tn-Hoop-277	994	480	1250	See Notes 1,3
TF20	324H01	Tn-Hoop-278	994	510	1310	See Notes 1,3
TF20	324H01	Tn-Hoop-279	994	510	1360	See Notes 1,3
TF20	324H01	Tn-Hoop-280	994	490	1310	See Notes 1,3
TF20	324H01	Tn-Hoop-281	994	490	1300	See Notes 1,3
Average				508	1314	
Standard Deviation				21	40	
COV				4%	3%	
TF20	324H04	Tn-Hoop-282	1234	520	1300	See Notes 1,3
TF20	324H04	Tn-Hoop-283	1234	500	1230	See Notes 1,3
TF20	324H04	Tn-Hoop-284	1234	490	1270	See Notes 1,3
TF20	324H04	Tn-Hoop-285	1234	470	1230	See Notes 1,3
TF20	324H04	Tn-Hoop-286	1234	240	620	See Notes 1,3
TF20	324H04	Tn-Hoop-287	1234	480	1230	See Notes 1,3
TF20	324H04	Tn-Hoop-288	1234	470	1240	See Notes 1,3
TF20	324H04	Tn-Hoop-289	1234	490	1320	See Notes 1,3
TF20	324H04	Tn-Hoop-290	1234	470	1250	See Notes 1,3
Average				459	1188	
Standard Deviation				79	203	
COV				17%	17%	

Table 5-4 (Page 4 of 4)

Room Temperature Hoop Tensile Strength of Schumacher TF20 and T10-20

Material	Candle	Specimen Number	Hours in Operation	Maximum Hydrostatic Pressure (psig)	Ultimate Strength (psi)	Remarks
T10-20	324H018	Tn-Hoop-91	1239	520	1310	See Note 1
T10-20	324H018	Tn-Hoop-92	1239	510	1300	See Note 1
T10-20	324H018	Tn-Hoop-93	1239	510	1300	See Note 1
T10-20	324H018	Tn-Hoop-94	1239	440	1150	See Note 1
T10-20	324H018	Tn-Hoop-95	1239	460	1210	See Note 1
T10-20	324H018	Tn-Hoop-96	1239	490	1270	See Note 1
T10-20	324H018	Tn-Hoop-97	1239	460	1230	See Note 1
T10-20	324H018	Tn-Hoop-98	1239	450	1200	See Note 1
T10-20	324H018	Tn-Hoop-99	1239	490	1300	See Note 1
Average				481	1252	
Standard Deviation				28	54	
COV				6%	4%	
T10-20	324H02	Tn-Hoop-291	1788	460	1160	See Note 1
T10-20	324H02	Tn-Hoop-292	1788	490	1240	See Note 1
T10-20	324H02	Tn-Hoop-293	1788	580	1490	See Note 1
T10-20	324H02	Tn-Hoop-294	1788	520	1360	See Note 1
T10-20	324H02	Tn-Hoop-295	1788	540	1400	See Note 1
T10-20	324H02	Tn-Hoop-296	1788	330	870	See Note 1
T10-20	324H02	Tn-Hoop-297	1788	500	1320	See Note 1
T10-20	324H02	Tn-Hoop-298	1788	560	1500	See Note 1
T10-20	324H02	Tn-Hoop-299	1788	550	1480	See Note 1
Average				503	1313	
Standard Deviation				71	191	
Coefficient of Variation (COV)				14%	15%	
T10-20	324H01	Tn-Hoop-300	1792	580	1460	See Notes 1,3
T10-20	324H01	Tn-Hoop-301	1792	570	1440	See Notes 1,3
T10-20	324H01	Tn-Hoop-302	1792	560	1430	See Notes 1,3
T10-20	324H01	Tn-Hoop-303	1792	500	1310	See Notes 1,3
T10-20	324H01	Tn-Hoop-304	1792	490	1260	See Notes 1,3
T10-20	324H01	Tn-Hoop-305	1792	500	1310	See Notes 1,3
T10-20	324H01	Tn-Hoop-306	1792	500	1310	See Notes 1,3
T10-20	324H01	Tn-Hoop-307	1792	510	1340	See Notes 1,3
T10-20	324H01	Tn-Hoop-308	1792	520	1380	See Notes 1,3
Average					1360	
Standard Deviation					66	
COV					5%	

Notes:

1. All operation at the SCS PSDF in combustion mode at a nominal-operating temperature of 1,400°F.
2. All operation in the Siemens Westinghouse advanced particulate filtration system at the Foster Wheeler PCFBC test facility in Karhula, Finland. Nominal-operating temperature was 1,550°F.
3. In operation during October 1998 PCD fire.

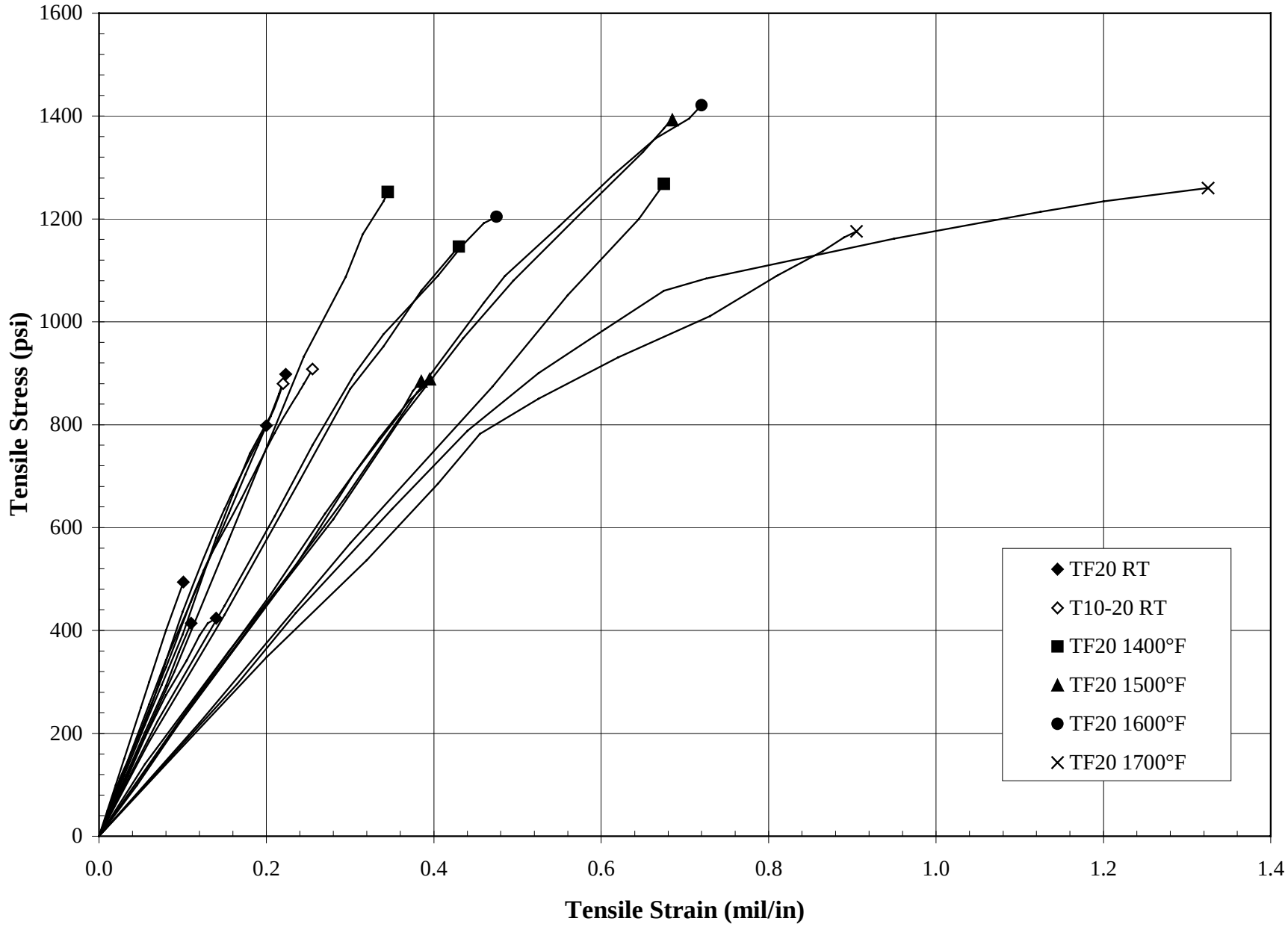

Figure 5-1 Room and Elevated Temperature Axial Tensile Stress-Strain Responses for Virgin Schumacher TF20 and T10-20

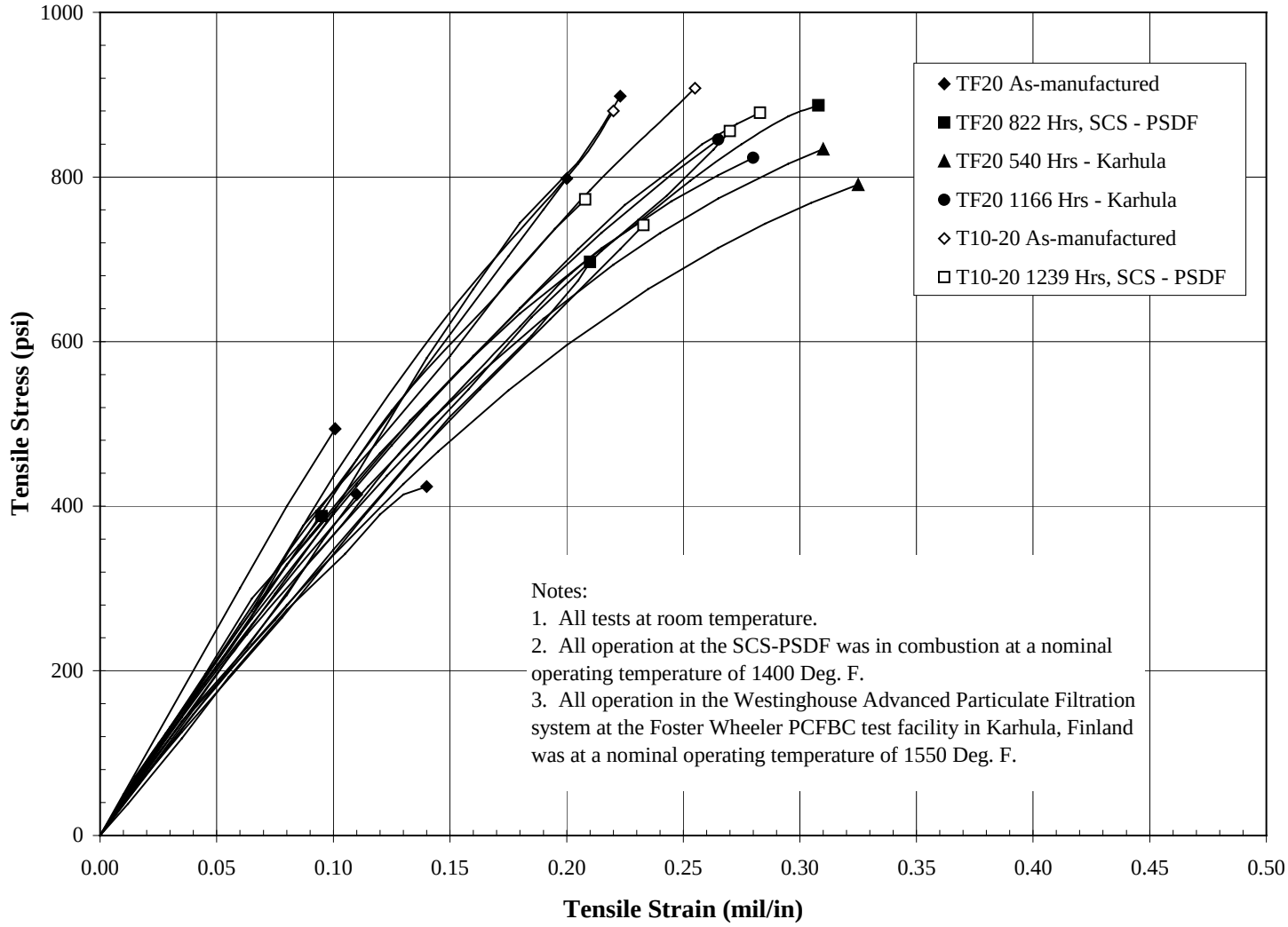

Figure 5-2 Room Temperature Tensile Stress-Strain Responses for Schumacher TF20 and T10-20 Virgin and After-Combustion Operation

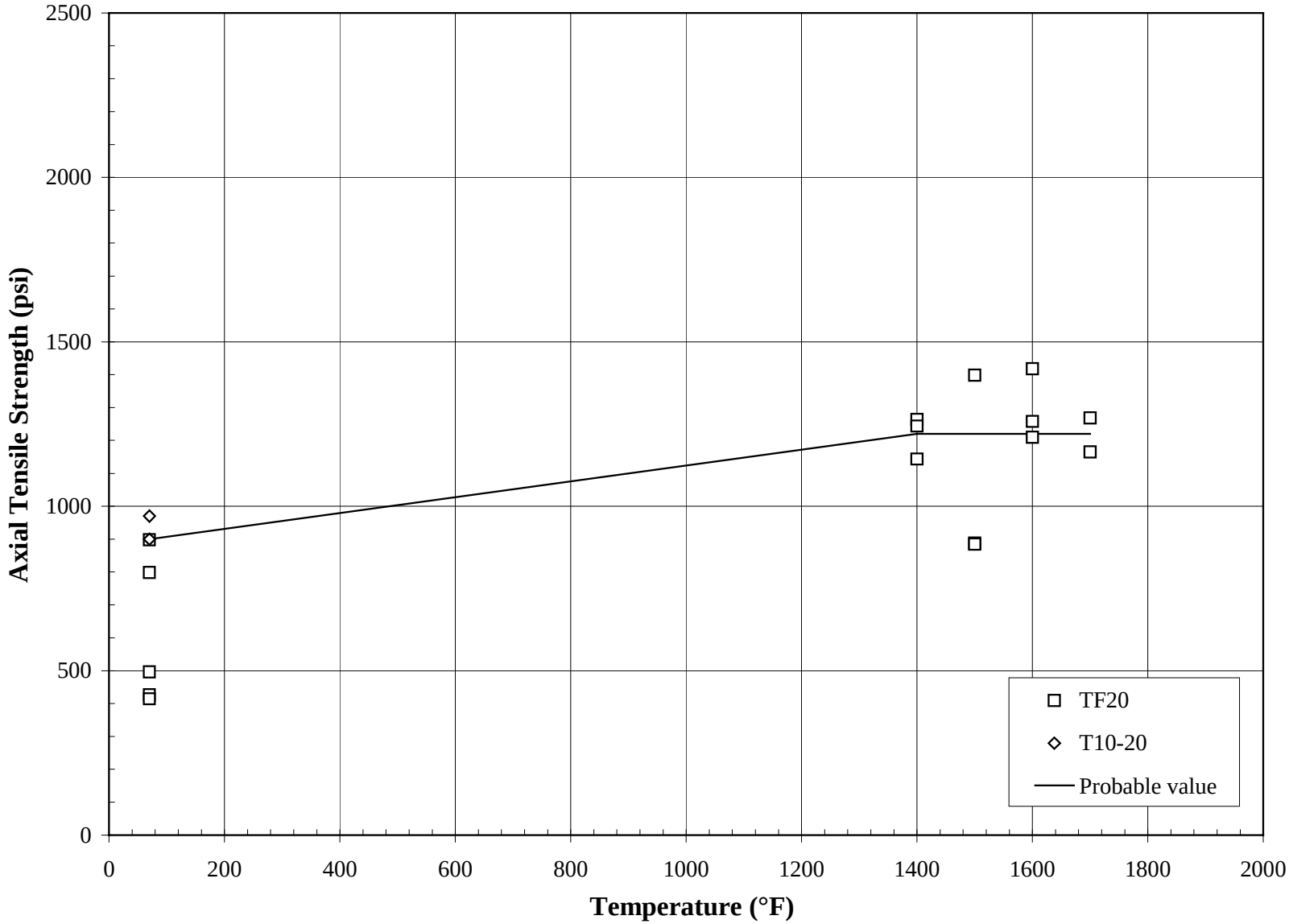

Figure 5-3 Axial Tensile Strength Versus Temperature for Virgin Schumacher TF20 and T10-20

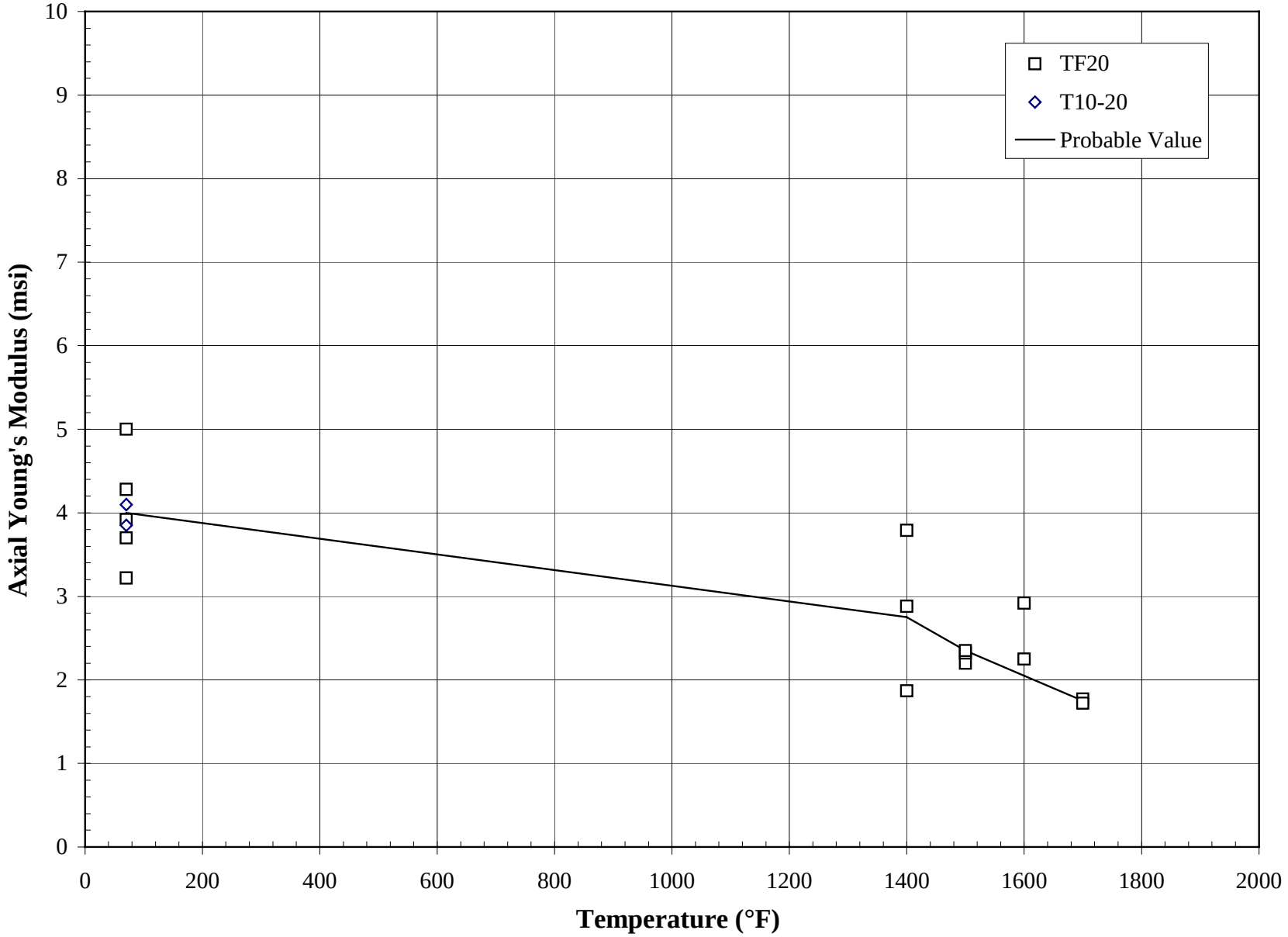

Figure 5-4 Young's Modulus Versus Temperature for Virgin Schumacher TF20 and T10-20

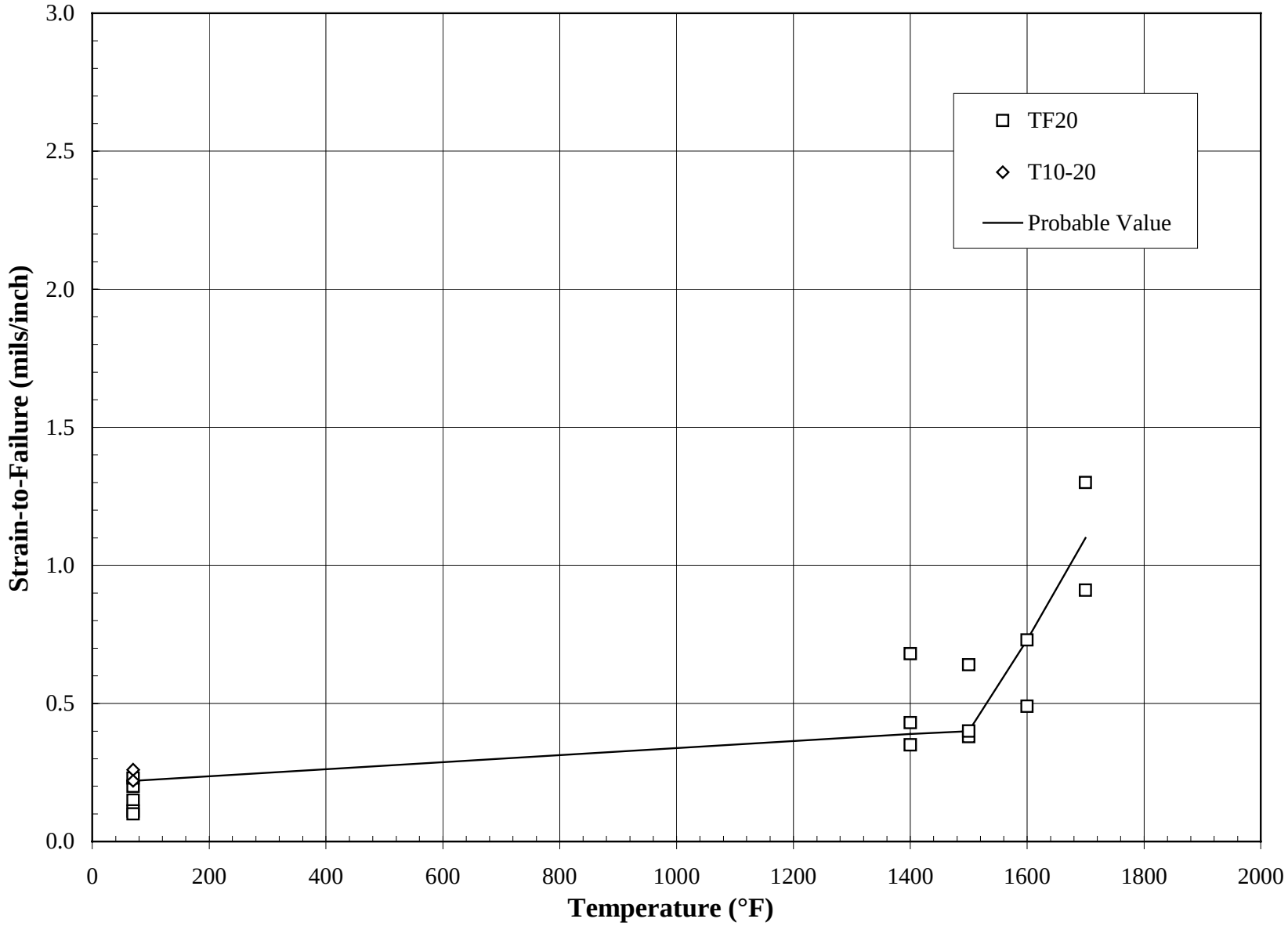

Figure 5-5 Axial Tensile Strain-to-Failure Versus Temperature for Virgin Schumacher TF20 and T10-20

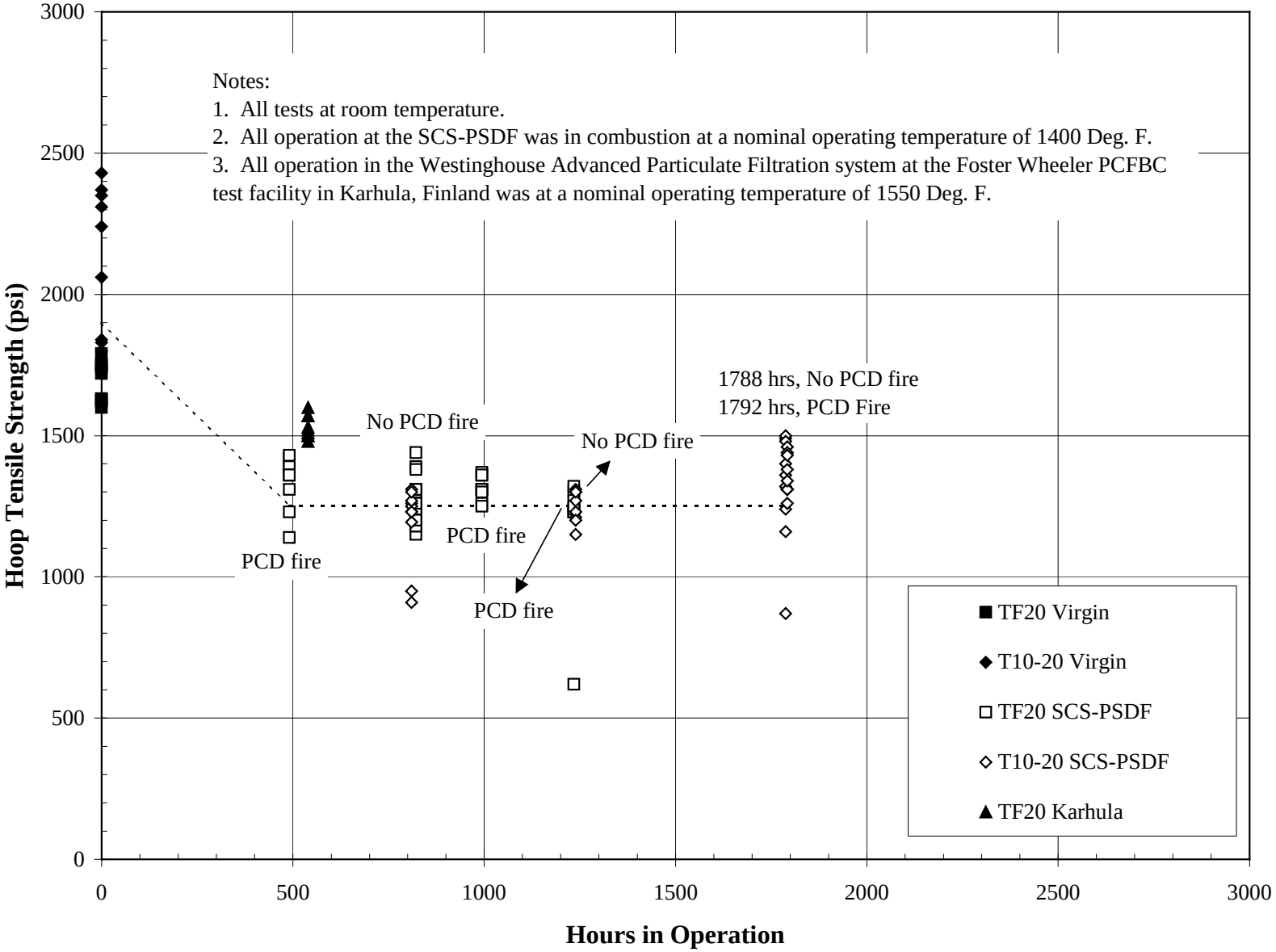

Figure 5-6 Room Temperature Hoop Tensile Strength Versus Hours in Operation for Schumacher TF20 and T10-20

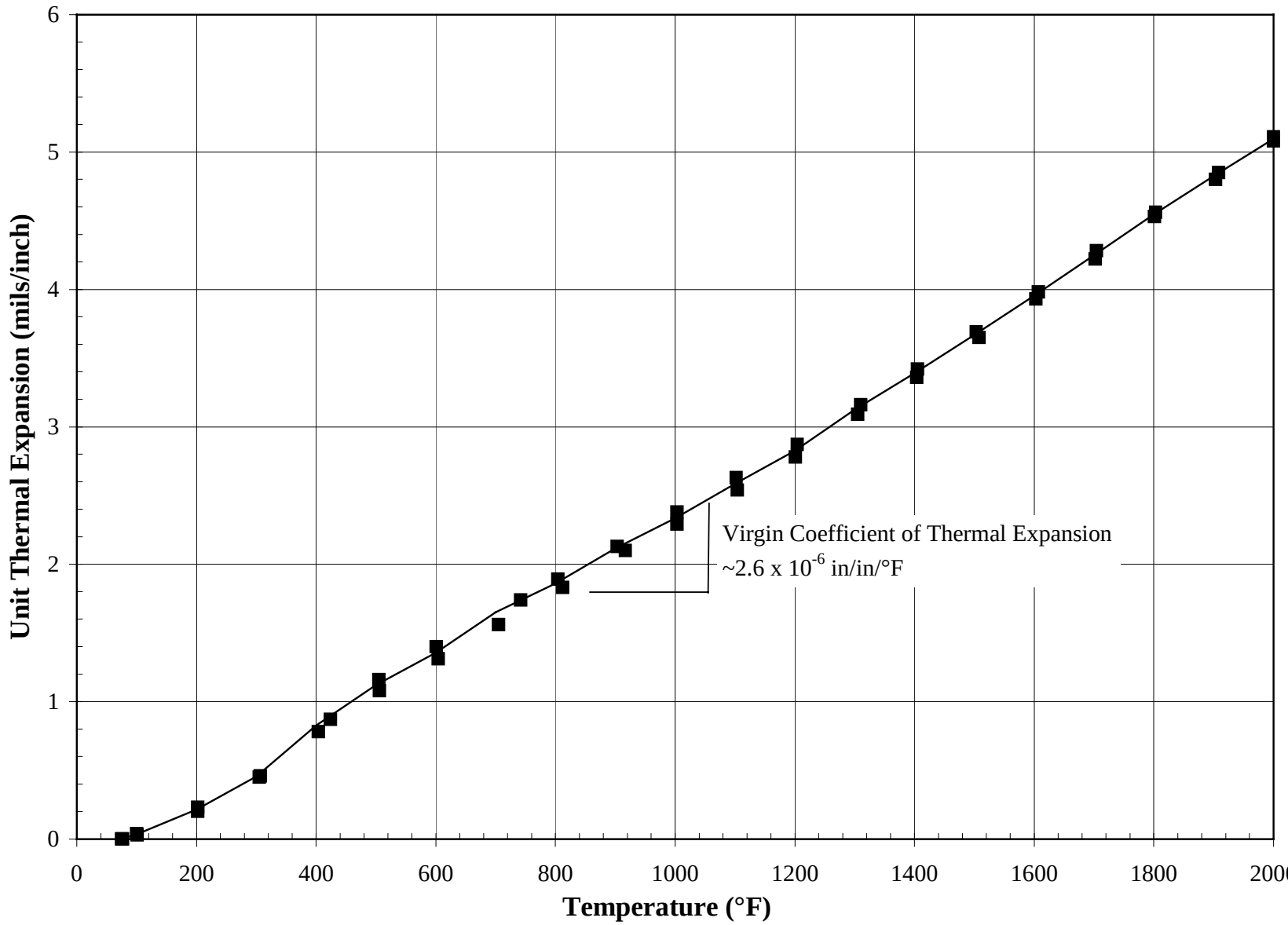

Figure 5-7 Unit Thermal Expansion of Virgin Schumacher TF20

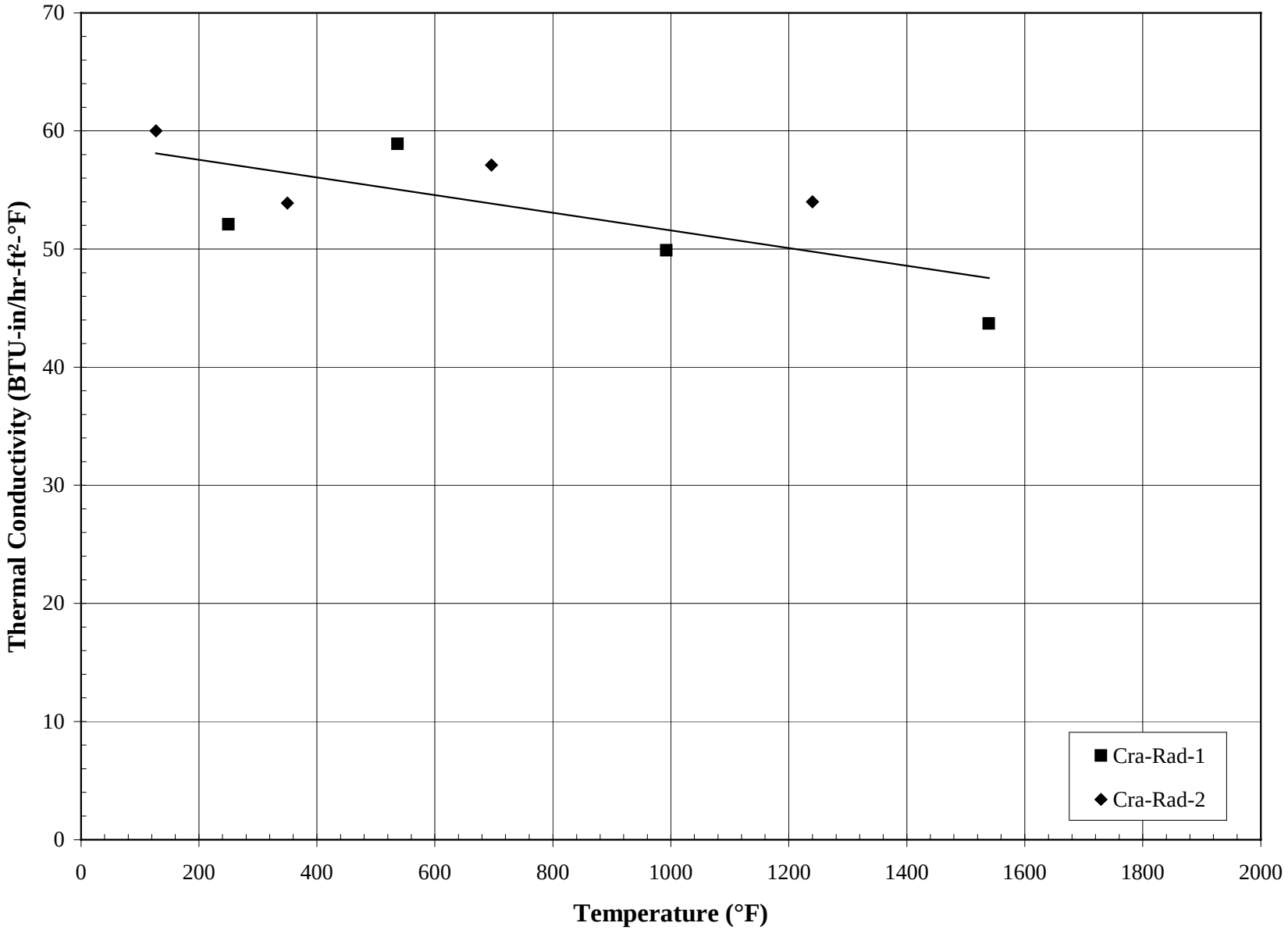

Figure 5-8 Radial Thermal Conductivity Versus Temperature for Virgin Schumacher TF20

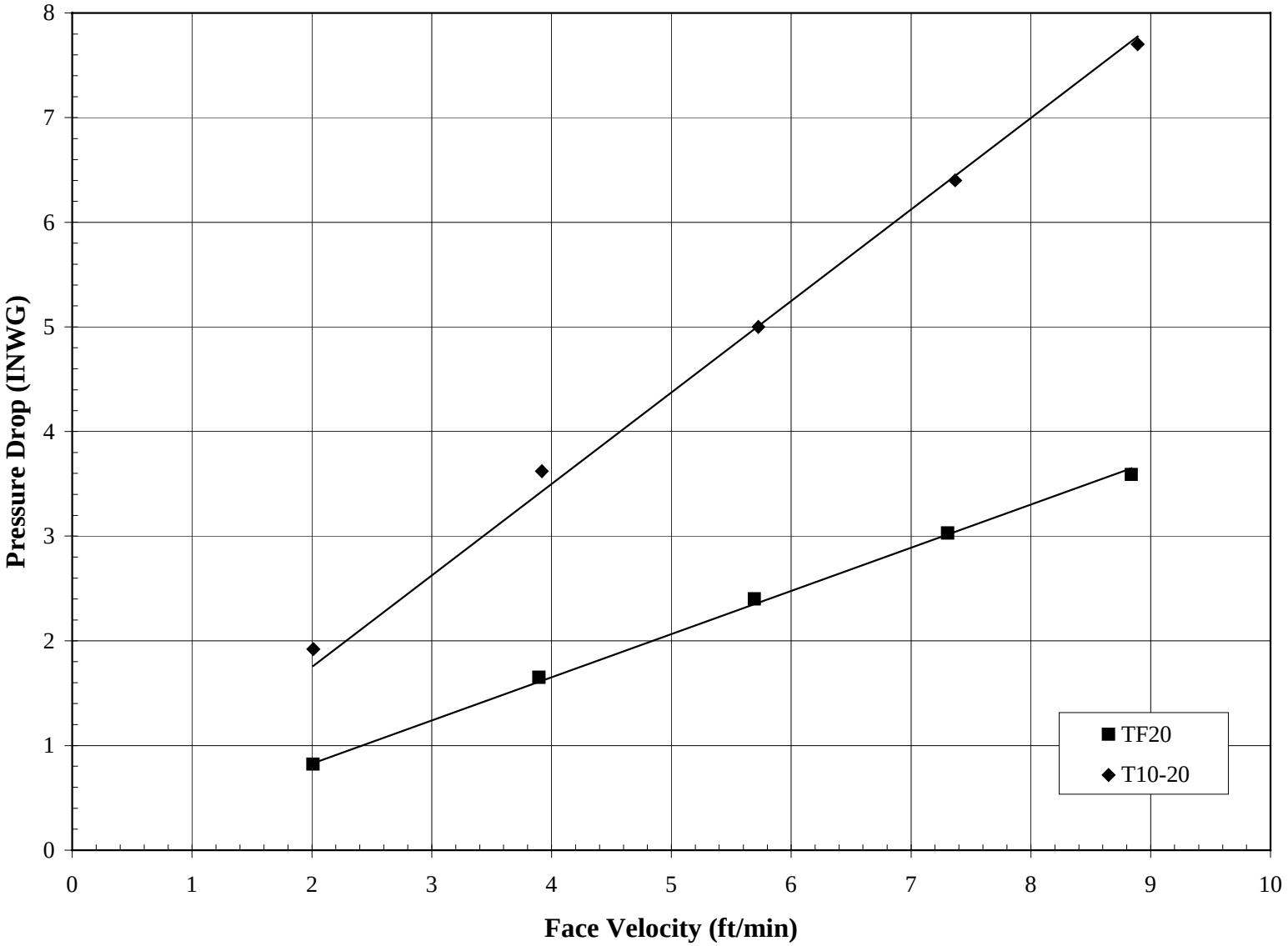

Figure 5-9 Pressure Drop Versus Face Velocity for Virgin Schumacher TF20 and T10-20 Using Air at Ambient Temperature and Pressure

6.0 SCHUMACHER N10-20

Schumacher N10-20 is a bonded SiC particle material with a microstructure similar to the clay-bonded SiC materials but with a different chemical composition of the binder. The binder system of the Schumacher clay-bonded materials was changed to try and improve corrosion resistance. The elements have a structural wall with a nominal I.D. of 1.575 in. (40 mm) and a nominal wall thickness of 0.40 in. (10 mm). Mechanical and thermal properties of the elements are controlled by the structural walls and a relatively thin membrane layer applied to the outside surface provides filtration. Probable values of selected properties of virgin Schumacher N10-20 filter elements are as follows:

Bulk Density (lbm/ft^3)	123
Hoop Tensile Strength at Room Temperature (psi)	2,530
Axial Coefficient of Thermal Expansion, 500 to 1,500°F (10^{-6} in./in./°F)	2.5
Radial Thermal Conductivity at 1,000°F (Btu-in./hr-ft^2-°F)	28

Table 6-1

Density of Schumacher N10-20

Element	Specimen Number	Hours in Operation	I.D. (in.)	O.D. (in.)	Density (gr/cm³)	Density (lb/ft³)	Remarks
354I2	Tn-hoop-1	Virgin	1.51	2.37	1.96	122	
354I2	Tn-hoop-2	Virgin	1.53	2.37	1.95	122	
354I2	Tn-hoop-3	Virgin	1.56	2.38	1.97	123	
354I2	Tn-hoop-4	Virgin	1.56	2.38	1.97	123	
354I2	Tn-hoop-5	Virgin	1.58	2.38	1.97	123	
354I2	Tn-hoop-6	Virgin	1.58	2.38	1.97	123	
Average					1.96	123	
Standard Deviation					0.01	0.52	
Coefficient of Variation (COV)					0.43%	0.43%	

Table 6-2

Room Temperature Hoop Tensile Strength of Schumacher N10-20

Element	Specimen Number	Hours in Operation	Maximum Hydrostatic Pressure (psig)	Ultimate Strength (psi)	Remarks
354I2	Tn-Hoop-1	Virgin	1110	2650	
354I2	Tn-Hoop-2	Virgin	1090	2640	
354I2	Tn-Hoop-3	Virgin	1010	2560	
354I2	Tn-Hoop-4	Virgin	1030	2590	
354I2	Tn-Hoop-5	Virgin	890	2280	
354I2	Tn-Hoop-6	Virgin	950	2450	
Average			1013	2528	
Standard Deviation			76	129	
Coefficient of Variation (COV)			8%	5%	

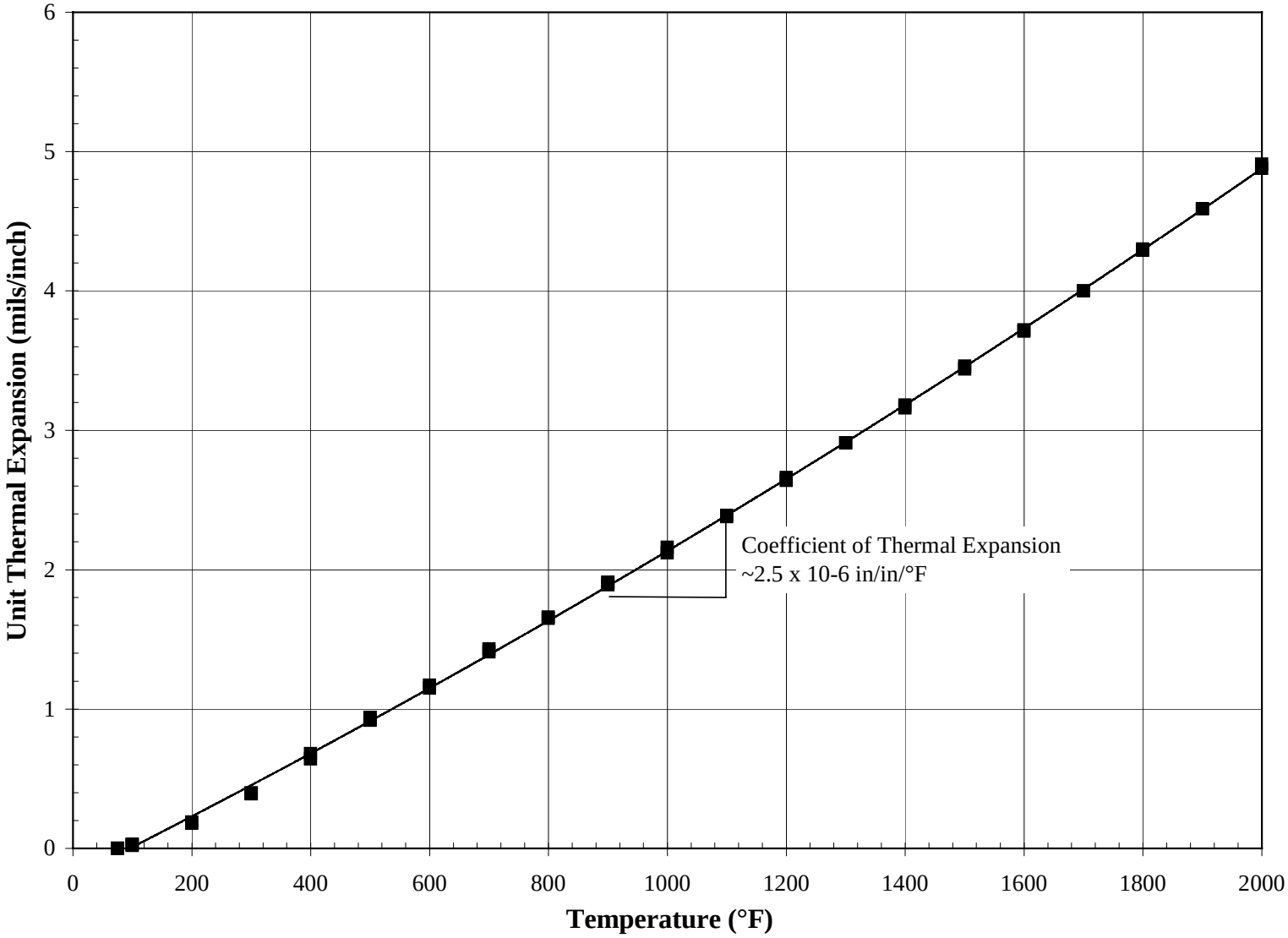

Figure 6-1 Unit Thermal Expansion of Virgin Schumacher N10-20

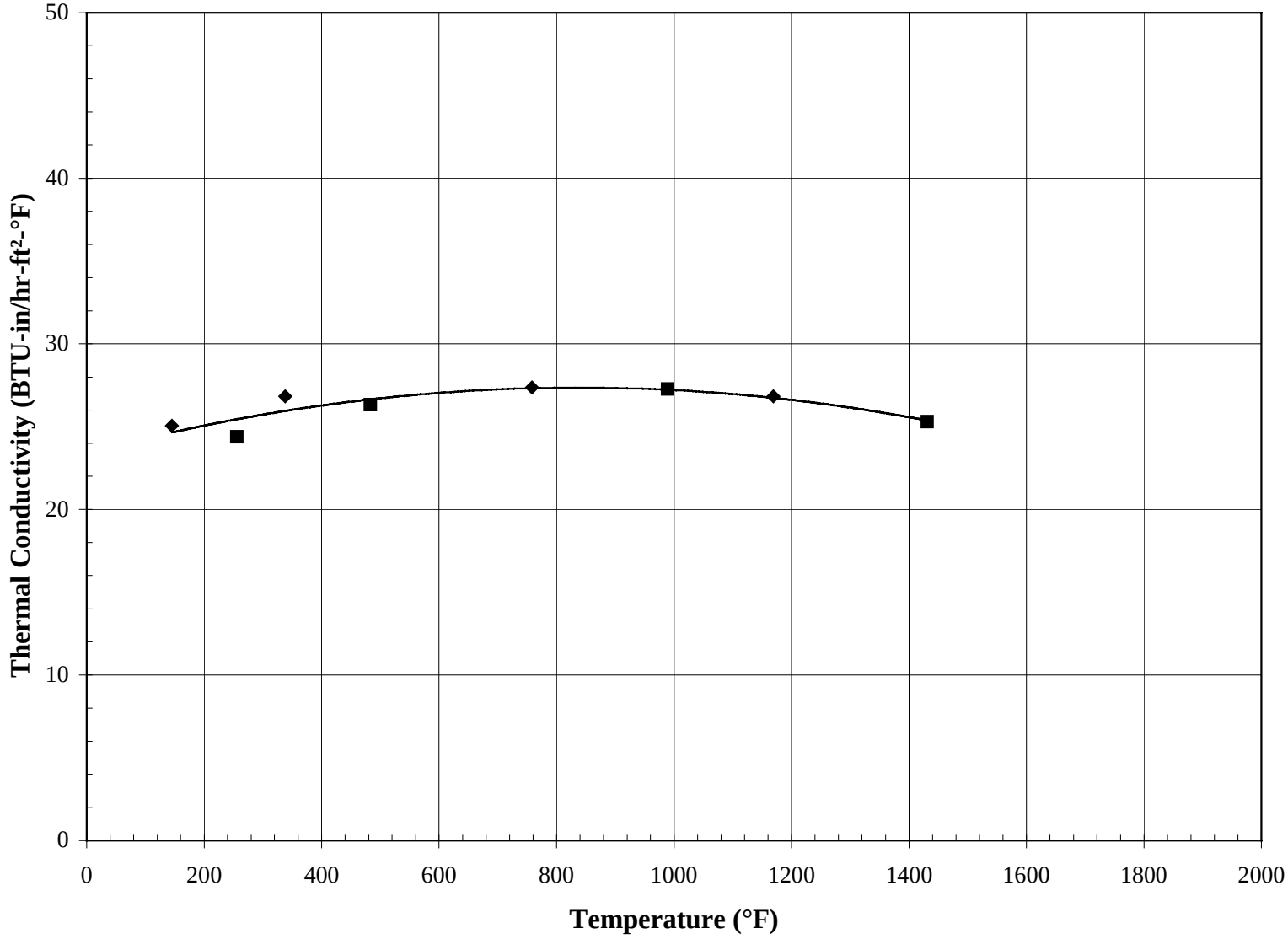

Figure 6-2 Radial Thermal Conductivity Versus Temperature of Virgin Schumacher N10-20

7.0 IF&P REECER™

IF&P REECER™ elements are manufactured of SiC grains fused together without the use of a glass or clay binder. Processing consists of heating to a temperature above 3,500°F (1930°C) in an inert environment so the grains fuse and form a monolithic material. The I.D. of the elements tested so far has ranged from 1.60 in. (41 mm) to 1.83 in. (46 mm). The O.D. has been much more consistent than the I.D. with a nominal dimension of 2.40 in. (61 mm). Probable values of selected properties of virgin IF&P REECER™ are as follows:

Bulk Density (lbm/ft^3)	137
Hoop Tensile Strength at Room Temperature (psi)	2,040
Axial Tensile Strength at Room Temperature (psi)	2,120
Axial Young's Modulus at Room Temperature (10^6 psi)	14
Axial Tensile Strain-to-Failure at Room Temperature (mils/in.)	0.16
Axial Tensile Strength at 1,500°F (psi)	1,980
Axial Young's Modulus at 1,500°F (10^6 psi)	18
Axial Tensile Strain-to-Failure at 1,500°F (mils/in.)	0.10
Axial Coefficient of Thermal Expansion, 500 to 1,500°F (10^{-6} in./in./°F)	2.4
Radial Thermal Conductivity at 1,000°F (Btu-in./hr-ft^2-°F)	120
Pressure Drop at 5 ft/min Face Velocity, Air at Ambient Conditions(inWG)	1.5

Table 7-1

Density of IF&P REECER

Candle	Specimen Number	Hours in Operation	I.D. (in.)	O.D. (in.)	Density (gr/cm³)	Density (lb/ft³)	Remarks
FE98073109	Te-Ax-1	Virgin			2.15	134	
FE98073109	CRA-Rad-1	Virgin			2.20	137	
FE98073109	CRA-Rad-2	Virgin			2.19	136	
FE98073110	Tn-Hoop-127	Virgin	1.612	2.419	2.30	144	
FE98073110	Te-Ax-4	Virgin			2.17	135	
FE98073105	Tn-Hoop-353	1420	1.574	2.395	2.46	153	See Notes 1,2
FE98073105	Tn-Hoop-354	1420	1.617	2.397	2.53	158	See Notes 1,2
FE98073105	Tn-Hoop-355	1420	1.574	2.394	2.42	151	See Notes 1,2
FE98073105	Tn-Hoop-356	1420	1.620	2.400	2.39	149	See Notes 1,2
FE98073105	Tn-Hoop-357	1420	1.623	2.398	2.38	149	See Notes 1,2
FE98073105	Tn-Hoop-358	1420	1.627	2.403	2.37	148	See Notes 1,2
FE98073105	Tn-Hoop-359	1420	1.663	2.399	2.38	149	See Notes 1,2
FE98073105	Tn-Hoop-360	1420	1.679	2.400	2.39	149	See Notes 1,2
FE98073105	Tn-Hoop-361	1420	1.679	2.397	2.39	149	See Notes 1,2
		Average			2.41	150	
		Standard Deviation			0.05	3.03	
		Coefficient of Variation (COV)			2.0%	2.0%	
FE98073102	Tn-Hoop-362	1424	1.602	2.407	2.38	149	See Notes 1,2,3
FE98073102	Tn-Hoop-363	1424	1.612	2.401	2.37	148	See Notes 1,2,3
FE98073102	Tn-Hoop-364	1424	1.645	2.409	2.38	149	See Notes 1,2,3
FE98073102	Tn-Hoop-365	1424	1.694	2.402	2.38	149	See Notes 1,2,3
FE98073102	Tn-Hoop-366	1424	1.707	2.401	2.40	149	See Notes 1,2,3
FE98073102	Tn-Hoop-367	1424	1.688	2.405	2.35	146	See Notes 1,2,3
FE98073102	Tn-Hoop-368	1424	1.743	2.400	2.36	147	See Notes 1,2,3
FE98073102	Tn-Hoop-369	1424	1.746	2.401	2.37	148	See Notes 1,2,3
FE98073102	Tn-Hoop-370	1424	1.738	2.400	2.36	147	See Notes 1,2,3
			Average		2.37	148	
			Standard Deviation		0.02	0.94	
			COV		0.6%	0.6%	

Notes:

1. Elements were water washed before density measurements but some ash remained in the pores. Density values were calculated based on weights measured with ash in the pores and, therefore, do not represent a material property. The values are for comparison only.
2. All operation at the SCS PSDF in combustion mode at a nominal-operating temperature of 1,400°F.
3. In operation during October 1998 PCD fire.

Table 7-2

Axial Tensile Properties of IF&P REECER

Element	Specimen Number	Test Temperature (°F)	Ultimate Strength (psi)	Young's Modulus (msi)	Strain-to-Failure (mils/in.)	Remarks
FE98073110	Tn-Ax-66	70	2150	12.8	0.17	
FE98073110	Tn-Ax-68	70	1990	16.3	0.12	
FE98073110	Tn-Ax-69	70	2240	14.5	0.16	
FE98073110	Tn-Ax-70	70				See Note 1
FE98073110	Tn-Ax-72	70				See Note 1
FE98073110	Tn-Ax-73	70				See Note 1
FE98073110	Tn-Ax-74	70	2110	11.1	0.19	
	Average		2123	13.7	0.16	
	Standard Deviation		90	1.9	0.03	
	COV		4%	14%	16%	
FE98073110	Tn-Ax-67	1500	1960	20.0	0.11	
FE98073110	Tn-Ax-71	1500	1990	20.0	0.09	
FE98073110	Tn-Ax-75	1500	950	16.3	0.06	See Note 2
	Average		1975	18.8	0.10	

Notes:
1. Specimen broke in handling.
2. Values not included in average.

Table 7-3 (Page 1 of 2)

Room Temperature Hoop Tensile Strength of IF&P REECER

Candle	Specimen Number	Hours in Operation	Maximum Hydrostatic Pressure (psig)	Ultimate Strength (psi)	Remarks
FE98073109	Tn-Hoop-118	Virgin	490	1530	See Note 1
FE98073109	Tn-Hoop-119	Virgin	590	1810	See Note 1
FE98073109	Tn-Hoop-120	Virgin	630	1980	See Note 1
FE98073109	Tn-Hoop-121	Virgin	660	2260	
FE98073109	Tn-Hoop-122	Virgin	710	2450	See Note 1
FE98073109	Tn-Hoop-123	Virgin	650	2300	See Note 1
FE98073109	Tn-Hoop-124	Virgin	560	2120	
FE98073109	Tn-Hoop-125	Virgin	630	2380	
FE98073109	Tn-Hoop-126	Virgin	520	1930	See Note 1
Average			604	2084	
Standard Deviation			67	282	
Coeffecient of Variation (COV)			11%	14%	
FE98073110	Tn-Hoop-127	Virgin	880	2260	
FE98073110	Tn-Hoop-128	Virgin	820	2130	
FE98073110	Tn-Hoop-129	Virgin	820	2130	
FE98073110	Tn-Hoop-130	Virgin	570	1660	See Note 1
FE98073110	Tn-Hoop-131	Virgin	600	1830	
FE98073110	Tn-Hoop-132	Virgin	670	2040	See Note 2
FE98073110	Tn-Hoop-133	Virgin	550	1800	
FE98073110	Tn-Hoop-134	Virgin	630	2070	
FE98073110	Tn-Hoop-135	Virgin	590	2060	
Average			681	1998	
Standard Deviation			118	181	
COV			17%	9%	

Table 7-3 (Page 2 of 2)

Room Temperature Hoop Tensile Strength of IF&P REECER

Candle	Specimen Number	Hours in Operation	Maximum Hydrostatic Pressure (psig)	Ultimate Strength (psi)	Remarks
FE98073105	Tn-Hoop-353	1420	1040	2633	See Note 1,3
FE98073105	Tn-Hoop-354	1420	1310	3487	See Note 1,3
FE98073105	Tn-Hoop-355	1420	960	2435	See Note 1,3
FE98073105	Tn-Hoop-356	1420	940	2501	See Note 1,3
FE98073105	Tn-Hoop-357	1420	970	2614	See Note 1,3
FE98073105	Tn-Hoop-358	1420	1230	3300	See Note 3
FE98073105	Tn-Hoop-359	1420	1190	3391	See Note 1,3
FE98073105	Tn-Hoop-360	1420	1010	2941	See Note 1,3
FE98073105	Tn-Hoop-361	1420	1030	3014	See Note 3
Average			1076	2924	
Standard Deviation			126	378	
COV			12%	13%	
FE98073102	Tn-Hoop-362	1424	1230	3174	See Notes 1,3,4
FE98073102	Tn-Hoop-363	1424	1110	2930	See Notes 1,3,4
FE98073102	Tn-Hoop-364	1424	1160	3187	See Note 3,4
FE98073102	Tn-Hoop-365	1424	1000	2982	See Notes 1,3,4
FE98073102	Tn-Hoop-366	1424	1070	3267	See Note 3,4
FE98073102	Tn-Hoop-367	1424	990	2901	See Notes 1,3,4
FE98073102	Tn-Hoop-368	1424	1000	3236	See Notes 1,3,4
FE98073102	Tn-Hoop-369	1424	840	2730	See Notes 1,3,4
FE98073102	Tn-Hoop-370	1424	1040	3325	See Note 3,4
Average			1049	3081	
Standard Deviation			106	190	
COV			10%	6%	

Notes:
1. Failed at "bubble."
2. Specimen had "bubbles" but did not fail at one.
3. All operation at the SCS PSDF in combustion mode at a nominal-operating temperature of 1,400°F.
4. In operation during October 1998 PCD fire.

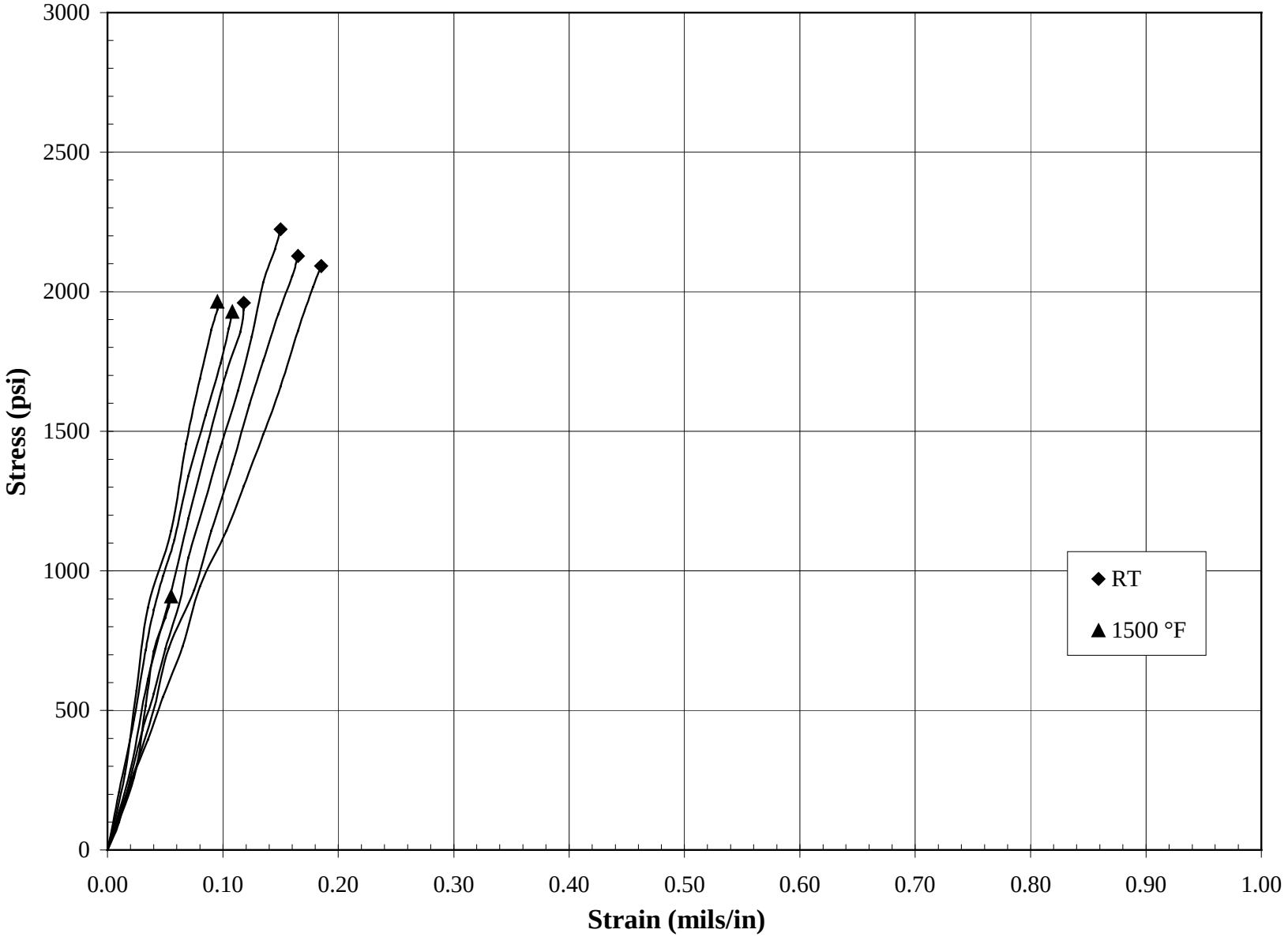

Figure 7-1 Axial Tensile Stress-Strain Responses of Virgin IF&P REECER

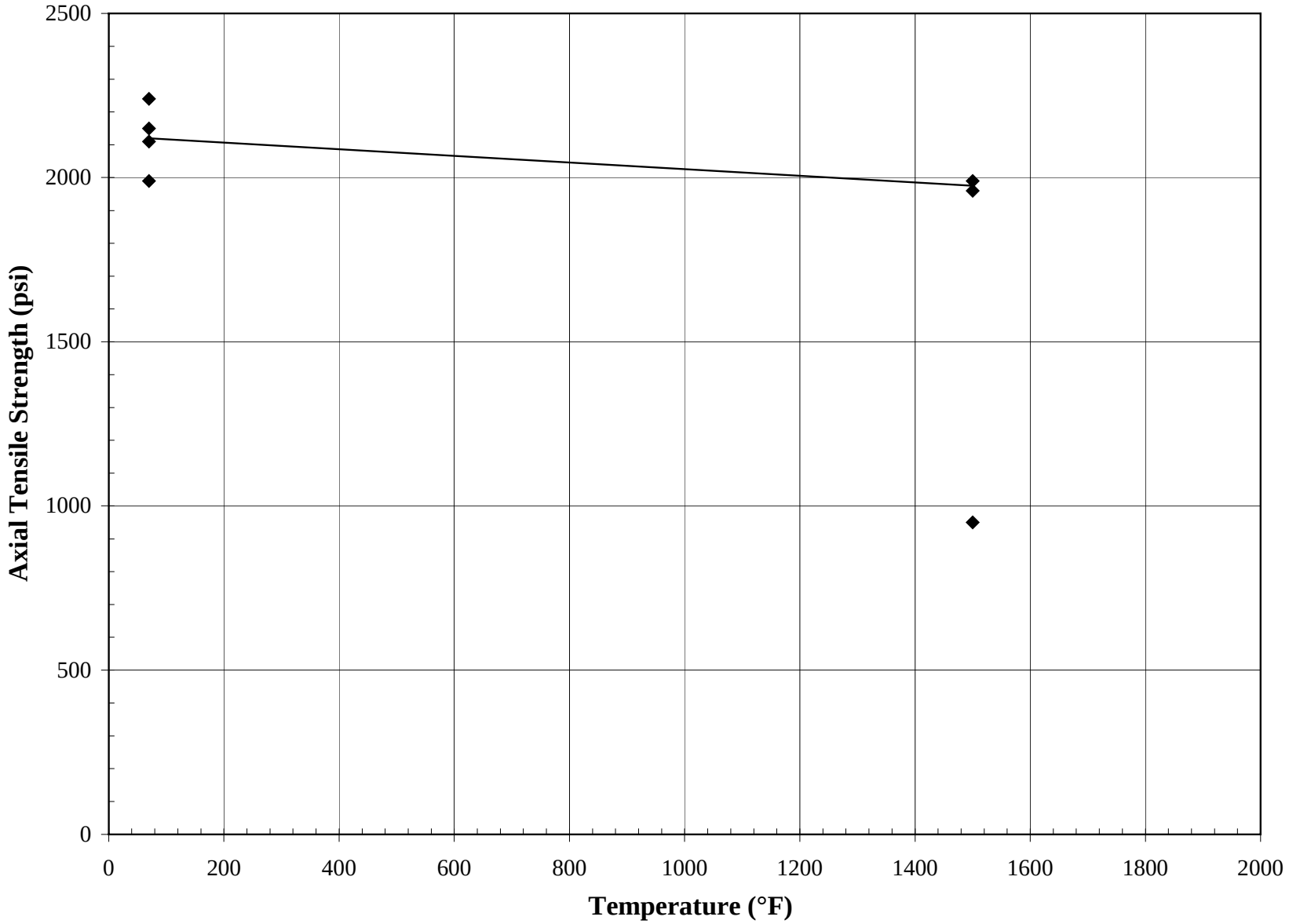

Figure 7-2 Axial Tensile Strength Versus Temperature for Virgin IF&P REECER

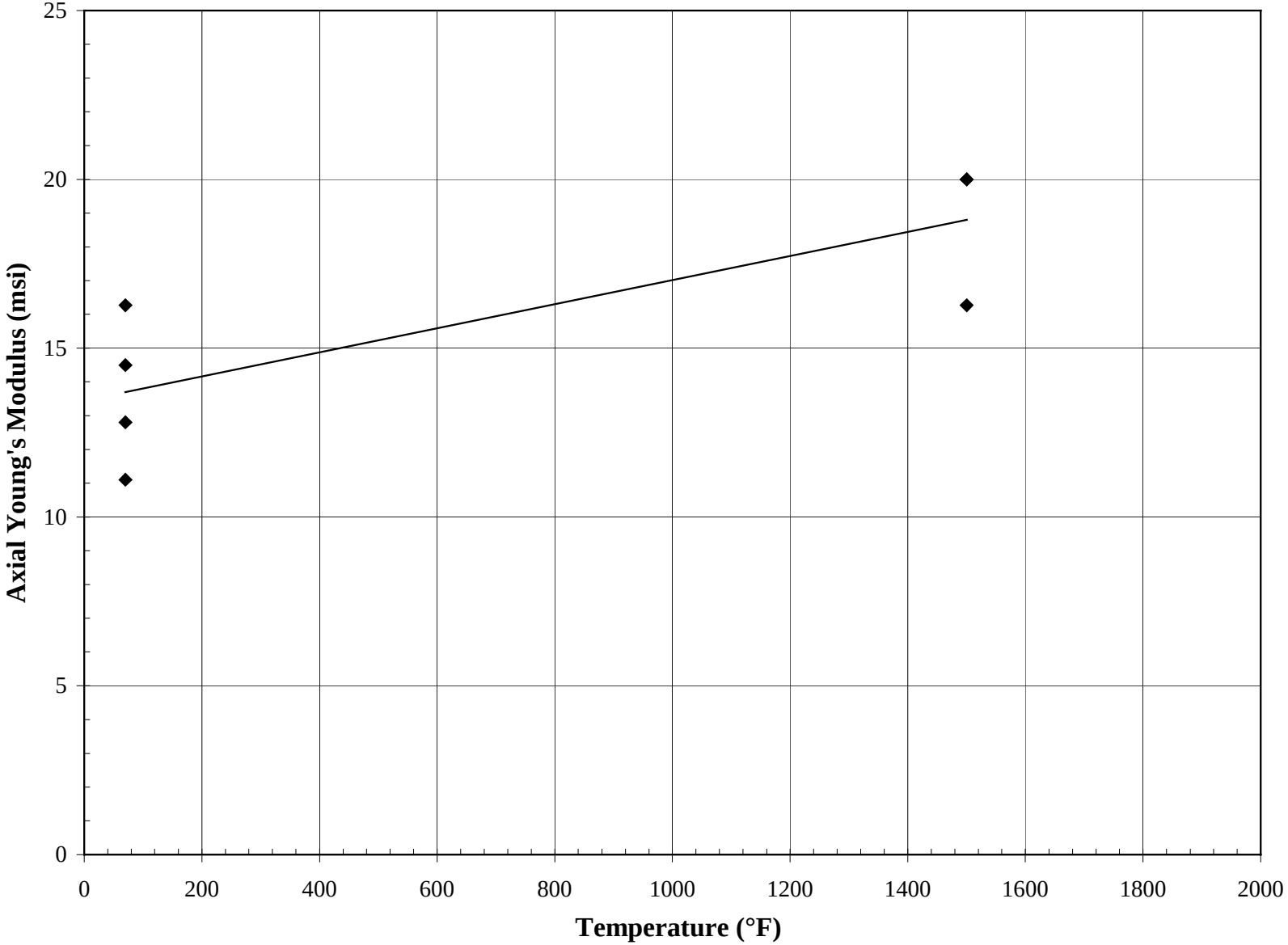

Figure 7-3 Young's Modulus Versus Temperature for Virgin IF&P REECER

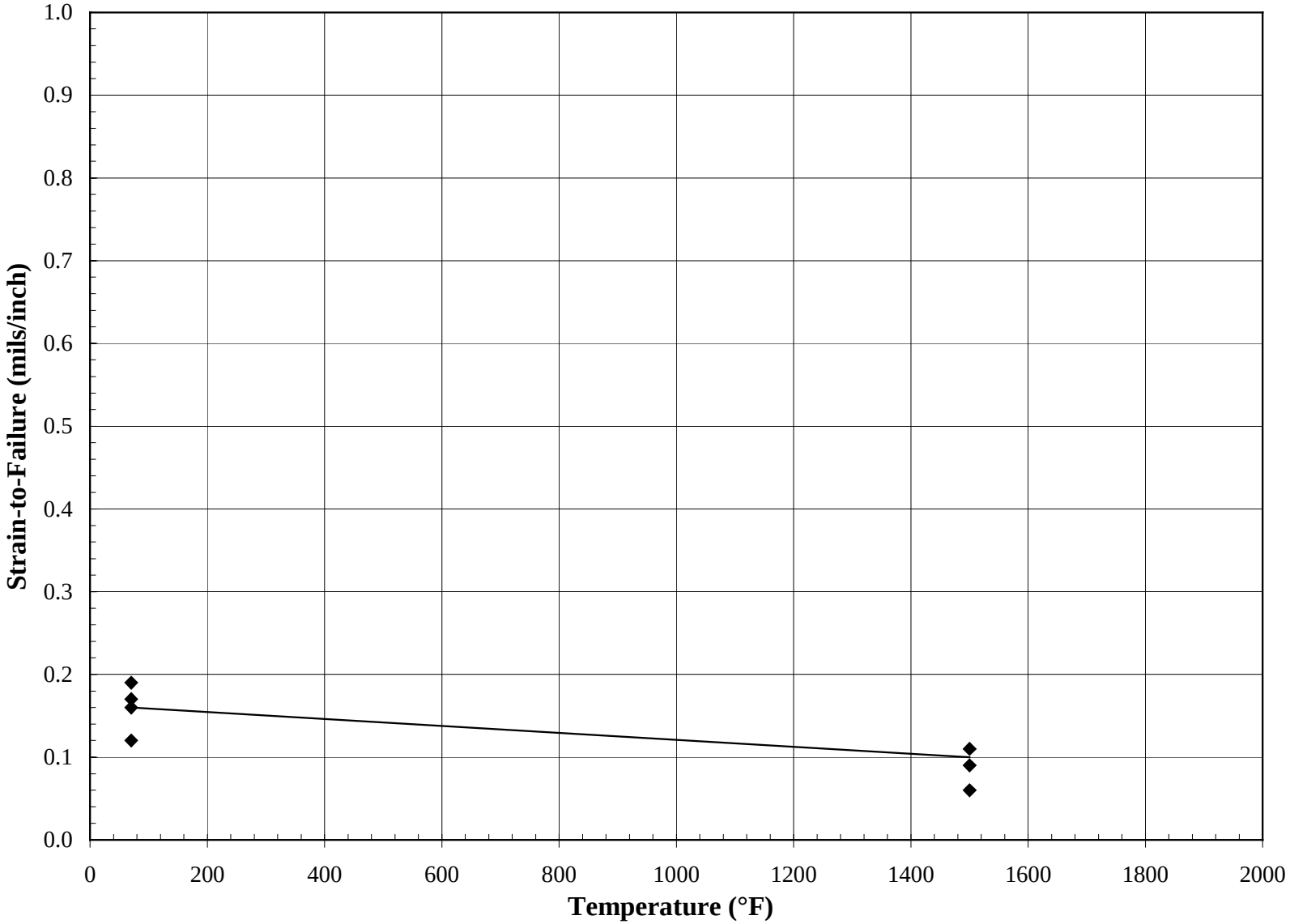

Figure 7-4 Axial Tensile Strain-to-Failure Versus Temperature for Virgin IF&P REECER

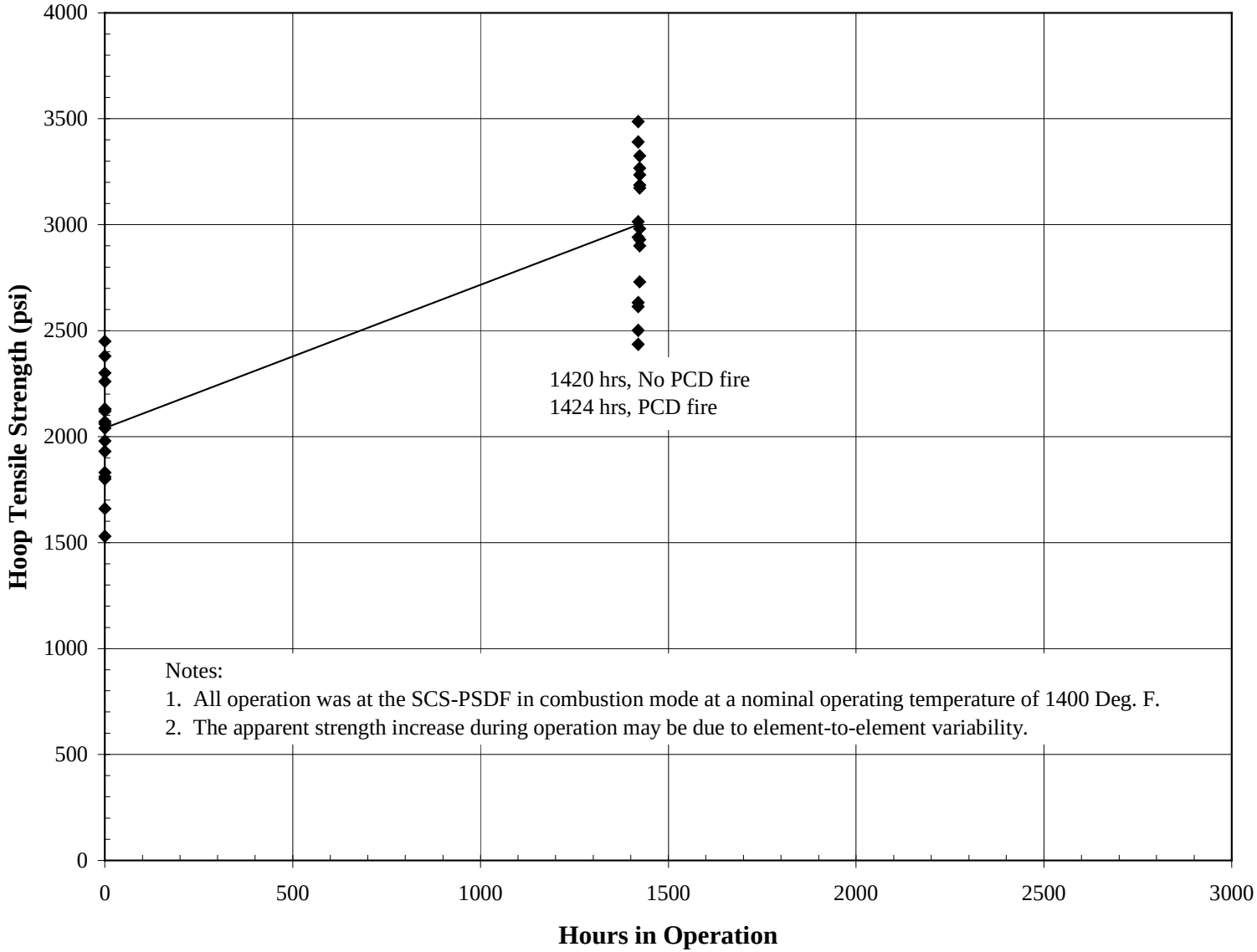

Figure 7-5 Room Temperature Hoop Tensile Strength Versus Hours in Operation for IF&P REECER

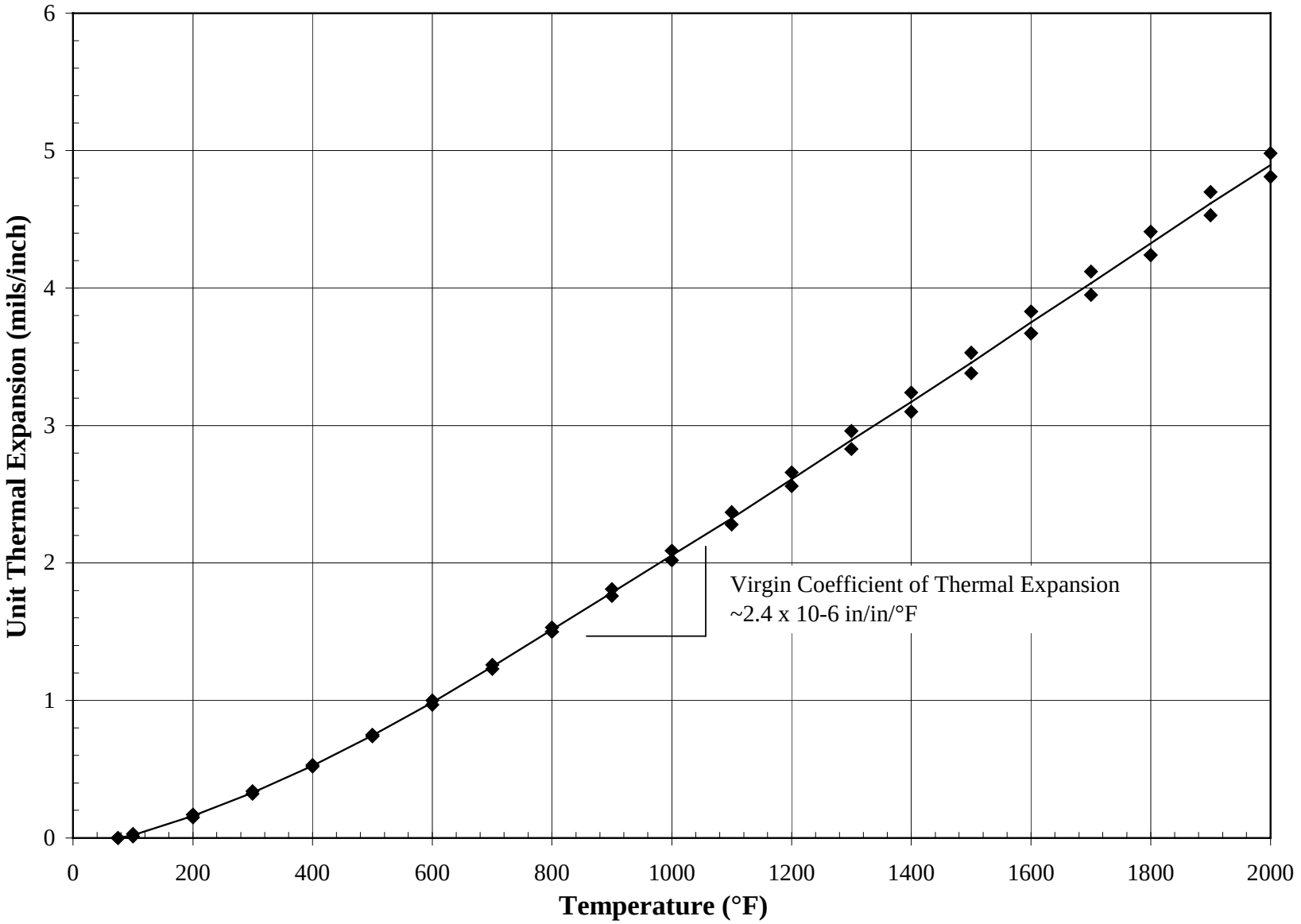

Figure 7-6 Unit Thermal Expansion of Virgin IF&P REECER

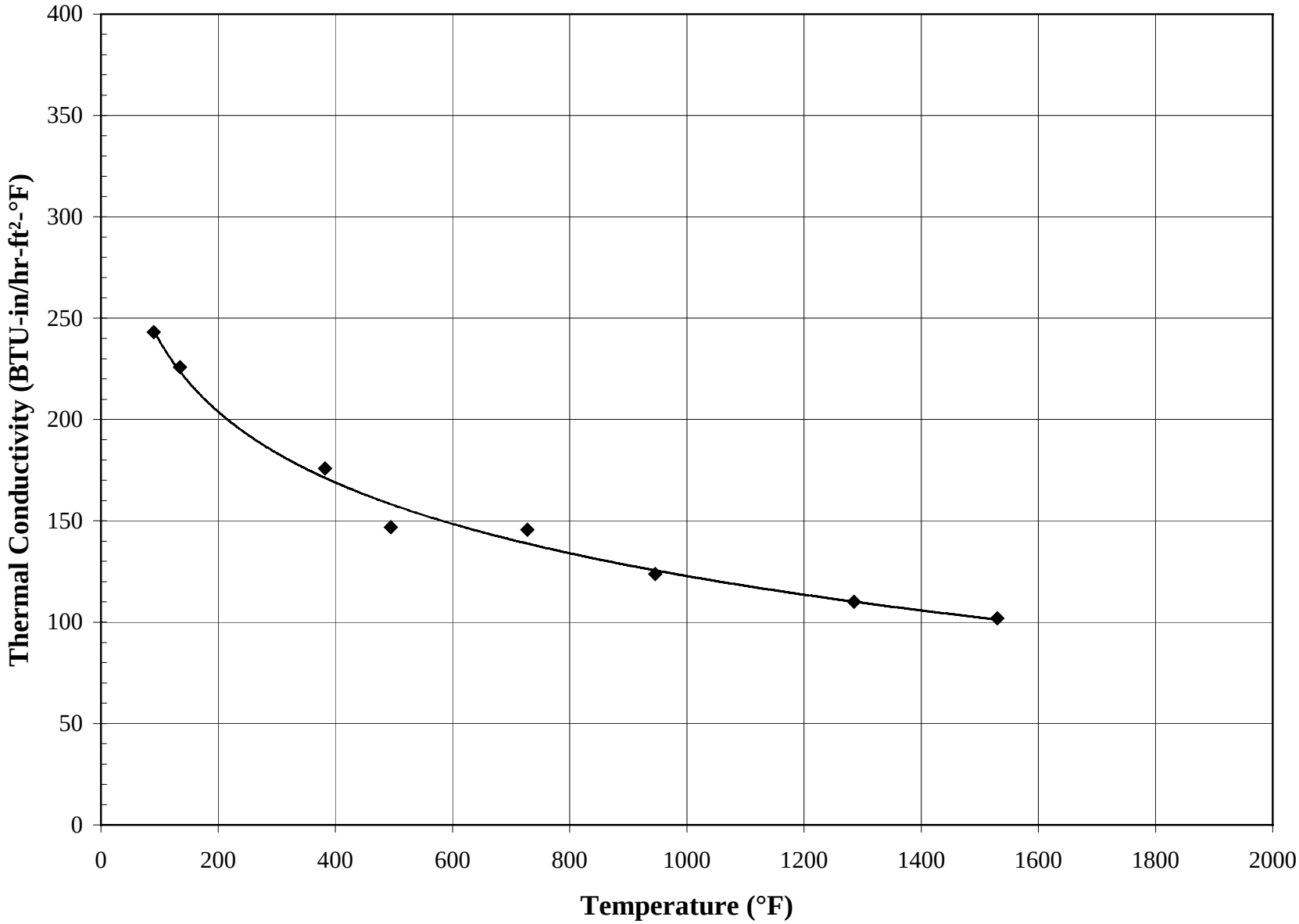

Figure 7-7 Radial Thermal Conductivity Versus Temperature for Virgin IF&P REECER

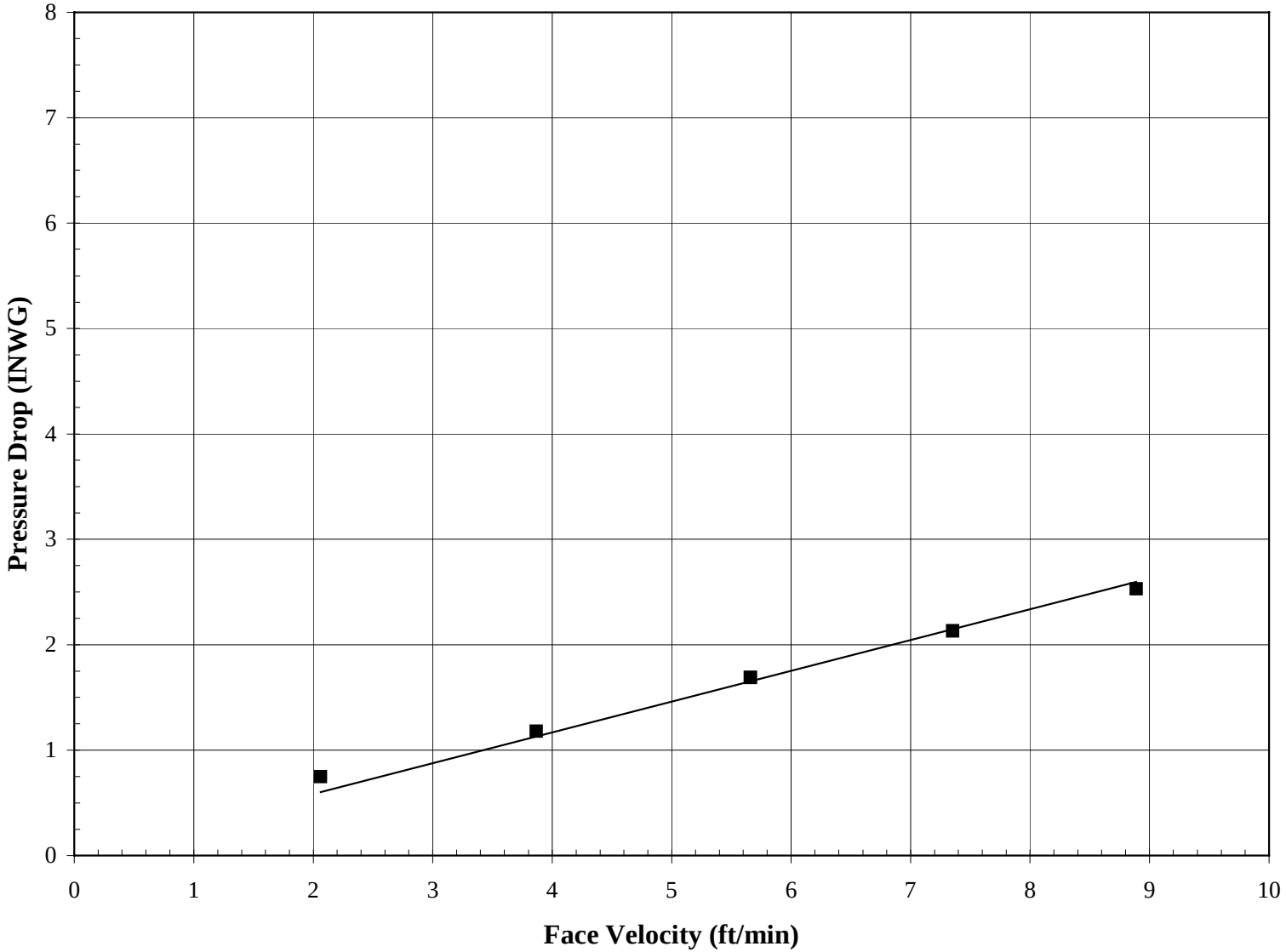

Figure 7-8 Pressure Drop Versus Face Velocity for Virgin IF&P REECER
Using Air at Ambient Temperature and Pressure

8.0 COORS P-100A-1

Coors P-100A-1 is a monolithic alumina/mullite filter material. Nominal dimensions of the filter elements are 1.575 in. (40 mm) I.D. and a nominal wall thickness of 0.40 in. (10 mm). Unlike the clay-bonded SiC elements, Coors is a depth filter with no membrane layer. Probable values of selected properties of virgin Coors P-100A-1 are as follows:

Bulk Density (lbm/ft^3)	103
Hoop Tensile Strength at Room Temperature (psi)	1,900
Axial Tensile Strength at Room Temperature (psi)	2,480
Axial Young's Modulus at Room Temperature (10^6 psi)	4.3
Axial Tensile Strain-to-Failure at Room Temperature (mils/in.)	0.62
Axial Tensile Strength at 1,500°F (psi)	2,390
Axial Young's Modulus at 1,500°F (10^6 psi)	2.5
Axial Tensile Strain-to-Failure at 1,500°F (mils/in.)	1.0
Axial Compressive Strength at Room Temperature (psi)	17,200
Axial Compressive Strain-to-Failure at Room Temperature (mils/in.)	4.4
Axial Coefficient of Thermal Expansion, 500 to 1,500°F (10^{-6} in./in./°F)	2.8
Radial Thermal Conductivity at 1,000°F (Btu-in./hr-ft^2-°F)	10
Pressure Drop at 5 ft/min Face Velocity, Air at Ambient Conditions(inWG)	3.3

Table 8-1 (Page 1 of 3)

Density of Coors P-100A-1

Candle	Specimen Number	Hours in Operation	I.D. (in.)	O.D. (in.)	Density (gr/cm³)	Density (lb/ft³)	Remarks
24	Cm-Ax-1	Virgin			1.69	105	See Note 1
24	Cm-Ax-2	Virgin			1.69	105	See Note 1
24	Cm-Ax-3	Virgin			1.68	105	See Note 1
24	Cm-Ax-4	Virgin			1.68	105	See Note 1
24	Cm-Ax-5	Virgin			1.68	105	See Note 1
24	Cm-Ax-6	Virgin			1.68	105	See Note 1
Average					1.68	105	
Standard Deviation					0.005	0.30	
Coefficient of Variation (COV)					0.28%	0.28%	
KC027	Tn-Hoop-4	Virgin	1.63	2.37	1.64	103	
KC027	Tn-Hoop-5	Virgin	1.63	2.37	1.65	103	
KC027	Tn-Hoop-6	Virgin	1.62	2.36	1.65	103	
KC027	Tn-Hoop-7	Virgin	1.63	2.37	1.64	102	
KC027	Tn-Hoop-8	Virgin	1.63	2.37	1.64	102	
KC027	Tn-Hoop-9	Virgin	1.63	2.37	1.64	102	
Average					1.64	102	
Standard Deviation					0.004	0.26	
COV					0.25%	0.25%	
LC026	Tn-Hoop-16	Virgin	1.62	2.35	1.66	104	
LC026	Tn-Hoop-17	Virgin	1.62	2.36	1.66	103	
LC026	Tn-Hoop-18	Virgin	1.63	2.36	1.65	103	
LC026	Tn-Hoop-19	Virgin	1.62	2.35	1.66	104	
LC026	Tn-Hoop-20	Virgin	1.63	2.36	1.66	103	
LC026	Tn-Hoop-21	Virgin	1.63	2.36	1.66	104	
LC026	Tn-Hoop-22	Virgin	1.62	2.36	1.65	103	
LC026	Tn-Hoop-23	Virgin	1.62	2.36	1.65	103	
LC026	Tn-Hoop-24	Virgin	1.63	2.37	1.64	102	
Average					1.65	103	
Standard Deviation					0.008	0.48	
COV					0.47%	0.47%	

Table 8-1 (Page 2 of 3)

Density of Coors P-100A-1

Candle	Specimen Number	Hours in Operation	I.D. (in.)	O.D. (in.)	Density (gr/cm^3)	Density (lb/ft^3)	Remarks
FC010	Tn-hoop-1	540	1.61	2.36	1.71	107	See Notes 2,3
FC010	Tn-hoop-2	540	1.61	2.37	1.71	107	See Notes 2,3
FC010	Tn-hoop-3	540	1.61	2.37	1.71	107	See Notes 2,3
FC010	Tn-hoop-4	540	1.61	2.37	1.70	106	See Notes 2,3
FC010	Tn-hoop-5	540	1.61	2.37	1.70	106	See Notes 2,3
FC010	Tn-hoop-6	540	1.61	2.37	1.70	106	See Notes 2,3
FC010	Tn-hoop-7	540	1.61	2.38	1.70	106	See Notes 2,3
FC010	Tn-hoop-8	540	1.61	2.37	1.70	106	See Notes 2,3
FC010	Tn-hoop-9	540	1.61	2.36	1.71	107	See Notes 2,3
Average					1.70	106	
Standard Deviation					0.004	0.26	
Coefficient of Variation (COV)					0.25%	0.25%	
KC005	Tn-Hoop-10	616	1.63	2.36	1.67	104	See Notes 2,4
KC005	Tn-Hoop-11	616	1.62	2.36	1.67	104	See Notes 2,4
KC005	Tn-Hoop-12	616	1.62	2.36	1.66	104	See Notes 2,4
KC005	Tn-Hoop-13	616	1.63	2.36	1.66	104	See Notes 2,4
KC005	Tn-Hoop-14	616	1.63	2.36	1.66	104	See Notes 2,4
KC005	Tn-Hoop-15	616	1.62	2.36	1.66	104	See Notes 2,4
KC005	Tn-Hoop-16	616	1.62	2.36	1.66	103	See Notes 2,4
KC005	Tn-Hoop-17	616	1.62	2.36	1.65	103	See Notes 2,4
KC005	Tn-Hoop-18	616	1.62	2.36	1.65	103	See Notes 2,4
Average					1.66	104	
Standard Deviation					0.004	0.27	
COV					0.26%	0.26%	
KC011	Tn-Hoop-19	616	1.62	2.37	1.65	103	See Notes 2,4
KC011	Tn-Hoop-20	616	1.62	2.37	1.65	103	See Notes 2,4
KC011	Tn-Hoop-21	616	1.63	2.37	1.65	103	See Notes 2,4
KC011	Tn-Hoop-22	616	1.63	2.37	1.65	103	See Notes 2,4
KC011	Tn-Hoop-23	616	1.63	2.37	1.65	103	See Notes 2,4
KC011	Tn-Hoop-24	616	1.63	2.37	1.65	103	See Notes 2,4
KC011	Tn-Hoop-25	616	1.63	2.37	1.65	103	See Notes 2,4
KC011	Tn-Hoop-26	616	1.63	2.37	1.65	103	See Notes 2,4
KC011	Tn-Hoop-27	616	1.63	2.37	1.65	103	See Notes 2,4
Average					1.65	103	
Standard Deviation					0.002	0.14	
COV					0.13%	0.13%	

Table 8-1 (Page 3 of 3)

Density of Coors P-100A-1

Candle	Specimen Number	Hours in Operation	I.D. (in.)	O.D. (in.)	Density (gr/cm^3)	Density (lb/ft^3)	Remarks
LC025	Tn-Hoop-28	616	1.62	2.35	1.65	103	See Notes 2,4
LC025	Tn-Hoop-29	616	1.62	2.35	1.65	103	See Notes 2,4
LC025	Tn-Hoop-30	616	1.62	2.35	1.66	104	See Notes 2,4
LC025	Tn-Hoop-31	616	1.62	2.35	1.66	104	See Notes 2,4
LC025	Tn-Hoop-32	616	1.62	2.35	1.66	104	See Notes 2,4
LC025	Tn-Hoop-33	616	1.62	2.35	1.65	103	See Notes 2,4
LC025	Tn-Hoop-34	616	1.62	2.36	1.65	103	See Notes 2,4
LC025	Tn-Hoop-35	616	1.62	2.35	1.65	103	See Notes 2,4
LC025	Tn-Hoop-36	616	1.62	2.36	1.64	103	See Notes 2,4
Average					1.65	103	
Standard Deviation					0.006	0.36	
COV					0.35%	0.35%	

Notes:

1. The "batch" was not identified for element 24.
2. Elements were water washed before density measurements but some ash remained in the pores. Density values were calculated based on weights measured with ash in the pores and, therefore, do not represent a material property. The values are for comparison only.
3. All operation in the Siemens Westinghouse advanced particulate filtration system at the Foster Wheeler PCFBC test facility in Karhula, Finland. Nominal-operating temperature was 1,550°F.
4. All operation at the SCS PSDF in combustion mode at a nominal-operating temperature of 1,400°F.

Table 8-2

Axial Tensile Properties of Virgin Coors P-100A-1

Candle Identification	Specimen Number	Temperature (°F)	Ultimate Strength (psi)	Young's Modulus (Msi)	Strain-to-Failure (mils/in.)	Remarks
24	Tn-ax-1	70	2850	4.22	0.73	
24	Tn-ax-4	70	2560	4.09	0.65	
24	Tn-ax-11	70	2140	4.40	0.50	
24	Tn-ax-19	70	2210	4.42	0.57	
24	Tn-ax-22	70	2630	4.25	0.65	
Average			2478	4.28	0.62	
Standard Deviation			266	0.1	0.08	
Coefficient of Variation (COV)			11%	3%	13%	
24	Tn-ax-10	1500	2460	2.65	0.99	
24	Tn-ax-14	1500	2450	2.02	1.30	
24	Tn-ax-17	1500	2430	2.76	0.96	
24	Tn-ax-18	1500	2220	2.50	0.93	
Average			2390	2.48	1.05	
Standard Deviation			99	0.3	0.15	
Coefficient of Variation (COV)			4%	11%	14%	
24	Tn-ax-5	1600	2060	2.35	0.95	
24	Tn-ax-8	1600	1830	2.04	0.95	
24	Tn-ax-13	1600	1680	1.94	0.87	
24	Tn-ax-16	1600	2210	2.28	1.05	
24	Tn-ax-24	1600	2040	2.32	0.91	
Average			1964	2.19	0.95	
Standard Deviation			187	0.2	0.06	
Coefficient of Variation (COV)			10%	8%	6%	
24	Tn-ax-3	1700	2120	1.96	1.31	
24	Tn-ax-12	1700	2000	1.99	1.10	
24	Tn-ax-15	1700	2200	2.09	1.20	
24	Tn-ax-21	1700	1970	1.97	1.10	
Average			2073	2.00	1.18	
Standard Deviation			93	0.1	0.09	
Coefficient of Variation (COV)			4%	3%	7%	

Notes:
1. The "batch" was not identified for element 24.

Table 8-3

Room Temperature Axial Properties of Coors P-100A-1
Virgin and After Combustion Operation

Candle Identification	Specimen Number	Hours in Operation	Ultimate Strength (psi)	Young's Modulus (Msi)	Strain-to-Failure (mils/in.)	Remarks
24	Tn-ax-1	Virgin	2850	4.22	0.73	See Note 1
24	Tn-ax-4	Virgin	2560	4.09	0.65	See Note 1
24	Tn-ax-11	Virgin	2140	4.40	0.50	See Note 1
24	Tn-ax-19	Virgin	2210	4.42	0.57	See Note 1
24	Tn-ax-22	Virgin	2630	4.25	0.65	See Note 1
Average			2478	4.28	0.62	
Standard Deviation			266	0.12	0.08	
Coefficient of Variation (COV)			11%	3%	13%	
FC007	Tn-ax-1	1166	1620	3.77	0.47	See Note 2
FC007	Tn-ax-2	1166	1740	3.96	0.48	See Note 2
FC007	Tn-ax-3	1166	1630	3.77	0.46	See Note 2
Average			1663	2.88	0.38	

Notes:

1. The "batch" was not identified for element 24.
2. All operation in the Siemens Westinghouse advanced particulate filtration system at the Foster Wheeler PCFBC test facility in Karhula, Finland. Nominal-operating temperature was 1,550°F.

Table 8-4 (Page 1 of 3)

Room Temperature Hoop Strength of Coors P-100A-1

Element	Specimen Number	Hours in Operation	Maximum Hydrostatic Pressure (psig)	Ultimate Strength (psi)	Remarks
24	Tn-Hoop-1	Virgin	860	2310	See Note 1
24	Tn-Hoop-2	Virgin	850	2230	See Note 1
24	Tn-Hoop-3	Virgin	810	2140	See Note 1
24	Tn-Hoop-4	Virgin	800	2140	See Note 1
24	Tn-Hoop-5	Virgin	830	2180	See Note 1
Average			830	2200	
Standard Deviation			23	64	
Coefficient of Variation (COV)			3%	3%	
KC027	Tn-Hoop-1	Virgin	540	1530	
KC027	Tn-Hoop-2	Virgin	600	1700	
KC027	Tn-Hoop-3	Virgin	610	1700	
KC027	Tn-Hoop-4	Virgin	590	1660	
KC027	Tn-Hoop-5	Virgin	560	1560	
KC027	Tn-Hoop-6	Virgin	580	1630	
KC027	Tn-Hoop-7	Virgin	650	1810	
KC027	Tn-Hoop-8	Virgin	620	1740	
KC027	Tn-Hoop-9	Virgin	630	1760	
Average			598	1677	
Standard Deviation			33	87	
COV			5%	5%	
LC026	Tn-Hoop-16	Virgin	700	1960	
LC026	Tn-Hoop-17	Virgin	690	1940	
LC026	Tn-Hoop-18	Virgin	680	1910	
LC026	Tn-Hoop-19	Virgin	730	2060	
LC026	Tn-Hoop-20	Virgin	630	1770	
LC026	Tn-Hoop-21	Virgin	670	1870	
LC026	Tn-Hoop-22	Virgin	610	1710	
LC026	Tn-Hoop-23	Virgin	790	2200	
LC026	Tn-Hoop-24	Virgin	730	2050	
Average			692	1941	
Standard Deviation			51	142	
COV			7%	7%	

Table 8-4 (Page 2 of 3)

Room Temperature Hoop Strength of Coors P-100A-1

Element	Specimen Number	Hours in Operation	Maximum Hydrostatic Pressure (psig)	Ultimate Strength (psi)	Remarks
FC010	Tn-Hoop-1	540	480	1310	See Note 2
FC010	Tn-Hoop-2	540	490	1330	See Note 2
FC010	Tn-Hoop-3	540	460	1260	See Note 2
FC010	Tn-Hoop-4	540	470	1270	See Note 2
FC010	Tn-Hoop-5	540	500	1340	See Note 2
FC010	Tn-Hoop-6	540	510	1360	See Note 2
FC010	Tn-Hoop-7	540	490	1330	See Note 2
FC010	Tn-Hoop-8	540	520	1410	See Note 2
FC010	Tn-Hoop-9	540	500	1370	See Note 2
Average			491	1331	
Standard Deviation			18	45	
COV			4%	3%	
KC005	Tn-Hoop-10	616	640	1800	See Note 3
KC005	Tn-Hoop-11	616	640	1780	See Note 3
KC005	Tn-Hoop-12	616	610	1710	See Note 3
KC005	Tn-Hoop-13	616	620	1720	See Note 3
KC005	Tn-Hoop-14	616	580	1620	See Note 3
KC005	Tn-Hoop-15	616	520	1460	See Note 3
KC005	Tn-Hoop-16	616	610	1710	See Note 3
KC005	Tn-Hoop-17	616	570	1600	See Note 3
KC005	Tn-Hoop-18	616	670	1870	See Note 3
Average			607	1697	
Standard Deviation			42	115	
COV			7%	7%	
KC011	Tn-Hoop-19	616	490	1350	See Note 3
KC011	Tn-Hoop-20	616	470	1310	See Note 3
KC011	Tn-Hoop-21	616	470	1320	See Note 3
KC011	Tn-Hoop-22	616	560	1570	See Note 3
KC011	Tn-Hoop-23	616	530	1490	See Note 3
KC011	Tn-Hoop-24	616	530	1470	See Note 3
KC011	Tn-Hoop-25	616	560	1560	See Note 3
KC011	Tn-Hoop-26	616	550	1530	See Note 3
KC011	Tn-Hoop-27	616	550	1540	See Note 3
Average			523	1460	
Standard Deviation			35	99	
COV			7%	7%	

Table 8-4 (Page 3 of 3)

Room Temperature Hoop Tensile Strength of Coors P-100A-1

Element	Specimen Number	Hours in Operation	Maximum Hydrostatic Pressure (psig)	Ultimate Strength (psi)	Remarks
LC025	Tn-Hoop-28	616	550	1540	See Note 3
LC025	Tn-Hoop-29	616	580	1620	See Note 3
LC025	Tn-Hoop-30	616	620	1740	See Note 3
LC025	Tn-Hoop-31	616	520	1470	See Note 3
LC025	Tn-Hoop-32	616	540	1520	See Note 3
LC025	Tn-Hoop-33	616	640	1790	See Note 3
LC025	Tn-Hoop-34	616	740	2060	See Note 3
LC025	Tn-Hoop-35	616	680	1890	See Note 3
LC025	Tn-Hoop-36	616	640	1800	See Note 3
Average			612	1714	
Standard Deviation			68	183	
COV			11%	11%	
KC007	Tn-Hoop-1	628	470	1270	See Notes 3,4
KC007	Tn-Hoop-2	628	520	1400	See Notes 3,4
KC007	Tn-Hoop-3	628	590	1610	See Notes 3,4
KC007	Tn-Hoop-4	628	540	1380	See Notes 3,4
KC007	Tn-Hoop-5	628	580	1570	See Notes 3,4
KC007	Tn-Hoop-6	628	580	1660	See Notes 3,4
KC007	Tn-Hoop-7	628	90	250	See Notes 3,4
KC007	Tn-Hoop-8	628	50	150	See Notes 3,4
KC007	Tn-Hoop-9	628	160	450	See Notes 3,4
Average			398	1482	
Standard Deviation			215	140	
COV			54%	9%	

Notes:
1. The "batch" was not identified for element 24.
2. All operation in the Siemens Westinghouse advanced particulate filtration system at the Foster Wheeler PCFBC test facility in Karhula, Finland. Nominal-operating temperature was 1,550°F.
3. All operation at the SCS PSDF in combustion mode at a nominal-operating temperature of 1,400°F.
4. In operation during PCD fire.

Table 8-5

Axial Compressive Properties of Virgin Coors P-100A-1

Candle Identification	Specimen Number	Temperature (°F)	Ultimate Strength (psi)	Young's Modulus (Msi)	Strain-to-Failure (mils/in.)	Remarks
24	Cm-ax-1	70	17660	4.27	4.5	
24	Cm-ax-3	70	16820	4.13	4.4	
24	Cm-ax-5	70	17070	4.16	4.4	
Average			17183	4.19	4.4	
24	Cm-ax-2	1700	9560	2.21	6.0	
24	Cm-ax-4	1700	10530	2.31	7.7	
24	Cm-ax-6	1700	9970	2.28	6.1	
Average			10020	2.27	6.6	

Notes:
1. The "batch" was not identified for element 24.

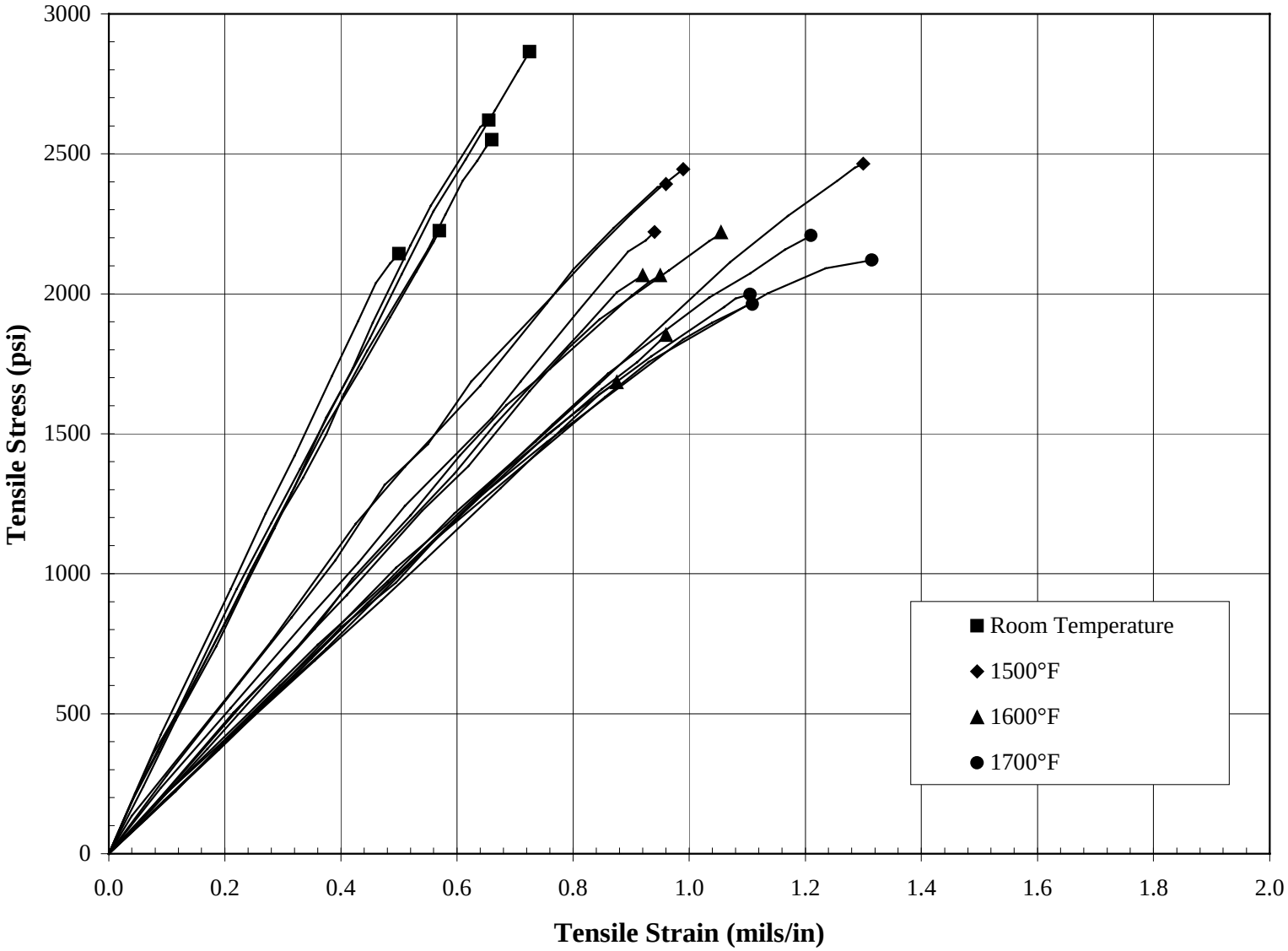

Figure 8-1 Room and Elevated Temperature Axial Tensile Stress-Strain Responses for Virgin Coors P-100A-1

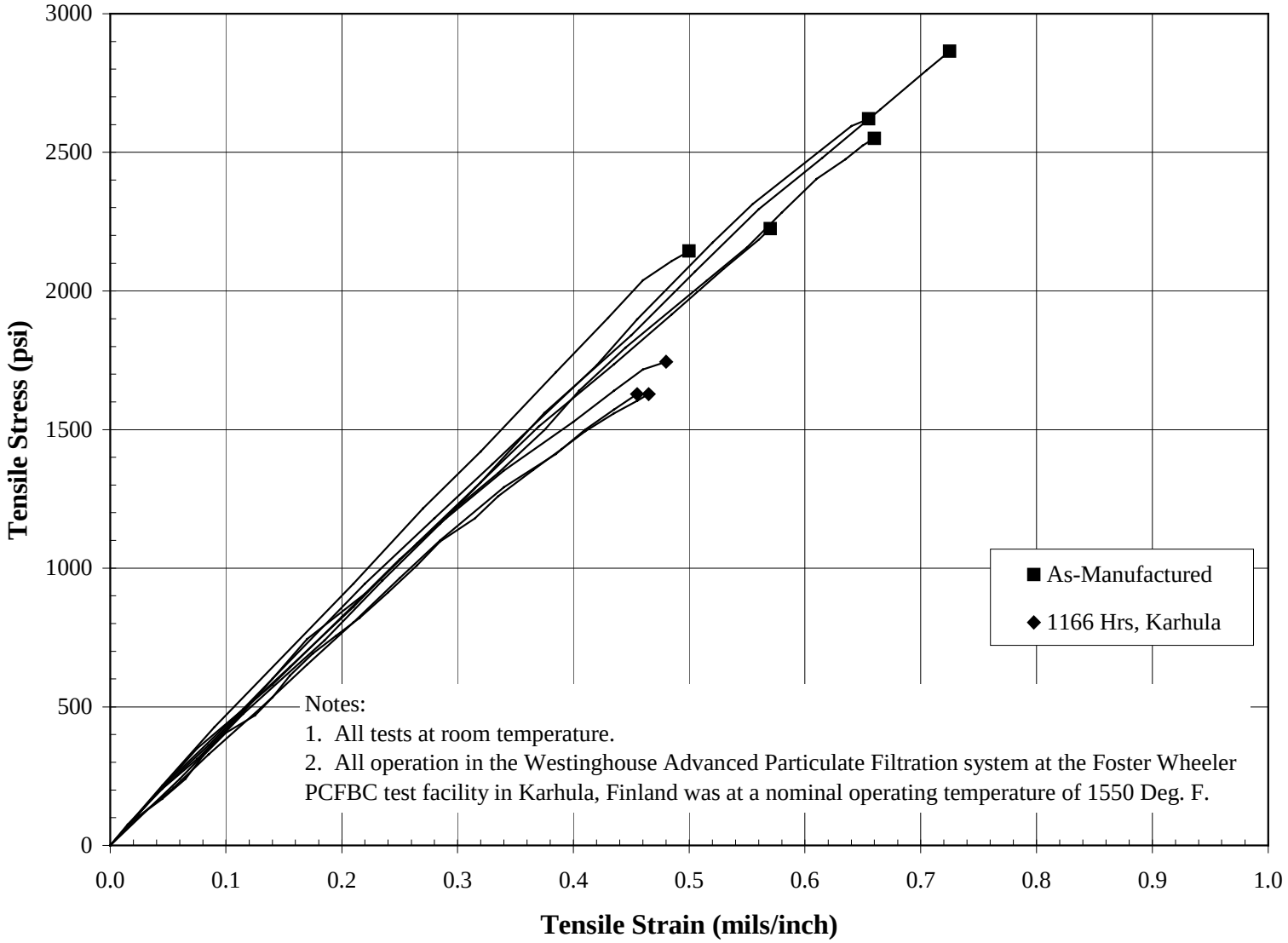

Figure 8-2 Room Temperature Axial Tensile Stress-Strain Responses for Coors P-100A-1 Virgin and After 1,166 Hours in Combustion Operation at Karhula

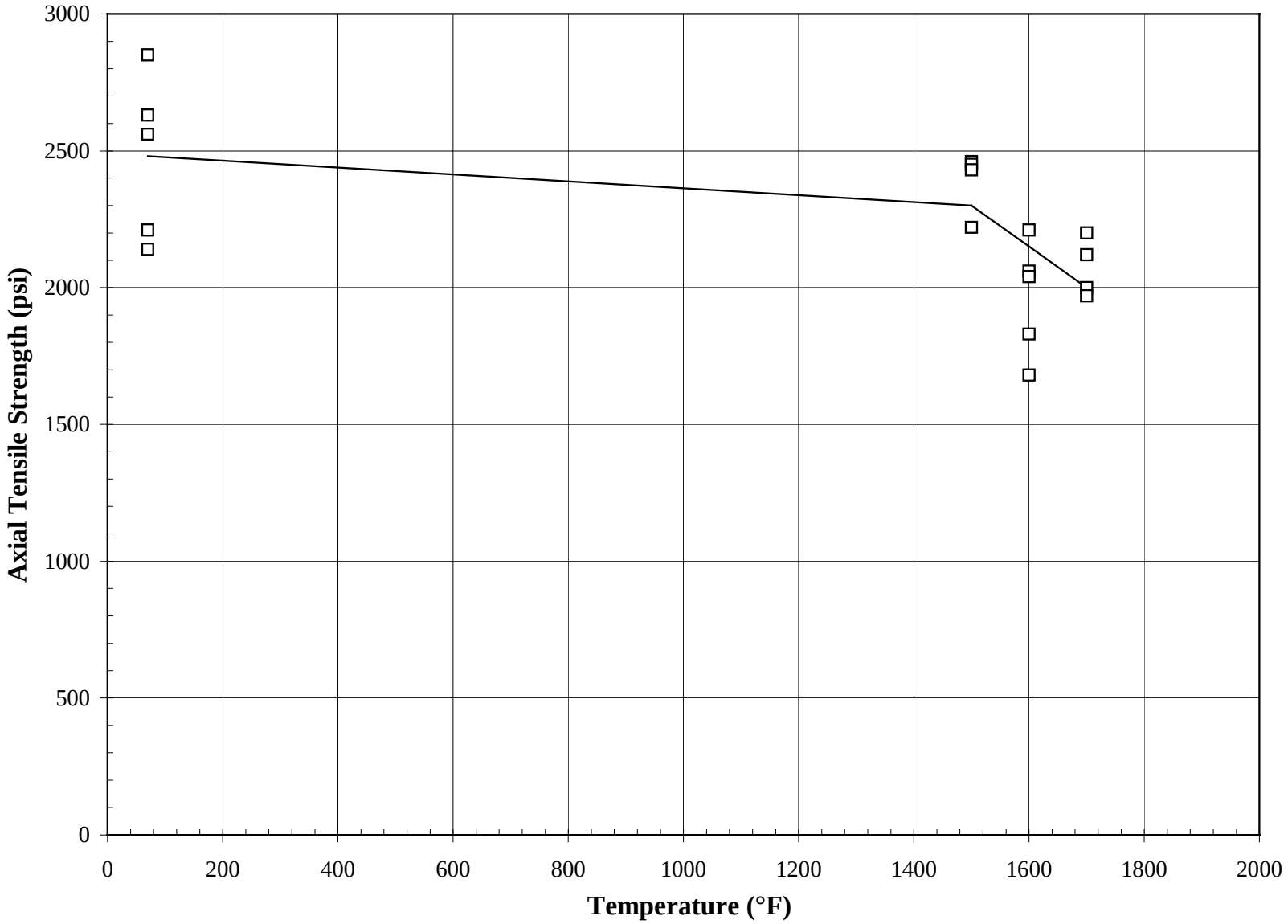

Figure 8-3 Axial Tensile Strength Versus Temperature for Virgin Coors P-100A-1

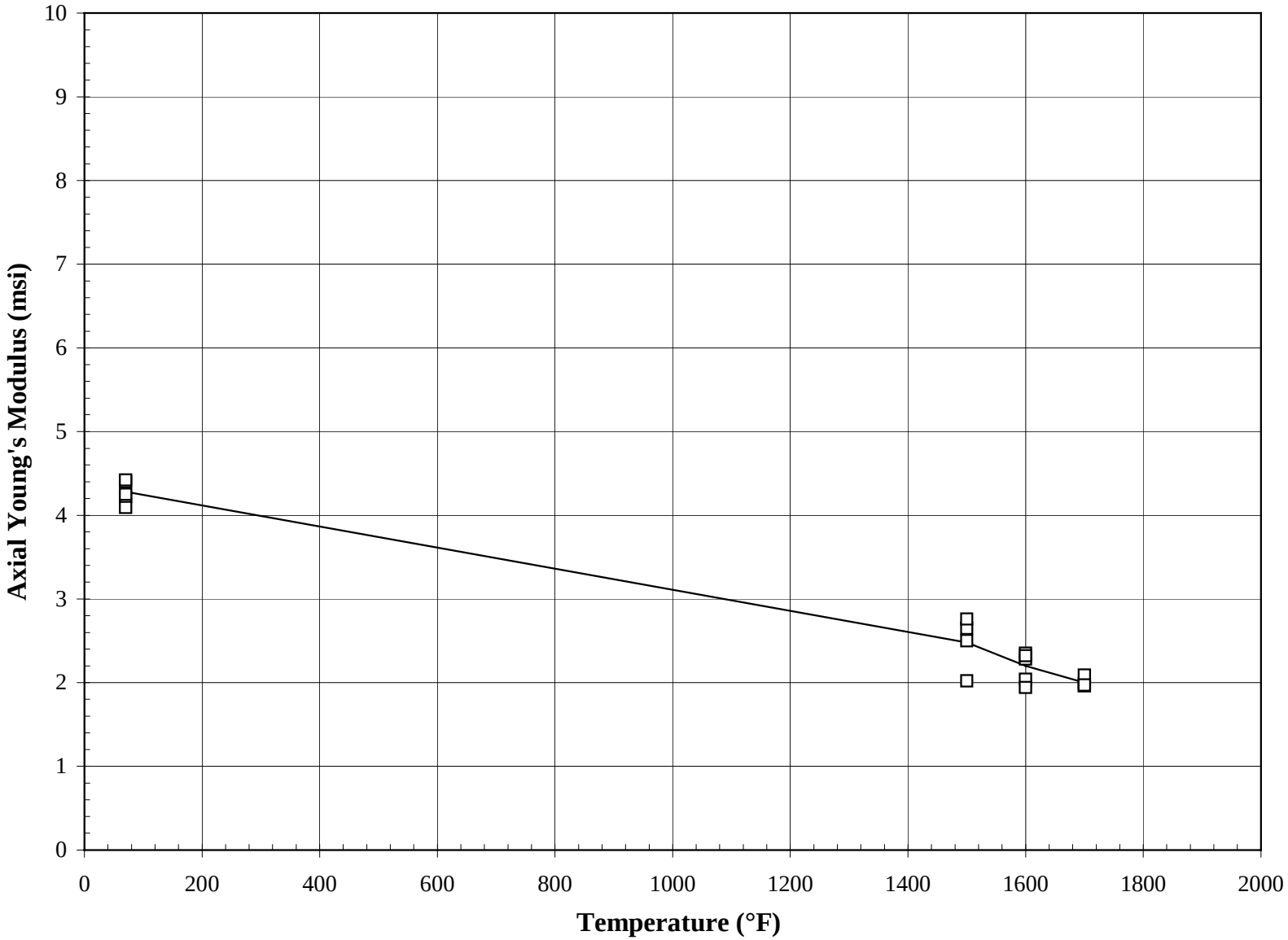

Figure 8-4 Axial Young's Modulus Versus Temperature for Virgin Coors P-100A-1

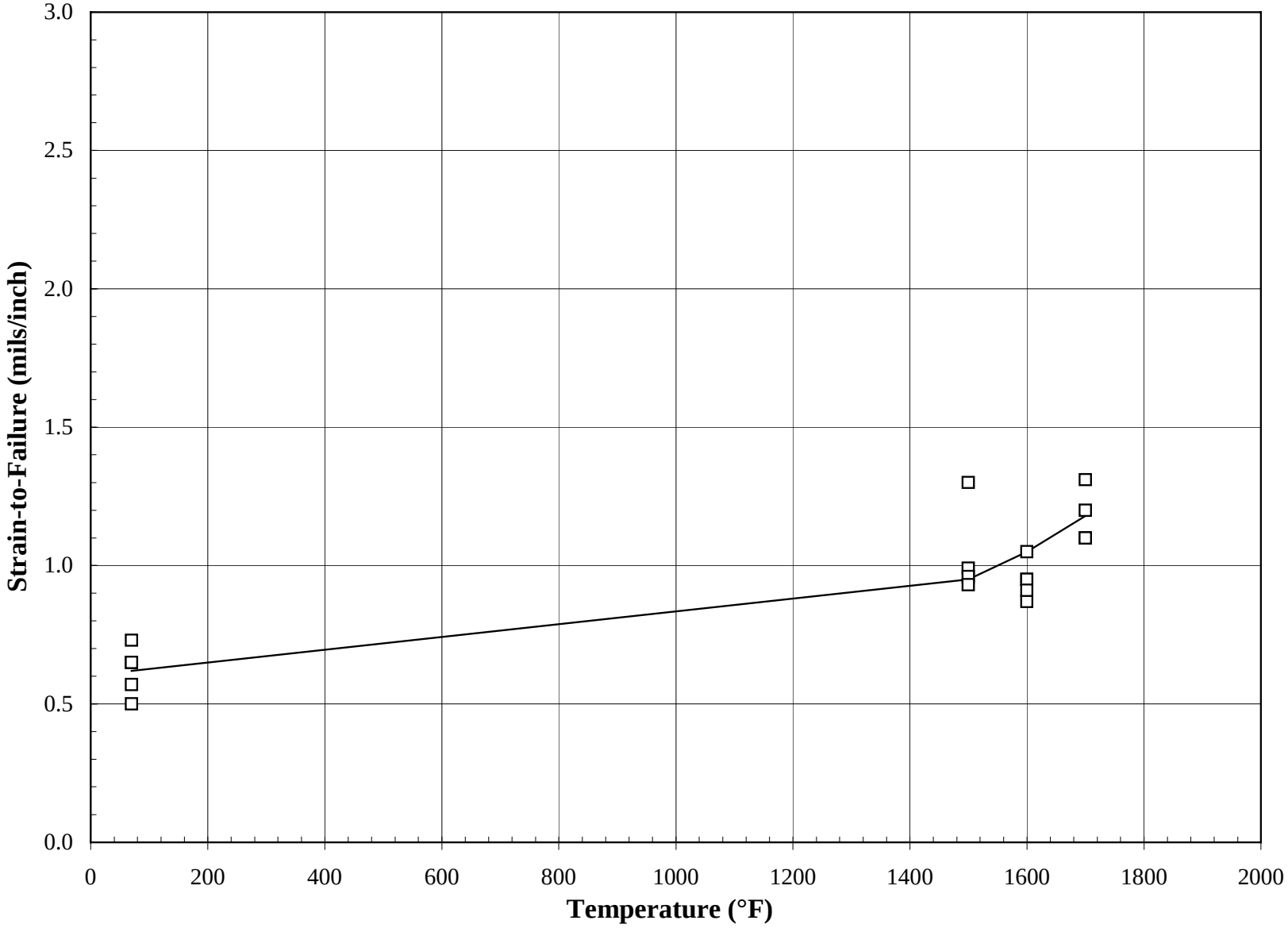

Figure 8-5 Axial Tensile Strain-to-Failure Versus Temperature for Virgin Coors P-100A-1

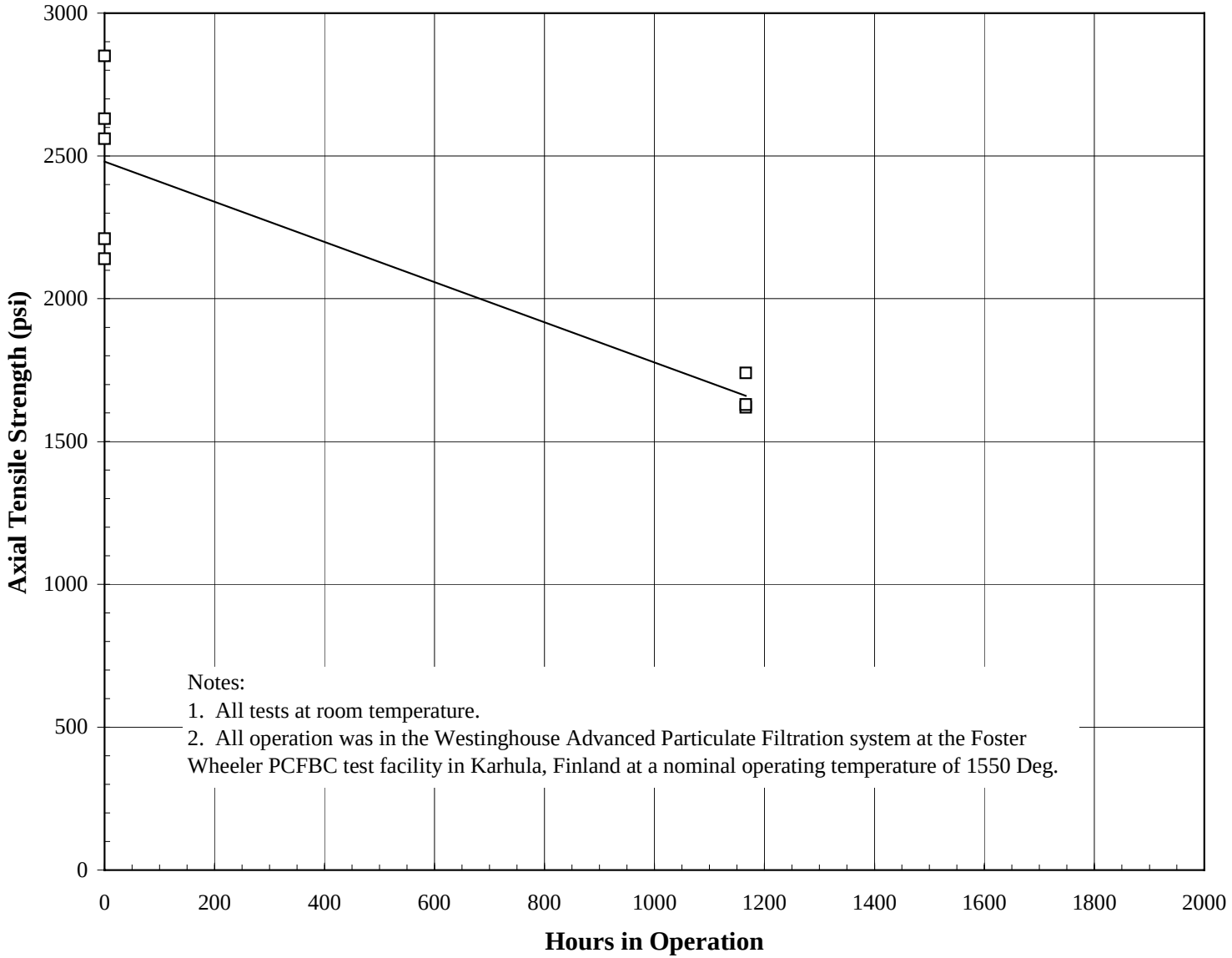

Figure 8-6 Room Temperature Axial Tensile Strength Versus Hours in Operation for Coors P-100A-1

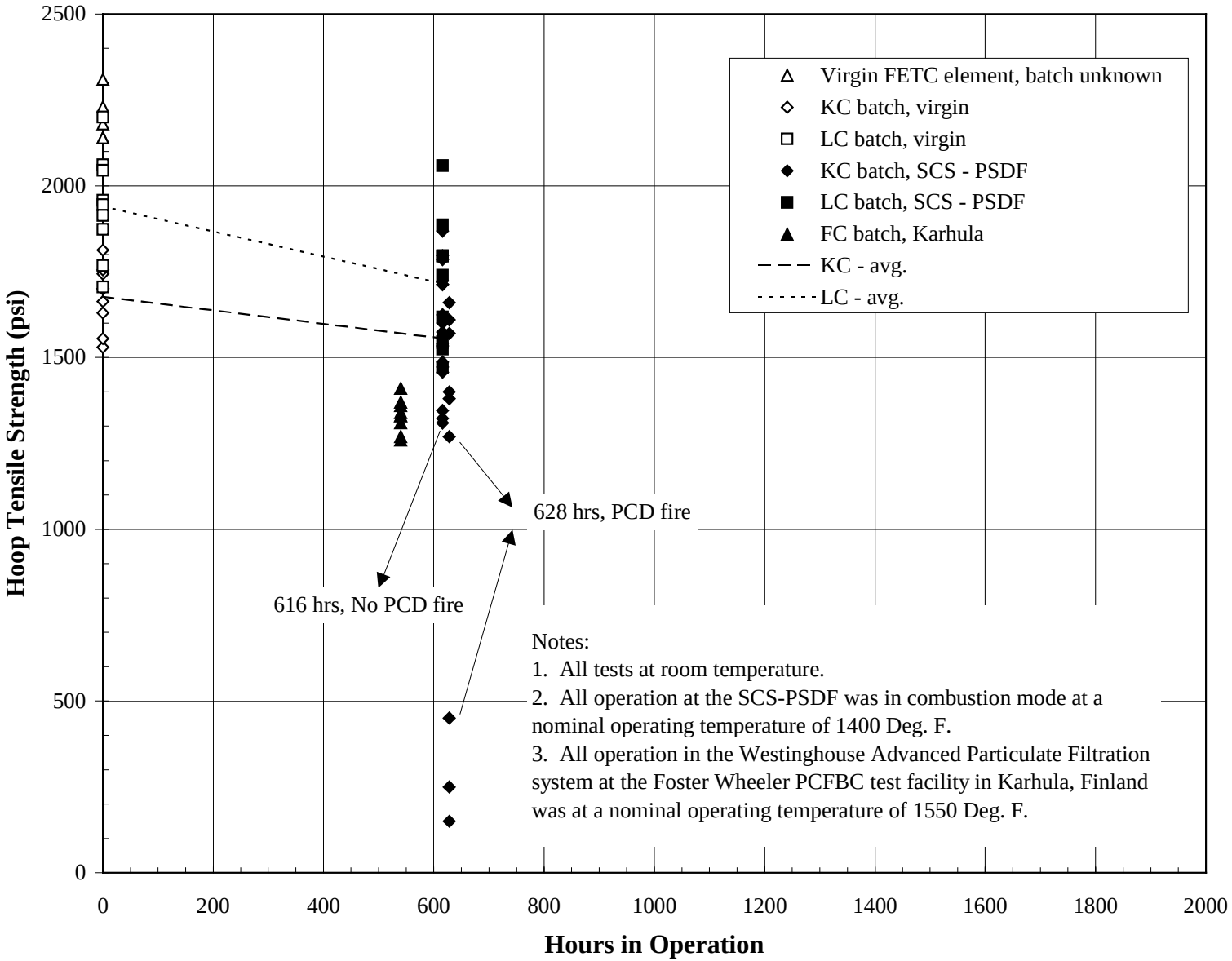

Figure 8-7 Room Temperature Hoop Tensile Strength Versus Hours in Combustion Operation for Coors P-100A-1

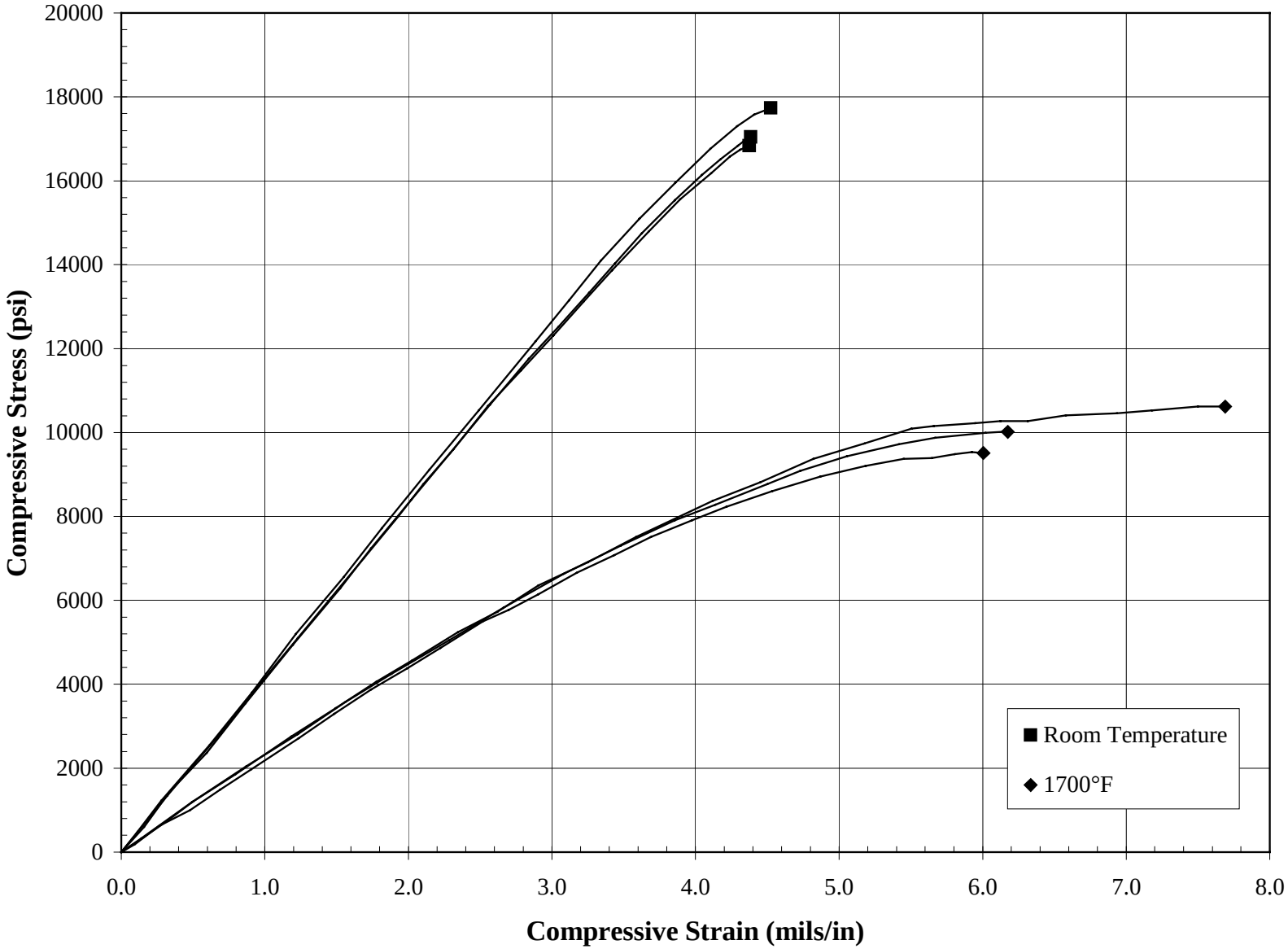

Figure 8-8 Room and Elevated Temperature Axial Compressive Stress-Strain Responses for Virgin Coors P-100A-1

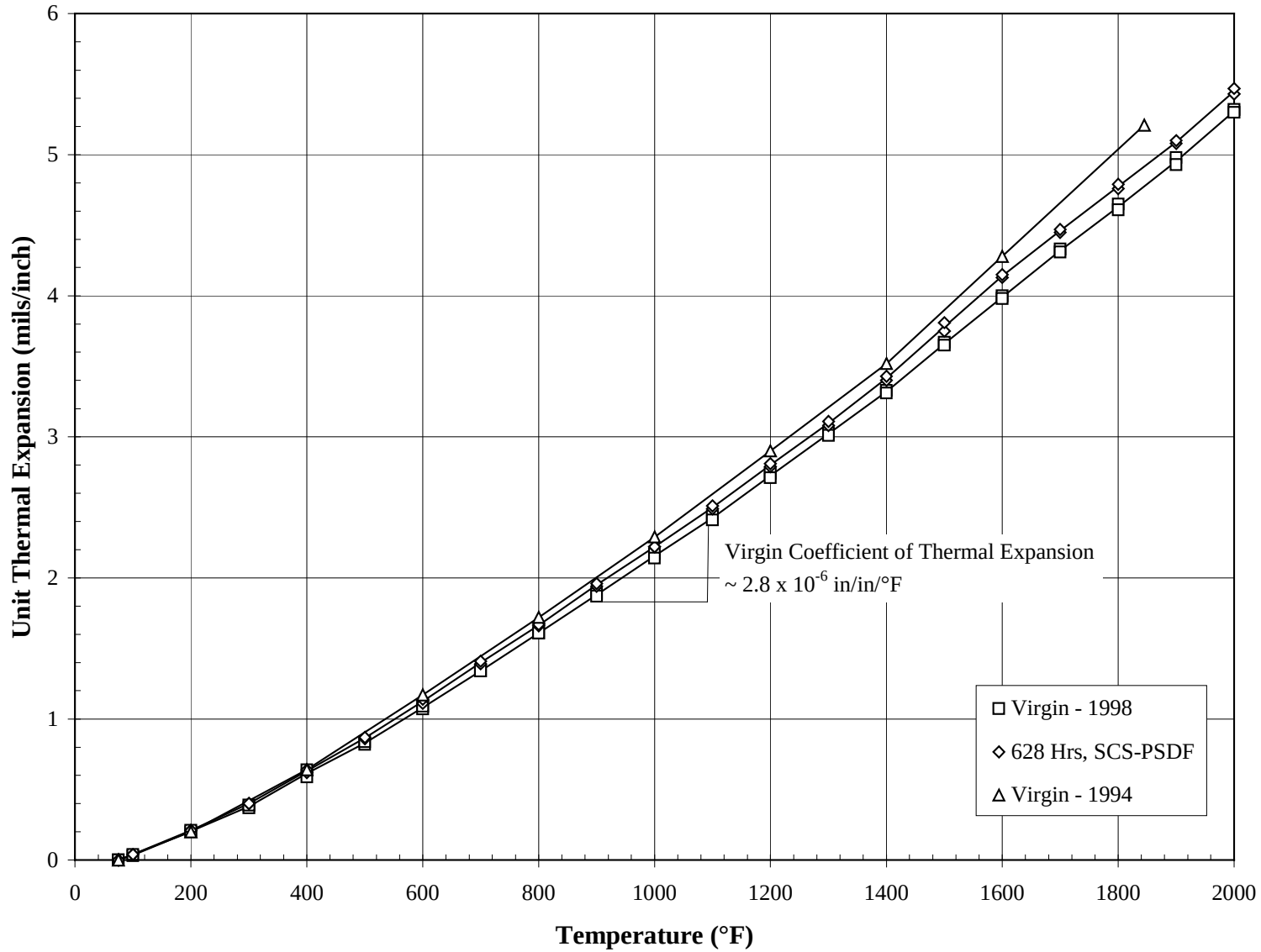

Figure 8-9 Unit Thermal Expansion of Coors P-100A-1

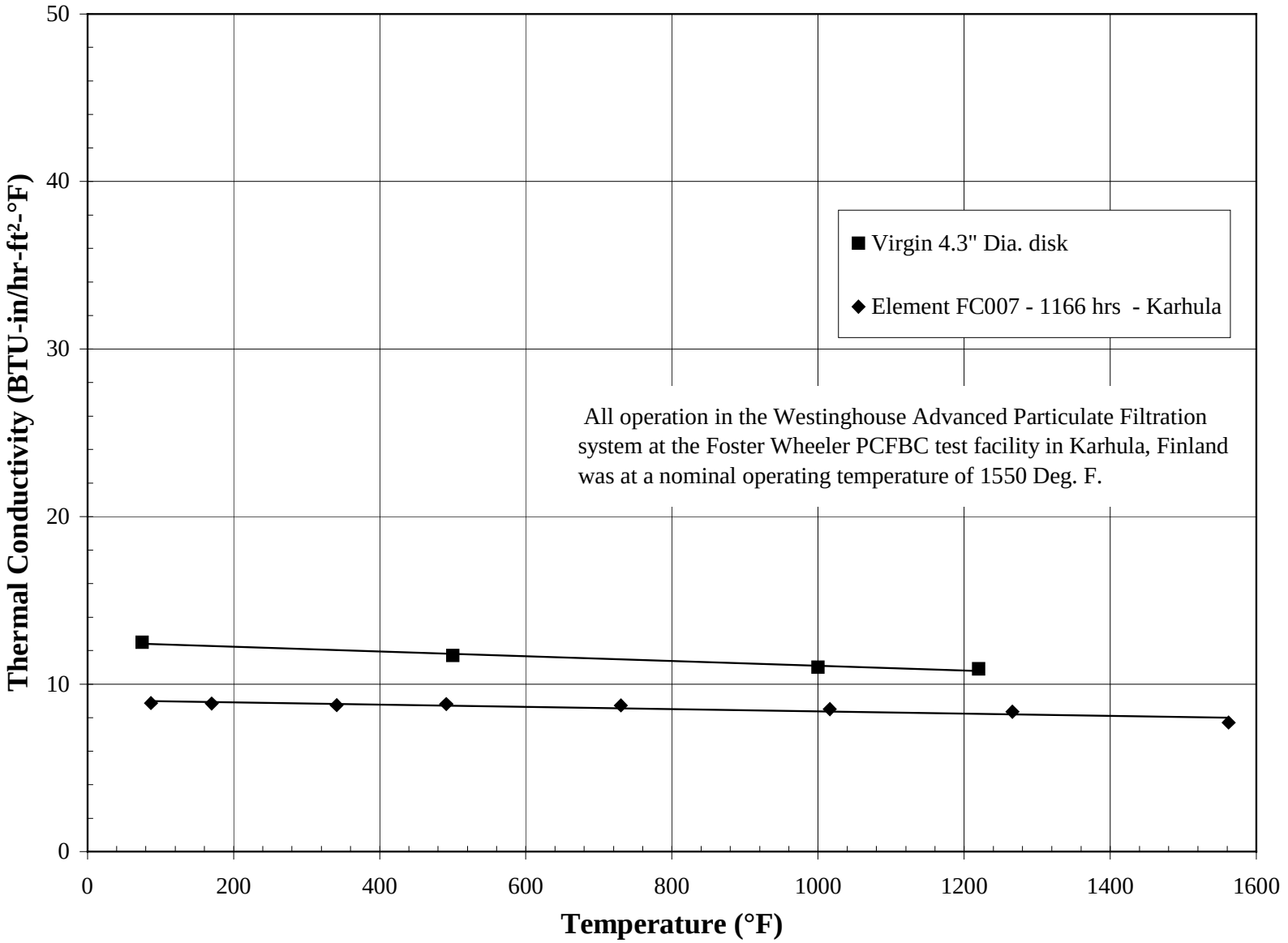

Figure 8-10 Thermal Conductivity Versus Temperature for Coors P-100A-1

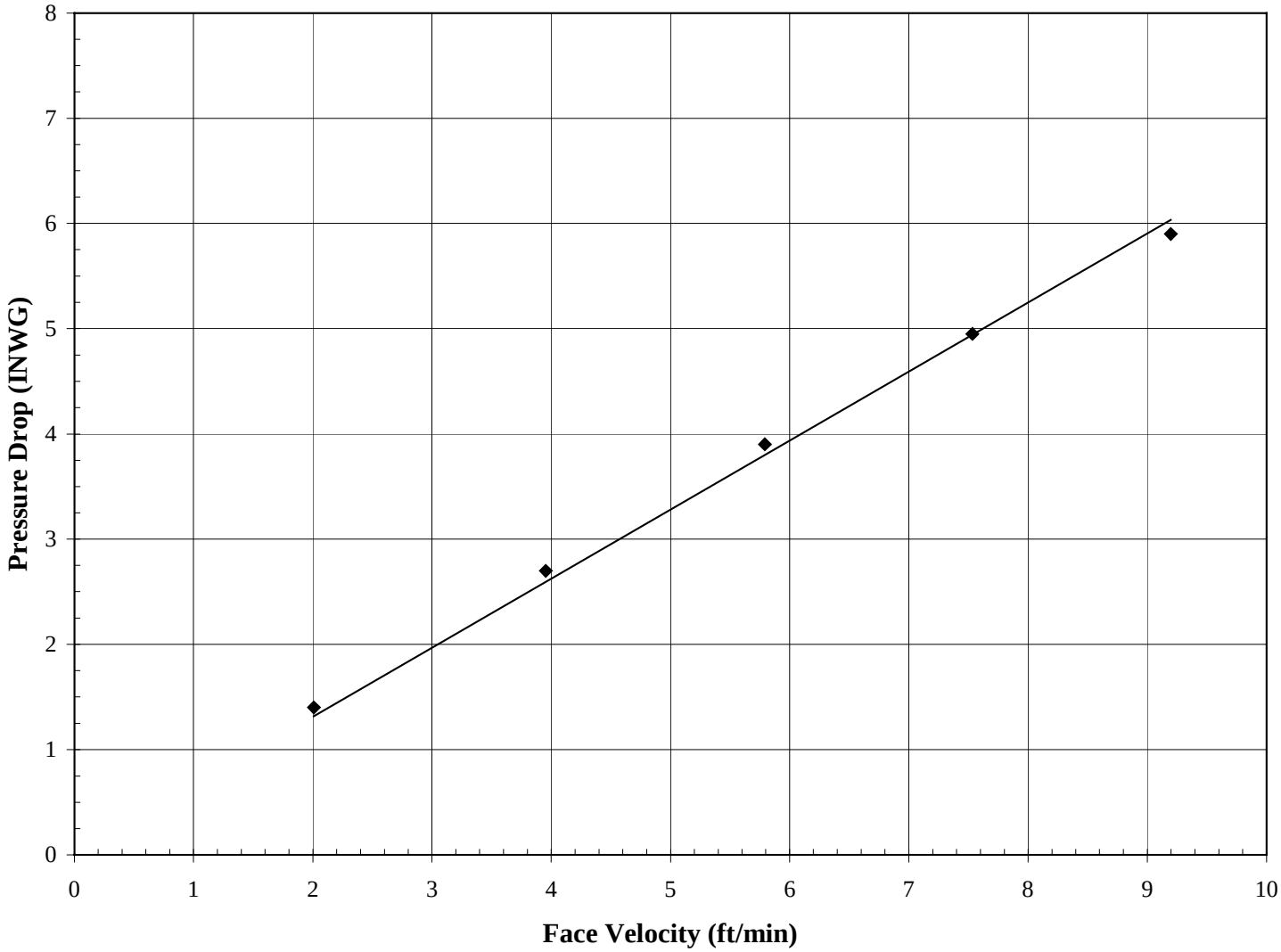

Figure 8-11 Pressure Drop Versus Face Velocity for Virgin Coors P-100A-1
Using Air at Ambient Temperature and Pressure

9.0 BLASCH 4-270

Blasch 4-270 is a monolithic mullite-bonded aluminum oxide with nominal dimensions of 1.52 in. (39 mm) I.D. and 0.42 in. (11 mm) wall thickness. Like the Coors material, Blasch is a depth filter with no membrane layer. Probable values of selected properties of virgin Blasch 4-270 are as follows:

Bulk Density (lbm/ft^3)	111
Hoop Tensile Strength at Room Temperature (psi)	500
Axial Tensile Strength at Room Temperature (psi)	270
Axial Young's Modulus at Room Temperature (10^6 psi)	0.9
Axial Tensile Strain-to-Failure at Room Temperature (mils/in.)	0.37
Axial Coefficient of Thermal Expansion, 500 to 1,500°F (10^{-6} in./in./°F)	4.1
Radial Thermal Conductivity at 1,000°F (Btu-in./hr-ft^2-°F)	5.2
Pressure Drop at 5 ft/min Face Velocity, Air at Ambient Conditions(inWG)	7.7

Table 9-1

Density of Blasch 4-270

Element	Specimen Number	Hours in Operation	I.D. (in.)	O.D. (in.)	Density (gr/cm³)	Density (lb/ft³)	Remarks
BPC-B14	Tn-Hoop-1	Virgin	1.46	2.36	1.84	115	
BPC-B14	Tn-Hoop-2	Virgin	1.46	2.36	1.80	112	
BPC-B14	Tn-Hoop-3	Virgin	1.46	2.36	1.74	108	
BPC-B14	Tn-Hoop-4	Virgin	1.52	2.37	1.79	111	
BPC-B14	Tn-Hoop-5	Virgin	1.53	2.36	1.78	111	
BPC-B14	Tn-Hoop-6	Virgin	1.53	2.37	1.74	109	
BPC-B14	Tn-Hoop-7	Virgin	1.56	2.37	1.79	112	
BPC-B14	Tn-Hoop-8	Virgin	1.57	2.37	1.78	111	
BPC-B14	Tn-Hoop-9	Virgin	1.57	2.36	1.79	111	
		Average			1.78	111	
		Standard Deviation			0.03	2	
		Coefficient of Variation (COV)			2%	2%	

Table 9-2

Axial Tensile Properties of Blasch 4-270

Filter Identification	Specimen Number	Test Temperature (°F)	Ultimate Tensile Strength (psi)	Young's Modulus (msi)	Strain-to-Failure (mils/in.)	Notes
BPC-B14	Tn-Ax-1					See Note 1
BPC-B14	Tn-Ax-2	70	260	0.96	0.30	
BPC-B14	Tn-Ax-3	70	410	0.67	0.67	
BPC-B14	Tn-Ax-4	70				See Note 1
BPC-B14	Tn-Ax-5	70	250	1.03	0.30	
BPC-B14	Tn-Ax-6	70	175	0.81	0.22	
		Average	274	0.87	0.37	

Notes:
1. Broke during machining.

Table 9-3

Hoop Tensile Strength of Virgin Blasch 4-270

Filter Identification	Specimen Number	Hours in Operation	Maximum Hydrostatic Pressure (psig)	Ultimate Tensile Strength (psi)	Notes
BPC-B14	Tn-Hoop-1	Virgin			See Note 1
BPC-B14	Tn-Hoop-2	Virgin	100	220	See Note 2
BPC-B14	Tn-Hoop-3	Virgin	130	300	See Note 2
BPC-B14	Tn-Hoop-4	Virgin	210	510	
BPC-B14	Tn-Hoop-5	Virgin	210	520	
BPC-B14	Tn-Hoop-6	Virgin	170	420	
BPC-B14	Tn-Hoop-7	Virgin	180	470	
BPC-B14	Tn-Hoop-8	Virgin	190	490	
BPC-B14	Tn-Hoop-9	Virgin	220	560	
			197	495	
			20	48	
			10%	10%	

Notes:
1. Broke in handling.
2. Not included in statistics.

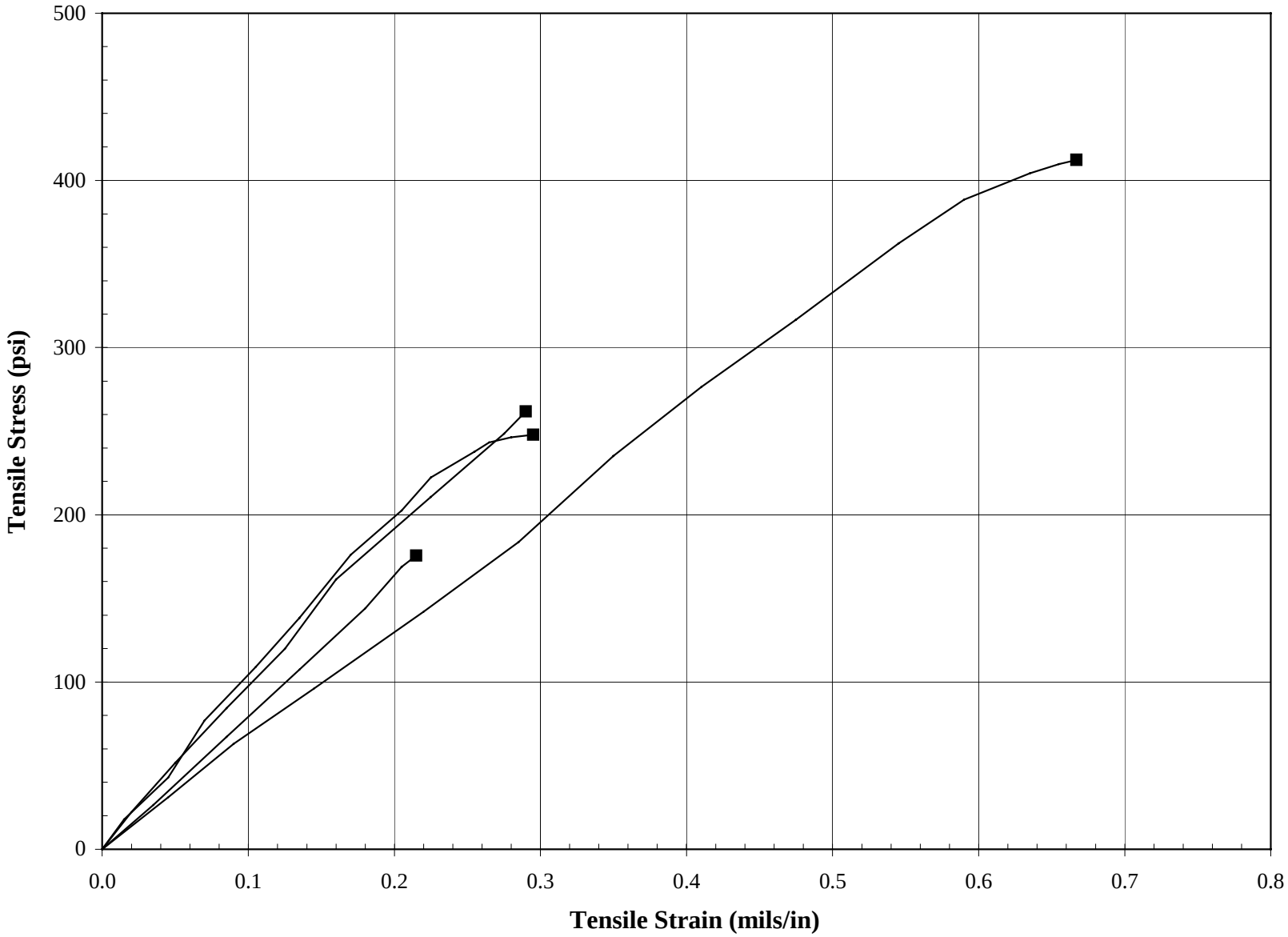

Figure 9-1 Room Temperature Axial Tensile Stress-Strain Responses of Virgin Blasch 4-270

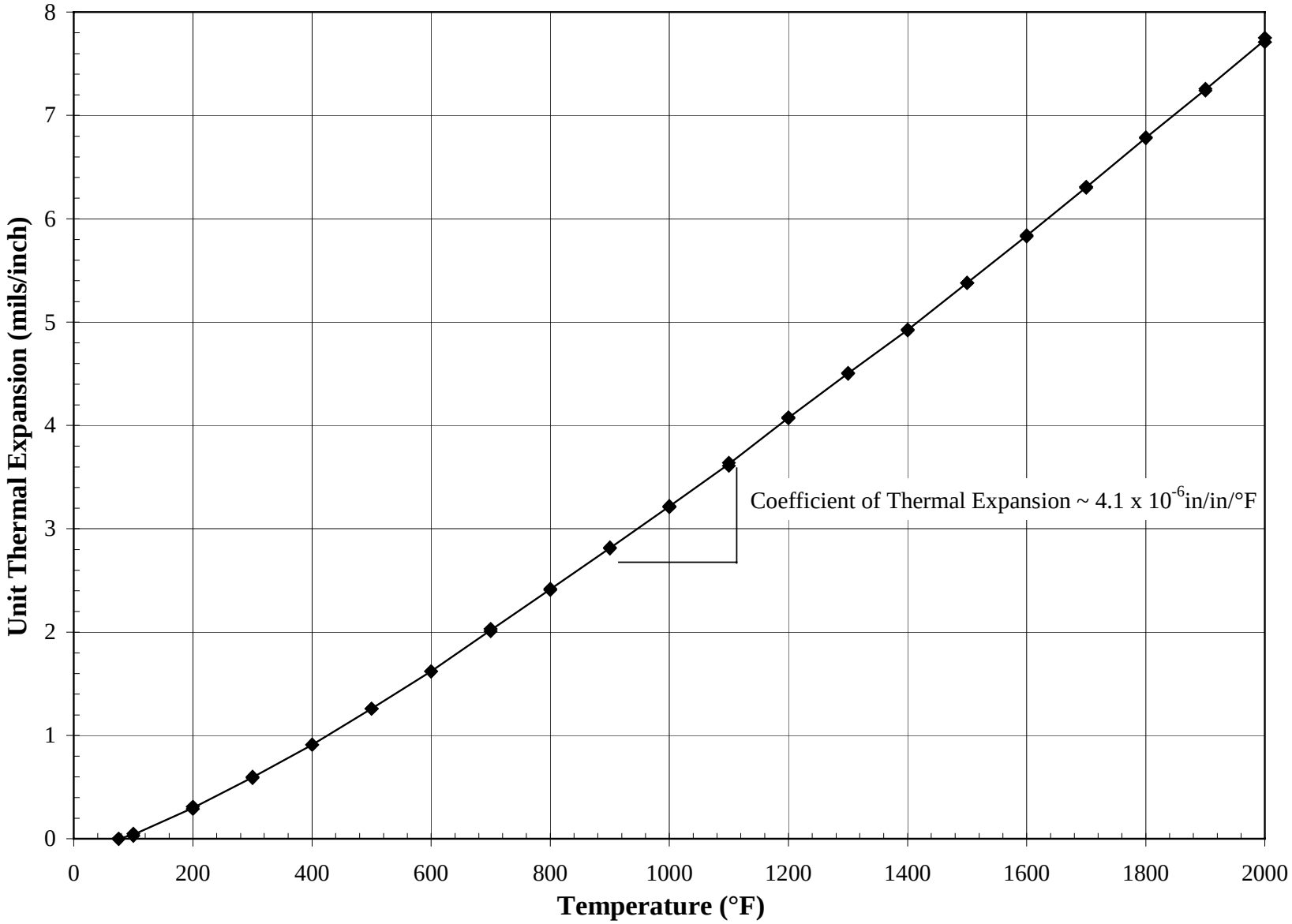

Figure 9-2 Unit Thermal Expansion of Virgin Blasch 4-270

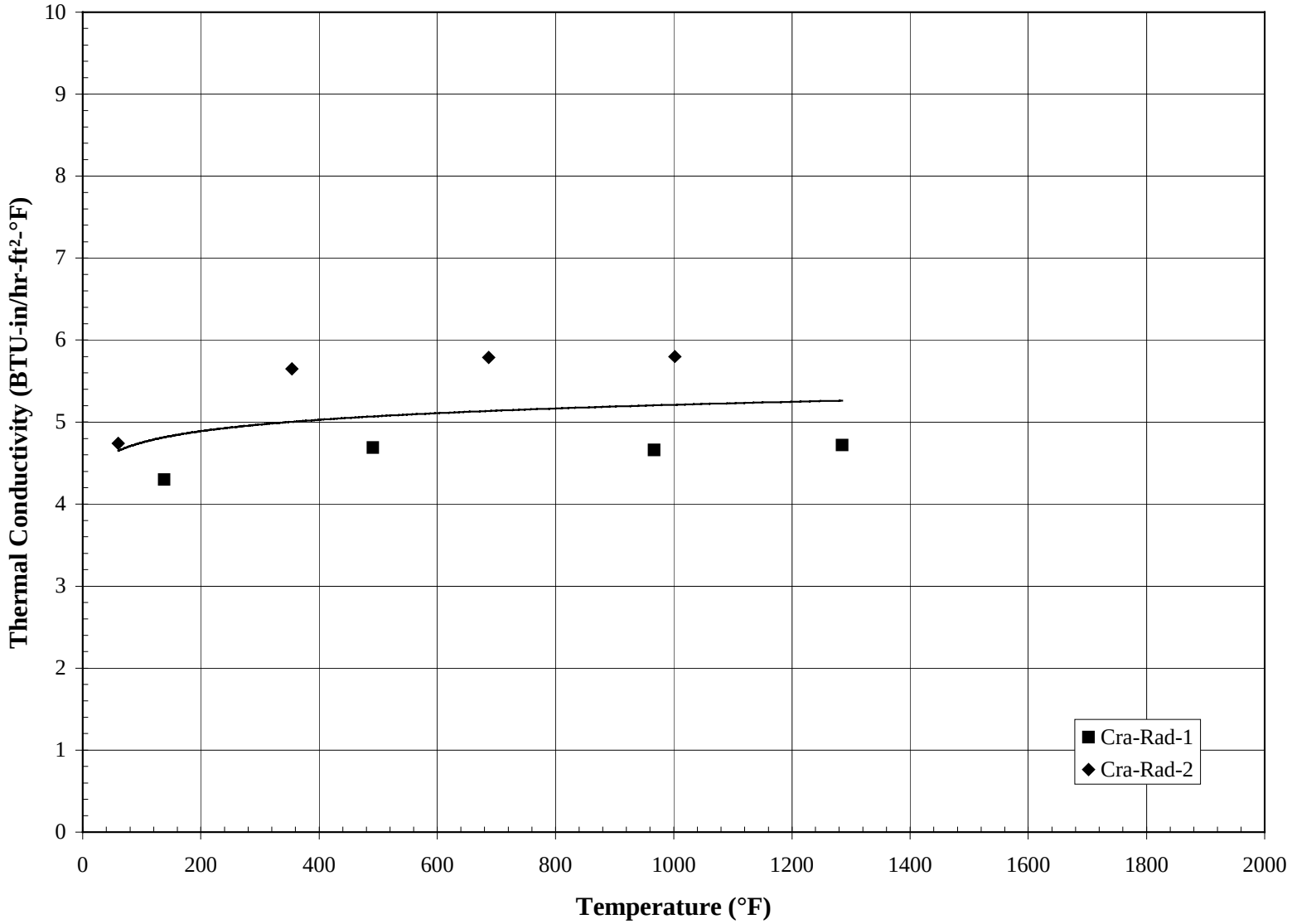

Figure 9-3 Radial Thermal Conductivity Versus Temperature for Virgin Blasch 4-270

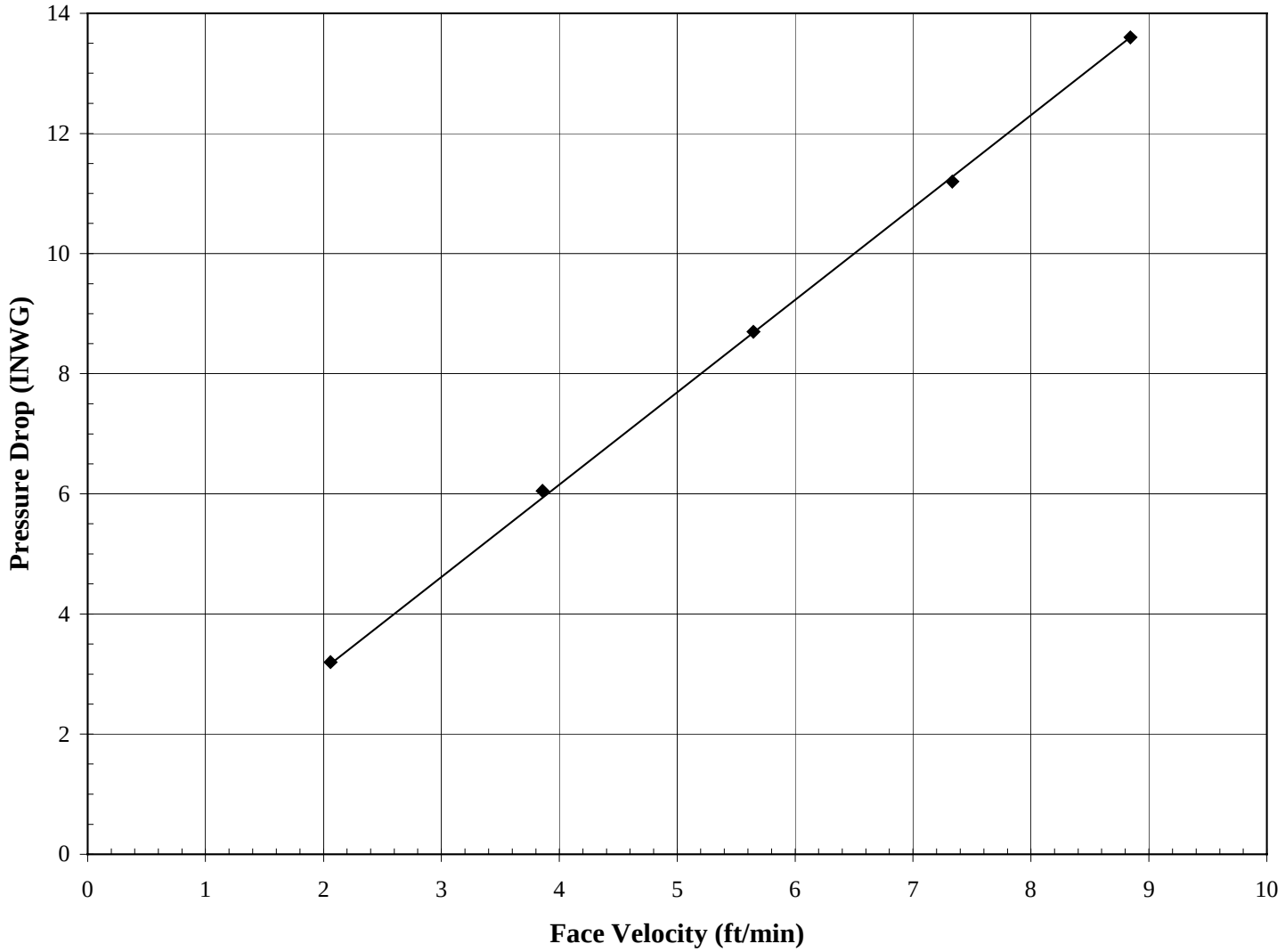

Figure 9-4 Pressure Drop Versus Face Velocity for Virgin Blasch 4-270
Using Air as Ambient Temperature and Pressure

10.0 ENSTO

Ensto elements are manufactured with aluminum oxide particles in a mullite binder to form a microstructure similar to the clay-bonded SiC materials. Nominal dimensions are 1.45 in. (37 mm) I.D. and 0.48 in. (12 mm) wall thickness. Like the Coors and Blasch materials, Ensto is a depth filter with no membrane layer. Probable values of selected properties of virgin Ensto 4-270 are as follows:

Bulk Density (lbm/ft^3)	118
Hoop Tensile Strength at Room Temperature (psi)	990
Axial Tensile Strength at Room Temperature (psi)	920
Axial Young's Modulus at Room Temperature (10^6 psi)	2.3
Axial Tensile Strain-to-Failure at Room Temperature (mils/in.)	0.50
Axial Tensile Strength at 1,500°F (psi)	900
Axial Young's Modulus at 1,500°F (10^6 psi)	2.3
Axial Tensile Strain-to-Failure at 1,500°F (mils/in.)	0.40
Axial Coefficient of Thermal Expansion, 500 to 1,500°F (10^{-6} in./in./°F)	3.9
Radial Thermal Conductivity at 1,000°F (BTU-in./hr-ft^2-°F)	6.0

Table 10-1

Density of Ensto Filter Element

Element	Specimen Number	Hours in Operation	I.D. (in.)	O.D. (in.)	Density (gr/cm^3)	Density (lb/ft^3)	Remarks
146-97	Tn-Hoop-100	Virgin	1.45	2.40	1.88	118	
146-97	Tn-Hoop-101	Virgin	1.45	2.40	1.89	118	
146-97	Tn-Hoop-102	Virgin	1.45	2.40	1.89	118	
146-97	Tn-Hoop-103	Virgin	1.45	2.39	1.88	118	
146-97	Tn-Hoop-104	Virgin	1.45	2.40	1.88	117	
146-97	Tn-Hoop-105	Virgin	1.45	2.39	1.89	118	
146-97	Tn-Hoop-106	Virgin	1.46	2.42	1.90	119	
146-97	Tn-Hoop-107	Virgin	1.46	2.42	1.90	119	
146-97	Tn-Hoop-108	Virgin	1.46	2.42	1.90	119	
		Average			1.88	118	
		Standard Deviation			0.002	0.150	
		Coefficient of Variation (COV)			0.13%	0.13%	

Table 10-2

Room and Elevated Axial Tensile Properties of Virgin Ensto

Element	Specimen Number	Test Temperature (°F)	Ultimate Strength (psi)	Young's Modulus (Msi)	Strain-to-Failure (mils/in.)	Notes
46-97	Tn-Ax-36	70	900	2.25	0.49	
46-97	Tn-Ax-39	70	960	2.18	0.55	
46-97	Tn-Ax-42	70				See Note 1
46-97	Tn-Ax-43	70	900	2.26	0.50	
46-97	Tn-Ax-45	70	920	2.44	0.47	
	Average		920	2.28	0.50	
	Standard Deviation		24	0.10	0.03	
	COV		3%	4%	6%	
46-97	Tn-Ax-37	1500	740	2.11	0.35	
46-97	Tn-Ax-38	1500	880	2.53	0.36	
46-97	Tn-Ax-40	1500	980	2.14	0.46	
46-97	Tn-Ax-44	1500	900	2.64	0.37	
	Average		875	2.36	0.39	
	Standard Deviation		86	0.23	0.04	
	COV		10%	10%	11%	

Notes: 1. Broke in handling.

Table 10-3

Room Temperature Hoop Tensile Strength of Ensto

Element	Specimen Number	Hours in Operation	Maximum Hydrostatic Pressure (psig)	Ultimate Strength (psi)	Remarks
146-97	Tn-Hoop-100	Virgin	420	900	
146-97	Tn-Hoop-101	Virgin	420	910	
146-97	Tn-Hoop-102	Virgin	440	950	
146-97	Tn-Hoop-103	Virgin	470	1000	
146-97	Tn-Hoop-104	Virgin	460	990	
146-97	Tn-Hoop-105	Virgin	410	890	
146-97	Tn-Hoop-106	Virgin	510	1090	
146-97	Tn-Hoop-107	Virgin	510	1100	
146-97	Tn-Hoop-108	Virgin	500	1070	
Average			460	989	
Standard Deviation			38	78	
Coefficient of Variation (COV)			8.2%	7.9%	

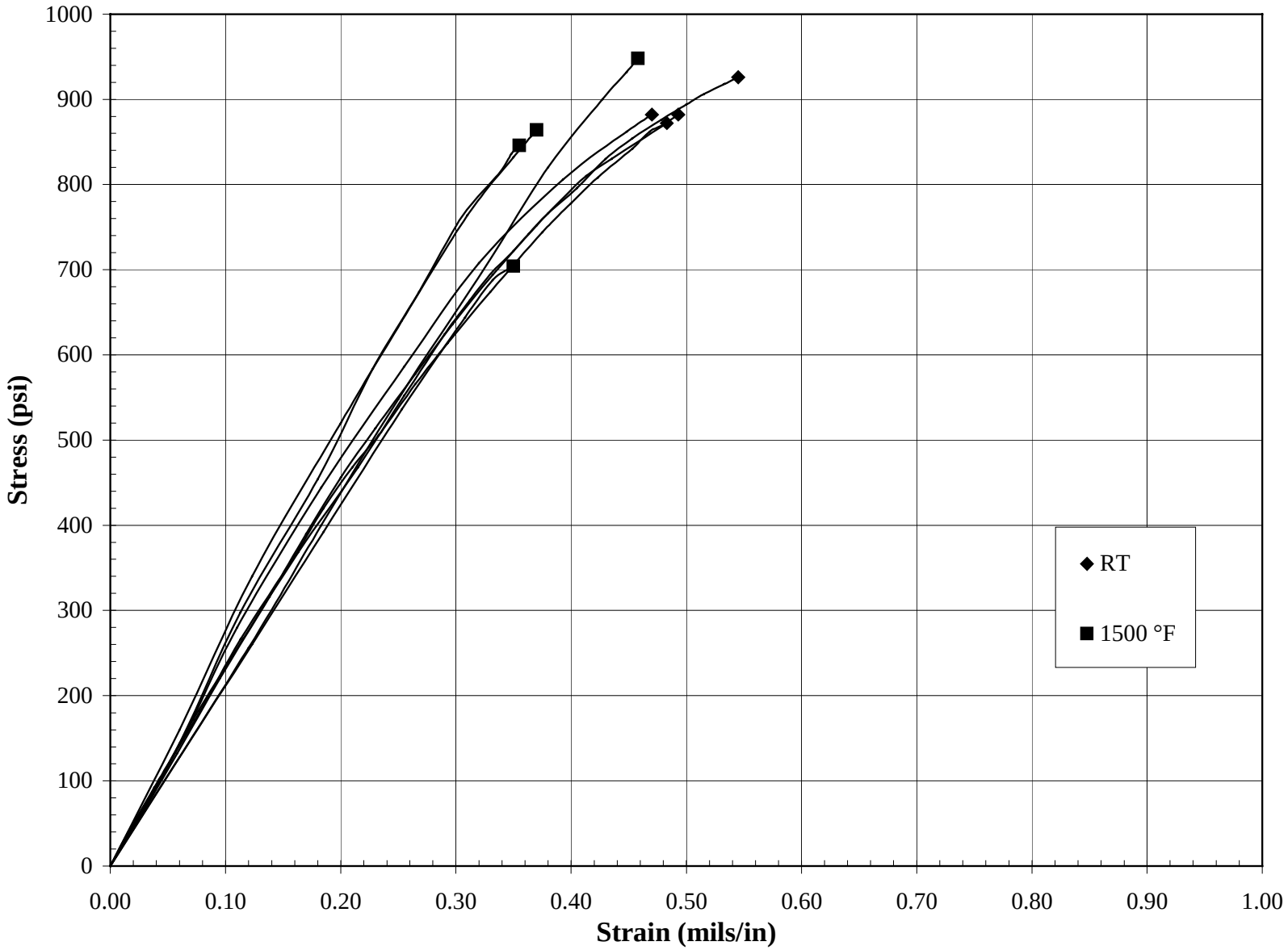

Figure 10-1 Room and Elevated Temperature Axial Tensile Stress-Strain Responses for Virgin Ensto

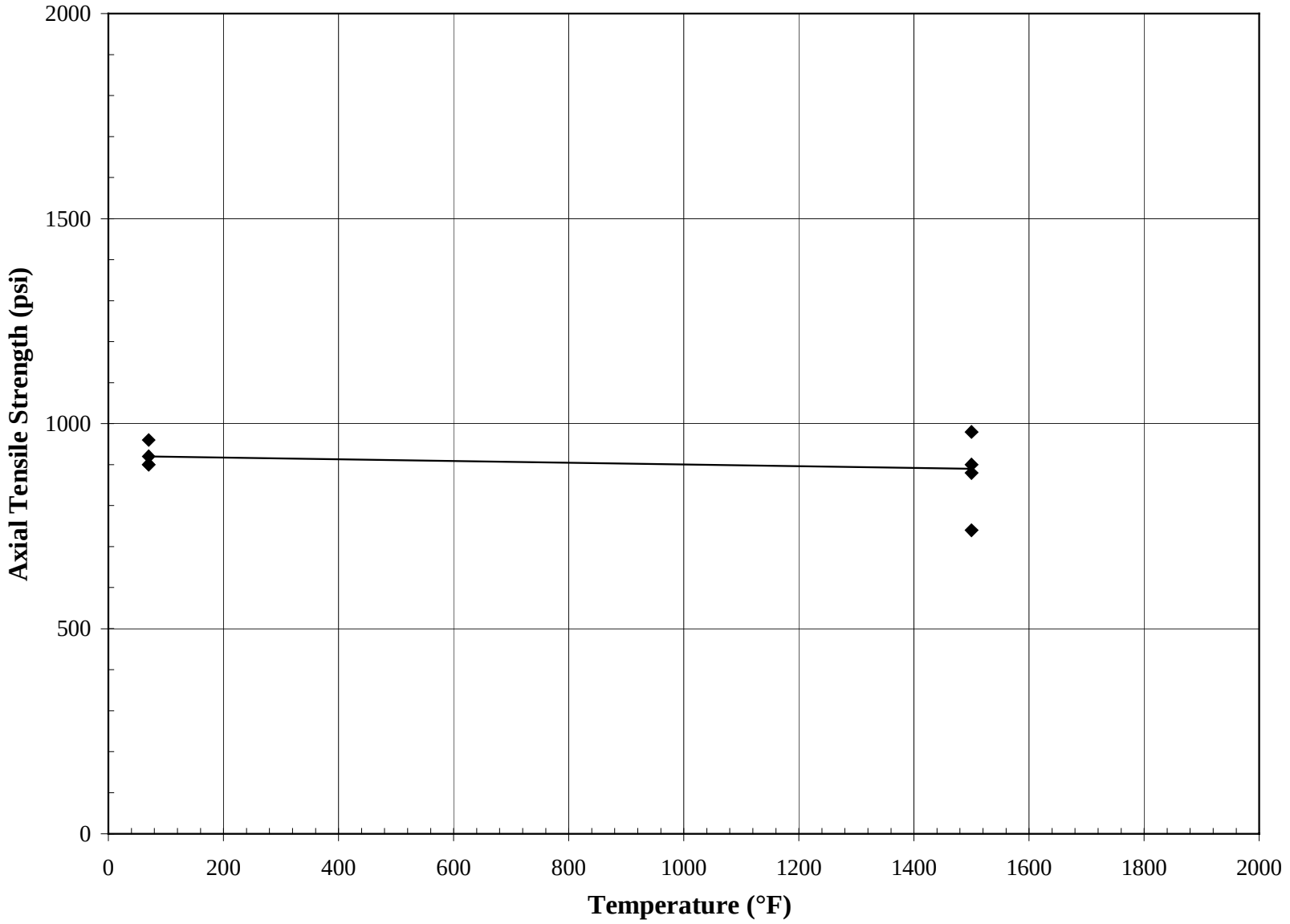

Figure 10-2 Axial Tensile Strength Versus Temperature for Virgin Ensto

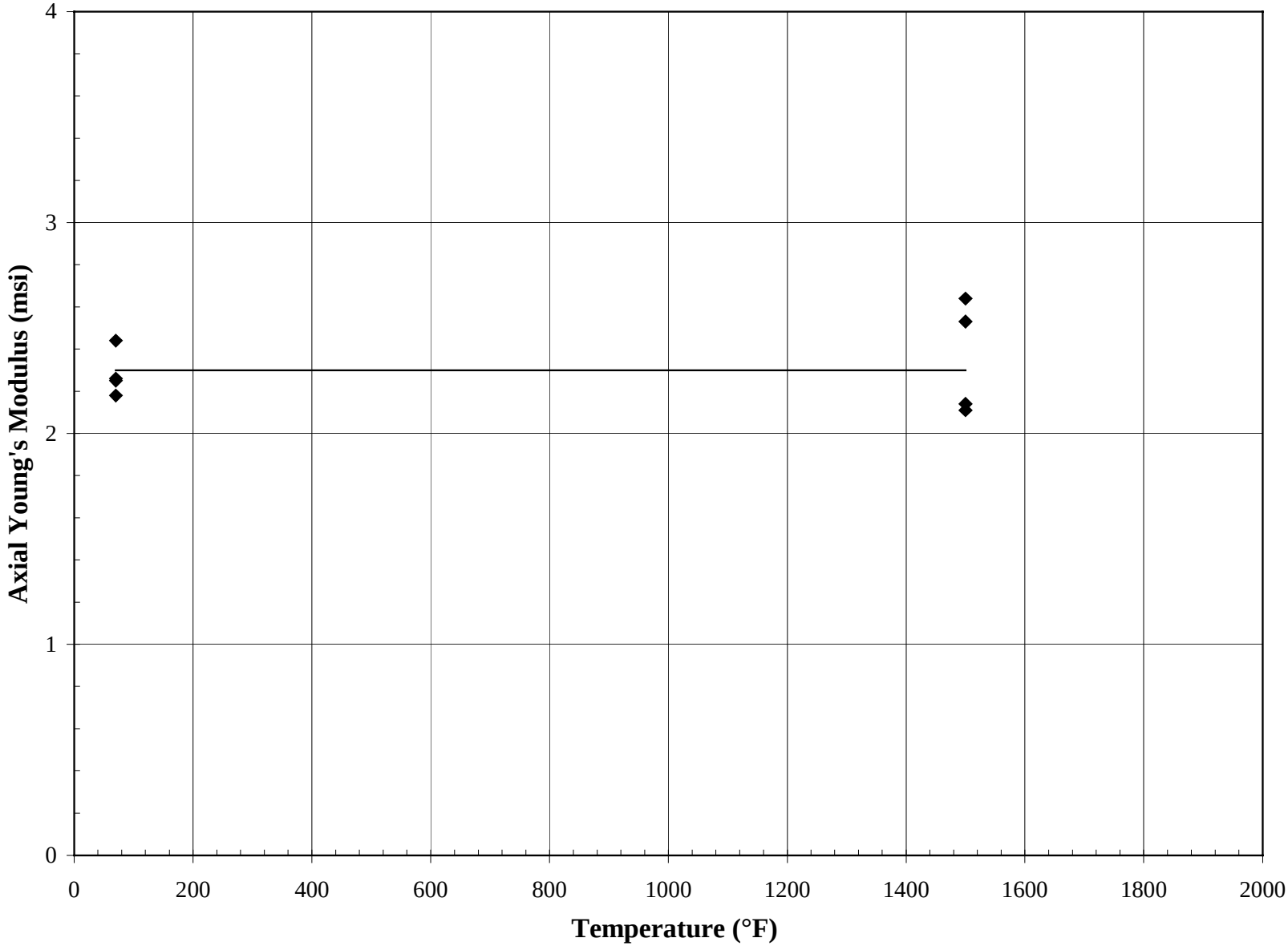

Figure 10-3 Axial Young's Modulus Versus Temperature for Virgin Ensto

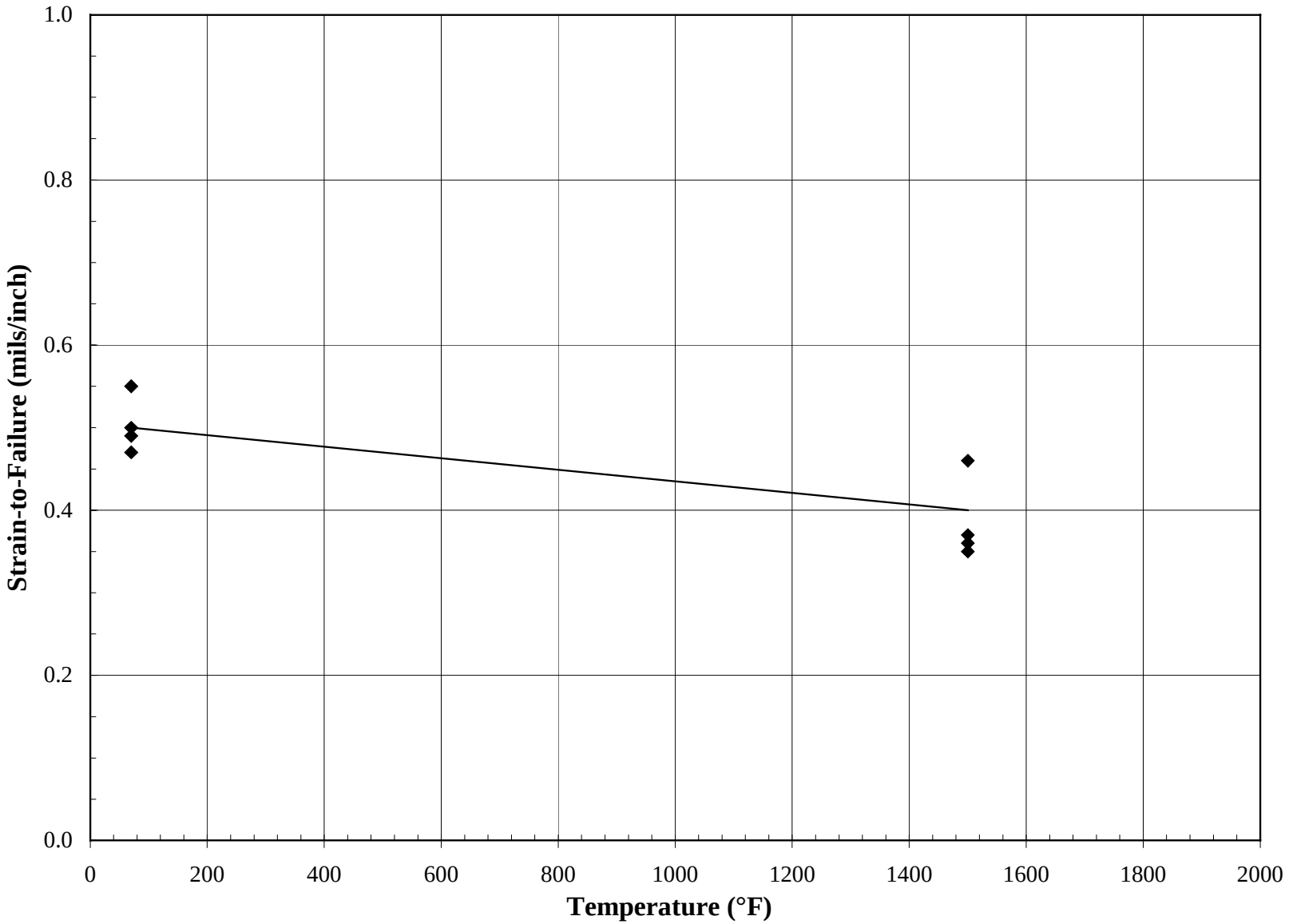

Figure 10-4 Axial Tensile Strain-to-Failure Versus Temperature for Virgin Ensto

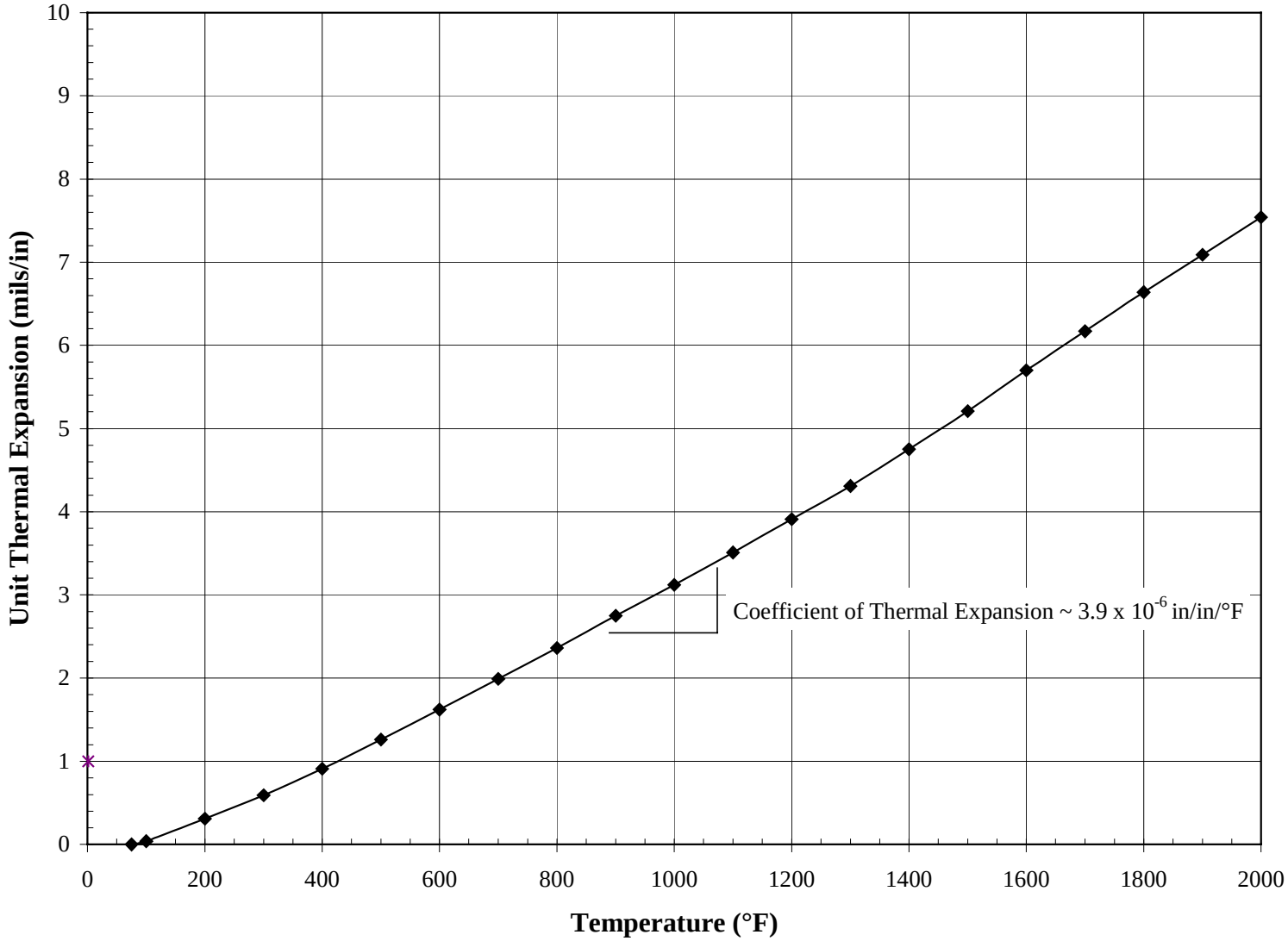

Figure 10-5 Unit Thermal Expansion of Ensto

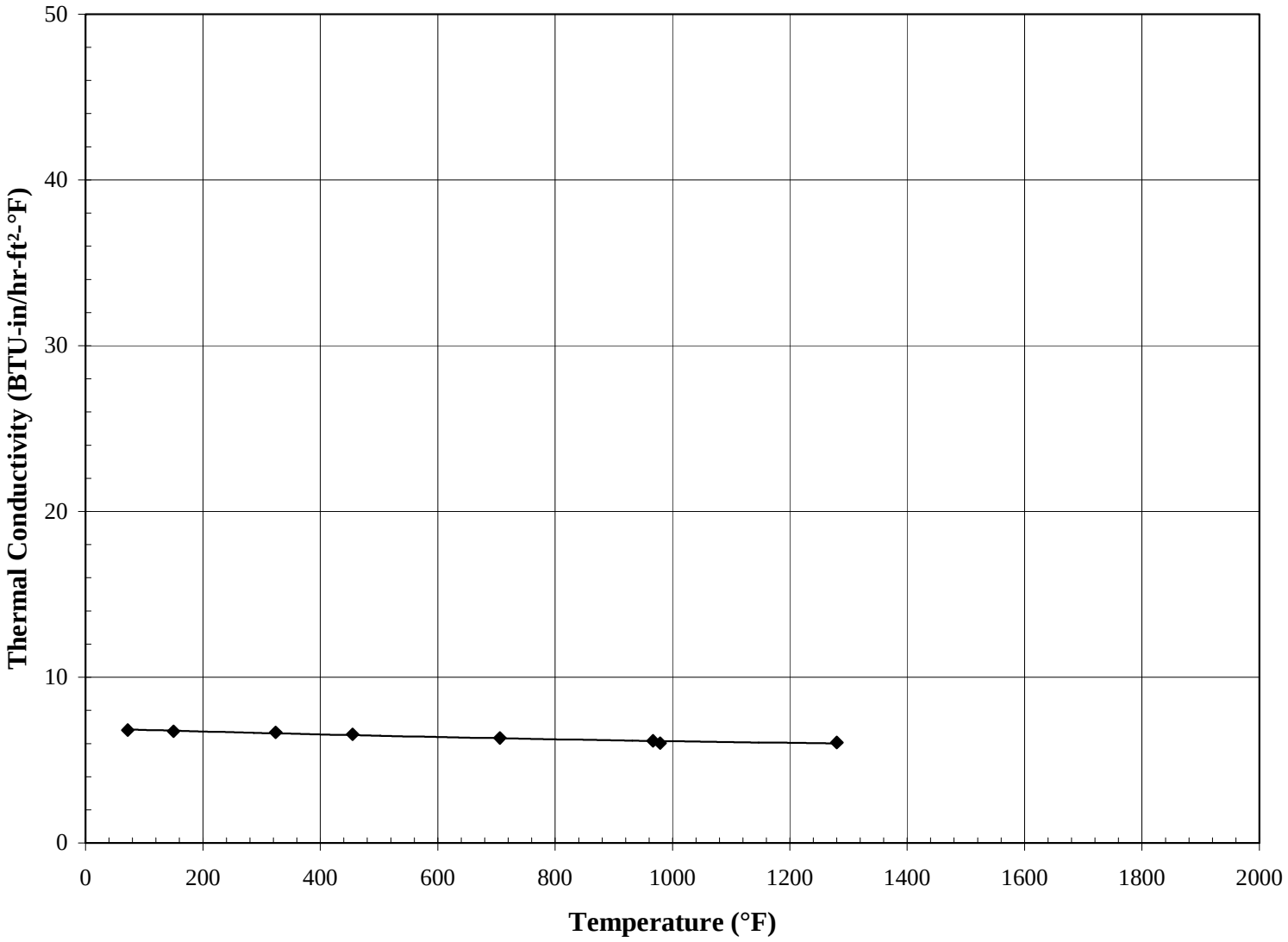

Figure 10-6 Radial Thermal Conductivity of Virgin Ensto

11.0 SPECIFIC SURFACE

Specific Surface is a monolithic cordierite element manufactured by a process where cordierite grains are laid down layer-by-layer to form the element and then sintered. The geometry of the elements tested in this program was of two concentric walls, like a sock with the toe tucked backed inside. Other shapes are possible with the Specific Surface process. The nominal O.D. of the elements was 2.40 in. (61 mm) and the nominal wall thickness (of both the outside and inside walls) was 0.20 in. (5mm). The Specific Surface element is a depth filter with no membrane layer. Probable values of selected properties of virgin specific surface cordierite material are as follows:

Bulk Density (lbm/ft^3)	77
Hoop Tensile Strength at Room Temperature (psi)	320
Axial Coefficient of Thermal Expansion, 500 to 1,500°F (10^{-6} in./in./°F)	1.0
Radial Thermal Conductivity at 1,000°F (Btu-in./hr-ft^2-°F)	3.8

Table 11-1

Density of Specific Surface Cordierite Filter Element

Element	Specimen Number	Hours in Operation	Density (gr/cm^3)	Density (lb/ft^3)	Remarks
3	Tn-Ax-1	Virgin	1.25	78.0	
3	Tn-Ax-2	Virgin	1.19	74.0	
3	Tn-Ax-3	Virgin	1.23	76.8	
3	Tn-Ax-4	Virgin	1.21	75.5	
3	Tn-Ax-5	Virgin	1.25	78.2	
Average			1.23	76.5	
Standard Deviation			0.03	1.59	
Coefficient of Variation (COV)			2.08%	2.08%	

Table 11-2

Room Temperature Hoop Tensile Strength of Specific Surface Cordierite Filter Element

Element	Specimen Number	Hours in Operation	Maximum Hydrostatic Pressure (psig)	Ultimate Strength (psi)	Remarks
3	Tn-Hoop-1	Virgin	70	370	
3	Tn-Hoop-2	Virgin	53	270	
3	Tn-Hoop-3	Virgin	10	50	See Note
3	Tn-Hoop-4	Virgin	7	30	See Note

Note: Specimen was adjacent to "stiffener."

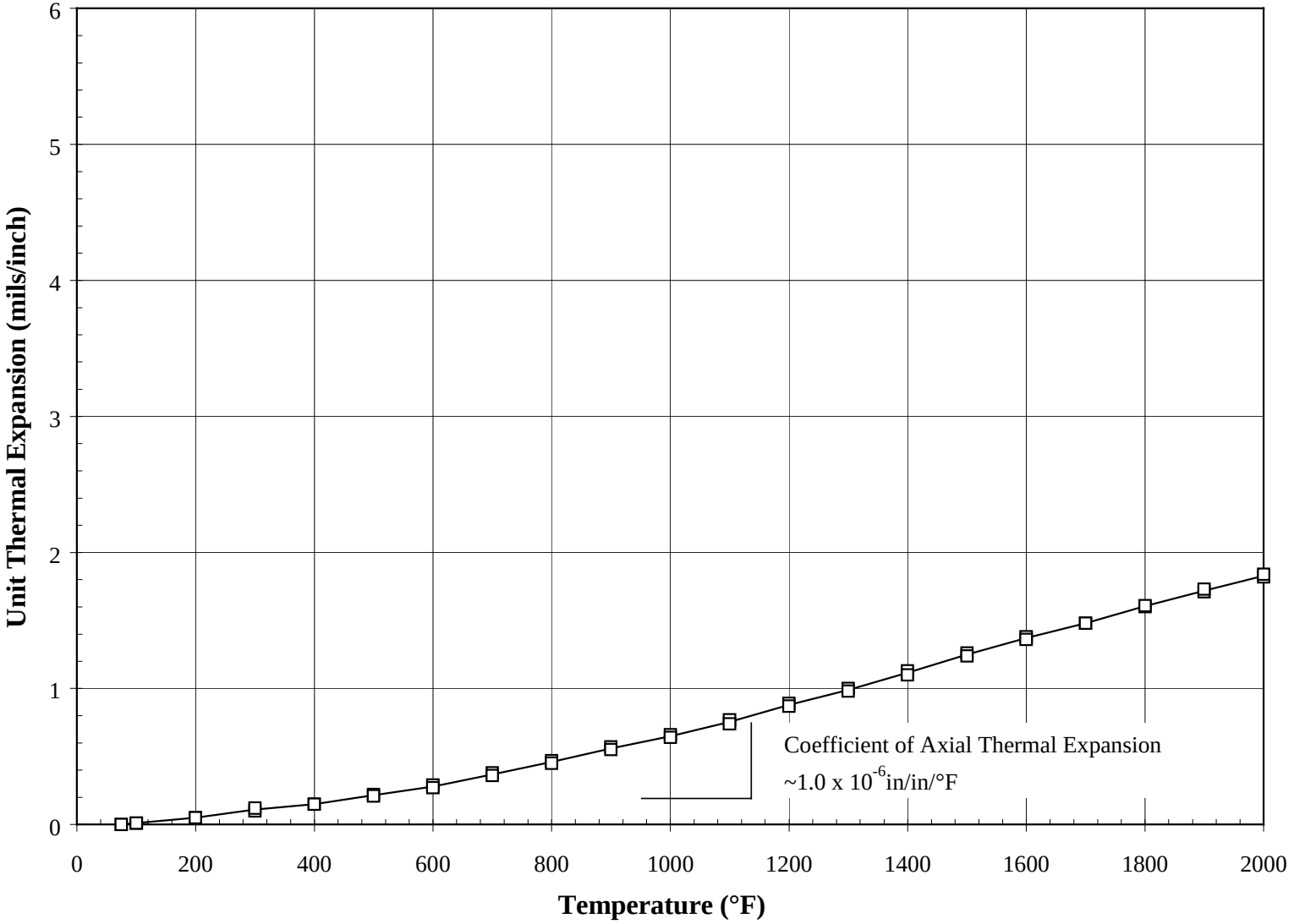

Figure 11-1 Unit Thermal Expansion of Specific Surface Filter Element Material

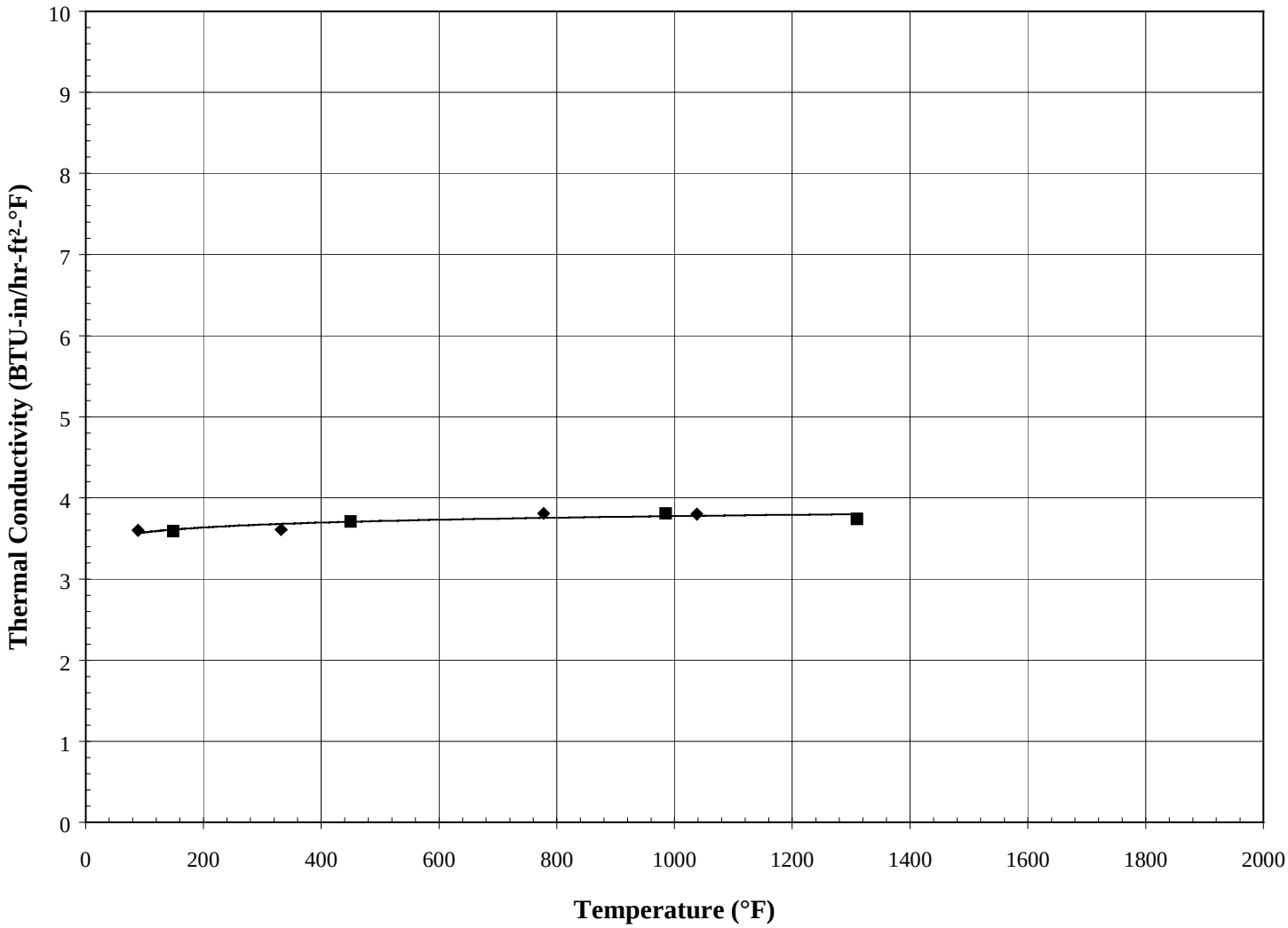

Figure 11-2 Radial Thermal Conductivity Versus Temperature for Specific Surface Filter Element Material

12.0 ALBANY INTERNATIONAL TECHNIWEAVE N610/MULLITE

Albany International Techniweave (AIT) N610/mullite elements are manufactured with Nextel™ 610 fibers in a mullite matrix using a 3D layer-to-layer interlock construction. Nominal dimensions are 2.15 in. (55 mm) I.D. and 0.125 in. (3 mm) wall thickness. Probable values of selected properties of virgin AIT N610/mullite are as follows:

Bulk Density (lbm/ft^3)	108
Hoop Tensile Strength at Room Temperature (psi)	3,460
Axial Tensile Strength at Room Temperature (psi)	5,450[1]
Axial Young's Modulus at Room Temperature (10^6 psi)	6.2
Axial Tensile Strain-to-Failure at Room Temperature (mils/in.)	0.84[1]
Axial Compressive Strength at Room Temperature (psi)	2,650
Axial Compressive Strain-to-Failure at Room Temperature (mils/in.)	0.53
Axial Coefficient of Thermal Expansion, 500 to 1,500°F (10^{-6} in./in./°F)	4.7
Radial Thermal Conductivity at 1,000°F (Btu-in./hr-ft^2-°F)	2.3

Notes: 1. Only one value.

Table 12-1

Density of AIT N610/Mullite

Element	Specimen Number	Hours in Operation	I.D. (in.)	O.D. (in.)	Density (gr/cm³)	Density (lb/ft³)	Remarks
9	Tn-Hoop-1	Virgin	2.15	2.41	1.69	105	
9	Tn-Hoop-2	Virgin	2.16	2.40	1.72	107	
9	Tn-Hoop-3	Virgin	2.16	2.40	1.76	110	
9	Cm-Ax-1	Virgin	2.15	2.41	1.69	105	
9	Cm-Ax-2	Virgin	2.16	2.39	1.79	112	
9	Tn-Ax-1	Virgin	2.16	2.41	1.72	107	
		Average			1.73	108	
		Standard Deviation			0.036	2.26	
		Coefficient of Variation (COV)			2.10%	2.10%	
PSDF 1247	Tn-Hoop-7	784	2.14	2.36	1.81	113	See Notes 1, 2, 3
PSDF 1247	Tn-Hoop-8	784	2.13	2.35	1.88	117	See Notes 1, 2, 3
PSDF 1247	Tn-Hoop-9	784	2.18	2.39	1.87	117	See Notes 1, 2, 3
PSDF 1247	Tn-Hoop-10	784	2.16	2.38	1.81	113	See Notes 1, 2, 3
PSDF 1247	Tn-Hoop-11	784	2.19	2.40	1.90	118	See Notes 1, 2, 3
PSDF 1247	Tn-Hoop-12	784	2.20	2.40	1.85	116	See Notes 1, 2, 3
		Average			1.85	116	
		Standard Deviation			0.034	2.14	
		Coefficient of Variation (COV)			1.85%	1.85%	

Notes:

1. Elements were water washed before density measurements but some ash remained in the pores. Density values were calculated based on weights measured with ash in the pores and, therefore, do not represent a material property. The values are for comparison only.
2. All operation at the SCS PSDF in combustion mode at a nominal-operating temperature of 1,400°F.
3. Candle number 1247 was assigned at the SCS PSDF. A manufacturer assigned I.D. number was not provided.

Table 12-2

Axial Tensile Properties of Virgin AIT N610/Mullite

Candle Identification	Specimen Number	Temperature (°F)	Ultimate Strength (psi)	Young's Modulus (Msi)	Strain-to-Failure (mils/in.)	Remarks
9	Tn-ax-1	70	5450	6.6	0.84	
9	Tn-ax-2	70	>1850	5.9	>0.31	See Note 1

Notes:
1. Tensile failure was not obtained. The glue bond between the specimen and the pullrod failed.

Table 12-3

Room Temperature Hoop Tensile Strength of AIT N610/Mullite

Element	Specimen Number	Hours in Operation	Maximum Hydrostatic Pressure (psig)	Tensile Strength[1] (psi)	Remarks
9	Tn-Hoop-1	virgin	365	3460	
9	Tn-Hoop-2	virgin	396	3670	
9	Tn-Hoop-3	virgin	427	4010	
	Average		396	3460	
PSDF 1247	Tn-Hoop-7	784	306	3140	See Notes 2,3
PSDF 1247	Tn-Hoop-8	784	340	3500	See Notes 2,3
PSDF 1247	Tn-Hoop-9	784	330	3680	See Notes 2,3
PSDF 1247	Tn-Hoop-10	784	358	3750	See Notes 2,3
PSDF 1247	Tn-Hoop-11	784	386	4380	See Notes 2,3
PSDF 1247	Tn-Hoop-12	784	356	3980	See Notes 2,3
	Average		346	3738	
	Standard Deviation		25	385	
	COV		7.2%	10.3%	

Notes:
1. Stress calculations by Lame's solution for isotropic materials.
2. All operation at the SCS PSDF in combustion mode at a nominal-operating temperature of 1,400°F.
3. Candle number 1247 was assigned at the SCS PSDF. A manufacturer assigned I.D. number was not provided.

Table 12-4

Room Temperature Axial Compressive Properties of Virgin AIT N610/Mullite

Filter Identification	Specimen Number	Ultimate Compressive Strength (psi)	Young's Modulus (msi)	Strain-to-Failure (mils/in.)
9	Cm-ax-1	3010	5.85	0.65
9	Cm-ax-2	2290	6.43	0.40
	Average	2650	6.14	0.53

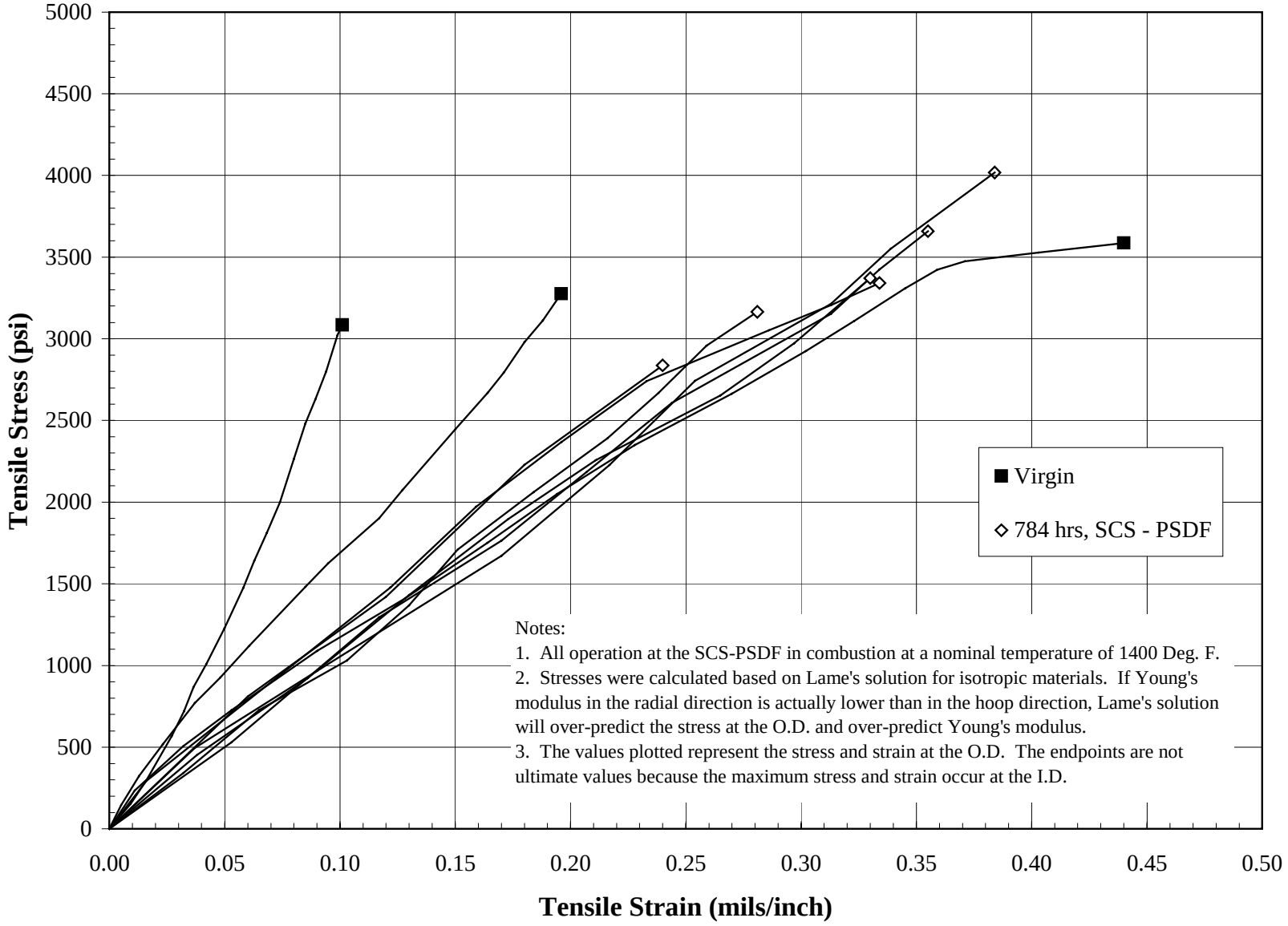

Figure 12-1 Room Temperature Hoop Tensile Stress-Strain Responses of AIT N610/Mullite-Virgin and After-Combustion Operation

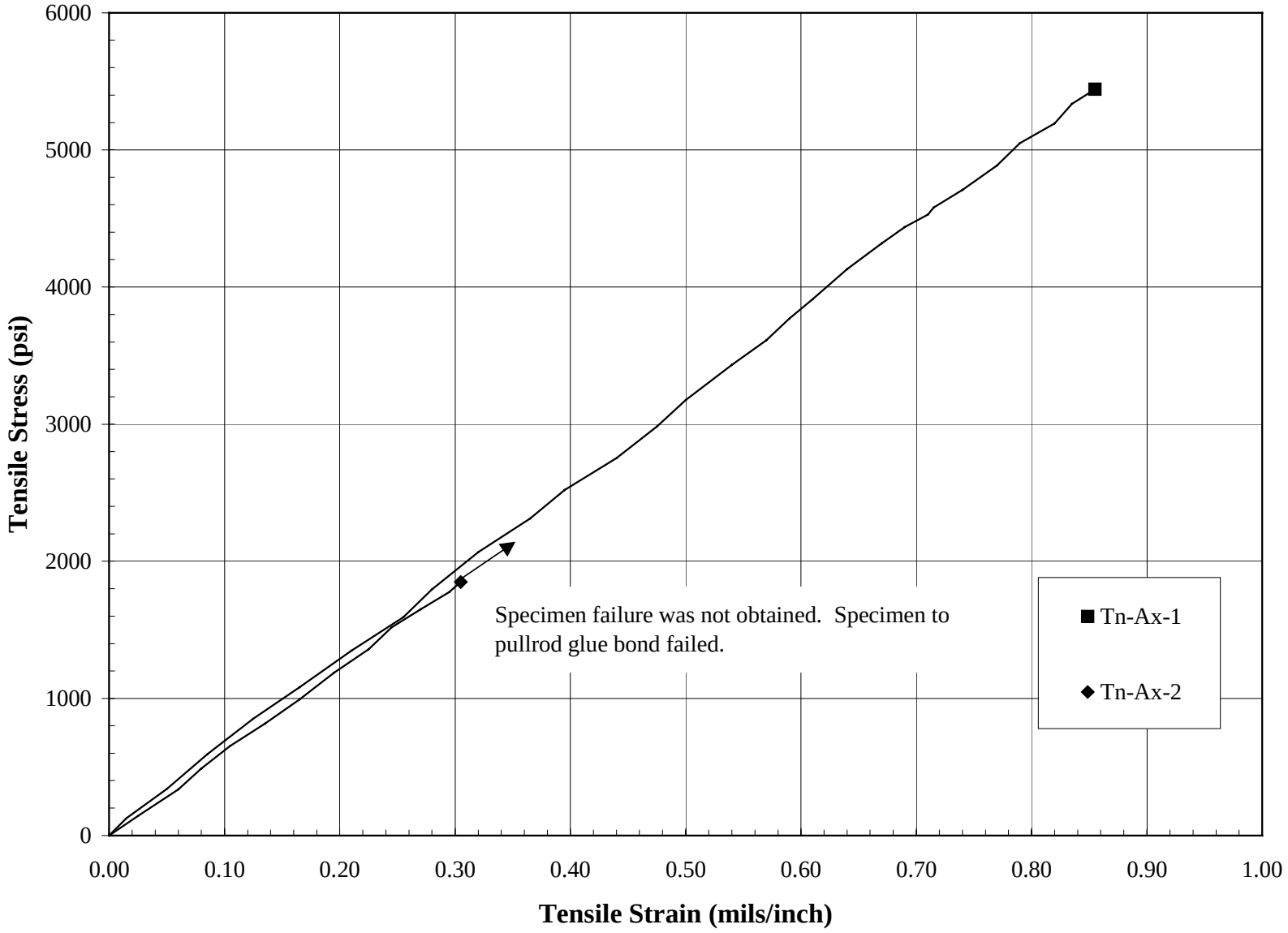

Figure 12-2 Room Temperature Axial Tensile Stress-Strain Responses of Virgin AIT N610/Mullite

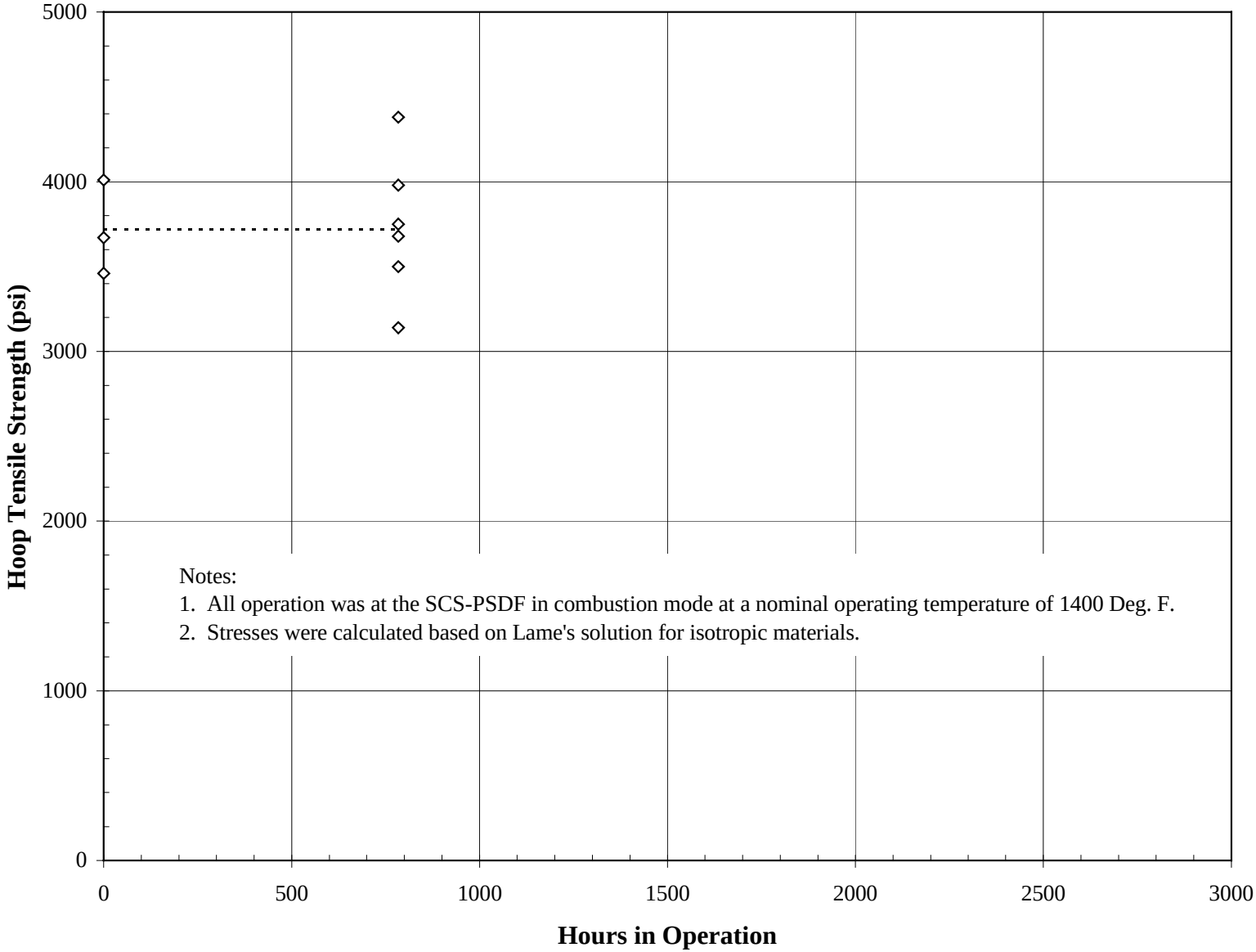

Figure 12-3 Room Temperature Hoop Tensile Strength Versus Hours in Operation for AIT N610/Mullite

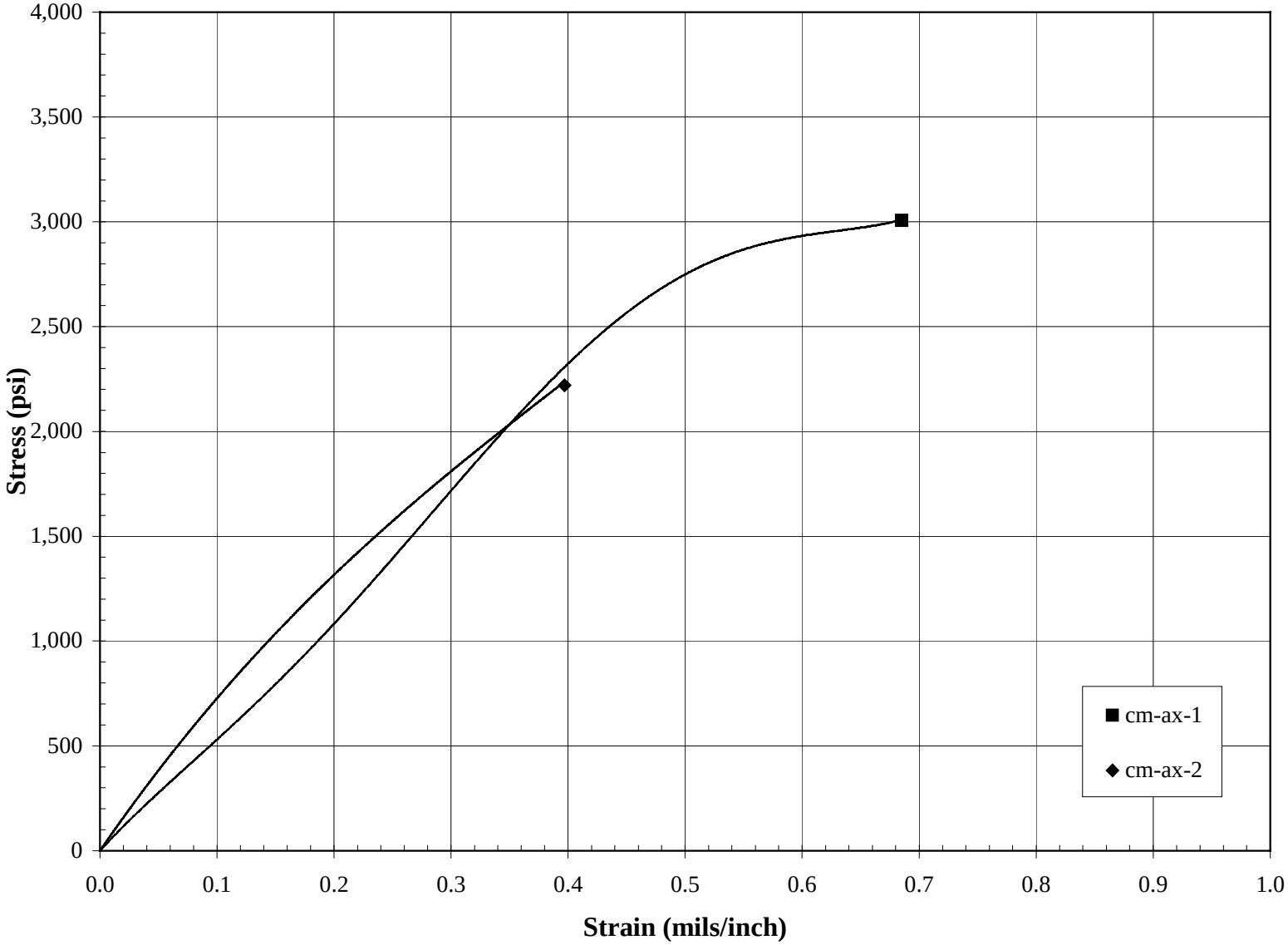

Figure 12-4 Room Temperature Axial Compressive Stress-Strain Responses for Virgin AITN610/Mullite

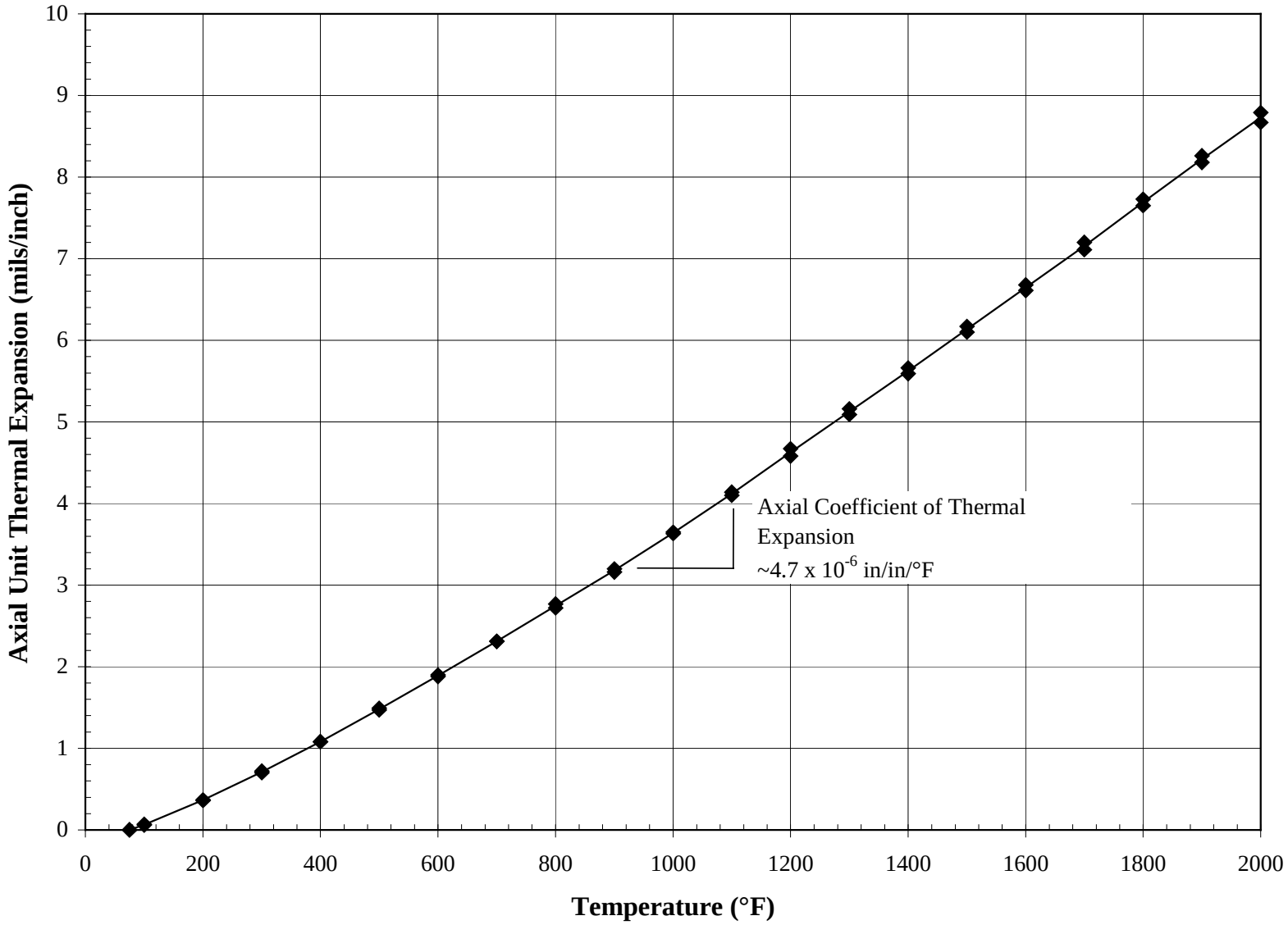

Figure 12-5 Axial Unit Thermal Expansion of Virgin N610/Mullite

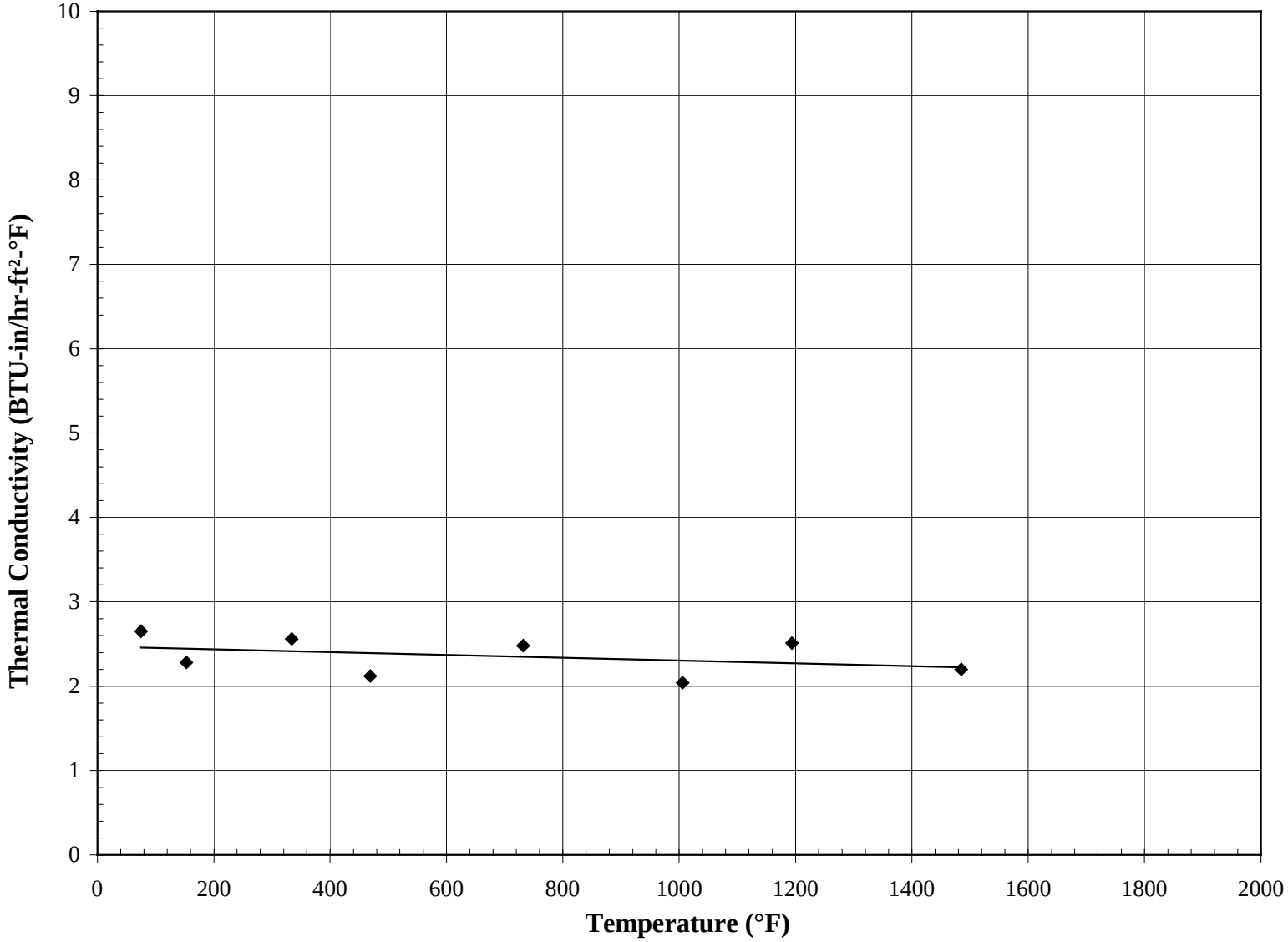

Figure 12-6 Radial Thermal Conductivity Versus Temperature for Virgin N610/Mullite

13.0 McDERMOTT CERAMIC COMPOSITE

McDermott continuous fiber ceramic composite elements are manufactured of continuous Nextel™ 610 fibers, chopped-saffil fibers, and an alumina binder in approximately equal amounts by a modified-winding process. The continuous Nextel™ fiber is wound at a 45° angle. These elements are depth filters with no filtration membrane. Nominal dimensions are 1.94 in. (49 mm) I.D. and 0.21 in. (5 mm) wall thickness. Probable values of selected properties of virgin McDermott ceramic composite are as follows:

Bulk Density (lbm/ft^3)	51
Hoop Tensile Strength at Room Temperature (psi)	700
Axial Tensile Strength at Room Temperature (psi)	600
Axial Young's Modulus at Room Temperature (10^6 psi)	0.45
Axial Tensile Strain-to-Failure at Room Temperature (mils/in.)	2.1
Axial Compressive Strength at Room Temperature (psi)	580
Axial Compressive Strain-to-Failure at Room Temperature (mils/in.)	2.3
Axial Coefficient of Thermal Expansion, 500 to 1,500°F (10^{-6} in./in./°F)	4.6
Radial Thermal Conductivity at 1,000°F (Btu-in./hr-ft^2-°F)	1.6
Pressure Drop at 5 ft/min Face Velocity, Air at Ambient Conditions(inWG)	1.7

Table 13-1

Density of McDermott Ceramic Composite

Element	Specimen Number	Hours in Operation	I.D. (in.)	O.D. (in.)	Density (gr/cm^3)	Density (lb/ft^3)	Remarks
8-1-2-3	Tn-Ax-1	Virgin	2.00	2.36	0.83	52	
8-1-2-3	Tn-Ax-2	Virgin	1.99	2.36	0.82	51	
8-1-2-3	Tn-Ax-3	Virgin	2.00	2.36	0.85	53	
8-1-2-3	Tn-Hoop-1	Virgin	2.01	2.43	0.70	43	
8-1-2-3	Tn-Hoop-2	Virgin	1.99	2.41	0.71	44	
8-1-2-3	Tn-Hoop-3	Virgin	1.99	2.39	0.75	47	
8-1-2-3	Tn-Hoop-4	Virgin	1.98	2.37	0.77	48	
8-1-2-3	Tn-Hoop-5	Virgin	1.97	2.37	0.76	48	
8-1-2-3	Tn-Hoop-6	Virgin	1.98	2.36	0.80	50	
8-1-2-3	Tn-Hoop-7	Virgin	1.97	2.36	0.81	51	
8-1-2-3	Tn-Hoop-8	Virgin	1.97	2.37	0.83	52	
8-1-2-3	Tn-Hoop-9	Virgin	1.98	2.38	0.83	52	
		Average			0.82	51	
		Standard Deviation			0.007	0.45	
		Coefficient of Variation (COV)			0.88%	0.88%	
8-1-30-1	Tn-Hoop-13	Virgin	1.99	2.36	0.78	49	
8-1-30-1	Tn-Hoop-14	Virgin	1.97	2.34	0.81	50	
8-1-30-1	Tn-Hoop-15	Virgin	1.98	2.34	0.83	52	
8-1-30-1	Tn-Hoop-16	Virgin	1.97	2.34	0.81	51	
8-1-30-1	Cm-Ax-4	Virgin	1.97	2.35	0.76	47	
8-1-30-1	Cm-Ax-5	Virgin	1.97	2.35	0.77	48	
8-1-30-1	Cm-Ax-6	Virgin	1.97	2.35	0.81	50	
8-1-30-1	Cm-Ax-7	Virgin	1.98	2.34	0.82	51	
		Average			0.80	50	
		Standard Deviation			0.03	1.6	
		Coefficient of Variation (COV)			3.2%	3.2%	
8-2-2-1	Tn-Hoop-101	1360	1.98	2.41	0.76	48	See Notes 1,2,3
8-2-2-1	Tn-Hoop-102	1360	1.97	2.37	0.81	51	See Notes 1,2,3
8-2-2-1	Tn-Hoop-103	1360	1.96	2.36	0.80	50	See Notes 1,2,3
8-2-2-1	Tn-Hoop-104	1360	1.98	2.35	0.85	53	See Notes 1,2,3
8-2-2-1	Tn-Hoop-105	1360	2.00	2.35	0.88	55	See Notes 1,2,3
8-2-2-1	Tn-Hoop-106	1360	1.99	2.34	0.89	55	See Notes 1,2,3
8-2-2-1	Tn-Hoop-107	1360	1.97	2.33	0.85	53	See Notes 1,2,3
8-2-2-1	Tn-Hoop-108	1360	1.97	2.33	0.86	53	See Notes 1,2,3
8-2-2-1	Tn-Hoop-109	1360	1.98	2.35	0.86	54	See Notes 1,2,3
		Average			0.84	52	
		Standard Deviation			0.04	2.6	
		Coefficient of Variation (COV)			4.9%	4.9%	
8-2-3-2	Tn-Hoop-110	1535	2.00	2.39	0.79	49	See Note 1,2
8-2-3-2	Tn-Hoop-111	1535	1.98	2.35	0.84	53	See Note 1,2
8-2-3-2	Tn-Hoop-112	1535	1.97	2.33	0.85	53	See Note 1,2
8-2-3-2	Tn-Hoop-113	1535	1.98	2.33	0.88	55	See Note 1,2
8-2-3-2	Tn-Hoop-114	1535	1.99	2.34	0.88	55	See Note 1,2
8-2-3-2	Tn-Hoop-115	1535	1.99	2.34	0.89	56	See Note 1,2
8-2-3-2	Tn-Hoop-116	1535	1.99	2.33	0.90	56	See Note 1,2
8-2-3-2	Tn-Hoop-117	1535	1.99	2.34	0.90	56	See Note 1,2
8-2-3-2	Tn-Hoop-118	1535	1.98	2.35	0.89	55	See Note 1,2
		Average			0.87	54	
		Standard Deviation			0.04	2.3	
		Coefficient of Variation (COV)			4.2%	4.2%	

Notes:

1. Elements were water washed before density measurements but some ash remained in the pores. Density values were calculated based on weights measured with ash in the pores and, therefore, do not represent a material property. The values are for comparison only.
2. All operation at the SCS PSDF in combustion mode at a nominal-operating temperature of 1,400°F.
3. In operation during October 1998 PCD fire.

Table 13-2

Axial Tensile Properties of Virgin McDermott Ceramic Composite

Filter Identification	Specimen Number	Test Temperature (°F)	Ultimate Strength (psi)	Young's Modulus (msi)	Strain-to-Failure (mils/in.)	Notes
8-1-23	Tn-Ax-2	70	625	0.48	1.96	
8-1-23	Tn-Ax-3	70	>520	0.46	>1.50	See Note 1
8-1-23	Tn-Ax-4	70	600	0.41	2.20	

Notes:
1. Specimen failure was not obtained. The glue bond between the specimen and the loading fixture failed.

Table 13-3

Room Temperature Hoop Tensile Strength of McDermott Ceramic Composite

Element	Specimen Number	Hours in Operation	Hydrostatic Pressure at Initial Failure (psig)	Tensile Stress at Initial Failure[1] (psi)	Young's Modulus[1] (msi)	Notes
8-1-30-1	Tn-Hoop-10	virgin	140	760	1.1	
8-1-30-1	Tn-Hoop-11	virgin	140	720	1.5	
8-1-30-1	Tn-Hoop-12	virgin	140	650		See Note 2
8-1-30-1	Tn-Hoop-13	virgin	140	820	0.8	
8-1-30-1	Tn-Hoop-14	virgin	130	750	1.2	
8-1-30-1	Tn-Hoop-15	virgin	130	750	2.0	
8-1-30-1	Tn-Hoop-16	virgin	110	670	1.1	
8-1-30-1	Tn-Hoop-20	virgin	100	490	1.1	
Average			129	701	1.2	
Standard Deviation			16	101	0.4	
Coeficient of Variation (COV)			12%	14%	30%	
8-2-2-1	Tn-Hoop-101	1360	80	430	1.7	See Notes 3,4
8-2-2-1	Tn-Hoop-103	1360	110	580	1.1	See Notes 3,4
8-2-2-1	Tn-Hoop-104	1360	90	520	1.3	See Notes 3,4
8-2-2-1	Tn-Hoop-105	1360	80	510	1.2	See Notes 3,4
8-2-2-1	Tn-Hoop-106	1360	80	480	1.2	See Notes 3,4
8-2-2-1	Tn-Hoop-107	1360	80	470	1.1	See Notes 3,4
8-2-2-1	Tn-Hoop-109	1360	90	550	1.2	See Notes 3,4
Average			87	506	1.2	
Standard Deviation			11	51	0.2	
Coeficient of Variation (COV)			13%	10%	17%	
8-2-3-2	Tn-Hoop-110	1535	>80	>440	>1.3	See Notes 3,5
8-2-3-2	Tn-Hoop-111	1535	120	710	1.5	See Note 3
8-2-3-2	Tn-Hoop-112	1535	120	720	1.8	See Note 3
8-2-3-2	Tn-Hoop-113	1535	100	650	1.1	See Note 3
8-2-3-2	Tn-Hoop-114	1535	100	630	1.1	See Note 3
8-2-3-2	Tn-Hoop-115	1535	110	660	1.6	See Note 3
8-2-3-2	Tn-Hoop-116	1535	100	620	1.2	See Note 3
8-2-3-2	Tn-Hoop-117	1535	>70	>440		See Note 2,3,5
8-2-3-2	Tn-Hoop-118	1535	110	670	1.7	See Note 3
Average			109	666	1.4	
Standard Deviation			9	38	0.3	
Coeficient of Variation (COV)			8%	6%	19%	

Notes:

1. Stress calculations by Lame's solution for isotropic materials. If Young's modulus in the thickness direction is lower than in the hoop direction Lame's solution will understate the tensile stress at initial failure and overstate Young's modulus.
2. Strain measurements were not obtained.
3. All operation was at the SCS PSDF in combustion mode at a nominal-temperature of 1,400°F.
4. In operation during PCD fire.
5. Tensile failure not obtained because of hydraulic fluid leak.

Table 13-4

Axial Compressive Properties of Virgin McDermott Ceramic Composite

Filter Identification	Specimen Number	Test Temperature (°F)	Ultimate Strength (psi)	Young's Modulus (msi)	Strain-to-Failure (mils/in.)
8-1-30-1	Cm-ax-1	70	550	0.37	1.8
8-1-30-1	Cm-ax-2	70	500	0.38	1.4
8-1-30-1	Cm-ax-3	70	560	0.33	1.9
8-1-30-1	Cm-ax-4	70	540	0.26	2.0
8-1-30-1	Cm-ax-5	70	610	0.34	2.3
8-1-30-1	Cm-ax-6	70	580	0.30	1.7
8-1-30-1	Cm-ax-7	70	730	0.27	5.0
Average			581	0.32	2.3
Standard Deviation			68.3	0.04	1.1
Coefficient of Variation (COV)			12%	13.5%	49.4%

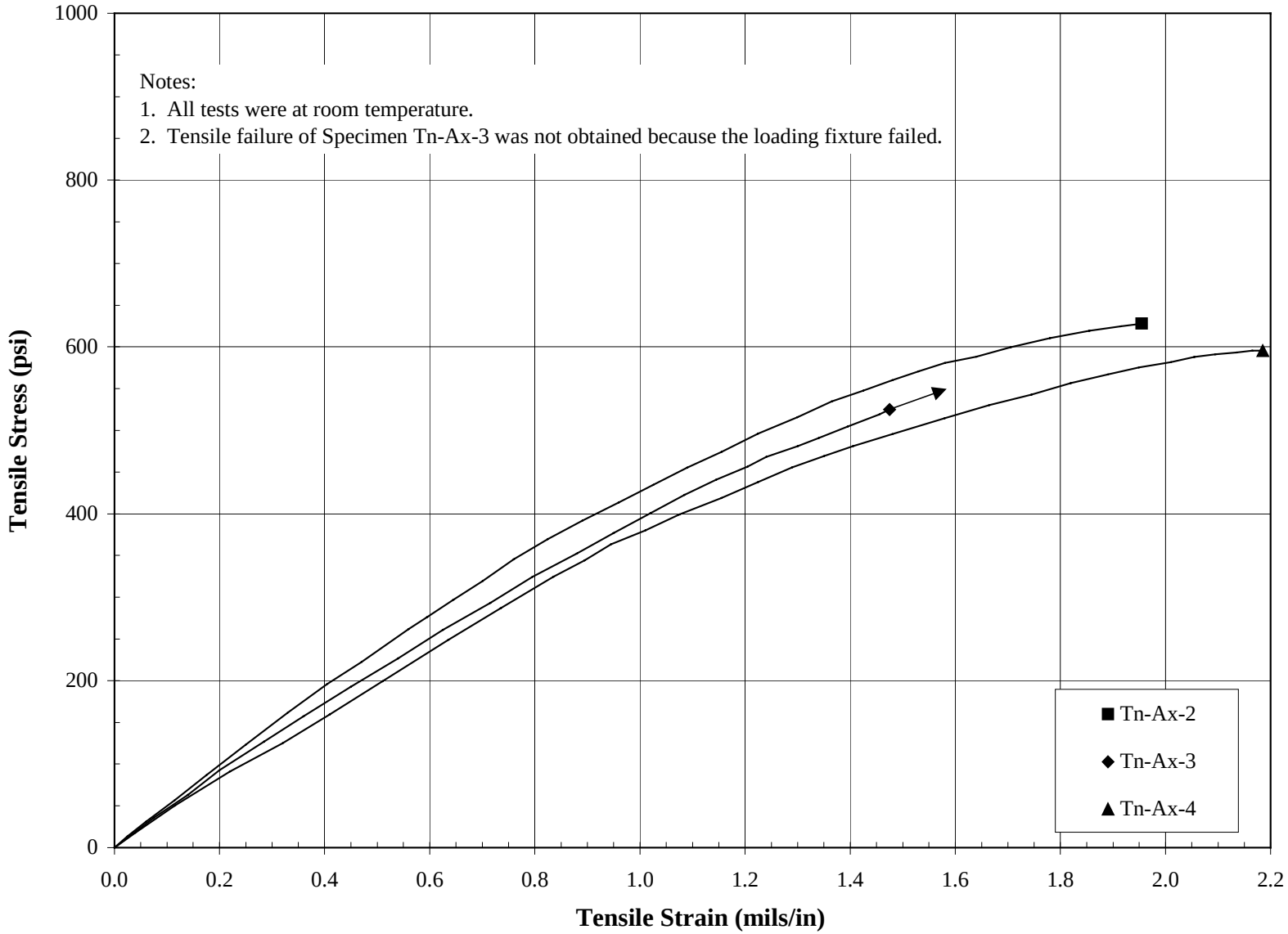

Figure 13-1 Room Temperature Axial Tensile Stress-Strain Responses for Virgin McDermott Ceramic Composite

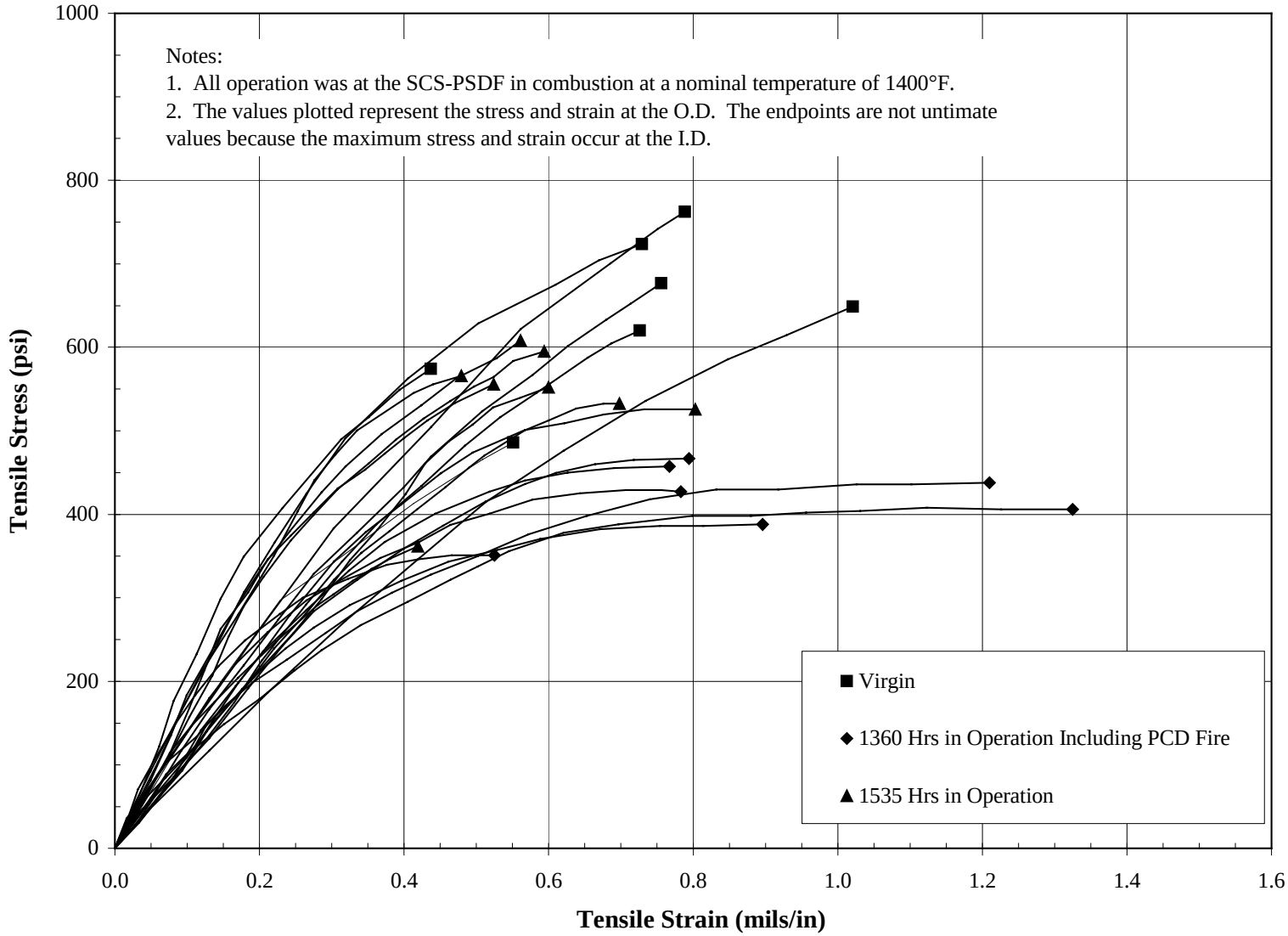

Figure 13-2 Room Temperature Hoop Tensile Stress-Strain Responses for McDermott Ceramic Composite Virgin and After-Combustion Operation

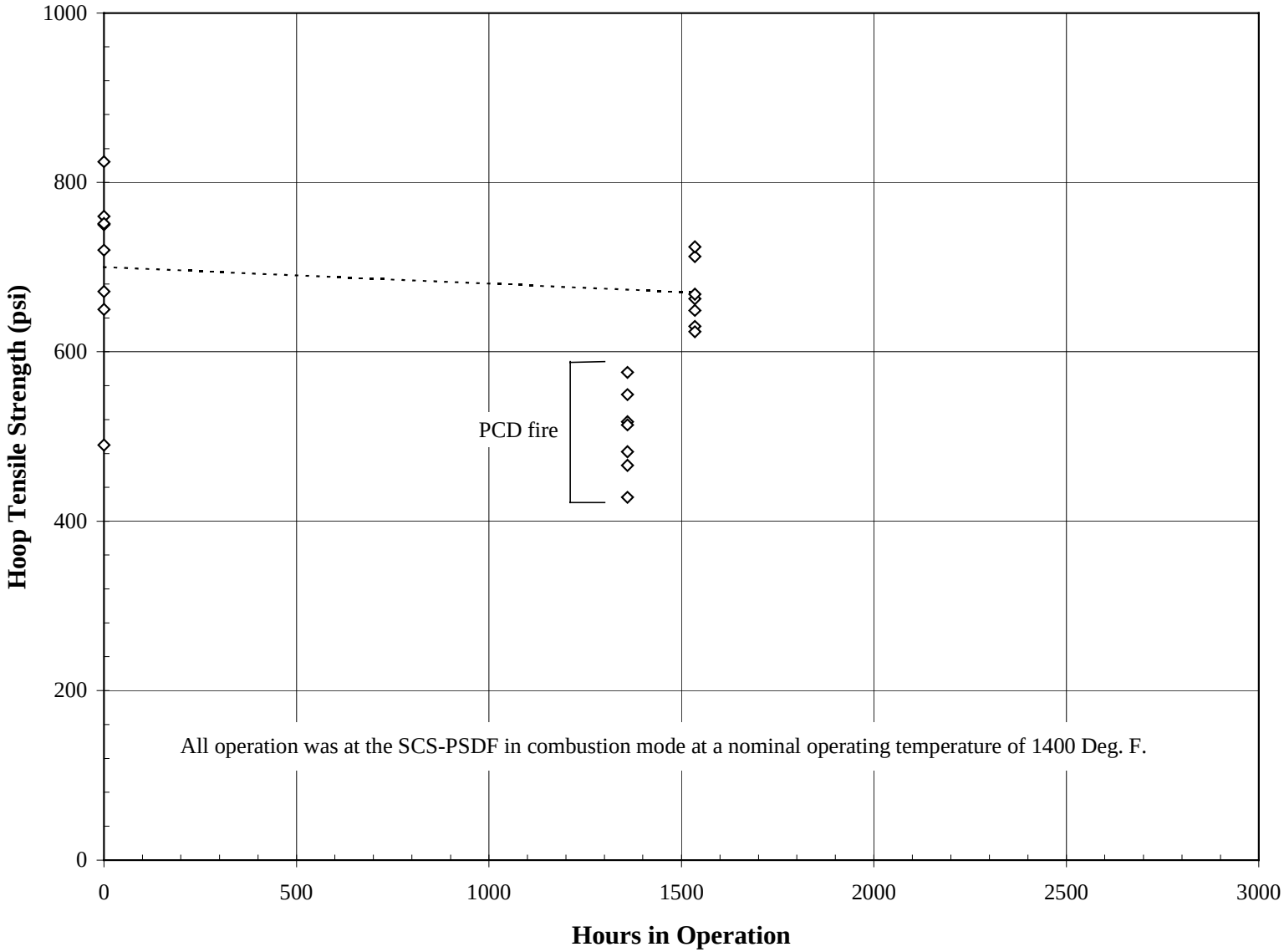

Figure 13-3 Room Temperature Hoop Tensile Strength Versus Hours in Operation for McDermott Ceramic Composite

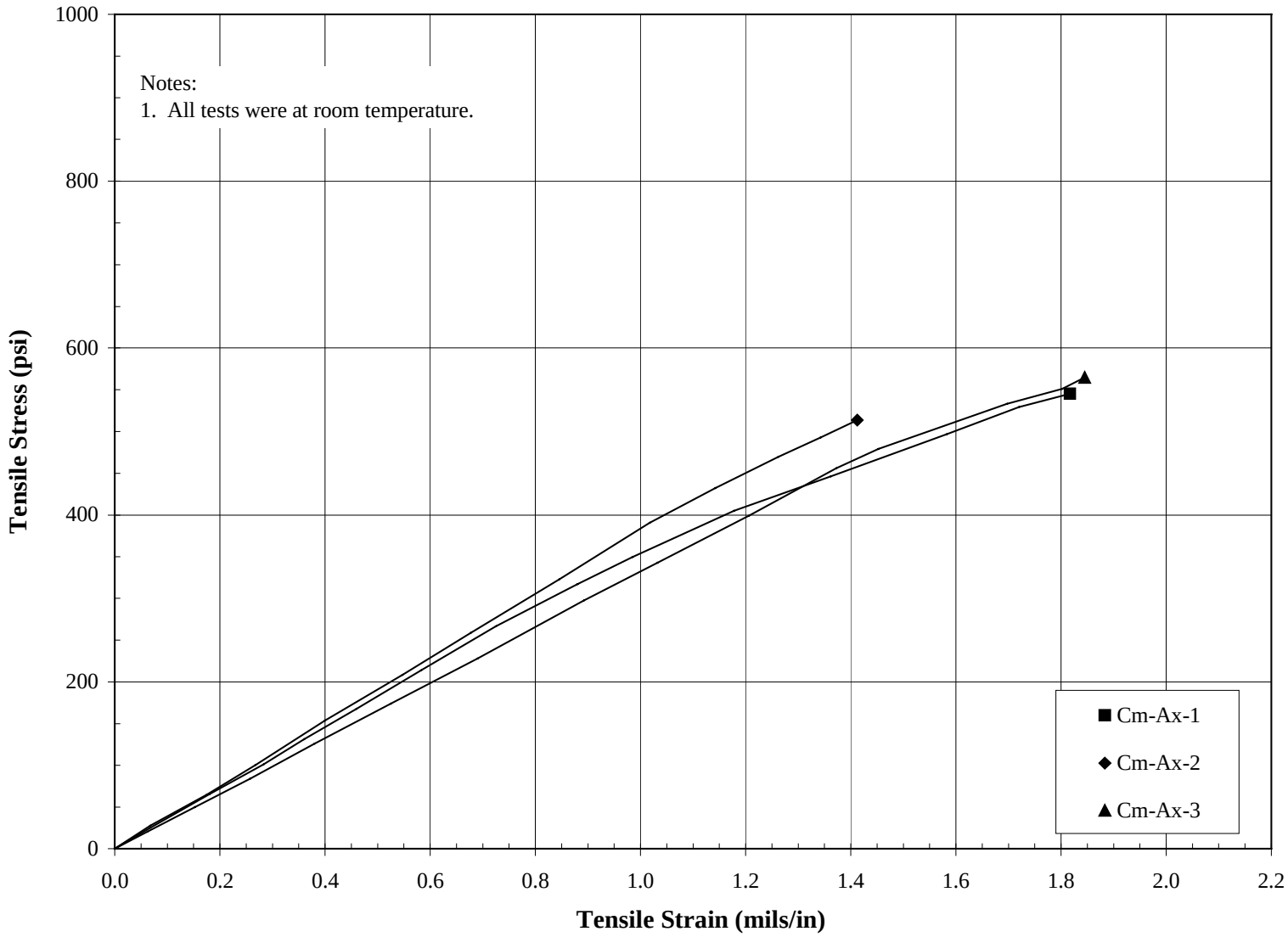

Figure 13-4 Room Temperature Axial Compressive Stress-Strain Responses for Virgin McDermott Ceramic Composite

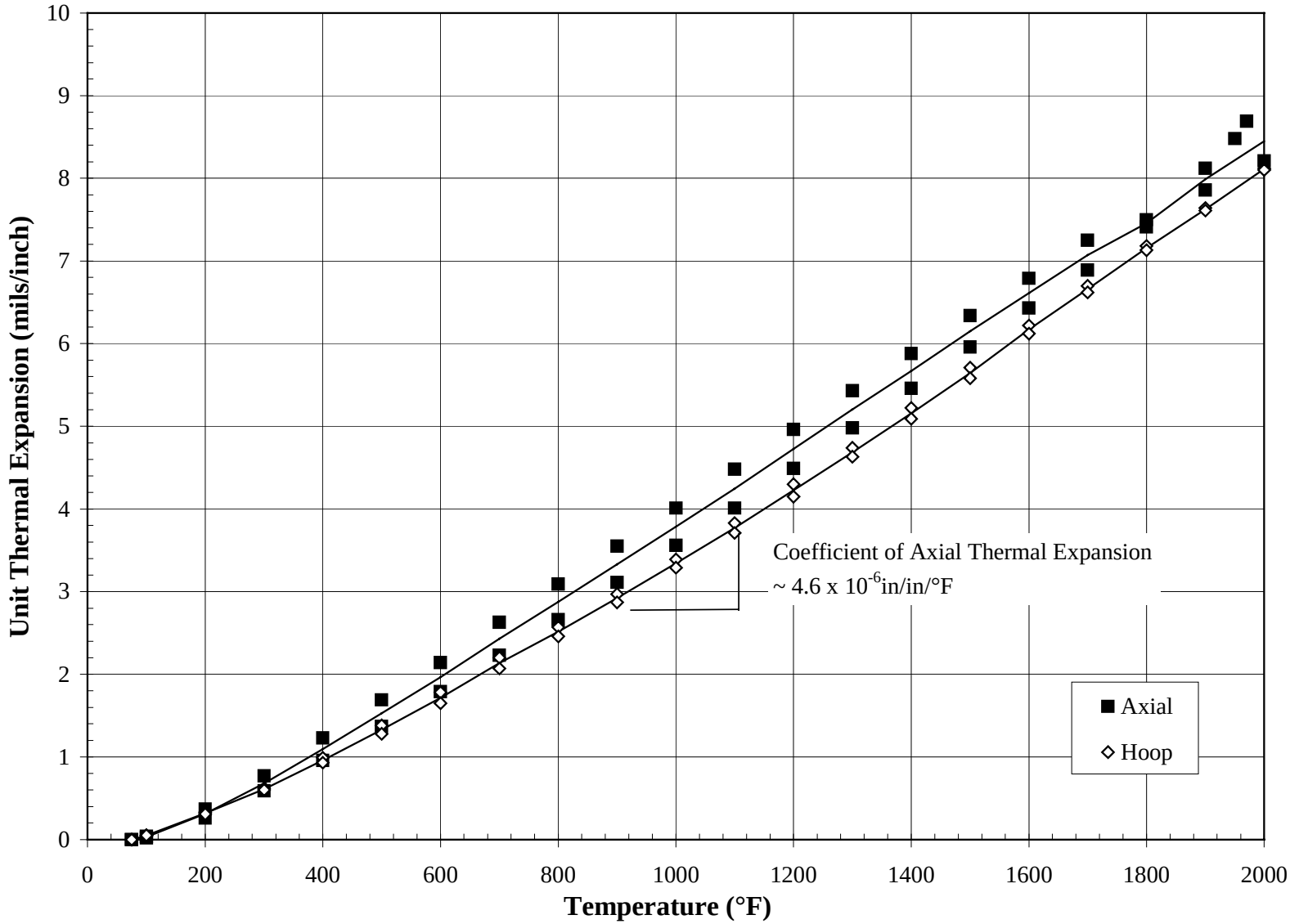

Figure 13-5 Unit Thermal Expansion of Virgin McDermott Ceramic Composite

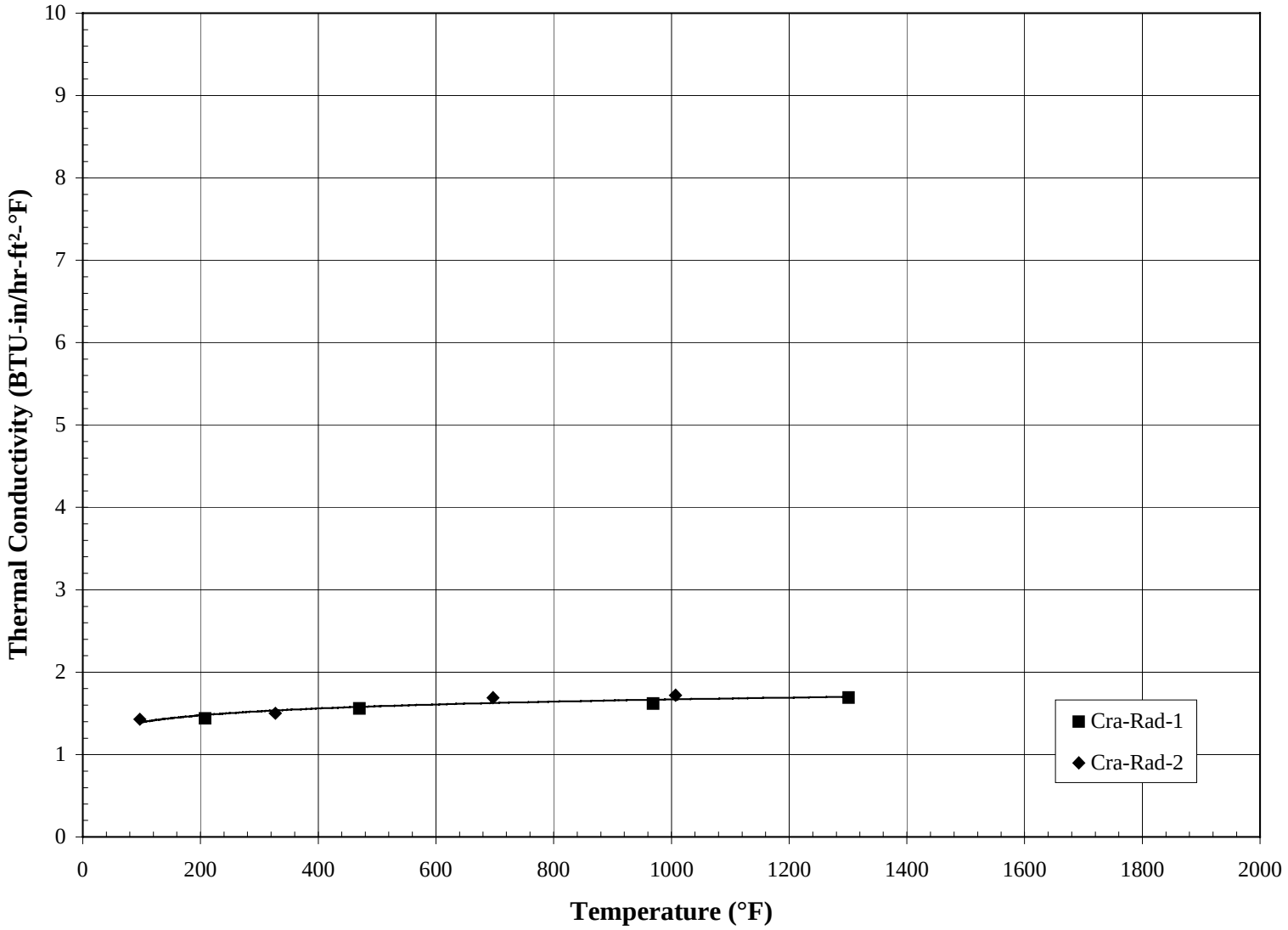

Figure 13-6 Radial Thermal Conductivity Versus Temperature for Virgin McDermott Ceramic Composite

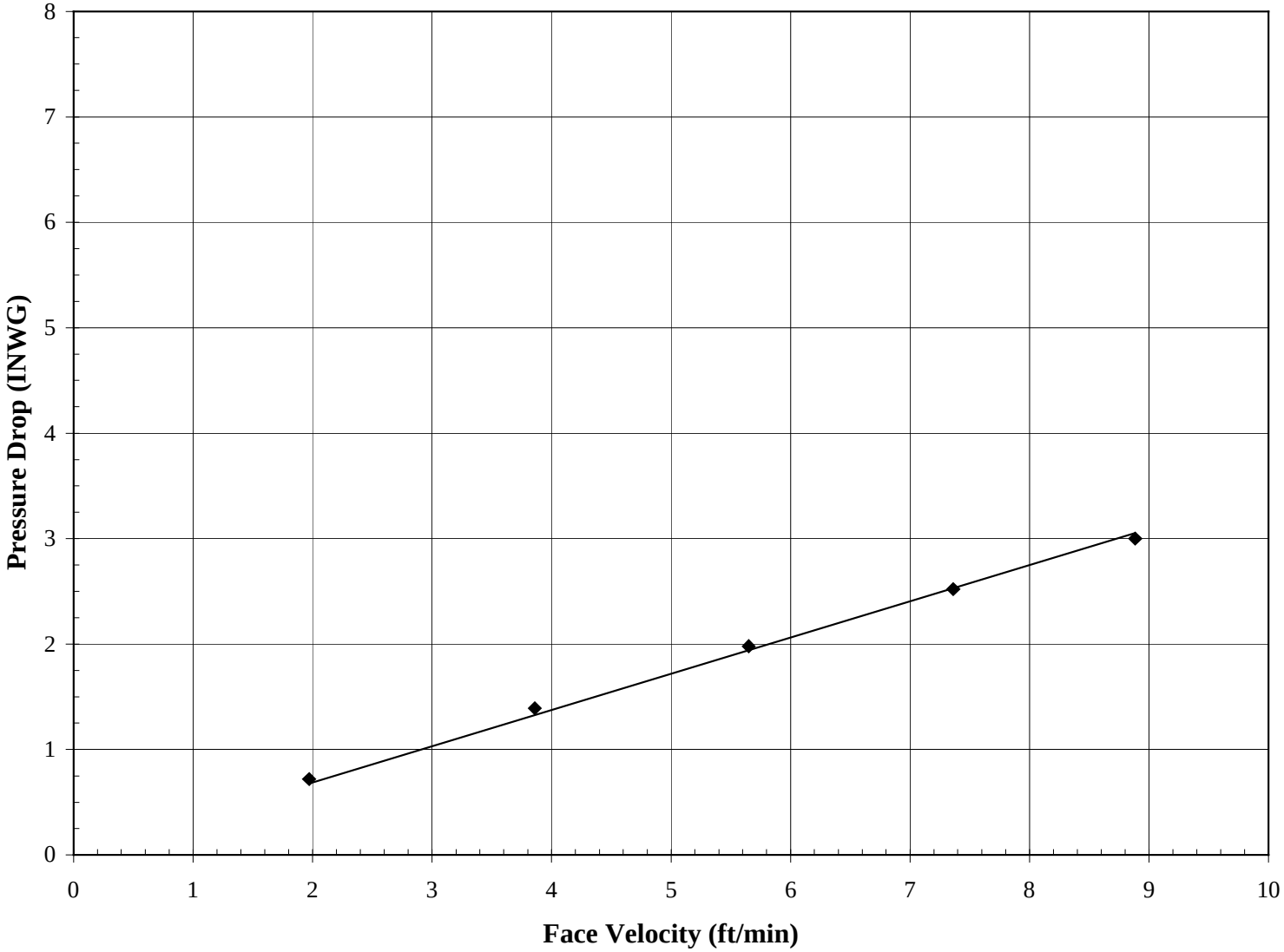

Figure 13-7 Pressure Drop Versus Face Velocity for McDermott Ceramic Composite Using Air at Ambient Temperature and Pressure

14.0 HONEYWELL PRD-66C

Honeywell PRD-66C elements contain a mixture of alumina, cordierite, mullite, and cristobalite. The elements are manufactured of textile-grade glass yarn, alumina particulate, and an Al_2O_3 precursor. A membrane layer is applied to the outside surface and provides the filtration. Nominal dimensions are 1.74 in. (44 mm) I.D. and 0.31 in. (8 mm) wall thickness. Probable values of selected properties of virgin Honeywell PRD-66C are as follows:

Bulk Density (lbm/ft^3)	89
Hoop Tensile Strength at Room Temperature (psi)	830
Axial Tensile Strength at Room Temperature (psi)	290
Axial Young's Modulus at Room Temperature (10^6 psi)	0.35
Axial Tensile Strain-to-Failure at Room Temperature (mils/in.)	1.5
Axial Coefficient of Thermal Expansion, 500 to 1,500°F (10^{-6} in./in./°F)	2.2
Radial Thermal Conductivity at 1,000°F (Btu-in./hr-ft^2-°F)	3.4
Pressure Drop at 5 ft/min Face Velocity, Air at Ambient Conditions(inWG)	0.9

Table 14-1

Density of Honeywell PRD-66C

Element	Specimen Number	Hours in Operation	I.D. (in.)	O.D. (in.)	Density (gr/cm³)	Density (lb/ft³)	Remarks
C631	Tn-Ax-1	Virgin	1.76	2.35	1.39	86.9	
C631	Tn-Ax-2	Virgin	1.76	2.35	1.40	87.1	
C631	Tn-Ax-3	Virgin	1.75	2.35	1.39	86.6	
C631	Tn-Hoop-1	Virgin	1.76	2.35	1.42	88.9	
C631	Tn-Hoop-2	Virgin	1.76	2.34	1.45	90.5	
C631	Tn-Hoop-3	Virgin	1.76	2.35	1.45	90.4	
C631	Tn-Hoop-4	Virgin	1.76	2.35	1.42	88.7	
C631	Tn-Hoop-5	Virgin	1.75	2.35	1.41	87.9	
C631	Tn-Hoop-6	Virgin	1.76	2.35	1.41	87.7	
C631	Tn-Hoop-7	Virgin	1.75	2.35	1.41	87.7	
C631	Tn-Hoop-8	Virgin	1.75	2.35	1.41	88.2	
C631	Tn-Hoop-9	Virgin	1.75	2.35	1.44	89.7	
		Average			1.42	88.5	
		Standard Deviation			0.014	0.86	
		Coefficient of Variation (COV)			0.97%	0.97%	
C638	Tn-Ax-4	Virgin	1.75	2.33	1.45	90.4	
C638	Tn-Ax-5	Virgin	1.75	2.34	1.42	88.6	
C638	Tn-Ax-6	Virgin	1.75	2.34	1.41	88.3	
C638	Tn-Hoop-10	Virgin	1.75	2.34	1.42	88.5	
C638	Tn-Hoop-11	Virgin	1.75	2.34	1.43	89.1	
C638	Tn-Hoop-12	Virgin	1.75	2.34	1.43	89.2	
C638	Tn-Hoop-13	Virgin	1.74	2.33	1.45	90.6	
C638	Tn-Hoop-14	Virgin	1.75	2.33	1.46	91.1	
C638	Tn-Hoop-15	Virgin	1.74	2.33	1.46	91.2	
C638	Tn-Hoop-16	Virgin	1.75	2.34	1.44	89.6	
C638	Tn-Hoop-17	Virgin	1.75	2.34	1.44	90.0	
C638	Tn-Hoop-18	Virgin	1.75	2.34	1.45	90.4	
		Average			1.44	90.0	
		Standard Deviation			0.005	0.33	
		Coefficient of Variation (COV)			0.37%	0.37%	
C732	Tn-Hoop-101	636	1.75	2.31	1.45	90.3	See Notes 1,2
C732	Tn-Hoop-102	636	1.75	2.31	1.44	89.6	See Notes 1,2
C732	Tn-Hoop-103	636	1.75	2.31	1.46	90.8	See Notes 1,2
C732	Tn-Hoop-104	636	1.75	2.31	1.42	88.5	See Notes 1,2
C732	Tn-Hoop-105	636	1.75	2.31	1.41	87.8	See Notes 1,2
C732	Tn-Hoop-106	636	1.75	2.31	1.41	87.7	See Notes 1,2
C732	Tn-Hoop-107	636	1.75	2.31	1.43	89.1	See Notes 1,2
C732	Tn-Hoop-108	636	1.75	2.32	1.43	89.4	See Notes 1,2
C732	Tn-Hoop-109	636	1.75	2.31	1.43	89.4	See Notes 1,2
		Average			1.43	89.3	
		Standard Deviation			0.003	0.16	
		Coefficient of Variation (COV)			0.18%	0.18%	

Notes:

1. Elements were water washed before density measurements but some ash remained in the pores. Density values were calculated based on weights measured with ash in the pores and, therefore, do not represent a material property. The values are for comparison only.
2. All operation at the SCS PSDF in combustion mode at a nominal-operating temperature of 1,400°F.

Table 14-2

Axial Tensile Properties of Virgin Honeywell PRD-66C

Element	Specimen Number	Temp. (°F)	Ultimate Strength (psi)	Young's Modulus (Msi)	Strain-to-Failure, (mils/in.)	Notes
C631	Tn-Ax-1	70	280	0.38	1.40	See Note 1
C631	Tn-Ax-2	70	290	0.35	1.56	
C631	Tn-Ax-3	70	290	0.36	1.59	See Note 1
C638	Tn-Ax-4	70	270	0.35	1.22	See Note 1
C638	Tn-Ax-5	70	280	0.30	1.57	See Note 1
C638	Tn-Ax-6	70	290	0.34	1.74	
Average			283	0.35	1.51	
Standard Deviation			8.2	0.03	0.18	
Coefficient of Variation (COV)			2.9%	7.7%	11.9%	

Notes:
1. Failed at the end of the grips.

Table 14-3

Room Temperature Hoop Tensile Strength of Virgin Honeywell PRD-66C

Element	Specimen Number	Hours in Operation	Maximum Hydrostatic Pressure (psig)	Ultimate Tensile Strength[1] (psi)	Notes
C631	Tn-Hoop-1	virgin	190	680	
C631	Tn-Hoop-2	virgin	190	660	
C631	Tn-Hoop-3	virgin	250	860	
C631	Tn-Hoop-4	virgin	250	870	
C631	Tn-Hoop-5	virgin	220	750	
C631	Tn-Hoop-6	virgin	240	830	
C631	Tn-Hoop-7	virgin	250	870	
C631	Tn-Hoop-8	virgin	200	670	
C631	Tn-Hoop-9	virgin	240	820	
Average			226	779	
Standard Deviation			26	90	
Coefficient of Variation (COV)			12%	11%	
C638	Tn-Hoop-10	virgin	260	870	
C638	Tn-Hoop-11	virgin	220	770	
C638	Tn-Hoop-12	virgin	280	950	
C638	Tn-Hoop-13	virgin	250	880	
C638	Tn-Hoop-14	virgin	250	890	
C638	Tn-Hoop-15	virgin	270	950	
C638	Tn-Hoop-16	virgin	270	920	
C638	Tn-Hoop-17	virgin	240	790	
C638	Tn-Hoop-18	virgin	270	930	
Average			257	883	
Standard Deviation			19	65	
Coefficient of Variation (COV)			7%	7%	
C732	Tn-Hoop-101	636	140	530	See Note 2
C732	Tn-Hoop-102	636	160	570	See Note 2
C732	Tn-Hoop-103	636	140	520	See Note 2
C732	Tn-Hoop-104	636	140	500	See Note 2
C732	Tn-Hoop-105	636	130	490	See Note 2
C732	Tn-Hoop-106	636	140	500	See Note 2
C732	Tn-Hoop-107	636	130	490	See Note 2
C732	Tn-Hoop-108	636	130	480	See Note 2
C732	Tn-Hoop-109	636	120	450	See Note 2
			137	503	
			11	34	
			8%	7%	

Notes:

1. Stress calculations by Lame's solution for isotropic materials. If Young's modulus in the thickness direction is lower than in the hoop direction Lame's solution will understate the tensile stress at initial failure.
2. All operation was at the SCS PSDF in combustion mode at a nominal temperature of 1,400°F.

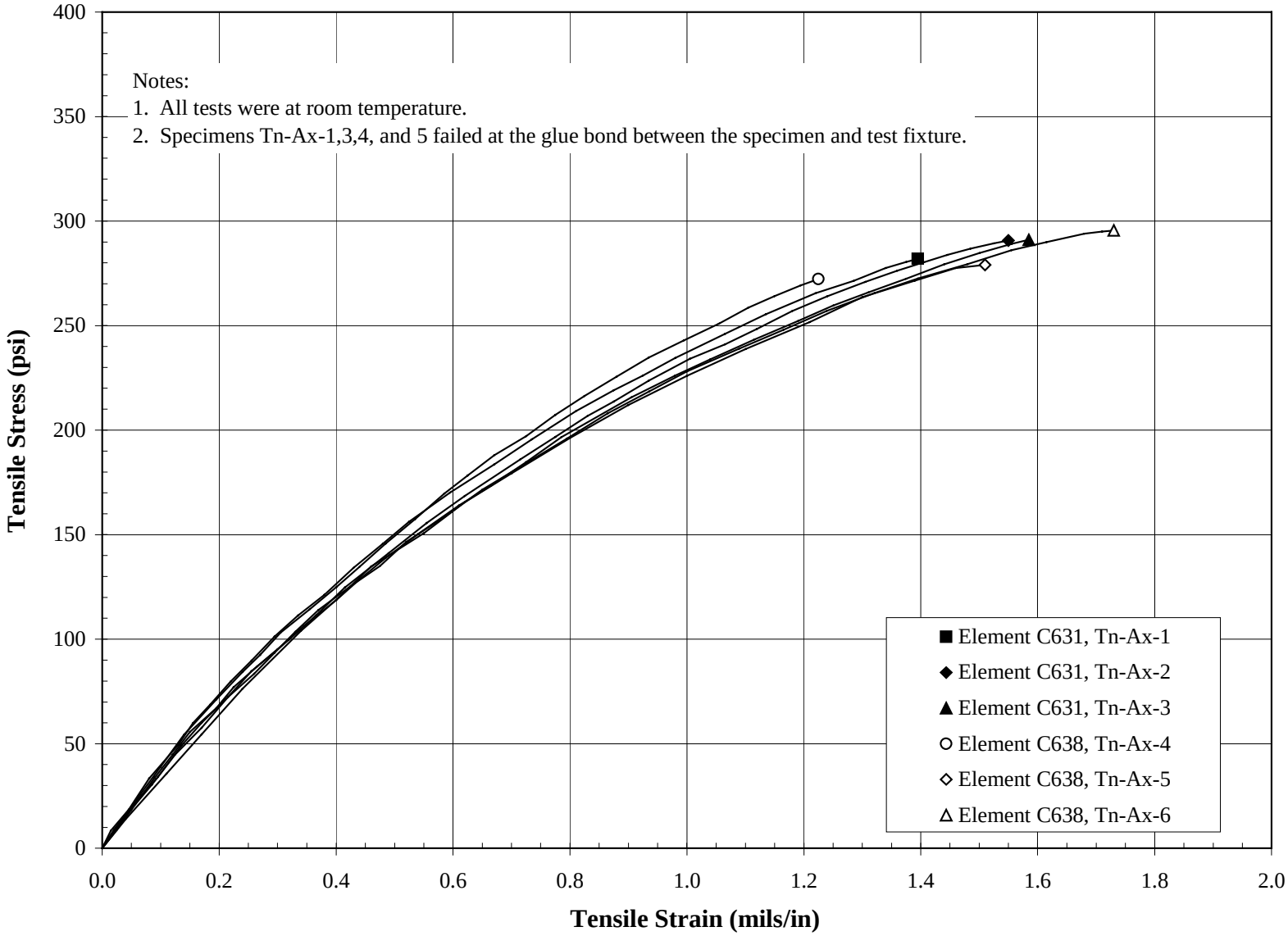

Figure 14-1 Room Temperature Axial Tensile Stress-Strain Responses for Virgin Honeywell PRD-66C

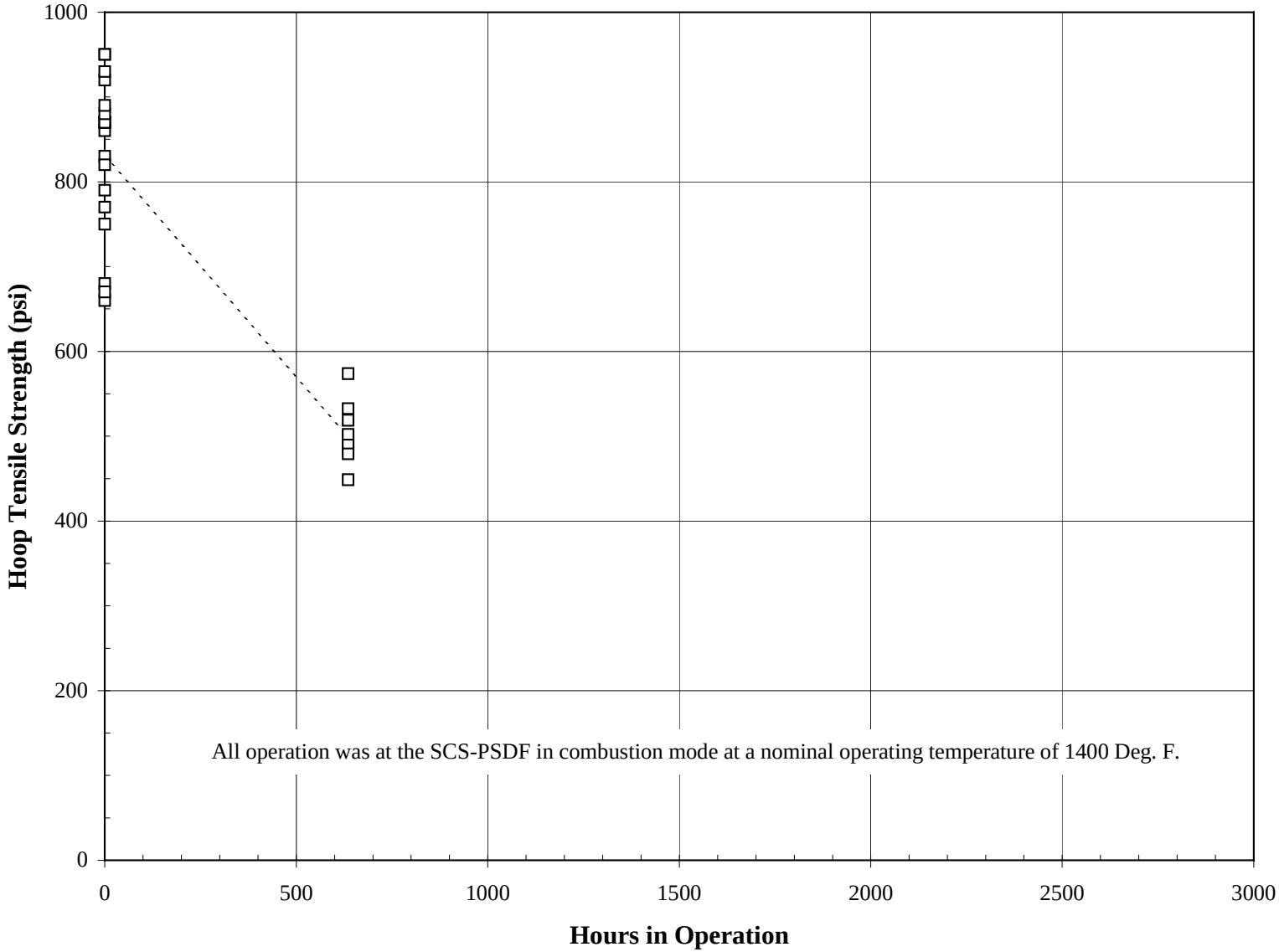

Figure 14-2 Room Temperature Hoop Tensile Strength Versus Hours in Operation for Honeywell PRD-66C

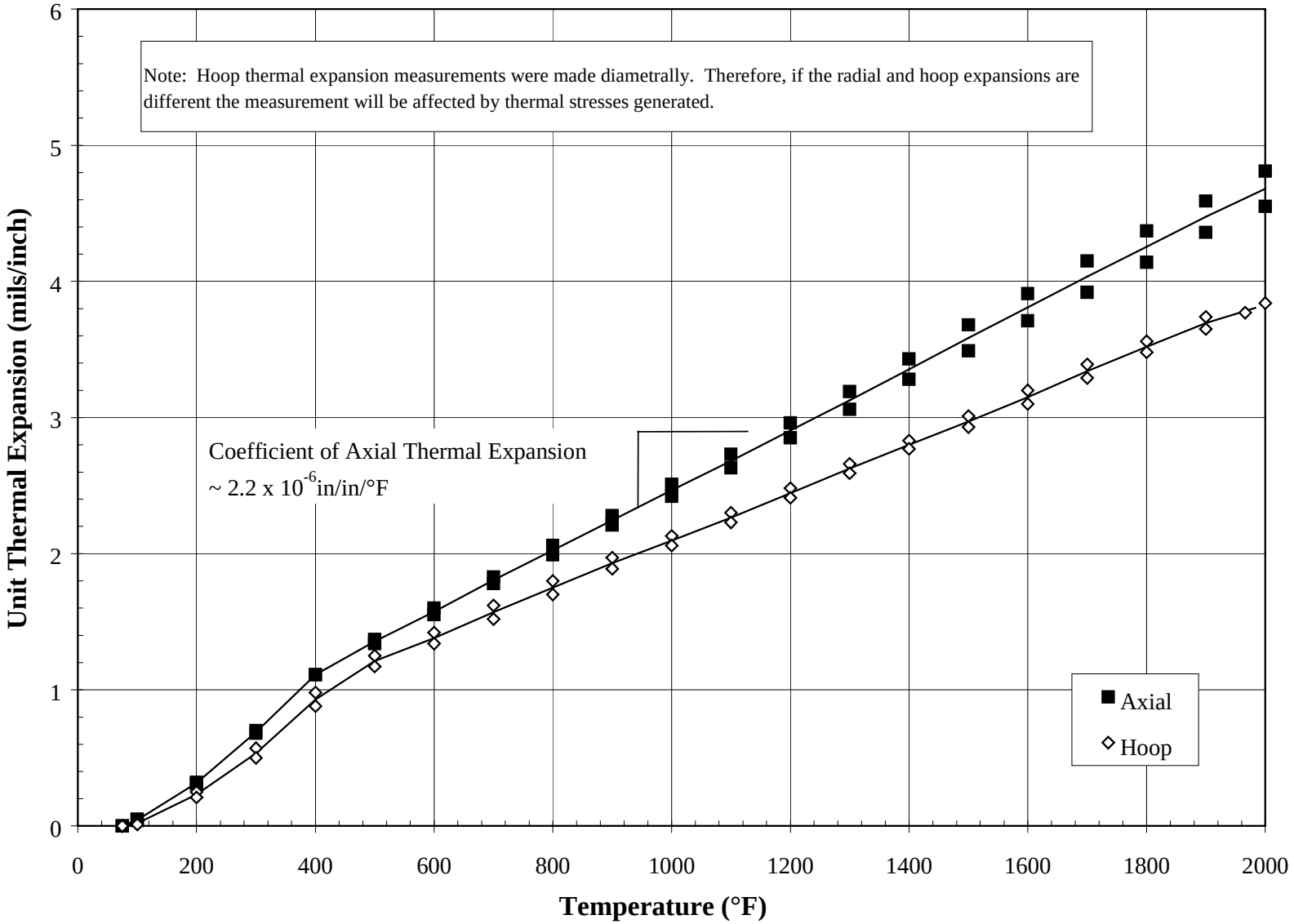

Figure 14-3 Unit Thermal Expansion of Virgin Honeywell PRD-66C

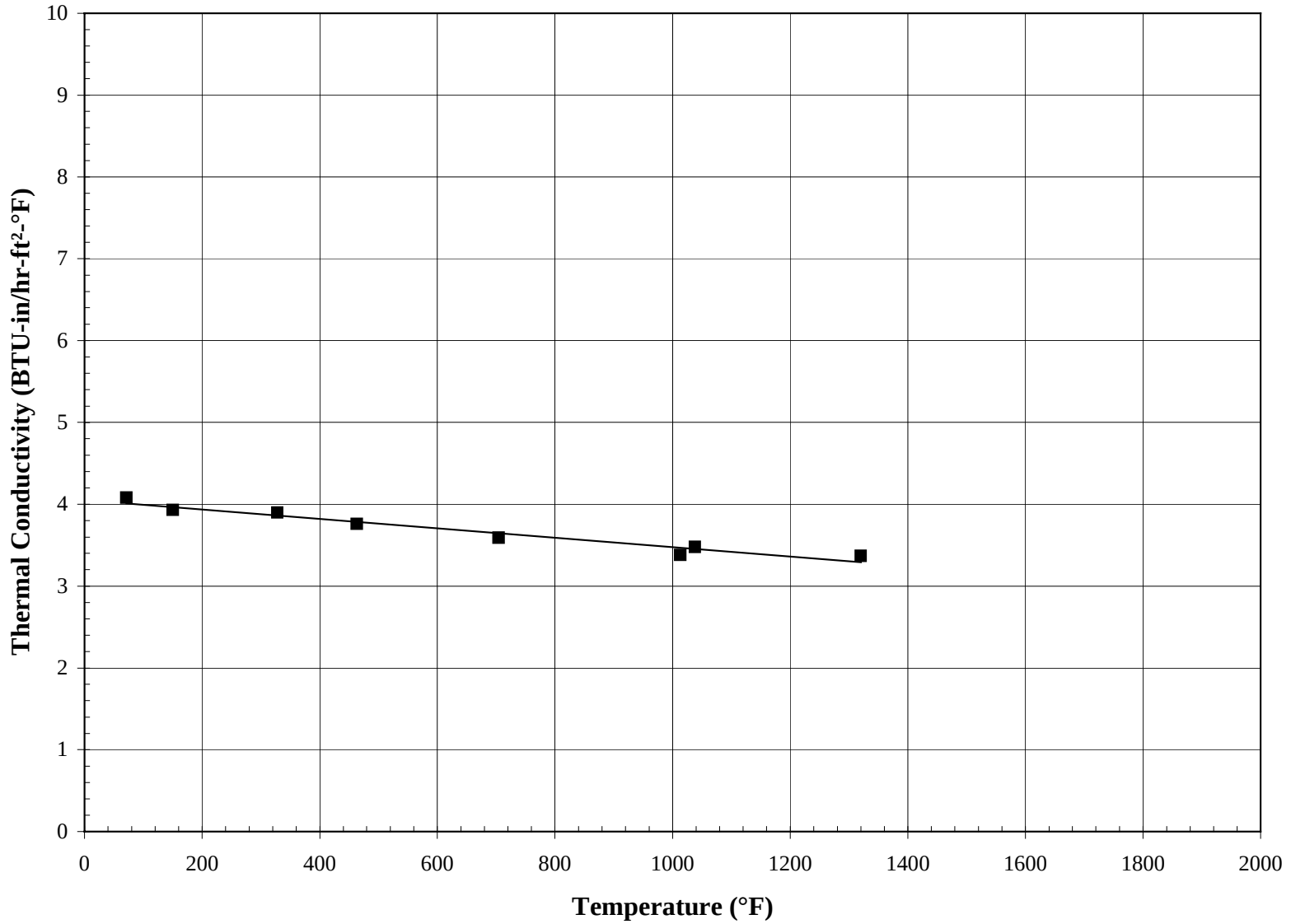

Figure 14-4 Radial Thermal Conductivity Versus Temperature for Virgin Honeywell PRD-66C

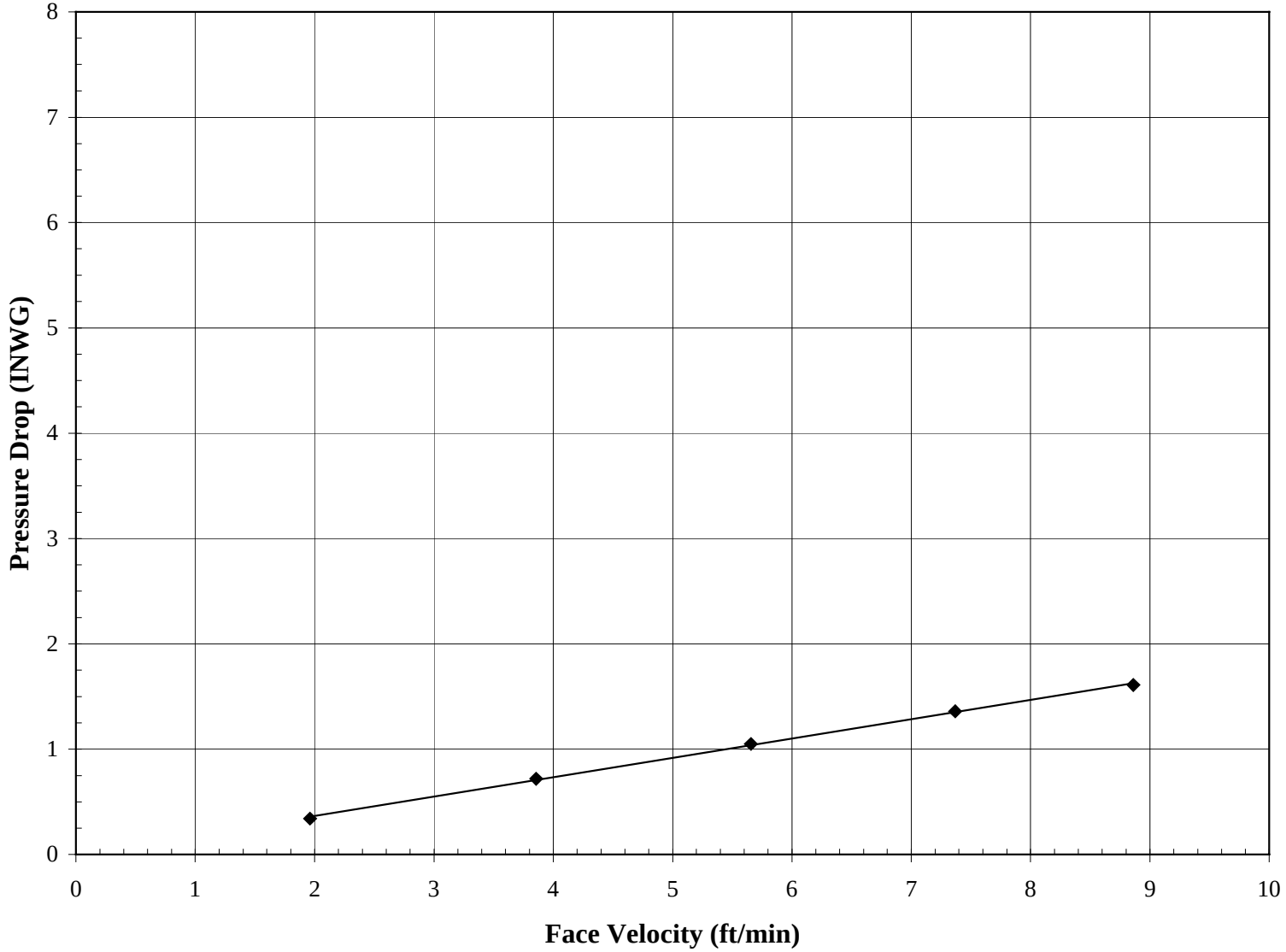

Figure 14-5 Pressure Drop Versus Face Velocity for Virgin Honeywell PRD-66C Using Air at Ambient Temperature and Pressure

15.0 3M OXIDE/OXIDE COMPOSITE

3M oxide/oxide is a three-layer composite element. The inside and outside layers provide structural support for the filtration mat in between. The inside- and outside-support layers are both Nextel™ 610 fiber (composition >99% Al_2O_3) in an alumino-silicate matrix. The filter mat is chopped-alumina fiber. Nominal overall dimensions are 2.22 in. (56 mm) I.D. and 2.38 in. (60 mm) O.D. Probable values of selected properties of virgin 3M oxide/oxide are as follows:

Hoop Tensile Strength at Room Temperature (psi)	2,530[1]
Hoop Young's Modulus at Room Temperature (10^6 psi)	3.1[1]
Axial Compressive Strength at Room Temperature (psi)	3,180[1]
Axial Compressive Strain-to-Failure at Room Temperature (mils/in.)	3.4
Pressure Drop at 5 ft/min Face Velocity, Air at Ambient Conditions(inWG)	1.1

Notes:

1. All stress calculations were based measured-specimen I.D. values and a nominal thickness of the inside structural wall of 0.055 in. The stress calculations assume that all load was carried by the inside structural wall.

Table 15-1

Room Temperature Hoop Strength of 3M Oxide-Oxide

Filter Identification	Specimen Number	Hours in Operation	Specimen I.D.[1] (in.)	Hydrostatic Pressure at Yield (psig)	Tensile Yield Strength (psi)	Maximum Hydrostatic Pressure (psig)	Tensile Strength (psi)	Young's Modulus[5] (msi)	Notes
8011	Tn-Hoop-145	Virgin	1.87	120	2120	140	2520	4.0	See Note 2
8011	Tn-Hoop-146	Virgin	1.89	130	2270	140	2570		See Note 3
8011	Te-ax-5	Virgin	1.91	100	1730	120	2210	2.1	See Note 2
8011	Te-ax-6	Virgin	2.00	90	1750	150	2840	3.3	See Note 2
Average				110	1968	138	2535	3.1	
Standard Deviation				16	234	11	224		
Coefficient of Variation (COV)				14%	12%	8%	9%		
8174	Tn-Hoop-330	1420	1.87	200	3550	230	4060	4.9	See Note 2
8174	Tn-Hoop-331	1420	1.89	200	3580	210	3720	2.7	See Note 2
8174	Tn-Hoop-332	1420	1.96	130	2400	150	2670	2.9	See Note 2
8174	Tn-Hoop-333	1420	1.95	130	2380	140	2480	2.6	See Note 2
8174	Tn-Hoop-334	1420	1.98	120	2300	130	2440	2.2	See Note 2
8174	Tn-Hoop-335	1420	1.99	130	2380	130	2470	4.1	See Note 2
Average				152	2765	165	2973	3.2	
Standard Deviation				34	567	40	660	0.9	
COV				23%	20%	24%	22%	29%	
8003	Tn-Hoop-324	1982	1.86			170	2870	3.2	See Note 4
8003	Tn-Hoop-325	1982	1.88			190	3270	3.0	See Note 4
8003	Tn-Hoop-326	1982	1.96			180	3220	3.4	See Note 4
8003	Tn-Hoop-327	1982	1.96			140	2490	2.9	See Note 4
8003	Tn-Hoop-328	1982	2.00			130	2480	3.3	See Note 4
8003	Tn-Hoop-329	1982	2.00			140	2600	3.0	See Note 4
Average						158	2822	3.1	
Standard Deviation						23	326	0.2	
COV						14%	12%	6%	

Notes:

1. The rough outside surface made accurate O.D. measurements impossible. All stress calculations were based on the measured I.D. and a nominal wall thickness of 0.055 in.
2. These stress-strain responses showed a definite "yield point" where large strains were seen with little increase in stress. No yield point was seen for the specimens in operation during the PCD fire.
3. Strain was not measured on this specimen. Yield strength was taken to be the point where a drop in internal pressure was seen on the load-time response.
4. In operation during PCD fire.
5. Young's modulus was obtained in the initial linear portion of the stress-strain curve. The values were calculated based on the same assumptions as the strength values and are intended for use only in comparison of elements (element-to-element variability, as-manufactured vs. used, etc.)
6. All specimens were 3 in. long. The ends were constrained with 5/16-in. hose clamps to prevent the bladder from extruding.

Table 15-2

Axial Compressive Properties of Virgin 3M Oxide-Oxide

Filter Identification	Specimen Number	Test Temperature (°F)	Specimen I.D.[1] (in.)	Compressive Yield Strength (psi)	Ultimate Compressive Strength (psi)	Young's Modulus (msi)
8011	Cm-ax-1	70	1.92	2550	3230	3.5
8011	Cm-ax-3	70	1.93	2550	3660	4.0
8011	Cm-ax-4	70	1.94	2900	2950	3.7
8011	Cm-ax-5	70	See Note 2	1730	2870	2.4
	Average			2433	3178	3.4
	Standard Deviation			430	309	0.6
	Coefficient of Variation (COV)			18%	10%	18%

Notes:

1. The rough outside surface made accurate O.D. measurements impossible. All stress calculations were based on a nominal wall thickness of 0.055 in.
2. The specimen I.D. was not measured on this specimen. The average value of the other specimens was used for the stress calculation.

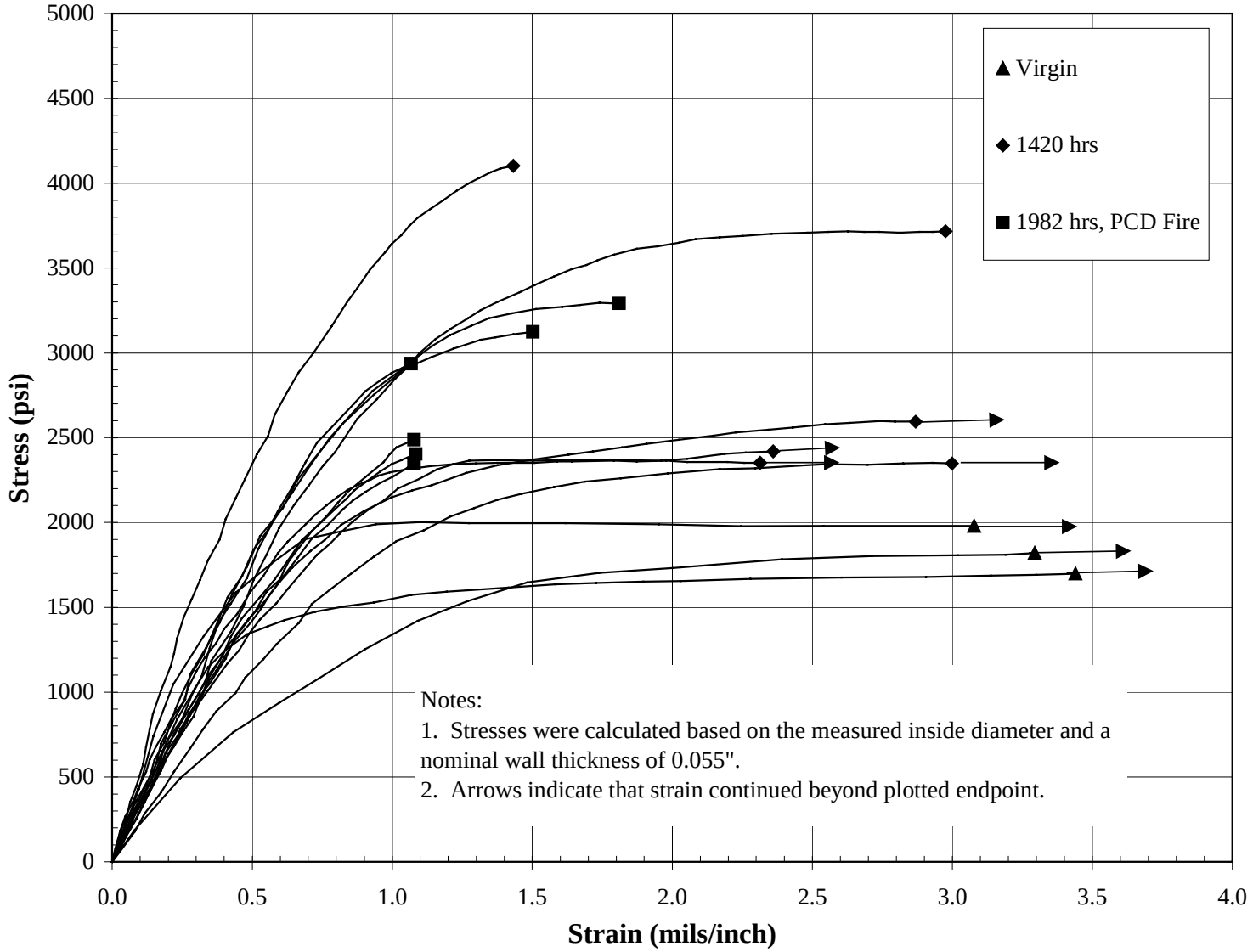

Figure 15-1 Room Temperature Hoop Tensile Stress-Strain Responses for 3M Oxide-Oxide Virgin and After Combustion Operation

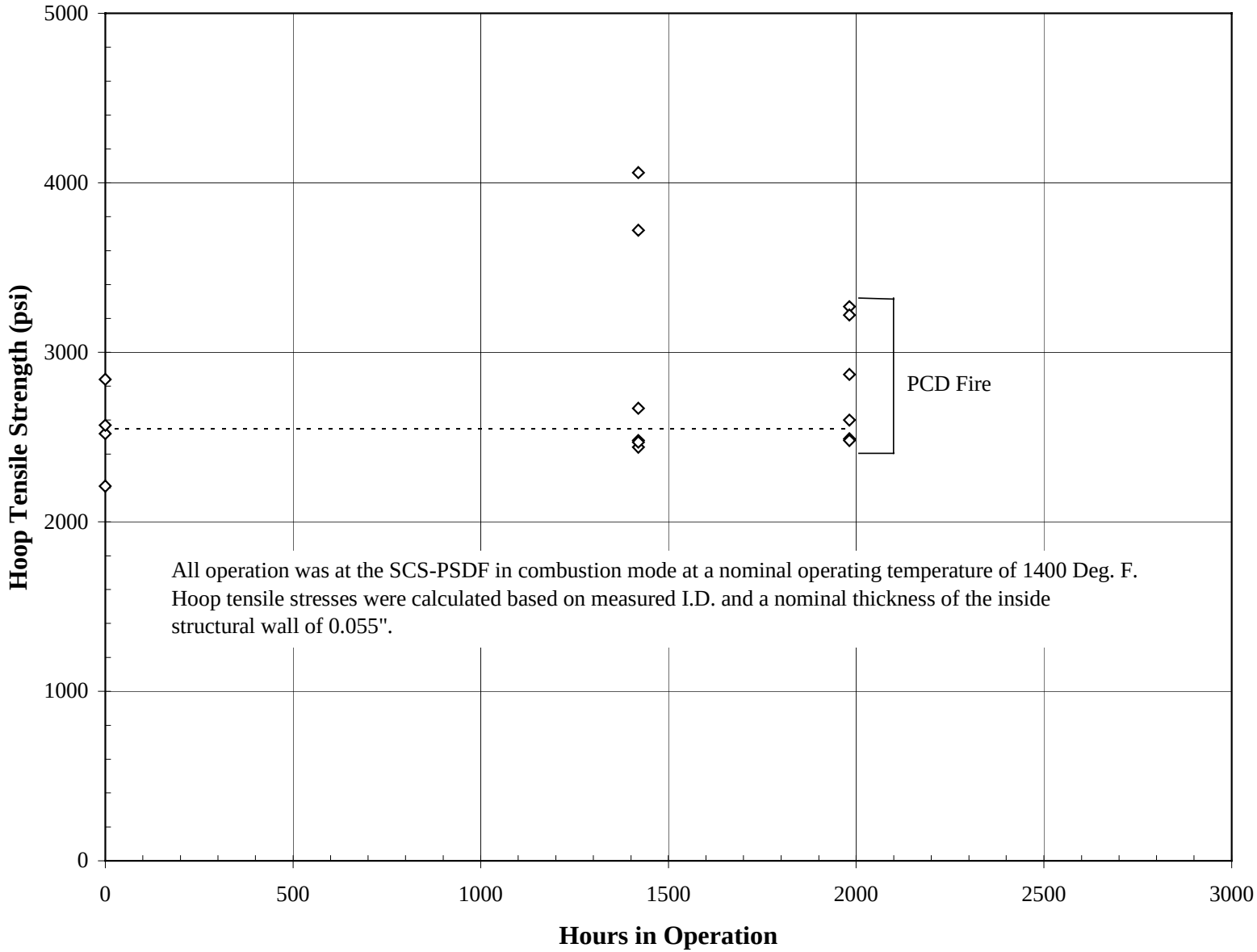

Figure 15-2 Room Temperature Hoop Tensile Strength Versus Hours Operation for 3M Oxide-Oxide

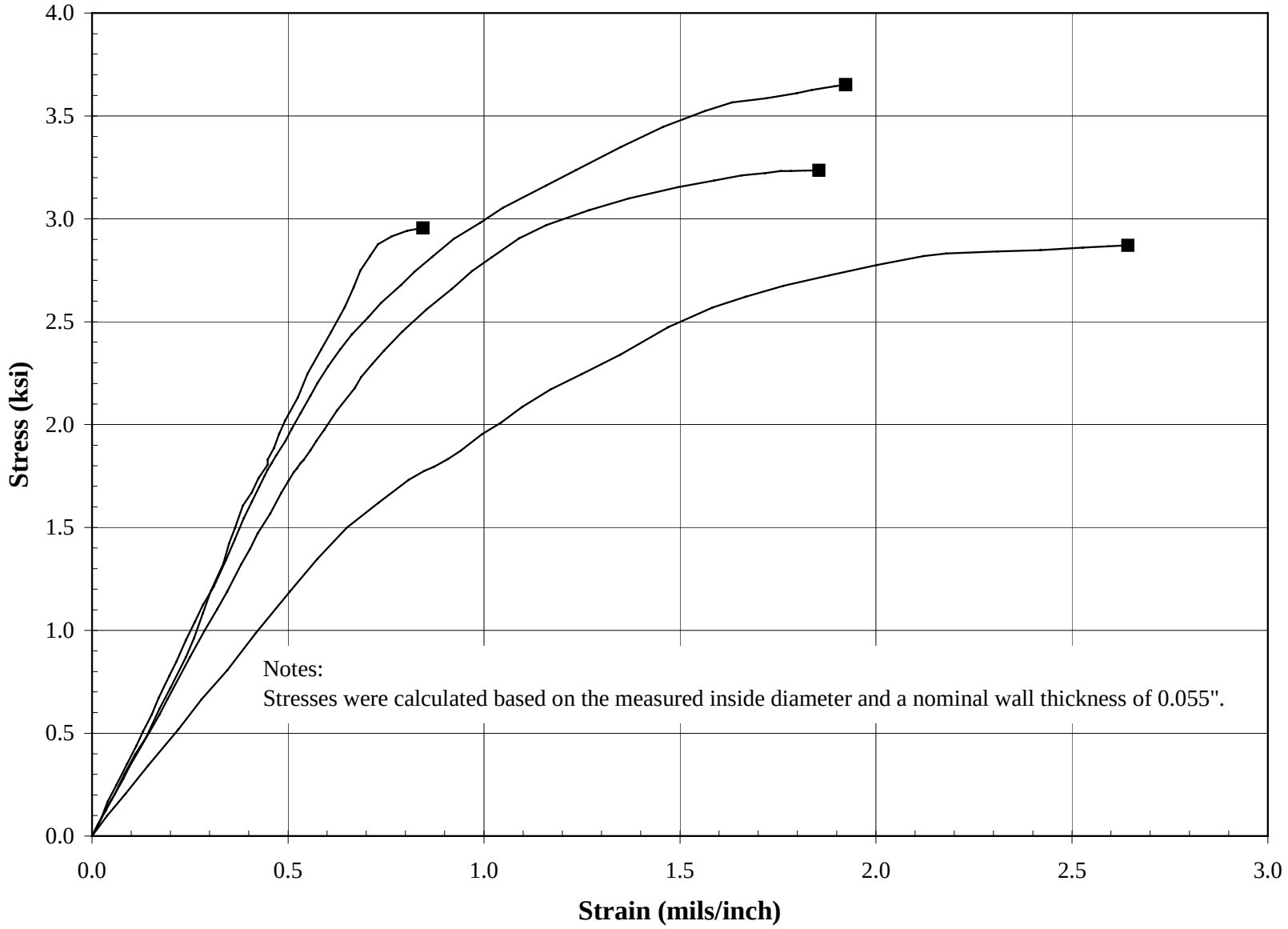

Figure 15-3 Room Temperature Axial Compressive Stress-Strain Responses for Virgin 3M Oxide-Oxide

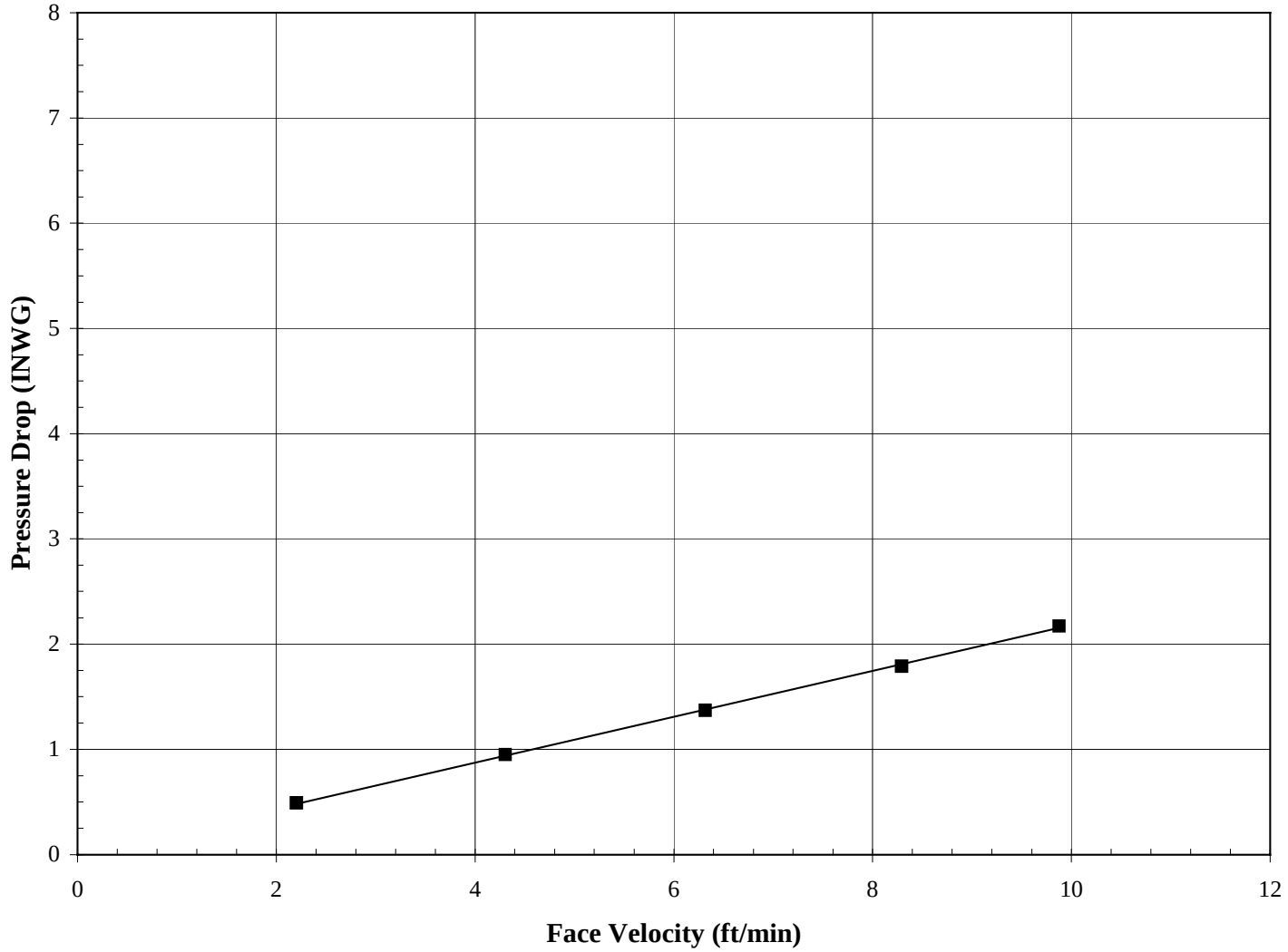

Figure 15-4 Pressure Drop Versus Face Velocity for Virgin 3M Oxide-Oxide Using Air at Ambient Temperature and Pressure

16.0 PALL IRON ALUMINIDE

Pall iron aluminide is a sintered-powder metal element. Each element consists of multiple 18-in. sections (three sections for a 1.5-meter element) welded together. The flange is welded to one end and an end cap to the other. Nominal dimensions are 2.22-in. (56 mm) I.D. and 0.065-in. (1.7 mm) wall thickness. Pall iron aluminide elements are depth filters with no membrane layer. Probable values of selected properties of virgin Pall iron aluminide are as follows:

Bulk Density (lbm/ft^3)	245
Hoop Tensile Strength at Room Temperature (psi)	17,300[1]
Axial Tensile Strength at Room Temperature (psi)	19,000[1]
Axial Young's Modulus at Room Temperature (10^6 psi)	5.2
Axial Tensile Strain-to-Failure at Room Temperature (mils/in.)	9.5
Axial Tensile Strength at 1,400°F (psi)	6,300[1]
Axial Young's Modulus at 1,400°F (10^6 psi)	3.6
Axial Tensile Strain-to-Failure at 1,400°F (mils/in.)	14.8
Axial Coefficient of Thermal Expansion, 500 to 1,500°F (10^{-6} in./in./°F)	13.1
Pressure Drop at 5 ft/min Face Velocity, Air at Ambient Conditions(inWG)	4.1

Notes:
1. Ultimate strength shown; yielding occurred at a lower stress level.

Table 16-1

Density of Pall Iron Aluminide

Element	Specimen Number	Hours in Operation	I.D. (in.)	O.D. (in.)	Density (gr/cm^3)	Density (lb/ft^3)	Remarks
034H-002	Tn-Hoop-309	virgin	2.22	2.37	3.91	244	
034H-002	Tn-Hoop-310	virgin	2.22	2.37	3.89	243	
034H-002	Tn-Hoop-311	virgin	2.22	2.37	3.90	243	
034H-002	Tn-Hoop-312	virgin	2.22	2.37	3.90	243	
034H-002	Tn-Hoop-313	virgin	2.22	2.37	3.93	245	
034H-002	Tn-Hoop-314	virgin	2.20	2.35	4.00	250	
034H-002	Tn-Hoop-315	virgin	2.23	2.37	3.92	245	
		Average			3.92	245	
		Standard Deviation			0.03	2.18	
		Coefficient of Variation (COV)			0.89%	0.89%	
034H-001	Tn-Hoop-316	1356	2.21	2.37	3.97	248	See Notes 1,2
034H-001	Tn-Hoop-317	1356	2.22	2.37	3.96	247	See Notes 1,2
034H-001	Tn-Hoop-318	1356	2.21	2.37	4.01	250	See Notes 1,2
034H-001	Tn-Hoop-320	1356	2.20	2.36	3.92	244	See Notes 1,2
034H-001	Tn-Hoop-321	1356	2.20	2.36	3.97	247	See Notes 1,2
034H-001	Tn-Hoop-322	1356	2.22	2.36	4.00	249	See Notes 1,2
034H-001	Tn-Hoop-323	1356	2.23	2.37	3.99	249	See Notes 1,2
		Average			3.97	248	
		Standard Deviation			0.03	1.84	
		COV			0.74%	0.74%	
504J	Tn-Hoop-336	1424	2.19	2.33	4.05	253	See Notes 1,2,3
504J	Tn-Hoop-337	1424	2.18	2.32	4.05	252	See Notes 1,2,3
504J	Tn-Hoop-338	1424	2.17	2.31	4.11	257	See Notes 1,2,3
504J	Tn-Hoop-339	1424	2.19	2.33	4.02	251	See Notes 1,2,3
504J	Tn-Hoop-340	1424	2.18	2.34	4.00	250	See Notes 1,2,3
504J	Tn-Hoop-341	1424	2.17	2.33	4.01	250	See Notes 1,2,3
		Average			4.04	252	
		Standard Deviation			0.04	2.38	
		COV			0.95%	0.95%	

Notes:

1. Elements were water washed before density measurements but some ash remained in the pores. Density values were calculated based on weights measured with ash in the pores and, therefore, do not represent a material property. The values are for comparison only.
2. All operation at the SCS PSDF in combustion mode at a nominal-operating temperature of 1,400°F.
3. In operation during October 1998 PCD fire.

Table 16-2

Axial Tensile Properties of Pall Iron Aluminide

Candle	Specimen Number	Hours in Operation	Test Temperature (°F)	0.05% Yield Strength (psi)	Ultimate Strength (psi)	Young's Modulus (msi)	Strain-to-Failure (mils/in.)	Remarks
034H-002	Tn-Ax-1	virgin	70	13400	20200	5.26	10.1	
034H-002	Tn-Ax-3	virgin	70	12770	18670	4.94	9.56	
034H-002	Tn-Ax-4	virgin	70	12160	18400	5.38	8.95	
			Average	12777	19090	5.19	9.54	
034H-002	Tn-Ax-2	virgin	1400	4140	6440	3.83	14.0	
034H-002	Tn-Ax-5	virgin	1400	4340	6110	3.29	15.6	
			Average	4240	6275	3.56	14.8	
034H-001	Tn-Ax-6	1356	70	10820	15680	5.36	6.71	See Note 1
034H-001	Tn-Ax-7	1356	70	10920	15100	5.36	5.76	See Note 1
034H-001	Tn-Ax-8	1356	70	11040	16440	5.28	8.32	See Note 1
034H-001	Tn-Ax-9	1356	70	11570	16950	4.89	8.45	See Note 1
			Average	11088	16043	5.22	7.31	

Notes:
1. All operation at the SCS PSDF in combustion mode at a nominal-operating temperature of 1,400°F.

Table 16-3

Room Temperature Hoop Tensile Strength of Pall Iron Aluminide

Candle	Specimen Number	Hours in Operation	Maximum Hydrostatic Pressure (psig)	Ultimate Strength (psi)	Young's Modulus (msi)	Maximum Strain at O.D. (mils/in.)	Remarks
034H-002	Tn-Hoop-309	virgin	1170	18000	6.09	5.63	
034H-002	Tn-Hoop-310	virgin	1150	17590	7.29	4.93	
034H-002	Tn-Hoop-311	virgin	1160	17460	5.84	5.18	
034H-002	Tn-Hoop-312	virgin	1110	17100	5.96	4.90	
034H-002	Tn-Hoop-313	virgin	1150	17720	5.64	5.69	
034H-002	Tn-Hoop-314	virgin	1060	16580	5.78	4.70	
034H-002	Tn-Hoop-315	virgin	1080	16750	5.84	4.82	
Average			1126	17314	6.06	5.12	
Standard Deviation			40	483	0.52	0.37	
Coefficient of Variation (COV)			4%	3%	9%	7%	
034H-001	Tn-Hoop-316	1356	790	11840	5.69	2.51	See Note 1
034H-001	Tn-Hoop-317	1356	970	14470	5.83	4.24	See Note 1
034H-001	Tn-Hoop-318	1356	900	13490	7.47	3.20	See Note 1
034H-001	Tn-Hoop-320	1356	1060	15220	5.78	4.79	See Note 1
034H-001	Tn-Hoop-321	1356	1030	15020	5.89	4.25	See Note 1
034H-001	Tn-Hoop-322	1356	910	15110	5.39	4.86	See Note 1
034H-001	Tn-Hoop-323	1356	870	14460	6.41	4.08	See Note 1
Average			933	14230	6.07	3.99	
Standard Deviation			87	1118	0.64	0.79	
COV			9%	8%	11%	20%	
504J	Tn-Hoop-336	1424	721	11260	6.10	1.86	See Notes 1,2
504J	Tn-Hoop-337	1424	755	11720	6.20	1.97	See Notes 1,2
504J	Tn-Hoop-338	1424	728	11260	6.30	1.88	See Notes 1,2
504J	Tn-Hoop-339	1424	891	13980	6.06	2.82	See Notes 1,2
504J	Tn-Hoop-340	1424	1068	15120	6.13	3.61	See Notes 1,2
504J	Tn-Hoop-341	1424	1061	15080	6.28	3.47	See Notes 1,2
Average			870	13070	6.18	2.60	
Standard Deviation			148	1705	0.09	0.74	
COV			17%	13%	1%	28%	

Notes:
1. All operation at the SCS PSDF in combustion mode at a nominal-operating temperature of 1,400°F.
2. In operation during October 1998 PCD fire.

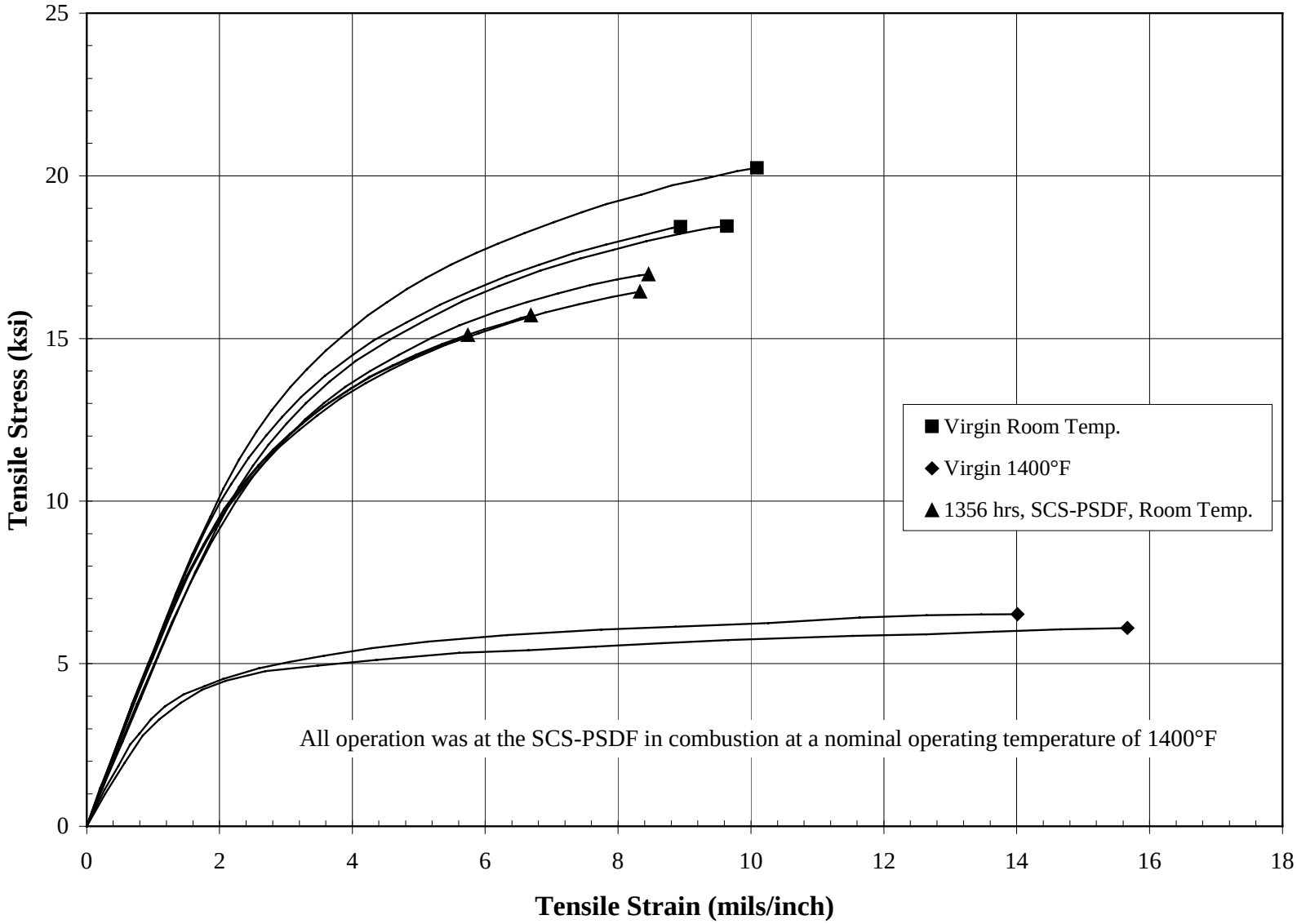

Figure 16-1 Axial Tensile Stress-Strain Responses for Pall Iron Aluminide Virgin and After-Combustion Operation

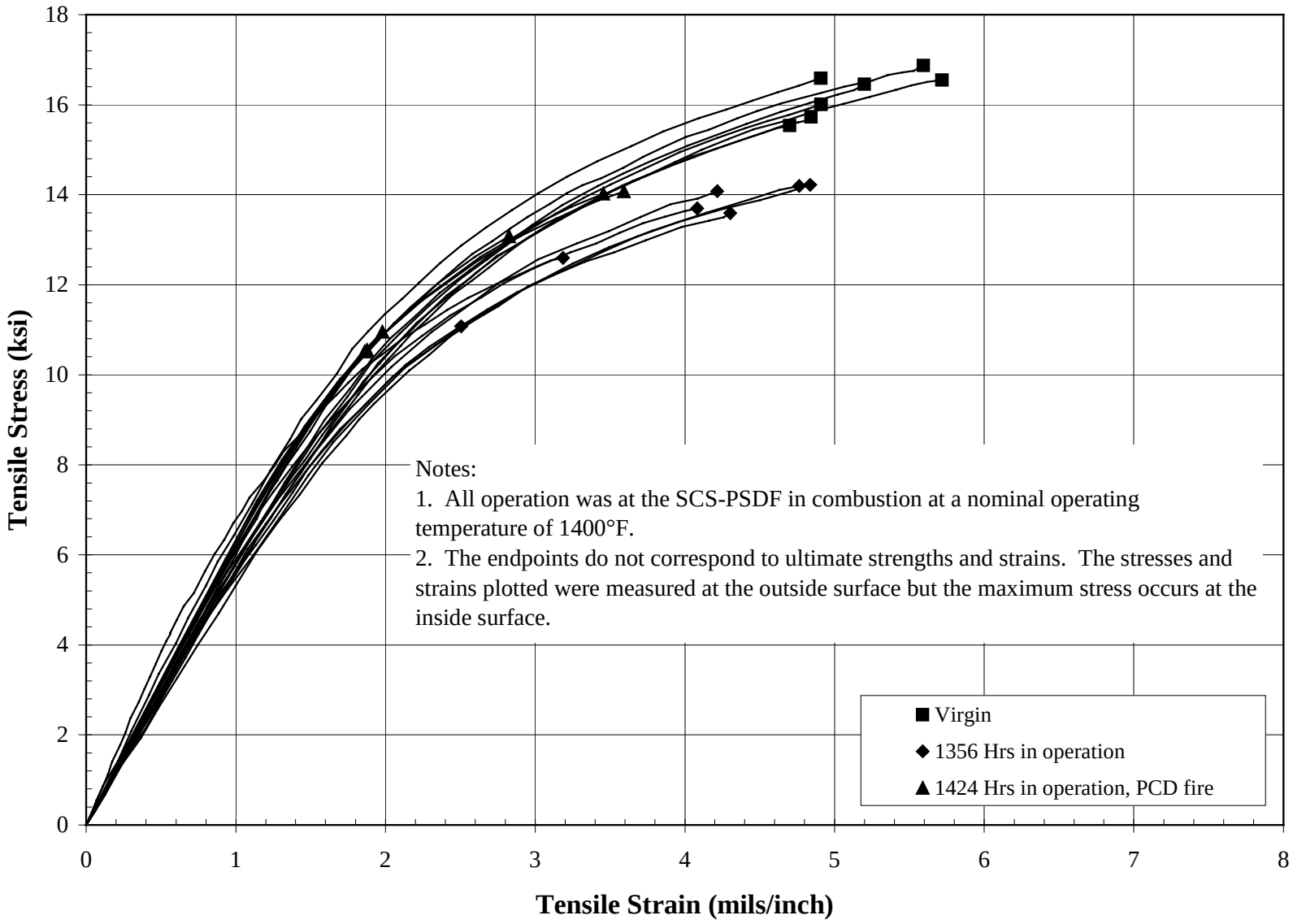

Figure 16-2 Room Temperature Hoop Tensile Stress-Strain Responses for Pall Iron Aluminide Virgin and After-Combustion Operation

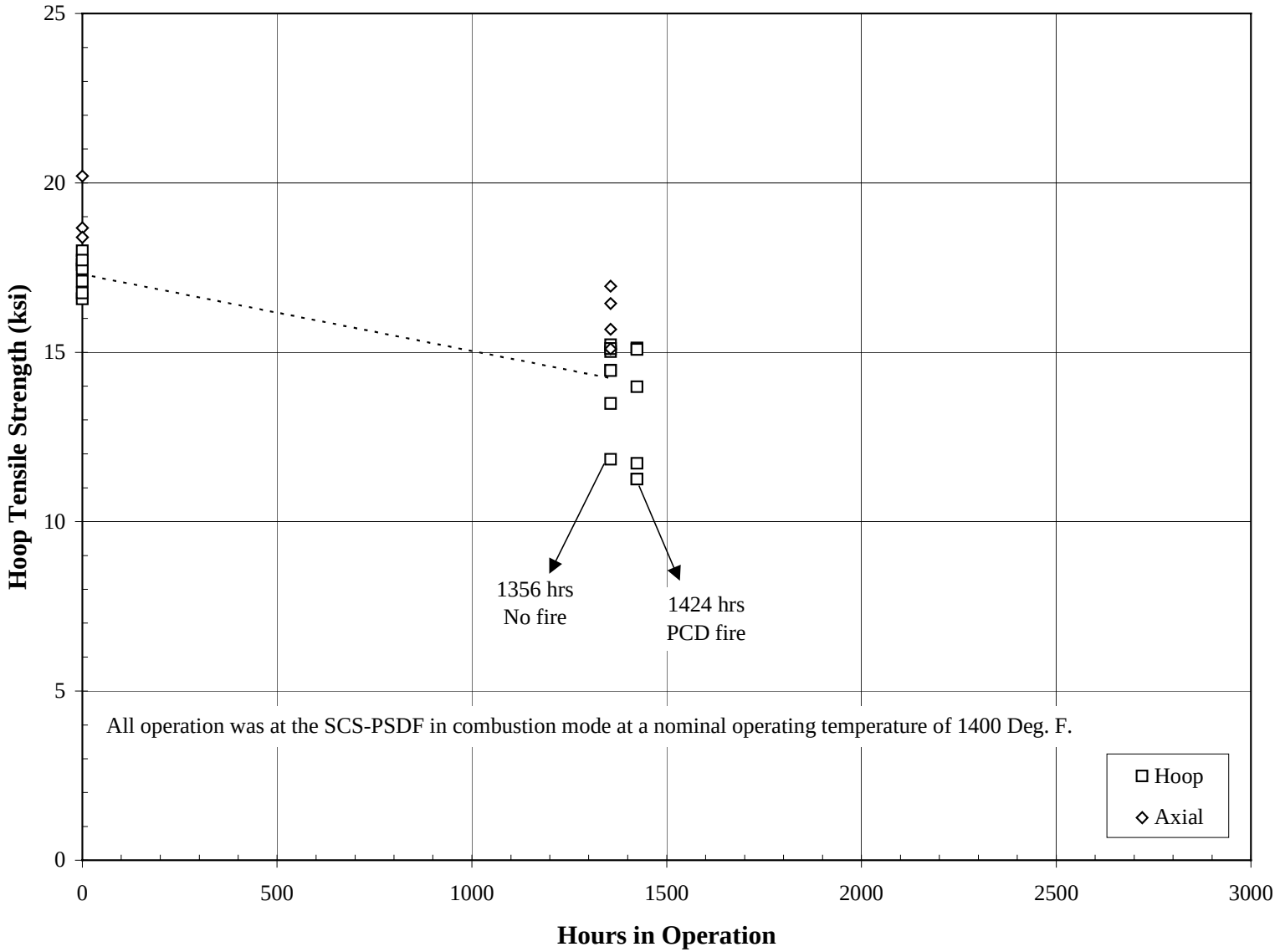

Figure 16-3 Room Temperature Hoop Tensile Strength Versus Hours in Operation for Pall Iron Aluminide

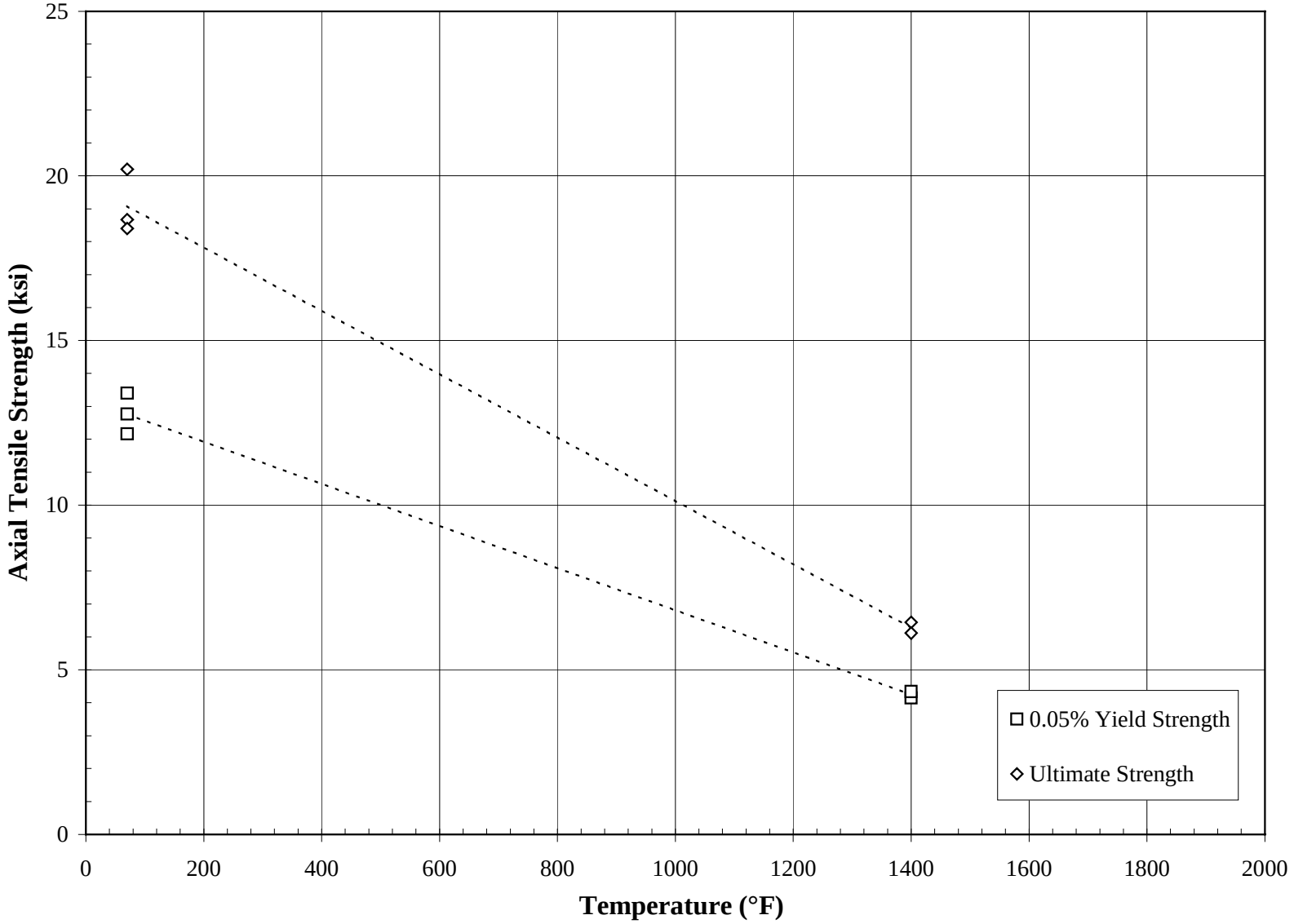

Figure 16-4 Axial Tensile Strength Versus Temperature for Virgin Pall Iron Aluminide

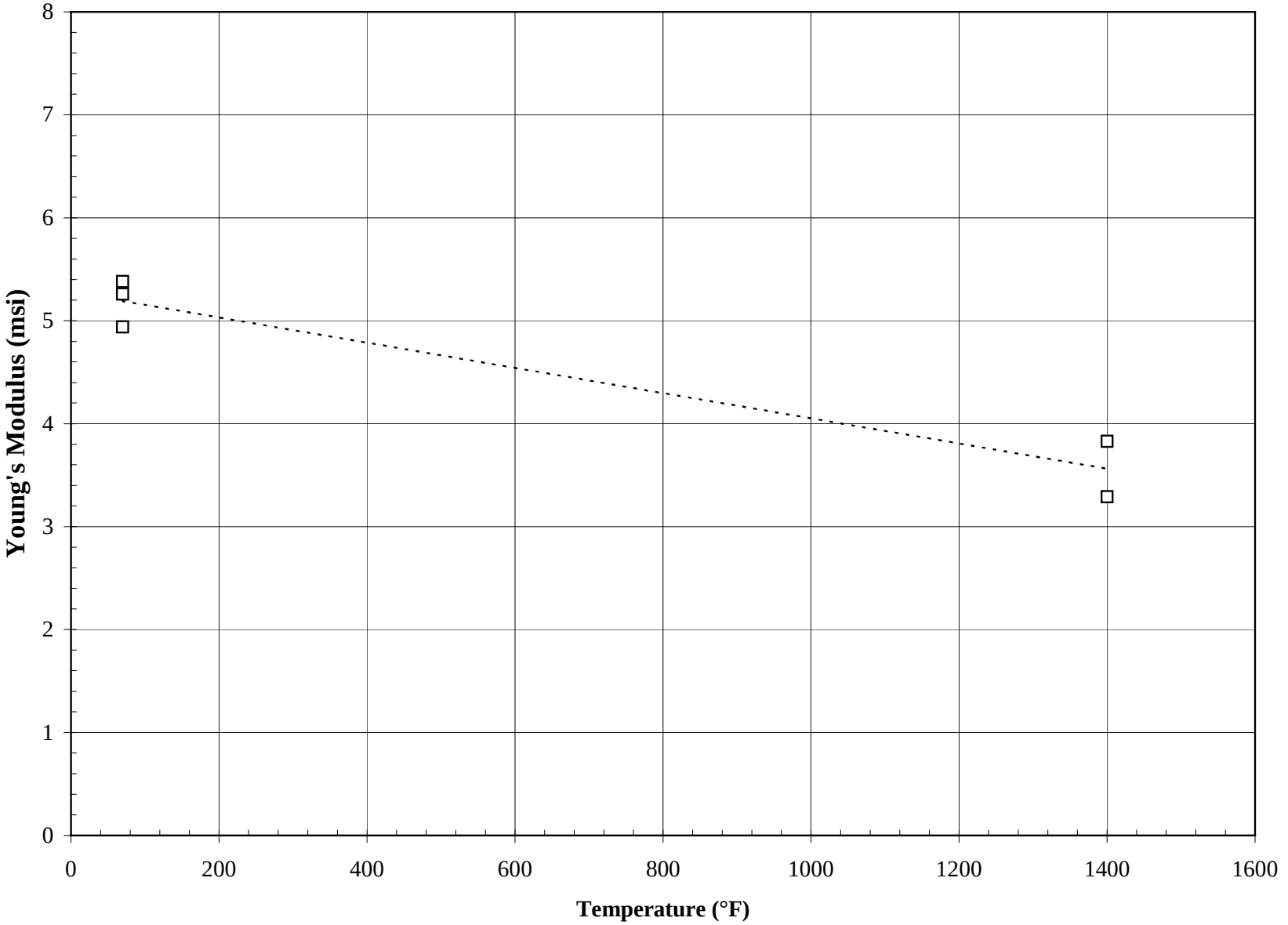

Figure 16-5 Axial Young's Modulus Versus Temperature for Virgin Pall Iron Aluminide

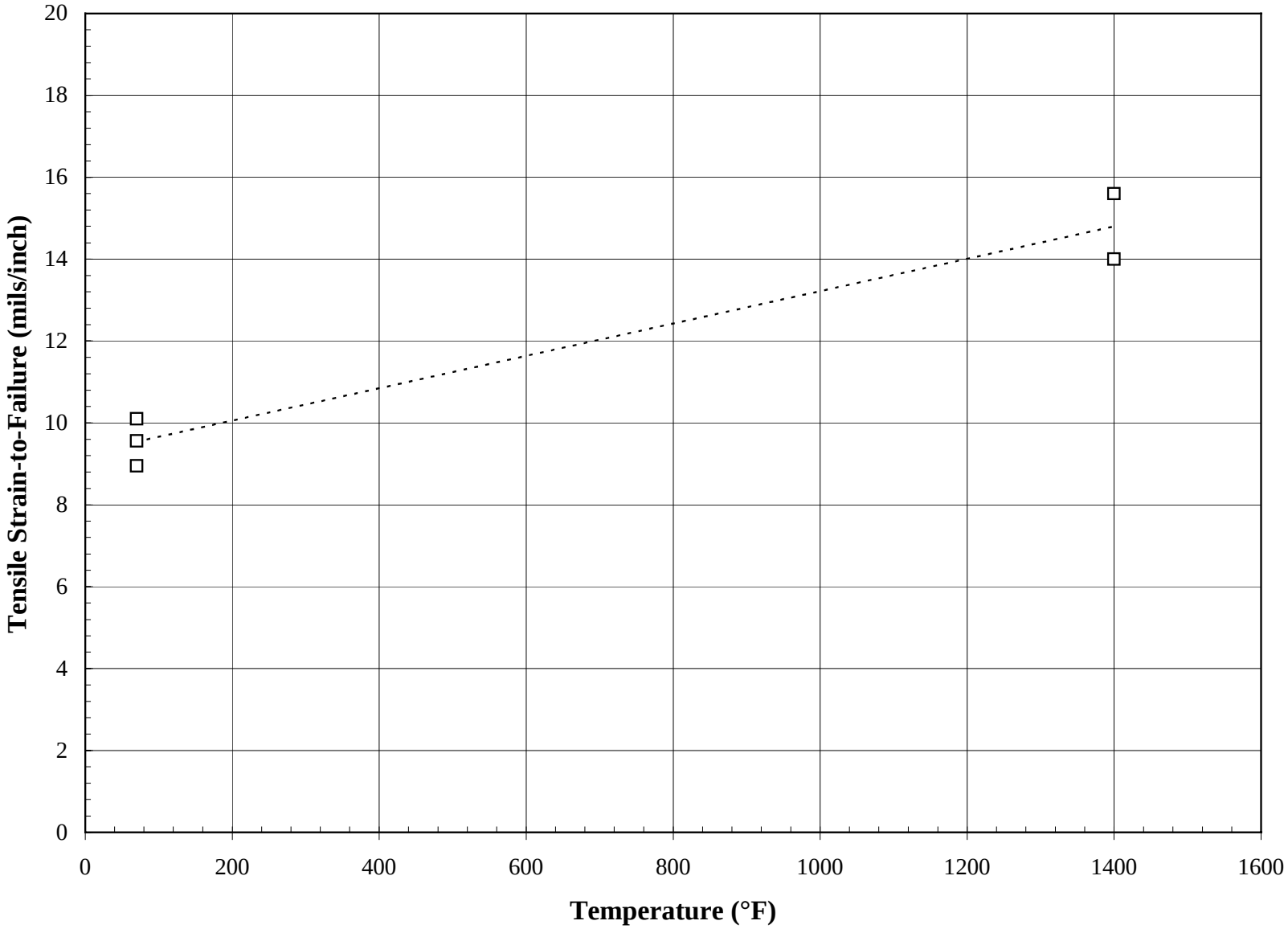

Figure 16-6 Axial Tensile Strain-to-Failure Versus Temperature for Virgin Pall Iron Aluminide

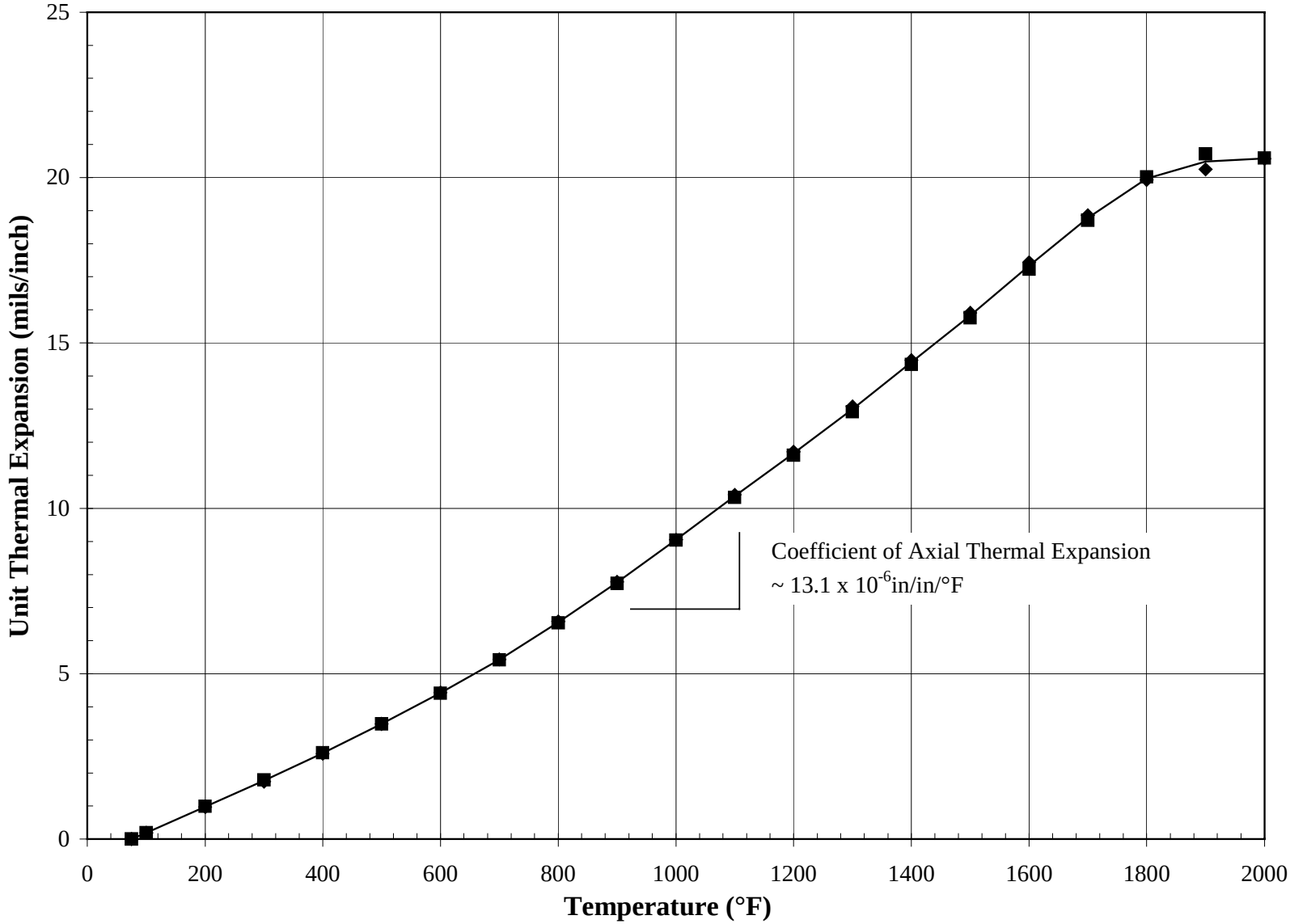

Figure 16-7 Unit Thermal Expansion of Virgin Pall Iron Aluminide

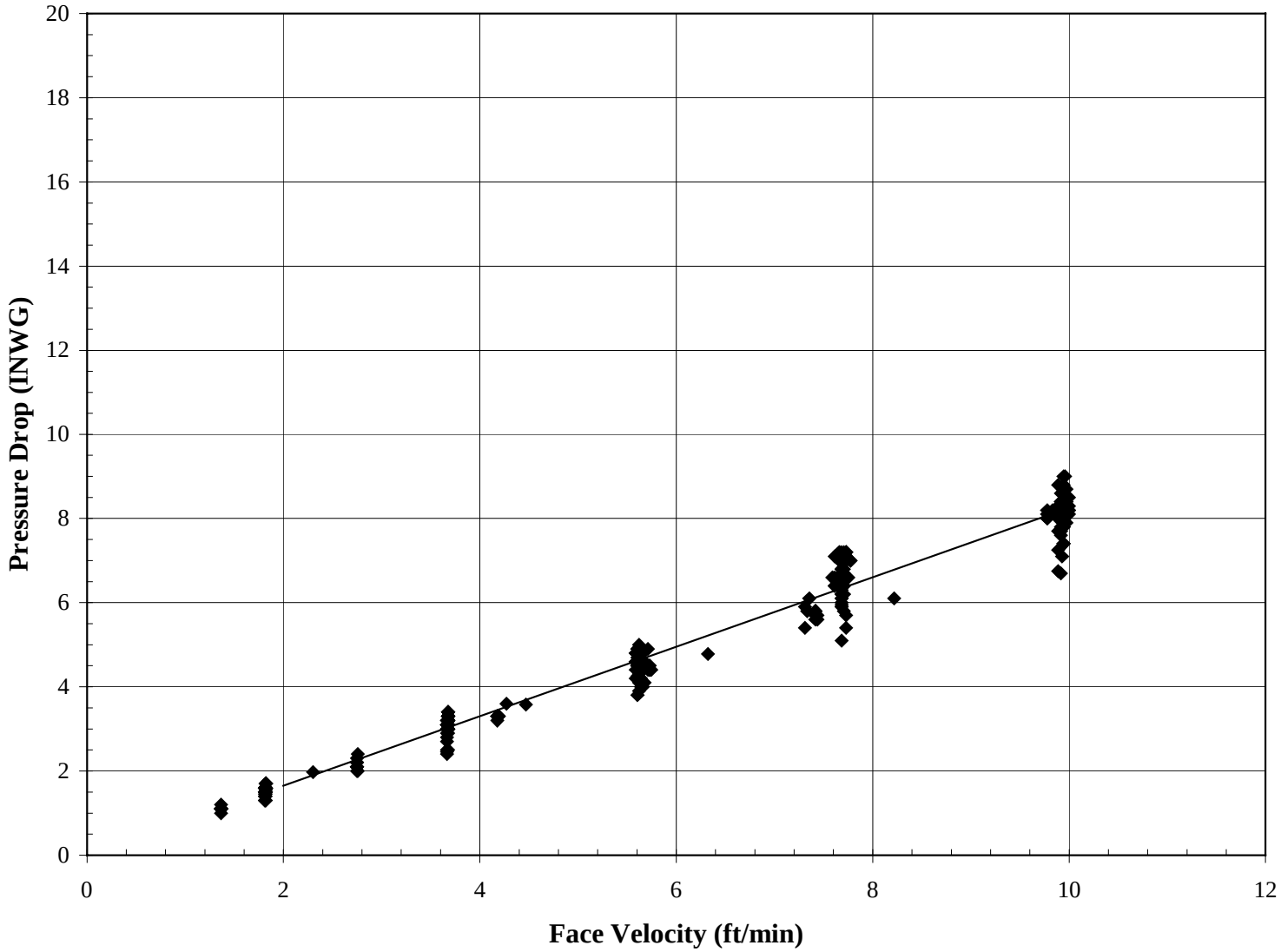

Figure 16-8 Pressure Drop Versus Face Velocity for Virgin Pall Iron Aluminide Using Air at Ambient Temperature and Pressure